

UNIVERSITY OF NAPLES FEDERICO II



Department of Civil, Building and Environmental Engineering (DICEA)

PhD Research in **Civil Systems Engineering**

XXXIII Cycle

Candidate

Luca Di Girolamo

Research Title

**EXPERIMENTAL INVESTIGATIONS AND ANALYSIS OF PILES
AS HEAT EXCHANGERS IN PYROCLASTIC SOILS**

PhD Coordinator:

Prof. Ing. Andrea Papola

Tutor:

Prof. Ing. Gianpiero Russo

Abstract

Sustainability and the greenhouse gases containment are the main purpose of the world policies to combat climate change. These are certainly in contrast with the world's growing demand for energy that is still too heavily based on fossil fuels, which are the main causes of gas emissions.

The European Energy policies for more than 20 years have been based on the reduction of the carbon dioxide emissions using renewable energy sources and the reducing the final energy consumption.

Shallow Geothermal Energy (SGE) is a rapidly growing technology all over Europe as a support for the Renewable Energy policies and European Directives because of its low greenhouse gas emissions into the atmosphere. It is considered a renewable source on the timescales of technological/societal systems because do not require the geological times of fossil fuel reserves such as coal, oil, and gas. Low enthalpy geothermal energy is used for heating and/or cooling building by exploiting the ground heat by ground heat exchangers connected to a geothermal source heat pump (GSHP).

Energy piles represents a rather innovative technology that couples the role of the structural foundation with the role of the heat exchangers for GSHP plants to satisfy the building heating and cooling needs. Compared to the traditional pile foundations, these structures are loaded both by mechanical and thermal loads, where for thermal loads is commonly intended the application of a thermal distortion. During the last years, thermal and thermomechanical behavior of energy piles has been investigated by different approaches.

In this PhD thesis the main aim was to investigate on the thermomechanical behavior of energy piles contextualized in Neapolitan context both by a geotechnical and energy point of view.

First of all, a general overview about the social and energy European context and about the geothermal energy, an introduction to energy piles, by both a mechanical and an energetical point of view, was reported.

The research was carried out following three different approaches: numerical modelling, small-scale tests, and field scale tests.

As regard the numerical modelling, two types of analyses were carried out. In the former case by an axisymmetric FEM model, the impact of different surface thermal boundary conditions on the thermomechanical behavior of a single end bearing energy pile embedded in pyroclastic multilayer soil is investigated. The latter case is about the study of the interaction factors for a couple of energy piles where only one is thermally loaded while the other is embedded as a passive element in the deformation field generated by the loaded pile. The results were obtained for different pile spacings and for different subsoil and are presented in the chapter 4.

Chapter 5 is dedicated to the small-scale test carried out on an aluminum energy prototype pile embedded in Neapolitan pyroclastic dry sand. Both thermal and thermomechanical tests were carried out considering a cyclical application of the thermal loads both in heating and in cooling mode and also considering the impact of different mechanical loads. The thermal loads provided to pile was obtained from a dynamic energy simulation of a building in the city of Naples. The results showed different axial forces distribution depending on the kind and magnitude of thermal and mechanical load applied on pile. Moreover, it was observed irreversible pile displacements during the application of cyclic thermal loads.

Finally, in the chapter 6 a field test was carried out in the province of Naples on a bored concrete energy pile 12 m in length and 0,60 m in diameter embedded in pyroclastic soil and equipped with a spiral heat exchanger configuration. Three heating thermal tests with different time duration were carried out. From the tests was observed that the null point of the pile was located at the same depth for all the tests. Anyway, the magnitude of the axial forces depended on the duration of the test and the magnitude of the inlet heat carrier fluid. The pile heating did not affect the surrounding soil temperatures during the tests and a high flow rate of heat power exchanged between the pile and soil was measured. The measured pile displacements ranged between the 75% and 78% of the theoretical free displacement. Moreover, a long-time monitoring of the pile and surrounding soil was carried out for about 7 months. The data collected allowed to study the site underground temperatures trend over the time and for different depth. It was also possible to find the mean value of the subsoil thermal diffusivity and consequently predict a yearly temperature trend over the time and for different depth for the site.

Table of contents

Chapter 1	1
1 An introduction to energy piles. The purpose of the research	1
1.1 Introduction	1
1.2 European Energy policy framework.....	2
1.3 A brief analysis of the main energy consumptions in the world	6
1.4 Shallow geothermal energy	8
1.4.1 Heat pump and geothermal heat pump	12
1.5 An overview on energy piles.....	16
1.5.1 Pile/soil thermomechanical interaction	17
1.6 Soil thermal properties, soil temperatures and heat transfer mechanisms	21
1.6.1 The mechanism of heat transfer	22
1.6.2 Heat transfer in soil	22
1.6.3 Soil thermal properties	23
1.6.3.1 The soil thermal conductivity	23
1.6.3.2 The volumetric heat capacity	24
1.6.3.3 The soil thermal diffusivity	25
1.6.4 Heat exchange between pile a soil – thermal behaviour.....	27
1.6.5 The underground temperature	29
1.6.5.1 Ground temperature prevision in function of the time and the depth: a mathematical approach	32
1.7 Conclusion: the role of energy geo-structures and the purpose of the research.....	34
1.8 References	35
Chapter 2	39
2 Literature review	39
2.1 Introduction	39
2.2 Mechanical behaviour of a single energy pile.....	39
2.2.1 Field tests	39
2.2.2 Small-scale tests	43
2.2.3 Axial response: vertical strain and vertical stress	46
2.2.4 The shaft response.....	49
2.2.5 The radial thermal response	49
2.2.6 Temperature induced displacements	50

2.3	Energy piles thermal performances	56
2.3.1	Heat flow rate: Thermal Performances Test (TPT)	57
2.3.2	TPT field test.....	61
2.3.3	Numerical model.....	65
2.3.4	Small scale test.....	69
2.3.5	The main design elements that affect thermal performances of energy piles	70
2.3.5.1	The pipes configuration	71
2.3.5.2	Aspect ratio and distance of pipes	74
2.3.5.3	Concrete cover	76
2.3.5.4	The effect of flow rate carrier fluid	77
2.3.5.5	Thermal conductivity of the pile materials	82
2.3.5.6	Effect of the operation mode on the heat exchange rate.....	85
2.3.5.7	The inlet temperature: the temperature difference between pile and soil.....	86
2.4	Conclusion.....	89
2.5	References	90
Chapter 3	98
3	Applications of EP in Neapolitan context.....	98
3.1	Introduction	98
3.2	The geological context of the city of Naples.....	98
3.2.1	Lithified facies: the Neapolitan Yellow Tuff.....	99
3.2.2	Unlithified facies: Neapolitan Pozzolana and Intracaldera Phlegrean pyroclastic Deposits.....	101
3.3	Thermal loads for building and for Geothermal Pumps.....	107
3.3.1	Neapolitan climate zone.....	108
3.3.2	Dynamic energy simulation: Design Builder.....	111
3.3.3	The building envelope.....	111
3.3.4	Indoor activities and design setpoint temperature.....	114
3.3.5	The building thermal plant design	116
3.3.5.1	Indoor heating design calculation.....	116
3.3.5.2	Indoor cooling design calculation.....	117
3.3.5.3	The geothermal plant	118
3.3.5.4	Energy simulation.....	121
3.4	Conclusion.....	122
3.5	References	123

Chapter 4.....	125
4 Numerical analysis on energy piles	125
4.1 Introduction	125
4.2 The effects of the boundary conditions on the energy pile behaviour embedded in pyroclastic soil	125
4.2.1 The 2D model.....	126
4.2.2 The 2D simulation.....	130
4.3 Interaction coefficient determination for a couple of energy piles	134
4.3.1 Background	134
4.3.2 The 3D model.....	135
4.3.3 The mathematical approach to the thermomechanical problem in FLAC3d	138
4.3.4 The material properties	140
4.3.5 The mechanical analysis	141
4.3.6 The thermal analysis	145
4.4 Conclusion.....	155
4.5 References	156
Chapter 5.....	158
5 Tests on small-scale model of energy pile embedded in pyroclastic soil	158
5.1 Introduction	158
5.2 Laboratory scale test layout.....	158
5.2.1 Test setup stages.....	158
5.2.2 The pile	161
5.2.3 The thermal and mechanical loading system	162
5.2.4 The water temperature and circulation control system	164
5.2.5 The soil – Pozzolana sand	165
5.2.5.1 Mechanical properties.....	166
5.2.5.2 Thermal aspects	172
5.2.6 The box	174
5.2.7 Sensors	176
5.2.7.1 Strain gauges.....	178
5.2.7.2 Strain gauge calibration: shunt calibration	183
5.2.7.3 Strain gauge thermal calibration	184
5.2.7.4 Thermocouples	185
5.3 Small-scale test program	186

5.3.1	Stresses in soil.....	188
5.3.2	Mechanical test. Determination of the ultimate capacity of the pile	189
5.3.3	Long-term thermomechanical heating test.....	191
5.3.3.1	Soil temperature distribution for Long-term thermomechanical heating test.....	192
5.3.3.2	Heat thermal power for Long-term thermomechanical heating test.....	194
5.3.3.3	Pile head displacements for Long-term thermomechanical heating test	195
5.3.3.4	Axial forces for Long-term thermomechanical heating test.....	196
5.3.4	Long-term thermomechanical cooling test	197
5.3.4.1	Soil temperature distribution for Long-term thermomechanical cooling test	198
5.3.4.2	Heat thermal power for Long-term thermomechanical cooling test.....	200
5.3.4.3	Pile head displacements for Long-term thermomechanical cooling test.....	200
5.3.4.4	Axial forces for Long-term thermomechanical cooling test.....	202
5.3.5	Regular cyclic tests	203
5.3.5.1	Soil temperature distribution for regular tests	204
5.3.5.2	Pile head displacements for regular tests.....	208
5.3.5.3	Heat power exchanged for regular tests.....	213
5.3.5.4	Axial forces for regular tests.....	215
5.4	General discussion.....	217
5.5	Conclusion.....	219
5.6	References	220
Chapter 6	222
6	Field tests: effects of thermal loads on a concrete energy pile	222
6.1	Introduction	222
6.2	The area of the field test	222
6.2.1	Test Pile.....	226
6.2.2	The mechanical resistance of the pile	229
6.2.3	Sensors and measuring instruments used for test.....	230
6.2.3.1	The vibrating wires	232
6.2.3.2	Thermistors strings	236
6.3	Parameters and interpretation of the thermal field test results	236
6.3.1	The concrete thermal expansion coefficient determination	236
6.3.2	The exchanged heat power between pile and soil.....	237
6.3.3	Axial forces and mobilized side shear stress	238
6.3.4	The degree of freedom	239

6.4	The test program.....	239
6.4.1	Test T1	240
6.4.2	Test T2	246
6.4.3	Test T3	253
6.5	Long term temperatures monitoring.....	260
6.6	Results discussion.....	266
6.7	Conclusion.....	267
6.8	References	268
	General conclusion.....	270

List of abbreviations

<i>AR</i>	Aspect Ratio
<i>CFA</i>	Continuous Flight Auger
<i>CFG</i>	Cement-fly ash-gravel
<i>COP</i>	Coefficient of Performance
<i>DTV</i>	Daily Thermal Variation
<i>EER</i>	Energy Efficiency Ratio
<i>EPs</i>	Energy piles
<i>EPBD</i>	Energy Performance Building Directive
<i>FEM</i>	Finite Element Model
<i>GF</i>	Geothermal Fluid
<i>GHEs</i>	Ground Heat Exchangers
<i>GSHP</i>	Ground Source Heat Pump
<i>gpm</i>	Gallon per minute
<i>HDPE</i>	High-density polyethylene
<i>HP</i>	Heat Pump
<i>H-S</i>	Hardening-Soil
<i>HTV</i>	Hourly Thermal Variation
<i>HVAC</i>	Heating Ventilation and Air Conditioning
<i>ILSM</i>	Infinite Line Source Method
<i>IPD</i>	Intracaldera Phlegrean pyroclastic Deposits
<i>LVDT</i>	Linear Variable Differential Transducer
<i>M-C</i>	Mohr-Coulomb
<i>NP</i>	Null point
<i>NTC</i>	Negative temperature coefficient
<i>(NYP)</i>	Neapolitan Yellow Pozzolana
<i>NYT</i>	Neapolitan Yellow Tuff
<i>NZEB</i>	Nearly Zero-Energy Building
<i>OC</i>	Overconsolidated
<i>PHC</i>	Precast high-strength concrete
<i>SCC</i>	Self-Compacting Concrete
<i>SPF</i>	Seasonal Performance Factor
<i>TPT</i>	Thermal Performances Test
<i>TRT</i>	Thermal Response Test
<i>VBHEs</i>	Vertical boreholes heat exchangers
<i>VW</i>	Vibrating wire

Chapter 1

1 An introduction to energy piles. The purpose of the research

1.1 Introduction

Nowadays, the world's growing demand for energy and its consequent environmental impact has prompted a change of course in the world politics if compared to previous years. The search for renewable primary energy sources other than fossil fuels was the driving force behind the Brundtland Report in 1987 and the Kyoto Protocol in 1997. From these acts, in fact, were introduced into the international policies, issues and concepts such as sustainability and the containment of greenhouse gases to combat climate change, a phenomenon which is still gripping our society today.

Greenhouse gas emissions are the main cause of climate changes and the fossil fuels are the main responsible of their production. Today a large part of energy electricity in the world is still generated from fossil fuels and some sectors, such as the residential and commercial buildings, are one the main responsible of these emissions. In fact, for these sectors, a large use of energy is provided by traditional heating and cooling systems responsible to generate significant amounts of carbon dioxide emissions. The decarbonization of energy supply can be achieved by maximizing the energy efficiency and the sustainability of heating, cooling, and electricity systems. As a matter of fact, the main options to reduce carbon dioxide emissions are the use of renewable energy sources and the reduction of the final energy consumption. The latter two aspects have been the basis of European energy policies for more than 20 years.

Since the early 2000s, indeed, a series of European Union (UE) directives were issued by European parliament, later transposed and transformed into law by each member country. The aim was to implement an energy policy in the civil construction sector aimed at limiting and reducing energy consumption, favoring as much as possible the supply of renewable energy sources.

In last decades, for its high energy efficiency, the Shallow Geothermal Energy (SGE) is rapidly increasing all over Europe as a support for the Renewable Energy policies and European Directives. With the replacement of traditional electric heating and cooling systems by shallow geothermal heat pumps it can be possible to significantly reduce the greenhouse gas emissions and the peak energy consumption. In fact, these systems based on SGE have generally higher energy performance than the traditional one.

To extract/inject heat from/to soil, a ground source heat pump (GSHP) connected to ground heat exchangers (GHEs) is needed. Generally, heat ground exchangers are installed in vertical boreholes approximately 100 m in depth or in horizontal loop bored in the shallow ground zone (about 1,5 m in

depth). Anyway, in the last decades a new technology is emerging among the various energy options. It is about energy geostructures, i.e., structures in contact with the ground in which the heat exchangers are installed.

In this chapter after an overview of the European directives and a brief description of the energy situation in Europe, the principles of geothermal energy and the operating mechanisms of a geothermal pump system are discussed. Moreover, a general overview about energy geostructures with a focus on energy piles is reported. Finally, the main thermal characteristic and property of the ground and the principal problems that affects geostructures design the are treated.

1.2 European Energy policy framework

The concept of sustainable development, introduced in 1987 with the Brundtland Report by the World Commission on Environment and Development (WCED), highlighted the strong relationship between development and the environment and the mutual influence between the former and the latter (World Commission On Environment And Development, 1987). Although all type of energy production causes an impact on the environment, the severity of the impact depends on the technology used to produce energy (Rybach, 2003). The Brundtland Report triggered a series of treaties born out of the need to make economic development and environmental protection compatible. During the United Nations Summits in Rio (1992), Kyoto (1997) and Johannesburg (2002), were defined the goals for the protection of the environment.

Kyoto Protocol of 1997 was the first to fix targets and limits for industrialised countries on the emission of greenhouse gases, the main contributors to the phenomenon of climate change that still grips our societies today.

Since the early 2000s, in fact, the European Union's policies, based on the objectives of the Kyoto Protocol, have promoted a sustainable, diversified, and low-energy economy that counteracts as much as possible the causes of global warming and climate change.

The studies and the analysis of the buildings potentialities to achieve the set targets, has led over the years to a series of directives for the energy management and the containment of greenhouse gas emissions.

An update of EU energy policy framework to facilitate the transition away from fossil fuels towards cleaner energy was made in 2019 to deliver on the EU's Paris Agreement commitments for reducing greenhouse gas emissions. "Clean energy for all Europeans package" was the name of the agreement on this new energy rulebook. It was marked a significant step towards the implementation of the energy union strategy, published in 2015. The *Clean energy for all Europeans package* is based on the Commission's proposals published in 2016 and consists of 8 legislative acts that bring significant

benefits from the perspective of consumers, the environment, and the economy fixing a long-term strategy of achieving carbon neutrality by 2050.

Because almost 50% of Union's final energy consumption is used for heating and cooling, of which 80% is used in buildings, efforts of Union were focused on the priority objective of energy efficiency in buildings and on the decarbonise of the building stock. The buildings sector, in fact, is the largest consumer of energy in the EU and one of the largest emitters of carbon dioxide. People spend most of their lives in different forms such as homes, schools, offices, public buildings and so on. The 40% of the EU's energy consumption and 36% of its greenhouse gas emissions come from buildings, including their construction, use, renovation, and demolition. Improving the energy efficiency of buildings is the key to achieving the ambitious goal of carbon neutrality by 2050. (European Commission - Department: energy, 2020).

The Union was committed to developing a sustainable, competitive, secure, and decarbonised energy system. The Energy Union and the Energy and Climate Policy Framework for 2030 establish ambitious Union commitments to reduce greenhouse gas emissions further by at least 40% by 2030 as compared with 1990, to increase the proportion of renewable energy consumed, to make energy savings in accordance with Union level ambitions, and to improve Europe's energy security, competitiveness, and sustainability. With the Paris Agreement on Climate Change in 2015 and the EU policy framework for climate and energy, the goals of EU energy policy to promote renewable forms of energy to reduce greenhouse gas emissions has become stronger than the approach taken under the 1997 Kyoto Protocol. It was set out a long-term goal in line with the objective to keep the global temperature increase well below 2 °C above pre-industrial levels and to pursue efforts to keep it to 1,5 °C above pre-industrial levels (Agreement, 1977; European Commission, 2016).

Specific EU's directives were issued for the buildings and civil construction sector called EPBD (Energy Performance Building Directive) while other directives were issued for the management and the containment of the greenhouse gas emissions. The EPBD are directives in the European regulatory framework covering both general criteria for calculating the energy performance of buildings and minimum efficiency requirements to be met when designing new buildings or renovating existing ones.

The first EPBD issued was the Directive 2002/91/EC "On the energy performances of the buildings". This directive deals with all issues related to the assessment of the energy performance of buildings emphasising the need to define harmonised methodologies for the estimation of energy consumption according to different climatic and microclimatic conditions, the intended use of the building or aspects related to local differences. It was characterized by some fundamental points. First of all, it was introduced the obligatory of the energy certification of buildings using energy classes, both for

new buildings and renovations, for the evaluation of the energy performance. Still used today, this approach allowed not only the assessment of energy performance, but also the possibility of comparing the performance of different buildings. A second aspect addressed by this directive was the gradual application of different minimum energy performance requirements between the case of new construction and renovation. Another fundamental aspect introduced was certainly a general framework for a calculation methodology of the integrated energy performance of buildings. Finally, the last point was the introduction of regular inspection of boilers and of air-conditioning systems in buildings.

The second EPBD issued was the Directive 2010/31/CE "On the energy performances of the buildings (recast)". This directive has abrogated the Directive 2002/91/EC and it sets even more stringent targets for reducing greenhouse gases and saving energy. This directive maintained the points introduced by the previous EPBD but extended them also to public buildings. Anyway, the most important concept introduced by the directive was the 'nearly zero-energy building' (NZEB), defined in article 2 of the directive as "a building that has a very high energy performance, as determined in accordance with Annex I. The nearly zero or very low amount of energy required should be covered to a very significant extent by energy from renewable sources, including energy from renewable sources produced on-site or nearby" (2010/31/EU, 2010). Furthermore, the Directive specified that new buildings had to meet the minimum energy performance requirements and to consider alternative systems such as decentralised energy supply systems based on energy from renewable sources, cogeneration, district or block heating or cooling, and heat pumps.

The third and last EPBD, up to the present day, is the Directive (EU) 2018/844 of 30 May 2018 that outlines specific measures for the building sector to tackle challenges, updating and amending many provisions from the Directive 2010/31/EU.

Regarding the management and the greenhouse gas emissions it is reported the evolution of the directives starting from 2006.

Through the improvement of energy end-use efficiency and cost-effectiveness, Directive 2006/32/EC "On energy end-use efficiency and energy services and repealing Council Directive 93/76/EEC" had as its main target set for member states to save 9% of energy by 2015. To achieve this target, the Directive placed the public sector at the heart of the matter by introducing energy efficiency and energy savings as a basis for awarding public contracts or tenders. In addition, it introduced energy audit systems to identify possible efficiency improvements for the civil, industrial, and commercial sectors.

The fundamental directive for the production and promotion of energy from renewable sources was the Directive 2009/28/EC "on the promotion of the use of energy from renewable sources and

amending and subsequently repealing Directives 2001/77/EC and 2003/30/EC" (European, 2009). This Directive set national targets for each member state of the European Union and obliged each state to adopt a national plan for renewable energy. It was also known as "20-20-20 package". This name come from the targets prefixed from the directive as well as the reduction of EU greenhouse gas emissions by 20% compared to 1990 levels, the improve of the EU's energy efficiency by 20% and the production from renewable sources of the 20% of the EU's energy. To reduce greenhouse gas emissions from the energy sector and major industries in a cost-effective way, a "cap and trade" policy was adopted by assigning a market price to emissions. For sectors other than those mentioned above, however, such as buildings, agriculture, waste, and transport, it set binding annual targets for 2013-2020, differentiated according to the relative wealth of each EU country, aimed at reducing their greenhouse gas emissions.

Directive 2012/27/EU replaced Directive 2006/32/EC and reinforced the energy efficiency and greenhouse gas emission reduction targets set for 2050 by incentivising, especially for the public sector, the rate of building renovations. The Directive detailed the framework of measures to improve energy efficiency by 20% by 2020 compared to 1990 levels and required all Member States to set national energy efficiency targets to achieve this goal. The Directive, moreover, through a common framework of measures covering every stage of the energy chain, energy efficiency in the EU, from generation to distribution and final consumption. The guidelines, while remaining like those of the directive it replaced, have been strengthened especially on the concept of energy diagnosis for the big companies and all energy-intensive enterprises and on the energy savings obligation.

The last updates regarding the Renewable energy and Energy efficiency European polices are represented respectively by the Directive 2018/2001 and the Directive 2018/2002. In fact, the EU set the ambitious target of 32% for renewable energy sources in the EU's energy mix by 2030 and the binding targets of at least 32,5% energy efficiency by 2030, relative to a 'business as usual' scenario considering the energy efficiency like the easiest way of saving money for consumers and for reducing greenhouse gas emissions.

The Directive 2018/2001 provides criteria for sustainability and greenhouse gas emissions saving criteria for biomass fuels, biofuels and bioliquids. Moreover, it establishes rules, on energy use from renewable sources in the heating and cooling sector and in the transport sector, on financial support for electricity from renewable sources and self-consumption of such electricity and on regional cooperation between Member States, and between Member States and third countries, on guarantees of origin, on administrative procedures and on information and training.

On the other hand, the Directive 2018/2002 revised Directive 2012/27/EU. The main changes to the 2012 Directive relate firstly to achieving the energy efficiency target of 32,5 % by 2030 and secondly

to anticipating further improvements by seeking to remove all barriers in the energy market that may obstruct efficiency in the supply and use of energy. Furthermore, the social aspects of energy efficiency have been strengthened by taking energy poverty into account when designing energy efficiency schemes and alternative measures. Finally, Member States are required to have transparent and publicly available national rules on the cost allocation of heating, cooling and hot water services in multi-apartment and multi-purpose buildings where these services are shared.

1.3 A brief analysis of the main energy consumptions in the world

The growing demand for energy for heating and cooling with the increased ownership of air conditioners and extreme weather events have caused energy-related CO₂ emissions from buildings to rise in recent years after flattening out between 2013 and 2016. The highest level ever was recorded in 2019 when direct and indirect emissions from electricity and commercial heat used in buildings rose to 10 GtCO₂. Counteracting this trend could be achieved mainly by decreasing fossil fuel-based goods and increasing investments in sustainable buildings. Focusing on the first aspect, although heat pumps and renewable heating equipment had an increase in sales in 2019 representing the 10% of the total, the market, with almost 80% of new sales, is still dominated by fossil fuel-based heating equipment and less efficient conventional electric heating technologies. By 2030, the share of heating technologies from clean sources should reach 50%. On the other hand, as far as cooling in buildings is concerned, data show that energy demand has more than tripled since 1990 and was responsible for emissions of about 1 GtCO₂ and almost 8,5% of total final electricity consumption in 2019 (*Heating – Tracking Buildings 2020 – Analysis - IEA*).

Analysing the data on total energy consumption at European level, from 1990 to 2018 the three most used energy sources were oil products, natural gas, and electricity. In percentage terms, over the years, the use of these energy sources was always much higher than the others. The final use of energy consumed by sector shows that the three most important sectors in Europe are Industry, Transport and Residential. However, since 1990, the transport and industrial sectors have had opposite trends, while the residential sector has had a fluctuating trend and, perhaps also due to European energy policies. In 2018 the residential sector showed the lowest value of energy consumed.

As mentioned, electricity is one of the most widely used energy resource in Europe. However, at European level, after nuclear power, fossil fuels are still the main resource with a consequent increase in CO₂ production.

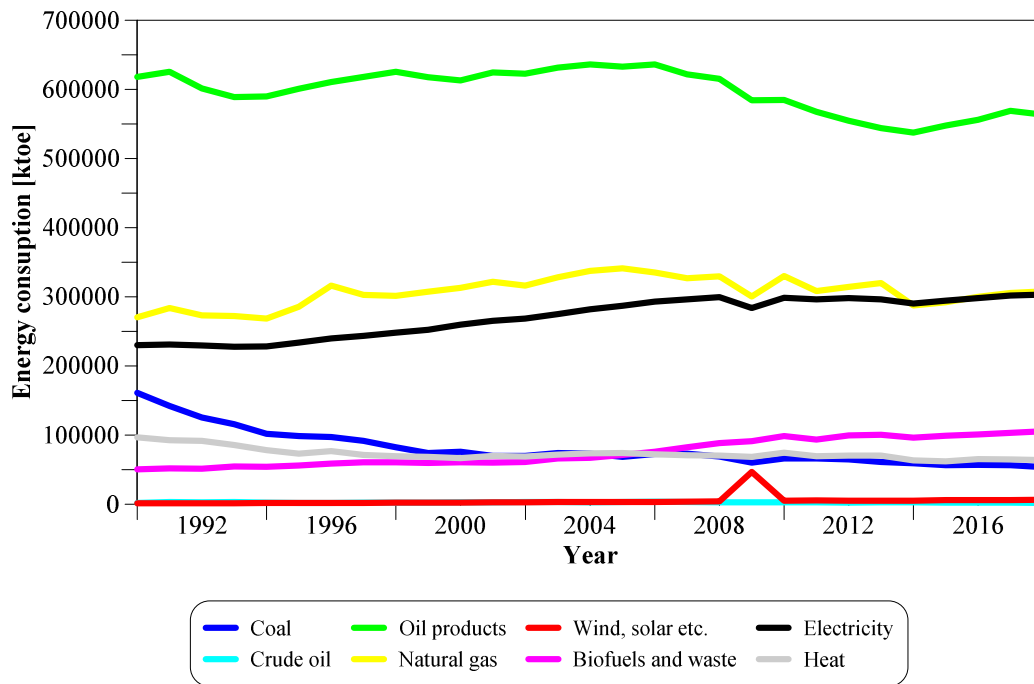


Figure 1-1 - Total final consumption by source in the World (Source: IEA World Energy Balances 2020 <https://www.iea.org/subscribe-to-data-services/world-energy-balances-and-statistics>)

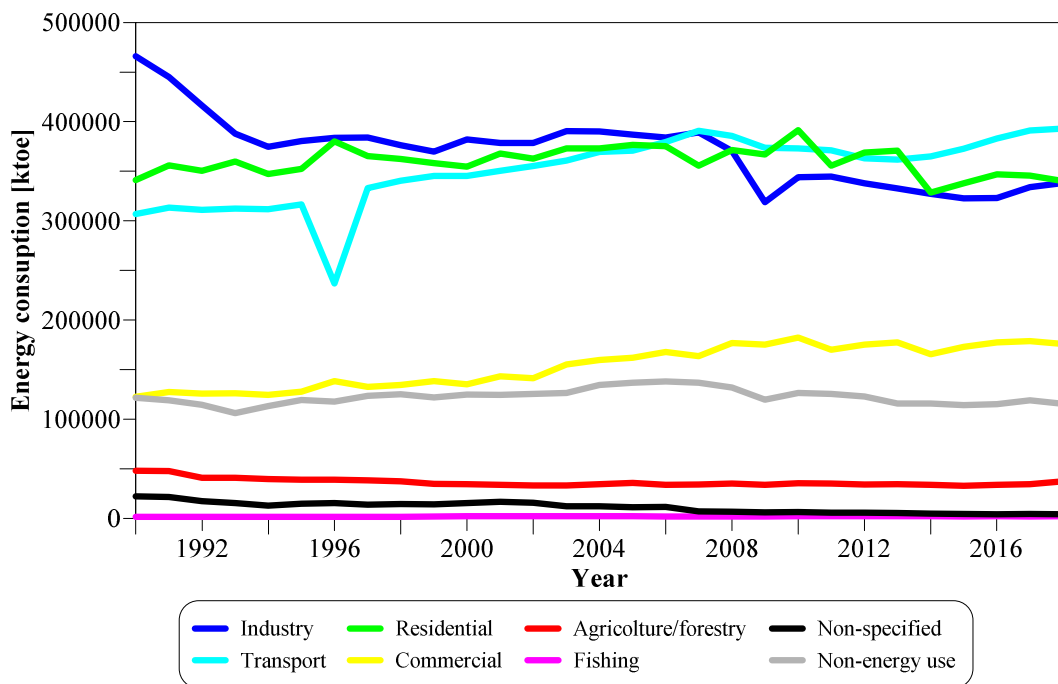


Figure 1-2 – Total final consumption by sector in the World (Source: IEA World Energy Balances 2020 <https://www.iea.org/subscribe-to-data-services/world-energy-balances-and-statistics>)

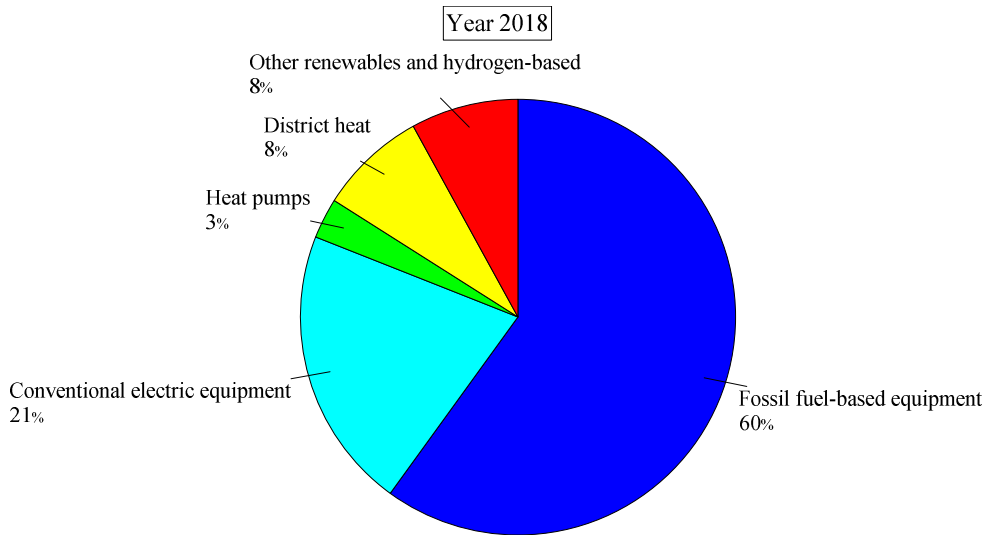


Figure 1-3 - Heating technology sales in the Sustainable Development Scenario, 2010-2030 (IEA, Heating technology sales in the Sustainable Development Scenario, 2010-2030, IEA, Paris <https://www.iea.org/data-and-statistics/charts/heating-technology-sales-in-the-sustainable-development-scenario-2010-2030>)

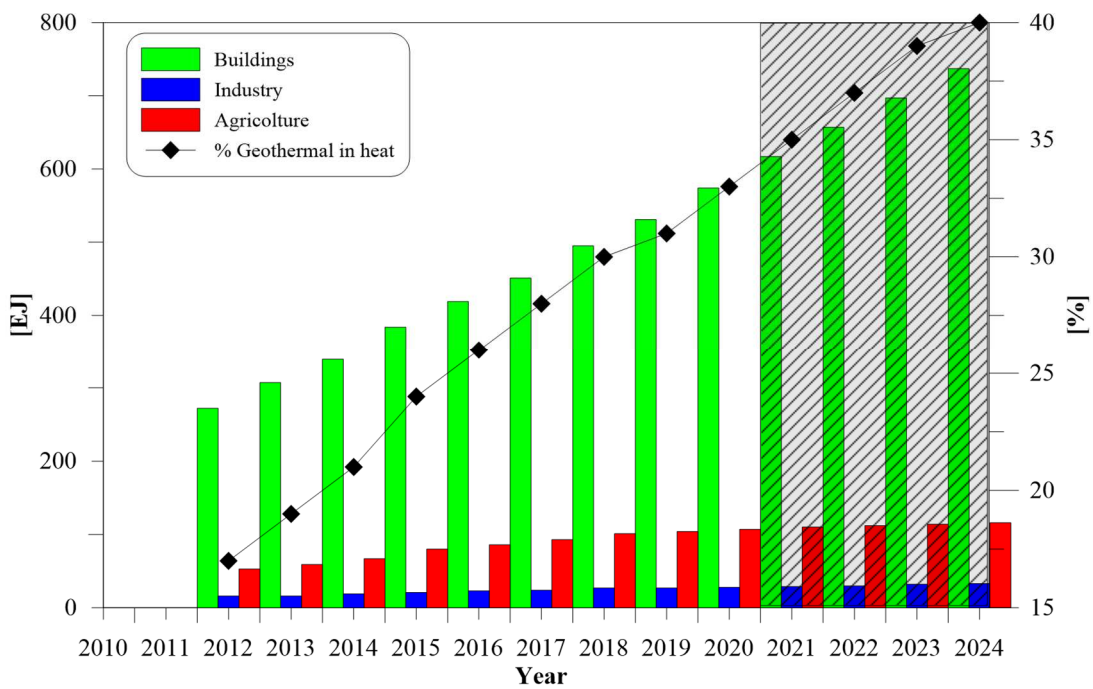


Figure 1-4 - Direct use of geothermal energy in the world during the period 2012-2024. The dashed zone represents future previsions. (IEA, Direct use of geothermal energy, world, 2012-2024, IEA, Paris <https://www.iea.org/data-and-statistics/charts/direct-use-of-geothermal-energy-world-2012-2024>)

1.4 Shallow geothermal energy

The geothermal energy is the source of energy from the heat stored in the Earth's crust, which is propagated to the surface, where it dissipates, through the rocks or through carrier fluids such as water or gas. In fact, there is a geothermal gradient between the internal part of the Earth's crust and surface with an average value of 30 °C/km, (Barbier, 2002).

The geothermal energy is considered a renewable source on the time-scales of technological/societal systems, do not require the geological times of fossil fuel reserves such as coal, oil, and gas and by virtue of its low greenhouse gas emissions into the atmosphere, it is promoted alongside other renewables in government programmes source of energy and an alternative to traditional energy sources (Rybach, 2003). It can be used both for power generation and to provide an energy efficient space heating and cooling for public, residential buildings, large architectural complexes, and other infrastructures (Gao, Zhang, Liu, K. Li, *et al.*, 2008; Johnston, Narsilio and Colls, 2011).

The difference between the uses of geothermal energy depends mainly on temperature of the geothermal fluid (GF) as shown in Figure 1-5. In fact, high-enthalpy resources are characterized by GF temperatures above 150 °C and are suitable for power generation while for temperatures below 150 °C of GF resources are called low-enthalpy and are suitable for the second aim (Barbier, 2002).

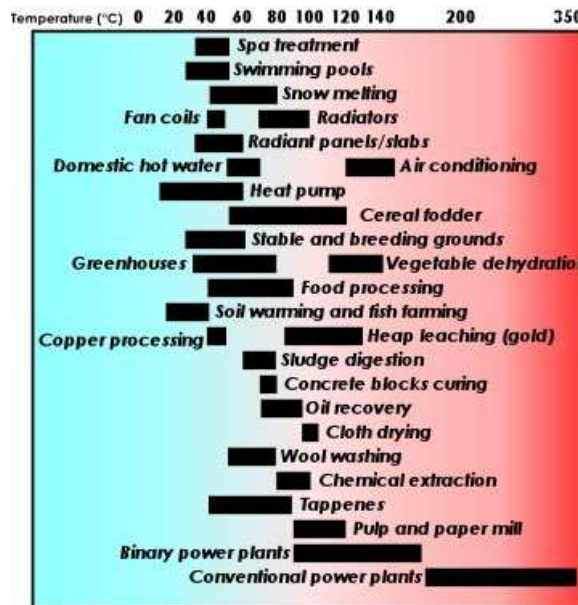


Figure 1-5 - The utilization of geothermal fluids derived from (Lindal, 1973)

Generally, high-enthalpy resources tap into high-temperature energy sources fluids to drive turbines for electricity production and often an interaction with kilometre-deep strata of rock is required. For this reason, they are also classified as deep resources. This technology is used above all for large scale application because its costs are generally very expensive. On the other hand, low-enthalpy resources make direct use of the shallow temperature of the soil, which at certain depths is constant and equal to the average annual air temperature. This solution, compared to the first one, shows great potential in terms of access, long-term sustainability, flexibility, and economics (Preene and Powrie, 2009; De Moel *et al.*, 2010).

While the deep geothermal energy can be used only in particular region of the world where there are hydrothermal resources, direct shallow geothermal energy can be used everywhere, and the heat can

be extracted using a device called Heat Pump. Even if it was invented by Lord Kelvin in 1852, it's only over the last two decades that Ground Source Heat Pumps (GSHPs) had had increased use in heating and cooling of buildings (Johnston, Narsilio and Colls, 2011).

Shallow Geothermal Energy (SGE) applications are increasing over the last decades all over Europe as a result to their high energy efficiency and support from the Renewable Energy policies and European Directives (Tsagarakis et al., 2020).

With this technology, a heat transfer fluid circulating inside geothermal heat exchangers (GHEs) installed in vertical boreholes, trenches or building foundations, can take or inject thermal energy from/to the ground depending on the heating or cooling phase of the building, respectively.

Heat can be extracted/injected from/in ground by different ways. It is possible to distinguish two main families of GHEs according to whether they form an open or a closed loop.

The first type can be used when there is a groundwater or artesian aquifer in the ground and therefore the thermal energy of the subsoil stored in the fluid could be taken directly and pumped to the surface through a well. After the water having completed its cycle, it is injected into the aquifer by a different injection well. Since the extraction well must guarantee a minimum flow rate to the heat pump, it is essential for this type of circuit, that the extraction and injection rates are balanced so as not to create imbalances in the source.

In closed loop, instead, a constant mass of heat carrier fluid circulates inside the GHEs transporting thermal energy from ground to GSHP or vice versa. Closed loop can be arranged both horizontally and vertically.

The horizontal typology is placed in a trench. It is a less expensive solution because it does not require deep excavations like boreholes or wells, but it is also less energy-efficient being installed in the shallowest part of the ground that is significantly affected by variations in air temperature. In addition, the surface area of the ground used for the installation of this type of GHE can be up to twice as large as the surface area to be conditioned.

The vertical typology, instead, unlike the horizontal type, develop their length vertically. This type of GHE has the advantage of being energy efficient by exchanging thermal energy with the ground at depths which are no longer affected by external climatic conditions occupying much less space than horizontal closed loops. At the same time, however, they have the disadvantage of having fairly high initial costs due to the excavation of the borehole (Wood, Liu and Riffat, 2010).

Nevertheless, energetic geo-structures and deep energetic foundations, such as piles, combine the advantages of vertical closed loops type with the elimination of the initial costs of boreholes excavation for GHEs. Energy foundations, with particular regard on energy piles, will be discussed extensively and in detail in the next paragraphs as they are the main topic of this research.

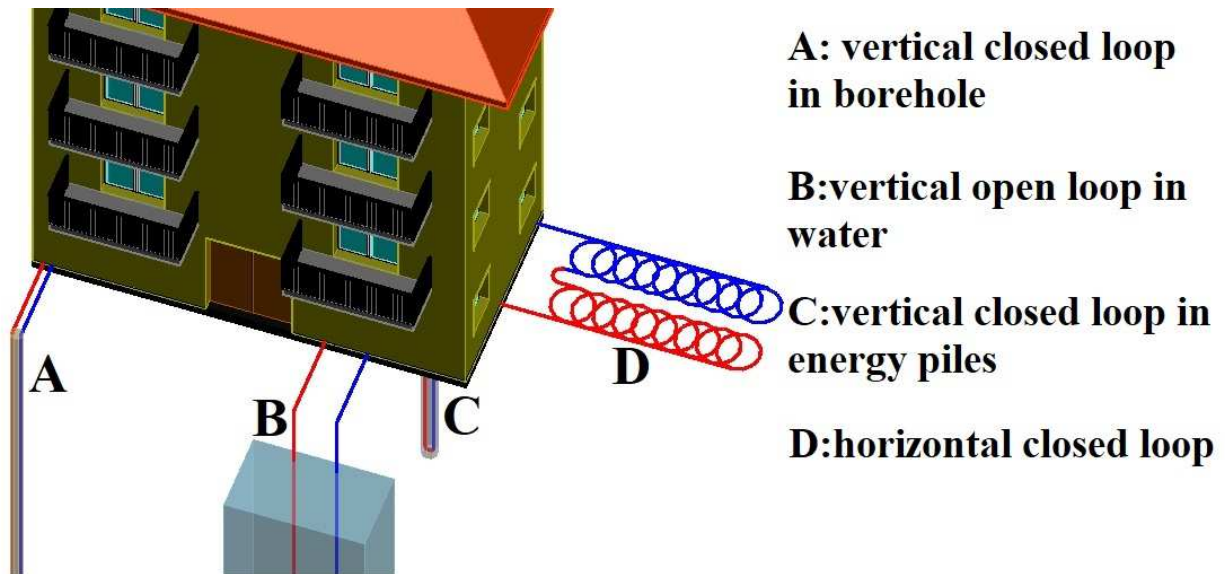


Figure 1-6 – Different type of heat exchangers

Regardless of the type of heat exchanger, conventionally systems for the heating and cooling with a direct use of geothermal energy are generally made by three distinct parts that could be categorized into three main components called primary circuit, secondary circuit and heat pump (Brandl, 2006). The primary circuit consists of GHE in direct contact with the ground or installed in structures that are in contact with the ground within which a heat carrier fluid circulates. The carrier fluid may be water or a mixture of water and antifreeze substances. The latter solution is often used for installations in colder regions where the temperature of the heat transfer fluid may reach temperatures close to 0 °C.

The secondary circuit, on the other hand, consists of a closed fluid-based building cooling or heating network installed inside the floors and/or walls of the structure if the geothermal plant serves a building or the secondary pipework could be installed also in bridge decks, road structures, platforms if the plant works for an infrastructure.

Because the ground temperature is usually not sufficient to reach the temperatures necessary to achieve indoor climate control, both in winter and summer season, a heat pump must be installed between the primary and secondary circuits. It is a machine capable to increase (or decrease) the temperature level. Heat pump system will be described in detail in the next section.

Recently, Preen and Powrie (2009) proposed an alternative subdivision of the ground energy system in source side, load side and heat transfer system. With this new subdivision the parts are characterized for the function and not for the component as in traditional classification.

However, in some county where the temperatures allow, it is possible to satisfy the upper structures cooling demand with a direct heat transfer from ground heat exchangers to soil without a passage of

the heat carrier fluid through a heat pump. This technique is so called “geocooling” or “freecooling” (Pahud, Belliardi and Caputo, 2012; Loveridge and Powrie, 2013).

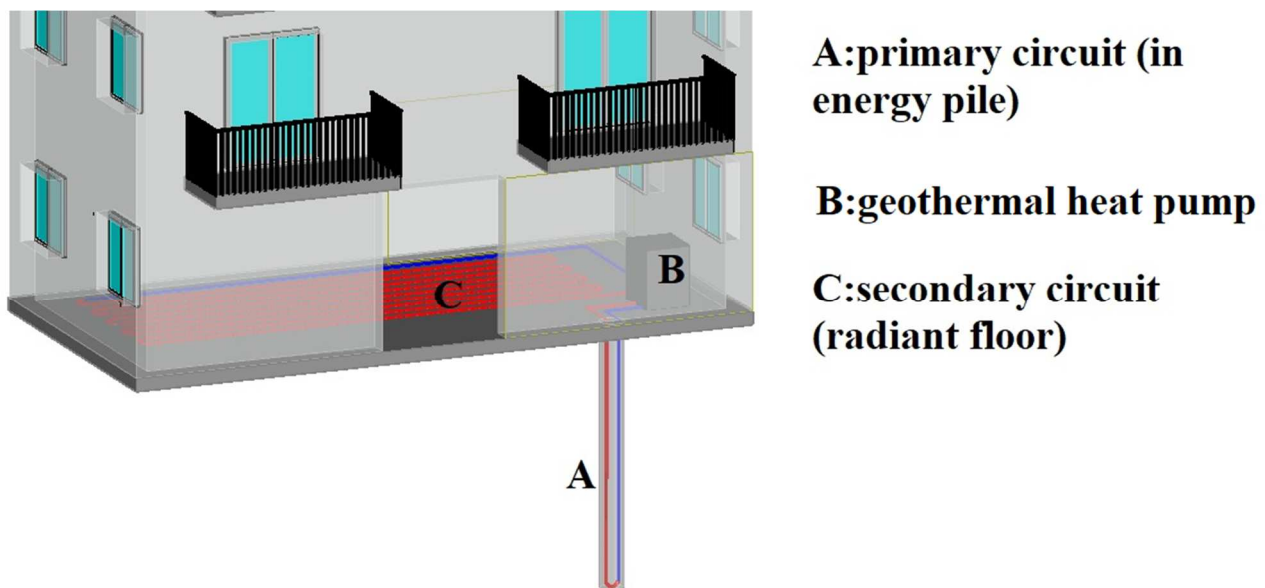


Figure 1-7 – Schematization of the components of a geothermal plant with energy piles

1.4.1 Heat pump and geothermal heat pump

To understand how a geothermal heat pump system works and what the real advantages are if compared to a traditional air source heat pump, it is necessary to explain the general operating principles of the heat pump.

Apparently contravening the second law of thermodynamics, a heat pump is a device that can transport heat from a lower temperature level to a higher one. In fact, the name “pump” is derived from the analogy with the hydraulic pump, which can lift a liquid from a lower to a higher level.

In the heat pump (as well as for water pump), however, the process can only take place with the use of external energy. The heat pumps, in comparison to traditional fossil energy systems that produce heat by burning fuel, use the energy in the environment such as air, water or soil, depending on the type of the heat pump, and transfer it with the help of electricity to where it is needed.

The heat pump consists of a refrigerant fluid, i.e. with a low boiling point, which circulates within pipes of a closed circuit made by four main components called respectively evaporator, compressor, condenser, and expansion valve.

Depending on the temperature, the refrigerant can be in a gaseous or liquid state. Within the heat pump circuit, in fact, what is commonly referred to as the thermodynamic cycle develops through changes in the state of the refrigerant fluid. The thermal cycle can occur in one direction or another depending on whether the heat pump is operating in heating or cooling mode. To explain the

functioning of the device, the operation of the cycle in which the heat pump is used for indoor space heating is described below.

- In the first step, into the evaporator, the refrigerant which is in a liquid state, evaporates by absorbing thermal energy (heat) from the external source (air, water, or ground).
- In the second step, into the compressor, the vapor, is brought to a higher pressure and temperature by using the external energy.
- In the third step, the high-temperature vapour arriving at the evaporator can supply its thermal energy to the heat-transfer fluid inside the space to be heated, with a new change of state of the refrigerant from vapour to liquid.
- In the fourth step, the fluid, which is still at high pressure, passes through an expansion valve to return to its initial pressure and to begin a new thermal cycle.

The phases of the thermodynamic cycle described are represented in the pressure-enthalpy diagram shown in Figure 1-9.

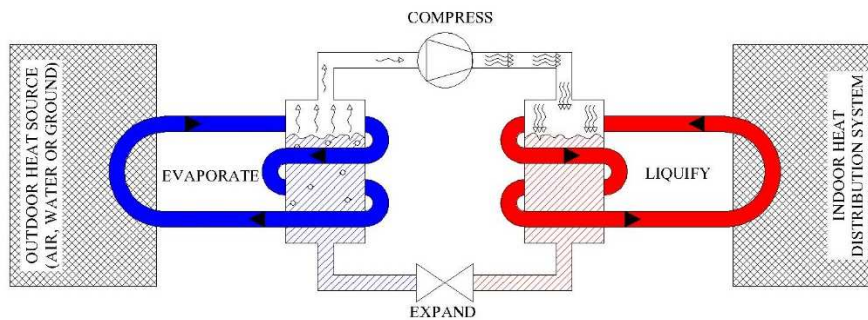


Figure 1-8 – Schematisation of the cycle of the heat pump internal fluid during the heating operation for indoor zones

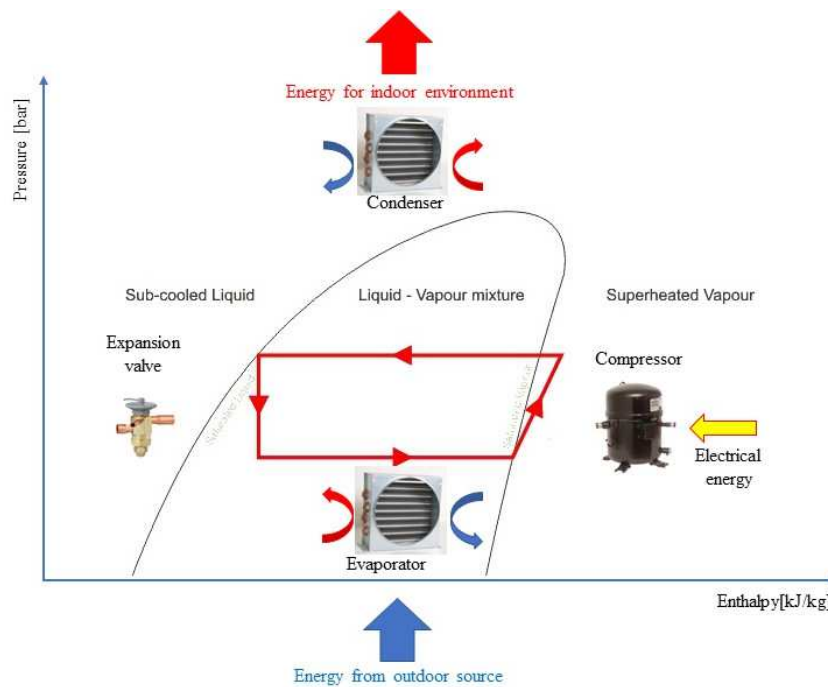


Figure 1-9 - Description of the different operating phases of a heat pump for an ideal refrigeration cycle plotted onto the pressure vs enthalpy diagram

The efficiency of the system, in the heating mode, is called Coefficient of Performance (COP). It is defined as:

$$COP = \frac{\text{energy output after heat pump [kW]}}{\text{energy input for operation [kW]}}$$

Equation 1-1

It represents the ratio between the thermal energy to be supplied to the source at higher temperature (indoor) and the mechanical energy to be supplied. Considering the ideal case in which the generated entropy is null (reversible transformations), for heat pump COP can be defined as the differences of source temperatures:

$$Q_{outd,rev} = \frac{Q_{ind}T_{outd}}{T_{ind}}$$

Equation 1-2

$$L_{rev} = Q_{ind} - Q_{outd,rev} = Q_{ind} \left(1 - \frac{T_{outd}}{T_{ind}} \right)$$

Equation 1-3

$$COP_{HP,rev} = \frac{Q_{ind}}{L_{rev}} = \frac{T_{ind}}{T_{ind} - T_{outd}}$$

Equation 1-4

In this case the indoor temperature was assumed to be the hot source while the outdoor was assumed to be the cold one because generally in winter, outdoor temperature is lower than indoor one.

Consequently, L_{rev} is the minimum work required to transfer the amount of indoor thermal energy Q_{ind} to the side with higher temperature. It is considered the minimum because of null generated entropy hypothesis (reversible transformations).

The meaning of the COP can be summarised with an example: a value COP of 4 means that four portions of usable energy are derived from one portion of electrical energy and three parts of external energy (Brandl, 2006).

In the case of a refrigerating machine the COP is replaced by the EER (Energy Efficiency Ratio). It is a way to differentiating the heap pump energy performances from that of the refrigerating machine, but the calculation criterion is the same for both. It represents the ratio between the thermal energy to be exported from the source at lower temperature (indoor) and the mechanical energy to be supplied. As well as in the case of COP, considering the ideal case in which the generate entropy is null (reversible transformations), for a refrigerating machine EER can be defined as the only differences of source temperatures:

$$Q_{outd,rev} = \frac{Q_{ind}T_{outd}}{T_{ind}}$$

Equation 1-5

$$L_{,rev} = Q_{outd,rev} - Q_{ind} = Q_{ind} \left(\frac{T_{outd}}{T_{ind}} - 1 \right)$$

Equation 1-6

$$EER_{,rev} = \frac{Q_{ind}}{L_{rev}} = \frac{T_{ind}}{T_{outd} - T_{ind}}$$

Equation 1-7

In this case, instead the indoor temperature was assumed to be the cold source while the outdoor was assumed to be the hot one because generally in summer, outdoor temperature is higher than indoor one and L_{rev} is the minimum work required to subtract the amount of thermal energy Q_{ind} from the lower temperature side. As before, it is considered the minimum because of null generated entropy hypothesis (reversible transformations).

The Seasonal Performance Factor (SPF) of a thermo-active system with heat pump, instead, is defined as:

$$SPF = \frac{\text{usable energy output of the energy system [kWh]}}{\text{energy input of the energy system [kWh]}}$$

Equation 1-8

Compared to COP and EER, SPF includes not only the energy consume of heat pump but also the other energy-consuming devices such as circulation pumps. SPF values between 3,8 and, 4,3 are achieved with standard electric pumps (Brandl, 2006).

Because, as mentioned, the smaller the temperature differences between the source and the space to be climate controlled, the greater the energy performance of the heat pump, it results that generally GSHPs have energy performances higher than traditional air heat pump. As will be explained in more detail in the following paragraphs, the temperatures of the subsoil remain constant at a temperature that approximates the average annual temperature of the outside air. It means that in summer season soil temperature is colder than air temperature and so soil can be used as reservoir and warmer temperatures from the building can be rejected. The opposite happens in winter where the soil can be used as a source of heat to heat the building because it results warmer than air temperature (Preene and Powrie, 2009). In this way the difference between the internal and external source temperatures is significantly reduced in geothermal heat pump if compared to air source heat pumps where external source is subject to hourly daily temperature fluctuations. The energy performance of geothermal heat

pumps, both in terms of COP and EER, is therefore generally much higher than that of conventional air source heat pumps.

1.5 An overview on energy piles

The energy geo-structures, also called thermo-active ground structures, are structural elements in contact with the ground, equipped with thermal energy exchangers and connected to a geothermal heat pump. Energy geo-structures may consist of shallow foundations such as slabs, or ground support works such as walls or diaphragms or using deep foundations such as piles. This is a relatively new sustainable and economically viable technology that uses renewable energy sources such as geothermal energy, providing long-term cost savings and minimised maintenance. The double purpose of the energy foundations is to support buildings and provide them the energy needed for heating and the cooling for building indoor environments during the year.

Chronologically, the application of this technology started at the beginning of the 1980s. The first applications of thermo-active ground structures are found in Austria and Switzerland where at first were used base slabs, then the piles (1984) and later diaphragm walls (1996) and tunnels (early-2000s) were also adapted (Brandl, 2006; Adam and Markiewicz, 2009). Nowadays geo-structures are widespread all around the world.

Focussing the attention exclusively on energy piles, they were used in many large construction projects in different country of Europe. As regarding the already mentioned example the first Austrian application, 59 bored energy piles 1,2 m in diameter and with an average length of 17,1 m were built for the foundation of the Lainzer Tunnel (Adam and Markiewicz, 2009). Other examples include the Frankfurt Main Tower in Germany where over 112 drilled energy piles 30 m in length were realised (Laloui, Nuth and Vulliet, 2006) and the Dock at Zürich airport in Switzerland where 315 energy piles were employed (Pahud *et al.*, 2008).

Energy piles (EPs) are a technology where heat exchangers, generally high-density polyethylene plastic pipes (HDPE) loops, are installed inside piles foundation (Brandl, 2006). Inside the pipes a heat carrier fluid flows inducing a heat exchange with surrounding soil. Over the years and in different parts of the world many different piles construction technologies have been used and/or tested such as concrete cast in situ (Gao, Zhang, Liu, K. S. Li, *et al.*, 2008; Park *et al.*, 2018), steel piles (Morino and Oka, 1994; Nagano *et al.*, 2005), precast high-strength concrete (PHC)(Park *et al.*, 2013; Go *et al.*, 2014), both for small and large diameter piles. EPs can have length from 10 m to 60 m and diameter from 0,15 m to 3,0 m (Bourne-Webb *et al.*, 2016). If compared with traditional vertical boreholes heat exchangers EPs reduces initial drilling costs and in the case of concrete piles the heat transfer is effective because of the good thermal properties of concrete (Wood, Liu and Riffat, 2010) (Brandl, 2006).

The double purpose of the energy foundations is to support buildings and provide them the renewable energy needed for heating and cooling of the building indoor environment during the year.

The design of energy piles should consider both serviceability and failure aspects of the system (Bourne-Webb *et al.*, 2016). The serviceability is linked to operational performances of the system like for example vertical and horizontal displacements of the pile or the satisfaction of thermal performances as required. On the other hand, the failure is linked to the complete collapse or loss of function of the pile foundation, or of the energy system or both. Regarding the thermal serviceability and failure, even if there are not so many indications on how should be measured, four criteria could be used:

- Energy delivered;
- Efficiency of the system;
- System temperatures;
- Environmental.

Regarding the geotechnical serviceability and failure aspects they are linked above all to the induced changes of the stress and strain regime in the pile structure due to changes in temperature. Three criteria could be used here based on:

- Deformation;
- Overstress;
- Resistance.

In the following paragraphs a short introductory literature review of the mechanical and thermal behaviour of energy piles will be dealt with, while in the chapter 2 a more careful and detailed review is presented showing how large is still the number of issues to be solved by researchers.

1.5.1 Pile/soil thermomechanical interaction

Pile and piles foundations are structural elements adopted when the mechanical properties of subsoil are not sufficient to build a shallow foundation or when the upper structure has characteristics that require the use of deep foundation. Generally, in service conditions, piles transmit vertical loads applied on their head to the subsoil partly by normal stresses developing at the toe and partly by shear stresses at the lateral pile-soil interface. The ratio between the two quantities depends both on the type and nature of subsoil and on the pile installation technique.

Energy piles, differently from traditional piles, are subjected both to mechanical and thermal loads. This can clearly change the load pattern of the pile. In fact, for an ordinary mechanically loaded pile the highest axial stress is expected at the head with decreasing value with the depth because of the shear stress mobilized at the soil-pile interface. If the shaft resistance is sufficient to support the

vertical load, the axial stress decreases to zero. On the other hand, if the shaft resistance is not sufficient non-zero values of the axial stress are measured at the pile toe. In the first case the pile is called “floating pile” while in the second case the pile is called “end-bearing pile”.

When an EP is heated it tends to expand, on the contrary, when is cooled it tends to contract. Along the pile shaft a neutral axis or so called “null point” (NP) is defined as the point where no thermal induced displacement is observed (Knellwolf, Peron and Laloui, 2011). In the top part the movements are directed upwards while in the bottom part the movements are directed downwards.

Anyway, a pile can expand or contract until a limiting value that is function of the thermal expansion coefficient of the pile material. In EP the so called “free-expansion” behaviour is the upper limit of the thermal strain and can be defined as:

$$\varepsilon_{T,free} = \alpha \cdot \Delta T$$

Equation 1-9

Where α is the thermal expansion coefficient of the pile material and ΔT is the change in temperature that occur in the pile.

However, an energy pile is not a free-standing column because restrains are provided by the surrounding soil that mobilize the shaft restraint at the pile-soil interface and/or by the upper structures or eventually stiff soil at the pile toe.

Usually, the observed strains due to a temperature change in a foundation pile ($\varepsilon_{T,obs}$) is less of the free-expansion strain ($\varepsilon_{T,free}$) and the difference between free-expansion and observed is the so called restrained axial strain ($\varepsilon_{T,Rest}$).

$$\varepsilon_{T,Obs} \leq \varepsilon_{T,free}$$

$$\varepsilon_{T,Rest} = \varepsilon_{T,free} - \varepsilon_{T,Obs}$$

Equation 1-10

Axial thermal stress (σ_{Th}) in the pile is created by the restrained axial strain ($\varepsilon_{T,Rest}$) and can be estimated as:

$$\sigma_{Th} = -E \cdot \varepsilon_{T,Rest} = -E \cdot (\varepsilon_{T,free} - \varepsilon_{T,Obs}) = -E \cdot (\alpha \cdot \Delta T - \varepsilon_{T,Obs})$$

Equation 1-11

with E equal to the Young’s modulus of the pile material.

Consequently, the thermally induced axial load (P_T) is estimated as:

$$P_T = -\sigma_{Th} \cdot A$$

Equation 1-12

where A is the section of the pile.

The distribution of the thermal stress and the position of the NP depend on the stiffness of the boundary restraints and whether the load applied to the energy pile is simply thermal or thermo-mechanical.

Often EP are subjected to both thermal and mechanical load simultaneously. In this case the total strain (ϵ_{Total}) can be estimated as:

$$\epsilon_{Total} = \epsilon_M + \epsilon_{T,Obs}$$

Equation 1-13

where ϵ_M is the mechanical strain caused by load on pile head and $\epsilon_{T,obs}$ is the thermal observed strain.

Mechanical induced axial load (P_M) is usually estimated as:

$$P_M = \epsilon_M \cdot AE$$

Equation 1-14

where A is the pile section and E is Young's modulus of the pile material.

The total axial load (P_{Tot}) of an EP subjected to both thermal and mechanical loading is:

$$P_{Total} = P_M + P_T$$

Equation 1-15

The mobilized coefficient of thermal expansion and the degree of freedom are two parameters that explain the thermomechanical behaviour of and energy pile.

The mobilized coefficient of thermal expansion (α_{mob}) is defined as the slopes of the observed thermal axial strain ($\epsilon_{T,obs}$) versus temperature (McCartney and Murphy, 2012).

$$\alpha_{mob} = \frac{\epsilon_{T,Obs}}{\Delta T}$$

Equation 1-16

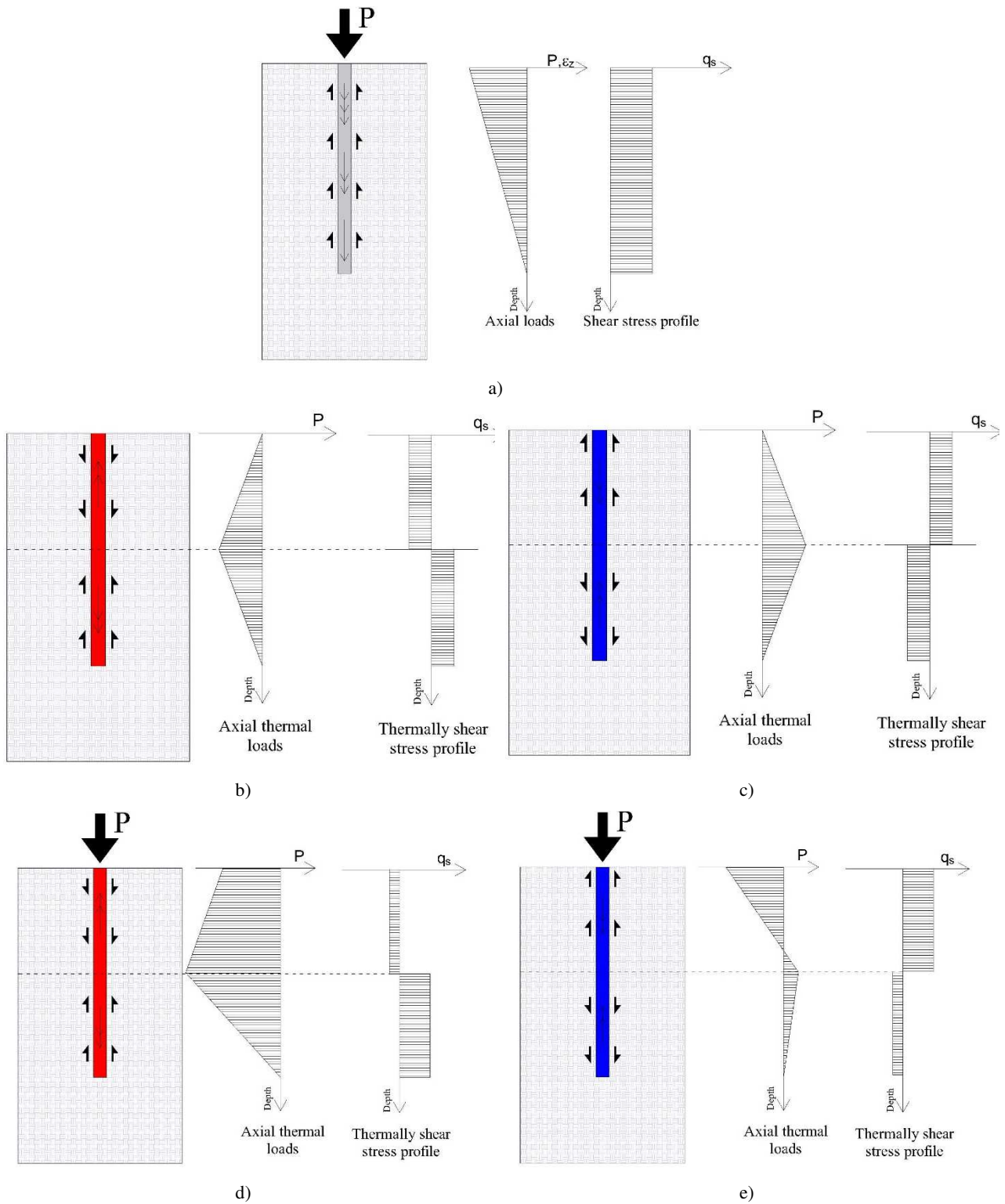
The ratio between the free and observed axial strains ($\epsilon_{t,obs}$) and the thermal free-expansion strain ($\epsilon_{t,free}$) is called degree of freedom of pile and is denoted as "n". The degree of freedom is a value in the range 0 and 1. For a null n the pile results completely blocked while for a unitary value of n the pile is completely free to move. By the way, in real cases, n is always an intermediate value between the two limits, and it depends on the restraint at the two extremities of the pile and moreover on the mobilized shaft friction (Knellwolf, Peron and Laloui, 2011)

$$n = \frac{\epsilon_{T,Obs}}{\epsilon_{T,free}}$$

Equation 1-17

A simple description of the behaviour of EP under thermal and thermomechanical loads was reported by P. J. Bourne-Webb et al. 2009 and Amatya et al. 2012. Replotted from literature, a scheme is reported in which strain, stress and interface shear stress are represented in function of restraint and

soil stiffness Figure 1-10. The schemes are rather simplified and self-explaining provided that the figure caption is kept in mind.



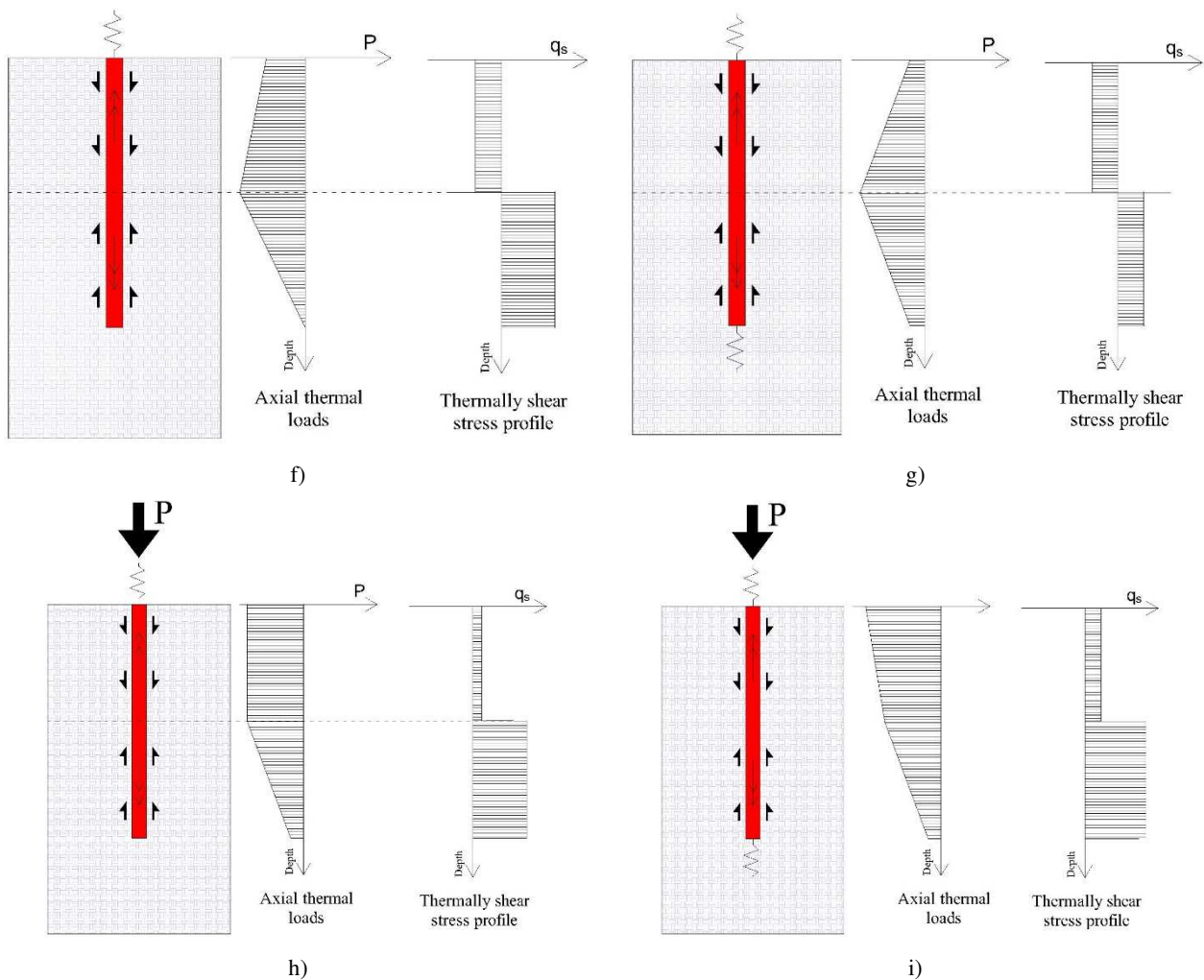


Figure 1-10 – Energy pile response mechanism under thermal and thermomechanical loads and different restraint conditions. a) mechanical load only; b) heating only; c) cooling only; d) combined mechanical loads and heating; e) combined mechanical loads and cooling; f) heating only with head restrained; g) heating only with head and toe restrained; h) combined mechanical loads and heating with head restrained; i) combined mechanical loads and heating with head and toe restrained

1.6 Soil thermal properties, soil temperatures and heat transfer mechanisms

Compared to traditional foundation piles, in the case of EPs, in addition to the knowledge of the mechanical properties of the soil, knowledge of its thermophysical properties and temperatures is also essential. In literature it was demonstrated that the ground temperature had an impact in terms of performances on geothermal heat pump and that vice versa energy piles could have an impact on ground temperature after some years of the plant operation (Morrone, Coppola and Raucci, 2014; Wu *et al.*, 2019). The subsoil temperature can vary in response to radiant, thermal, and latent energy exchange processes that occur mainly through the surface (Hillel, 1982). Anyway, it was shown that at about twenty meters from the surface, seasonal fluctuations can be neglected and the subsoil temperature stands at a value equal to that of the seasonal averages (Tinti *et al.*, 2014). The effects of the energy exchange on the soil profile depend on the time-variable and space-variable soil properties like the specific heat capacity, the thermal conductivity (λ), and the thermal diffusivity (α_s) (Hillel, 1982).

In the following section soil thermal properties, temperature soil trend and prediction with the depth and the main heat transfer mechanism are briefly recalled.

1.6.1 The mechanism of heat transfer

In nature the main heat transfer mechanisms are conduction, convection, and radiation. Conduction occurs when the heat transfer takes place with the transfer of kinetic energy from molecules located in a higher temperature area of the body to others in an adjacent lower temperature area. The heat transfer occurs in solid, liquid, or gaseous bodies with no mass transport.

Convection is the thermal energy transfer mechanism triggered by the combined action of conduction and mass transport. It is the most significant mechanism of heat transfer between a solid surface and a fluid. The transfer of energy as the particles of the fluid come through their motion in contact with other particles giving rise to different points of the fluid and has multiple conductive flows. An increase of the fluid velocity provides an increase of the transferred energy.

The thermal radiation occurs through the propagation of electromagnetic waves. It is based on absorption and emission phenomena for which each body, at a temperature different from 0 K, emits an electromagnetic radiation that propagates through the vacuum. This radiation is partly absorbed by another body and produces a transfer of energy between the two bodies.

1.6.2 Heat transfer in soil

In unfrozen soil the heat transfer occurs mainly by conduction and secondly by convection (Brandl, 2006).

The heat transfer mechanism of the conduction is governed by the Fourier's Law. It states that the flux of heat in a homogeneous body is in the direction of, and proportional to, the temperature gradient:

$$q_{cond} = -\lambda \nabla T$$

Equation 1-18

Where q_{cond} is the thermal flux [W/m^2], λ is the thermal conductivity [$W/m^\circ C$] and ∇T the spatial gradient of temperature. For a dimension, such as respect the depth of soil z , it becomes:

$$q_{cond} = -\lambda \frac{dT}{dz}$$

Equation 1-19

With dT/dz the gradient of temperature in vertical direction.

Fourier's Law represent a way to describe heat conduction under steady-state condition. Generally, the pile-soil thermal interaction is transient and so the heat transfer is affected not only by the geometry and thermal conductivity but also by the temperature change velocity. The heat capacity of soil governs the latter aspect (Loveridge and Powrie, 2013). For transient conditions, the equation that must be adopted is:

$$\frac{d^2T}{dx^2} + \frac{d^2T}{dy^2} + \frac{d^2T}{dz^2} = \frac{C}{\lambda} \frac{dT}{dt}$$

Equation 1-20

Where C_v ($J/m^3\text{°C}$) is the volumetric heat capacity, T is the temperature and λ is the thermal conductivity [$W/m\text{°C}$]. This equation is similar to the consolidation governing equation simply exchanging the temperature with the piezometric head.

The convection in soils occurs generally between the solid phase that is static and the water and/or gasses in the pore and the convection heat transfer is calculated as:

$$q_{w,conv} = c_w \rho_w v_w (T - T')$$

Equation 1-21

$$q_{v,conv} = c_v \rho_v v_v (T - T')$$

Equation 1-22

where the symbol w or v means water or vapour, respectively, c is the specific heat capacity, v is the velocity vector and ρ is the density. Finally, T' is the reference temperature.

Sometime the water can also undergo the phenomenon of the vaporisation. It is well known that it consists in a water phase change providing a latent heat transfer that can be quantified as:

$$q_{Lat} = L_0 \rho_w v_v$$

Equation 1-23

where L_0 is the latent vaporisation heat at the temperature T' .

The overall process of heat transfer in a soil volume is thus governed by the equation:

$$q_{tot} = q_{cond} + q_{w,conv} + q_{v,conv} + q_{lat}$$

Equation 1-24

1.6.3 Soil thermal properties

The heat transfer in the soil is affected by some soil thermal properties such as the thermal conductivity, the volumetric heat capacity and the thermal diffusivity. Briefly the thermal conductivity can be seen as the capacity of material to conduct the heat from zones where the temperature is higher to zones where the temperature is lower. The volumetric heat capacity is the energy needed to increase in a material the temperature of 1 K (or 1 °C). Finally, the thermal diffusivity is the parameter that indirectly affected the thermal conductivity law in transient condition. These thermal properties are all described in detail in the next sections.

1.6.3.1 The soil thermal conductivity

As already reported before, thermal conductivity λ [$W/m\text{°C}$] is defined as the quantity of heat transferred through a unit area of the conducting body in the unit time under a unit temperature gradient. It is the most important thermal soil parameter (Brandl, 2006).

Density of soil and its water content, and so also mineralogical components and chemical properties of pore water, influence the thermal conductivity of soil. It is also influenced by the state of water inside the pore. In fact, freezing increases the thermal conductivity significantly because of the higher thermal conductivity of ice (2,18 W/m°C) compared to the lower thermal conductivity of the water at liquid state (0,57 W/m°C) (Brandl, 2006).

Thermal conductivity is variable in time, because the proportions of air and water in soil continuously change and is variable with depth because seldom soil composition is uniform in depth (Hillel, 1982). The internal structure of soil matrix and the mode of transmission of heat from particle to particle and from phase to phase could change the relationship between the specific thermal conductivities of the constituent of soil and the overall thermal conductivity of soil.

Because of the multiphasic nature of the soil (solid, water and air), the parallel and the series theoretical model were both developed to define a likely upper bound and lower bound for the soil aggregate at its natural status. The parallel theoretical model defines the upper bound thermal conductivity as in the following equation:

$$\lambda_s = \lambda_g(1 - n) + S\lambda_w n + n(1 - S)\lambda_a$$

Equation 1-25

On the other hand, the series theoretical model for the lower bound correspond to the following overall conductivity:

$$\lambda_s = \frac{1}{\left(\frac{1-n}{\lambda_g}\right) + \left(\frac{n}{\left(\frac{S}{\lambda_w}\right) + \left(\frac{1-s}{\lambda_a}\right)}\right)}$$

Equation 1-26

where the symbol s, g, w and a means soil, grain (soil solid phase), water and air respectively, S is the degree of saturation, n is the porosity.

1.6.3.2 The volumetric heat capacity

The soil volumetric heat capacity C_v (J/m³°C) is defined as the change in heat content of a unit bulk volume of soil per unit change in temperature. It is the product of the soil density (kg/m³) and the specific heat extraction c, i.e. the skill of a material to store heat energy.

$$C_v = \rho c$$

Equation 1-27

C_v of a soil aggregate depends on some soil characteristics such as the wetness, the density and the mineral and/or organic composition of the solid phase. Its value for soil can be estimated as the sum of the volumetric heat capacity of soil various components in relation of the state of the soil

$$C_{v,s} = (1 - n)\rho_g c_g + nS\rho_w c_w + n(1 - S)\rho_v c_v$$

Equation 1-28

Where the symbol s, g, w and a means soil, grain (soil solid phase), water and air respectively, S is the degree of saturation, n is the porosity.

1.6.3.3 The soil thermal diffusivity

The thermal diffusivity α_s can be defined as the change in temperature produced in a unit volume by the quantity of heat flowing through the volume in unit time under a unit temperature gradient or as the ratio between the soil thermal conductivity and the product of the soil density and its specific heat.

$$\alpha_s = \frac{\lambda}{c_s \rho} = \frac{\lambda}{C_{v,s}}$$

Equation 1-29

In the following tables the recommendations coming from different handbooks or regulations on the average thermal properties for soils and rocks are summarized. Of course, these are simply general indications and cannot be considered as alternative to site and laboratory testing for measuring the thermal properties of a specific soil aggregate.

Table 1-1 - Some thermal properties for soils and rocks from handbook (ASHRAE, 2011)

		Thermal conductivity [W/m°C]	Thermal diffusivity [m²/day]
Soil			
Heavy clay	15% water	1,4-1,9	0,042-0,061
	5% water	1,0-1,4	0,047-0,061
Light clay	15% water	0,7-1,0	0,047-0,055
	5% water	0,5-0,9	0,056
Heavy sand	15% water	2,8-3,8	0,084-0,11
	5% water	2,1-2,3	0,093-0,14
Light sand	15% water	1,0-2,1	0,047-0,093
	5% water	0,9-1,0	0,055-0,12
Rocks			
Granite		2,3-3,7	0,084-0,13
Limestone		2,4-3,8	0,084-0,13
Sandstone		2,1-3,5	0,11-0,65
Shale	wet	1,44-2,4	0,065-0,084
	dry	1,0-2,1	0,55-0,074

Table 1-2 - Thermal properties for soils from (VDI 4640, 2001)

	Thermal conductivity [W/m°C]		Volumetric heat capacity [MJ/m ³ /°C]		Density [kg/m ³]	
	min	max	min	max	min	max
Dry clay	0,4	1	1,5	1,6	1,8	2
Water saturated clay	1,1	3,1	2	2,8	2	2,2
Dry sand	0,3	0,9	1,3	1,6	1,8	2,2
Water saturated sand	2	3	2,2	2,8	1,9	2,3
Dry gravel	0,4	0,9	1,3	1,6	1,8	2,2
Water saturated gravel	1,6	2,5	2,2	2,6	1,9	2,3
Quartzite rock	5	6	2,1	2,1	2,5	2,7

Table 1-3 - Thermal diffusivity values derived from the thermal property of VDI 4640, 2001

	Thermal Diffusivity [m ² /s]			Thermal Diffusivity [m ² /day]		
	min	max	ave	min	max	ave
Dry clay	2,67E-07	6,25E-07	4,46E-07	0,023	0,054	0,039
Water saturated clay	5,50E-07	1,11E-06	8,29E-07	0,048	0,096	0,072
Dry sand	2,31E-07	5,63E-07	3,97E-07	0,020	0,049	0,034
Water saturated sand	9,09E-07	1,07E-06	9,90E-07	0,079	0,093	0,086
Dry gravel	3,08E-07	5,63E-07	4,35E-07	0,027	0,049	0,038
Water saturated gravel	7,27E-07	9,62E-07	8,44E-07	0,063	0,083	0,073
Quartzite rock	2,38E-06	2,86E-06	2,62E-06	0,206	0,247	0,226

Table 1-4 – Thermal conductivity ranges for some soils and rocks. Replotted from (Microgeneration Certification Scheme - Biomass WG, 2015)

	Type of rock		Thermal conductivity [W/m°C]		
			Min	Max	Recommended
Unconsolidated rock	Sand, dry		0,3	0,8	0,4
	Gravel, dry		0,4	0,5	0,4
	Peat, soft lignite		0,2	0,7	0,4
	Clay/silt, dry		0,4	1,0	0,5
	Clay/silt, water saturated		0,9	2,3	1,7
	Gravel. water saturated		1,6	2,0	1,8

	Claystone, siltstone		1,1	3,5	2,2
	Sand, water saturated		1,5	4,0	2,4
Solid Sediments	Hard coal		0,3	0,6	0,4
	Gypsum		1,3	2,8	1,6
	Marl		1,5	3,5	2,1
	Sandstone		1,3	5,1	2,3
	Conglomerates		1,3	5,1	2,3
	Limestone		2,5	4,0	2,8
	Dolomite		2,8	4,3	3,2
	Anhydrite		1,5	7,7	4,1
	Salt		5,3	6,4	5,4
		Tuff		1,1	1,1
Magmatites	Vulcanite, alkaline to ultra-alkaline	e.g. andesite, basalt	1,3	2,3	1,7
	Plutonite, alkaline to ultra-alkaline	Gabbro	1,7	2,5	1,9
		Diorite	2,0	2,9	2,6
	Vulcanite, acid to intermediate	e.g. Latite, dacite	2,0	2,9	2,6
		e.g. Rhyolite, trachyte	3,1	3,4	3,3
	Plutonite, acid to intermediate	Syenite	1,7	3,5	2,6
Granite		2,1	4,1	3,4	
Metamorphic rock	Slight metamorphic	Clay shale	1,5	2,6	2,1
		Chert	4,5	5,0	4,5
		Mica schist	1,5	3,1	2,2
	Moderately to highly metamorphic	Gneiss	1,5	3,1	2,2
		Marble	1,3	3,1	2,5
	Vulcanite, acid to intermediate	Amphibolite	1,9	4,0	2,9
		e.g. Rhyolite, trachyte	2,1	3,6	2,9
Quartzite		5,0	6,0	5,5	

1.6.4 Heat exchange between pile a soil – thermal behaviour

The heat exchange between the energy piles and the surrounding soil occurs mainly through mechanisms of conduction and convection. The heat transfer in a concrete energy pile occurs by heat convection between carrier fluid and wall of pipes and heat conduction between pipes' wall and concrete of pile and between concrete and soil. For these reasons usually the heat exchange between pile and soil is simplified and the convection and radiation mechanisms are considered as negligible (Rees *et al.*, 2000).

Heat transfer mechanism from the primary circuit of EPs to surrounding soil and vice versa during heating or cooling phases is a complex mechanism that involves all the underground components of geothermal system.

The HDPE loops heat exchanging incorporated within the energy piles, the heat exchangers fluid that flows inside pipes loops and finally the concrete of the pile, constitute the primary circuit. Between the fluid circulating into the pipes inside the pile and the surrounding soil there is of course a thermal gradient which is influenced by the pile-soil thermal interaction (Faizal, Bouazza and Singh, 2016). The larger dimensions of the diameter of the energy piles compared to traditional geothermal wells ensure that it cannot be considered a thermal steady state (Loveridge *et al.*, 2015). In fact, since the concrete around the pipes can take several days to reach the steady state, the difference in the average temperature between the heat exchanger fluid and the average soil temperature on the edge of the exchanger cannot be considered constant. For this reason, thermal resistance of concrete could become a fundamental parameter to improve thermal performances of energy piles.

The heat transfer between the primary circuit fluid and the soil is summarized by equation (Faizal, Bouazza and Singh, 2016):

$$Q = \frac{T_1 - T_5}{R_{tot}}$$

Equation 1-30

Where T_1 and T_5 are fluid and soil temperatures, respectively, and R_{Tot} is the total thermal resistance transfer, given as:

$$R_{tot} = +R_{fluid} + R_{pipe} + R_{concrete} + R_{ground}$$

Equation 1-31

The resistance of the fluid is usually expressed as:

$$R_{fluid} = \frac{1}{2n\pi r_i h}$$

Equation 1-32

Where r_i is the internal pipe radius, n is the number of pipes, and h is the convective heat transfer coefficient [$W/m^2\text{°C}$]. The pipe thermal resistance is given as:

$$R_{pipe} = \frac{\ln(r_o/r_i)}{2n\pi\lambda_p}$$

Equation 1-33

Where r_o is the pipe outer radius and λ_p is the thermal conductivity of the pipe material [$W/m\text{°C}$].

Regarding thermal resistance of the concrete annular section, its steady state value could be calculated with the equation of the thermal resistance of a cylinder, but an assumption must be made for the effective inner radius of that cylinder r_{eff} .

The concrete thermal resistance using the equivalent diameter approach is given as:

$$R_{concrete} = \frac{\ln(r_b/r_{eff})}{2\pi\lambda_c}$$

Equation 1-34

where r_b is pile radius, λ_c is concrete thermal conductivity [W/m°C], and r_{eff} is the effective radius.

$$R_{eff} = r_0\sqrt{n}$$

Equation 1-35

Where n is the number of pipes. The equivalent cylinder approach does not consider actual positioning of pipes. The mechanism is explained in Figure 1-11.

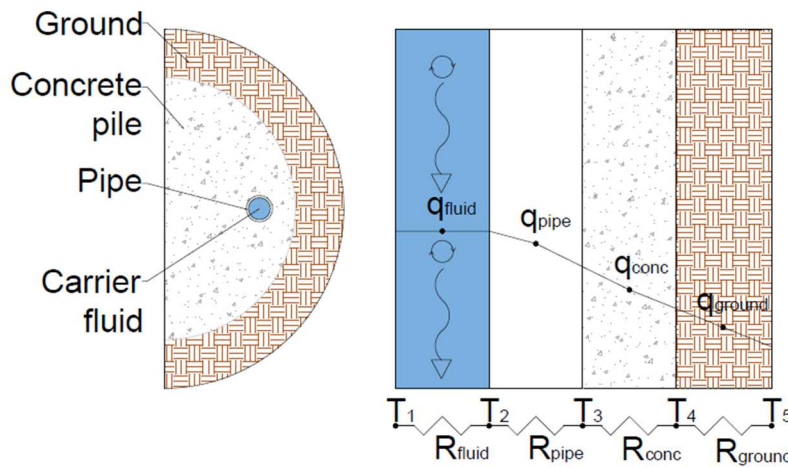


Figure 1-11 – Simplified scheme of the heat transfer mechanism from the heat carrier fluid to the surrounding soil in energy pile

In this section only a very schematic description of the heat transfer process is done. In the following chapters a critical review of the literature on the mentioned properties and on the heat transfer processes is proposed. Some hints about the possibility to improve the heat transfer are also provided.

1.6.5 The underground temperature

To provide an optimal design for energy piles, the soil temperature at relatively shallow depth below the ground surface should be known. In fact, because EPs use ground as a heat source, the amount of energy exchanged between piles and soil and vice versa, is directly proportional to the temperature difference between the ground and the piles. Moreover, because the temperature field in the ground and in the pile may affect mechanical behaviour of both elements to know temperatures in soil is fundamental for the global performances of EPs.

The ground temperature is affected by some factors such as the structure and physical properties of the ground, external air temperature variations, climatic factors, topography, position of surface of soil with regards to the sun, solar radiation, wind, rainfall, and surface cover (van Manen and Wallin, 2012).

Because of the local influences of the mentioned factors, during the year the temperature of the soil does not follow the same pattern everywhere (Islam, 2017).

If compared to the average annual air temperature wave valued monthly, the annual thermal wave in the soil shows a greater damping in amplitude and a phase-shift with the increase of the depth. Only for the upper crust made by the first few tens of cm the average annual temperature wave of the soil tends to coincide with the air one (Baggs, 1983).

The soil temperature is constant at certain depths, and around 15 m in depth it is equal to the mean annual air temperature (Rybach and Sanner, 2000). For this reason, at a given time the soil shows lower temperatures compared to the air temperatures in the summer period. The reverse occurs in the winter period.

In literature, generally three temperature zones can be distinguished subdivided for depth. The surface zone between 0 m and 2 m, the shallow zone between 2 m and 15 m and finally the deep zone between 15 m and 50 m.

In the surface zone, the ground temperature is sensitive to diurnal variations. In this zone thermal parameters of soil are important, but the temperature is affected above all by surface condition like for example soil cover, wind velocity and the interaction with structures.

In the shallow zone, the ground is sensitive to seasonal weather variations. External climatic conditions and details tend to become negligible but the presence of a groundwater and the interaction with upper structures and buildings must be taken in account for thermal exchanges.

In the deep zone, the ground temperature is nearly constant and depends in the upper 20-30 m by the geographic location.

Under 50 m the temperature behaviour is completely affected by the geothermal heat flux.

This subdivision is fundamental for the design of the energy piles because the main part of the energy piles is installed in the shallow zone and results very important to know the yearly temperature trends and cycles.

To determine design parameters, as well as the detailed soil properties, long-term soil temperature measurement at different soil depths and over the time are needed. This process often results lengthy, complicated, and expensive.

Because a detailed site survey is not always possible, to minimize costs and time designers and researchers are in the need of more practical tools (Ozgener, Ozgener and Tester, 2013).

Over the years, many studies were carried out about the subsoil temperatures for different aims.

Kasuda and Achemback (1965) compiled and analysed 63 sets of data of 48 states of the USA for the annual variations of monthly average earth temperatures at different depths. From this data, the authors, through the least-squared method, calculated the annual average amplitude and the phase

angle of the soil temperature distribution with the depth. The thermal diffusivity of soil was also computed from the observed temperatures data.

Baggs (1983) developed a semi-empirical formula for assessing soil temperature as a function of time and depth. Using coefficient data derived from the temperature measurement of 20 Australian experimental sites, the author adapted for the southern hemisphere the mathematical models for predicting the temperature profiles in the subsoil, already published for the northern hemisphere. This formula was calibrated so that the result of the algorithm had the best fitting with the experimental curve. The data needed to use the formula was provided by Baggs both through a map of Australia showing temperatures in different areas and through a table showing the lag time between wave air temperature and soil wave temperature in relationships of the thermal diffusivity (Figure 1-12).

The effects of the upper structures on soil surfaces were investigated by Mihalakakou et al. (1995) and Popiel et al. (2001). In the first case, the aim was to research an accurate transient numerical method to calculate ground temperature at different depth starting from the calculation of the heat flow towards the ground from a building foundation. In the second case, instead, the investigation was carried out comparing both a paver car park surface and a grass covered surface. It was found that for bare soil (car park) in summer at depth of 1 m the temperature was higher than 4 °C in comparison with the lawn underground, while in winter the temperature was the same. Moreover, the experimental data showed a good agreement with Baggs's formula.

A study to predict soil temperature for geothermal heat exchangers application was carried out by Ozgener et al. (2013). The model was determined using principles of transient heat flow with the assumption of one-dimensional heat flow, constant thermal diffusivity, and homogenous soil. To validate the accuracy of the model, the predicted temperature was compared with temperature measured in field test performed at the Ede University (Turkey) at depth of 5 cm, 10 cm, 20 cm, and 300 cm.

Soil Thermal Diffusivity $10^{-2} \text{ cm}^2 \text{ sec}^{-1}$	B.*	1000'	1500'	2000'	3000'	3500'	4000'	5000'
		mm						
		(day)						
0.22	(0.20)*	40	59	79	116	138	158	199
0.27	(0.25)*	36	53	71	106	124	141	177
0.32	(0.30)*	32	48	65	97	113	129	161
0.38	(0.35)*	30	45	60	90	105	120	148
0.43	(0.40)*	28	42	56	84	98	112	140
0.48	(0.45)*	26	40	52	79	92	105	132
0.54	(0.50)*	25	38	50	75	89	100	125
0.59	(0.55)*	24	36	48	72	83	95	119
0.65	(0.60)*	23	34	46	69	80	91	114
0.70	(0.65)*	22	33	44	66	77	88	110
0.75	(0.70)*	21	32	42	63	74	85	106
0.81	(0.75)*	20	31	41	61	71	82	102
0.86	(0.80)*	20	30	40	59	69	79	99
0.92	(0.85)*	19	29	38	58	67	77	96

* Column B. Converted to $(\text{ft}^2 \text{ day}^{-1})$
 ** Zone A. : All figures to the right and above broken line shown thus:  indicate a seasonal lag of four months or more (122-198 days).
 *** Zone B. : All figures below the broken line of Zone A. and above the broken line of Zone B. shown thus:  indicate a seasonal lag of three/four months (91-121 days).

Figure 1-12 – Baggs (1983). Time delay in relationship of soil depth and thermal diffusivity

Many other studies about the temperature soil distribution prediction over the time were carried out by authors in many parts of the world such as Chow et al. (2011) in China, Van Manen et al. (2012) in New Zealand, Pouloupatis et al. (2011) in Cyprus, Tinti et al. (2014) in Italy or Islam (2017) in Bangladesh.

1.6.5.1 Ground temperature prevision in function of the time and the depth: a mathematical approach

Because of the connection between the soil-surface and external environmental temperature conditions and the irregular weather episodic phenomena, to predict the temperature soil profile is not a simple task.

A pure harmonic (sinusoidal) function of time around an average value is the easiest mathematic way to represent the fluctuating thermal regime of nature for all depth in soil.

The following equation is thus widely applied and especially if it is calibrated with field data can give a good approximation for the thermal regime of the soil (Hillel, 1982):

$$T(z, t) = T_m + A_z \sin[\omega t + \varphi(z)]$$

Equation 1-36

where:

T(z, t) is the temperature of soil at time t and depth z;

T_m is the average temperature of the soil;

z is the considered soil depth;

t is the considered time;

A_z is the amplitude at depth z ;

$\varphi(z)$ is the phase angle at depth z .

A_z and $\varphi(z)$ are function of depth but not of time. The sinusoidal function derived by solving annual variation of daily average soil temperature at various depths (Hillel, 1982):

$$\frac{\partial T(z, t)}{\partial t} = \alpha \frac{\partial^2 T(z, t)}{\partial z^2}$$

Equation 1-37

where α is the thermal diffusivity.

The boundary condition used to solve Equation 1-37 regarding temperature at surface:

$$T(0, t) = T_m + A_0 \sin(\omega t)$$

Equation 1-38

and temperature at infinite depth is constant and equal to T_m :

$$T(\infty, t) = T_m$$

Equation 1-39

the solution is (Hillel,1982):

$$T(z, t) = T_m + A_0 e^{-z/d} \left[\sin\left(\omega t - \frac{z}{d}\right) \right]$$

Equation 1-40

where:

ω is the radial frequency defined as $2\pi/P$;

P is the period;

d is called damping depth and it is defined as the depth at which the temperature amplitude decreases to the fraction $1/e$ (37%) of the A_0 . Damping depth is linked to thermal diffusivity and radial frequency ω :

$$d = \sqrt{\frac{2\alpha}{\omega}}$$

Equation 1-41

when an arbitrary zero point is introduced (t_0) and because the addition of constants does not affect the Equation 1-40, become:

$$T(z, t) = T_m + A_0 e^{-z/d} \left[\sin\left(\omega(t - t_0) - \frac{z}{d} - \frac{\pi}{2}\right) \right]$$

Equation 1-42

For any depth, the amplitude of the wave temperature is smaller of the quantity $e^{z/d}$ compared to the amplitude of the wave temperature at the soil surface and the phase shift of $-z/d$.

Analysing the sinusoidal function, it can be decomposed in three parts: an average steady temperature, a sinusoidal annual variation and a transient variation. While the last term depends on climatic change during the period of calculation, the first two depend on geographical location and annual variations. From the differences of amplitudes and the phases of the waves at two different depths, it is possible to calculate thermal diffusivity:

$$\alpha_{\varphi} = \left(\frac{\omega}{2}\right) (z_2 - z_1)^2 \left(\frac{1}{(\varphi(z_1) - \varphi(z_2))}\right)^2$$

Equation 1-43

$$\alpha_A = \left(\frac{\omega}{2}\right) \left(\frac{z_2 - z_1}{\ln\left(\frac{|A(z_1, \omega)|}{|A(z_2, \omega)|}\right)}\right)$$

Equation 1-44

where z_1 and z_2 are the selected depth, φ is the phase, ω is the radial frequency and A is the amplitude of wave temperatures at the different depths.

1.7 Conclusion: the role of energy geo-structures and the purpose of the research

In recent decades, the world's energy policies have been aimed at combating the sudden phenomenon of climate change on the one hand and an ever-increasing demand for energy on the other. The main problem is the still strong dependence on fossil fuels, both for direct energy consumption and to produce derived energy sources such as electricity. It has been demonstrated that the heating and cooling of the indoor spaces, is the largest energy sector in the world as well as one of the main contributors to direct and indirect emissions of CO₂ and other climate-changing gases that contribute to global warming. Moreover, the large amount of energy expended in this sector is very often caused by energy-inefficient heating/conditioning systems. One possible answer to this problem can be the installation of high-performance systems that do not use fossil fuels directly. Geothermal heat pump systems meet these requirements exactly. In recent years, the increasingly binding energy design criteria imposed by the EU have led to the rapid development of this type of technology. However, it does have its limitations, such as the space required for the installation of underground heat exchangers or the drilling costs for installing them.

Energy piles represent a new technology currently available in which geothermal heat exchangers are inserted into the pile foundations. In this way, in addition to the dead and live loads of the upper structures, energy piles are subjected also to thermal loads during the heat exchangers between the piles and the surrounding ground. that should be taken into account both in Ultimate Limit State (ULS) and in Serviceability Limit State (SLS) checks.

- Faizal, M., Bouazza, A. and Singh, R. M. (2016) 'Heat transfer enhancement of geothermal energy piles', *Renewable and Sustainable Energy Reviews*. Elsevier, 57, pp. 16–33. doi: 10.1016/j.rser.2015.12.065.
- Gao, J., Zhang, X., Liu, J., Li, K., et al. (2008) 'Numerical and experimental assessment of thermal performance of vertical energy piles: An application', *Applied Energy*, 85(10), pp. 901–910. doi: 10.1016/j.apenergy.2008.02.010.
- Gao, J., Zhang, X., Liu, J., Li, K. S., et al. (2008) 'Thermal performance and ground temperature of vertical pile-foundation heat exchangers: A case study', *Applied Thermal Engineering*, 28(17–18), pp. 2295–2304. doi: 10.1016/j.applthermaleng.2008.01.013.
- Go, G. H. et al. (2014) 'Design of spiral coil PHC energy pile considering effective borehole thermal resistance and groundwater advection effects', *Applied Energy*. Elsevier Ltd, 125, pp. 165–178. doi: 10.1016/j.apenergy.2014.03.059.
- Heating – Tracking Buildings 2020 – Analysis - IEA (no date). Available at: <https://www.iea.org/reports/tracking-buildings-2020/heating#abstract> (Accessed: 28 February 2021).
- Hillel, D. (1982) 'Soil Temperature and Heat Flow', *Introduction to Soil Physics*, pp. 155–175. doi: 10.1016/b978-0-08-091869-3.50013-5.
- Islam, R. (2017) 'A comparative study on the variation of soil temperature at different depths', 8(7), pp. 444–446.
- Johnston, I. W., Narsilio, G. A. and Colls, S. (2011) 'Emerging geothermal energy technologies', *KSCE Journal of Civil Engineering*, 15(4), pp. 643–653. doi: 10.1007/s12205-011-0005-7.
- Kasuda, T. and Achenboch, P. R. (1965) 'The classified or limited status of this report applies to each page, unless otherwise marked. Separate page printouts MUST be marked accordingly.'
- Knellwolf, C., Peron, H. and Laloui, L. (2011) 'Geotechnical Analysis of Heat Exchanger Piles', *Journal of Geotechnical and Geoenvironmental Engineering*, 137(10), pp. 890–902. doi: 10.1061/(asce)gt.1943-5606.0000513.
- Laloui, L., Nuth, M. and Vulliet, L. (2006) 'Experimental and numerical investigations of the behaviour of a heat exchanger pile', *International Journal for Numerical and Analytical Methods in Geomechanics*, 30(8), pp. 763–781. doi: 10.1002/nag.499.
- Lindal, B. (1973) 'Industrial and other applications of geothermal energy.', *Geothermal energy*, pp. 135-148.
- Loveridge, F. et al. (2015) 'The Thermal Behaviour of Three Different Auger Pressure Grouted Piles Used as Heat Exchangers', *Geotechnical and Geological Engineering*, 33(2), pp. 273–289. doi: 10.1007/s10706-014-9757-4.
- Loveridge, F. and Powrie, W. (2013) 'Pile heat exchangers: Thermal behaviour and interactions', *Proceedings of the Institution of Civil Engineers: Geotechnical Engineering*, 166(2), pp. 178–196. doi: 10.1680/geng.11.00042.
- van Manen, S. M. and Wallin, E. (2012) 'Ground temperature profiles and thermal rock properties at Wairakei, New Zealand', *Renewable Energy*. Elsevier Ltd, 43, pp. 313–321. doi: 10.1016/j.renene.2011.11.032.
- McCartney, J. S. and Murphy, K. D. (2012) 'Strain Distributions in Full-Scale Energy Foundations (DFI Young Professor Paper Competition 2012)', *DFI Journal - The Journal of the Deep Foundations Institute*, 6(2), pp. 26–38. doi: 10.1179/dfi.2012.008.
- Microgeneration Certification Scheme - Biomass WG (2015) 'MIS 3004 - Requirements for MCS

contractors undertaking the supply, design, installation, set to work, commissioning and handover of solid fuel heating systems', (4.2), p. 57.

- Mihalakakou, G. et al. (1995) 'On the ground temperature below buildings', *Solar Energy*, 55(5), pp. 355–362. doi: 10.1016/0038-092X(95)00060-5.
- De Moel, M. et al. (2010) 'Technological advances and applications of geothermal energy pile foundations and their feasibility in Australia', *Renewable and Sustainable Energy Reviews*. Elsevier Ltd, 14(9), pp. 2683–2696. doi: 10.1016/j.rser.2010.07.027.
- Morino, K. and Oka, T. (1994) 'Study on heat exchanged in soil by circulating water in a steel pile', *Energy and Buildings*, 21(1), pp. 65–78. doi: 10.1016/0378-7788(94)90017-5.
- Morrone, B., Coppola, G. and Raucci, V. (2014) 'Energy and economic savings using geothermal heat pumps in different climates', *Energy Conversion and Management*. Elsevier Ltd, 88, pp. 189–198. doi: 10.1016/j.enconman.2014.08.007.
- Nagano, K. et al. (2005) 'Thermal Characteristics of Steel Foundation Piles As Ground Heat Exchangers', IEA Heat Pump Conference, 8th.
- Ozgener, O., Ozgener, L. and Tester, J. W. (2013) 'A practical approach to predict soil temperature variations for geothermal (ground) heat exchangers applications', *International Journal of Heat and Mass Transfer*. Elsevier Ltd, 62(1), pp. 473–480. doi: 10.1016/j.ijheatmasstransfer.2013.03.031.
- Pahud, D. et al. (2008) 'Measured thermal performances of the Dock Midfield energy pile system at Zürich airport', *Proceedings of 9th IEA Heat Pump Conference*, 20-22 May, 2(June), pp. 1–11.
- Pahud, D., Belliardi, M. and Caputo, P. (2012) 'Geocooling potential of borehole heat exchangers' systems applied to low energy office buildings', *Renewable Energy*. Elsevier Ltd, 45, pp. 197–204. doi: 10.1016/j.renene.2012.03.008.
- Park, H. et al. (2013) 'Evaluation of thermal response and performance of PHC energy pile: Field experiments and numerical simulation', *Applied Energy*. Elsevier Ltd, 103, pp. 12–24. doi: 10.1016/j.apenergy.2012.10.012.
- Park, S. et al. (2018) 'Engineering chart for thermal performance of cast-in-place energy pile considering thermal resistance', *Applied Thermal Engineering*. Elsevier Ltd, 130, pp. 899–921. doi: 10.1016/j.applthermaleng.2017.11.065.
- Popiel, C. O. Wojtkowiak, J. Biernacka, B. (2001) 'Measurements of temperature distribution in ground', *Experimental Thermal and Fluid Science*, 25, pp. 301–309. doi: 10.1023/A:1012520601587.
- Pouloupatis, P. D., Florides, G. and Tassou, S. (2011) 'Measurements of ground temperatures in Cyprus for ground thermal applications', *Renewable Energy*. Elsevier Ltd, 36(2), pp. 804–814. doi: 10.1016/j.renene.2010.07.029.
- Preene, M. and Powrie, W. (2009) 'Ground energy systems: From analysis to geotechnical design', *Geotechnique*, 59(3), pp. 261–271. doi: 10.1680/geot.2009.59.3.261.
- Rees, S. W. et al. (2000) 'Ground heat transfer effects on the thermal performance of earth-contact structures', *Renewable & sustainable energy reviews*, 4(3), pp. 213–265. doi: 10.1016/S1364-0321(99)00018-0.
- Rybach, L. (2003) 'Geothermal energy: Sustainability and the environment', *Geothermics*, 32(4), pp. 463–470. doi: 10.1016/S0375-6505(03)00057-9.
- Rybach, L. and Sanner, B. (2000) 'Ground-source heat pump systems - the European Experience', *GHC Bulletin*, (March), pp. 16–26. Available at: <http://www.sanner-geo.de/media/art4.pdf>.

- Tinti, F. et al. (2014) 'Experimental analysis of shallow underground temperature for the assessment of energy efficiency potential of underground wine cellars', *Energy and Buildings*. Elsevier B.V., 80, pp. 451–460. doi: 10.1016/j.enbuild.2014.06.002.
- Tsagarakis, K. P. et al. (2020) 'A review of the legal framework in shallow geothermal energy in selected European countries: Need for guidelines', *Renewable Energy*, 147, pp. 2556–2571. doi: 10.1016/j.renene.2018.10.007.
- VDI 4640 (2001) 'VDI 4640 Part 2. Thermal Use of the Underground: Ground source heat pump systems', p. 52.
- Wood, C. J., Liu, H. and Riffat, S. B. (2010) 'Comparison of a modelled and field tested piled ground heat exchanger system for a residential building and the simulated effect of assisted ground heat recharge', *International Journal of Low-Carbon Technologies*, 5(3), pp. 137–143. doi: 10.1093/ijlct/ctq015.
- World Commission On Environment And Development (1987) 'Vol. 17 - doc. 149', World Commission on Environment and Development, 17, pp. 1–91.
- Wu, D. et al. (2019) 'Thermo-mechanical behavior of energy pile under different climatic conditions', *Acta Geotechnica*, 14(5), pp. 1495–1508. doi: 10.1007/s11440-018-0731-9.

Chapter 2

2 Literature review

2.1 Introduction

In this chapter a literature review about energy piles was proposed. The chapter was divided in two main parts. In the first one, the mechanical aspects of energy piles were investigated while in the second one the energy aspects and the thermal performances were analysed. After a brief description of the tests the data collected by the literature both for mechanical and energy aspects were analysed and discussed. The aim of the analysis of the mechanical tests, both for full scale and small-scale tests, was to investigate the main change respect a traditional pile in terms of stress, strain and displacements. On the other hand, the aim of the review of the energy performances of the energy piles was to investigate on the main factors that affects the thermal performance during the pile work and the effects of these factors on the mechanical behaviour of the pile.

2.2 Mechanical behaviour of a single energy pile

In this section the main results collected from the literature by field scale and small-scale tests were summarized and analysed. After a separate review between full and small scale about the methodology of the tests carried out, the main mechanical behaviours of the energy pile for both the types of test were analysed. The results were collected with the aim of investigating the mechanical behaviour about the axial response, shaft response, radial response and head displacements.

2.2.1 Field tests

Field tests represent the most direct and closest experimental choice to the real thermomechanical behaviour of an energy pile.

Over the years, field scale mechanical tests were conducted and published. The data and results have been collected, synthesised, and compared.

The tests were carried out on piles installed with different technologies (both bored and driven concrete piles), with different aspect ratios and embedded in different soils. Some tests were conducted on single energy piles and others on energy piles that were part of a group of piles. Some piles were tested by means of dedicated load tests, others, instead, were tested with the real weight force of the building above. In this analysis only well-documented cases were reported. A brief description of the collected tests is given below, and the main data are summarised in Table 2-1.

One out of the first tests on the behaviour of energy pile and its bearing capacity under thermal loads were carried out by Brandl (2006) on an instrumented concrete bored pile, 9 m in length and 1,2 m in diameter, forming part of an operational GSHP system of 143 piles installed during the construction of a rehabilitation centre in Bad Schallerbach, Austria.

The effects of thermal load on shaft resistance of the pile and the energy extraction were analysed. Subsequently, first Laloui et al. (2006), then Bourne-Webb et al. (2009) in Switzerland and United Kingdom, respectively, carried out field tests on energy piles.

In the first case, at the Ecole Polytechnique Fédérale de Lausanne (EPFL) the tests were performed on a drilled pile 0,88 m in diameter and 25,8 m in length equipped with a U-shaped configuration pipe system for heat carrier fluid circulation located in the edge of a group of 97 piles. Mechanical and thermal loads were applied on the pile separately and alternately to decouple the thermal and mechanical effects. The mechanical load was applied by the weight of the building under construction under which the piles were installed.

In the second case, Bourne-Webb et al. (2009) carried out a thermo-mechanical test on an energy pile in the Clapham Centre of Lambeth College in South London. The test was carried out in a main test pile 23 m in length and 0,60 m in diameter installed in a first thin layer of sand and gravel (about 4 m) and the remaining part of the pile in a layer of stiff, fissured silty clay. A vertical load of 1200 kN applied against the reaction beam and anchor pile system on the main test pile was held 46 of the 53 days. It was observed by the strain profiles a thermal-elastic response of the pile under the applied loads. The mobilised shaft capacity was smaller than the ultimate resistance.

Singh et al (2015) and Wang et al. (2013, 2015), on the other hand, investigated on the effect of heating and cooling cycles on the shaft capacity and the radial thermal strain. In both cases it was observed that heating and cooling cycles did not affect the side shear capacity of the energy pile and that after a gain of strength of the pile shaft resistance during the heating phase it was observed a return to initial values when the pile was cooled.

Field tests at Denver Housing Authority Senior Living Facility in Denver, Colorado were carried out by McCartney and Murphy (2012) first and by Murphy and McCartney (2015) later. In both cases, two different energy piles of the same foundation placed beneath an 8-story building were tested. The drilled concrete energy piles, called A and B, were both 0,91 m in diameter and respectively 14,8 m and 13,4 m in length. It was observed that the side shear stresses provided resistance to thermally induced movements. It was also observed that for complex soil layers it is not always possible to appreciate a thermo-elastic behaviour of the system. According to the authors a thermo-elasto-plastic model for the soil could better capture the observed behaviour.

The thermo-mechanical response during a heating and cooling test of three of eight full-scale energy foundations constructed for a new building at the US Air Force Academy, were analysed in USA (Kyle D. Murphy, McCartney, and Henry 2015). The drilled shaft instrumented piles were called Foundation 1, Foundation 3, and Foundation 4, and were 0,61 m in diameter and 15,2 m in length.

Santiago et al. (2016) carried out a field test on a reinforced concrete square cross section driven pile. The pile had a length of 17,4 m and a section of 0,35 m side fully instrumented with vibrating wire strain gauges with thermistors and optical fibre sensors. In the centre of the pile a double U-shaped configuration of HDPE pipes were installed. It was a thermomechanical test in which the pile was first subjected to a mechanical load of 1000 kN, and after to a thermomechanical test where mechanical load was maintained and heating and cooling thermal loads were applied to the foundation. The subsoil consisted of an alternation of sandy gravel, stiff and soft clay.

In the city of Xinyang in Henan Province, China, Luo et al. (2019) carried out a field test on two different drilled energy piles equipped with double U-loop pipe configuration and spiral configuration, respectively and embedded in stiff sandstone. The U-loop pipe configuration EP was 0,6 m in diameter and 18,5 m in length while the other one was 0,8 m in diameter and 13,0 m in length. The authors observed the axial and radial movements of the piles and the radial-strain development and its contribution to pile settlement subjecting the pile to a heating-recovery-cooling-recovery cycle. It was observed that during the heating cycles, shaft friction was mobilized, and consequently measured strains was less than free conditions strains. In cooling phase, on the other hand, if the pile was not subjected to mechanical loads, the axial strains measured were close to free expansion condition while, with the application of the external mechanical load, the strains decreased. The radial stress and the behaviour of EPs under cyclic thermal loads were analysed by Faizal et al. (2018, 2019a, 2019b). By the tests it was observed that a minimal resistance was provide by the surrounding soil. For this reason, radial stress was not considered a problem for pile/soil interaction for the typical setting of cast-in-place concrete energy piles. The same conclusion was also found when the mechanical load on the pile reached values approximately equal to 52% of the ultimate capacity of the pile or considering daily cyclic thermomechanical loads. In fact, in these cases, the radial thermal stresses had negligible values if compared to the axial one and the skin friction of the pile was not affected by the radial thermal expansion/contraction of the pile. Moreover, it was observed that thermal axial strain resulted uniform along the pile but, when the mechanical load was applied an increase of stresses near the pile head was observed. Consequently, the stress distribution was not uniform as the purely thermal case.

The field tests carried out by Sutman et al. (2015, 2019) in USA (Texas), highlighted that during heating and cooling tests, the location of the dominant restriction affected the induced axial stresses and the mobilization of shaft resistance distribution. Moreover, the effects of the end-restrain disappeared moving away from the dominant restriction.

Finally, a full-scale test on driven energy pile was carried out by Jiang et al. (2021). The pile, 0,4 m in diameter and 15 m in length embedded in medium dense silt was subjected to heating-recovery

and cooling-recovery cycles under different mechanical loading levels. From the test the authors found that for thermal cycles the pile settlements were affected by the level of the mechanical loading and that the thermal cycle history affected the pile settlement rate provided by mechanical loads. A comparison in difference between driven and bored pile was also done.

Table 2-1 - Field tests on single energy piles

Author	L [m]	D [m]	Constructive technique	Single/piled raft	End restrains (Floating/End-Bearing)	Soil	Mech. load applic.	Applied mechanical load [kN]	Thermal load
(Brandl 2006)	9,0	1,2	Bored	Piled raft	Floating	Clayey-sandy silt	Building	500 - 900	$\Delta T_{min} = -14\text{ }^{\circ}\text{C}$ $\Delta T_{max} = 7\text{ }^{\circ}\text{C}$
(Laloui, Nuth, and Vulliet 2006)	25,8	0,88	Bored	Piled raft	End-Bearing	Soft clay/sandstone	Building	0 (T1) 1183 (T2-T6) 1088 (T7)	$\Delta T = 21\text{ }^{\circ}\text{C}$ (T1) $\Delta T = 15\text{ }^{\circ}\text{C}$ (T2-T7)
(P. J. Bourne-Webb et al. 2009)	23	0,60	Bored	Single	Floating	London clay	Standard load test	1200	$\Delta T_{min} = -19\text{ }^{\circ}\text{C}$ $\Delta T_{max} = 29,4\text{ }^{\circ}\text{C}$
(McCartney and Murphy 2012)	14,8 (A) 13,4 (B)	0,91	Bored	Piled raft	End-Bearing	Clayrock	Building	3840 (A) 3640 (B)	$\Delta T_{min} = -5\text{ }^{\circ}\text{C}$ $\Delta T_{max} = 14\text{ }^{\circ}\text{C}$
(K. D. Murphy and McCartney 2015)									
(Kyle D. Murphy, McCartney, and Henry 2015)	15,2	0,61	Bored	Piled raft	End-Bearing	Sandstone	Building	883	$\Delta T_{max} = 18\text{ }^{\circ}\text{C}$
(Bill Wang et al. 2015)	16,1	0,60	Bored	Single	End-Bearing	Very dense sand	Bottom-up	1700 1750	$T_{in} = 38\text{ }^{\circ}\text{C}$ $T_{in} = 46\text{ }^{\circ}\text{C}$
(Luo et al. 2019)	13 (2U) 18,5 (S)	0,80 0,60	Bored	Single	End-Bearing	Stiff sandstone	Standard load test	0 1600	(2U) $\Delta T_{min} = -6,8\text{ }^{\circ}\text{C}$ $\Delta T_{max} = 12,9\text{ }^{\circ}\text{C}$ (S) $\Delta T_{min} = -12,4\text{ }^{\circ}\text{C}$ $\Delta T_{max} = 24,4\text{ }^{\circ}\text{C}$
(Sutman, Olgun, and Brettmann 2015) (Sutman, Brettmann, and Olgun 2019)	(P1) 15,24 (P2) 9,14 (P3) 15,24	0,457	Bored	Single	(P1) E-Bearing (P2) Floating (P3) E-Bearing	(P1) Very dense sand (P2) stiff clay (P3) Very dense sand	Standard load test	0	$T_{max} = 45\text{ }^{\circ}\text{C}$ $T_{min} = 8\text{ }^{\circ}\text{C}$
(Singh et al. 2015)	16,1	0,60	Bored	Single	Floating	Sandy soil	Standard load test	1650 1850	$T_{max} = 41\text{ }^{\circ}\text{C}$
(Santiago et al. 2016)	17,4	0,35 (square section)	Driven	Single	End-Bearing	Sandy gravel	Standard load test	1000	$\Delta T_{max} = 17\text{ }^{\circ}\text{C}$
(Akrouh, Sánchez, and Briaud 2014)	5,50	0,18	Bored	Piled raft	Floating	Stiff clay	Tensile Load	40 – 100 – 150 – 200 – 256	$\Delta T = 10\text{--}15\text{ }^{\circ}\text{C}$

(Faizal et al. 2018)	16,1	0,60	Bored	Single	Floating	Dense sand	No load	-	Monotonic heating T=45°C Monotonic cooling T=5°C Heating cycle T=30-55°C Cooling cycle T=7-16°C
(Faizal et al. 2019a)	16,1	0,60	Bored	Piled raft	End-Bearing	Unsaturated sand	Building	1404	$\Delta T=24,1^{\circ}\text{C}$
(Faizal et al. 2019b)	16,1	0,60	Bored	Piled raft	End-Bearing	Unsaturated sand	Building	1404	Cycles $\Delta T=-8^{\circ}\text{C}; 5^{\circ}\text{C}$
(Jiang et al. 2021)	15	0,40	Driven	Single	Floating	Medium dense silt	Standard load test	0, 315, 630, 945, 1260	$\Delta T=30^{\circ}\text{C}; \Delta T=-9^{\circ}\text{C};$

2.2.2 Small-scale tests

Although field tests are more representative of the real behaviour of an energy pile, for several reasons such as the expensive costs or the impossibility of checking the boundary conditions, the small-scale tests represent a possible alternative to field test. Small-scale test can be carried out by centrifuge or by 1-g physical model.

The centrifuge method has the advantage respect the 1-g physical model to be able to reproduce satisfactorily more realistic stress field in the subsoil surrounding the pile. On the other hand, centrifuge test needs specific equipment to be carried out and are of course more expensive than 1-g physical model.

Centrifuge tests were carried out both on small-scale concrete piles (McCartney and Rosenberg 2011), (Stewart and McCartney 2012, 2014), (Goode and McCartney 2015), and small-scale aluminium piles (Ng et al. 2014).

During the tests the thermo-mechanical effects on the side shear capacity was investigated, and the measurement of the load-settlement curves were evaluated using load transfer analysis (McCartney and Rosenberg 2011). Also the axial strains, the head displacements and stress distributions considering fixed-end boundary condition were analysed (Stewart and McCartney 2012, 2014) observing a gain of compressive stress near the pile toe during the heating phases.

The effects of different soils (dry sand or unsaturated silt layers) and different boundary condition of the pile end-restraining (floating and end bearing pile) were investigated by Goode and McCartney (2015). The aim of the test was to quantify the end restraint boundary conditions impact on the distribution of the thermal axial displacement and stress of the foundation.

The effects on pile behaviour considering different soils (overconsolidated kaolin clay and heavily overconsolidated kaolin clay) were investigated also by Ng et al. (2014) on two small-scale tests in centrifuge on floating energy piles using an aluminium pile. The aim was to investigate about the pile behaviour under the influence of the induced temperature variations.

1-g model small-scale tests were carried out both on aluminium/steel and concrete piles embedded both in dry sand and clay.

In tests carried out on aluminium piles in dry sand (Kalantidou et al. 2012), (Neda Yavari et al. 2014) (Nguyen, Tang, and Pereira 2017), the thermomechanical behaviour of the pile subjected to thermal cycles under different constant mechanical axial loads was investigated. From the experiments, all the authors found a thermo-elastic behaviour of the pile subjected to thermal cycles when the mechanical loads did not reach some values in percentage than the pile bearing capacity. On the contrary, irreversible pile settlements were observed when the mechanical loads limit was surpassed. Moreover, it seemed also that under a constant mechanical load, pile settlements increased with the increase of the number of cycles (Nguyen, Tang, and Pereira 2017).

The change in pile behaviours compared to the mechanical loads applied on the pile head was also investigated by Yavari et al. (2016) for an aluminium pile embedded in clay. Wu et al. (2019) adopting a steel small-scale model embedded in normally consolidated clay and subjected to thermomechanical cyclical loads also investigated the effects of different climatic conditions considering both end-bearing and floating piles. In addition, were assigned boundary conditions that simulated warm/cold balanced climate, warm-dominated climate regions, and cold-dominated climate, respectively.

Adopting concrete small-scale model of energy piles, in some case it was possible also to investigate the effects of different pipes configurations on the energy pile thermomechanical behaviour.

Two small-scale tests were carried out by Wang et al. (2016, 2017) to study the behaviour of concrete energy pile with or without mechanical load and considering different heat exchanger configuration in dry sand. In the first test (Cheng long Wang et al. 2016) the authors carried out a small-scale test to evaluate the difference in behaviour of the energy pile during the heating and the cooling with and without the presence of a vertical mechanical load on pile head. It was found residual thermal stress after a heating and cooling cycle. Moreover, the vertical load also affected the pile displacements. As a matter of fact, the pile head heaved under heating loads 143% compared to the case with vertical load. The same occurred during cooling test. In the second study the thermomechanical behaviour of semi-floating concrete energy piles subjected to heating–cooling cycles was investigated by authors (Cheng-long Wang et al. 2017). The test was carried out comparing piles equipped with different pipe configuration embedded in dry sand. It was observed the pile equipped with the W-shaped pipe configuration had the larger settlements values compared to other piles. Finally, Elzeiny et al. (2020) investigated on the thermo-mechanical performances of a small-scale concrete energy pile embedded in dry sand and subjected to different number of heating cycles followed by axial pull-out load. From the test the authors found that after 5 and 100 heating cycles, the peak pull-out load increase of 30% and 27% then the baseline value. It was attributed to effects of ratcheting.

In Table 2-2 small-scale test on energy piles are summarized.

Table 2-2 - Small-scale tests on energy piles

Author	L [m]	D [m]	Pile Material	Soil	Type of test	Mechanical load	Thermal load
(McCartney and Rosenberg 2011)	0,381	0,0762	Concrete	Bonny silt	Centrifuge	0,2 mm/min	Monotonic $\Delta T=35^{\circ}C$ Monotonic $\Delta T=45^{\circ}C$
(Stewart and McCartney 2012)	0,5334	0,0508	Concrete	Unsat. silt	Centrifuge	303 kN	Monotonic ΔT max= $22^{\circ}C$
(Stewart and McCartney 2014)	0,5334	0,0508	Concrete	Unsat. silt	Centrifuge	443 kN	Monotonic ΔT max= $30^{\circ}C$
(Ng et al. 2014)	0,420	0,022	Aluminium	Lightly OC clay	Centrifuge	96 kN	5 cycles $\Delta T = 11^{\circ}C - \Delta T = -9^{\circ}C$
				Heavily OC clay		192 kN	
(Goode and McCartney 2015)	0,3429	0,0635	Concrete	Dry sand	Centrifuge	360 kN	Monotonic $\Delta T = 0^{\circ}C$
							Monotonic $\Delta T = 7^{\circ}C$
							Monotonic $\Delta T = 12^{\circ}C$
							Monotonic $\Delta T = 18^{\circ}C$
	0,5334			Monotonic $\Delta T = 11,1^{\circ}C$			
				Monotonic $\Delta T = 11,8^{\circ}C$			
	0,3429			Monotonic $\Delta T = 0^{\circ}C$			
				Monotonic $\Delta T = 10^{\circ}C$			
0,5334	Monotonic $\Delta T = 18^{\circ}C$						
Story $\Delta T = 0^{\circ}C - 9,5^{\circ}C - 14,7^{\circ}C - 15,9^{\circ}C - 6,1^{\circ}C$							
(Kalantidou et al. 2012)	0,6	0,002	Aluminium	Fontainebleau dry sand	1g model	0 kN	2 cycles $\Delta T = 25^{\circ}C - \Delta T = -25^{\circ}C$
						0,2 kN	
						0,4 kN	
						0,5 kN	
(Neda Yavari et al. 2014)	0,6	0,002	Aluminium	Fontainebleau dry sand	1g model	0 kN	2 cycles $\Delta T = 15^{\circ}C - \Delta T = -15^{\circ}C$
						0,1 kN	
						0,15 kN	
						0,2 kN	
						0,25 kN	
0,3 kN							
(N. Yavari et al. 2016)	0,6	0,002	Aluminium	Saturated clay	1g model	0,1 kN	2 cycles $\Delta T = 5^{\circ}C - \Delta T = -5^{\circ}C$
						0,15 kN	
						0,2 kN	
						0,25 kN	
(Nguyen, Tang, and Pereira 2017)	0,6	0,002	Aluminium	Dry sand	1g model	0 kN	30 cycles $\Delta T = 1^{\circ}C - \Delta T = -1^{\circ}C$
						0,1 kN	
						0,2 kN	
						0,3 kN	
(Cheng long Wang et al. 2016)	1,4	0,104	Concrete	Dry Nanjing sand	1g model	0 kN	$\Delta T = 30^{\circ}C - \Delta T = -10^{\circ}C$
						10 kN	
(Cheng-long Wang et al. 2017)	1,4	0,104	Concrete	Dry Nanjing sand	1g model	10 kN	3 cycles $T_{in}=55^{\circ}C - T_{inti}=11^{\circ}C$
(Liu et al. 2018)	1,4	0,104	Concrete	Dry Nanjing sand	1g model	0 kN	$\Delta T = 9^{\circ}C - \Delta T = -1,5^{\circ}C$
						10 kN	
(Wu et al. 2019)	0,45	0,023	Steel	Normally consolidated clay	1g model	0,147 kN	5 cycles $\Delta T = 20^{\circ}C - \Delta T = -20^{\circ}C$
							$\Delta T = 20^{\circ}C$
							$\Delta T = -20^{\circ}C$
							No thermal load
(Elzeiny et al. 2020)	1,098	0,102	Concrete	Dry sand	1g model	Various tensile forces	100 cycles $\Delta T = 20^{\circ}C$

2.2.3 Axial response: vertical strain and vertical stress

The distributions of vertical strain and stress along the pile, depend on the boundary conditions of the pile end restraint and on the surrounding soil stiffness (Laloui, Nuth, and Vulliet 2006). Generally, the pile heating induces expansive strain and, vice versa, the cooling induces a contraction of the pile.

In the semi-floating pile studied in the field test carried out in Lausanne (Laloui, Nuth, and Vulliet 2006) it was observed that at the pile toe thermal axial stress was much larger than the mechanical one. Moreover, while the mechanical axial stress tended to decrease with depth (almost zero at the toe) the thermal stress was uniform with depth. It was found that for the only thermal load test (free displacements for pile head), strain during the heating period were non-uniform and influenced by the friction along the pile shaft. During the cooling phase, a thermo-elastic linear behaviour was observed, and the magnitude of the strains depended on the type of surrounding soil. It was observed that the axial force induced by the thermal loads were larger and quite uniform compared to the force induced by the mechanical one, which was maximum at the pile head and almost zero at the toe. A temperature increment of 1 °C resulted in an additional temperature-induced vertical force on the order of 100 kN and consequently, the total axial load in the pile was twice as large as the one due to purely mechanical loading, with a large stress at the pile tip. Even if it was not possible to determinate the influence of thermal cycles on the ultimate resistance of the pile, also in the test carried out by Bourne-Webb et al. (2009), it was observed by the strain profiles a thermal-elastic response of the pile under the applied loads. Moreover, the mobilised shaft capacity was smaller than the ultimate resistance.

Some conclusions can be found in Faizal et al. (2019a, 2019b) where for thermal loads, the energy pile showed an elastic behaviour and strains at the end of the thermal cycles returned to the initial values. Moreover, the authors observed a substantial difference between thermal and thermomechanical loads in terms of stress distribution along the pile. The former, in fact, provided a rather uniform distribution of strain along the pile. When the mechanical load was added to thermal one, near the pile head were recorded the higher axial stresses for the pile.

The distribution of stress/strain is affected by the position of the dominant restriction. It was well showed both in the field test carried out by Sutman et al. (2019) and in the field test carried out by Murphy et al. (2015) where it was observed that for the three foundation, even if the heating provided a uniform distribution of the temperature along the piles, the maximum compressive thermal axial stress occurred at a depth between the 72-78% of the pile length.

Anyway, differently from field scale, the main portion of 1 g small-scale physical model in dry sand (Neda Yavari et al. 2014; N. Yavari et al. 2016; Cheng long Wang et al. 2016; Kalantidou et al. 2012;

Nguyen, Tang, and Pereira 2017) found that mechanical load induced irreversible axial strains and stresses during the application of the thermal load (cyclic or monotonic).

On the other hand, for the centrifuge models was found that strains along the pile were function of the mobilised side friction and, that the heating thermal loads induced in the pile compressive strains larger than the strains induced by mechanical load. End-bearing piles in compacted silt showed larger values of thermal axial stresses than semi-floating piles in sand. It was attributed to the restraint of the toe and the stiffness of the compacted silt (McCartney and Rosenberg 2011; Stewart and McCartney 2012; Goode and McCartney 2015).

A possible explain to this contrast between 1g model and field scale could be found in the difference in the initial stress boundary condition due to installation technique of the pile or more on the way in which the soil was prepared for the small-scale model. In addition, Faizal et al. (2019b) outlined the difference in the safety factor of the full-scale piles designed for building dead load compared to the small-scale piles. The authors supposed also that the difference in pile behaviour could be attributed to the soil stiffness. They concluded that the dense sand found in the site test contributed to the reversible energy pile thermal responses through a higher resistance to thermal strain.

In Figure 2-1 the axial stress versus the temperature change in heating phase were plotted for some field tests. To consider the difference of stiffness of surrounding soil with depth, the data also reported the normalized depth, i.e. the ratio between the depth and the pile length at which the data was collected. The data included both thermomechanical tests and only thermal one. An increasing trend of axial stresses could be observed with increasing temperature. In any case, the value of the stress also depended on the degree of restraint possessed by the pile at the depth considered and by the test i.e. if only thermal loads were applied on pile or thermal and mechanical at the same time.

It was clear that thermomechanical tests had an axial stress increment almost three times than the only thermal load tests (333 kPa/°C and 244 kPa/°C for thermomechanical tests versus 121 kPa/°C and 106 kPa/°C for the only thermal load tests).

Moreover, the difference between the results depended also on the degree of restraint of the pile.

To consider this variable, in Figure 2-2 the axial tension was normalised with respect to the maximum theoretical stress value attainable by each pile under perfect restraint conditions and calculated as:

$$\sigma_{theo, fixed} = \alpha_{pile} E_{pile} \Delta T$$

Equation 2-1

Where α_{pile} is the coefficient of thermal expansion of the pile, E_{pile} is the Young modulus of the pile and ΔT is the difference of temperature considered.

As shown in Figure 2-2 the value of the normalized axial stress is variable with the temperature increase. It could be observed, in fact, that some piles tended to have a constant value of the degree

of restrain, while in other cases the values tended to increase with the temperature with different trends.

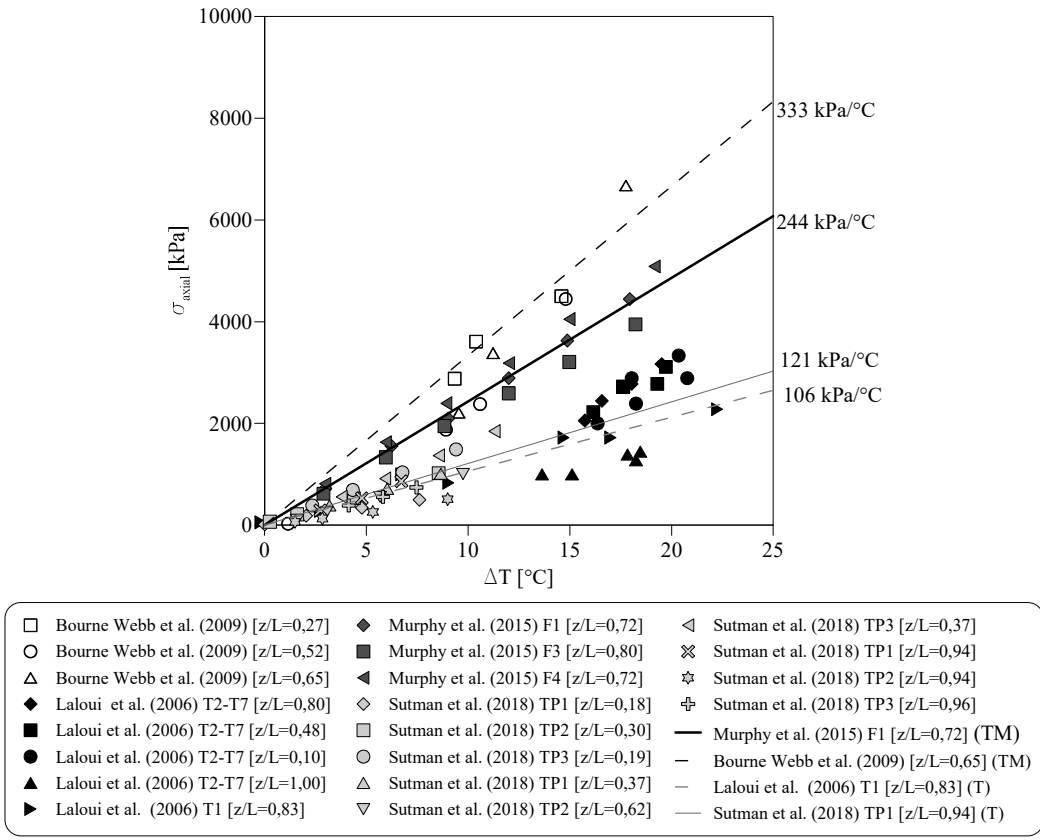


Figure 2-1 Axial stress vs the temperature increment for some field tests

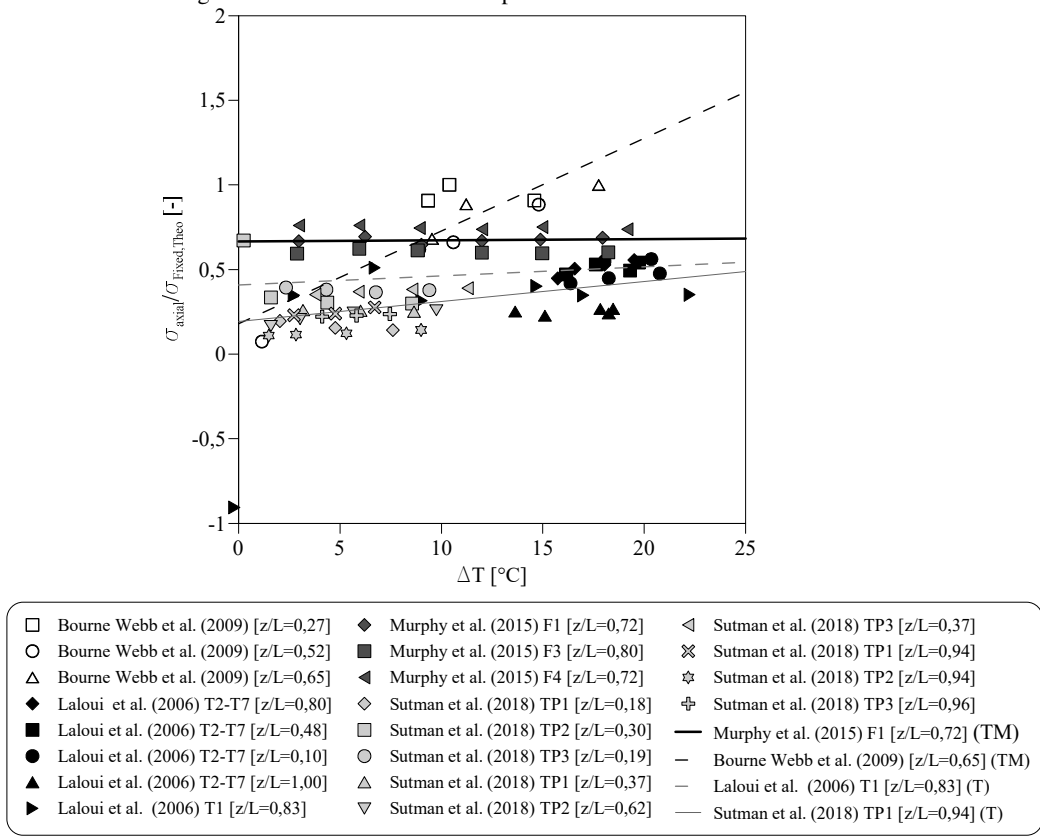


Figure 2-2 – Normalized axial stress vs the temperature increment for some field tests

2.2.4 The shaft response

Thermal strain induced by thermal loads alters the initial stress at the interface between pile and soil even changing the mobilized shaft resistance direction (P. J. Bourne-Webb et al. 2009). When the pile is heated, in fact, it tends to expand around the null point and the opposite effect is induced by the cooling. To ensure the equilibrium, shear stress at the pile shaft is mobilized in opposite direction of piles thermal displacements. The value and magnitude of the shear stress depend on the applied thermal loads and on the pile restrain boundary conditions.

In field test carried out in Lausanne (Laloui, Nuth, and Vulliet 2006) and London (P. J. Bourne-Webb et al. 2009), semi-floating and a floating pile were tested, respectively. Laloui et al. (2006) concluded that temperature did not affected the friction resistance and that during heating a relief of side friction mobilization was observed. On the other hand, Borne-Webb et al. (2009) observed that the shaft resistance increased and decreased when the temperature changed. In particular, the shaft resistance mobilization resulted greater in heating than in cooling mode. Amatya et al. (2012) attributed this phenomenon to the radial expansion of the pile diameter during the heating phase that contributed to increase the horizontal normal stresses at the pile/soil interface and so the shaft resistance of the pile. The opposite effect was induced by the pile cooling where the contraction of the pile section reduced the normal axial stress decreasing so the shaft resistance.

Anyway, a reduction of the shear resistance in cooling phases was not observed in the case of overconsolidated soil in which, the soil tended to return to its initial state (Mimouni and Laloui 2015). The same results of Bourne-Webb (P. J. Bourne-Webb et al. 2009) was achieved also in small-scale centrifuge test for a pile model in unsaturated silt (Stewart and McCartney 2014), or for pile model in dry sand (Cheng long Wang et al. 2016).

Wang et al. (2015) observed that for a full-scale pile embedded in very dense sand there was an increase of the pile shaft resistance during the heating and that the shaft capacity returned to initial conditions when the pile was cooled. This elastic behaviour was also confirmed by the test carried out by Faizal et al. (2019b) for a similar pile, embedded in a similar soil and loaded by a residential building.

An increase of the pile load capacity after a heating phase was found during the field test carried out by Shing et al. (2015). The authors attributed it to an increase of the pile side shear load capacity due to pile expansion and to a possible frictional resistance increase because of the drying.

2.2.5 The radial thermal response

As said in previous sections, the radial expansion/contraction of the pile under thermal loads could be a reason for the ultimate capacity increase/decrease because of the change in the pile/soil interface stresses.

This phenomenon was considered both for field test in cohesive soils (Laloui, Nuth, and Vulliet 2006; Mimouni and Laloui 2015) and cohesionless soil (Bill Wang et al. 2015; Faizal et al. 2018, 2019a, 2019b; Luo et al. 2019) and for small-scale centrifuge tests in compacted silt (McCartney and Rosenberg 2011; Goode and McCartney 2015).

Contrasting results were found. Wang et al. (2015) observed a thermoelastic behaviour of the pile embedded in very dense sand. At the end of the heating and cooling periods the average circumferential strains of the pile were relatively uniform and no change with depth of them was observed. In addition, there was a full recovery during the cooling period of the initial strain.

The same pile behaviour was observed by Faizal et al. (2018, 2019a, 2019b). In any case, it was found that axial strain was more restricted than the radial one with measured radial strains 40% higher than axial strains at the same depth.

In the field test carried out by Laloui et al. (2006) also the thermal radial strains resulted larger than the axial one. In fact, it was found that at a depth of 16 m with a pile temperature of 21 °C the axial thermal strain was about 160 $\mu\epsilon$ while the radial one was 450 $\mu\epsilon$. For a pile temperature change of 3 °C, instead, at the same depth, it was observed radial thermal strains of 100 $\mu\epsilon$ and axial thermal strain of 30 $\mu\epsilon$.

McCartney and Rosenberg (2011) and Goode and McCartney (2015) observed that in energy piles the radial thermal expansion could affect the pile ultimate capacity for monotonic heating thermal loads. In the small-scale physic model 1-g carried out by Wang et al. (2017) was observed that after each of the three thermal cycles imposed in the test, there was no recovery of the horizontal effective stresses because of a non-recovery of initial temperature conditions. Anyway, the pile equipped with the W-shaped configuration showed the greater horizontal stresses values. At the end of the cycles the peak of horizontal stress was observed but at the end of the tests the horizontal stress resulted nearly recovered.

2.2.6 Temperature induced displacements

The serviceability and safety of structures on piles is affected by settlements/displacements of the foundation. The magnitude of EPs displacements depends both on the Null Point (NP) location (and consequently on the type and the stiffness of external restraints) and obviously on the thermal or thermomechanical loads conditions. Moreover, thermal displacements are directly proportional to the linear/volumetric thermal expansion coefficient and to the pile geometry. Material and length of pile, for instance, play a fundamental role for the final displacement value.

As already discussed in previous sections, heating loads always induce to a heave of the EP head. The opposite happens for the cooling mode. When a compressive load, provided directly by the superstructure or by a hydraulic jack during a test, is added to thermal loads, the pile behaviour could

change. In this case, the mechanical load provides additional settlements of pile head. So, when a pile is heated, the effects of the expansion tend to reduce the head settlements, on the other hand, when it is cooled the verse of the mechanical and thermal displacements are in accordance and settlements are amplified.

In the field test carried out by Santiago et al. (2016) it was observed that for a square section concrete pile embedded in sandy gravel, after a heating phase of about five days the pile achieved a maximum displacement of 1,4 mm. Anyway, after stopping the heating the pile head had a residual upward displacement of 0,4 mm. In cooling phase Jiang et al. (2021) observed an elastic-plastic pile behaviour of a full-scale driven pile. The authors observed also that the mechanical loads magnitude and the cycles history of thermal loads affected both the pile heave in heating and the pile head settlement in cooling phase. Moreover, it was also noticed that the pile construction technique affected the head displacements result with less normalized thermal-induced settlement developed for the driven energy pile compared to bored one. It was attributed to the different effects of the pile construction techniques on surrounding subsoil.

In small-scale tests, also, the magnitude of the mechanical load and the thermal history seemed to play a principal role.

For physical 1-g model of pile embedded in dry sand, also, similar results were found (Kalantidou et al. 2012; Neda Yavari et al. 2014; Cheng-long Wang et al. 2017; Nguyen, Tang, and Pereira 2017).

In small-scale test carried out by Kalantidou et al. (2012) the behaviour of the energy pile subjected to thermal cycles and four different constant axial loads was investigated. It was found a thermo-elastic behaviour for a pile subjected to thermal cycles and axial loads below the 40% of the ultimate capacity. Anyway, during the heating phases the pile heave was lower than the free thermal expansion of the pile. According to authors it was due to the settlements of the pile toe.

The same approach was followed in the test carried out by Yavari et al. (2014). The pile was subjected to seven different axial loads and thermal cycles. It was observed that only for axial load below 30% of the pile estimated bearing capacity the energy pile had a thermo-elastic behaviour both for heating phases and cooling one. Anyway, over this axial load limit, the pile changed the behaviour and significant cumulative settlement was observed and axial force at pile toe gradually increased over the cycles.

From the small-scale test on aluminium piles carried out by Nguyen et al. (2017), instead, longer thermal cycles were considered to observe the long-term behaviour of the pile. It was subjected to 30 cycles and different axial loads. In this test, also, was observed that the magnitude of the applied axial load changed the final head pile displacements. Irreversible pile head settlements were provided in

any case during the first heating/cooling cycle and the greater the mechanical load applied to the pile head the larger the irreversible part of the settlements.

Anyway, also for small-scale concrete pile similar results were observed (Cheng-long Wang et al. 2017). From this test, indeed, was observed that the piles axially loaded up to the 50% of the failure load and subjected to three circles of heating-cooling, presented irreversible increasing settlement for each cycle.

In the test carried out by Yavari et al. (2016) the pile embedded in saturated clay was subjected to incremental loads. It was found irreversible settlements for lower percentages of load relative to the ultimate pile load than those seen for dry sand tests. In fact, irreversible settlements were already recorded when an axial load of more than 20% of the ultimate load was imposed. After one cycle, the magnitude of the irreversible settlement was less than the 0,5% of the pile diameter.

In the test carried out by Wu et al. (2019) a pile was subjected to different inlet temperatures to simulate warm-dominated, cold-dominated or balanced climate considering both floating piles and end-bearing pile. It was found after five cycles larger irreversible displacements of floating piles compared to the end-bearing one under warm/cold balanced climate while the smallest irreversible displacement was recorded under cold-dominated climate.

As regarding the small-scale test in centrifuge similar tests were carried out both in clay and silt (Ng et al. 2014; Stewart and McCartney 2014).

Ng et al. (2014) studied the displacements of a pile embedded both in lightly and heavily overconsolidated (OC) clay. The piles were subjected to five heating/cooling cycles under constant working load. In any case cumulative irreversible displacement was found. In the case of lightly OC clay, it corresponded to 3,8% of the pile diameter while for the heavily case it corresponded to 2,1% of pile diameter.

On the other hand, in the test carried out by Stewart and McCartney (2014) on an end-bearing pile in unsaturated silt no irreversible settlements were found during heating and cooling cycles. A possible explain was provided by the authors which referred the occurrence to the end-bearing status of the pile.

The effect of the thermal cycles on full scale and small-scale pile was summarized in next graphs.

Regarding the full-scale tests, in Figure 2-3 the piles head displacements versus the temperature during the heating phase of the tests were plotted. It was possible to notice a linearity between the head pile heave and the increase of the applied thermal loads. Anyway, the magnitude of the displacements for the considered tests depended on some external factors such as the presentence of the mechanical load with the thermal one and on the degree of restrain of the pile. By the graphs, in fact, it was possible to notice that the larger values of displacements were obtained for the T1 test

carried out by Laloui et al. (2006) where only thermal loads were applied on the pile. On the other hand, when a thermomechanical load was applied the values of the displacements was lower. In Figure 2-4 the displacements were normalized respect the maximum theoretical displacements for each pile. The graph confirmed that the test where only thermal loads were applied was the nearest to condition of free pile both in heating and cooling phase. Anyway, for all the piles, a certain difference in behaviour was observed between the heating phase of the test (full symbols) and the cooling phase (empty symbols) for the same temperature.

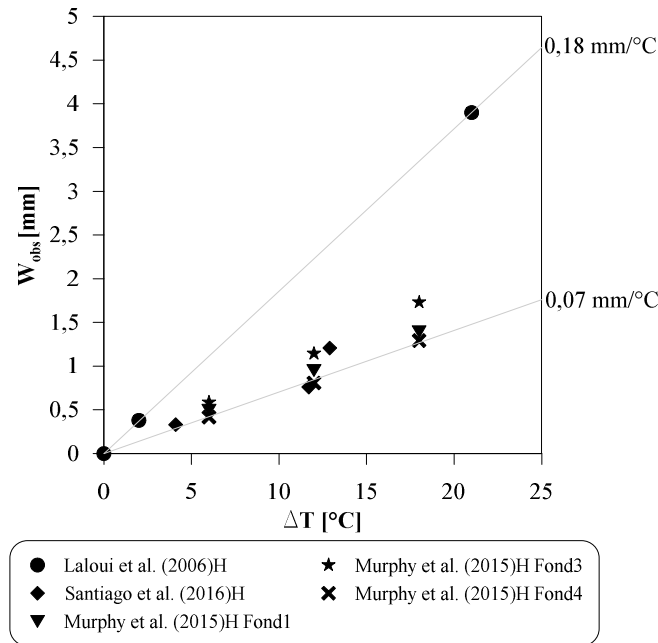


Figure 2-3 – Pile head displacements against the temperature variation for field tests (H=heating)

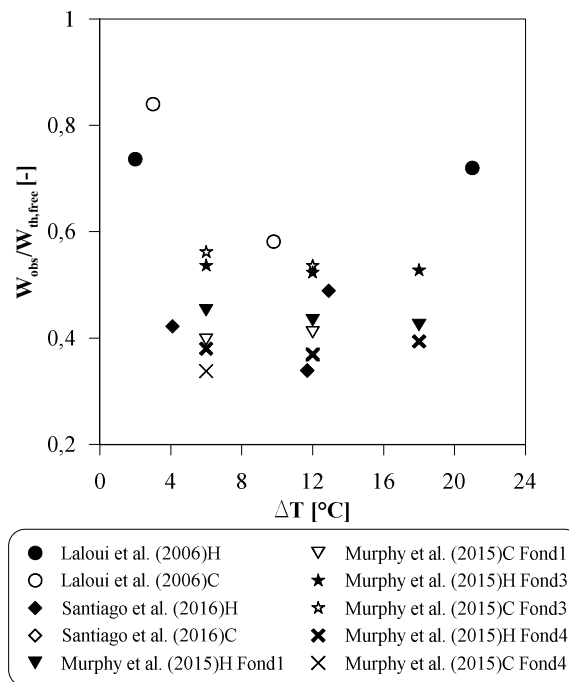


Figure 2-4 Normalized pile head displacements against the temperature variation for field tests both for heating and cooling phase (H=heating, C=cooling)

1g small-scale tests of pile embedded in sand and piles embedded in clay are summarized.

In Figure 2-5 the normalized displacement versus the temperature differences are represented for the heating (full symbols) and cooling phase (empty symbols), respectively for the tests in sand. For each test the mechanical load applied on the pile was reported in terms of percentage respect the ultimate capacity bearing, in the breakers in the legend of the graph. It was observed that as the mechanical load applied to the pile head increases, the normalised values of the displacements during heating are always smaller than the unit value (theoretical case). The test carried out by Yavari et al. (2014) shows negative values because it was the only test in which the cooling thermal load was applied before heating. On the other hand, it was observed that in the cooling phase, the normalized displacements values were higher than the unit and in some cases, were the applied mechanical load were very close to the ultimate capacity (95%) the value of the normalized displacements had approximately an order of magnitude greater than other cases.

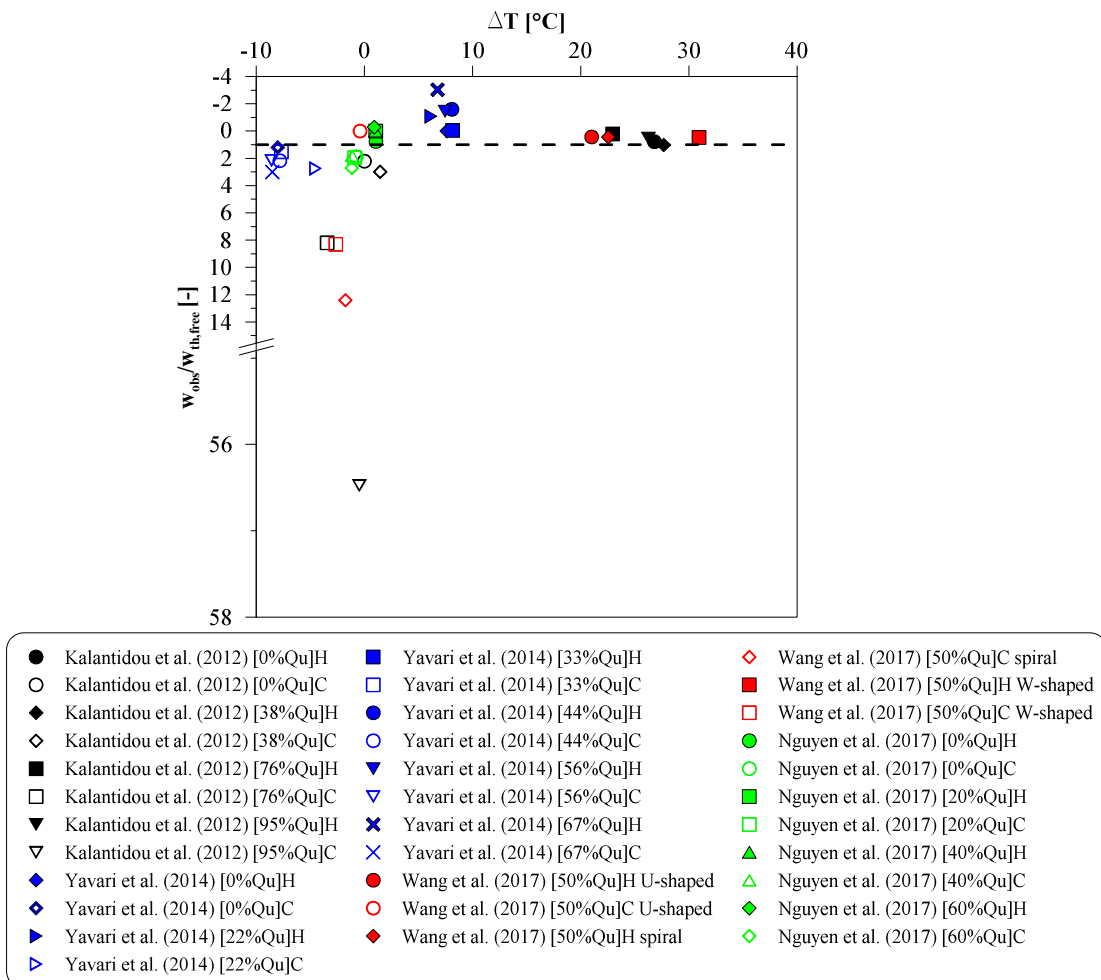


Figure 2-5 - Small-scale tests in sand. Normalized displacements against the temperature (H=heating, C=cooling, Qu=Ultimate load)

Considering the number of the cycles, in Figure 2-6 it was possible to notice the impact of the mechanical loads on the displacement trend. In fact, it was observed that for many cycles, as the load applied to the pile head increased, so did the displacements.

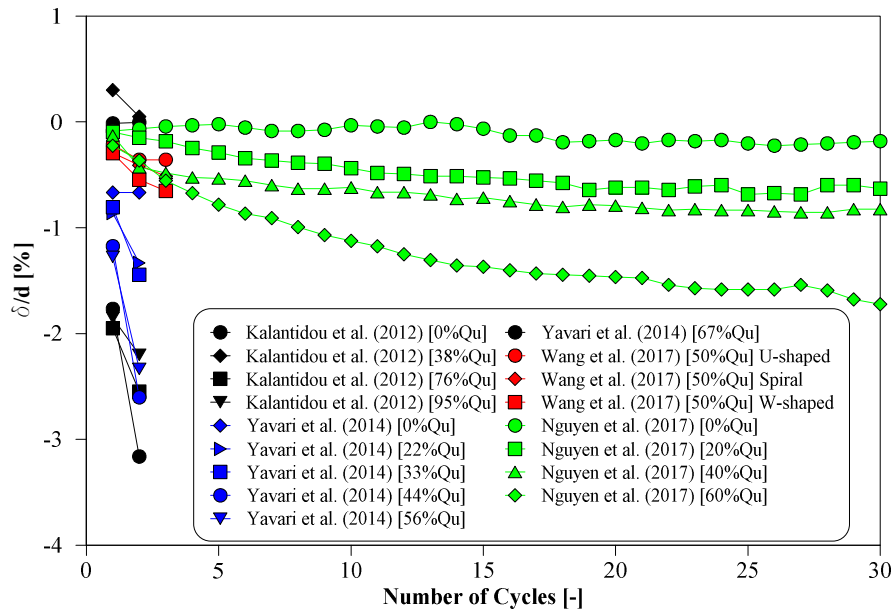


Figure 2-6 - Small-scale tests in sand. Displacements percentage against the number of cycles (Qu=Ultimate load)

The effects of the number of the cycles were considered also for the small-scale piles embedded in clay. In this case, the applied mechanical loads were the same in percentage, but the degree of constrain of the pile changed (Figure 2-7). To compare the different tests, the displacements were normalized respect the pile diameters. It was possible to observe the impact of the soil stiffness already at the end of the first cycle. Moreover, it was observed that the end bearing piles tended to have less displacements than the floating one at the end of the cycles.

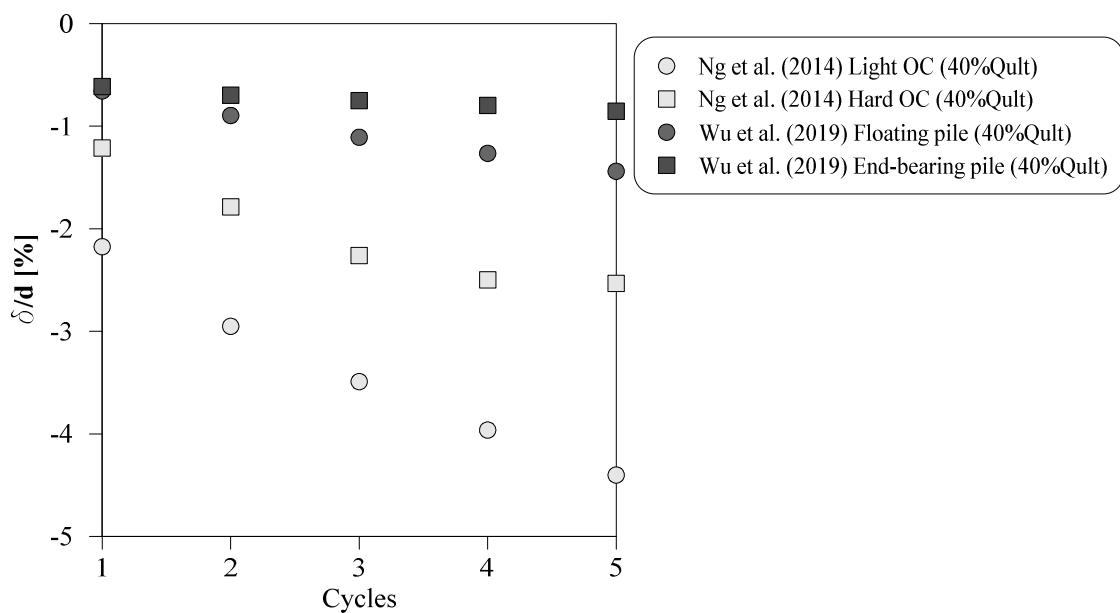


Figure 2-7 – Small-scale tests in clay. Displacements percentage against the number of cycles (OC=overconsolidated)

2.3 Energy piles thermal performances

Due to its dual intrinsic structural and energetic nature, the energy pile needs special care in the design stage. Differences in heat transfer performance and in temperature cycles bring to different thermo-mechanical behaviours due to an alteration of the soil and soil/pile interaction that could affect the thermo-mechanical structural and geotechnical behaviour of axially loaded EP (Brandl 2006; Elzeiny et al. 2020; Cheng-long Wang et al. 2017).

Heat performances in EPs depend on different factors that could be investigated starting from the experience on vertical boreholes heat exchangers (VBHEs).

The temperature level in heat exchangers depends on two groups of parameters (Eskilson 1987; Hellström 1991). The first group is related to soil thermal conditions and properties such as the undisturbed soil temperature, the amount of heat rejected or absorbed from the ground over time or the thermal conductivity and the thermal diffusivity of the soil. The second group, instead, is related to the design and construction of the borehole i.e. the diameter of the borehole, the diameter and thickness of pipes, the number and the arrangement of pipes in the borehole, pipe and grout thermal conductivities and the convection heat transfer characteristics at the inner surfaces of the pipes.

As regarding EPs, instead, according to Bozis et al. (2011) thermal performances of energy pile depends on the number of pipes, configuration, dimensions of pipes and the flow specifications inside the pipe.

According to Suryatriyastuti et al. (2012) the heat transfer rate depends on energy performances (COP) of heat pumps and the soil thermal and hydrology properties such as saturation degree, thermal conductivity, and specific heat extraction.

According to Park S. et al. (2016) because conduction is the main mechanism of heat transfer from energy piles and soil, the energy performance is linked to the thermal conductivity of medium, temperature difference between ground and fluid, the contact area of heat exchange pipe, and the length and diameter of borehole. Also flow rate of the carrier fluid has an important role because the rate of heat transfer from the fluid to the pipe wall largely depends on the convective condition of the fluid.

According to Batini et al. (2015), the energy and geotechnical performances of energy piles are affected by different factors such as different site layout, foundation geometry, pipe configuration and soil and foundation material property while geotechnical performances vary for restrain condition and applied thermal loads. Energy demand of the superstructures and thermal performances of energy piles affect thermal loads.

According to Brandl (2006) diameter and length of pipes, roughness of pipe wall, thermal property, density, viscosity, flow velocity and flow conditions (laminar or turbulent) of the carrier fluid that flow in pipes should be considerate in order to optimize the absorber pipes system.

The heat flow rate of an EP is the ratio between the heat power extracted or injected from/into ground by an EP and the pile length [W/m]. It represents a simple way to evaluate and compare thermal performances of different EPs. The heat flow ratio can be evaluated directly with Thermal Performances Tests (TPTs).

2.3.1 Heat flow rate: Thermal Performances Test (TPT)

Thermal Performances Test (TPT) and Thermal Response Test (TRT) are two kind of test to determine or thermal parameters (and in some cases also the undisturbed initial temperature of soil), or the thermal performances (of energy piles), respectively. Generally, TPT is a faster method compared to TRT. In any case, before a TRT, it is necessary to obtain thermal properties of soil and pile to comprehensively analyse the heat exchange capacity of the EPs (Gao et al. 2008b).

Because the apparent similitude with VBHEs, the TRT technique was applied also for EPs.

TRT was first presented in 1983 by Mogensen (C. Zhang et al. 2014). With this kind of test it is possible to determine the borehole/pile thermal resistance (R_b) and the thermal conductivity of surrounding soil (λ_s) applying a controlled amount of heating power to heat exchangers and monitoring the temperature response of the carrier fluid (Loveridge et al. 2015).

The inlet and outlet heat carrier fluid temperature gradually increases, and a heat exchange balance is reached after a long time (You et al. 2014).

TRT is based on the theory of Infinite Line Source Method (ILSM). It is among the most used mathematical model to evaluate TRT data for sufficiently large times (C. Zhang et al. 2014).

ILSM returns the temperature in an infinite homogenous body heated along an ideal thin infinite line with a constant heating rate q released as a constant per unit length and time and only moving along a radial direction (Zarrella et al. 2017).

According to this model, the temperature at time t and at the distance r from the line is:

$$\Delta T_f(r, t) = \frac{q}{4\pi\lambda_s} \cdot \int_{\frac{r^2}{4at}}^{\infty} \frac{e^{-\beta^2}}{\beta} d\beta = \frac{q}{4\pi\lambda_s} \cdot E\left(\frac{r^2}{4at}\right)$$

Equation 2-2

For large values of the parameter at/r^2 , the exponential integral can be approximated as (Carslaw 1959):

$$E\left(\frac{r^2}{4at}\right) = \ln\left(\frac{4at}{r^2}\right) - \gamma$$

Equation 2-3

With this simplification Equation 2-2 becomes:

$$\Delta T_f = \frac{q}{4\pi\lambda_s} \cdot \left(\ln\left(\frac{4at}{r^2}\right) - \gamma \right) + q \cdot R_b$$

Equation 2-4

Where:

$\Delta T_f = T_f - T_g$ is a function of radius of pile/borehole [°C];

T_f is the average temperature of the fluid [°C];

T_g is the undisturbed soil temperature [°C];

Q is the heating power for length [W/m];

T is the time of the test [s];

λ_s is thermal conductivity of the soil [W/m°C];

a is thermal diffusivity of the soil [m²/s];

r is the radius of the borehole/pile [m];

γ is the Euler's constant (0,5772);

R_b is the thermal resistance of the borehole/pile;

Equation 2-4 is applicable if $t > 5r_b^2/a$. In fact, when $t > 5r_b^2/a$, 10% is the error of the approximation of Equation (Equation 2-2).

The thermal resistance R_b and thermal conductivity of the soil λ_s can be determinate from a graph where are plotted changes of temperature of the carrier fluid against the logarithm of time using the log-linear relationship equation for the infinite line source (Equation 2-2) (Loveridge et al. 2015).

When a heat flow is injected a transient process start:

$$T_f = \frac{Q}{4\pi\lambda_s H} \cdot \ln(t) + \left[\frac{Q}{H} \cdot \left(\frac{1}{4\pi\lambda_s} \cdot \left(\ln\left(\frac{4at}{r^2}\right) - \gamma \right) + R_b \right) T_g \right]$$

Equation 2-5

Equation 2-5 is the evolution of (Equation 2-4) considering the total length of heat exchanger H [m] and the total heat power Q [W] (always for $t > 5r_b^2/a$).

Introducing:

$$K = \frac{Q}{4 \cdot \pi \cdot \lambda \cdot H}$$

Equation 2-6

And

$$m = \frac{Q}{H} \left(\frac{1}{4 \cdot \pi \cdot \lambda} \left(\ln \left(\frac{4at}{r^2} \right) - \gamma \right) + R_b \right) + T_g$$

Equation 2-7

The Equation 2-7 can be expressed in linear form:

$$T_f = K \cdot \ln(t) + m$$

Equation 2-8

With the Equation 2-8 it is possible to estimate the mean thermal conductivity of the soil through the slope K on a plot T_f against $\ln(t)$. The estimated thermal conductivity is independent from R_b and so using λ_s it is possible to also find the borehole thermal resistance according to the following relationships.

$$\lambda = \frac{Q}{4 \cdot \pi \cdot K \cdot H}$$

Equation 2-9

$$R_b = \frac{1}{q} (T_f - T_b) = \frac{1}{q} (T_f - T_g) - \frac{1}{4 \cdot \pi \cdot \lambda} \cdot \left(\ln(t) + \ln \left(\frac{4at}{r^2} \right) - \gamma \right)$$

Equation 2-10

TRT method is subject to uncertainties because results depend on, via the slope K, the time of the test duration to determine the effective thermal conductivity. A recommendation for a minimum of 50 h is recommended (Gao et al. 2008b).

To consider EPs like VBHEs could bring to large errors in evaluation of thermal properties. Indeed, EPs are similar to traditional boreholes heat exchangers but have some peculiarities that should be always taken into consideration during the tests. First, the aspect ratios for EPs (the ratio between length and diameter of pile) are smaller than VBHEs. In fact, usually lengths of piles are shorter, and diameters are larger than those of vertical boreholes. For piles AR are in a range between 15 and 50 while for boreholes between 500 and 2000 (P. Bourne-Webb et al. 2016; Hu et al. 2014).

Then, thermal properties of the materials of the two technologies, concrete and the reinforce steel cages for concrete piles and grout in traditional boreholes, are another important difference. Moreover, the larger diameter of EPs compared to the VBHEs create a substantial difference between the two technologies. On the one hand, it makes possible the introduction of multiple pipes and multiple configurations in EPs, but on the other hand it represents a significant thermal mass with different thermal properties compared to the surrounding soil. In this way, concrete of energy pile can control the heat transfer potential of the pile-soil system (Singh, Bouazza, and Wang 2015; Peter J. Bourne-Webb 2013).

The infinite line source model represents the steady-state performance of boreholes reasonably well but tends to under predict the thermal response of piles for periods out to a few days to weeks depending on the diameter of the pile because of the dependence of the time on the radius square (Loveridge and Powrie 2013). Moreover, while for traditional boreholes heat exchangers ground surface is usually modelled as adiabatic due the length of the boreholes, in energy piles modelling ground surface could play an important role because the pile works in the shallow zone of ground where climatic condition affects the heat extraction/injection (Fadejev et al. 2017).

To compare the heat exchange performance of coil-type cast-in-place energy pile in TRT, Park et al. (2015) introduced the concept of relative heat exchange efficiency (eff) normalized for length of piles and for length of pipes taking into account the coil pitch:

$$eff_{pile} = \frac{Q}{slope \cdot L_{pile}}$$

Equation 2-11

$$eff_{pipe} = \frac{Q}{slope \cdot L_{pipe}}$$

Equation 2-12

The same equipment used for TRT can be used to carry out a TPT. Unlike the TRT, with TPT is possible to calculate the heat exchange rate per meter of the borehole/pile through the injection of a constant inlet temperature carrier fluid in heat exchanger and measuring circulating water flow velocity and the outlet water temperature (You et al. 2014):

$$Q = \dot{m}c_p(t_{out} - t_{in})$$

Equation 2-13

$$q = \frac{Q}{H}$$

Equation 2-14

Where:

Q is the heat exchange rate [W];

q is the average heat exchange rate per meter [W/m]

\dot{m} is the mass flow [kg/s];

c_p is the heat capacity of the circulating water [J/(kg°C)];

t_{out} is the outlet temperature of the circulating water [°C];

t_{in} is the inlet temperature of the circulating water [°C];

H is the borehole/pile depth [m].

Generally, TPT are carried out in field test and, depending on the duration, can be classified in short or long tests. Generally, short tests have an operation time of few days and no more of three months. Vice versa, long tests have more longer time of observation and could run also for the full operation

of the system. Even if short tests can lead to an overestimate of thermal performances of EPs are anyway used to evaluate design parameters of piles and pipes.

Anyway, the evaluation of thermal performances of and energy pile was tested also by small scale model and numerical analysis if carried out with principia of TPT.

To compare different thermal design solutions for energy piles, below were summarized the results from the principal field short TPT, small scale tests and numerical analysis. Only short-term field TPTs were analysed because a direct comparison between the different long-time tests was not possible. Indeed, long time TPT often provide results of heat exchange rate at the end of a time in which both inlet temperature and carrier fluid flow rate were varied in time.

2.3.2 TPT field test

The results of short TPTs collected regarded different types of pile and different pipes configurations. One on the first TPT in field was carried out in Japan in 1987 using steel piles (Morino and Oka 1994). Subsequently other authors used carried out steel piles for TPT in Japan (Katsura et al. 2009; Nagano et al. 2005; Jalaluddin et al. 2011).

Hamada et al. (2007) described performances of energy piles applied for both residential and office use during a field test. TPT was carried out on a 9 m in length precast high-strength concrete (PHC) energy piles filled with water. Three different pipes configurations (U-shaped, double U-shaped and indirect double pipe) were analysed.

TPT on a cast in situ concrete pile 1,5 in diameter and 20 m in length equipped with 8 pair of U tube all around was carried out by Sekine et al. (2007). The authors investigated also on economic feasibility of the solution and on change of underground.

In South Korea Park S. et al. (2015) and (2016) carried out many experiments to study thermal performances of energy piles. In the first two studies the authors investigated thermal performance of energy piles before with field tests and after with numerical analysis. The piles were equipped with spiral coil pipes and influences of spiral pitch was investigated. In the second study, instead, was carried out on large diameter (1,5 m) cast in situ concrete energy piles equipped with a W-shaped pipe only for the half section of the pile. Park et al. (2017) evaluated the applicability of this kind of pile comparing it with the thermal performances of other types of piles presented in literature. On the other hand, Yoon et al. (2015) carried out an experimental and numerical study to investigate on thermal performances and a cost analysis of precast high-strength concrete (PHC) energy piles equipped with W and coil-type pipes configuration. TPT was carried out for 4 days heating the pile with a constant inlet temperature of 30 °C under the operating condition of an 8 h on and a 16 h off cycle. Subsequently the prediction of the heat flow rate for three months operation was carried out to compare the performances of the two configurations in long time by a 3D FEM simulation.

In China Gao et al. (2008a, 2008b) and You et al. (2014) carried out field TPT on cast in situ and CGC concrete energy piles respectively.

Gao et al. (2008a, 2008b) analysed and comparing the thermal performance of cast in situ energy piles equipped with U-configuration (single U, double U and triple U) and W-shaped configuration heat exchangers by field tests and numerical simulations.

You et al. (2014) carried out field tests on the heat exchange capacity of energy piles cement-fly ash-gravel (CFG) 18 m in length and 0,42 m in diameter equipped with W-shaped pipes 25 mm in diameter connected in series. TPTs were conducted changing water flow velocities (0,26 m/s, 0,51 m/s and 1,02 m/s), water inlet temperatures (5 °C, 35 °C, and 60 °C) and considering intermittent operation and continuous operation.

Li et al. (2006) set up field tests on the thermal performance of single U-pipe with cement backfills and single or double U-pipes with sandstone backfills. Different parameters were considered during tests such as the water flow rate, the operation modes, the inlet water temperature, the backfill materials, the soil types and the number of U-pipes were.

Luo et al. (2016) investigated on the thermal performances of double-U, triple-U, double-W and spiral configurations in energy piles through an experimental and numerical study. Also, a cost-benefits analysis was developed. The tests were carried out in the Henan province on two type of cast in situ pile that had length of 12 m and diameter of 0,8 m or pile 18,5 m in length and 0,6 m in diameter. The type of the pile depended on type of pipes configurations. The thermal performances were determined both for cooling mode and heating mode considering an intermittent operation mode made by 7 days on for cooling, 26 days off, 7 days on for heating.

In Melbourne (Australia) Singh et al. (2015) investigated on thermal performances of concrete bored cast in situ energy piles 0,6 m in diameter and 16,1 m in length equipped with U and W-shaped pipes configurations. Three different heating tests were carried out considering different operation time. On the other hand, Faizal et al. (2016a) analysed with a full scale test the thermal behaviour of a single geothermal bored pile 16,10 m long and 0,60 m in diameter subjected to intermittent and continuous operating cooling modes. Three different operating modes were analysed over a period of one year and results of only 20 days of the experimentation were reported by authors. The pile was tested with two intermittent modes, 8 h and 16 h with natural ground recovery and a continuous daily mode (24 h).

In USA Murphy et al. (Kyle D. Murphy, McCartney, and Henry 2015) investigated on eight drilled shafts, each 15,2 m in length and 0,61 m in diameter equipped with different pipes configurations such as single U, W-shaped and triple U shaped. The different results in terms of heat flow rate [W/m] were compared by author considering the heat exchange through the horizontal portion of the loop.

The field tests mentioned above are classified as “short terms TPT” because the time of the operation mode was not longer than 3 months. Anyway, in literature there were also test where the thermal performances were observed and investigated for a time much longer often on real plants that have not been explicitly addressed in this review for the reasons explained in the previous section (C. J. Wood, Liu, and Riffat 2010; Pahud et al. 2008; Christopher J. Wood, Liu, and Riffat 2010; Ruíz 2015; Sekine et al. 1997).

In Table 2-3 results of field TPT test are summarized.

Table 2-3 – Energy piles thermal performances - field test (C=continuous operation mode; I=intermittent operation mode)

Reference	Pipe configuration	Tin [°C]	Water flow rate [l/min]	Pitch [mm] (only for elical)	ΔT [°C]	Pile type	Pile lenght [m]	Pile diameter [m]	Aspect ratio L/D	Operation time	Thermal flow rate [W/m]
(Gao et al. 2008a) (Gao et al. 2008b)	U tube	35,13	5,7	-	16,93	Concrete-cast in situ	25	0,6	41,7	ND	57,84
	Double U-tube	35,08	11,4		16,88						89,53
	Triple U-tube	34,88	17,1		16,68						108,07
	W-shaped	35,02	5,7		16,82						83,05
	W-shaped	34,79	11,4		16,59						94,25
(Jalaluddin et al. 2011)	U tube	27,00	2	-	10	Steel - sand filled	20	0,14	142,9	C for 1 day	24,9
			4								30,4
			8								31,5
	Double Tube	27,00	2								36,9
			4								49,6
			8								54,8
	Multi-Tube	27,00	2								26,6
			4								34,8
			8								40,2
(Hamada et al. 2007)	U tube	17,79	4,38	-	8,49	Concrete-PHC	9	0,302	29,8	ND	53,81
	Double U-tube	18,90	4,06		9,6						54,76
	Indirect double pipe	21,07	4,6		11,77						68,71
(Yoon et al. 2015)	W-shaped	30,00	11,4	-	13	Concrete-PHC	13,27	0,4	33,175	I 8h on -16h off (4 days average value)	95
	Helical (Coil Type)			50			12,8	0,4	32		120
(You et al. 2014)	W-shaped	35,00	15,01	-	19,00	Concrete -CFG	18	0,42	42,9	C 50h	116
			15,01		44,00					C 50h	258
			15,01		-11					C 130h	-58
			7,65		19,00					C 28h	84
			15,01		19,00					C 28h	116
			30,02		19,00					C 28h	94
			15,01		19,00					C 120 h	116
			15,01		19,00					I 120h (24on and 24h off)	139
			15,01		19,00						
(Singh, Bouazza, and Wang 2015)	U tube	50,5	10	-	41,2	Concrete-Bored pile	16,1	0,6	26,8	C 3 days	190
	W-shaped	41	10		31,7					C 9 days	229
	W-shaped	48	10		38,7					C 52 days	181

(S. Park et al. 2015)	Helical (Coil Type)	30,00	20	200 mm	13	Concrete-cast in situ	14	1,5	9,3	I (8h on-16h off) for 7 days	285,4	
	Helical (Coil Type)	30,00	20	500 mm			12,5	1,5	8,3	I (8h on-16h off) for 7 days	252,2	
(Sekine et al. 1997)	8 U-shaped all around	ND	ND	-	-	Concrete-Cast in situ	20	1,5	13,3	I 9h on -15 off for 4 months	100	
		ND	ND								120	
		ND	ND								186	
		ND	ND								201	
		ND	ND								-44	
		ND	ND								-52	
(Kyle D. Murphy, McCartney, and Henry 2015)	W-shaped	ND	6,48	-	-	Concrete - Bored cast in situ	15,2	0,61	24,9	ND	105,2	
		ND	7,14								8,8	101,6
		ND	8,22								6,9	109,4
		ND	6,36								4,8	97,9
	Triple U-tube	ND	8,46								6	139,2
	U tube	ND	6,48								4,8	126,9
		ND	7,56								4,5	120
		ND	20,82								3,9	90,1
		ND	13,56								2	55,8
		ND	13,56								1,6	55,4
		ND	11,34								1,6	44,6
		ND	11,34								1,3	44,8
		ND	11,34								1,3	44,8
		ND	11,34								1,9	56,9
ND		11,34	1,9	56,9								
(S. Park et al. 2016)	Helical (Coil Type)	5,00	10	200 mm	-12	Concrete-cast in situ	14	1,5	9,3	I (8h on-16h off) for 7 days	-140,4	
		5,00	10	500 mm			12,5	1,5	8,3	I (8h on-16h off) for 7 days	-132,9	
(Nagano et al. 2005)	Direct	2	5	-	-	Steel pile, water filled	40	0,4	100,0	C 10 days	-27,2	
	Direct	-5	30								-7,3	-94,9
	U tube	2	30								-14,3	-24,3
	U tube	-5	12								-7,3	-54,7
	Double U-tube	2	30								-14,3	-19,9
	Direct	2	30								-7,3	-19,8
	Direct	-5	30								-7,3	-61,6
	U tube	2	30								-14,3	-13,7
	U tube	-5	10								-7,3	-38,9
	Double U-tube	2	30								-14,3	-17,9
	Direct	2	5								-7,3	-20,4
	Direct	-5	30								-14,3	-64,6
	U tube	2	30								-7,3	-17
	U tube	-5	12								-14,3	-41,9
	Double U-tube	2	30								-7,3	-19,9
	Direct	2	30								-7,3	-14,9
	Direct	-5	30								-14,3	-45,2
	U tube	2	30								-7,3	-14,3
	U tube	-5	10								-14,3	-29,9
	Double U-tube	2	30								-7,3	-18,9

2.3.3 Numerical model

Numerical model simulation could be a valid support to investigate on thermal performances tests of EPs, often validated on previous field tests results, and very often allow to carry out parametrical analysis to compare different design parameters.

Park H. et al (2013) analysed the thermal performances of precast high-strength concrete (PHC) energy piles 400 mm in diameter and 180 mm in thickness installed in partially saturated weathered granite soil deposit equipped with W-shaped and triple U configuration. W-shaped pipes and triple U-pipes configuration thermal performances were compared through a 3D numerical analysis validated on a previous TRT field measure. In the simulation, an initial soil temperature of 17 °C, an inlet temperature of water of 30 °C and a flow rate of 7,2 l/min were considered. The simulations were conducted an intermittent operation mode of 8 hours and a continuous operation mode considering a period of operation 3 months long.

Zarella et al. (2013) carried out a comparative analysis on thermal performances between the triple U-shaped pipes configuration (coupled in parallel) and helical pipes configuration. The comparison of the two configurations was developed for the same boundary conditions for both the piles through a numerical simulation using an equivalent electrical circuit of suitable thermal resistances and capacitance to solve the heat transfer problem. The model was compared with a field test carried out in Mestre (Italy) on two energy piles 12 m in length and 500 mm in diameter, equipped with the two pipes configuration and during the test the peak loads were measured and the behaviour in the short term was investigated.

Hu P. et al. (2014) presented a composite cylindrical model for large diameter piles based on the composite line source and cylindrical model taking into account the heat capacity of energy piles in GSHP. This model was validated with a 3-D numerical model calibrated with field measured data sets. A parametrical analysis on pipes number and layout was carried out. An energy pile 0,6 m in diameter and 45 m in length was considered equipped with different pipes configurations (2-U, W-shaped and 3-U.)

Batini et al. (2015) developed parametrical numerical analyses to investigate the full-scale energy pile thermo-mechanical response considering different pipes configurations (U-shaped, double U-shaped and W-shaped type), foundation aspect ratio, mass flow rate of the carrier fluid and the carrier fluid mixture composition. The simulation was carried out considering the characteristics of energy pile and surrounding soil from the study developed in the experimental site in the Swiss Federal Institute of Technology in Lausanne (EPFL) under the Swiss Tech Convention Centre. The pile had a length of 28 m and a diameter of 0,90 m.

Carotenuto et al. (2017) developed a 3D numerical model, verified, and validated against experimental and numerical data available in the literature (You et al. 2014; Bezyan, Porkhial, and Mehrizi 2015), to investigate the heat transfer performance of different configurations of energy piles. The authors carried out a parametrical analysis to evaluate the effects of design and operating parameters like different diameter of pipes and pile, different properties of the materials, different flow rate and pipes configurations such as U-tube, Double U-tubes, Triple U-tubes, spiral coil.

Cecinato and Loveridge (2015) developed a FE model to analyse the factors that mostly influence the thermal behaviour of energy piles through a parametric analysis. In particular, the effects of pile length concrete conductivity, pile diameter and concrete cover, diameter and number of pipes, carrier fluid flow velocity were investigated.

Bezyan et al. (2015) developed a 3D-fluid-solid coupled numerical simulation in order to investigate the best performance in heat transfer rate and efficiency in energy pile equipped with 1-U-shaped and 1-W-shaped and vertical Spiral-shaped in cooling mode of water. Moreover, the authors also compared three different pitch sizes for spiral configuration to establish the best design of spiral coil for thermal performances. Finally, the analysis focused on the connection of multiple energy piles in parallel and serially simulating a large-scale plant.

Three types of vertical pile-foundation heat exchangers (U-shaped, W-shaped and a W-shaped-all round type which 6-U pipes) were analysed and compared by Mehrizi et al. (2016) by a 3D numerical simulation in order to determine the most efficient configuration in terms performance in heat transfer rate. The three different configurations were investigated considering three different pile length for each configuration (20 m, 25 m and 30 m). From the analysis resulted that the W-shaped-all round type configuration had the best performances. After, the authors carried out another analysis to compare performances of serial and parallel connection of pile-foundations in cooling. The result was that the best efficiency in heat transfer rate was achieved by pile-foundation with W-shaped- all round configuration in serial connection.

Luo et al. (2016) investigated on the thermal performances of double-U, triple-U, double-W and spiral configurations in energy piles through an experimental and numerical study. Also, a cost-benefits analysis was developed. The tests were carried out in the Henan province on two type of cast in situ pile that had length of 12 m and diameter of 0,8 m or pile 18,5 m in length and 0,6 m in diameter. The type of the pile depended on type of pipes configurations. The thermal performances were determined both for cooling mode and heating mode considering an intermittent operation mode made by 7 days on for cooling, 26 days off, 7 days on for heating.

Zhang et al. (2017) carried out a numerical simulation in order to investigate on the heat transfer performance of the single energy pile and 3x3 energy piles equipped with a triple U pipes configuration.

Abdelaziz et al. (2011) carried out a series of numerical analyses using a three-dimensional finite element model to investigate on various factors on the thermal performance of GEPs using the pile geometry (23 m long and 60 cm in diameter) from the field test reported in Bourne-Webb et al. (2009) and a double loop of 19 mm diameter circulation tubes extended to a depth of 22,5 m. Form the simulation the heat exchange rate was calculated for each case of configuration considering as parameters thermal conductivities of different in-situ soils, pile materials, and flow conditions.

In Table 2-4 the results of the numerical analysis are summarized.

Table 2-4 - Energy piles thermal performances - Numerical analysis (C=continuous operation mode; I=intermittent operation mode)

Reference	Pipe configuration	Tin [°C]	Water flow rate [l/min]	Pitch [mm] (only for helical)	ΔT [°C]	Pile type	Pile length [m]	Pile diameter [m]	Aspect ratio L/D	Operation Time	Thermal flow rate [W/m]	
(Mehrizi et al. 2016)	U tube	35,00	5,7	-	16,80	Concrete	20	0,6	33,3	ND	49,345	
							25	0,6	41,7		44,45	
							30	0,6	50,0		40,65	
	W-shaped						20	0,6	33,3		63,084	
							25	0,6	41,7		54,28	
							30	0,6	50,0		51,23	
							Six U-Tube (W-shape all around)	20	0,6		33,3	72,27
								25	0,6		41,7	68,4
								30	0,6		50,0	63,5
(Bezyan, Porkhial, and Mehrizi 2015)	U tube	35,00	5,7	-	16,80	Concrete	25	0,6	41,7	ND	44,45	
	W-shaped	35,00	5,7								54,28	
	Helical (Coil Type)	35,00	5,7								200	102,5
	Helical (Coil Type)	35,00	5,7								400	123,06
	Helical (Coil Type)	35,00	5,7								600	92,84
(Batini et al. 2015)	U tube	5,00	9,7	-	-8,20	Concrete	28	0,9	31,1	C 15 days	-16,9	
							9		10,0		-12,5	
							18		20,0		-16,5	
							28		31,1		-16,9	
							36		40,0		-16,1	
							28		31,1		-15,8	
			31,1					-16,9				
			31,1					-17,3				
			31,1					-17,2				
			31,1					-18,1				
			31,1					-18,1				
			Double U-tube				5,00	19,3	-		-8,20	Concrete

			11,8				9		10,0		-20,3
			18				20,0		-26,3		
			28				31,1		-26,5		
			36				40,0		-25,9		
			28				31,1		-25		
									-26,5		
									-27,1		
									-27,4		
	W-shaped	5,00	9,7	-	-8,20	Concrete	28	0,9	31,1	C 15 days	-26,1
							9		10,0		-21
							18		20,0		-26,6
							28		31,1		-26,1
							36		40,0		-24,9
							28		31,1		-24,2
-26,1											
-27											
-27,9											
(Carotenuto et al. 2017)	Double U-tube	35,13	-	-	Concrete	25		0,6	41,7	C6h	163,88
								0,5	50,0		156,36
								0,7	35,7		167,36
								0,9	27,8		169,72
								1	25,0		170,2
								0,6	41,7		148,84
								0,6	41,7		170,4
								0,6	41,7		175,56
	Triple U-tube	35,13	30	-	-	Concrete	25	0,6	41,7	C6h	222,32
	Helical (Coil Type)	35,13	10	-	-	Concrete	25	0,6	41,7	C6h	700 mm
500 mm											152,6
250 mm											215,9
100 mm											276,1
(Luo et al. 2016)	Double U-tube	ND	98,4	-	ND	Concrete	18,5	0,6	30,8	C 7 days	147,1
	Double U-tube	5,00	98,4		-11,00	Concrete	18,5	0,6	30,8	C 7 days	-115,5
	Triple U-tube	ND	94,8		ND	Concrete	18,5	0,6	30,8	C 7 days	252
	Triple U-tube	5,00	94,8		-11,00	Concrete	18,5	0,6	30,8	C 7 days	-157,1
	Helical (Coil Type)	5,00	111	300 mm	-11,00	Concrete	12	0,8	15,0	C 7 days	ND
	Helical (Coil Type)	5,00	94,2	300 mm	-11,00	Concrete	12	0,8	15,0	C 7 days	-145,7
	Helical (Coil Type)	ND	111	300 mm	ND	Concrete	12	0,8	15,0	C 7 days	296,3
	Helical (Coil Type)	ND	94,2	300 mm	ND	Concrete	12	0,8	15,0	C 7 days	224,7
(H. Park et al. 2013)	Triple U-tube	30,00	7,2	-	13,00	Concrete	13,75	0,4	34,4	C 3 months	42
	Triple U-tube	30,00	7,2		13,00	PHC	13,75	0,4	34,4	1 8h on-16h off for 3 months	87

	W-shaped	30,00	7,2		13,00		13,25	0,4	33,1	C 3 months	40
	W-shaped	30,00	7,2		13,00		13,25	0,4	33,1	1 8h on-16h off for 3 months	76
(Zarrella, De Carli, and Galgaro 2013)	Triple U-tube	30,00	5,4	-	17,00	Concrete	12	0,5	24,0	C 3 days	107
	Helical (Coil Type)			75 mm						C 3 days	123
				150 mm						C 3 days	120
				300 mm						C 3 days	113
(Yoon et al. 2015)	W-shaped	30,00	11,4		17,00	Concrete PHC	13,27	0,4	33,2	1 8h on-16h off for 3 months	74,8
	Helical (Coil Type)			50 mm			12,8	0,4	32,0	1 8h on-16h off for 3 months	94
(S. Park et al. 2016)	Helical (Coil Type)	30,00	20	500 mm	17	Concrete CIS	14	1,5	9,3	1 8h on-16h off for 1 months	143,9
				350 mm							184,9
				200 mm							235,9
				100 mm							292,4
(H. Zhang and Chen 2017)	Triple U-tube	35,00	11,3	-	17	Concrete	28	0,6	46,7	C for 1 month	60

2.3.4 Small scale test

In this section the main results obtained by TPT on small-scale energy pile are described. Wang et al. (2017) through a comparative analysis investigated different thermo-mechanical performances of small-scale concrete energy piles equipped with U-shaped, W-shaped and spiral coil configuration of piles. The tests were carried out considering a cycle of 72 hours where the piles were before heated and after cooled.

Yang et al. (2016) carried out small scale test to study the different conditions that could affect the thermal performance of a PVC hollow pile filled with concrete equipped with a spiral coil pipe. The authors investigated on the effects of spiral pitch, temperature of inlet fluid, operation mode and pile materials.

In the small-scale test carried out by Kramer et al. (2015) a concrete pile equipped with a U pipe configuration was heated for 7 days in continuous operation mode. The effects of temperature difference in temperature between carrier fluid and surrounding soil and of the fluid circulation velocity on heat transfer performance were investigated by authors.

Elzeiny et al. (2020) investigated on thermo-mechanical performances of a small-scale concrete energy pile equipped with a double U pipes configuration. During the test, the pile was subjected to 5 heating cycles and 100 cooling cycles. The maximum heat exchange rate for both tests was developed at the beginning of the first cycle and decreased towards the end of heating of the first 15 cycle.

In Table 2-5 the small-scale tests results are summarized.

Table 2-5 - Energy piles thermal performances - Small-scale test (C=continuous operation mode; I=intermittent operation mode)

Reference	Pipe configuration	Tin [°C]	Water flow rate [l/min]	Pitch [mm] (only for helical)	ΔT [°C]	Pile type	Pile length [m]	Pile diameter [m]	Aspect ratio L/D	Operation time	Thermal flow rate [W/m]
Wang et al. (2017)	U tube	55	3,27	-	44,00	Concrete	1,6	0,104	15,4	5 h heat - 8h rest - 5h cooling for 72h	ND
	W-shaped	55	2,68		44,00						
	Helical (Coil Type)	55	2,83		44,00						
	U tube	4	3,27		-7,00						
	W-shaped	4	2,68		-7,00						
	Helical (Coil Type)	4	2,83		-7,00						
Yang et al. (2016)	Helical (Coil Type)	37	0,67	20	25,8	PVC cement filled	0,8	0,2	4	C 10h	404,4
	Helical (Coil Type)	32	0,67	20	20,8					C 10h	339,3
	Helical (Coil Type)	27	0,67	20	15,8					C 10h	275,1
	Helical (Coil Type)	37	0,67	20	25,8					I 1h on - 1h off for 10h	570,25
	Helical (Coil Type)	37	0,67	20	25,8					I 80min on - 40min off for 10h	496,6
	Helical (Coil Type)	37	0,67	20	25,8					C 10h	429,4
	Helical (Coil Type)	37	0,67	60	25,8					C 10h	250
	Helical (Coil Type)	37	0,67	40	25,8					C 10h	312,5
	Helical (Coil Type)	37	0,67	20	25,8					C 10h	337,5
	Helical (Coil Type)	37	0,67	20	25,8					C 10h	225,6
	Helical (Coil Type)	37	0,67	20	24,8					C 10h	285,9
	Helical (Coil Type)	37	0,67	20	23,8					C 10h	326,6
Kramer et al. (2014)	U tube	39	0,8	-	20	Concrete	1,38	0,1	13,8	C for 7 days	13,04
			2,39								39,09
			4,78								76,08
Elzeiny et al. (2020)	Double U-tube	36	0,8	-	20	Concrete	1,383	0,102	13,6	I 1h on - 15 min off for 5 times	125
										I 1h on - 15 min off for 100 times	148

2.3.5 The main design elements that affect thermal performances of energy piles

There are some design parameters that affect the energy piles thermal performances in terms of heat flow rate. They are detailed described in next sections.

2.3.5.1 *The pipes configuration*

The heat exchangers surface affects the short-term specific heat extraction/rejection rate. Because there is a substantial difference in lengths between energy piles and traditional VBHEs, it could subsist a clear difference in terms of energy performances between the two technologies.

To solve this problem it is necessary to enhance the heat transfer of energy piles by increasing the total length of heat exchangers (S. Park et al. 2015).

Larger dimeters of EPs than the VBHEs allow installing a larger number of heat exchangers inside the structure with different possible shapes and configurations of pipes.

The configuration pipes design leads to different thermal performances but could leads also to different mechanical behaviours of the pile. A not balanced area of heat exchangers in the section of pile could cause non-uniform heating/cooling and consequently bending strains in the pile (Singh, Bouazza, and Wang 2015). On the other hand it was demonstrate that the reduction of the pile cross-sectional area due to the presence of the pipe is negligible in terms of bearing capacity of the pile (You et al. 2016).

The types and the shapes of pipes inside the EPs can also affect the Coefficient of Performance (COP) of a GSHP system (Christopher J. Wood, Liu, and Riffat 2012).

The velocity and the pressure loss of carrier fluid depend on pipes shapes and sections and affect the heat exchange flow rate that can achieve the pile.

Single U-shape, W-shape, double U-shape, triple U-shape, spiral or helical shape, direct double-pipe type and indirect double-pipe type are some of the most common configurations of pipes for concrete EPs (Gao et al. 2008a; Hamada et al. 2007; Nagano et al. 2005; H. Park et al. 2013; S. Park et al. 2015; You et al. 2016).

Due to simplicity of mounting to reinforcements bars and for ease of pouring concrete especially for bored piles, the most common configurations of pipes in EPs are U-shaped arrangements that in large diameter energy piles may commonly exceed two (Faizal, Bouazza, and Singh 2016b).

The single U-tube configuration is used both in VBHEs and in concrete energy piles. The U-tube configuration results the most economic feasibility and workability solution. In addition, the differences in terms of thermal performances respect other solution such as double U-shaped and indirect double pipe types are negligible (Hamada et al. 2007). Anyway, energy piles are not so depth than the VBHEs it does not result the best solution in terms of energy performances because it would result a too little heat exchanger surface.

An upgrade of the U-tube configuration can be represented by the double-U or triple-U (if the U-shaped pipes are parallel connected) or W-shaped configuration (if the U-shaped pipes are serially connected). It should be noticed that when these configurations are compared in terms of energy

performances, also the amount of carrier fluid flow rate should be considered. In fact, because of the parallel connection, in double or triple U the total flow is the sum of each U configuration. On the other hand, the flow rate for W-shaped configuration is the inlet flow rate. In fact, in absolute terms triple and double-U configuration had higher performances than W-shaped and single U, but, considering the effective flow rate in terms of thermal performances, W-shaped configuration should be more preferred (Gao et al. 2008a, 2008b). Anyway, this type of configuration is affected by higher installation costs and the risk of air accumulation on the top of the circuit (Wenke Zhang et al. 2017). The better thermal performances of the triple-U than the W-shaped in the short-time was also confirmed by Park et al. (2013), but for long-term operation the differences between triple-U and the W-shaped configurations were negligible. Moreover, also the numerical analysis carried out by Batini et al. (2015) (Batini et al. 2015) this trend comparing double-U configuration with the W-shaped and single U. The Double-U resulted the best in terms of thermal performances also because the double flow rate during the simulated 15 days of operation. On the other hand, a W-shaped-all round configuration had the best thermal performance in terms of in heat transfer than other configurations compared to U-shaped and 1-W-shaped types (Mehrizi et al. 2016).

As regarding the spiral or helical coil configuration, a lot of studies and comparisons with the previous configurations were carried out in literature.

A comparison on thermal performances between double-U, triple-U, double-W and spiral configurations in energy piles was carried out by Luo et al. (2016). From the analysis resulted that triple U tube was the best configuration both for thermal performances both in cooling mode and heating mode and from an economical point of view. Anyway, also the double U-configuration was the cheapest configurations after triple U but in terms of thermal performances it was only 67%-69% than spiral or double W-shaped configuration. The spiral type with 0,4 m pitch, with 123,0645 W/m of heat exchange rate was, the best pipes configuration compare with 1-W-shaped and 1-U-shaped (Bezryan, Porkhial, and Mehrizi 2015).

In terms of specific heat flow values, an energy pile equipped with helical pipe reached values of 120 W/m while a pile equipped with the triple U-tube configuration reached values of 107 W/m (Zarrella, De Carli, and Galgaro 2013). According to authors a helical-pipe configuration in pile also reduce the installing costs because needs a shorter total borehole length for the same thermal performances of a U configuration. The latter aspect is confirmed also by Christopher et al. 2012. According to Park et al. (2013) spiral coil-type enhanced the heat efficiency because had largest heat exchange area compared to U-type. Consequently, for the same heat power to extract/inject from/into soil, pile equipped with coil type pipes could be shorter than others.

When the pitch decreased from 0,15 m to 0,075 m, the peak load increased by about 13% and when it increased from 0,15 m to 0,3 m, the peak load decreased by about 14% (Zarrella, De Carli, and Galgaro 2013). From the numerical analysis carried out by Carotenuto et al. (2017) resulted that in terms of temperature distribution along the pipes the spiral coil ensured the largest temperature difference between inlet and outlet than double and triple U configurations and found that the heat transfer rate per unit of length of pile and the outlet water temperature increase as the pitch decreases. Anyway, too small pitch was not a good solution because there was not a linear proportionality between the pitch size and the heat transfer rate because the thermal interference between each loop of pipe increase.

An improvement of the energy efficiency and the applicability of a GSHP system could be obtained by a decrease of the spiral pitch (Zhao et al. 2017). Indeed, the authors found that increasing the spiral pitch from 0,25 m to 2,0 m resulted a reduction of the mean COPs from 0,77 to 16,49%. Increasing the coil pitch the heat exchange improved (S. Park et al. 2015). Anyway, it was a not-linear relationship between pitch and thermal performances. Indeed, for a coil pitch of 500 mm was obtained a heat exchange rate of 248,19 W/m, while, with a coil pitch of 200 mm resulted 285,36 W/m.

The relationship between the coil pitch and the thermal performances were evident also in the small-scale test carried out by Yang et al. (2016). The heat exchange increased from 200 W to 270 W when the coil pitch passed from 6 cm to 20 cm respectively.

With coil-type heat exchangers it was possible to achieve highest heat rejection rates. Anyway, because the potential ground extracted energy amount depends on ground initial temperature and ground source system application, for long time operation mode high heat extraction/rejection potential may not be optimal solution because excessive heating/cooling of the soil (Fadejev et al. 2017).

Anyway, not only concrete piles were tested in literature. As regarding the steel pile and the comparison between direct use and indirect use (inside pipes) of carrier fluid, Nagano et al. (2005) carried out a field test where direct circulating heat exchange, U-tube and double U-tube configurations were compared. Two different diameters of 400 mm and 165 mm were adopted for steel piles. It was observed that for long time operation, single U-tube configuration had the 83% of the heat exchange rate of direct circulation type for pile of 400 mm in diameter while for piles with smaller diameter, direct circulation type was still better than U-tube configuration but the difference in heat exchange rate was only 96%. On the other hand, from the comparison between direct configuration and double U type resulted that for large diameter the heat exchange rate of double U configuration was 96% of the direct configuration but, considering the smaller diameter double U configuration was had a heat exchange rate 127% than direct configuration.

In TPT carried out by Jalaluddin et al. (2011), for a flow rate of 4 l/min, the heat exchange rate were 49,6 W/m, 34,8 W/m, and 30,4 W/m respectively for the double-tube, for the for the multi-tube and for the U-tube in steel piles and filled. The results indicated that the most important factor for the heat exchange rate was the heat exchange surface. As a matter of fact, the double-tube had the larger contact surface area with the ground (8,73 m²) compared to that of the other GHEs (6,28 m² for multi-tube and 4,15 m² for U-tube). Moreover, for high water flow rate the heat exchange rates of the double-tube and multi-tube GHEs tended to increase while the U-tube tends to be constant.

2.3.5.2 Aspect ratio and distance of pipes

The aspect ratio (AR), is the ratio between length and diameter of the EP. Because of the double nature of EP, generally length and diameter are chosen based on the structural and geotechnical design of piles. From an energy point of view, EPs length should be enough to overcome the most superficial area of the soil affected by ambient temperatures (Suryatriyastuti, Mroueh, and Burlon 2012). On the other hand, Brandl (2006) proposed a minimum length of the pile of 6 m because, from an economical point of view, to obtain 1 kW of energy occur 20 m² for EPs in saturated soil and 50 m² for dry soil, respectively.

Anyway, with diameters that are at least 300 mm (Loveridge and Powrie 2013), EPs result larger than traditional VBEHs. Even if the greater space allows the possibility to install more pipes in the pile section, the thermal performance does not improve linearly with the number of pipes used.

In numerical analysis carried out by Batini et al. (2015) it was observed that an increment of the aspect ratio corresponded to an increase of the difference in temperature between inlet and outlet fluid. An increase of heat exchange surface resulted and a consequently increase of energy exchange. Moreover, according to the authors, depending on the pipes configurations, doubling AR from 10 to 20 the heat exchange rate increased between 152% and 170% while an increase between 87% and 100% was found doubling of AR from 20 to 40. The last result was attributed to the tendency to saturation of the heat exchangers with the increase of heat transfer surface.

While Batini et al. (2015) carried out their analysis varying the AR with a constant diameter length, Carotenuto et al. (2017) in their numerical model analysed the effects of different AR with a constant length of piles and varying diameter dimensions using a double U configuration of pipes. From the simulation resulted that increasing the diameter (i.e. decreasing the AR) the heat exchange rate increased but not linearly. An increase of 7% of thermal performance resulted passing from a pile diameter 0,5 m to a pile diameter of 0,7 m while an increase only of 9% of the thermal performances was found passing from a pile 0,5 m in diameter to a pile 1,0 m diameter. According to the authors, the reason of the increase of thermal performances was the smaller thermal interferences between in and out pipes.

In the parametric simulation carried out by Mehrizi et al. (2016) a pile 0,6 m in diameter was equipped with different pipes configurations and three different lengths for the piles were considered. From the analysis resulted that in terms of absolute power [W], longest piles (i.e., with a larger AR) resulted the best for every configuration of pipes because of the larger difference in temperature of carrier fluid between inlet and outlet.

A study about the effects of the distances between pipes legs was, instead, carried out with a numerical simulation by Hu et al. (2014). According to the authors, even if triple U pipes configuration resulted the best solution compared to the double U and W-shaped configuration, it was found that the larger distances between pipes that are typical of U configurations provided fewer thermal interferences between pipes and so higher thermal performances.

The effects of different volumes of pipes installed in a large diameter concrete EP were investigated by Park S. et al. (2017). After a TPT in field on a concrete pile 1,5 m in diameter and 60 m in length equipped with a W-shaped pipe for half section and for 30 m in length, the authors carried out a numerical parametric simulation validated based on the field test, to compare other possible configurations. It was found that the improving of thermal performances is not only proportional to pipes length but also the pipes proximity should be considered because of thermal interferences.

From data collected both for field and small-scale tests (Figure 2-8 and Figure 2-9), it is possible to notice that spiral pipes configuration and low AR values given the best performances both for field scale and small-scale tests. Comparable results in field tests can be obtained by W-shaped configuration installed in concrete bored pile with an A/R approximately 2,5 time greater or by W-shaped configuration installed in cement fly-ash gravel (CFG) pile with an A/R approximately 4 time greater that spiral configuration. The result more evident in the small-scale tests is that also with a low flow rate of heat carried fluid a small AR combined with the spiral configuration results the better solution in terms of heat flow rate exchanged between pile and soil.

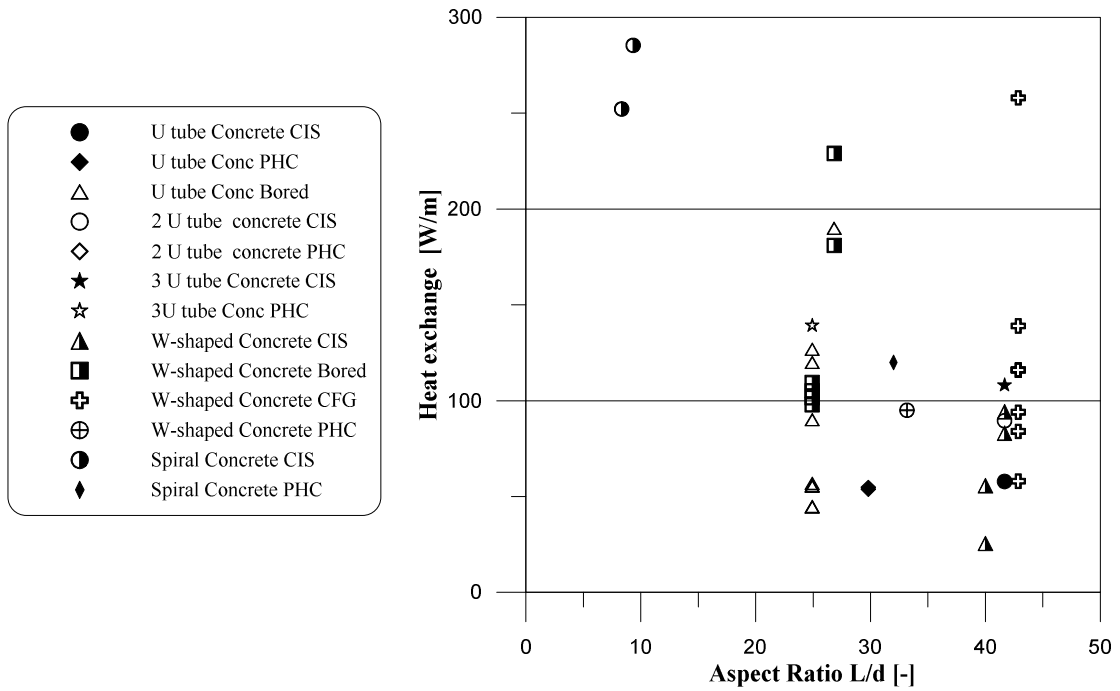


Figure 2-8 - Field test results: heat exchange vs pile aspect ratio for different pipes configurations and pile types

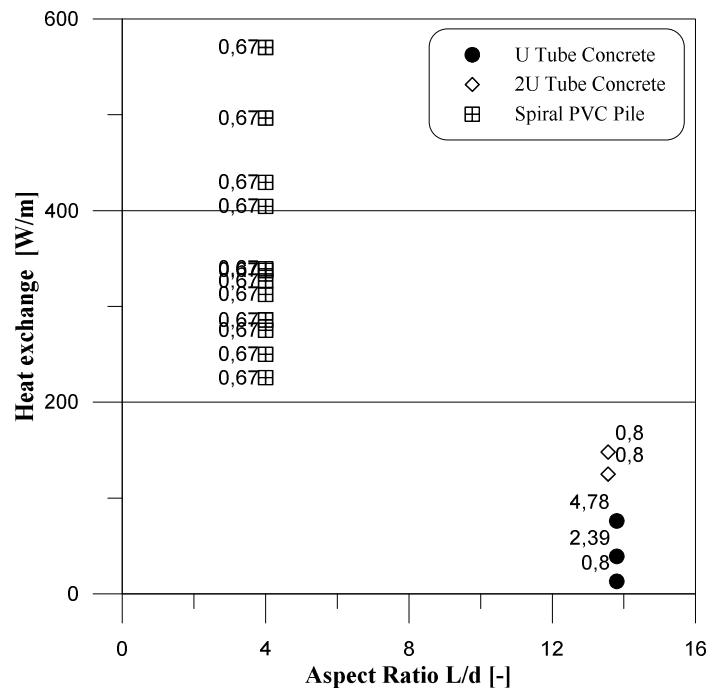


Figure 2-9 – Small-scale results: Heat exchange vs pile aspect ratio for different pipes configurations and pile types. The values of the carrier fluid flow rate during the test are also reported

2.3.5.3 Concrete cover

For concrete piles, the concrete cover between pipes and soil could play a role in the heat exchange rate.

For an EP 600 mm diameter equipped with heat exchangers pipe 25 mm in diameter, the thermal resistance decreased with the number of pipes and increased with the concrete cover decrease

(Loveridge and Powrie 2014). It was observed that the concrete cover was a factor much more important than the number of pipes. In fact, a configuration with many pipes and large cover of concrete had a high thermal resistance. The authors also investigated on the effects of not symmetrical installation of pipes in a 600 mm diameter CFA pile attached to a 40 mm steel bar for installation with a concrete cover of 255 mm. As for the previous case cover of concrete was yet the most important parameter to consider also than the symmetry of pipes. Another parametric analysis was carried out considering the effect of different size of diameters of pile and pipes considering a constant value of concrete cover depth. From the study resulted that smaller pile diameters typically gave lower thermal resistance shape factors but, however, larger piles with a lot of pipes and small cover had a low thermal resistance.

The pile length and number of pipes was the most important parameter combination to energy efficiency of an energy pile. Number of pipes could be chosen independently from structural and geotechnical design but, it was limited by geometrical restraints like pile diameter, concrete cover, the space needed for accommodate several pipes in the pile section and by thermal interaction between the pipes. In fact, reducing the interaction potential is maximized the energy output (Cecinato and Loveridge 2015). Anyway, because thermal performances are non-directly proportional to number of piles as resulted by the numerical analysis of Cecinato et al. (2015), an optimum should be found.

2.3.5.4 The effect of flow rate carrier fluid

An analysis about the best design approach on fluid velocity and pipes diameter considering also economic aspects were carried out in this section.

The heat exchange between carrier fluid and pipes wall is a complex thermal problem that could be simplified considering as an only thing the pipes walls of heat exchangers and surrounding soil, in the case of VBHE, or surrounding concrete, in the case of EPs. In this case, the only factor that could affect the heat exchange is the flow behaviour of the fluid. In fact, it can be laminar or turbulent.

For higher flow rate results an intense turbulent flow and consequently the heat convection between the carrier fluid and pipe wall is enhanced.

Laminar or turbulent flow depends on Reynolds number. If Reynolds number is less than 2300 flow is laminar, from 2300 to 4000 flow is transient while over 4000 flow is turbulent. Reynolds number is the ratio between inertial forces and viscous forces within a fluid (Brandl 2006).

$$Re = \frac{\rho v D}{\mu}$$

Equation 2-15

Where:

v is the velocity [m/s];

ρ is the fluid density [kg/m³]

D is the diameter of pipe [m]

μ dynamic viscosity of the fluid [Kg/ms]

From the formula it is possible to notice that considering the same fluid, a turbulent flow is achieved increasing diameter of pipes, velocity of fluid or both.

Diffusive transfer energy, impulse and mass are increased by turbulence (Brandl 2006).

According to Abdelaziz et al. (2011) laminar or turbulent flow of the carrier fluid in pipes have different effects on temperature distribution in the ground. For laminar flow, the effects can be considered negligible. On the other hand, they result significantly pronounced when the flow becomes turbulent.

From an analytic point of view, in fact, the thermal resistance of the heat carrier fluid that flow inside the pipes is:

$$R_{fluid} = \frac{1}{2\pi r_{inner} L h_{fluid}}$$

Equation 2-16

Where:

r_{inner} is the internal radius of the pipe [m];

L is the EP length [m];

h_{fluid} is the convective heat transfer of the heat carrier fluid [W/m²°C] that is calculated as:

$$h_{fluid} = \frac{Nu \cdot \lambda_{fluid}}{2r_{inner}}$$

Equation 2-17

Where λ_{fluid} is the thermal resistance of the heat carrier fluid [W/m²°C] and Nu is the Nusselt number explained as:

$$Nu = \frac{(f/8) \cdot (Re - 1000) \cdot Pr}{1 + 12,7 \cdot \sqrt{\left(\frac{f}{8}\right)} \cdot (Pr^{2/3} - 1)}$$

Equation 2-18

f is the Darcy friction factor:

$$f = [0,790 \cdot \ln(Re) - 1,64]^{-2}$$

Equation 2-19

Pr is Prandtl number:

$$Pr = \frac{c_{fluid} \cdot \mu_{fluid}}{\lambda_{fluid}}$$

Equation 2-20

Where c_{fluid} is the specific heat of the fluid [J/kg°C] and μ is the dynamic viscosity [Ns/m²]. Re, finally, is the Reynolds number explained before.

From the formula it is possible to notice that the fluid thermal conductivity (the inverse of the resistance) is directly proportional to the convective heat transfer of the heat carrier fluid that depends on Reynolds number.

Flow rate can be changed both by variation of the carrier fluid velocity and by variation of pipe diameter (Batini et al. 2015). A reasonable circulating carrier fluid flow velocity is needed to find to achieve both the thermal performance and economic feasibility. As a matter of fact, the amount of heat exchange is not directly proportional to the flow rate (S. Park et al. 2018). Moreover, a too large velocity brings to an insufficient heat exchange between heat exchangers and the surrounding soil and a waste of electrical energy. Vice versa, a too small velocity bring to a too long time despite sufficient heat transfer without that the total heat exchange will meet the requirements for use (You et al. 2014).

By literature results, it is evident that the increase of heat flow rate is not proportional linearly with the carrier fluid flow rate increase.

You et al. (2014) heating a CFG pile with a constant temperature of 35 °C and three different carrier fluid flow velocities (0,26 m/s, 0,51 m/s, and 1,02 m/s) found final heat exchange flow rate of 84 W/m 116 W/m and 94 W/m respectively. Similar results were obtained by Gao et al. (2008a, 2008b). The authors found that the increased relative heat rejection rate of the W-shaped from half to the reference rate and from the reference to double were 49% and 11%. According to Li et al. (2006) under the same condition of flow rate and inlet temperature, the heat exchange rate of double U-pipes was about 50% higher than that of single U-pipe. A doubled flow rate increased by about 10% thermal flow rate both types of U-pipes. In experiment carried out by Jalaluddin et al. (2011) the increase of carrier fluid flow rate led to an increase of the heat exchange rate of the GHEs. Significantly the heat exchange rate increased from 2 l/min to 4 l/min, but not so much from 4 l/min to 8 l/min.

Batini et al. (2015) (Batini et al. 2015) investigated the effects of different carrier fluid flow rates analysing the variation of the tube diameter and the change of the fluid velocity for different pipes configurations. In the first case, considering a constant velocity of carrier fluid, diameters 25 mm and 40 mm were compared to a reference diameter of 32 mm. In the second case, considering a constant diameter, velocities of the carrier of 0,5 m/s and 1 m/s were compared with a reference velocity of 0,2 m/s. According to the authors, only for the W-shaped pipes configuration was obtained

appreciable results. In fact, thermal power extracted from the soil was gained up to 10% of the heat transfer rate when the diameter of the pipes was increased from 25 to 40 mm. When the velocity increased from 0,2 to 0,5 m/s and from 0,2 to 1 m/s an increase of the heat transfer efficiency of 7% and 11% respectively was observed.

Abdelaziz et al. (2011) observed that while a flow gain from 3 gpm to 15 gpm (laminar flow) led to an increase in power output of 21% (from 1166 W to 1416 W). On the other hand, a flow rate of 40 gpm (turbulent flow) led to an increase of power of 154% (from 1166 W to 2963 W). In addition, according to the authors, for the same flow, the diameter of pipes did not affect the temperature distribution but, after a week of operation, the power output increased by 10-19% considering a pipe diameter of 2,54 cm than 1,90 cm.

Carotenuto et al. (2017) investigated on the influence of the variation of the pipes diameter and the variation of volumetric carrier fluid flow rate on thermal performance of energy piles. As regarding the first case the energy performance increased proportionally to the diameter increase (an increase of 11% of heat transfer passing from a diameter of 20 mm to 40 mm). According to the authors, this phenomenon was due to a larger contact time between fluid and solid domains because the slower velocity of the same fluid flow rate in a larger diameter. In the second case, it was found that an increase of the heat transfer rate was sprung by an increase of the fluid flow rate and a reduction of temperature difference between inlet and outlet fluid was observed. Anyway, benefits in terms of improved thermal performances were not directly proportional to volumetric flow rate and were evident until a value of about 1 m³/h. Indeed, considering a flow rate of 1,0 m³/h than 0,3 m³/h, heat transfer rate increase of about 15% while considering a flow rate of 2,0 m³/h only 3% more was appreciated than 1 m³/h (18%).

Larger diameter of the pipes involved a bigger area of heat exchange, larger diameter had important effects on flow rate and costs aspects should be always considered (Luo et al. 2016).

In the numerical analysis of Cecinato and Loveridge (2015), the fluid velocity and the volumetric flow rate had a negligible effect on thermal performances of the energy piles. The reason was due to the velocities chosen by authors for the parametrical analysis that always gave a Reynolds numbers greater than 8000 and so carrying out the analysis always in turbulent flow. Sensible changes of thermal performances were obtained, instead, for a passage from laminar to turbulent flow.

The effects of flow rate also characterized the results of field tests for steel pile and large diameter concrete piles (Nagano et al. 2005; S. Park et al. 2017). From the comparison between direct circulating heat exchange, U-tube and double U-tube configurations in steel energy piles, Nagano et al (2005) found that, in terms of heat exchange rate, for smaller diameter piles, the double U configuration was better than direct circulating because the presence of the turbulent flow in the U-

tube. In the field test carried out on large-diameter cast-in-place pile by Park et al. (2017)., instead, the authors found that in a thermal test two weeks long, increasing the flow rate in the second week from 1,68 l/m to 2,46 l/m, an increase of 264 W in heat exchange rate was obtained.

In Figure 2-10 and Figure 2-11 the results of heat exchange rate obtained by different authors by field and small-scale tests in function of the carrier fluid flow rate are represented. For some cases also the difference of temperature from pile and soil is represented for small-scale tests. It is observed that for field scale tests, concrete piles equipped with a spiral configuration and a flow rate of about 20 l/min present the better energy performances also for tests in which the initial temperature difference between the surrounding soil and the inlet fluid was not so high. Moreover, it is evident that concrete piles have better performances if compared to steel EP because the same energy performances of concrete energy piles are obtained with the steel piles for values of flow rate 4 or more times greater. More evident is the influence of the flow rate carrier fluid for the small-scale tests. In fact, as can be observed from the trend of the tests on piles equipped with U-shaped configuration, it is possible to notice a linear increasing trend with the increase of the flow rate. Anyway, also in this case, the spiral configuration of the pipes seems to be the better energy solution for the same flow rate if compared to other solutions.

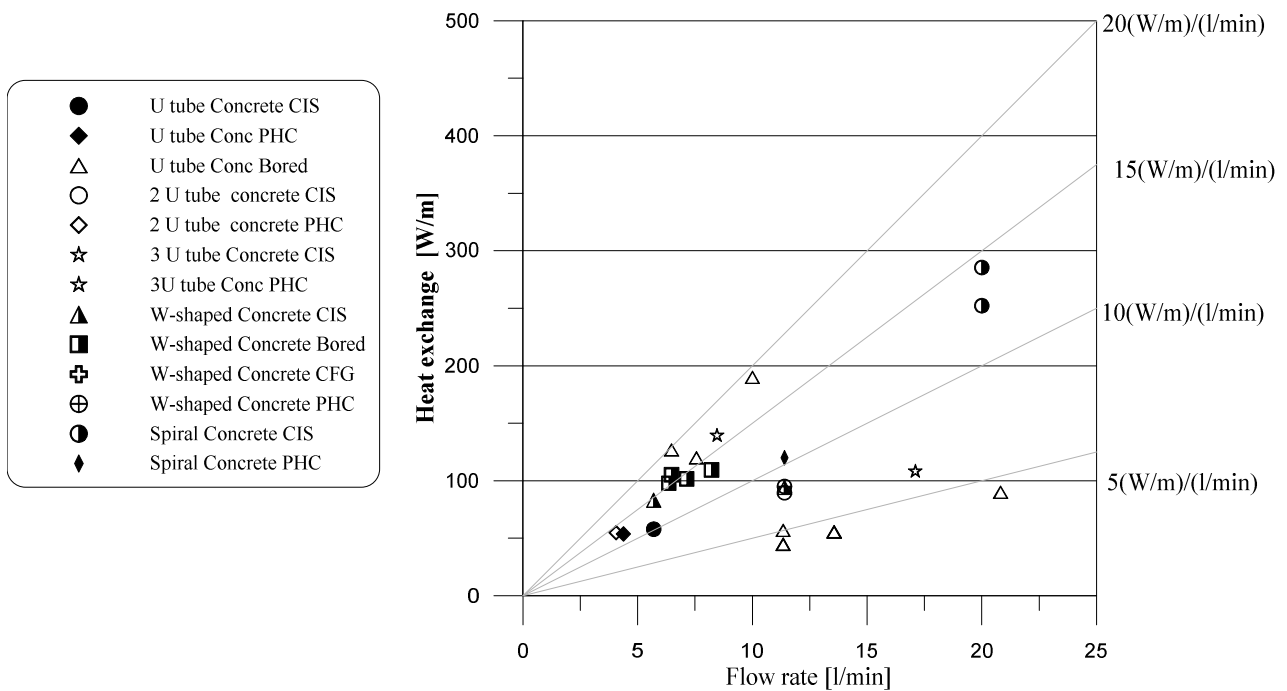


Figure 2-10 – Field test results: Heat exchange vs carrier fluid flow rate for different pipes configurations and pile types.

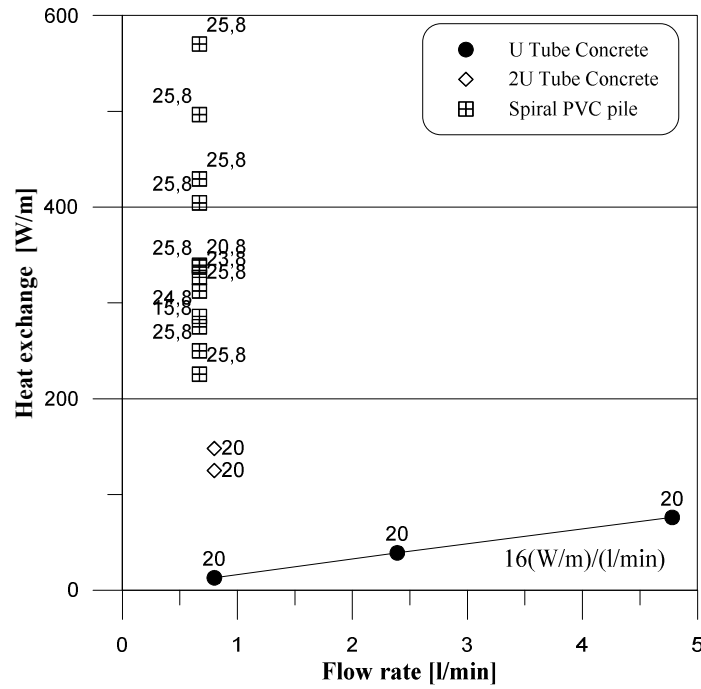


Figure 2-11 - Small-scale results: Heat exchange vs carrier fluid flow rate for different pipes configurations and pile types. The values of the difference of temperature between the pile and soil during the test are also reported

In conclusion, the heat carrier fluid flow rate in heat exchangers is a critical factor for the EPs thermal performances. Anyway, it is a design factor function of other parameters such as thermal loads, characteristic of heat pumps operation costs and so on. Moreover, this analysis evidenced that thermal performances are not proportional to carrier fluid flow rate, but an optimum point is needed to find between performances and operation costs.

2.3.5.5 Thermal conductivity of the pile materials

Increasing foundation thermal conductivity reduces the heating and cooling energy demands of a building (Kwag and Krarti 2013) as shown in Figure 2-12.

The thermal conductivity of the pile materials components also play an important role in the global thermal performances of the EPs.

By the thermal resistance equation, it is possible to calculate the total heat transfer coefficient:

$$U = \frac{1}{R_{tot}}$$

Equation 2-21

$$R_{tot} = R_{fluid} + R_{pipe} + R_{pile} + R_{soil}$$

Equation 2-22

The thermal resistances of fluid and soil were already explained in previous sections.

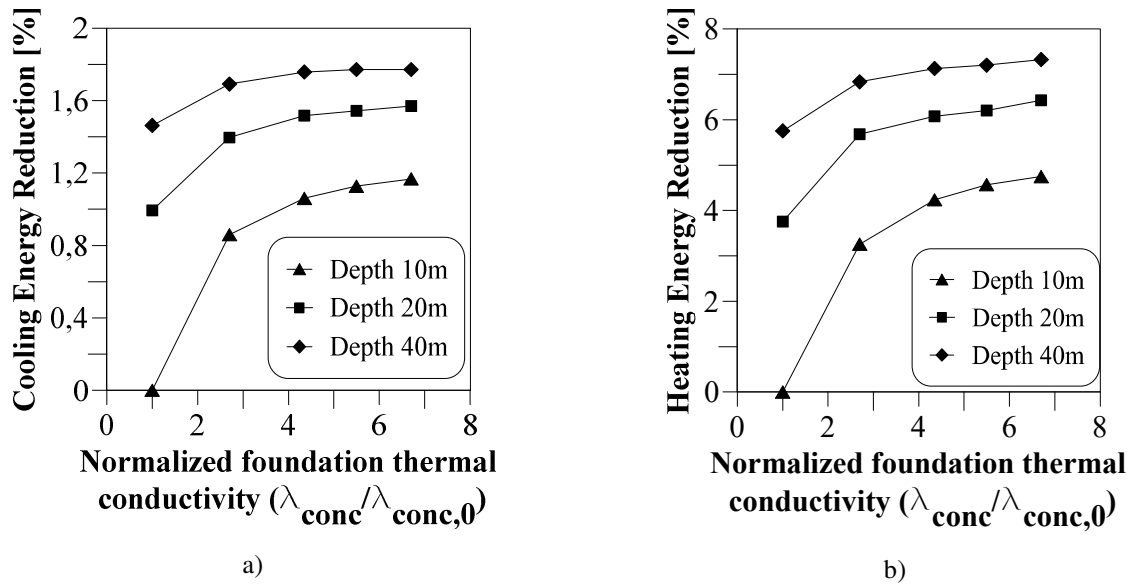


Figure 2-12 - Energy reduction with the increase of concrete thermal conductivity a)in cooling mode b) in heating mode [image replotted from (Kwag and Krarti 2013)]

The thermal resistance of the pipes, can be calculated with the well-known equation of the radial conduction in a cylindrical wall (thermal resistance of a hollow cylinder):

$$R_{pipe} = \frac{\ln\left(\frac{r_{out}}{r_{in}}\right)}{2\pi L \lambda_{pipe}}$$

Equation 2-23

With r_{out} and r_{in} the outer and inner radius of the pipe respectively [m], L is the pipe length [m] and λ_{pipe} is the thermal conductivity of the pipe [W/m°C]. Regarding the latter aspect, usually pipes are made of high-density polyethylene (HDPE) (Brandl 2006). From the literature review of thermal field test carried out during the years, it was observed that pipes the thermal conductivity was a value between 0,35 W/m°C and 0,51 W/m°C.

For the pile, on the other hand, the thermal resistance can be estimated as:

$$R_{pile} = \frac{1}{2\pi L \lambda_{pile}} \ln \frac{r_{EP}}{r_{out} \sqrt{n}}$$

Equation 2-24

With r_{out} the outer radius of the pipe [m], r_{EP} the radius of the pile [m] L is the pile length [m] and λ_{pile} is the thermal conductivity of the pipe [W/m°C] and n the number of the pipes.

Usually, assuming a turbulent flow, R_{fluid} and R_{pipe} tend to be small, in total around 0,01 m°C/W for four pipes in parallel and the greater part of the pile thermal resistance is due to pile construction material (Loveridge and Powrie 2013).

EPs can be built in concrete or steel. Regarding the steel, it is generally an industrial product with well-known and easily available thermal and mechanical properties. The concrete thermal resistance, instead, is strongly affected by its mix design and may change from case to case.

The main factors that influence concrete thermal conductivity are moisture, the specimen's condition, and aggregate volume fraction (Asadi et al. 2018). Anyway, the water/cement ratio and type of admixture result the most effective factors on the concrete thermal conductivity playing a key role in terms of the overall compactness and density of the concrete. It was observed that an increase of density and compactness increase not only the concrete thermal conductivity, but also its mechanical resistance and durability, two aspects very important for deep foundation elements such as EPs.

Because the most important mechanism of heat transfer for concrete is the conduction, the porosity of the mix affects its thermal (and mechanical) properties (Chung et al. 2016).

As a matter of fact, the water, that is present into mix, is responsible for the formation of the voids created after its natural evaporation. Therefore, a lower w/c ratio corresponds to a lower porosity of the concrete.

Considering that steel thermal conductivity and steel density are approximately 50 and 3 times respectively greater than that of concrete, the use of steel fibers may be another aspect to consider into EPs concrete mix design.

The Fiber Reinforced Concrete (FRC) with steel fibers reaches high levels of thermal conductivity, of about 2,0-2,5 W/m°C compared to 1,0-1,3 W/m°C of a concrete without fibers, with increases well above 100%, increasing, moreover the mix density (Adeyanju and Manohar 2011).

Comparing various steel fibers FRCs, Nagy, Nehme and Szagri (2015) found that thermal conductivity values ranged from 2,0 to W/m°C 3,2 W/m°C. These values were gained by the tests carried out by Khaliq and Kodur (2011) on Self Compacting Concrete (SCC) reinforced with steel fiber where the thermal conductivity values ranged from 3,0 W/m°C to 3,5 W/m°C.

The formation of the voids in concrete is also affected by the quantity and size of steel fibers. A large quantity of fibres, indeed, bring to the formation of voids. Too much steel fibers start to decrease the thermal conductivity (Nagy, Nehme, and Szagri 2015).

Anyway, the concrete thermal conductivity increases when voids are filled with water instead than air. Under saturated conditions thermal conductivity increases by at least 50% (Weiping Zhang et al. 2015). Another study (Abdou 2004) provides reports to parameterize the increases in the λ value as a function of the humidity and of the weight of the concrete both due to the absorption of water. Therefore, the same mix design could have two different values of thermal conductivity because of different boundary conditions of the installation. In this case, for example, pile foundations made by concrete directly cast in place in soils below the groundwater table can boast greater thermal performance.

Regarding the relationships between the components of the mix larger the amount of coarse aggregate in a concrete mix the higher the thermal conductivity of the mixture because of the well-known higher

thermal conductivity value of aggregate than other constituents of the concrete mix (Xiao, Song, and Zhang 2010). In addition, also the nature of component plays role in thermal performances (Lie, T.T. Kodur 1996). The more regular molecular structure (crystallinity) of the siliceous aggregate, bring to a higher thermal conductivity if compared to the carbonate aggregate. Even with an increase in the fine aggregate, an increase in thermal conductivity is obtained (Xiao, Song, and Zhang 2010).

Relating the thermal conductivity of SCC concrete with the increase in temperature, for large temperature ranges, thermal conductivity decreases linearly with temperature (Asadi et al. 2018). Anyway, EPs works always in temperature range very lower that compared to those considered in the literature and so the dependence of the conductivity from the temperature may be considered nearly negligible.

By the FE numerical analysis carried out by Di Girolamo et al. (2021) it was observed that the enhance of the pile concrete thermal conductivity, for a short time analysis, do not determine significant axial thermal load variation along the pile shaft. So, the structural performance is not affected by the change of the pile concrete thermal conductivity for short periods of operation.

2.3.5.6 Effect of the operation mode on the heat exchange rate

The operation mode of a GSHP plant depends on the type of building that must be cooled or heated and/or to environmental boundary conditions of the geographical area. For example, for residential building operation mode, generally, is intermittent and the plant work for only some hours for day. Vice versa, if hospitals industrial buildings or commercial buildings are considered, the operation mode of the plant may be continuous for all 24 hours of a day (Faizal, Bouazza, and Singh 2016a).

In literature intermittent and continuous operation mode were compared through field tests, small-scale tests, and numerical model all over the world.

From the review of the different tests carried out it was observed that for continuous operation mode there was a decrease of thermal performances because the heat exchange system tends to steady state with a difference in temperatures between heat carrier fluid of pile and surrounding soil which consequently tends to zero. On the other hand, for intermittent operation mode it was found that it performs better the longer the recovery time between uses.

At the beginning of the operation the heat exchange rates are higher because the constant undisturbed temperature of surrounding soil (Jalaluddin et al. 2011). Over time, the heat exchange from the carrier fluid and soil tends to create a thermal equilibrium between the two media decreasing, consequently the heat exchange.

Vice versa, according to You et al. (2014) the better performances of intermittent mode are to research after that pump stop to working. In fact, the heat exchange between the pile and surrounding soil continue and consequently, the pile tends to return to undisturbed temperature condition. According

to the authors, intermittent operation mode should be considered during the TPT to simulate the real operation of GSHP over the time of their life.

Moreover, considering a long-term view of plant operation, it results that system that works only in one way of heat extraction/injection (only cooling or only heating of the pile and surrounding soil), tends to decrease thermal performances during their life cycle because of the change in temperature of surrounding soil than the undisturbed condition (Sutman et al. 2020).

It is an important aspect which should be considered when designing energy piles for buildings working with continuous operation mode.

2.3.5.7 The inlet temperature: the temperature difference between pile and soil

The thermal resistance and the temperature difference between the pile and the soil are the two main factors affect the heat transfer from the heat carrier fluid inside pipes and the pile edge. Thermal resistance of the soil and of the various components of the pile were already explained in previous sections.

The main mechanism of heat transfer because the pile and the surrounding soil is the conduction (S. Park et al. 2018). Therefore, the heat exchange rate is proportional to the contact area and temperature difference between pile and ground.

$$q = \frac{T_f - T_s}{R_{pile}}$$

Equation 2-25

Where:

R_{pile} is the thermal resistance of an energy pile system ($m^{\circ}C/W$);

T_f is the mean temperature of fluid ($^{\circ}C$);

T_s is the initial ground temperature ($^{\circ}C$);

q is the heat exchange rate per unit pile length (W/m).

Generally, in field TPT, to obtain the heat exchange capacity rate of the geothermal heat exchanger, the operation mode in summer is simulated and heating tests for the pile are carried out.

Operation mode in winter, and so cooling mode for the piles, is not conducted very often because the temperature cannot be controlled easily. As resulted from literature, tests carried out with winter operation mode led to smaller geothermal heat exchanger than in a summer operation mode. If energy pile design is relied solely on heat exchange rate results calculated with a heating test for the pile, may led to a length of the geothermal heat exchanger not long enough for the winter mode. In fact, generally, the difference in temperature between soil and carrier fluid are smaller in winter season (cooling mode for pile) and so, longer heat exchangers or larger area of them could be required to

satisfy the energy needs of upper building because the heat exchange depends on the difference in temperature between soil and carrier fluid (You et al. 2014).

The heat exchange linearly increases with temperature difference increase but, anyway, the heat exchange tends to decrease with time (S. Park et al. 2018). Moreover, while heat rejection rate was strongly influenced to the inlet temperature, the heat resistance was not so sensitive and heat rejection rate increased almost linearly with the increase of inlet temperature (Gao et al. 2008a, 2008b). The same result was found by Li et al. (2006). The authors, in fact, that maintaining a constant carrier fluid flow rate, increasing the inlet temperature from 30 °C to 35 °C increased the heat flow rate of about 20 % for single U-pipes and almost 100% for double U-pipes.

In test carried out by Park S. et al. (2017) it was evident the almost linear dependency of difference in temperature with heat rate for same boundary conditions. As a matter of fact, in a large diameter concrete energy pile, after two weeks of intermittent operation mode, from a difference of 7 °C in heating mode resulted a heat rate injection of 25,5 W/m. On the other hand, in cooling mode, with a difference in temperature of 13,5 °C resulted a heat rate extraction of -55,7 W/m for the same boundary conditions. Some investigations were carried out also in small scale tests. Yang et al. (2016) compared the heat transfer performance of a small-scale pile equipped with a spiral coil pipe under different inlet temperatures. The authors demonstrated that an increase of inlet temperature, in heating mode, led to improve heat transfer performance of spiral coil energy pile. Indeed, the performances were better than 49,9% when the inlet temperature passed from 27 °C to 37 °C. An approximately linearly increases with the inlet temperature was observed for the heat release rate. It should be noted that, the changes in temperature in pile and surrounding soil lead to additional concrete stresses and displacements within the pile-soil system. As a matter of fact, it is one of the most important design parameters for the structural safety to control and verify that do not led to stresses over design safety factors and/or additional displacements that may affects the buildings serviceability (Loveridge and Powrie 2013). Moreover, severe temperature can affect soil properties. In fact, thermal variation on soil inducted by the heat exchange with energy pile, induce a migration of water inside the ground from warmer to colder zones. This process can bring in fine-grained sensitive soils to a gradually shrinkage of the warmer zones and an expansion of the colder. The water pressure is increased by the pore water thermal expansion with a consequent soil effective stress decreasing. The shear resistance is reduced by an increase of temperature because of the reduction of the internal viscosity. As regarding silt and sand it was observed from oedometric tests that for higher temperatures resulted larger settlements. On the other hand, the temperature seems to do not affected affect the load bearing of energy system embedded in clay, even if its organic constituents increase the temperature sensitivity of this kind of soils (Brandl 2006).

Comparing the results of heat exchange obtained in literature with the difference of temperature, both for field scale and small tests, it is possible to notice a certain linear dependence between the difference temperature increase and the thermal flow increase as observed in field scale tests (Figure 2-13 and Figure 2-14). Anyway, both from field and the small-scale tests, it is evident that the pipe configurations play a fundamental role also in this case. In fact, especially for the small-scale tests, were also the value of the flow rate carrier fluid was provided, for the same temperature difference, the U-shaped pipes had the lower energy performance while the spiral configuration the higher. This is more evident in the field scale tests where for a difference of temperature of about 15 °C the large part of the tests record an energy performance under 100 W/m. On the other hand, the spiral configuration has an energy performance over 250 W/m.

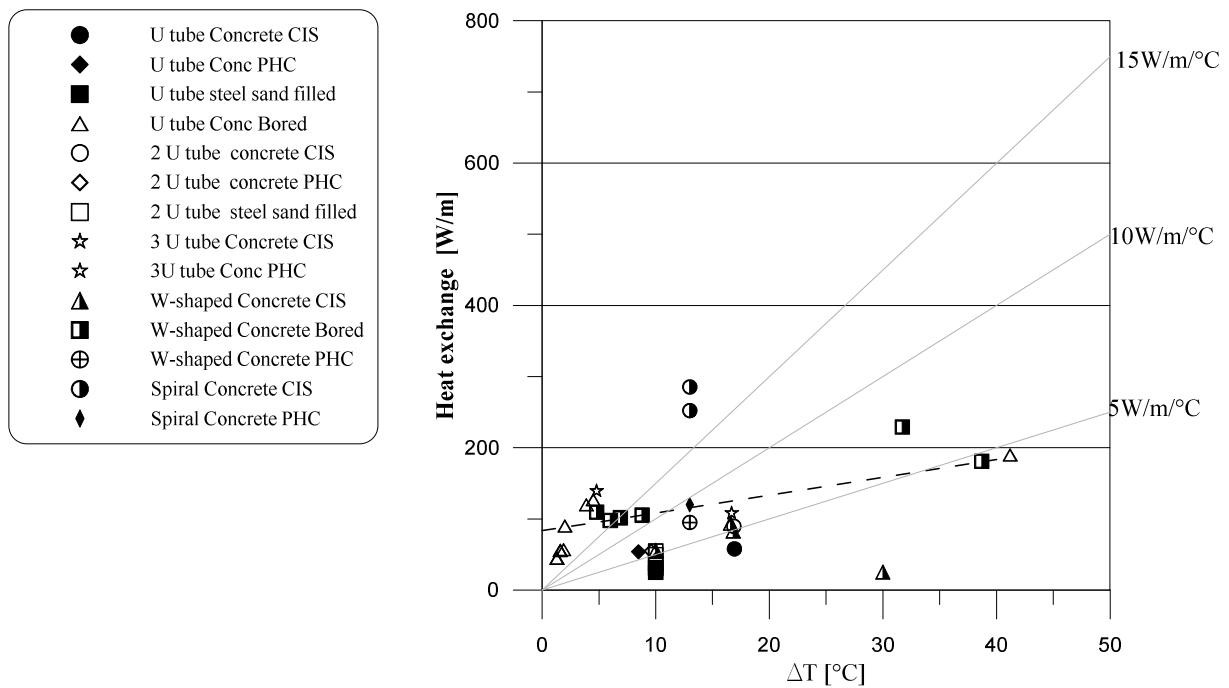


Figure 2-13 - Field test results: Heat exchange vs ΔT for different pipes configurations and pile types

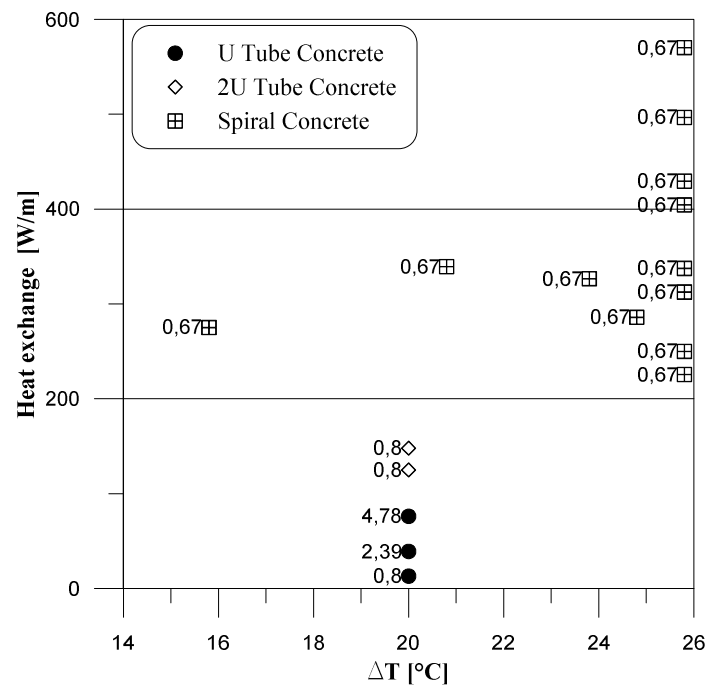


Figure 2-14 - Small-scale results: Heat exchange vs ΔT for different pipes configurations and pile types. Heat carrier fluid flow rate values are also reported in the graph.

2.4 Conclusion

In this chapter a literature review of the mechanical and energy behavior of single energy piles was carried out. Literature results obtained from field tests, small-scale tests and numerical analysis were compared. The chapter was subdivided in two main parts. In the first one the mechanical aspects were reported while in the second one the main aspects about the energy performances were investigated. Regarding the mechanical aspects it was observed that the impact of the additional thermal loads on the pile behavior was very variable both in terms of stress/strain and in terms of displacements and depended above all on the degree of restraint of the pile and by the magnitude of the applied loads. Generally, it was observed that piles with a lower degree of restraint allowed larger displacements and were subjected to lower stress. On the other hand, the opposite happened for pile strongly restrained by the surrounding soil and/or external restrains. In the first case, with low degree of freedom for the pile, the design should be based on admissible displacements of the foundation. Conversely, for the second case, the pile design should be focused on the range of stresses and forced at which the energy pile could be subjected in its life.

It was observed that the energy performances of energy piles depend on the design of some aspects. In this chapter the correlation between the impact of the pipes shapes and the energy performances was crossing with a lot of other parameters such as the pile aspect ratio, the carrier fluid flow rate, the inlet water temperature, the operation mode, the thermal conductivity of the material of the pile and so on. The results highlighted that the Eps energy is strongly influenced by the heat exchangers

surface employed inside the pile. In fact, in any case, the spiral shaped configuration resulted the solution with the best energy performances.

In conclusion, from this literature review it was observed that the design of energy piles is closely linked to the context in which they are to be built, both from a climatic and structural/geotechnical point of view, taking into account also the economic variable. Therefore, a specific design for each individual case is necessary to obtain the maximum yield from this technology.

2.5 References

- Abdelaziz, S. L. Olgun, C. G. Martin II, J.R. 2011. "Design and Operational Considerations of Geothermal Energy Piles." *Geo-Frontiers 2011* © ASCE 2011, 450–59.
- Abdou, A.A. Budaiwi I.M. 2004. "Comparison of Thermal Conductivity Measurements of Building Insulation Materials under Various Operating Temperatures" 29 (2): 171–84. <https://doi.org/10.1177/1744259105056291>.
- Adeyanju, A A, and K Manohar. 2011. "Effects of Steel Fibers and Iron Filings on Thermal and Mechanical Properties of Concrete for Energy Storage Application" 10 (15): 1429–48.
- Akrouch, Ghassan Anis, Marcelo Sánchez, and Jean Louis Briaud. 2014. "Thermo-Mechanical Behavior of Energy Piles in High Plasticity Clays." *Acta Geotechnica* 9 (3): 399–412. <https://doi.org/10.1007/s11440-014-0312-5>.
- Amatya, B. L., K. Soga, P. J. Bourne-Webb, T. Amis, and L. Laloui. 2012. "Thermo-Mechanical Behaviour of Energy Piles." *Geotechnique* 62 (6): 503–19. <https://doi.org/10.1680/geot.10.P.116>.
- Asadi, Iman, Payam Sha, Zahiruddin Fitri, and Bin Abu. 2018. "Thermal Conductivity of Concrete – A Review" 20 (July): 81–93. <https://doi.org/10.1016/j.job.2018.07.002>.
- Batini, Niccolò, Alessandro F. Rotta Loria, Paolo Conti, Daniele Testi, Walter Grassi, and Lyesse Laloui. 2015. "Energy and Geotechnical Behaviour of Energy Piles for Different Design Solutions." *Applied Thermal Engineering* 86: 199–213. <https://doi.org/10.1016/j.applthermaleng.2015.04.050>.
- Bezyan, Behrad, Soheil Porkhial, and Abbasali Aboui Mehrizi. 2015. "3-D Simulation of Heat Transfer Rate in Geothermal Pile-Foundation Heat Exchangers with Spiral Pipe Configuration." *Applied Thermal Engineering* 87: 655–68. <https://doi.org/10.1016/j.applthermaleng.2015.05.051>.
- Bourne-Webb, P. J., B. Amatya, K. Soga, T. Amis, C. Davidson, and P. Payne. 2009. "Energy Pile Test at Lambeth College, London: Geotechnical and Thermodynamic Aspects of Pile Response to Heat Cycles." *Geotechnique* 59 (3): 237–48. <https://doi.org/10.1680/geot.2009.59.3.237>.
- Bourne-Webb, Peter, Sebastien Burlon, Saqib Javed, Sylvia Kürten, and Fleur Loveridge. 2016. "Analysis and Design Methods for Energy Geostructures." *Renewable and Sustainable Energy Reviews* 65: 402–19. <https://doi.org/10.1016/j.rser.2016.06.046>.
- Bourne-Webb, Peter J. 2013. "An Overview of Observed Thermal and Thermo-Mechanical Response of Piled Energy Foundations." *Proc. European Geothermal Conference*, no. June: 1–8.
- Bozis, D., K. Papakostas, and N. Kyriakis. 2011. "On the Evaluation of Design Parameters Effects on the Heat Transfer Efficiency of Energy Piles." *Energy and Buildings* 43 (4): 1020–29.

<https://doi.org/10.1016/j.enbuild.2010.12.028>.

- Brandl, H. 2006. "Energy Foundations and Other Thermo-Active Ground Structures." *Geotechnique* 56 (2): 81–122. <https://doi.org/10.1680/geot.2006.56.2.81>.
- Carotenuto, Alberto, Pasquale Marotta, Nicola Massarotti, Alessandro Mauro, and Gennaro Normino. 2017. "Energy Piles for Ground Source Heat Pump Applications: Comparison of Heat Transfer Performance for Different Design and Operating Parameters." *Applied Thermal Engineering* 124: 1492–1504. <https://doi.org/10.1016/j.applthermaleng.2017.06.038>.
- Carslaw, H S. 1959. "CONDUCTION OF HEAT IN SOLIDS."
- Cecinato, Francesco, and Fleur A. Loveridge. 2015. "Influences on the Thermal Efficiency of Energy Piles." *Energy* 82: 1021–33. <https://doi.org/10.1016/j.energy.2015.02.001>.
- Chung, Sang-yeop, Tong-seok Han, Se-yun Kim, Jang-ho Jay Kim, Kwang Soo, and Jae-hong Lim. 2016. "Evaluation of Effect of Glass Beads on Thermal Conductivity of Insulating Concrete Using Micro CT Images and Probability Functions." *Cement and Concrete Composites* 65: 150–62. <https://doi.org/10.1016/j.cemconcomp.2015.10.011>.
- Di Girolamo, L., Ausiello, G., Russo, G., Marone, G. "High Thermal Conductivity Concrete for Energy Piles". Fib International Conference on Concrete Sustainability. 8-10 September 2021, Prague, czech Republic. (Accepted)
- Elzeiny, Rehab, Muhannad T. Suleiman, Suguang Xiao, Mu’Ath Abu Qamar, and Mohammed Al-Khawaja. 2020. "Laboratory-Scale Pull-out Tests on a Geothermal Energy Pile in Dry Sand Subjected to Heating Cycles." *Canadian Geotechnical Journal* 57 (11): 1754–66. <https://doi.org/10.1139/cgj-2019-0143>.
- Eskilson, P. 1987. "Thermal Analysis of Heat Extraction Boreholes." *Response*, 222.
- Fadejev, Jevgeni, Raimo Simson, Jarek Kurnitski, and Fariborz Haghghat. 2017. "A Review on Energy Piles Design, Sizing and Modelling." *Energy* 122: 390–407. <https://doi.org/10.1016/j.energy.2017.01.097>.
- Faizal, Mohammed, Abdelmalek Bouazza, Chris Haberfield, and John S. McCartney. 2018. "Axial and Radial Thermal Responses of a Field-Scale Energy Pile under Monotonic and Cyclic Temperature Changes." *Journal of Geotechnical and Geoenvironmental Engineering* 144 (10): 04018072. [https://doi.org/10.1061/\(asce\)gt.1943-5606.0001952](https://doi.org/10.1061/(asce)gt.1943-5606.0001952).
- Faizal, Mohammed, Abdelmalek Bouazza, John S. McCartney, and Chris Haberfield. 2019a. "Axial and Radial Thermal Responses of Energy Pile under Six Storey Residential Building." *Canadian Geotechnical Journal* 56 (7): 1019–33. <https://doi.org/10.1139/cgj-2018-0246>.
- Faizal, Mohammed, Abdelmalek Bouazza, John S. McCartney, and Chris Haberfield. 2019b. "Effects of Cyclic Temperature Variations on Thermal Response of an Energy Pile under a Residential Building." *Journal of Geotechnical and Geoenvironmental Engineering* 145 (10): 04019066. [https://doi.org/10.1061/\(asce\)gt.1943-5606.0002147](https://doi.org/10.1061/(asce)gt.1943-5606.0002147).
- Faizal, Mohammed, Abdelmalek Bouazza, and Rao M. Singh. 2016a. "An Experimental Investigation of the Influence of Intermittent and Continuous Operating Modes on the Thermal Behaviour of a Full Scale Geothermal Energy Pile." *Geomechanics for Energy and the Environment* 8: 8–29. <https://doi.org/10.1016/j.gete.2016.08.001>.
- Faizal, Mohammed, Abdelmalek Bouazza, and Rao M. Singh. 2016b. "Heat Transfer Enhancement of Geothermal Energy Piles." *Renewable and Sustainable Energy Reviews* 57: 16–33. <https://doi.org/10.1016/j.rser.2015.12.065>.

- Gao, Jun, Xu Zhang, Jun Liu, Kui Shan Li, and Jie Yang. 2008a. "Thermal Performance and Ground Temperature of Vertical Pile-Foundation Heat Exchangers: A Case Study." *Applied Thermal Engineering* 28 (17–18): 2295–2304. <https://doi.org/10.1016/j.applthermaleng.2008.01.013>.
- Gao, Jun, Xu Zhang, Jun Liu, Kuishan Li, and Jie Yang. 2008b. "Numerical and Experimental Assessment of Thermal Performance of Vertical Energy Piles: An Application." *Applied Energy* 85 (10): 901–10. <https://doi.org/10.1016/j.apenergy.2008.02.010>.
- Goode, J. C., and John S. McCartney. 2015. "Centrifuge Modeling of End-Restraint Effects in Energy Foundations." *Journal of Geotechnical and Geoenvironmental Engineering* 141 (8): 04015034. [https://doi.org/10.1061/\(asce\)gt.1943-5606.0001333](https://doi.org/10.1061/(asce)gt.1943-5606.0001333).
- Hamada, Yasuhiro, Hisashi Saitoh, Makoto Nakamura, Hideki Kubota, and Kiyoshi Ochifuji. 2007. "Field Performance of an Energy Pile System for Space Heating." *Energy and Buildings* 39 (5): 517–24. <https://doi.org/10.1016/j.enbuild.2006.09.006>.
- Hellström, G. 1991. "Ground Heat Storage: Thermal Analyses of Duct Storage Systems." *Lund University*, 310. <http://search.proquest.com/docview/303983441?accountid=14357>.
- Hu, Pingfang, Jing Zha, Fei Lei, Na Zhu, and Tianhua Wu. 2014. "A Composite Cylindrical Model and Its Application in Analysis of Thermal Response and Performance for Energy Pile." *Energy and Buildings* 84: 324–32. <https://doi.org/10.1016/j.enbuild.2014.07.046>.
- Jalaluddin, Akio Miyara, Koutaro Tsubaki, Shuntaro Inoue, and Kentaro Yoshida. 2011. "Experimental Study of Several Types of Ground Heat Exchanger Using a Steel Pile Foundation." *Renewable Energy* 36 (2): 764–71. <https://doi.org/10.1016/j.renene.2010.08.011>.
- Jiang, Gang, Cheng Lin, Dong Shao, Mian Huang, Hongwei Lu, Gen Chen, and Chenfeng Zong. 2021. "Thermo-Mechanical Behavior of Driven Energy Piles from Full-Scale Load Tests." *Energy and Buildings* 233: 110668. <https://doi.org/10.1016/j.enbuild.2020.110668>.
- Kalantidou, Argyro, Anh Minh Tang, J. M. Pereira, and G. Hassen. 2012. "Preliminary Study on the Mechanical Behaviour of Heat Exchanger Pile in Physical Model." *Geotechnique*. <https://doi.org/10.1680/geot.11.T.013>.
- Katsura, T, Y Nakamura, Nippon Steel Engineering, T Okawada, S Hori, and K Nagano. 2009. "Field Test on Heat Extraction or Injection Performance of Energy Piles and Its Application," no. January.
- Khaliq, Wasim, and Venkatesh Kodur. 2011. "Cement and Concrete Research Thermal and Mechanical Properties of Fiber Reinforced High Performance Self-Consolidating Concrete at Elevated Temperatures." *Cement and Concrete Research* 41 (11): 1112–22. <https://doi.org/10.1016/j.cemconres.2011.06.012>.
- Kramer, Cory A., Omid Ghasemi-Fare, and Prasenjit Basu. 2015. "Laboratory Thermal Performance Tests on a Model Heat Exchanger Pile in Sand." *Geotechnical and Geological Engineering* 33 (2): 253–71. <https://doi.org/10.1007/s10706-014-9786-z>.
- Kwag, Byung Chang, and Moncef Krarti. 2013. "Performance of Thermoactive Foundations for Commercial Buildings" 135 (November). <https://doi.org/10.1115/1.4025587>.
- Laloui, Lyesse, Mathieu Nuth, and Laurent Vulliet. 2006. "Experimental and Numerical Investigations of the Behaviour of a Heat Exchanger Pile." *International Journal for Numerical and Analytical Methods in Geomechanics* 30 (8): 763–81. <https://doi.org/10.1002/nag.499>.
- Li, Xinguo, Yan Chen, Zhihao Chen, and Jun Zhao. 2006. "Thermal Performances of Different Types of Underground Heat Exchangers." *Energy and Buildings* 38 (5): 543–47.

<https://doi.org/10.1016/j.enbuild.2005.09.002>.

- Lie, T.T. Kodur, V.K.R. 1996. “Thermal and Mechanical Properties of Lightweight Foamed Concrete at Elevated Temperatures.” *Canadian Journal of Civil Engineering* 23 (4): 511–17. <https://doi.org/10.1680/macrcr.10.00162>.
- Liu, Han long, Cheng long Wang, Gang qiang Kong, Charles W.W. Ng, and Ping Che. 2018. “Model Tests on Thermo-Mechanical Behavior of an Improved Energy Pile.” *European Journal of Environmental and Civil Engineering*. Taylor & Francis. <https://doi.org/10.1080/19648189.2016.1248792>.
- Loveridge, Fleur, C. Guney Olgun, Tracy Brettmann, and William Powrie. 2015. “The Thermal Behaviour of Three Different Auger Pressure Grouted Piles Used as Heat Exchangers.” *Geotechnical and Geological Engineering* 33 (2): 273–89. <https://doi.org/10.1007/s10706-014-9757-4>.
- Loveridge, Fleur, and William Powrie. 2013. “Pile Heat Exchangers: Thermal Behaviour and Interactions.” *Proceedings of the Institution of Civil Engineers: Geotechnical Engineering* 166 (2): 178–96. <https://doi.org/10.1680/geng.11.00042>.
- Loveridge, Fleur, and William Powrie. 2014. “2D Thermal Resistance of Pile Heat Exchangers.” *Geothermics* 50: 122–35. <https://doi.org/10.1016/j.geothermics.2013.09.015>.
- Luo, Jin, Qi Zhang, Haifeng Zhao, Shuqiang Gui, Wei Xiang, Joachim Rohn, and Kenichi Soga. 2019. “Thermal and Thermomechanical Performance of Energy Piles with Double U-Loop and Spiral Loop Heat Exchangers.” *Journal of Geotechnical and Geoenvironmental Engineering* 145 (12): 04019109. [https://doi.org/10.1061/\(asce\)gt.1943-5606.0002175](https://doi.org/10.1061/(asce)gt.1943-5606.0002175).
- Luo, Jin, Haifeng Zhao, Shuqiang Gui, Wei Xiang, Joachim Rohn, and Philipp Blum. 2016. “Thermo-Economic Analysis of Four Different Types of Ground Heat Exchangers in Energy Piles.” *Applied Thermal Engineering* 108: 11–19. <https://doi.org/10.1016/j.applthermaleng.2016.07.085>.
- McCartney, John S., and Kyle D. Murphy. 2012. “Strain Distributions in Full-Scale Energy Foundations (DFI Young Professor Paper Competition 2012).” *DFI Journal - The Journal of the Deep Foundations Institute* 6 (2): 26–38. <https://doi.org/10.1179/dfi.2012.008>.
- McCartney, John S., and Joshua E. Rosenberg. 2011. “Impact of Heat Exchange on Side Shear in Thermo-Active Foundations,” 488–98. [https://doi.org/10.1061/41165\(397\)51](https://doi.org/10.1061/41165(397)51).
- Mehrzi, Abbasali Abouei, Soheil Porkhial, Behrad Bezyan, and Hossein Lotfizadeh. 2016. “Energy Pile Foundation Simulation for Different Configurations of Ground Source Heat Exchanger.” *International Communications in Heat and Mass Transfer* 70: 105–14. <https://doi.org/10.1016/j.icheatmasstransfer.2015.12.001>.
- Mimouni, Thomas, and Lyesse Laloui. 2015. “Behaviour of a Group of Energy Piles.” *Canadian Geotechnical Journal* 52 (12): 1913–29. <https://doi.org/10.1139/cgj-2014-0403>.
- Morino, K., and T. Oka. 1994. “Study on Heat Exchanged in Soil by Circulating Water in a Steel Pile.” *Energy and Buildings* 21 (1): 65–78. [https://doi.org/10.1016/0378-7788\(94\)90017-5](https://doi.org/10.1016/0378-7788(94)90017-5).
- Murphy, K. D., and John S. McCartney. 2015. “Seasonal Response of Energy Foundations During Building Operation.” *Geotechnical and Geological Engineering* 33 (2): 343–56. <https://doi.org/10.1007/s10706-014-9802-3>.
- Murphy, Kyle D., John S. McCartney, and Karen S. Henry. 2015. “Evaluation of Thermo-Mechanical and Thermal Behavior of Full-Scale Energy Foundations.” *Acta Geotechnica* 10 (2): 179–95.

<https://doi.org/10.1007/s11440-013-0298-4>.

- Nagano, Katsunori, T Katsura, Sayaka Takeda, E Saeki, Nippon Steel Corporation, Y Nakamura, A Okamoto, and S Narita. 2005. "Thermal Characteristics of Steel Foundation Piles As Ground Heat Exchangers." *IEA Heat Pump Conference* 8th.
- Nagy, Balázs, Salem Georges Nehme, and Dóra Szagri. 2015. "Thermal Properties and Modeling of Fiber Reinforced Concretes." *Energy Procedia* 78: 2742–47. <https://doi.org/10.1016/j.egypro.2015.11.616>.
- Ng, C. W.W., C. Shi, A. Gunawan, and L. Laloui. 2014. "Centrifuge Modelling of Energy Piles Subjected to Heating and Cooling Cycles in Clay." *Proceedings of the Institution of Civil Engineers: Structures and Buildings* 4: 310–16. <https://doi.org/10.1680/geolett.14.00063>.
- Nguyen, Van Tri, Anh Minh Tang, and Jean Michel Pereira. 2017. "Long-Term Thermo-Mechanical Behavior of Energy Pile in Dry Sand." *Acta Geotechnica* 12 (4): 729–37. <https://doi.org/10.1007/s11440-017-0539-z>.
- Pahud, Daniel, Das Dock, Der Terminal, E Flughafen, and Von Zürich In. 2008. "Measured Thermal Performances of the Dock Midfield Energy Pile System at Zürich Airport." *Proceedings of 9th IEA Heat Pump Conference, 20-22 May 2 (June)*: 1–11.
- Park, Hyunku, Seung Rae Lee, Seok Yoon, and Jung Chan Choi. 2013. "Evaluation of Thermal Response and Performance of PHC Energy Pile: Field Experiments and Numerical Simulation." *Applied Energy* 103: 12–24. <https://doi.org/10.1016/j.apenergy.2012.10.012>.
- Park, Sangwoo, Dongseop Lee, Hyun Jun Choi, Kyoungsik Jung, and Hangseok Choi. 2015. "Relative Constructability and Thermal Performance of Cast-in-Place Concrete Energy Pile: Coil-Type GHEX (Ground Heat Exchanger)." *Energy* 81: 56–66. <https://doi.org/10.1016/j.energy.2014.08.012>.
- Park, Sangwoo, Dongseop Lee, Seokjae Lee, Alexis Chauchois, and Hangseok Choi. 2017. "Experimental and Numerical Analysis on Thermal Performance of Large-Diameter Cast-in-Place Energy Pile Constructed in Soft Ground." *Energy* 118: 297–311. <https://doi.org/10.1016/j.energy.2016.12.045>.
- Park, Sangwoo, Seokjae Lee, Dongseop Lee, Sean S. Lee, and Hangseok Choi. 2016. "Influence of Coil Pitch on Thermal Performance of Coil-Type Cast-in-Place Energy Piles." *Energy and Buildings* 129: 344–56. <https://doi.org/10.1016/j.enbuild.2016.08.005>.
- Park, Sangwoo, Seokjae Lee, Kwanggeun Oh, Dongku Kim, and Hangseok Choi. 2018. "Engineering Chart for Thermal Performance of Cast-in-Place Energy Pile Considering Thermal Resistance." *Applied Thermal Engineering* 130: 899–921. <https://doi.org/10.1016/j.applthermaleng.2017.11.065>.
- Santiago, C De, F Pardo De Santayana, M De Groot, J Urchueguía, B Badenes, T Magraner, J L Arcos, and Francisco Martín. 2016. "Thermo-Mechanical Behavior of a Thermo-Active Precast Pile." *European Geothermal Congress 2016* 48 (E): 41–54. http://gateway.webofknowledge.com/gateway/Gateway.cgi?GWVersion=2&SrcAuth=ORCID&SrcApp=OrcidOrg&DestLinkType=FullRecord&DestApp=WOS_CPL&KeyUT=WOS:000392370100006&KeyUID=WOS:000392370100006.
- Sekine, Kentaro, Ryoza Ooka, Mutsumi Yokoi, and Y Shiba. 1997. "Development of a Ground Source Heat Pump System with Ground Heat Exchanger" 2005 (September): 1–11.
- Sekine, Kentaro, Ryoza Ooka, Mutsumi Yokoi, Yoshiro Shiba, and Suck Ho Hwang. 2007.

- “Development of a Ground-Source Heat Pump System with Ground Heat Exchanger Utilizing the Cast-in-Place Concrete Pile Foundations of Buildings.” *ASHRAE Transactions* 113 PART 1: 558–66.
- Singh, Rao Martand, Abdelmalek Bouazza, and Bill Wang. 2015. “Near-Field Ground Thermal Response to Heating of a Geothermal Energy Pile: Observations from a Field Test.” *Soils and Foundations* 55 (6): 1412–26. <https://doi.org/10.1016/j.sandf.2015.10.007>.
- Singh, Rao Martand, Abdelmalek Bouazza, Bill Wang, C. H. Haberfield, S. Baycan, and Y. Carden. 2015. “Thermal and Thermo-Mechanical Response of a Geothermal Energy Pile.” *World Geothermal Congress 2015*, no. April: 7.
- Stewart, Melissa A., and John S. McCartney. 2012. “Strain Distributions in Centrifuge Model Energy Foundations,” no. 2006: 4376–85. <https://doi.org/10.1061/9780784412121.450>.
- Stewart, Melissa A., and John S. McCartney. 2014. “Centrifuge Modeling of Soil-Structure Interaction in Energy Foundations.” *Journal of Geotechnical and Geoenvironmental Engineering* 140 (4): 04013044. [https://doi.org/10.1061/\(asce\)gt.1943-5606.0001061](https://doi.org/10.1061/(asce)gt.1943-5606.0001061).
- Suryatriyastuti, M. E., H. Mroueh, and S. Burlon. 2012. “Understanding the Temperature-Induced Mechanical Behaviour of Energy Pile Foundations.” *Renewable and Sustainable Energy Reviews* 16 (5): 3344–54. <https://doi.org/10.1016/j.rser.2012.02.062>.
- Sutman, Melis, Tracy Brettmann, and C. Guney Olgun. 2019. “Full-Scale in-Situ Tests on Energy Piles: Head and Base-Restraining Effects on the Structural Behaviour of Three Energy Piles.” *Geomechanics for Energy and the Environment* 18: 56–68. <https://doi.org/10.1016/j.gete.2018.08.002>.
- Sutman, Melis, C. Guney Olgun, and Tracy Brettmann. 2015. “Full-Scale Field Testing of Energy Piles,” 1638–47. <https://doi.org/10.1061/9780784479087.148>.
- Sutman, Melis, Gianluca Speranza, Alessio Ferrari, Pyrène Larrey-Lassalle, and Lyesse Laloui. 2020. “Long-Term Performance and Life Cycle Assessment of Energy Piles in Three Different Climatic Conditions.” *Renewable Energy* 146: 1177–91. <https://doi.org/10.1016/j.renene.2019.07.035>.
- Wang, B., A. Bouazza, R. M. Singh, D. Barry-Macaulay, C. Haberfeld, G. Chapman, and S. Baycan. 2013. “Field Investigation of a Geothermal Energy Pile: Initial Observations.” *18th International Conference on Soil Mechanics and Geotechnical Engineering: Challenges and Innovations in Geotechnics, ICSMGE 2013* 4: 3415–18.
- Wang, Bill, Abdelmalek Bouazza, Rao Martand Singh, Chris Haberfield, David Barry-Macaulay, and Serhat Baycan. 2015. “Posttemperature Effects on Shaft Capacity of a Full-Scale Geothermal Energy Pile.” *Journal of Geotechnical and Geoenvironmental Engineering* 141 (4): 04014125. [https://doi.org/10.1061/\(asce\)gt.1943-5606.0001266](https://doi.org/10.1061/(asce)gt.1943-5606.0001266).
- Wang, Cheng-long, Han-long Liu, Gang-qiang Kong, and Charles Wang Wai Ng. 2017. “Different Types of Energy Piles with Heating–Cooling Cycles.” *Proceedings of the Institution of Civil Engineers - Geotechnical Engineering* 170 (3): 220–31. <https://doi.org/10.1680/jgeen.16.00061>.
- Wang, Cheng long, Charles W.W. Ng, Han long Liu, Di Wu, and Gang qiang Kong. 2016. “Model Tests of Energy Piles with and without a Vertical Load.” *Environmental Geotechnics* 3 (4): 203–13. <https://doi.org/10.1680/jenge.15.00020>.
- Wood, C. J., H. Liu, and S. B. Riffat. 2010. “Comparison of a Modelled and Field Tested Piled Ground Heat Exchanger System for a Residential Building and the Simulated Effect of Assisted

- Ground Heat Recharge.” *International Journal of Low-Carbon Technologies* 5 (3): 137–43. <https://doi.org/10.1093/ijlct/ctq015>.
- Wood, Christopher J., Hao Liu, and Saffa B. Riffat. 2010. “An Investigation of the Heat Pump Performance and Ground Temperature of a Piled Foundation Heat Exchanger System for a Residential Building.” *Energy* 35 (12): 4932–40. <https://doi.org/10.1016/j.energy.2010.08.032>.
- Wood, Christopher J., Hao Liu, and Saffa B. Riffat. 2012. “Comparative Performance of ‘U-Tube’ and ‘Coaxial’ Loop Designs for Use with a Ground Source Heat Pump.” *Applied Thermal Engineering* 37: 190–95. <https://doi.org/10.1016/j.applthermaleng.2011.11.015>.
- Wu, Di, Hanlong Liu, Gangqinag Kong, and Chao Li. 2019. “Thermo-Mechanical Behavior of Energy Pile under Different Climatic Conditions.” *Acta Geotechnica* 14 (5): 1495–1508. <https://doi.org/10.1007/s11440-018-0731-9>.
- Xiao, Jian Zhuang, Zhi Wen Song, and Feng Zhang. 2010. “An Experimental Study on Thermal Conductivity of Concrete.” *Jianzhu Cailiao Xuebao/Journal of Building Materials* 13 (1): 17–21. <https://doi.org/10.3969/j.issn.1007-9629.2010.01.004>.
- Yang, Weibo, Pengfei Lu, and Yongping Chen. 2016. “Laboratory Investigations of the Thermal Performance of an Energy Pile with Spiral Coil Ground Heat Exchanger.” *Energy and Buildings* 128: 491–502. <https://doi.org/10.1016/j.enbuild.2016.07.012>.
- Yavari, N., A. M. Tang, J. M. Pereira, and G. Hassen. 2016. “Mechanical Behaviour of a Small-Scale Energy Pile in Saturated Clay.” *Géotechnique* 66 (11): 878–87. <https://doi.org/10.1680/jgeot.15.t.026>.
- Yavari, Neda, Anh Minh Tang, Jean Michel Pereira, and Ghazi Hassen. 2014. “Experimental Study on the Mechanical Behaviour of a Heat Exchanger Pile Using Physical Modelling.” *Acta Geotechnica* 9 (3): 385–98. <https://doi.org/10.1007/s11440-014-0310-7>.
- Yoon, Seok, Seung Rae Lee, Jianfeng Xue, Kai Zosseder, Gyu Hyun Go, and Hyunku Park. 2015. “Evaluation of the Thermal Efficiency and a Cost Analysis of Different Types of Ground Heat Exchangers in Energy Piles.” *Energy Conversion and Management* 105: 393–402. <https://doi.org/10.1016/j.enconman.2015.08.002>.
- You, Shuang, Xiaohui Cheng, Hongxian Guo, and Zhiquan Yao. 2014. “In-Situ Experimental Study of Heat Exchange Capacity of CFG Pile Geothermal Exchangers.” *Energy and Buildings* 79: 23–31. <https://doi.org/10.1016/j.enbuild.2014.04.021>.
- You, Shuang, Xiaohui Cheng, Hongxian Guo, and Zhiquan Yao. 2016. “Experimental Study on Structural Response of CFG Energy Piles.” *Applied Thermal Engineering* 96: 640–51. <https://doi.org/10.1016/j.applthermaleng.2015.11.127>.
- Zarella, Angelo, Michele De Carli, and Antonio Galgaro. 2013. “Thermal Performance of Two Types of Energy Foundation Pile: Helical Pipe and Triple U-Tube.” *Applied Thermal Engineering* 61 (2): 301–10. <https://doi.org/10.1016/j.applthermaleng.2013.08.011>.
- Zarella, Angelo, Giuseppe Emmi, Samantha Graci, Michele De Carli, Matteo Cultrera, Giorgia Dalla Santa, Antonio Galgaro, et al. 2017. “Thermal Response Testing Results of Different Types of Borehole Heat Exchangers: An Analysis and Comparison of Interpretation Methods.” *Energies* 10 (6): 0–18. <https://doi.org/10.3390/en10060801>.
- Zhang, Changxing, Zhanjun Guo, Yufeng Liu, Xiaochun Cong, and Donggen Peng. 2014. “A Review on Thermal Response Test of Ground-Coupled Heat Pump Systems.” *Renewable and Sustainable Energy Reviews* 40: 851–67. <https://doi.org/10.1016/j.rser.2014.08.018>.

- Zhang, Hezhi, and Zhenqian Chen. 2017. "Study on Heat Transfer Performance of Energy Pile in GSHP System." *Procedia Engineering* 205: 2393–2400. <https://doi.org/10.1016/j.proeng.2017.09.861>.
- Zhang, Weiping, Hongguang Min, Xianglin Gu, Yunping Xi, and Yishan Xing. 2015. "Mesoscale Model for Thermal Conductivity of Concrete." *Construction and Building Materials* 98: 8–16. <https://doi.org/10.1016/j.conbuildmat.2015.08.106>.
- Zhang, Wenke, Ping Cui, Junhong Liu, and Xueting Liu. 2017. "Study on Heat Transfer Experiments and Mathematical Models of the Energy Pile of Building." *Energy and Buildings* 152: 643–52. <https://doi.org/10.1016/j.enbuild.2017.07.041>.
- Zhao, Qiang, Baoming Chen, and Fang Liu. 2016. "Study on the Thermal Performance of Several Types of Energy Pile Ground Heat Exchangers: U-Shaped, W-Shaped and Spiral-Shaped." *Energy and Buildings* 133: 335–44. <https://doi.org/10.1016/j.enbuild.2016.09.055>.
- Zhao, Qiang, Fang Liu, Chunwei Liu, Maocheng Tian, and Baoming Chen. 2017. "Influence of Spiral Pitch on the Thermal Behaviors of Energy Piles with Spiral-Tube Heat Exchanger." *Applied Thermal Engineering* 125 (July 2017): 1280–90. <https://doi.org/10.1016/j.applthermaleng.2017.07.099>.

Chapter 3

3 Applications of EP in Neapolitan context

3.1 Introduction

In this chapter, an overview on the soils and climate main characteristic of the Neapolitan context were presented. The aim was to introduce the issue of geotechnical and energy design of energy piles within the well-defined context of the city of Naples. In this regard, an initial analysis of the geological and geotechnical aspects of the Neapolitan subsoil was carried out, summarizing the main mechanical and thermal characteristics of the main geological formations in the examined area. Then, a brief analysis about the Mediterranean and Neapolitan climate context was introduced. These aspects were fundamental to analyze the energy demand and the energy design of geothermal energy pumps and energy piles for a sample building in Neapolitan context. As a matter of fact, in the literature review chapter it was outlined that many researches on the energy piles do not take into account realistic energy demand and temperature conditions

3.2 The geological context of the city of Naples

Naples is a city of the Campania Region located on the western coast of the south of Italy facing the Tyrrhenian Sea. It is a zone characterized by the presence of three volcanos. Ischia Island, Campi Flegrei and the Somma-Vesuvius are the most important volcanic structures surrounding the study area. The volcanic activity that has taken place over the millennia has in fact characterized the Neapolitan geological context and the stratigraphic succession is the result of the superimposition of different eruptive events.



Figure 3-1 - Location of the city of Naples and surrounding volcanic structures

The most ancient geological formations are the Campanian Ignimbrite (35000 years b.p.) that cover an area of approximately 10000 km² with thickness often exceeding 50 m, Ancient Neapolitan Yellow

Tuff (35000-12000 years b.p.), Neapolitan Yellow Tuff (12000 years b.p.) that cover an area approximately of 300 km² and finally the pyroclastic sandy soils from the last Phlegrean activity (<12000 years b.p.) that can have variable thickness from a few meters to a few tens of meters (Aversa et al. 2013).

In the urban area of Naples, it is possible to find both lithified and unlithified facies of pyroclastic deposits, the unlithified Neapolitan Yellow Tuff, also called Pozzolana (NYP), and the Intracaldera Phlegrean pyroclastic Deposits (IPD) i.e. Campi Flegrei pyroclastic products younger than 15 ky. The Neapolitan Yellow Tuff present different degree of cementation also depending on the distance of the pyroclastic deposit from the Campi Flegrei volcano. On the other hand, the thickness reached by the IPD can vary from 20 m for the areas closest to the Campi Flegrei to only a few meters for the furthest areas (Picarelli et al. 2006).

It should be noted that the pyroclastic deposits of the Neapolitan subsoil do not exclusively characterize the geotechnical behavior of the city. In fact, over the centuries, they Yellow Tuff has been largely quarried and used as construction material in squared blocks.

On the other hand, also Pozzolana had a wide use already in the Roman era. In fact, Roman *opus caementicium* structures were originally made with mortars of aerial lime and sand. This type of mixture did not guarantee great mechanical performance and, above all, could not be used for works in which curing had to take place in anaerobic conditions, as for example in constructions in contact with water or underwater. The ancient Romans solved this problem by using *Pulvis Puteolana* (Pozzolana). Although pozzolana is a sand, it does not behave like a simple inert material. It is, in fact, capable of reacting with the lime present in the mixture and producing chemical reactions for which the presence of CO₂ is no longer necessary for the setting and hardening phases. Finally, the resulting compound had a porous binder matrix that was more compact compared to binders with only hydraulic lime. This resulted in a much stronger and more durable mixture.

In next sections the mechanical and thermal properties of the three main pyroclastic deposit of the city of Naples are discussed.

3.2.1 Lithified facies: the Neapolitan Yellow Tuff.

In this section just some information on the Neapolitan Yellow Tuff features and behaviors as deduced by some major research paper on the topic. Both mechanical and thermal properties are briefly described.

An ashy matrix, pumices and/or scoriae inclusions (highly porous) and lithic inclusions are the main components of the lithified Neapolitan Yellow Tuff. As shown from various tests carried out on this material, it was observed that dry density strongly affected the uniaxial compressive strength (Figure 3-2). Higher mechanical capacities were achieved for higher dry densities. However, as different

values of mechanical capacity were recorded for the same density, the structure of the material also seemed to play a key role (Evangelista 2000).

Two different stress domains characterized the behavior of this soft rock. In fact, as shown the results obtained from triaxial test the NYT exhibited a so called “rock-like behavior” and a “soil-like behavior” (Picarelli et al. 2006). The former was typical for tests at small stress states while the latter was shown for tests with high confining stress state. The so called destructuration phenomenon (Leroueil and Vaughan 1990), i.e. the progressive transformation of the rock into fragments assembly because of the bonds breaking, is associated to the transition between the two kind of behaviors. The friction angle for this material is between 22° and 30°.

The soaking of the soft rock in the water provided material volumetric strain inversely proportional to the initial degree of saturation of the tuff specimen (Evangelista 1980). It was also observed that the saturation provided a reduction of the peak strength and a contraction of the elastic domain. According to the author it was attributed to suction decrease and to interaction of water and zeolitic minerals.

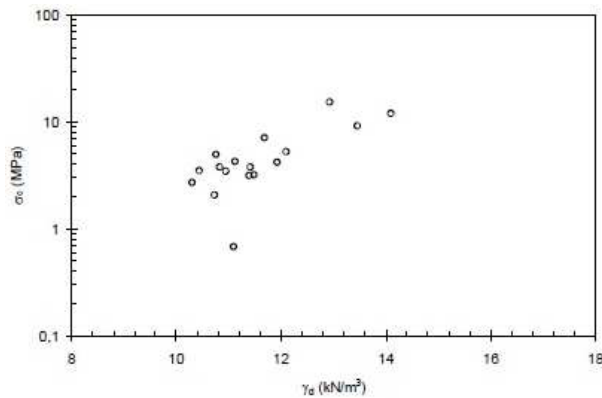


Figure 3-2 Lithified Neapolitan Yellow Tuff: uniaxial compressive strength vs. dry density. After (Picarelli et al. 2006)

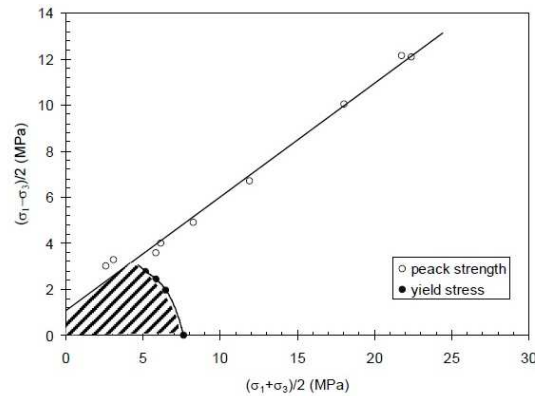


Figure 3-3 - Lithified Neapolitan Yellow Tuff: “rock-like behaviour” and “soil-like behaviour domains”. After (Picarelli et al. 2006)

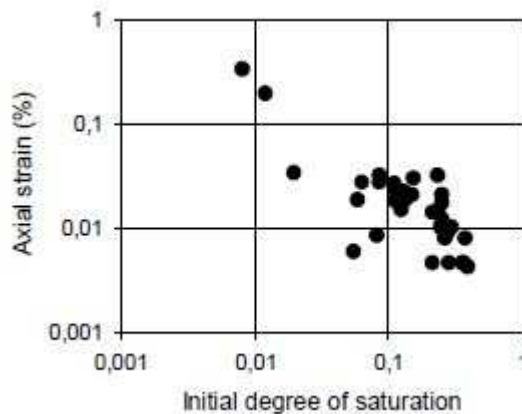


Figure 3-4 - Uniaxial expansion in function of degree of saturation for lithified tuff. After (Picarelli et al. 2006)

The thermal characteristics of Neapolitan Yellow Tuff have been extrapolated from the literature. From the study carried out by Colombo (Colombo 2010) the minimum and the maximum values of main thermal characteristics were obtained for this material. The values are summarized in Table 3-1.

Table 3-1 – Yellow Neapolitan Tuff thermal conductivity after (Colombo 2010)

	min	Max
Thermal conductivity of soil particles [W/m°C]	4,500	4,500
Thermal conductivity of dry soil [W/m°C]	0,160	0,160
Thermal conductivity saturated soil not frozen [W/m°C]	1,470	1,500
Thermal conductivity saturated soil frozen [W/m°C]	3,060	3,080

Aversa and Evangelista (Aversa and Evangelista 1993) carried out a study on the thermal expansion of the Neapolitan yellow tuff. Some different tests were carried out by the authors. The thermal expansion coefficient was determined for drained conditions when the material was saturated with water. From the analysis resulted an average thermal expansion coefficient of $5 \times 10^{-5} \text{ }^\circ\text{C}^{-1}$.

3.2.2 Unlithified facies: Neapolitan Pozzolana and Intracaldera Phlegrean pyroclastic Deposits

In this section as for the Yellow tuff a short description of the main features of the volcanic uncemented material as Pozzolana and IPD are summarized starting from some major research paper on the topic. Both mechanical and thermal properties are briefly described.

Pozzolana deposits are intended as an uncemented deposit. Typical grain size distribution for Pozzolana and IPD deposits are reported in figure 5 and 6 respectively. In Figure 3-7 and Figure 3-8 the main physical property of the Pozzolana and of IPD are summarized for a typical subsoil in the city area (Picarelli et al. 2006). In any case, except than for the sandy silt, the clay fraction is usually less than 10%. On the other hand, except than for the sandy gravel the sandy friction is usually less than 40% (Figure 3-6). According to authors the way the material was originated was the cause of this variability. A collection of standard oedometer tests on unsaturated specimens for Pozzolana is reported in Figure 3-9. In Figure 3-10 results of 125 standard triaxial compression tests on natural samples are summarized. The tests were subdivided in four categories depending on the initial dry unit weight. It can be noticed that after a certain initial dry unit weight the linear regression show a significant cohesive intercept of the strength linear envelope. Because it was assumed the absence of cementation bonds it could depend on the combined effect of expansion and matric suction.

Some direct shear tests (Nicotera 1998; 2000) to study the mechanical behavior of Pozzolana upon wetting are also reported. Two different tests were performed. In a kind test the natural specimen wetted during the test at the peak strength, in the other kind the natural specimen saturated in the

consolidation stage. Three different vertical stresses were used for the tests. The results of the test are reported in Figure 3-11. It was observed that the specimens with a natural content of water showed a brittle behavior for lower and medium vertical stress levels while a hardening behavior was noticed for higher vertical stress or for saturated specimens. Moreover, wetting the sample at the peak strength caused a sudden and relevant decrease of it and a volumetric compression.

Regarding the IPD the shear strength was determined from the results of 175 triaxial tests (CID) both on specimens with natural water content (132) and on saturated specimens (43). The test carried out on saturated specimens showed a brittle and dilative behavior in case of dense specimens and ductile and contractive behavior for loose specimens. Anyway, the initial degree of saturation affected the behavior of specimens. In fact, as shown in Figure 3-12 for a same specimen subjected to the same test only the unsaturated showed the peak strength. As for the case of the Pozzolana, also for the IPD triaxial tests were carried out subdividing the specimens in four categories depending on the dry unit weight. Also, for this case was noticed that the peak friction increased the density increased. It was noticed that the value of the critical angle was approximately 35° (Figure 3-13).

Moreover, direct shear tests were carried out on IPD specimens. Four types of test were considered. One was carried out on specimens wetted at the peak strength during the shear test, another was carried out on specimens saturated in the consolidation stage, the third carried out on specimens at their natural content and finally tests carried out on specimens dried in the pressure plate apparatus at different matric suction values (Scotto di Santolo, 2000). In Figure 3-14 the results of the shear test for different saturation condition are shown. It was noticed that increasing the degree of saturation the behavior of the specimen tends to pass from brittle to ductile and that wetting the specimen at the peak caused a relevant strength to decrease and a volume compression. Continuing with the test a progressive recovery of the shear strength until a steady state value was observed.

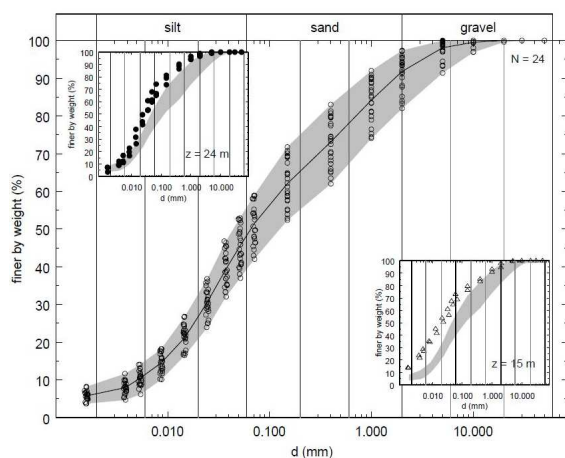


Figure 3-5 - Pozzolana grain size distribution. After (Picarelli et al. 2006)

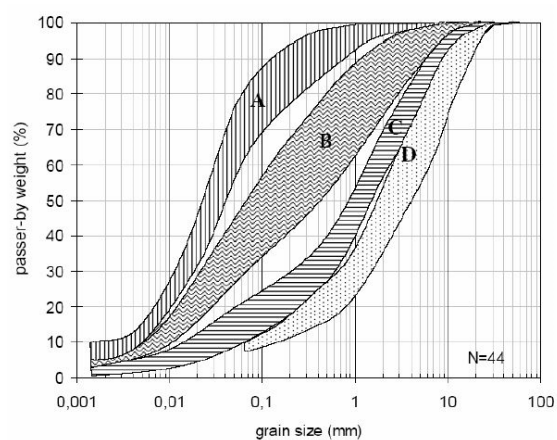


Figure 3-6 - IPD grain size distribution. After (Picarelli et al. 2006)

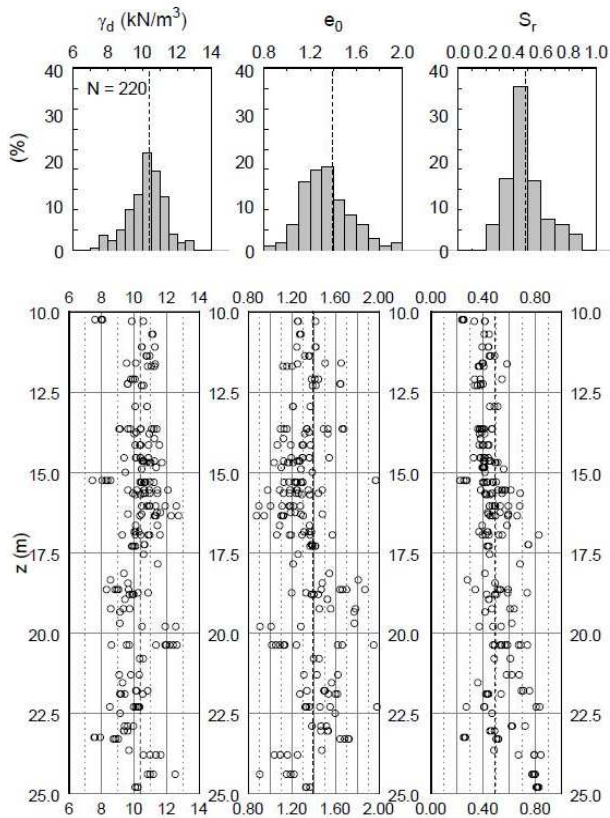


Figure 3-7 - Pozzolana main physical property. After (Picarelli et al. 2006)

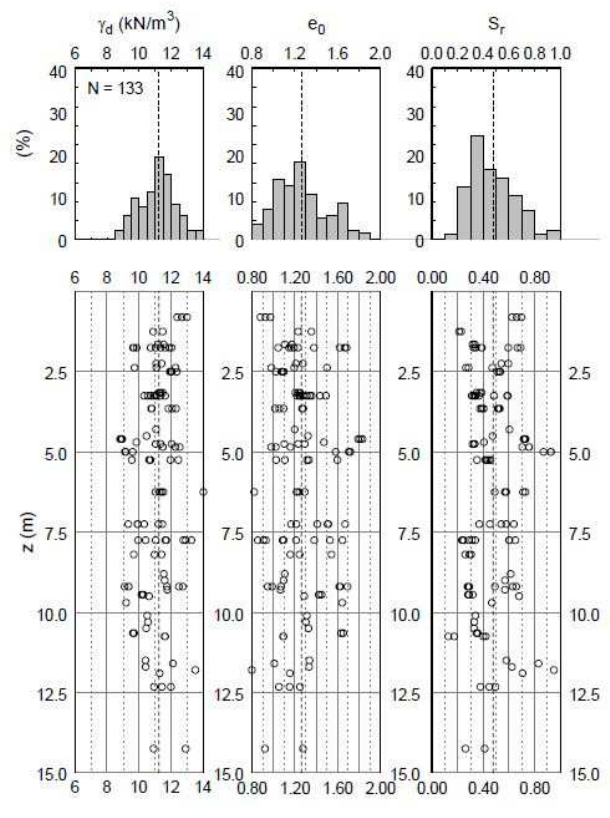


Figure 3-8 - IPD main physical property. After (Picarelli et al. 2006)

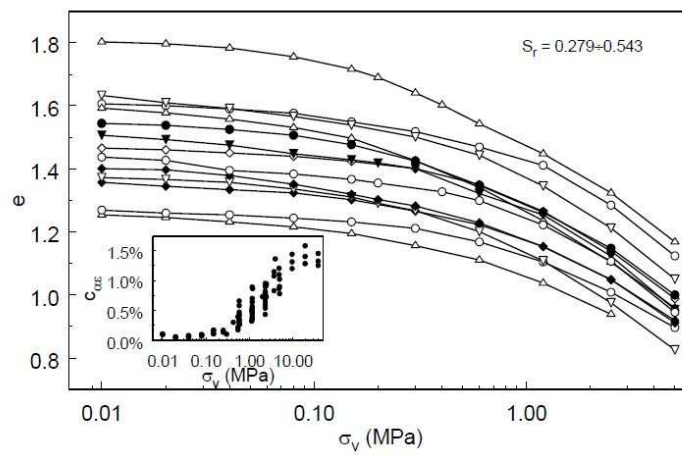


Figure 3-9 - Standard oedometric tests on unsaturated pozzolana after (Picarelli et al. 2006)

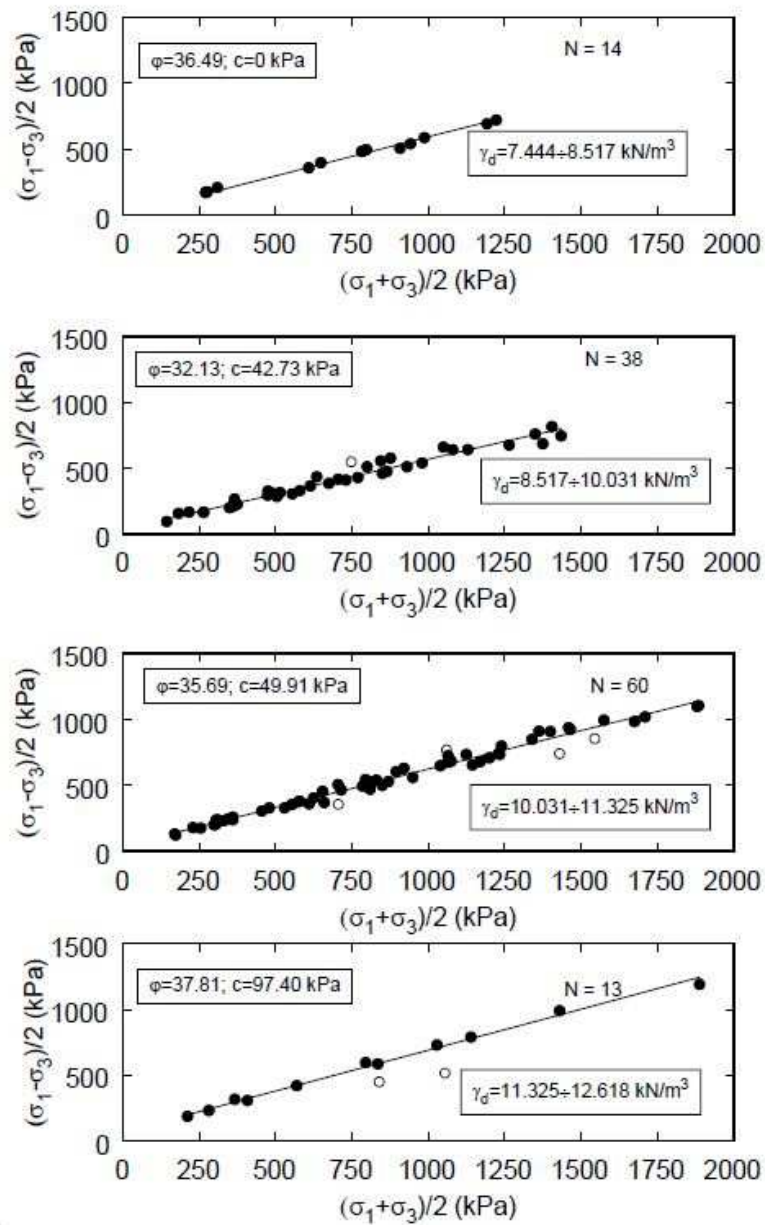


Figure 3-10 - Strength envelopes for unsaturated undisturbed pozzolana specimens. the empty circles indicate outliers data identified by the regression analysis. After (Picarelli et al. 2006)

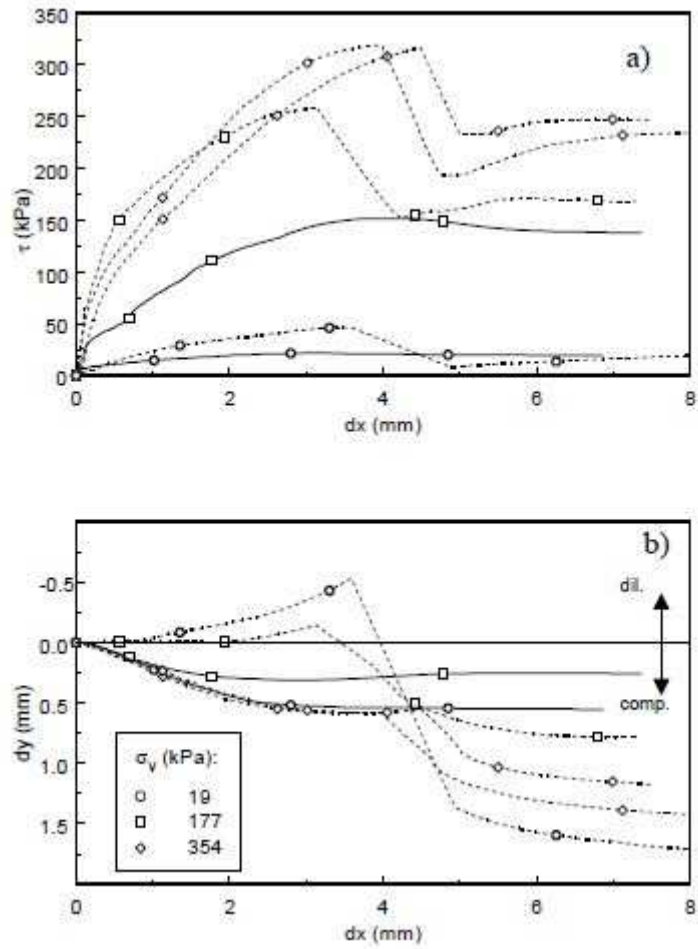


Figure 3-11 - Pozzolana direct shear test results. With the continuous line the saturated specimens are represented, with the dashed line specimens wetted at peak are represented. After (Picarelli et al. 2006)

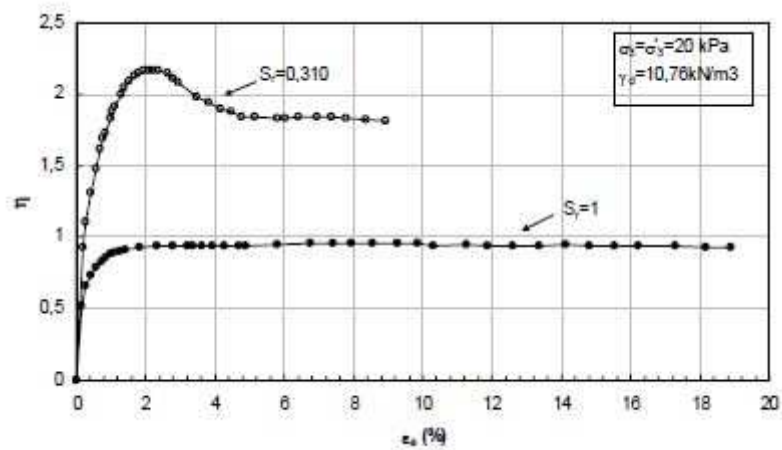


Figure 3-12 - Stress-strain response in triaxial test of two specimens of IPD with the same dry density and different degree of saturation. After (Picarelli et al. 2006)

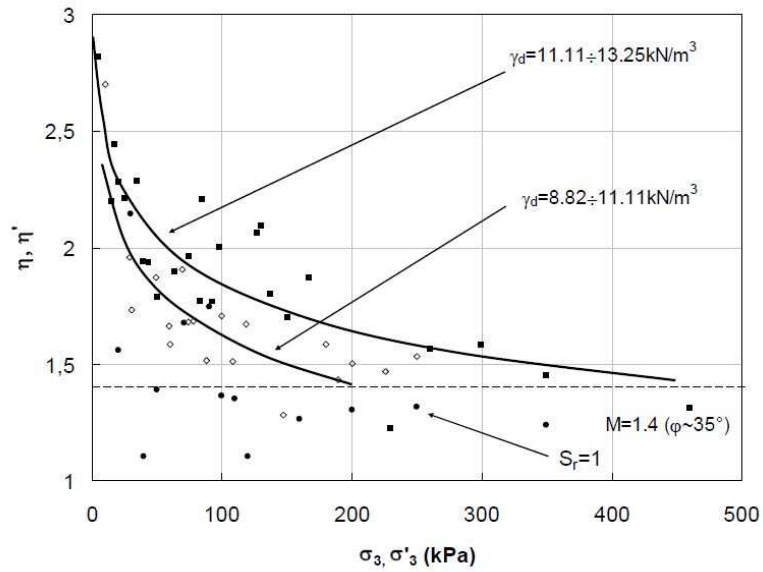


Figure 3-13 – Stress ratio vs confining stress for IPD specimens characterized by a different density and degree of saturation. After (Picarelli et al. 2006)

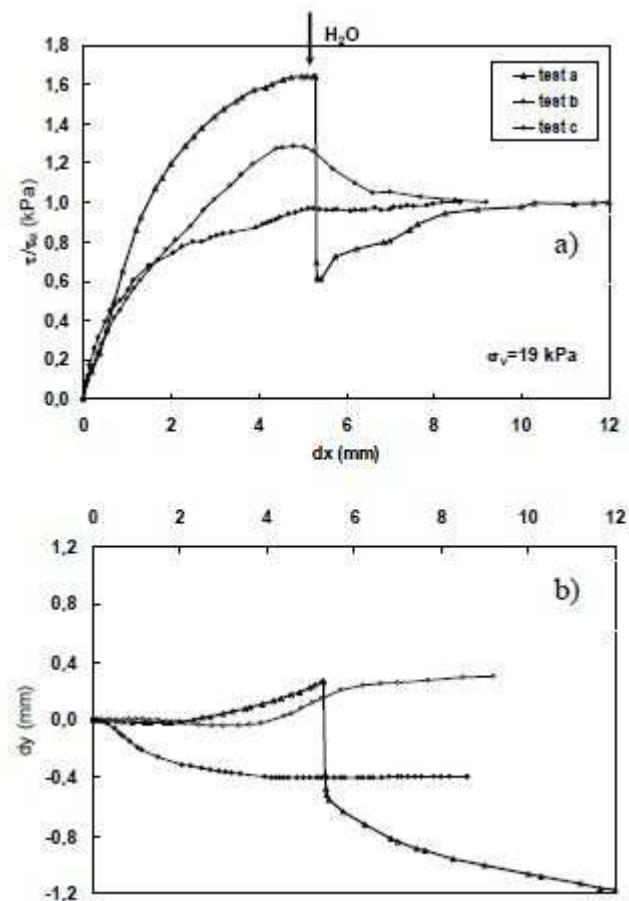


Figure 3-14 – IPD direct shear test results for different condition of saturation. After (Picarelli et al. 2006)

A study about the thermal properties of pozzolana was carried out by McCombie 2017 et al. (McCombie et al. 2017). The authors carried out tests on the thermal conductivity of the Pozzolana sand considering two different porosities and six different degree of saturation. It was observed that the conductivity increased with the saturation increase as it could be expected and the experimental results obtained by these authors are summarized in the plot of Figure 3-15.

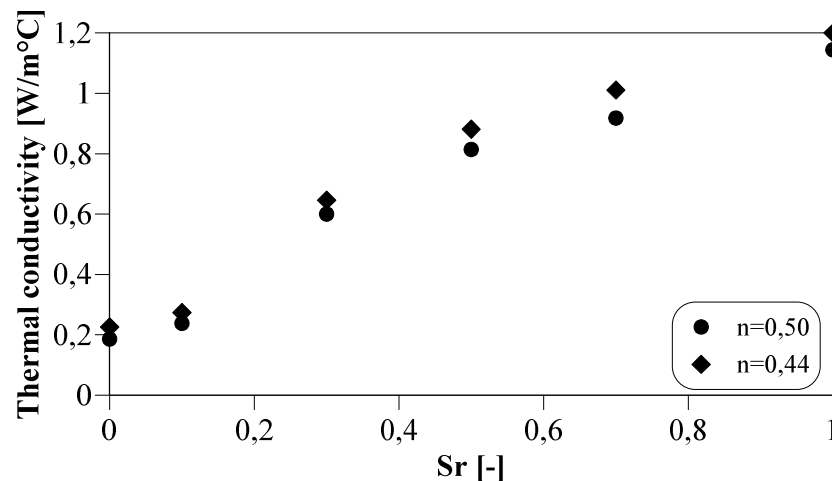


Figure 3-15 - Pozzolana thermal conductivity vs the degree of saturation for different porosity. Replotted from (McCombie et al. 2017)

From the results the authors obtained a thermal conductivity for the solid part (sandy grain) of approximately $2,14 \pm 0,09$ W/m°C.

3.3 Thermal loads for building and for Geothermal Pumps

To simulate realistic conditions for the temperature boundaries conditions in the soil-energy piles interaction problem, an analysis about the building energy demand is opportune. The building geographic location, its urbanistic usage and the human activities carried out in the indoor spaces, affect the thermal loads for the GSHP and consequently, also the heat carried fluid of the ground heat exchangers present into energy piles. But, also the choice of the heat pump, the design of ground heat exchangers affects the energy piles thermal loads and consequently their energetic and/or structural performances.

It is very important the analysis of the building energy demand also to verify that the peak of thermal loads is into reasonable limits both for the cooling phase (risk of water freezing) and for the heating phase (risk of too high stress/strain into pile).

Some software allows to design the components both of GSHP and of the energy distribution system and to simulate the behaviour of these system integrated into a building.

To establish a thermal loads range in terms of magnitude of temperatures for energy piles in the Neapolitan area, a dynamic energy simulation was carried out with Design Builder software to

analyse the energy behaviour of a plant operating over a period of one year under the thermal boundary conditions of the Neapolitan context.

3.3.1 Neapolitan climate zone

The city of Naples is placed in the centre of the Mediterranean area on the western coast in the South of Italy.

The Mediterranean climate is intermediate between warm and hot and substantially dry during the summer and mild, wet during the winter because it is a zone included between the rainy climate of central Europe and arid climate of North Africa (Giorgi and Lionello 2008).



Figure 3-16 - Naples in the Mediterranean region. Replotted from (Castro-jiménez et al. 2013)

Very often in Mediterranean coastal regions the real challenge is especially in the summer season when it is necessary to ensure thermo-hygrometric comfort inside the buildings with the rather high temperatures that the air can reach in the warmer months.

The climate in Italy can differ very much passing from the north to the south of the country. The energy design approach of the building and consequently of the energy piles depend on the Italian region. These differences were already observed by Morrone et al. (2014) who compared the energy results for the same residential building equipped with a geothermal heat pump and energy piles for the heating and the cooling of the indoor spaces. The building was numerically simulated in a cold climate (area of Milan) and in mild climate (area of Naples) for 20 years of operations. The aim was to evaluate the technical and economic feasibility of the design. The authors observed that the knowledge of the magnitude of injected and extracted heat was a fundamental component for the analysis of the global energy performances of the system in the long term. In fact, it was found that for buildings in mild climates, where the heat pump is mainly used to cool the indoor spaces, the

temperature of the subsoil increased 10 °C after many operational years. On the other hand, the change was negligible for buildings in cold climates.

Italy is subdivided in six climate zones (Figure 3-17) introduced by the Italian Law n. 412 26/08/1993. The difference between a zone and another zone is due to the evaluation of the Daily Degrees (DD) defined as the sum extended every day of a conventional annual heating period, of only the daily positive differences between the indoor temperature, conventionally set at $T_i = 20$ °C and the daily average outdoor temperature T_o (Equation 3-1).

$$DD = \sum_{i=1}^n (T_i - T_o)$$

Equation 3-1

Climate zones are used for the energy design of the buildings. Naples with 1034 DD is in the climate zone C. Based on the climate zone, the Italian Law establishes, for the building heating mode, the time limit to set up for the thermal plan. For Naples, the period is from the 15 of November to the 31 of March. On the other hand, the Italian Law does not establish anything about the buildings cooling and so it is the designer's task to analyse the energy requirements needed to ensure proper indoor thermohydrometric comfort. A way, also used in this research, to evaluate the period of building cooling, is to analyse in which part of the year the indoor temperature is over the prefixed setpoint temperature of design to ensure the comfort.

The following Figure 3-18 shows the daily average, maximum and minimum temperatures recorded for the city of Naples from the year 2017 to the year 2020. In Figure 3-19 are compared the temperature from 2017 to 2020 obtained from network archive (“Che Tempo Faceva a Napoli - Archivio Meteo Napoli » ILMETEO.It” n.d.) and the simulated temperature by the software Design Builder according to the ASHRAE 2013 (Design Builder Templates)..

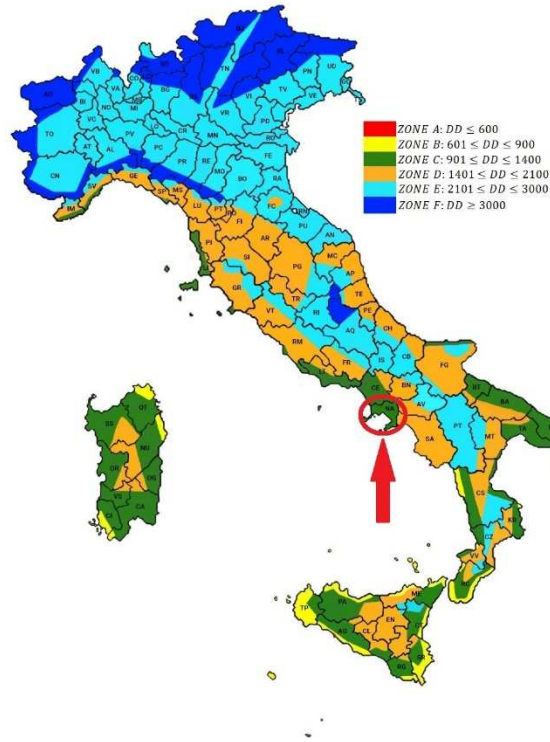


Figure 3-17 - Italian climate zones with the indication of the city of Naples in the Zone C

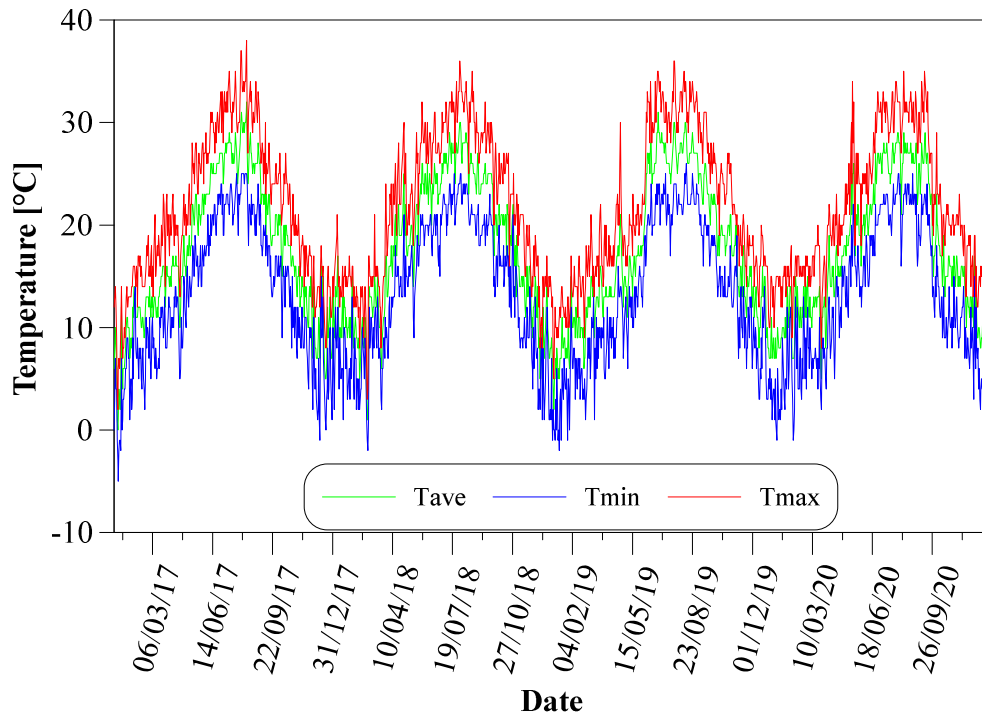


Figure 3-18 - Average, Maximum and minimum air temperature from the 01/01/2017 to 31/12/2020 (data from ("Che Tempo Faceva a Napoli - Archivio Meteo Napoli » ILMETEO.IT" n.d.)

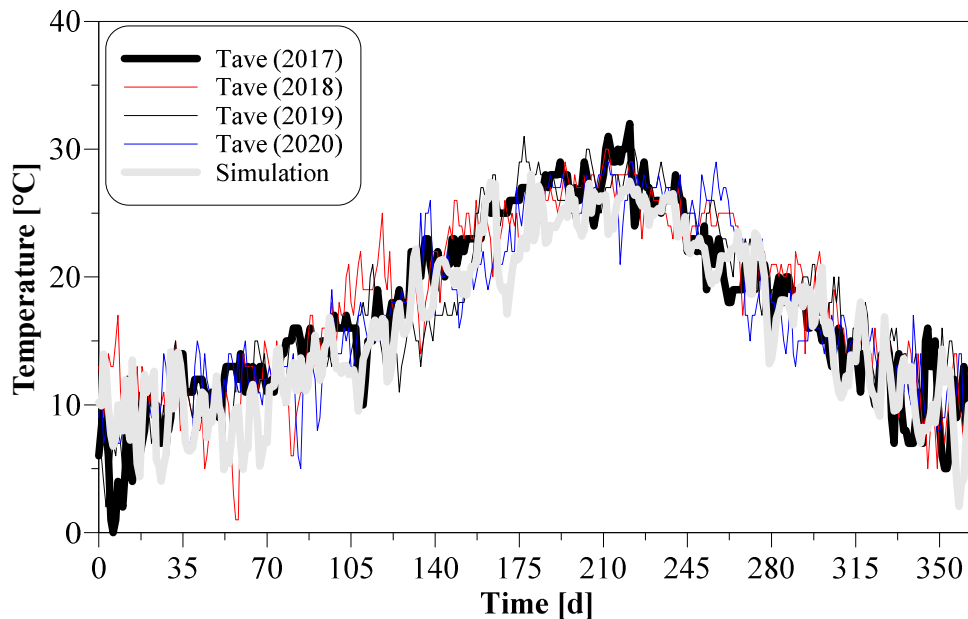


Figure 3-19 - Comparison from different annual air temperature recorded in Naples and simulated temperature according to ASHRAE 2013

3.3.2 Dynamic energy simulation: Design Builder

To evaluate a realistic magnitude of thermal loads to apply to the energy pile in Neapolitan climate context, a dynamic energy simulation was carried out by the software Design Builder. This software includes the “Energy-Plus tool” capable to model and analyse the overall building energy exchange taking into account cooling, heating, lighting, ventilation, and other energy flow (DesignBuilder intro). The aim of the simulation was to determine the inlet water temperature in the primary circuit of the energy pile induced by the heat pump for a plant operating over a period of one year. Design Builder is the user-friendly graphical interface of the thermal simulation engine Energy-Plus. With Design Builder it was possible to model in a three-dimensional environment the geometry of the building, modelling the external envelope and the internal partitions and taking into account the difference between the opaque elements and the transparent one. It was possible also to assign a specific geographical location and the connected weather data choosing from the internal software database. Moreover, it was possible to consider in the model either simple or detailed HVAC (Heating Ventilation and Air Conditioning) system. Further independent HVAC model options were available such as Natural Ventilation, Earth Tubes Domestic Hot Water and Air Temperature Distribution. As regarding the output, it was possible to choose from General outputs, Heating Design, Cooling Design, or energy Dynamic simulation.

In the next section will be better explained how these options were used for the energy model.

3.3.3 The building envelope

To determinate the thermal loads to use for energy pile thermo-mechanical design, a dynamic energy analyses was carried out on a hypothesized building. It was a four-storey building with a rectangular

plan 9,00 m x 16,25 m for a total area of around 146 m² per floor. Office destination was selected for a total of four storeys. The choice of a building office instead of a more generic residential usage was due to the possibility of a simpler determination of the hours and days office usage.

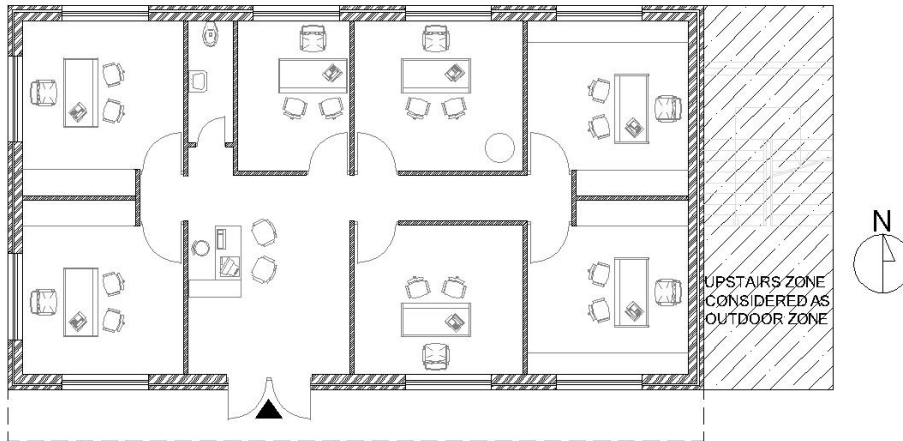
About the architectural/plant engineering part, the model was created assuming a new construction intervention and therefore taking into consideration the regulatory aspects and the limit parameters in terms of transmittance of the parts of the building envelope such as walls, slabs, windows and so on. The design strata of vertical and horizontal envelope, in fact, was affected by the transmittance limits provided by the Table 3-2 replotted from Appendix A, Annex 1 of the Italian Law D.M. 26/06/2015 for “reference” or “target” building. In Table 3-2 the limit transmittance parameters for the envelope and for the Neapolitan climate zone values are summarized.

Table 3-2 –Thermal transmittance limit values according to the Appendix A of the Italian Law D.M. 26/06/2015

Type of structure	Transmittance [W/m ² °C]
Vertical opaques – separation from indoor and outdoor	0,34
Top horizontal or inclined opaques - separation from indoor and outdoor	0,33
Floor horizontal opaques - separation from indoor and outdoor	0,38
Windows and glasses door (both transparent and opaque parts)	2,20

It was assumed that each floor consists of a single “Thermal Zone”, i.e. a thermally homogeneous zone both for the activities carried out and for the minimum and maximum set point temperatures to be considered during the summer and winter seasons (Figure 3-21).

GROUND FLOOR



PLANT TYPE

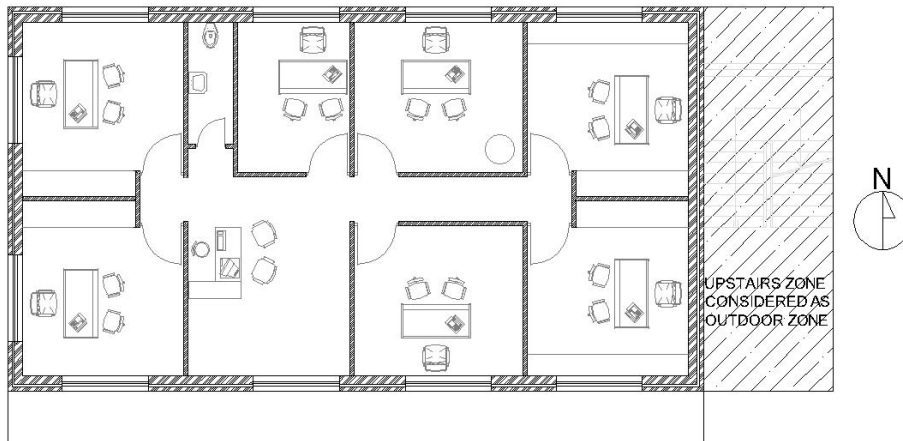
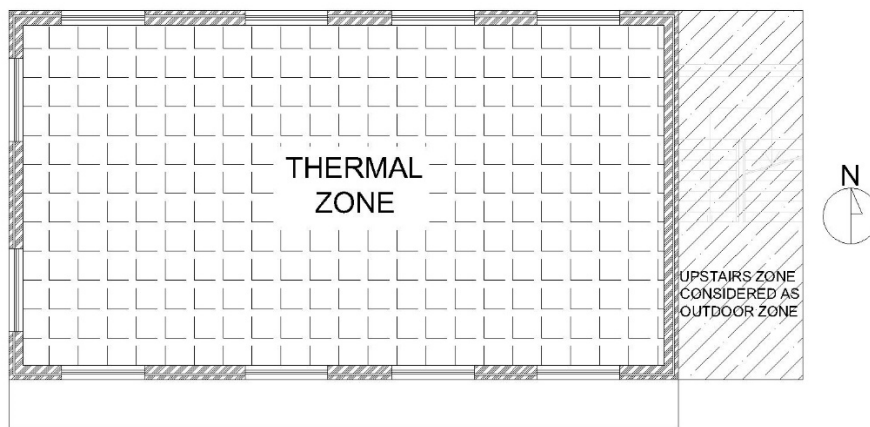


Figure 3-20 - Architectural plans of the office building considered for the energy simulation

THERMAL ZONE PLANT



a)

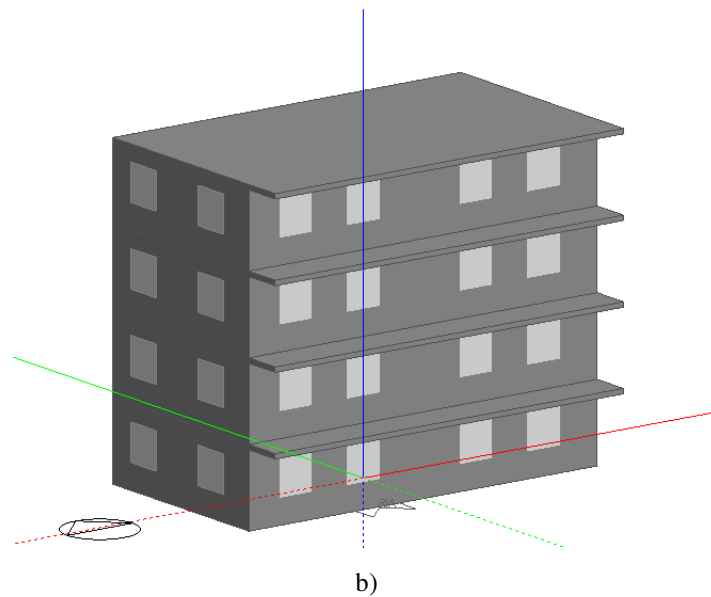


Figure 3-21 - Design Builder model. a) the thermal zone; b) three-dimensional view of the building

3.3.4 Indoor activities and design setpoint temperature

Once the architectural modelling and assignment of the thermal properties of the building envelope was done, it was necessary to define the indoor activities of the building, the urban usage, the occupancy people rate for the thermal zone and above all the setpoint temperatures to define the limits for which thermal systems must work.

The use of the building as a private office was established to be able to outline a hypothetical operation of the air conditioning system during the day, during the week and during the year. In fact, it was established that the thermal plant worked in a daily “on/off” mode from 8:00 a.m. to 18:00 p.m., from Monday to Friday. Furthermore, during the year was established that in April, May and October the plant did not work. The activities in the building were set to “Generic Office Area” with a density of occupation scenario of 0,111 person/m². The indoor setpoint temperatures of the building were assumed equal to 20 °C for heating in the wintertime and 26 °C for cooling in the summertime according to the provisions of UNI / TS 113000.

The on/off operation mode was established because from literature review (see chapter 2) it was observed that this option provides typically the best energy performance of the system but also the bigger initial thermal loads for the heat exchangers. As regards the annual switching system on and off, this derives from regulatory considerations, as seen in the previous paragraph, and from design considerations. The heating mode was established from the criteria of Italian law. On the other hand, the period for the cooling mode was established based on the analysis of the difference in temperature between the indoor side and the outdoor. As a matter of fact, a first simulation of a building model without thermal plant was carried out, in Figure 3-22 the indoor and outdoor temperature were shown. It was observed that in cold season the respect of the transmittance limits for the building envelope

imposed by the Law allows for internal temperatures that are certainly not sufficient for thermal comfort but are nevertheless acceptable. Moreover, in cold season the greenhouse effect provided by the transparent elements (windows) allow an internal heat gain during the day. On the other hand, in warm season the problems affecting Mediterranean areas are fully manifested. As shown, indoor temperatures were well above the limit of 26 °C set as the warm season set point temperature. This phenomenon starts right around the beginning of June and ends towards the end of September. So, from this analysis it was designed that the air-conditioning system would operate during this period.

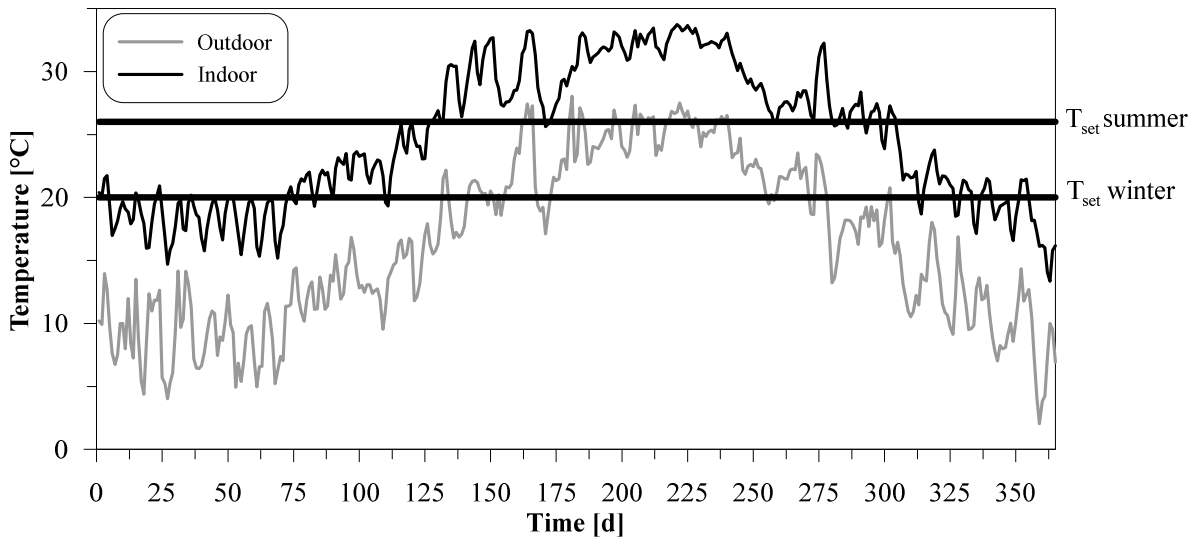


Figure 3-22 - Indoor and outdoor temperature simulated by Design Builder

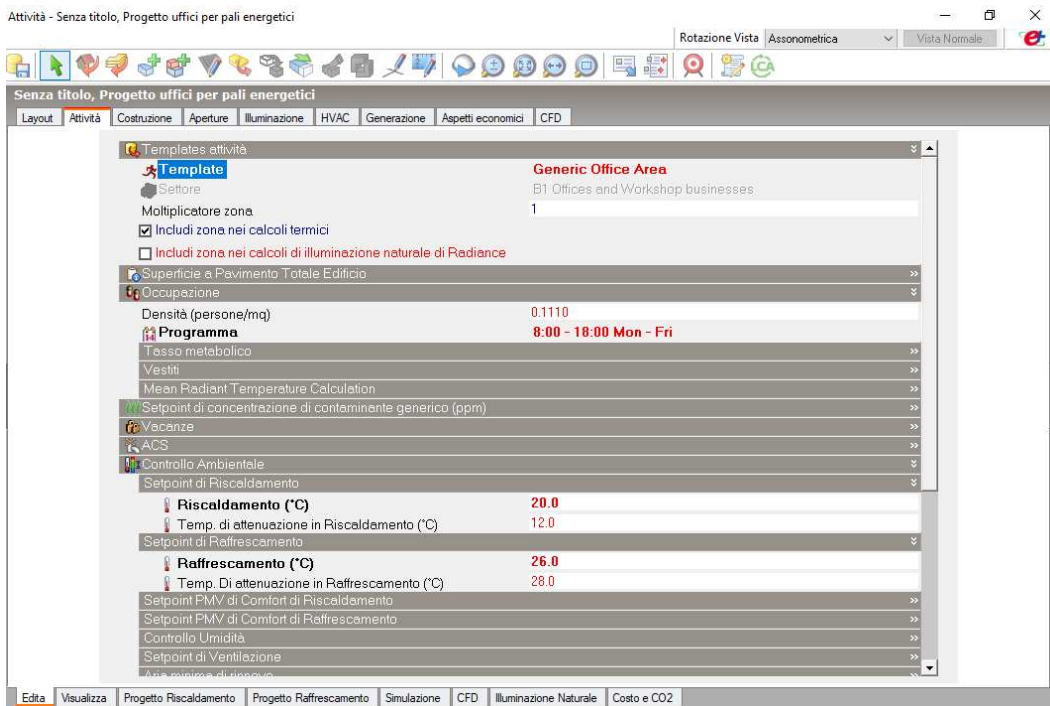


Figure 3-23 - Input parameter provided to the software

3.3.5 The building thermal plant design

The last step for the input data phase was the model of the HVAC system. Obviously for the aim of this research, a system with a geothermal heat pump and underground heat exchangers was selected and designed.

The first step to design the plant was to size the geothermal heat pump according to the energy peaks of the building in both cold and warm seasons.

To obtain the energy peaks in the winter season, an indoor heating design calculation was carried out. On the other hand, the summer energy peaks were obtained by an indoor cooling design calculation. These calculation methods were described in detail in the following subsections.

3.3.5.1 Indoor heating design calculation

To determine the size of heating equipment and heating design calculations were carried out by Design Builder. The software, through the Energy Plus dynamic thermal simulation engine, carried out a transient analysis to meet even the coldest winter design weather conditions likely to be encountered at the site location (Naples). The winter design weather is based on a worst-case design day in which the software considers the minimum outside dry-bulb temperature and a corresponding wind speed. The latter factor is needed to calculate external convective heat transfer. The Energy Plus dynamic thermal simulation engine was used to carry out heating design simulations. To maximise the heating power demand, the software did not consider the solar gain and other internal gain such as lighting, equipment or occupancy. The zones were heated constantly to achieve the heating temperature set point. Moreover, the software considered the heat exchange of the indoor zones not only with the outdoor but with all the zones with a lower temperature.

The simulation continued until the engine converged towards a stable solution in terms of temperatures and heat flows in each zone and towards any component of the system.

The total heat loss in each zone is multiplied by a Safety factor that is assumed with a default value of 1,5 to give a recommended heating Design Capacity.

From the analyses a peak heating load of 30,5 kW was obtained (Figure 3-24).

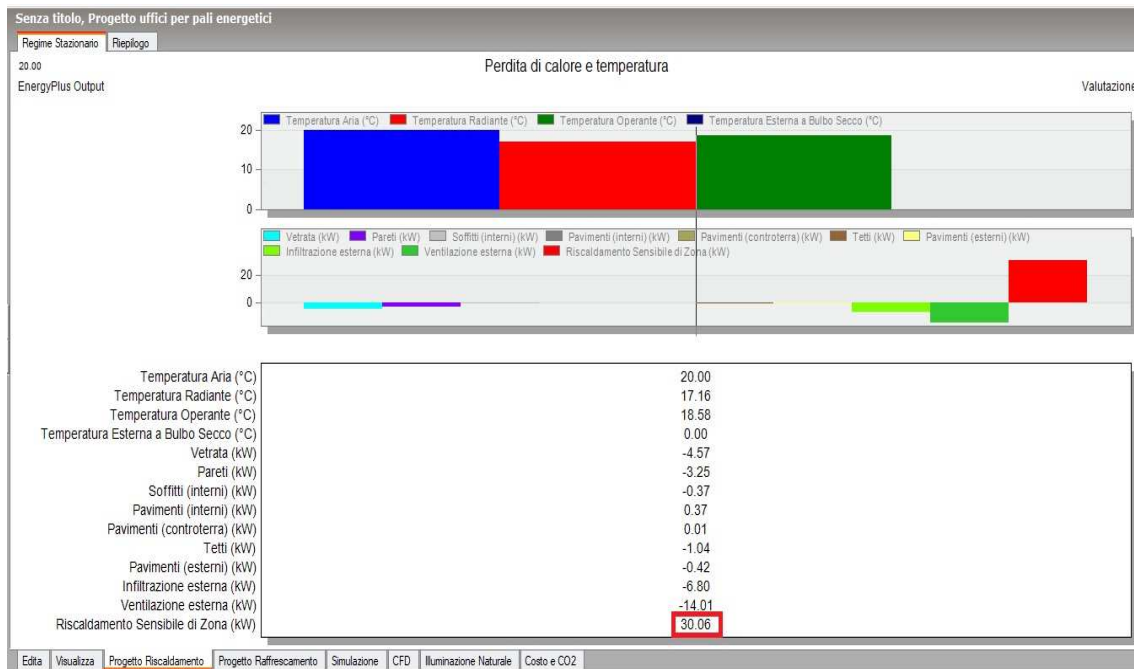


Figure 3-24 - Indoor heating design calculation results

3.3.5.2 Indoor cooling design calculation

The cooling design was needed to determine the capacity of cooling equipment required to meet the hottest summer design wheatear conditions likely to be encountered at the site location. In this case for the summer design wheatear conditions in the software was considered the maximum dry bulb air temperature over the day, the minimum dry bulb air temperature (in the night-time) and the wet-bulb temperature at the time of the maximum dry-bulb temperature. The default parameters for the daily temperature profile used in the cooling design calculations were calculated from the maximum and minimum values using a modified sinusoidal curve and assuming that the maximum temperature occurs at 15:00 p.m. and the minimum at 5:00 a.m.

Generally, the indoor cooling design calculation are carried out using periodic steady-state methods such as the admittance and response factor methods. With the use of Design Builder, it was possible to use for the same purpose the Energy Plus dynamic thermal simulation engine.

Energy Plus for the indoor cooling design has different features compared to the case for the indoor heating design. The periodic steady-state external temperatures were calculated using maximum and minimum values obtained by the design summer weather. Moreover, to maximize the cooling thermal loads, no wind was considered. On the other hand, for the same previous purpose, the solar gains through windows and scheduled natural ventilation, were included as well as internal gains from occupants, lighting and other equipment. The conduction and convection between zones of different temperatures were always considered. The simulation continued until temperatures and heat flows in each zone converged to stable values. For each zone the simulation calculated half-hourly temperatures and heat flows and determined the cooling capacities required to maintain any cooling

temperature set points. The maximum cooling load in each zone was multiplied by a safety factor with a default value of 1,3 to give the design cooling capacity.

From the analyses a peak cooling load of -51,25 kW was obtained (Figure 3-25)

Senza titolo, Progetto uffici per pali energetici												
Apporti di calore e temperatura - Senza titolo, Progetto uffici per pali energetici												
EnergyPlus	Tempo	2:00	4:00	6:00	8:00	10:00	12:00	14:00	16:00	18:00	20:00	22:00
Temperatura Aria (°C)		29.09	28.86	26.00	26.00	26.00	26.00	26.00	26.00	26.00	30.26	29.73
Temperatura Radiante (°C)		29.74	29.57	29.31	29.54	29.84	30.07	30.28	30.37	30.25	30.24	30.08
Temperatura Operante (°C)		29.42	29.21	27.65	27.77	27.92	28.03	28.14	28.18	28.12	30.25	29.90
Temperatura Esterna e Bulbo Secco (°C)		24.52	23.83	23.83	26.69	30.73	33.60	35.10	34.41	32.34	29.36	27.28
Vetrata (kW)		-1.51	-1.60	0.38	1.01	1.75	1.92	2.47	2.38	1.74	-0.77	-1.09
Pareti (kW)		1.86	1.94	3.12	0.99	0.20	-0.01	-0.19	0.10	0.91	0.27	1.08
Soffitti (intemi) (kW)		0.91	0.97	1.13	-0.55	-0.90	-0.79	-0.87	-0.62	-0.02	0.30	0.61
Pavimenti (intemi) (kW)		0.44	0.60	0.68	0.07	-0.52	-0.59	-0.74	-0.47	0.09	-0.68	-0.16
Pavimenti (esterni) (kW)		-0.28	-0.24	-0.46	-0.37	-0.43	-0.43	-0.47	-0.46	-0.41	-0.37	-0.36
Tetti (kW)		-0.40	-0.47	-0.51	-0.30	0.93	2.07	2.48	2.37	1.78	0.62	0.04
Pavimenti (esterni) (kW)		-0.07	-0.09	-0.23	-0.05	0.14	0.34	0.44	0.45	0.34	0.20	0.04
Infiltrazione esterna (kW)		-1.50	-1.65	-0.72	0.18	1.50	2.40	2.95	2.64	2.00	-0.30	-0.80
Ventilazione esterna (kW)		0.00	0.00	0.00	0.22	4.43	5.78	9.99	9.11	1.21	0.00	0.00
Illuminazione Generale (kW)		0.00	0.00	0.00	10.95	10.95	10.95	10.95	10.95	10.95	0.00	0.00
Computer + Dispositivi (kW)		0.35	0.35	0.35	6.44	6.44	6.44	6.44	6.44	6.44	0.35	0.35
Occupazione (kW)		0.00	0.00	0.00	1.79	3.58	2.69	3.58	3.58	0.90	0.00	0.00
Apporti Solari attraverso Finestra Esterna (kW)		0.00	0.00	6.60	2.81	3.14	2.99	3.14	2.89	2.43	0.00	0.00
Raffrescamento Sensibile di Zona (kW)		0.00	0.00	-10.17	-22.44	-27.14	-28.98	-32.75	-32.60	-26.76	0.00	0.00
Raffrescamento Sensibile (kW)		0.00	0.00	-10.17	-22.67	-30.70	-33.26	-39.67	-38.91	-27.95	0.00	0.00
Raffrescamento Totale (kW)		0.00	0.00	-12.26	-31.39	-42.00	-43.20	-51.25	-50.65	-33.36	0.00	0.00
Umidità Relativa (%)		48.06	48.76	46.70	48.13	49.34	47.86	48.33	48.30	45.69	40.85	45.54
Vent. Mecc + Vent. Nat + Infiltrazioni (vol/h)		0.71	0.71	0.71	1.80	3.84	3.05	3.83	3.83	1.47	0.70	0.71

Figure 3-25 - Indoor cooling design calculation results

3.3.5.3 The geothermal plant

In Design Builder software to create a system with a geothermal pump it was necessary to active the HVAC detailed option to define the system components in detail. It was possible to choose if a single water to water heat pump provided either heating only, cooling only or both heating and cooling. These configurations were represented in Design Builder using so called “heat pump – heating” and “heat pump – cooling” components connected to hot and chilled water plant loops, respectively. The aim of the plant designed for the case study building was to satisfy with the same heat pump both the summer and winter needs. For this reason, both heating and cooling heat pumps were included in the HVAC layout and the data entry for the heat pumps were coordinated. The primary circuit analysed consisted of U-shaped heat exchanger composed by 16 wells 76 m in length. It was connected to the heat pump system to supply the thermal energy from the ground. As regarding the secondary circuit, it consisted of radiant panel floors for the heating mode and cold beams for cooling mode. The size of the heat pump was chosen to satisfy the heating and cooling peaks loads calculated previously.

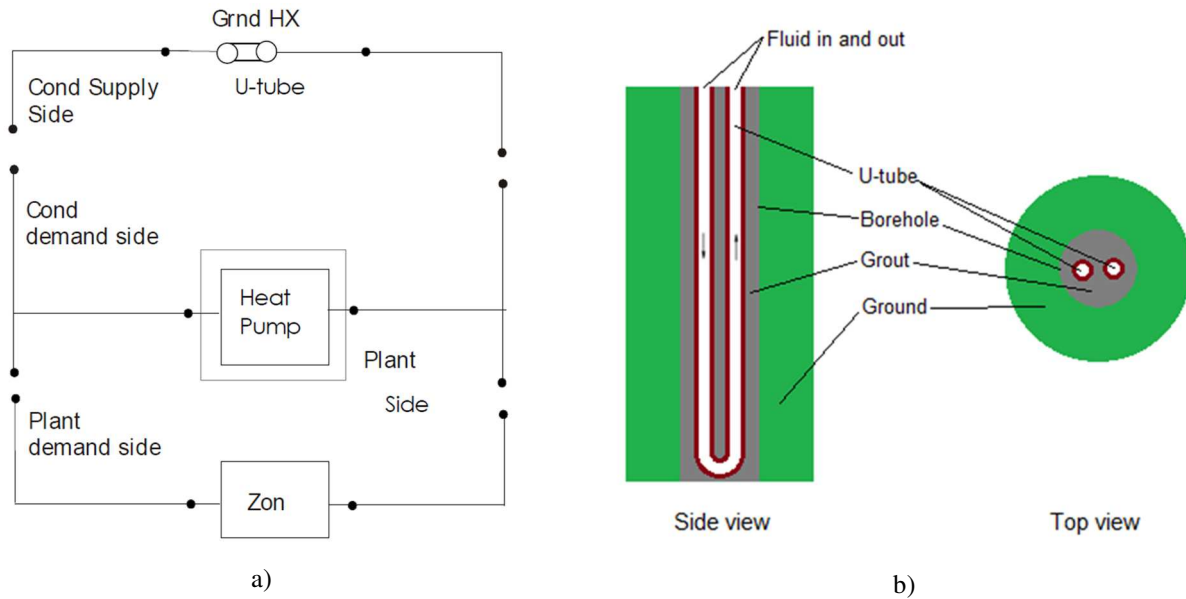


Figure 3-26 - GSHP plant design a) scheme of the components of the plant; b) the type of ground heat exchangers used in Design Builder

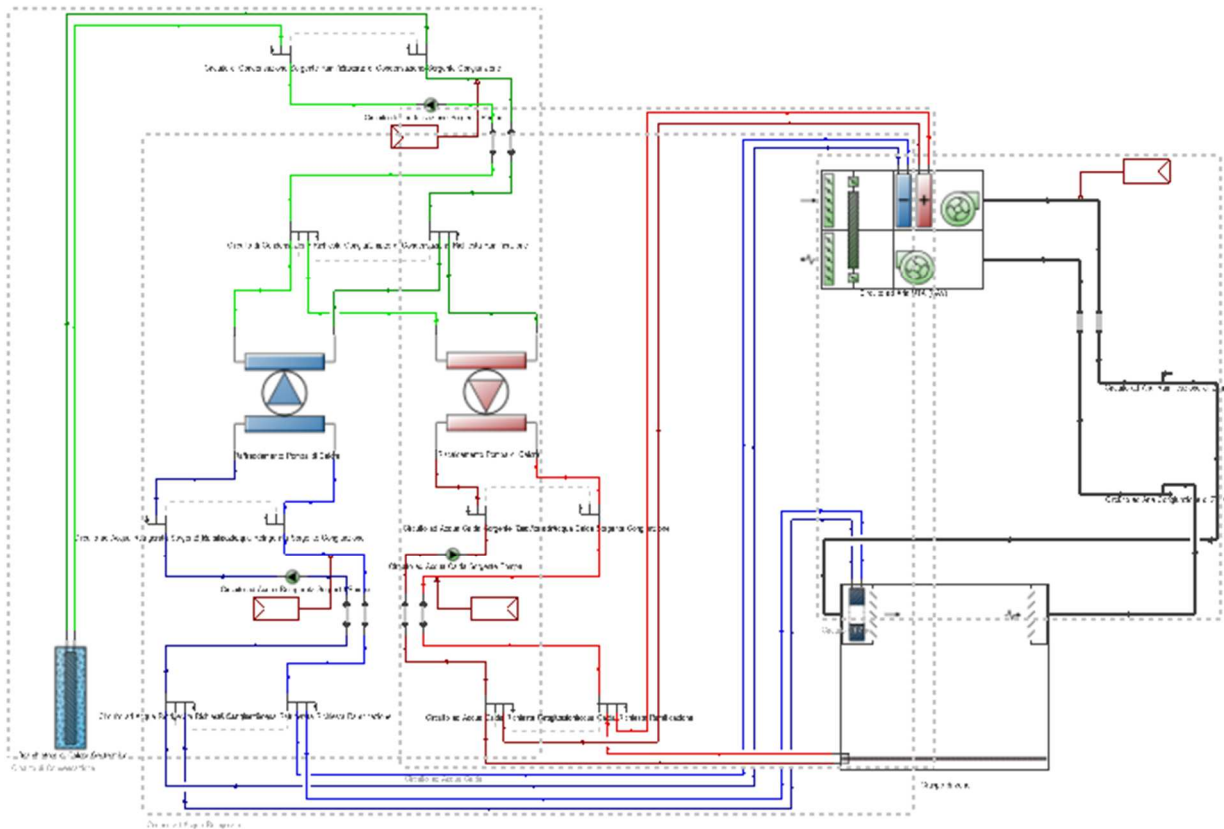


Figure 3-27 - Detailed scheme of the GSHP plant from the indoor spaces to ground heat exchangers

Based on the peak loads, a simplified method proposed by the software guide was adopted to choose the number of boreholes and the length of the ground heat exchangers. It consisted of a matrix in which crossing heating and cooling peak loads the number of boreholes was obtained.

It should be clear that the number of boreholes and the length of U-shaped GHEs were used only to know the required approximate length of GHEs. In fact, in energy piles, as said in previous sections,

an equivalent length of GHEs can be obtained even using other shapes than U and other depth of excavation.

		Peak cooling load (kW)									
		10	20	30	40	50	60	70	80	90	100
Peak heating load (kW)	10	4	4	8	8	8	12	12	12	16	16
	20	8	8	8	12	12	12	12	12	16	16
	30	12	12	12	12	16	16	16	16	16	16
	40	16	16	16	16	16	24	24	24	24	24
	50	24	24	24	24	24	24	24	24	24	24
	60	24	24	24	24	24	24	24	24	24	40
	70	40	40	40	40	40	40	40	40	40	40
	80	40	40	40	40	40	40	40	40	40	40
	90	40	40	40	40	40	40	40	40	40	40
	100	40	40	40	40	40	40	40	40	40	40

Figure 3-28 - Simplified matrix method to design the boreholes number

After this preliminary sizing to complete the input data for the model important parameters for the heat exchangers such as the thermal parameters of both grout and soil were fixed. The heat carrier fluid flow rate also was imposed according to the heat pump chosen. To simulate an energy pile as a GHE the concrete thermal properties were inserted in the grout field.

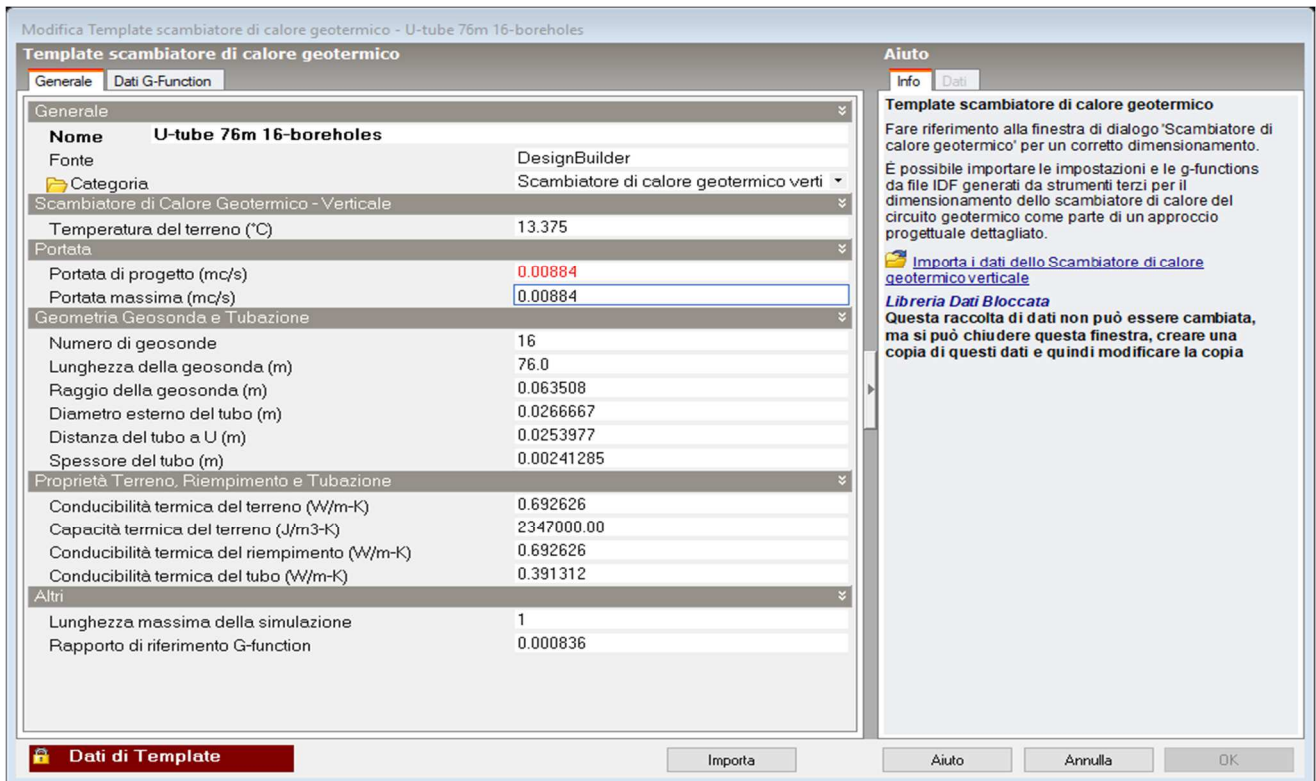


Figure 3-29 - Input parameters for the ground heat exchangers

3.3.5.4 Energy simulation

From the above analyses it was possible to obtain the final energy model of the building provided with the geothermal plant. On this model an annual dynamic simulation was carried out and the inlet temperature in the ground heat exchangers was obtained. It represented a realistic thermal load to apply to an energy pile with the above assumptions related to the climate conditions of the Neapolitan area, for a typical building occupied by offices.

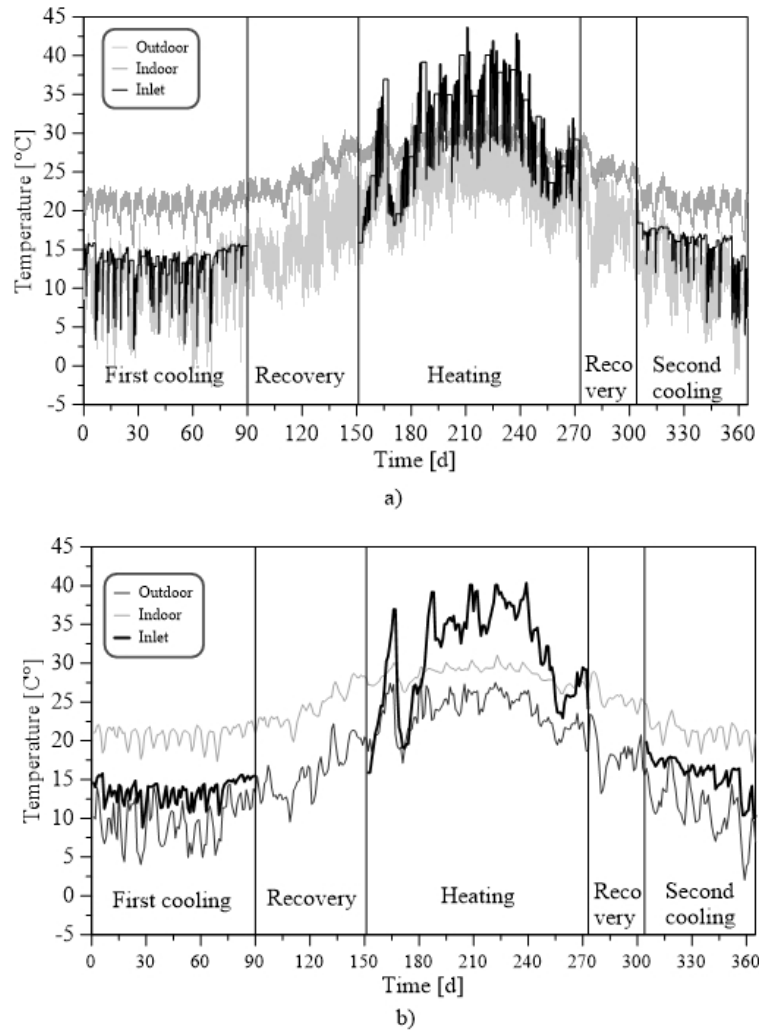


Figure 3-30 - a) Hourly and b) daily values of temperature of the water entering (inlet) the underground collector; outdoor and indoor temperatures.

The inlet temperature trend is described for the whole year in the above figures. In terms of daily cycles, the winter and the summer working temperatures show different features. In fact, it is clearly shown that in winter generally the most severe temperatures (colder) supplied to ground heat exchangers are recorded from the start to the middle of the daily system operation. On the other hand, in summer season generally the most severe temperatures (warmer) are recorded from the middle to the end of the daily operation. In Figure 3-31 a zoom view of the trend of the inlet temperatures for

10 hours of work of a plant with an on-off operation mode is plotted. The system starts at 8:00 a.m. and finishes at 18:00 p.m. both for a winter's day and a summer's day.

The reason of this different behaviour could depend on the outdoor temperature. As a matter of fact, the plant works at the same hours of the day for the whole year. In winter when the plant starts to work it must heat the cold temperatures accumulated during the night when the plant was off. Moreover, until the middle of the operation, the plant is working with the morning outdoor temperatures that resulted generally colder than those recorded in the middle of day. The opposite occurred in summer season. In fact, at the start of the operation the plant must work to cool the building starting from the indoor temperatures accumulated during the night that are obviously colder than those experienced during the daytime. In this way the system supplies higher inlet temperature to the heat exchanger from the middle to the end of the work.

It is possible to observe by Figure 3-31, as it could be expected in a Mediterranean city like Naples, that the higher thermal loads are provided to heat exchangers in the indoor spaces cooling mode. In this mode, in fact, the inlet temperature for the energy pile can overcome the 40 °C. In the simulation of pile-soil interaction under thermal loads the cyclic nature of the load is important. The thermal analysis carried in the building provides a realistic estimate of the thermal loads moving from a detailed hourly variation up to the scale of a whole year. On this aspect and on the importance of the cyclic nature of the thermal loads a detailed discussion can be found in the paper by Marone et al. (2020).

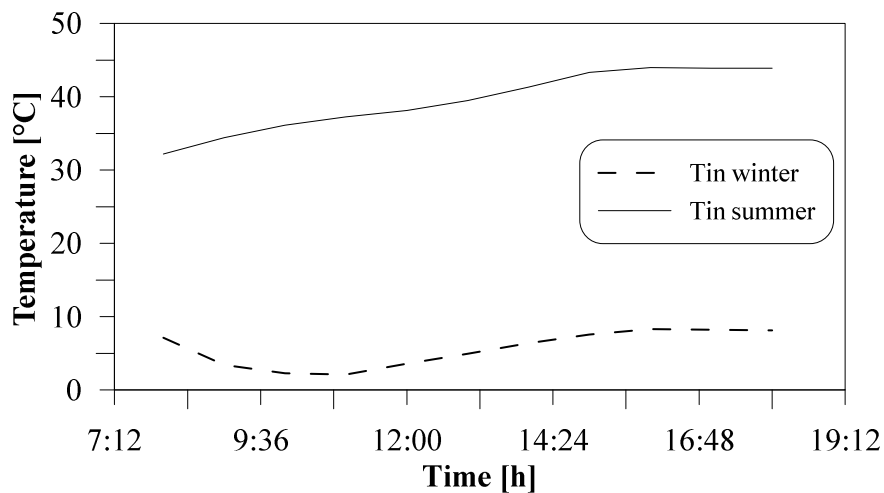


Figure 3-31 - An example of inlet temperature trend for the operation time of the GSPH in summer and winter season

3.4 Conclusion

The aim of this brief chapter was to describe the main features of the energy piles applications in the city of Naples and its surroundings. For such a reason the context of the area was first described by a geological point of view outlining the main volcanic formations likely to find in the subsoil. For these formations a brief and obviously not exhaustive discussion of the main geotechnical and thermal

properties is carried out. Typical climate conditions are presented and a simplified thermal analysis of a schematic office building in the city of Naples is carried out.

Using this partially coupled approach a magnitude of the thermal loads to apply to the energy piles is obtained. It was observed that for the Mediterranean Neapolitan climate the cooling demand of the building during a year was slightly higher than the heating one. In terms of thermal loads for energy piles it means that more attention in the design should be paid for the heating case even because the differences in temperature resulted higher and kept constant for a longer time compared to the cooling ones.

3.5 References

- Aversa, S., and A. Evangelista. 1993. "Thermal Expansion of Neapolitan Yellow Tuff." *Rock Mechanics and Rock Engineering* 26 (4): 281–306. <https://doi.org/10.1007/BF01027114>.
- Aversa, S., Evangelista, A. and Nicotera, M.V. 1998. Experimental determination of characteristics curves and permeability functions of partially saturated pyroclastic soil. In *Unsaturated Soils, Proc. 2nd Int. Conf., Beijing*, 1:13-18.
- Aversa, S., Evangelista, A. and Scotto di Santolo, A. 2013. Influence of the subsoil on the urban development of Napoli. *Geotechnical Engineering for the Preservation of Monuments and Historic Sites – Bilotta, Flora Lirer & Viggiani (eds)*. Taylor & Francis Group, London, ISBN 978-1-138-00055-1
- Castro-jiménez, Javier, Naiara Berrojalbiz, Laurance Mejanelle, and Jordi Dachs. 2013. "Sources , Transport and Deposition of Mediterranean Sea."
- "Che Tempo Faceva a Napoli - Archivio Meteo Napoli » ILMETEO.It." n.d. Accessed March 30, 2021. <https://www.ilmeteo.it/portale/archivio-meteo/Napoli>.
- Colombo, Giuseppe. 2010. "Il Congelamento Artificiale Del Terreno Negli Scavi Della Metropolitana Di Napoli : Valutazioni Teoriche e Risultati Sperimentali."
- Evangelista, A. 1980. Influenza del contenuto d'acqua sul comportamento del tufo giallo napoletano. In *proc. 14th Italian Geotechnical Conf, Firenze*
- Evangelista, A., Aversa, S., Pescatore, T.S., and Pinto, F. 2000. Soft rocks in southern Italy and role of volcanic tuffs in the urbanization of Naples. *Proc. Of the II Int. Symp. On "The Geotechnics of Hard Soils and Soft Rocks"*, Napoli, Vol.3: 1243-1267. Rotterdam: Balkema.
- Giorgi, Filippo, and Piero Lionello. 2008. "Climate Change Projections for the Mediterranean Region" 63: 90–104. <https://doi.org/10.1016/j.gloplacha.2007.09.005>.
- Guide DesignBuilder, help. n.d. "DesignBuilder Help - Welcome to DesignBuilder V6." Accessed April 5, 2021. <https://designbuilder.co.uk/helpv6.0/>.
- Leroueil, S. & Vaughan, P.R. 1990. The general and congruent effects of the structure in natural soils and weak rocks. *Géotechnique*, 40 (3): 467-488
- Marone, Gabriella, Luca Di Girolamo, Marianna Pirone, and Gianpiero Russo. 2020. "Numerical Modelling of Heat Exchanger Pile in Pyroclastic Soil." *E3S Web of Conferences* 205: 1–7. <https://doi.org/10.1051/e3sconf/202020505014>.
- McCombie, M. L., V. R. Tarnawski, G. Bovesecchi, P. Coppa, and W. H. Leong. 2017. "Thermal

- Conductivity of Pyroclastic Soil (Pozzolana) from the Environs of Rome.” *International Journal of Thermophysics* 38 (2). <https://doi.org/10.1007/s10765-016-2161-y>.
- Morrone, Biagio, Gaetano Coppola, and Vincenzo Raucci. 2014. “Energy and Economic Savings Using Geothermal Heat Pumps in Different Climates.” *Energy Conversion and Management* 88: 189–98. <https://doi.org/10.1016/j.enconman.2014.08.007>.
- Nicotera, M. V. 1998 Effetti del grado di saturazione sul comportamento meccanico di una pozzolana del napoletano, PhD Thesis, Università di Napoli Federico II
- Nicotera, M.V., Evangelista, A. and Aversa, S. 1999. Osservazioni di una pozzolana in condizioni lontane dalla saturazione. In *proc. 20th Italian Geotechnical Conf.*, Parma:222-230. Bologna: Pàtron.
- Nicotera, M. V. 2000. Interpretation of shear response upon wetting of natural unsaturated pyroclastic soils. In Tarantino and Mancuso (eds.) *proc. int. workshop on Unsaturated Soils*, Trento: 177-192. Balkema, Rotterdam
- Picarelli, L, A Evangelista, G Rolandi, A Paone, M V Nicotera, A Scotto Santolo, S Lampitiello, and M Rolandi. 2006. “Mechanical Properties of Pyroclastic Soils in Campania Region.” In *Proc. Int. Workshop on Characterisation & Engineering Properties of Natural Soils*, edited by Tayloer&Francis Group Plc., 2331–83. ISBN 978-0-415-47692-8.
- Scotto di Santolo, A. 2000. *Analisi geotecnica dei fenomeni franosi nelle coltri piroclastiche della Provincia di Napoli*. Ph.D. Thesis, Università di Napoli Federico II.
- Templates, DesignBuilder Help - Location. n.d. “DesignBuilder Help - Location Templates.” Accessed April 5, 2021. https://designbuilder.co.uk/helpv6.0/#Location_Templates.htm%23kanchor2196.

Chapter 4

4 Numerical analysis on energy piles

4.1 Introduction

The numerical methods are powerful tools to analyse the behaviour of a soil-pile interaction model under thermal and mechanical loadings. By numerical analysis it is certainly possible to analyse the impact of different design elements of an energy pile such as geometry, thermal and mechanical material properties, thermal boundary conditions.

Two different software have been used with different aims.

The first part of the chapter is dedicated to the numerical analysis carried out with the finite element software Plaxis 2D. An axisymmetric 2D model is used with the final aim to establish the effects of different assumptions on the boundary conditions at ground surface on the thermomechanical behaviour of a single energy pile embedded in Neapolitan pyroclastic soils. The importance of this aspect is generally underestimated

In the second part a parametric study is presented carried out by the commercial software FLAC3D and using a 3D model. The aim is to investigate the behaviour of energy pile groups via the interaction factors method (Poulos, 1968), (Poulos et al., 1971), (Russo, 1998). For this reason, a couple of energy piles was modelled considering them embedded in different soil layering and at different spacing. One of the piles was subjected to mechanical loads only and the effects on the adjacent unloaded pile were evaluated. The same analysis was repeated applying a thermal load on one of the two piles. By the analysis a coefficient of interaction between the pile was determined for the different parameters chosen both for the mechanical case and the thermal one. Moreover, it was compared with literature results.

4.2 The effects of the boundary conditions on the energy pile behaviour embedded in pyroclastic soil

This chapter summarizes the results presented in 2nd International Conference on Energy Geotechnics ICEGT 2020 (Marone et al., 2020).

An investigation about energy piles mechanical behaviour contextualized in Neapolitan area was carried out by a FE thermomechanical axisymmetric numerical analysis using the commercial software Plaxis 2D.

A Continuous Flight Auger (CFA) energy pile 13 m in length and 0,60 m in diameter embedded in a typical Neapolitan pyroclastic soil deposit subjected to thermomechanical loads was simulated. The material properties and the mechanical load was determinate by a field test. On the other hand, the thermal loads and the climatic context were determinate by an energy dynamic simulation of a

prototype building, as already detailed described in chapter 3. In this way the annual energy pile thermal loads corresponded to a realistic heating and cooling demand of the designed building for Neapolitan context.

In addition, to the thermal loads provided by the designed GSHP to the energy pile by the energy simulation it was also possible to evaluate the indoor and outdoor annual temperature trends.

The aim was to establish the effects of the different surface thermal boundary conditions, i.e. considering the indoor or outdoor annual temperature trend on the mechanical pile behaviour and to investigate the differences in results obtained with an hourly or daily simulation.

4.2.1 The 2D model

The soil and pile mechanical property adopted in the model were determinate by a trial and error procedure based on experimental data of a site investigation and conventional design pile load test reported by Russo (2013).

The site was in the plain east on Naples. In this zone, Vesuvius and Phlegrean volcanos deposits constituted the subsoil and the groundwater was close to the ground surface.

5 load tests to failure and 12 proof load tests were carried out in the framework of the foundation design of a new big trade centre. Three conventional top-down maintained stage load tests on piles with different length and diameters and two Osterberg's cell load tests on pile with similar geometry and length were carried out (Russo et al., 2018a).

To investigate the site stratigraphy, moreover, 6 CPT and 11 boreholes were carried out. From boreholes the stratigraphy was detected. Made ground with a thickness ranged between 1 m and 3 m was the first layer. The second layer was made by pyroclastic sandy soil with a thickness ranged between 8 m and 11 m. Finally, the bedrock of volcanic grey tuff was detected for depth from the ground surface ranged between 10 m and 12 m. The tuff layer was 20 m in thickness. In Figure 4-1 the CPT and SPT results and the variation of the specific weight and friction angle with the depth are reported (Russo, 2013).

The friction angle was obtained by Schmertmann (1975) deriving the soil densities from the CPTs and SPTs results (Kulhawy and Mayne 1990). By the obtained results the friction angle ranged between 31° and 37° for the pyroclastic sandy soil upper the tuff bedrock. The upper bound of the angle friction values were reached in the upper and in the lower part of the soil profile. On the other hand, in the middle part of the soil profile, the lower bound of the friction angle values were detected. Even if the tuff layer was not directly investigated it, it was well-known deposit of the Neapolitan area, as said in previous chapter 3. A Mohr-Coulomb (M-C) envelope characterize the tuff strength with c' (effective cohesion) ranged between 400 kPa and 800 kPa and a friction angle of 28° (Russo, 2013).

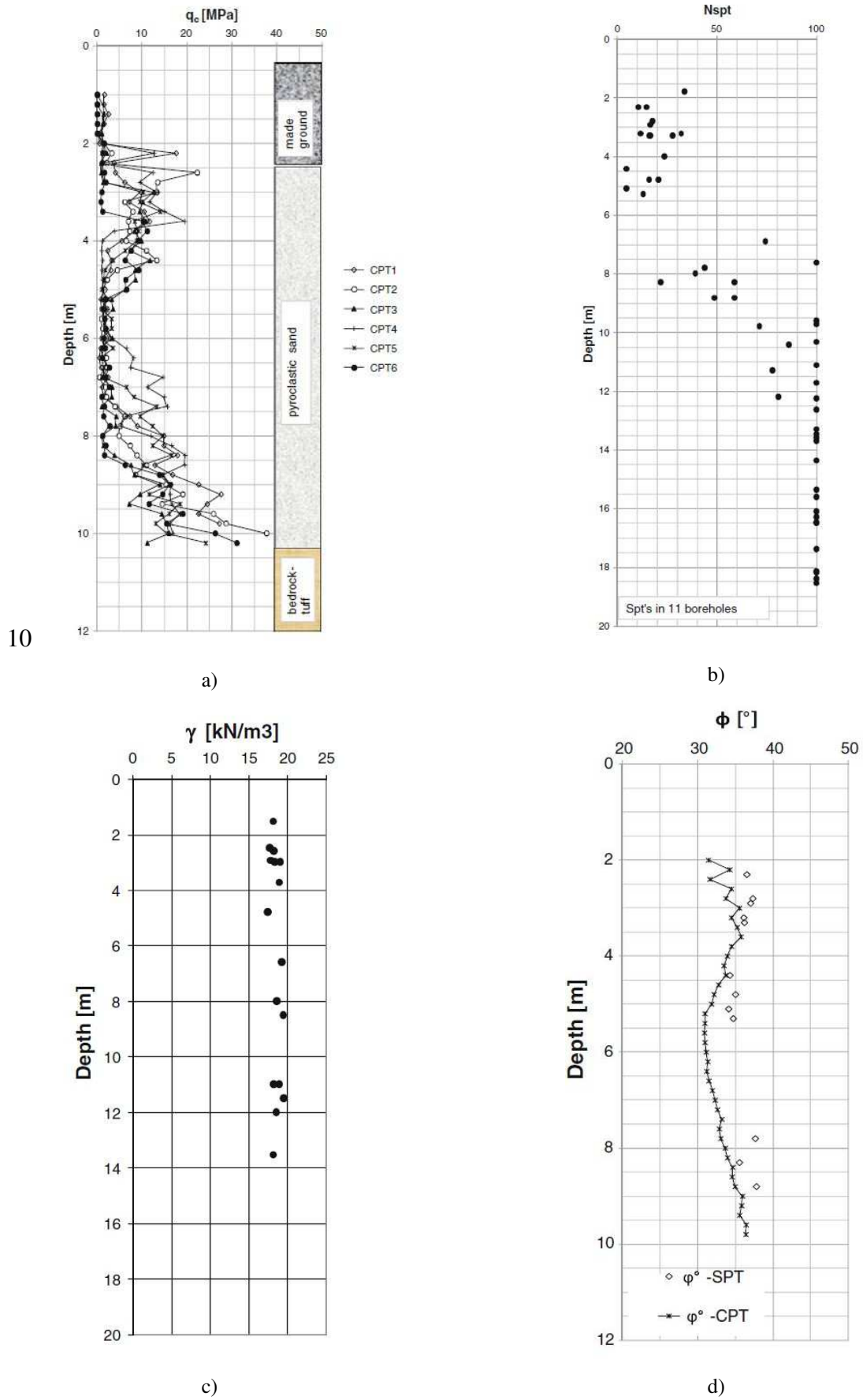


Figure 4-1 – a) CPT results; b) SPT results; c) Unit weight deduced by penetration test; d) friction angle deduced by penetration test (after Russo 2013)

By obtained site results, the stratigraphy was modelled. The geotechnical model used in the numerical simulation was made by three different layers of pyroclastic sand for the first 10 m and a grey tuff layer from 10 m to 30 m. The ground water was 1 m below the ground surface. The first three layers were called Upper sand, middle sand and lower sand and had thickness of 4 m, 3 m and 3 m, respectively.

From the back analysis of the site load test on a continuous flight auger (CFA) pile 13 m in length and 0,6 m in diameter, the mechanical parameters of soil were calibrated using an Hardening-Soil (H-S) constitutive model for the pyroclastic sands and a Mohr-Coulomb model (M-C) constitutive model for the tuff. Between the pile and the surrounding soil and interface was included with a M-C constitutive model.

In Figure 4-2 the comparison between the experimental and simulated load settlements curve obtained with the calibrated parameters is shown. It can be observed a sudden settlement for a load value of approximately 6000 kN, reaching a maximum settlement value of almost 0,03 m. The failure can be considered representative of the mobilisation of both the lateral and the tip resistance of the tuff pile. The pile and the soil thermal properties were assigned on the basis of the literature values as explained in previous chapters 2 and 3 considering the presence of the water table and its effects on the thermal conductivity of soil.

The mechanical and thermal parameters assigned in the model are reported in Table 4-1.

Table 4-1 - Pile and soil mechanical and thermal parameters

	Pile	Upper sand	Intermediate sand	Lower sand	Tuff
Unit weight (γ) [kN/m³]	24	19	18	19	17
Young's modulus (E_{50}) [MPa]	30000	31.85	9.10	53.30	5000
Young's modulus (E_{ur}) [MPa]	-	95.55	27.30	159.90	-
Thermal expansion coefficient (α_s) [$10^{-5} \text{ }^\circ\text{C}^{-1}$]	1.2	4	4	4	4
Thermal conductivity (λ) [$\text{W m}^{-1}\text{ }^\circ\text{C}^{-1}$]	2.4	2.4	2.4	2.4	1.4
Specific heat capacity (c_s) [$\text{J kg}^{-1} \text{ }^\circ\text{C}^{-1}$]	100	1000	1000	1000	1300
Cohesion (c') [kPa]	-	1	-	-	
Friction angle (ϕ') [$^\circ$]	-	37	32	37	28
Dilatancy angle (ψ) [$^\circ$]	-	7	2	7	-

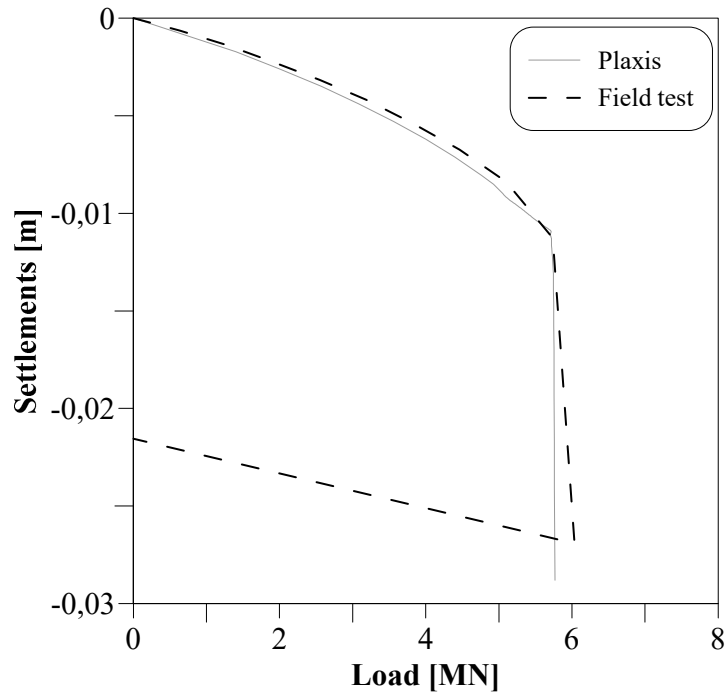


Figure 4-2 – Load-Settlements curve. Comparison between experimental and simulated results

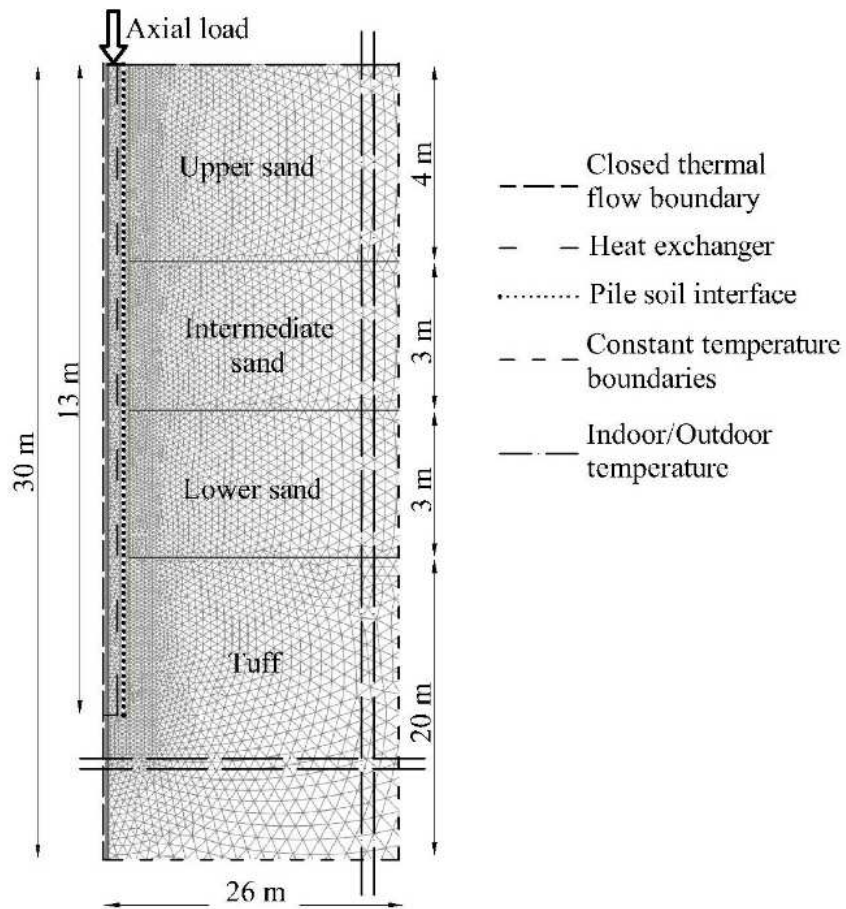


Figure 4-3 - The adopted model

To analyse the energy pile mechanical behaviour an axisymmetric model 30 m in length and 26 m in width with a triangular fine mesh of 15 nodes elements was setup.

Different thermal boundary conditions were adopted around the model box. A closed thermal flow boundary was inserted in correspondence of the pile axis edge to take into account the axial symmetry of the model. On the other vertical boundary, constant temperature boundary was adopted. The temperature chosen for this boundary was 17 °C, temperature assumed for the initial and undisturbed condition of the soil in Neapolitan context. It should be noted that assuming a constant temperature for the lateral edge of the model was a simplification because of the previously discussed natural soil temperature variation with the depth. However, the distance between the boundary and the pile (approximately 43 times the pile diameter) was large enough to not influence the soil/pile thermomechanical interaction.

On the top of the model the effects of two boundary conditions were explored: the “indoor” or the “outdoor” constant temperatures were assigned. An imposed constant temperature vertical line was imposed at 0,25 m from the pile axis to simulate the location of the heat exchanger pipes inside the pile. The temperature assigned to this boundary depended on the results obtained from the energy simulation and was variable over the time.

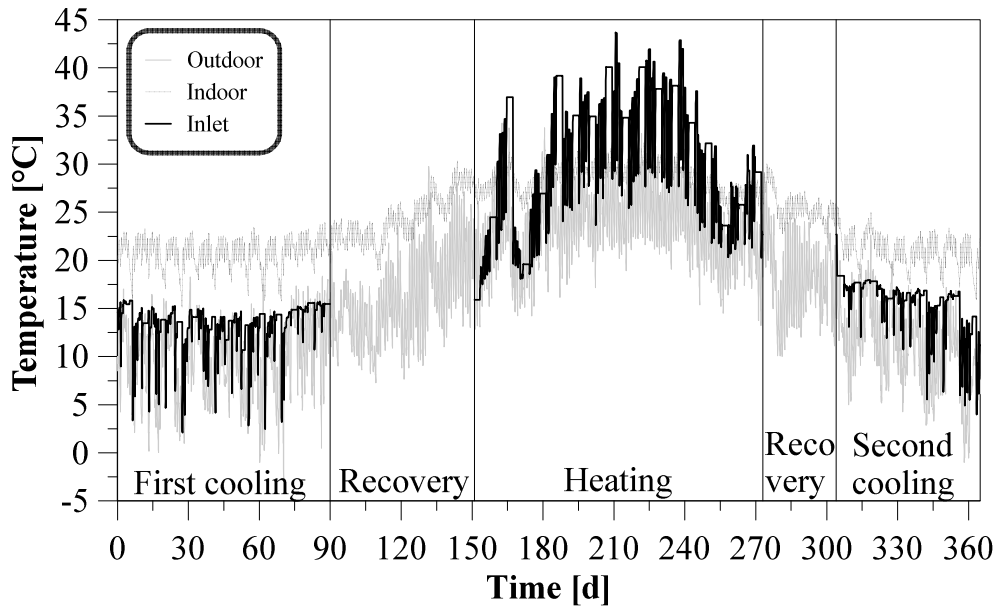
A fully coupled thermo-hydro-mechanical analysis, for the same pile and the same subsoil conditions, was carried out. A constant service load of 2400 kN equal to the 40% of the ultimate pile’s capacity was applied on the pile head and coupled with the variable thermal loads provided by the building energetical simulation.

4.2.2 The 2D simulation

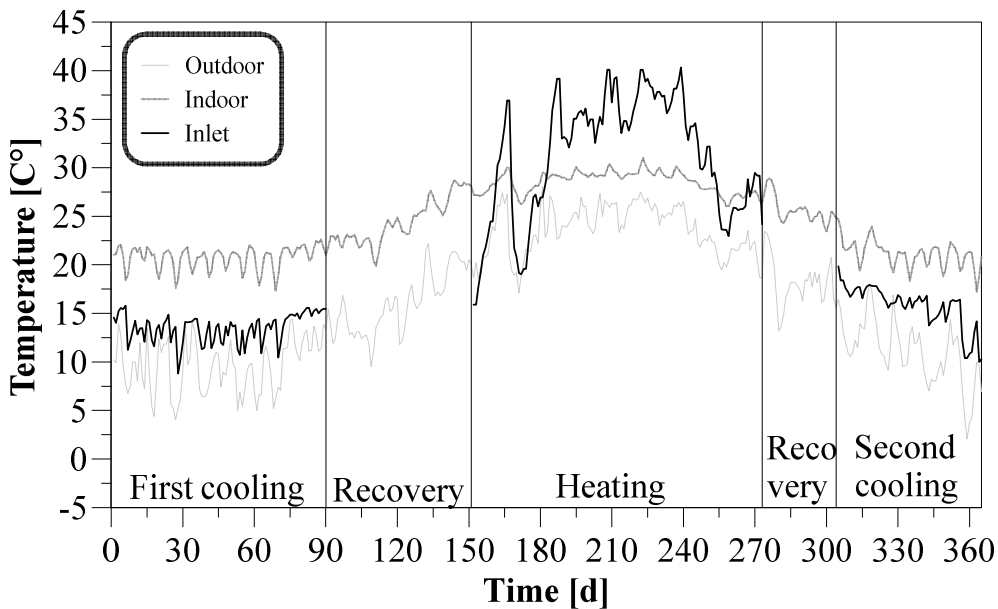
The numerical analysis was carried out considering one year of the GSHP operation. For the system it was hypothesised a daily “on-off” operation mode from the 8:00 a.m to 18:00 p.m., from Monday to Friday. Moreover, it was also assumed that the plant did not work continuously for all the year. In fact, in April, May and October it was considered turned off. The reasons of these choices were already described in chapter 3.

The thermal loads cycle was subdivided in 5 steps according to the following list: (Figure 4-4):

1. First cooling cycle. Duration 90 days;
2. First recovery phase. Duration 61 days;
3. Heating cycle. Duration 122 days;
4. Second recovery phase. Duration 31 days;
5. Second cooling cycle. Duration 61 days.



a)



b)

Figure 4-4 – Outdoor, indoor and inlet carrier fluid temperature values a) hourly; b) daily

First a simulation comparing different kinds of thermal loading was carried out. Cycles with hourly or daily thermal variation, HTV and DTV, respectively, were considered.

The comparison was carried out comparing both the pile head displacements and the axial forces of the two condition.

In Figure 4-5 the pile head displacements are reported. First of all, an obvious trend of the pile head to settle for cooling load phases and to heave for the heating phase should be noticed. During the first recovery, the tendency of the temperature is to increase because of the surface temperature. Moreover, also the pile/surrounding soil system, when the cooling phase is finished, tends to return to the undisturbed soil temperature. It corresponds to a heating for the pile. Vice versa, the opposite can be

observed in the second recovery where from the warm season the simulation is continuing to the cold one. In this case, the heated system (pile and the surrounding soil) tend to return to the undisturbed temperature.

Two analyses are compared: one is based on an inlet temperature defined on an hourly basis and the other on a daily basis. The maximum incremental displacement obtained for the hourly simulation is 4,86 mm while for the daily simulation is 4,40 mm. Because the settlements due to mechanical effects are equal to 3,21 the impact on the settlements increase of the thermal loads are 37% and 51% for the hourly and daily variation, respectively (Figure 4-5).

However, comparing the maximum displacements obtained with the two simulations, the difference results less than 0,5 mm, which is a magnitude that can be considered nearly negligible for engineering purposes.

At some predetermined time along the thermal cycle, the axial forces were evaluated both for daily and hourly temperature variation. The thermomechanical axial force trends are compared with the axial forces provided by the mechanical case (Figure 4-6 a). In the heating phase, as expected, the compressive axial loads increased than the mechanical phase and the effects are more evident in the hourly simulation. On the other hand, the cooling phase decrease the compressive stress. In this case the axial force values of the daily and hourly simulation are not so far. In Figure 4-6 a) the second recovery rest is also reported. In fact, it is interesting to notice that, also without the application of thermal loads to the pile, the axial force trend do not correspond to purely mechanical one as expected because of a thermal variation into the pile linked to the previous phase. Finally, it can be observed that at the end of the yearly cycle, both for the case of daily and the hourly thermal variation simulation the axial forces are smaller than the mechanical case. This occurs since at the end of the cycle temperatures lower than the initial ones are recorded.

The results confirm also for the axial forces that a great difference between the hourly and daily simulation is not found. It can be concluded that the greater computational efforts to carry out an hourly simulation on a whole year is not needed. A simpler and less demanding daily simulation on a whole year period is a good compromise.

After, considering the obtained results, a comparison between daily variation simulations was carried out by comparing indoor and outdoor temperatures on the top surface boundary.

The aim was to investigate the different energy pile behaviour under different boundary conditions. The effects on the pile head displacements versus the time have already investigated before. Now, the effects on the axial forces are described.

As the previous case, the axial forces were evaluated in different phases of the yearly cycle. In Figure 4-6 b) the axial force trends for the different cycle phase and the mechanical trend is plotted.

It is possible to notice that by applying the outdoor temperature, axial forces in the heating phase are more compressive than the indoor case. On the other hand, in the cooling phases, the indoor temperature boundary condition seems to produce smaller axial force values if compared to the outdoor boundary but anyway comparable. A large difference, instead, is noted in the second rest where both the outdoor and indoor boundary trend show smaller values if compared to the mechanical case.

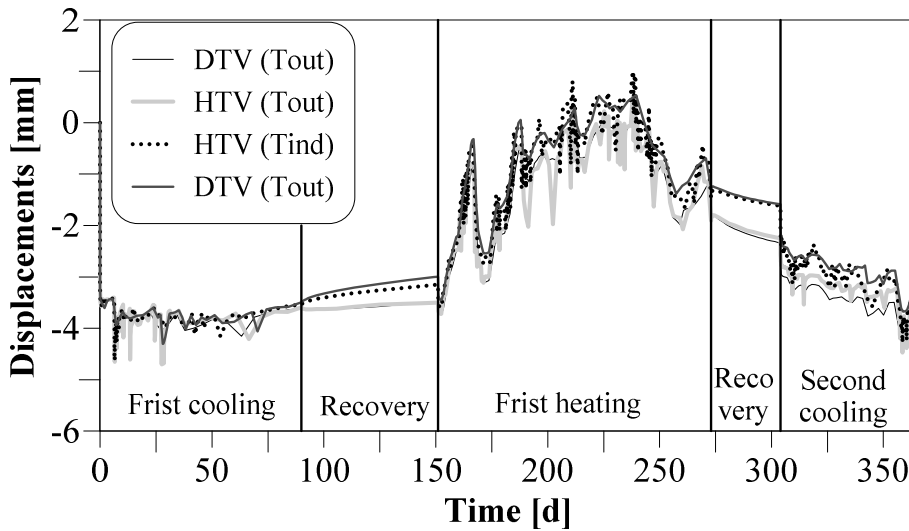


Figure 4-5 -Thermomechanical displacements for the different cases

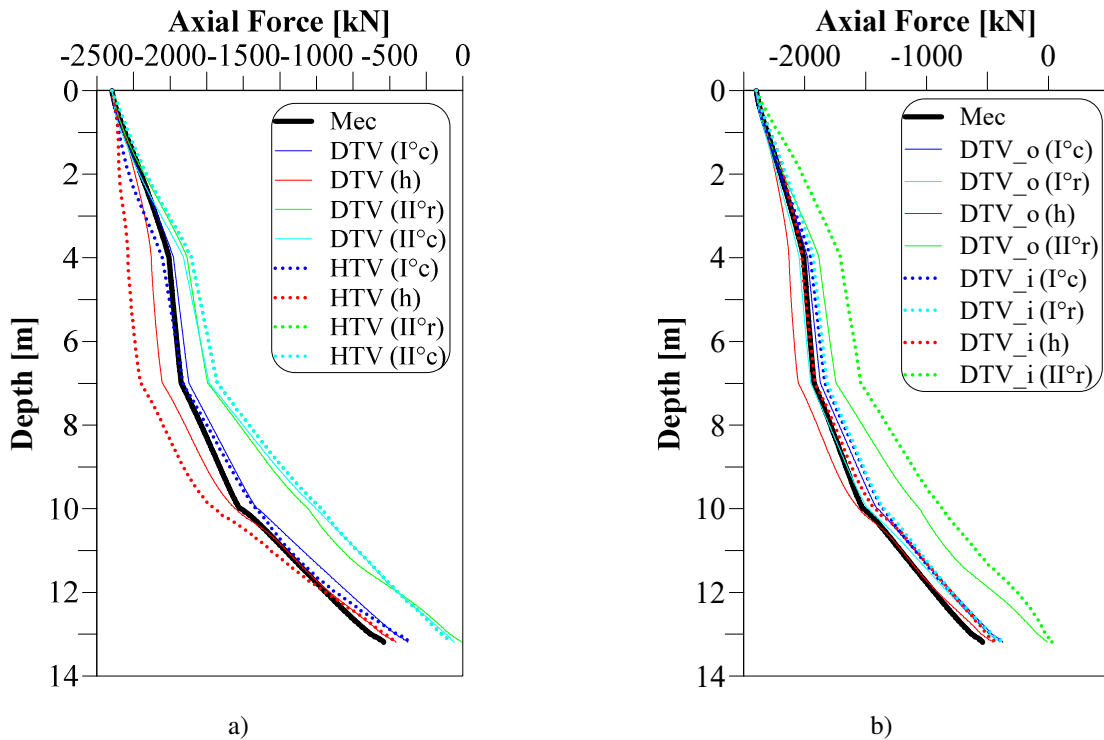


Figure 4-6 - Axial forces trend comparison between a) daily and hourly temperature variation with the application of outdoor temperature on the top boundary; b) daily temperature variation with different external temperature on the top boundary (“i” = indoor temperature, “o” = outdoor temperature, “h”= heating, “c”= cooling and “r”= recovery)

4.3 Interaction coefficient determination for a couple of energy piles

The interaction factor is a simplified method introduced by (Poulos, 1968) and (Poulos et al., 1971). Based on hypothesis of linearly elastic soil behaviour, this method allows the displacement analysis of a pile group on the basis of the knowledge of the interaction factor between a couple of two identical piles at different spacings. The linearly elastic assumption allows to make use of the superposition effect.

Numerical analysis was carried out to study the behaviour of a group of energy piles. The numerical model was developed using the finite difference software FLAC3D. The aim was to analyse the interaction in a couple of energy piles in dry pyroclastic soils by a parametric analysis.

The analysis was carried out considering two concrete piles 15 m in length and 0,60 m in diameter not mechanically loaded and with no head restraint.

Four different spacings were analysed, i.e. 2d, 3d, 4d and 5d. Both a loose sand and a dense sand subsoil profile were considered in the analyses. In both cases two different subsoil profiles were considered. In one case a stiffness constant with depth was assumed while in the other a linearly variable with depth soil stiffness was considered.

The analysis was subdivided in two main parts. In the first part, the piles were only subjected to mechanical loads. Subsequently load-settlements curves were determined for the different parameters considered. The results were also compared with the literature results obtained by Poulos. In the second part of the analysis, the same procedure implemented for mechanical case were carried out considering only thermal loads on piles.

The analysis was carried out considering a linear-elastic constitutive model both for the concrete piles and for the surrounding soil.

4.3.1 Background

When energy piles are sufficiently close each other, a “group effects” could occur both for thermal and for thermomechanical loads. Due to the interaction the pile group settlement is larger than the settlement of a single pile subjected to a load equal to the average load per pile of the group.

In the last years, some studies by numerical analysis were carried out about the behaviour of groups of energy piles.

FEM analyses were carried out by Tsetoulidis et al. (2016) with model validated on the field test carried out in Lambeth College (Bourne-Webb et al., 2009). A 3x3 pile group embedded in clay was analysed. The authors found a significant compressive force of the piles both in the cooling and in the heating phase in the case of all piles thermoactivated in the same time. Moreover, the compressive force gained in cooling phase could be attributed to the lower thermal expansion coefficient of the

concrete pile compared to the clay one. Vice versa, when only the central pile was thermo-activated, in cooling and heating phase very large axial force decrease or increase were found, respectively.

Rotta Loria et al (Rotta Loria et al., 2018; Rotta Loria and Laloui, 2018, 2017a, 2017b, 2016) carried out a series of studies about energy piles group. In this studies Finite element analyses were carried out to investigate the behaviour of a group of energy pile for different number of thermo-activated piles, the interaction factor method, and the equivalent pier method.

4.3.2 The 3D model

The numerical box was taken large enough in order to have the behaviour of the pile or of the pile couple not affected by the rigid model boundaries. The minimum distance between the piles axis and the lateral surfaces was greater than 10 diameters (6 m) and the distance between the piles toe and the bottom of the model was greater than 8 diameters (4,8 m). Consequently, the model adopted was a parallelepiped with a square plan of 20 m x 20 m and a total height of 30 m.

As said before, 4 spacings in function of the piles diameters where chosen to study the behaviour of the pile group. In Figure 4-7 plan views of the four analysed models are sketched.

The subdivision and the size of the zones of the model in plan were carried out to obtain the maximum of the discretization in the pile and in the areas immediately surrounding the group. For areas further away from the above, the zones were left wider. The motivation was due to the search for the right balance between the accuracy of the final results and the onerousness of the calculation. In this way it was possible to use a lean but precise model for the intended purpose. In the vertical side, on the other hand, for the same reasons explained before, the high of the zones were 0,50 m (Figure 4-8).

About the boundary conditions imposed on the model, in addition to geometric conditions, constraining conditions were imposed. To apply a given displacement to a boundary, it was necessary to prescribe the boundary's velocity. It was imposed that the boundary faces of the model, except for the upper face, had zero velocity in direction of the normal exiting their plane. In this way a condition equivalent to a system of constraints was imposed around the model (Figure 4-9).

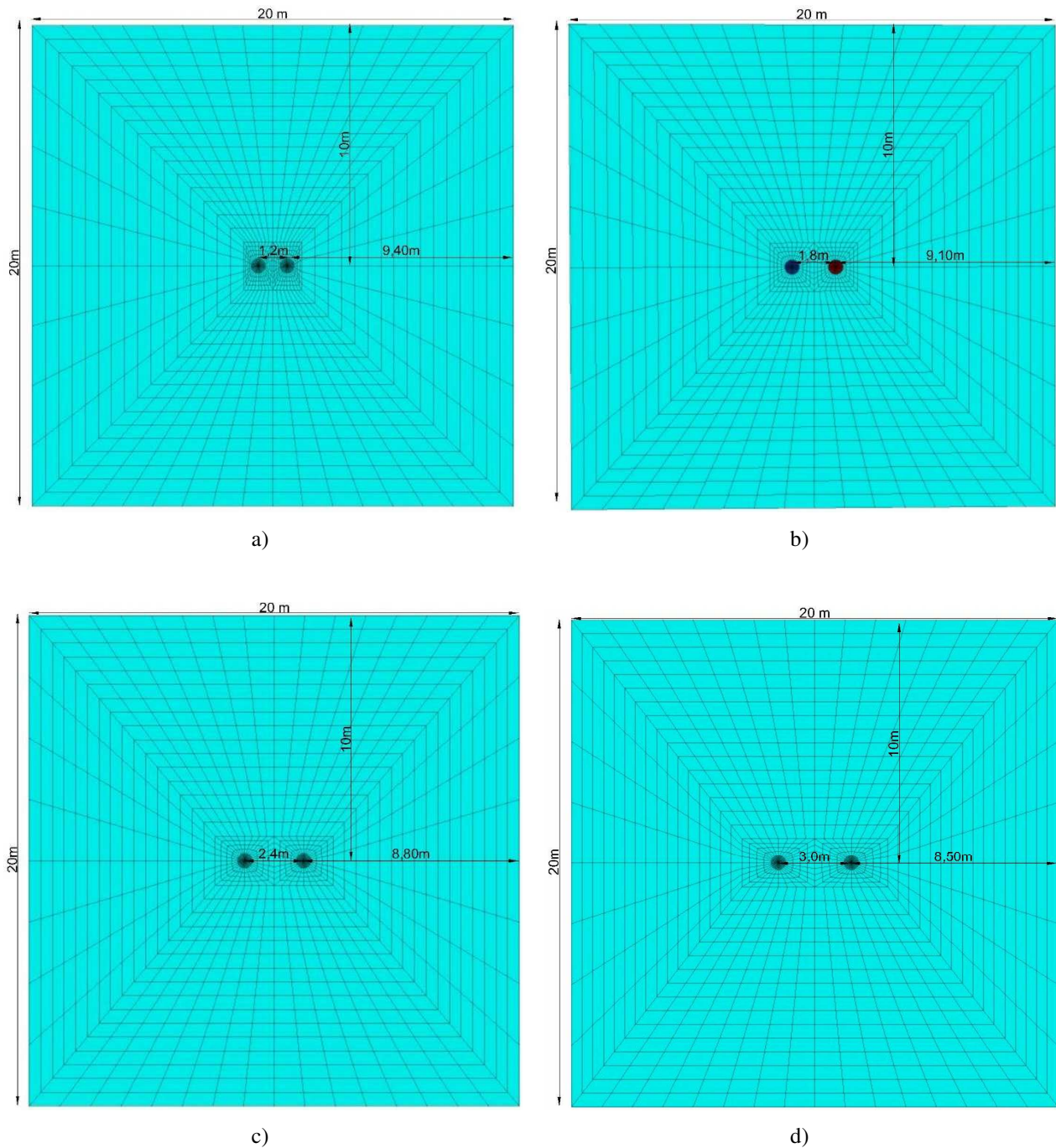


Figure 4-7 – Plan view of the geometries of the adopted model for distances between the piles of a) 2 diameters; b) 3 diameters; c) 4 diameters; d) 5 diameters

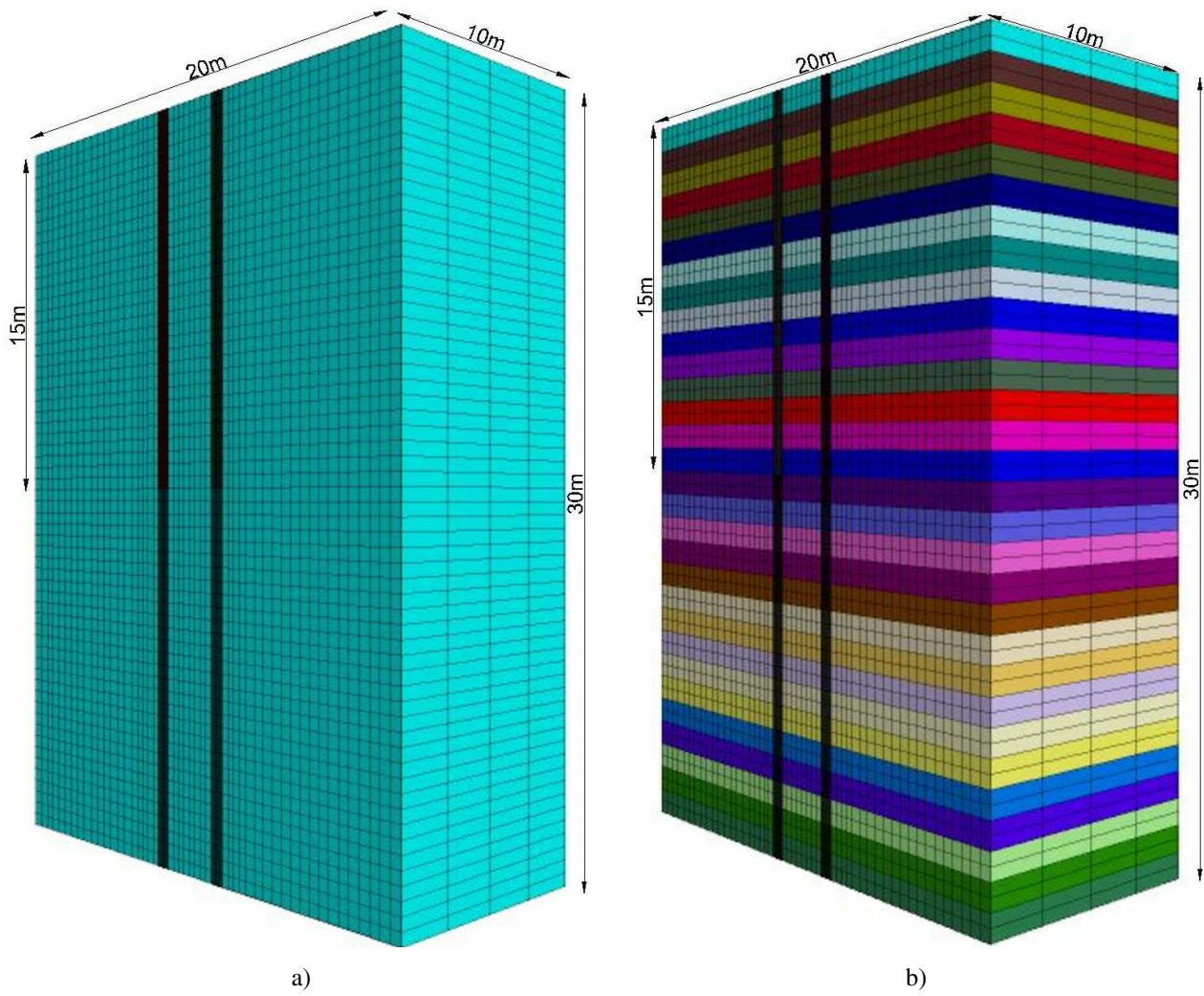


Figure 4-8 - Geometry and discretisation of zones of the adopted model a) with homogeneous soil properties with depth; b) with soil properties varying with depth

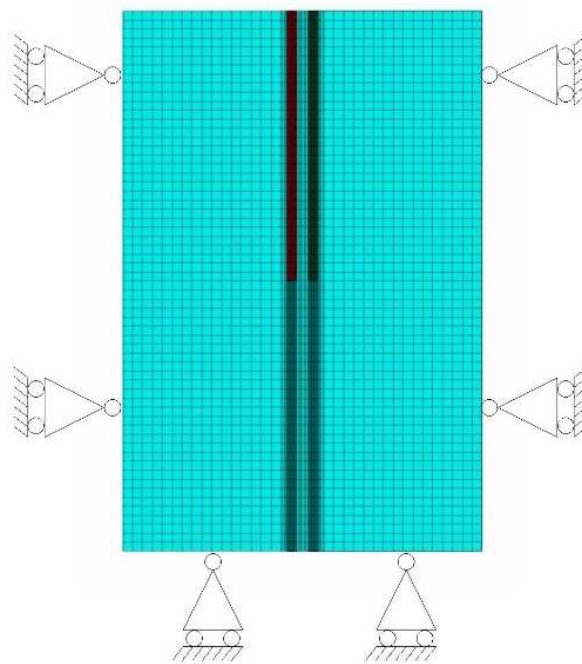


Figure 4-9 - Schematisation of the boundary conditions of the adopted model

4.3.3 The mathematical approach to the thermomechanical problem in FLAC3d

In FLAC3D a thermomechanical analysis was carried out using the thermal option of conduction models. This kind of model, in fact, allow simulation of transient heat conduction in materials, and the development of thermally induced displacements and stresses.

The relation between the heat-flux vector and the temperature gradient is linked by the Fourier's law.

In the case of stationary, homogeneous, isotropic solid, the law is:

$$q_i = -\lambda T_i$$

Equation 4-1

Where T is the temperature [°C] and λ is the thermal conductivity [W/m°C].

An isotropic conduction material model was adopted both for pile and surrounding soil.

For isotropic conduction the thermal conductivity matrix is:

$$\lambda = \lambda \cdot \begin{bmatrix} 1 & 0 & 0 \\ 0 & 1 & 0 \\ 0 & 0 & 1 \end{bmatrix}$$

Equation 4-2

For this model one conductivity scalar parameter is sufficient.

Anyway, in isotropic model in addition to the thermal conductivity, it will also be necessary to provide the scaled value of the thermal expansion coefficient and the specific heat for each material of the model.

The temperature and the three components of the heat flux are the variables involved in FLAC3D in heat conduction related through the energy-balance equation and transport laws derived from Fourier's law of heat conduction. The differential expression of the energy balance is:

$$-q_{i,j} + q_v = \frac{\partial \zeta}{\partial t}$$

Equation 4-3

Where:

q_i is the heat flux vector [W/m²];

q_v is the volumetric heat-source intensity [W/m³];

and ζ is the heat stored per unit volume [J/m³];

t is the time [s].

Generally, a change in temperature could be caused by changes both in volumetric strain ϵ and energy storage. Relating those parameters, the thermal constitutive law can be expressed as:

$$\frac{\partial T}{\partial t} = M_{th} \left(\frac{\partial \zeta}{\partial t} - \beta_{th} \frac{\partial \epsilon}{\partial t} \right)$$

Equation 4-4

Where M_{th} and β_{th} are material constants and T is the temperature. FLAC3D consider the particular case in which $M_{th}=1/(C_v\rho)$ and $\beta_{th}=0$ where ρ is the mass density of the medium [kg/m^3] and C_v is the specific heat at constant volume [$\text{J}/\text{kg}^\circ\text{C}$]. The basic assumption is that strain changes play a negligible role in influencing the temperature, a valid assumption for quasi-static mechanical problems involving solids and liquids. So:

$$\frac{\partial \zeta}{\partial t} = \rho C_v \frac{\partial T}{\partial t}$$

Equation 4-5

By substituting Equation 4-5 in Equation 4-3 the energy-balance equation became

$$-q_{i,j} + q_v = \rho C_v \frac{\partial T}{\partial t}$$

Equation 4-6

A reformulation of the incremental stress-strain relations is required for the solution of thermal-stress problems, which is accomplished by subtracting the portion due to temperature change from the total strain increment. Since free thermal expansion does not cause any angular distortion in an isotropic material, the shearing-strain increments are unaffected. The thermal-strain increments associated with the free expansion corresponding to temperature increment is:

$$\Delta \varepsilon_{i,j} = \alpha_t \Delta T \delta_{ij}$$

Equation 4-7

Where α_t is the coefficient of linear thermal expansion, and δ_{ij} is the Kronecker delta.

On the other hand, during a transient simulation, the heat transfer can be coupled to thermal-stress calculations at any time. As said before, the relationship between stress and temperature is only in one way i.e. the temperature can affect the stress change, but it is not possible the contrary. The stress change in a triangular zone, assuming a constant temperature in each triangular zone that is interpolated from the surrounding grid points is:

$$\Delta \sigma_{i,j} = -3K\alpha_t \Delta T \delta_{ij}$$

Equation 4-8

where K is the bulk modulus [Pa]. This stress is added to the zone stress state prior to application of the constitutive law.

4.3.4 The material properties

One of the aims of this section is to determine the coefficient of interaction between piles. Both the piles and the surrounding sand were modelled with a linear elastic model. Bulk and shear modulus were the only two properties to fix.

In Figure 4-10 the trend of the bulk and the shear moduli were reported both for dense and loose soil considering both homogeneous soil and not homogeneous one.

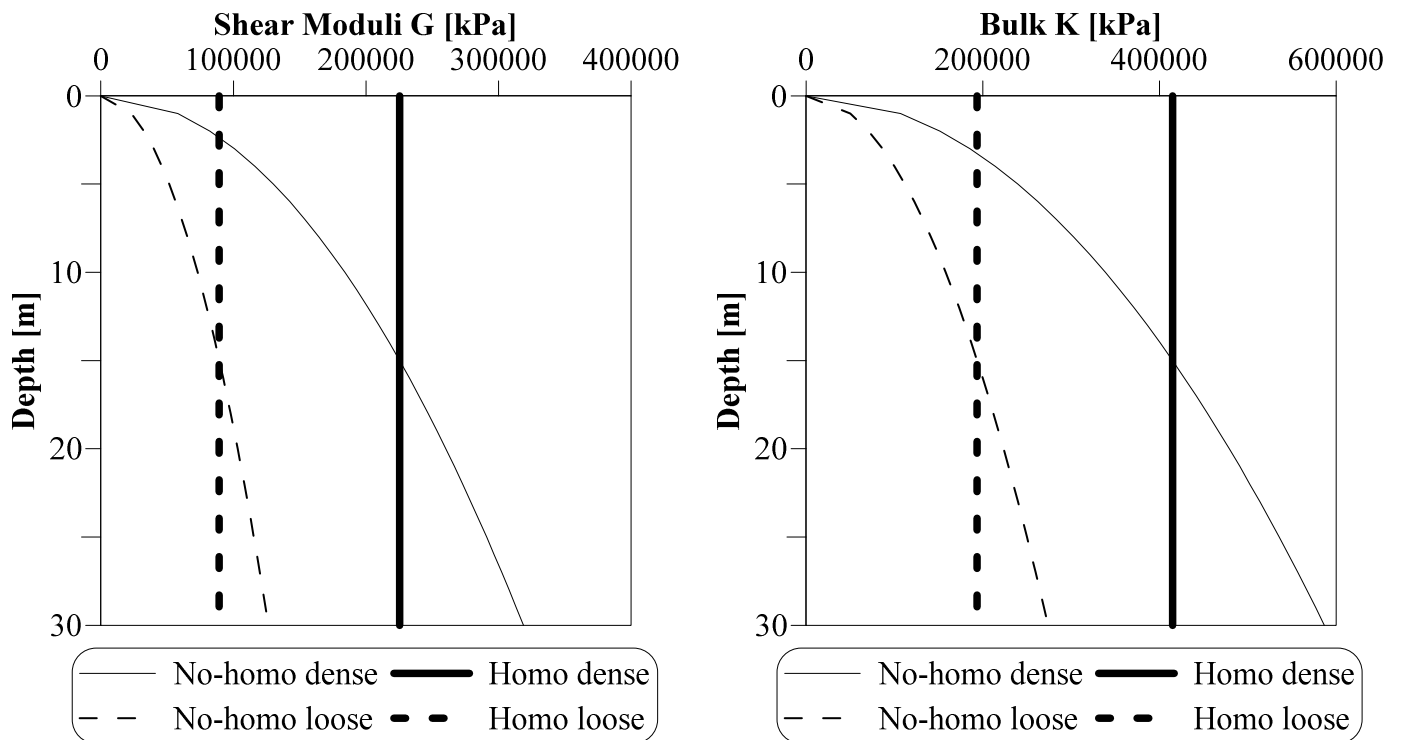


Figure 4-10 - Soil properties for the different model used in the numerical analysis a) shear moduli b) bulk

In Table 4-2 the mechanical parameters are summarized both for the dense soil and for the loose one. On the other hand. In Table 4-3 the concrete mechanical parameters used for the piles were summarized.

Table 4-2 – Soil parameters for dense and loose soils

	ρ	ν
SOIL	[kg/m ³]	[-]
dense	2200	0,27
loose	2000	0,3

Table 4-3 – Concrete parameters for the piles

Concrete		
K	G	v
[kPa]	[kPa]	[-]
1,67E+07	1,25E+07	0,2

4.3.5 The mechanical analysis

During the mechanical analysis for the interaction factor determination, only one pile of the couple was mechanically loaded and the head displacements of both the active and the passive piles were determined. Conventionally, for these analyses the loaded pile was named pile A while the unloaded pile was named “pile B”.

The coefficient of interaction between the two piles was calculated as:

$$\alpha = \frac{w_B}{w_A}$$

Equation 4-9

where w_B was the pile B head displacements while w_A was the pile A head displacements.

The pile A was loaded by a velocity applied on pile head of 1×10^{-6} m/s. It was established that the analyses carried out in 60000 steps (every step corresponded to 1 second). In this way, the analysis was carried out imposing a final pile settlement of 0,06 m. This value corresponded to a displacement equal to the 10% of the pile diameter. Of course, it is evident that being the analyses limited to the elastic model the fixed final settlement has no particular meaning.

In Figure 4-11 the linear load settlement relationships are plotted. The aim of the plot is obviously only to compare the different inclination of the lines. From the plots on the side A it is possible to outline the stiffening effect due to the presence of the passive pile. This effect tends to keep nearly constant independently from the spacing increase. Anyway, the differences in behaviour between the couple of piles and the single pile is more evident in not-homogeneous soils. In dense homogeneous soil this difference is the minimum.

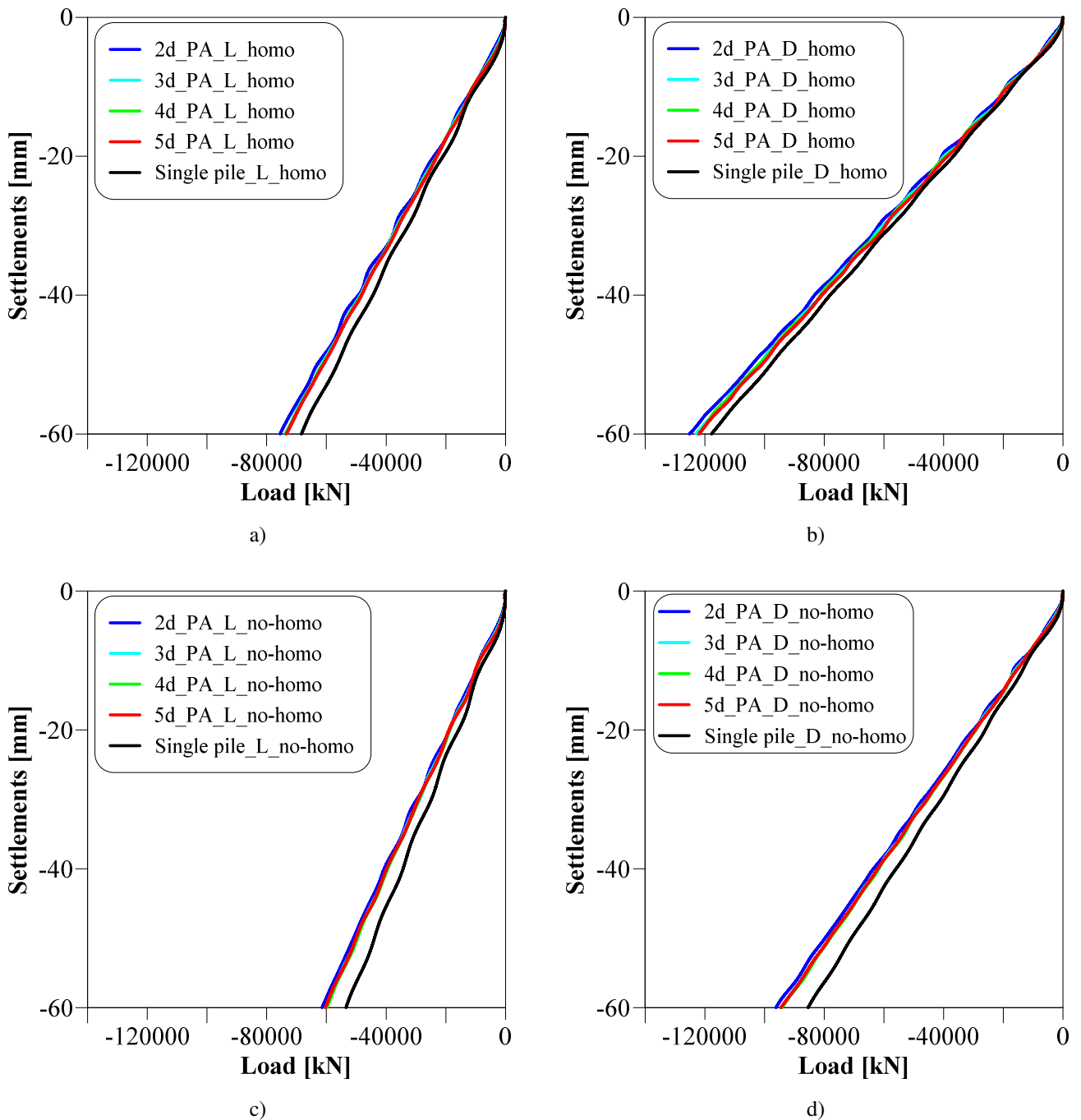


Figure 4-11 – Load/Settlements curves comparing for different distances between the piles a) Pile A in loose homogeneous soil; b) Pile A in dense homogeneous soil; c) Pile A in loose not-homogeneous soil; d) Pile A in dense not-homogeneous soil;

From these data should be noticed a significant difference between model with homogeneous properties and not-homogeneous one even if the values of mechanical properties for the homogeneous model were chosen as the property of the soil at the middle of the depth (as shown in Figure 4-10). The data collected from these analyses were sufficient to obtain the coefficient of interaction between the couple of the piles for the different scenarios considered in the numerical analyses.

According to Poulos the coefficient of interaction varied in function of the s/d ratio i.e. the ratio between the piles distances and the piles diameter, in function of the aspect ratio of the pile, i.e. the ratio between the pile length and its diameter, and finally, in function of the K coefficient. It is a

parameter defined as the ratio between the elastic modulus of the pile and the elastic modulus of the soil. In Figure 4-12 the Poulos abacus is replotted and the coefficient of interaction found from the numerical analysis are reported. In the legend of the graph, in addition to the type of soil, the K coefficients, determined by the properties of the materials considered in the analysis, are also indicated in brackets. It is possible to notice that a great accord is found above all when homogeneous soil was considered into the numerical analysis. On the other hand, when the soil parameters were function of the depth, lower coefficients values were found. This result is in line with Poulos' theory. According to the author, in fact, when interaction coefficients are calculated for soils with stiffnesses increasing with depth, values of interaction coefficients 20-25% lower were obtained.

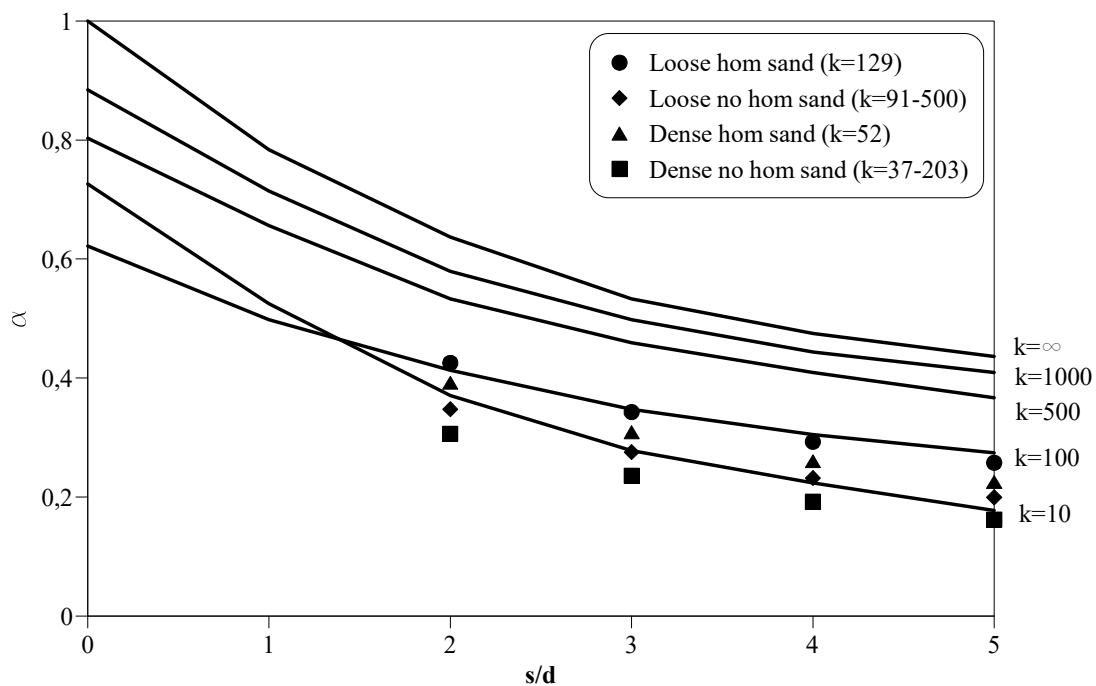


Figure 4-12 - Coefficient of interaction for the different scenarios considered in the numerical analysis. Black lines are replotted from the Poulos abacus

Finally, pile A axial forces with the depth are plotted. To compare the different scenarios of the parametric analysis, the axial force N calculated at the end of the steps was normalized with the maximum axial force at the same time instant found for a depth of 0,5 m.

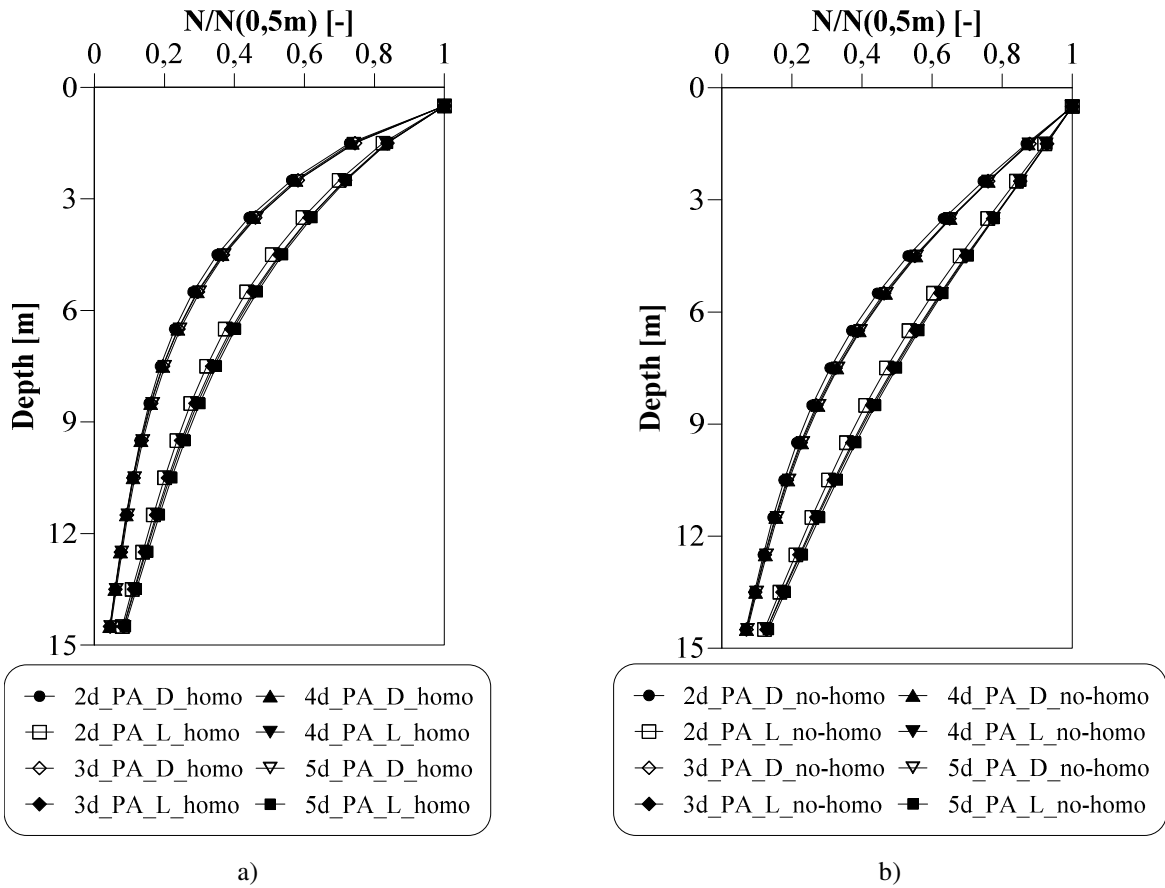


Figure 4-13 – normalized axial forces for pile A according to different criteria

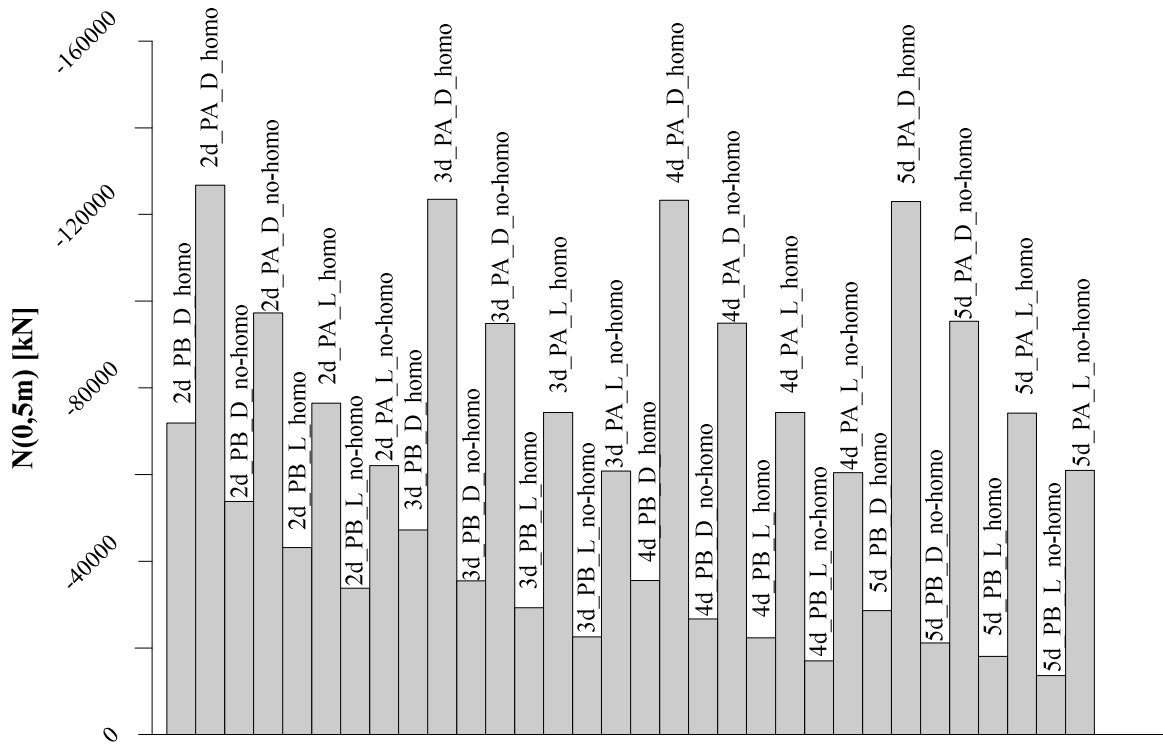


Figure 4-14 – Axial forces at depth 0,5 m for all cases of the numerical analysis

In Figure 4-13 the normalized axial forces of the pile A are compared considering different s/d ratios for loose and dense soil in homogeneous and not-homogeneous case.

By the graphs of the Figure 4-13 it is possible to notice that piles embedded in loose homogeneous soil had the maximum axial forces if compared with the same piles distances. Moreover, there is a clear difference in curves trend for the same pile and the same soil concept (homogeneous or not homogeneous) between the dense and the loose sand. In fact, in both two cases the loose sands have always higher values of normalized axial forces.

In Figure 4-14 the values of the axial forces at a depth of 0,5 m obtained at the end of any case of the numerical analysis were reported.

4.3.6 The thermal analysis

A procedure like that applied for the mechanical case was then implemented for the evaluation of the interaction coefficients of the couple of piles subjected to thermal loads. In this case the pile A was subjected to a constant heating thermal load with the time and the effects in terms of displacements and stresses were evaluated both on pile A and on pile B. Compared to the mechanical case, in thermal model the piles were equipped with a new annular zone inside the concrete section. It was placed 0,5 m from the pile external edge and had a thickness of 0,025 m. These zones simulate the insertion of spiral shaped heat exchangers inside the pile (Figure 4-15).

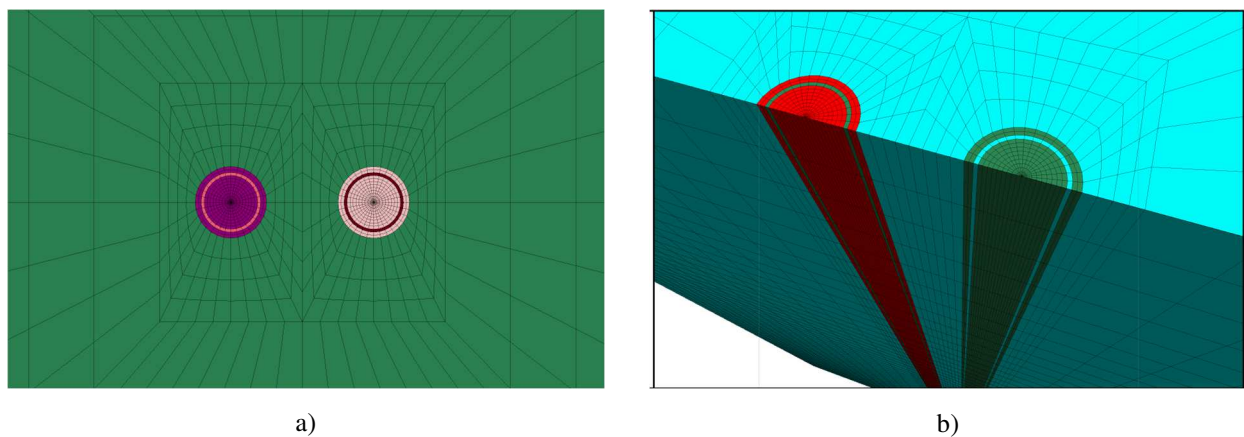


Figure 4-15 - Insertion of the heat exchangers inside the model a) plan view b) section view

The numerical analysis was carried out considering an initial soil and pile temperature of 17 °C. Then a constant temperature of 35 °C for one week was applied on the heat exchanger of the pile A.

The pile and the soil thermal properties were assigned on the basis of the literature values as explained in previous chapters 2 and 3 and are shown in Table 4-4. The values of soil thermal conductivity have been assigned considering the different soil state (loose or dense) and dry state.

Table 4-4 – Thermal properties for the materials of the model

Element	Thermal conductivity [W/m°C]	Specific heat [J/kg°C]	Linear expansion coefficient [1/°C]
Concrete	2,00	850	1x10 ⁻⁵
Heat exchangers	0,42	600	1x10 ⁻⁵
Dry dense sand	0,266	800	4x10 ⁻⁵
Dry loose sand	0,226	800	4x10 ⁻⁵

Heating the pile, A, a heave of the pile B was observed. For the thermal case, also, an increase of displacement was observed in unload pile. The displacement magnitude varied, as the mechanical case, in function of a coefficient of interaction. The coefficient values depended on the different parameters considered in the numerical analysis.

Despite the mechanical case, in thermal case the coefficient of interaction α was calculated as the ratio between the thermal displacements of the pile B due to the interaction of the pile A and the displacement of a single pile in the same soil

$$\alpha = \frac{w_B}{w_{single\ pile}}$$

Equation 4-10

In Figure 4-16 the trend of the coefficient of interaction for the thermal case was plotted and compared both with the mechanical case and with the Poulos abacus for a couple of pile with an aspect ratio of 25.

It could be observed that, as for the mechanical case, increasing the distance from piles the coefficient decreased. Anyway, despite the mechanical case the trend of the interaction factor for the thermal case is opposite considering the K coefficient. Not homogeneous sands make exception. In this case seemed that also for the thermal case the non-uniformity of the soil modulus with the depth played a role in the coefficient of interaction. As observed for the mechanical case and in agreement with literature (Poulos et al., 1971) when the modulus varied with the depth lower values were found. This result was also observed by (Rotta Loria and Laloui, 2016).

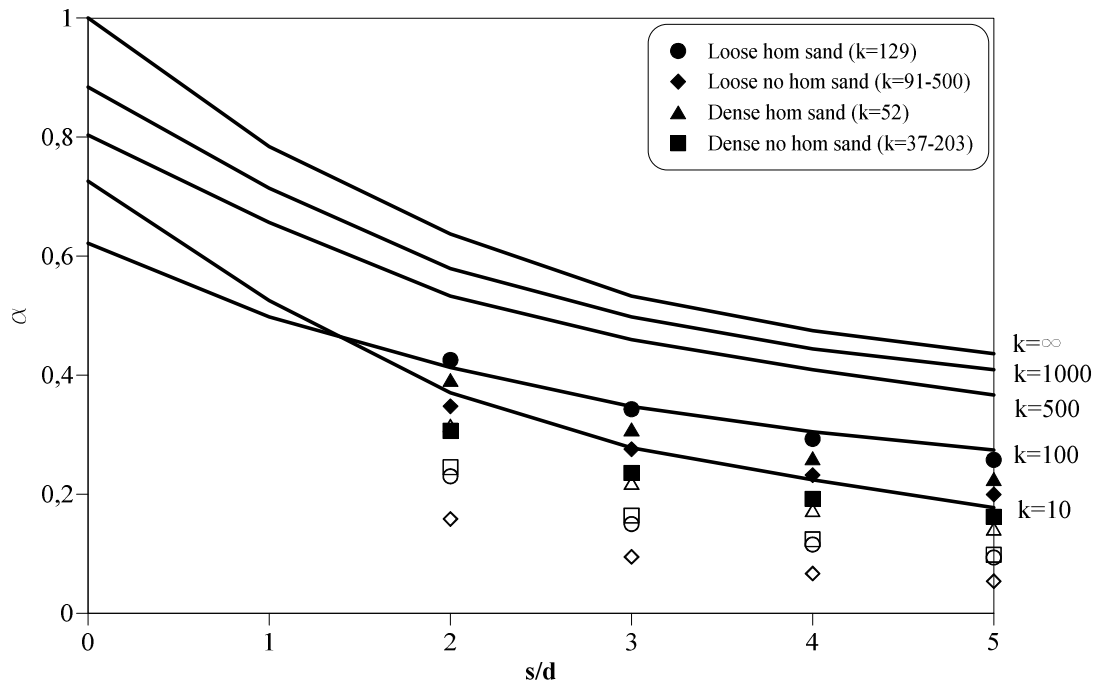


Figure 4-16 - Coefficient of interaction for the different scenarios considered in the numerical analysis. Full symbols represent the mechanical case while empty symbol thermal case for the same K parameter. Black lines are replotted from the Poulos abacus

The shaft resistance, the shaft stress, and the axial forces of the pile A are also analysed for the different parameters considered in the numerical analysis.

The pile was loaded only by thermal loads and no mechanical loads were applied on pile heads both for A and B. Consequently, the axial forces provided into pile are due only by the lateral and pile toe soil restrain.

First the lateral forces and lateral stress trend were analysed over the time, with the depth and in different location of the pile circumference.

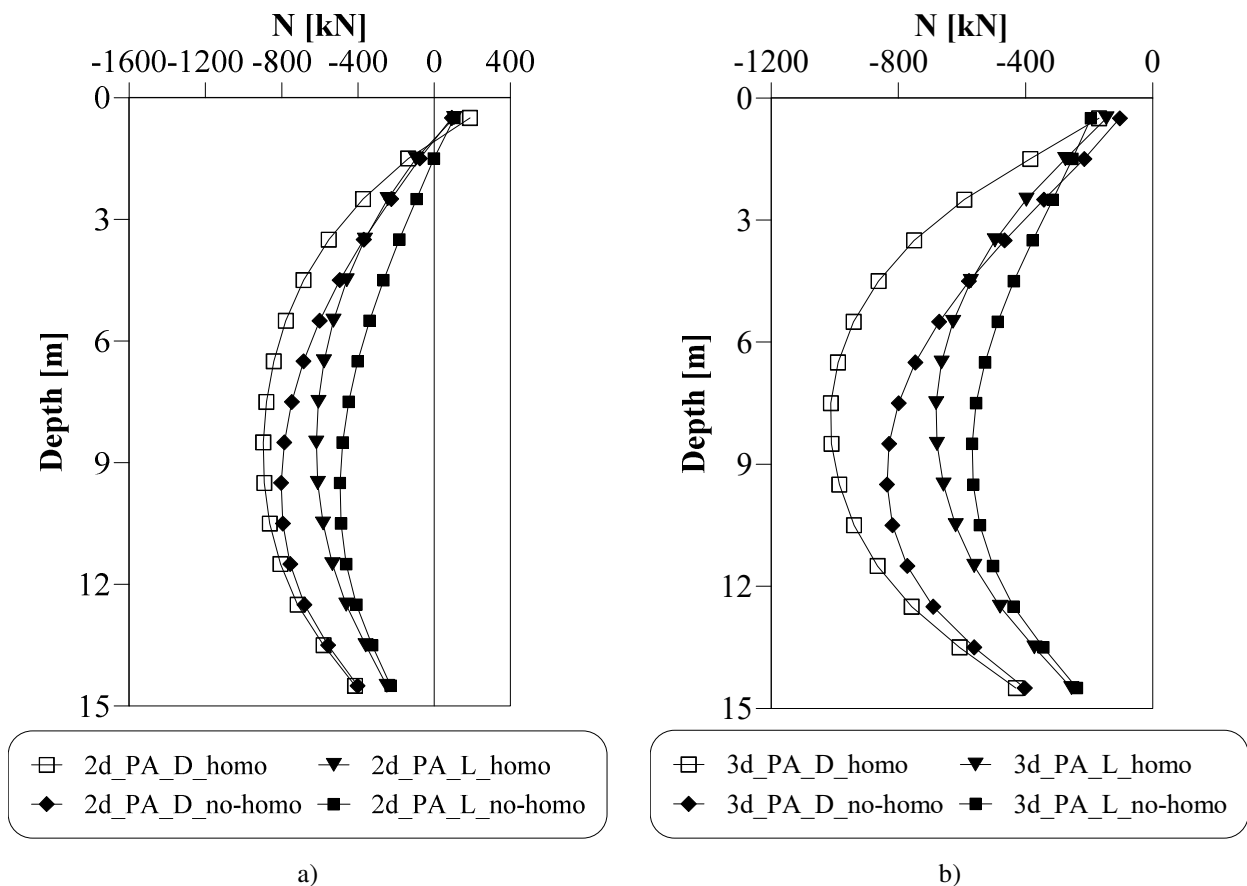
Comparing the axial forces for different pile distance and different soils it is observed that the couple of pile in dense homogeneous soil with s/d ratio of 3 had the maximum compressive values for a depth approximately in the middle of the pile. Anyway, the couple with 3 s/d ratio is the only one that showed exclusively compressive axial forces. The other pile couples in the higher zones shows axial forces nearly to null or very small tensile values. Only the pile couple with 2 s/d ratio shows higher tensile axial forces values in the upper part of the pile.

Figure 4-18 shows the shaft resistance distribution with the pile depth comparing for the same soil different s/d ratio. A difference in curve shapes is observed between the homogeneous and not-homogeneous soils with greater values for the former than the latter. Moreover, it should be noticed that while for homogeneous soil the upper and lower shaft resistance values are approximately opposite values with similar magnitude, in the other cases shaft resistance at the pile toe results greater than the values obtained at the pile head. It is due to the stiffness soil increase with the depth.

In Figure 4-19 and Figure 4-20 the case of the couple of pile with a s/d ratio 2 embedded in dense homogeneous soil was chosen to show the evolution of the shaft stress along the pile circumference for different depth and the shaft resistance over the time for different depth.

From Figure 4-19 it is possible to notice that τ_{xz} and τ_{yz} for the same angle at centre of the pile circumference had always an opposite phase of the trend. Moreover, the greater value and most definite trend were found in extreme zones of the pile. Towards the central pile zones, the values became smaller and the trend was less defined.

The same considerations could be appreciated with Figure 4-20. Considering the shaft resistance over the time, it could be observed how the extreme zones, the upper and the lower, had the greater values while toward the pile middle the values tend to zero. Moreover, after 7 days for the extreme zones the values tended to decrease with the time. So, the same analysis was carried out considering a longer time of thermal load application of 28 days. From Figure 4-20 b) a strong shaft resistance values decrease, especially of the upper zone, is appreciate.



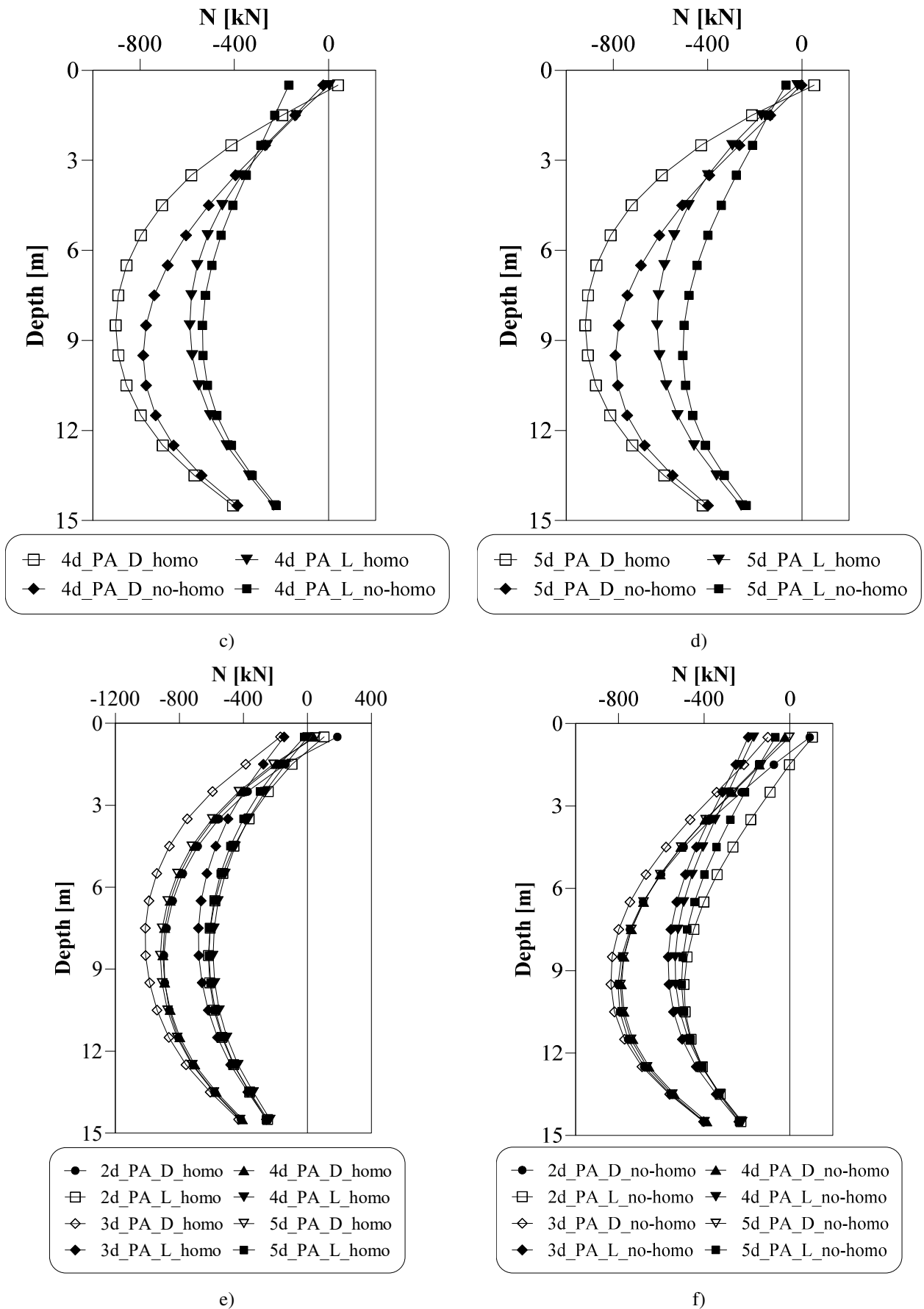


Figure 4-17 – Thermal axial forces grouped according to different criteria

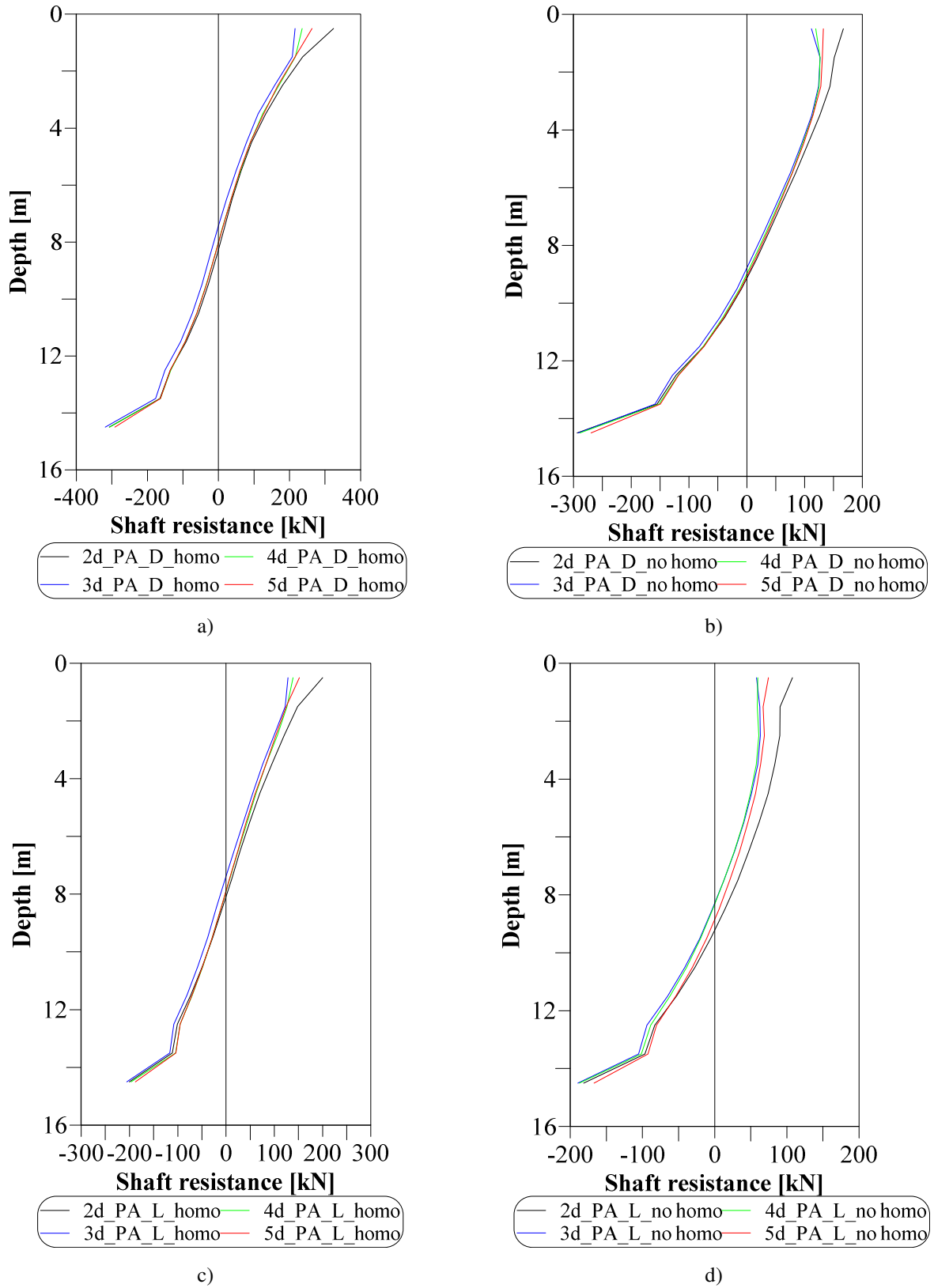
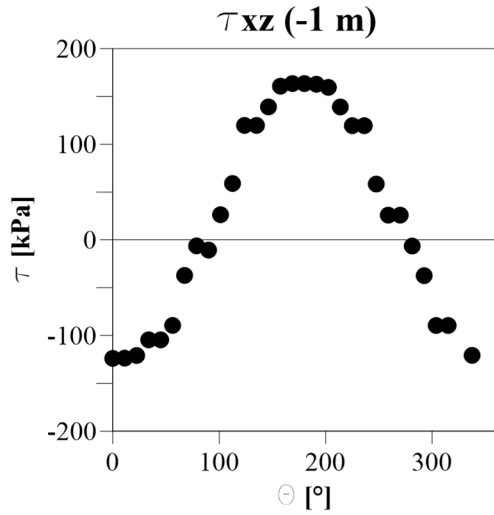
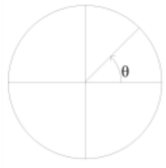
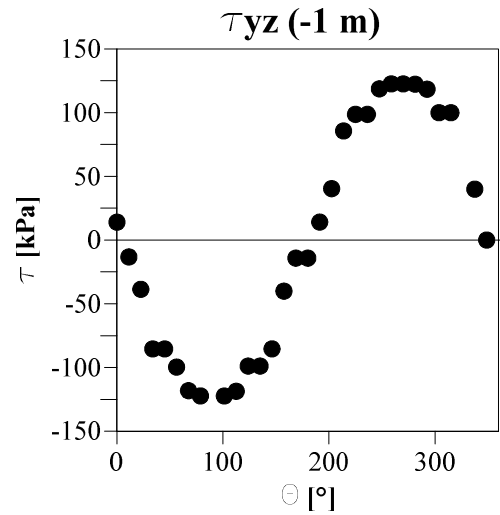


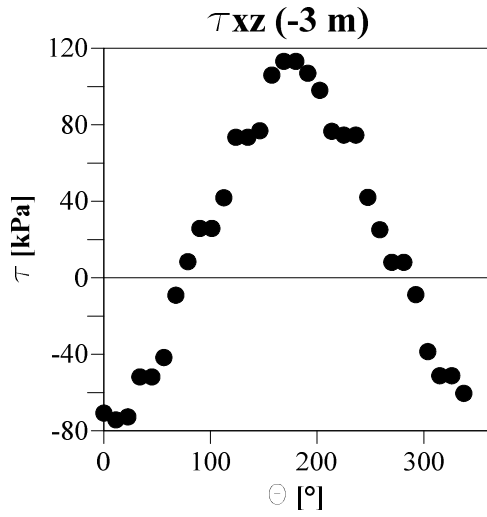
Figure 4-18 – Comparison of the shaft resistance along the pile for a) homogeneous dense soil; b) not-homogeneous dense soil; c) homogenous loose soil; d) not-homogeneous loose soil



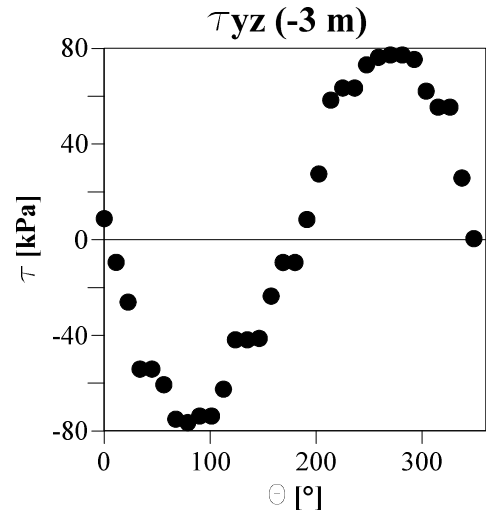
a)



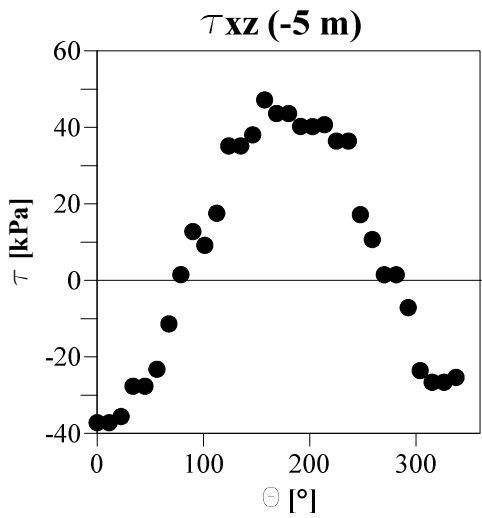
b)



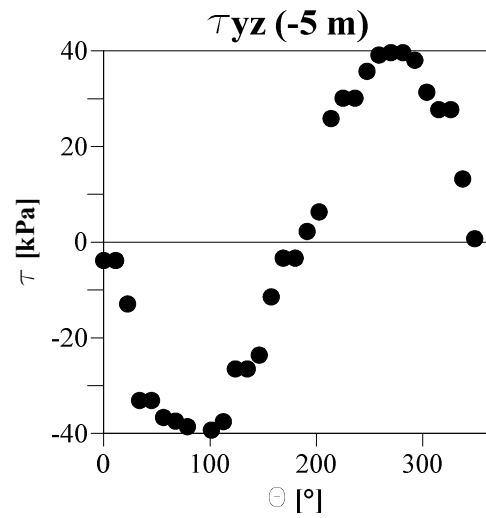
c)



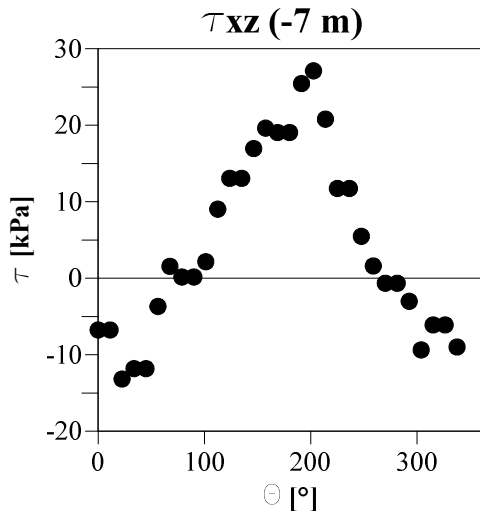
d)



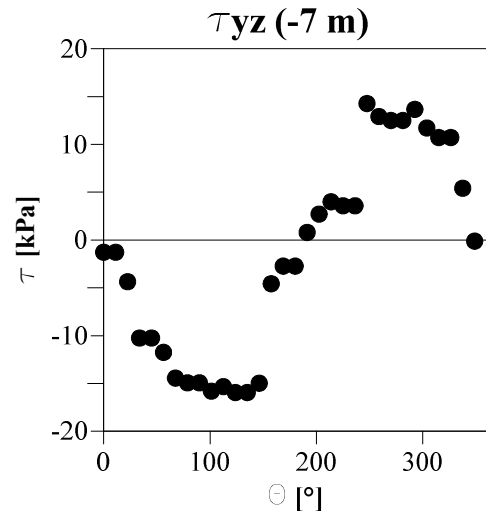
e)



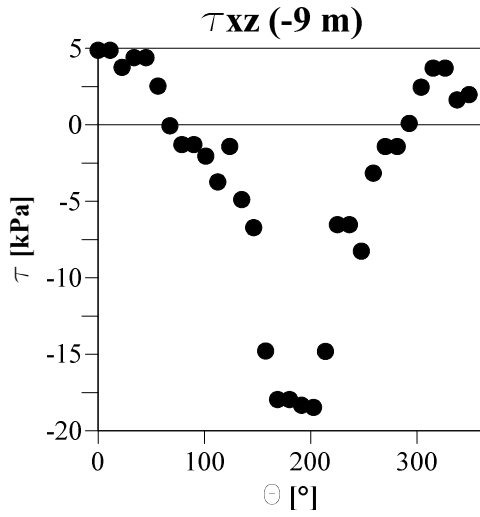
f)



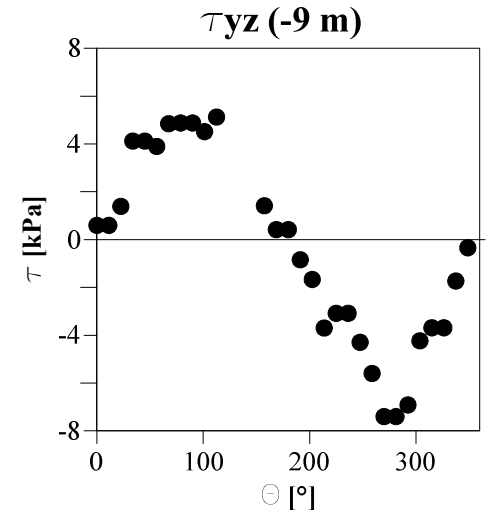
g)



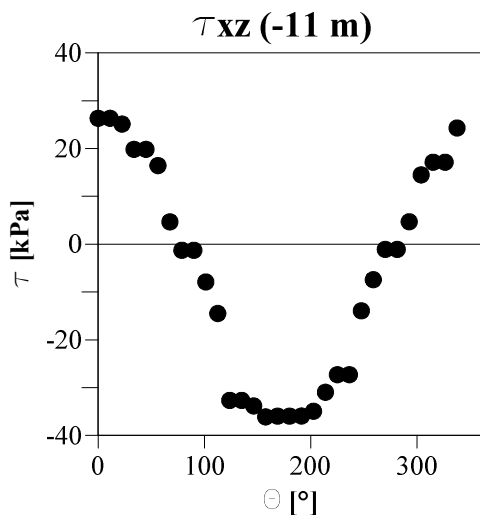
h)



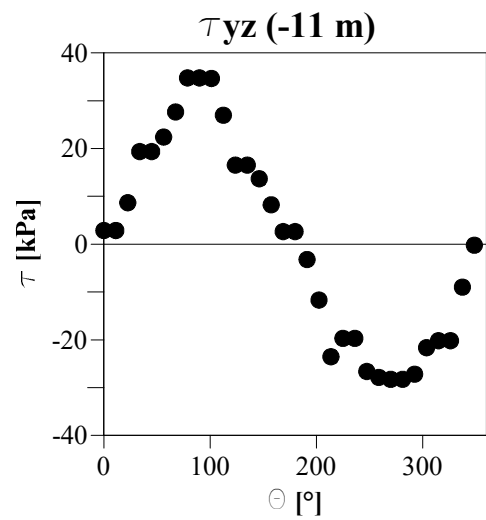
i)



j)



k)



l)

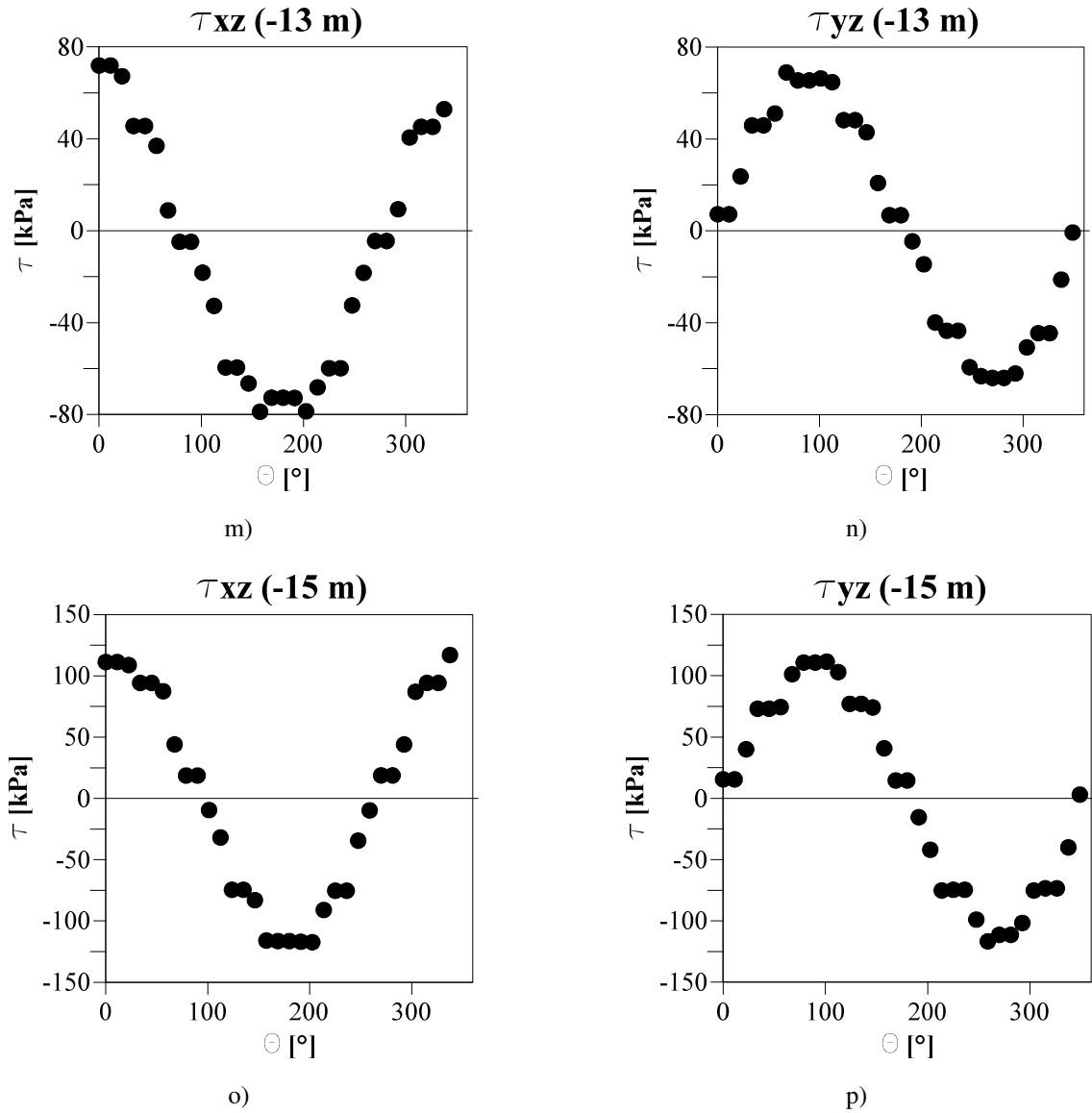
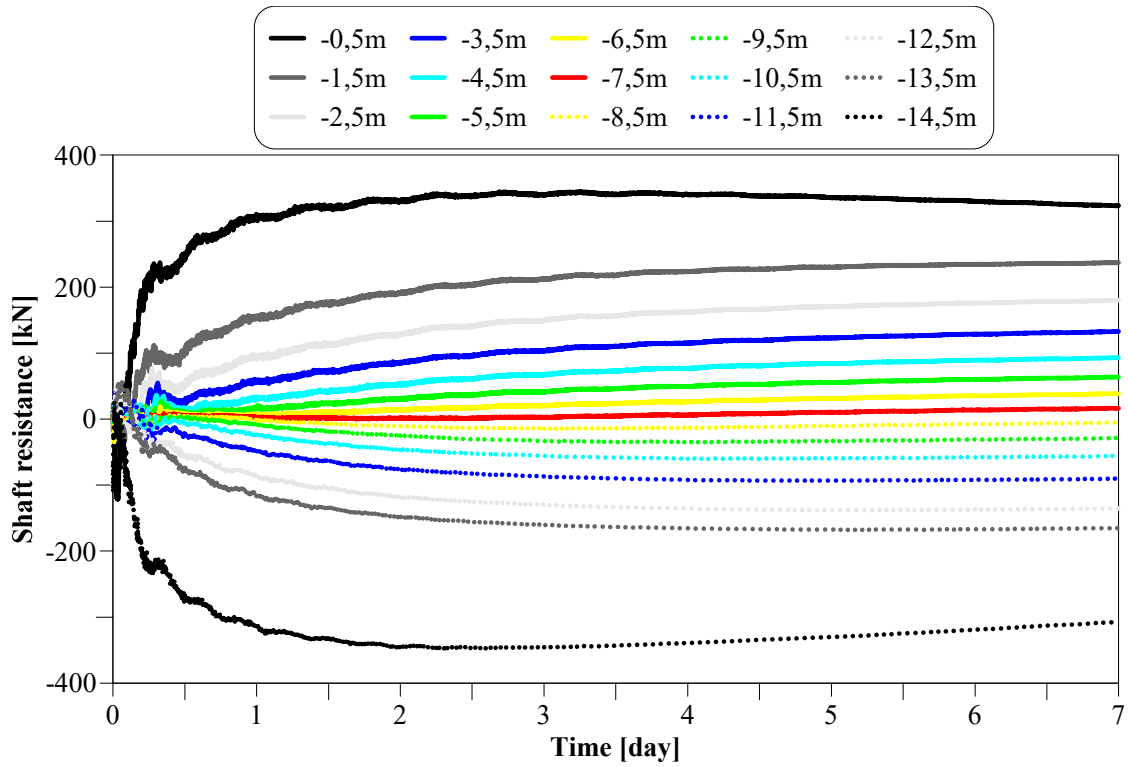
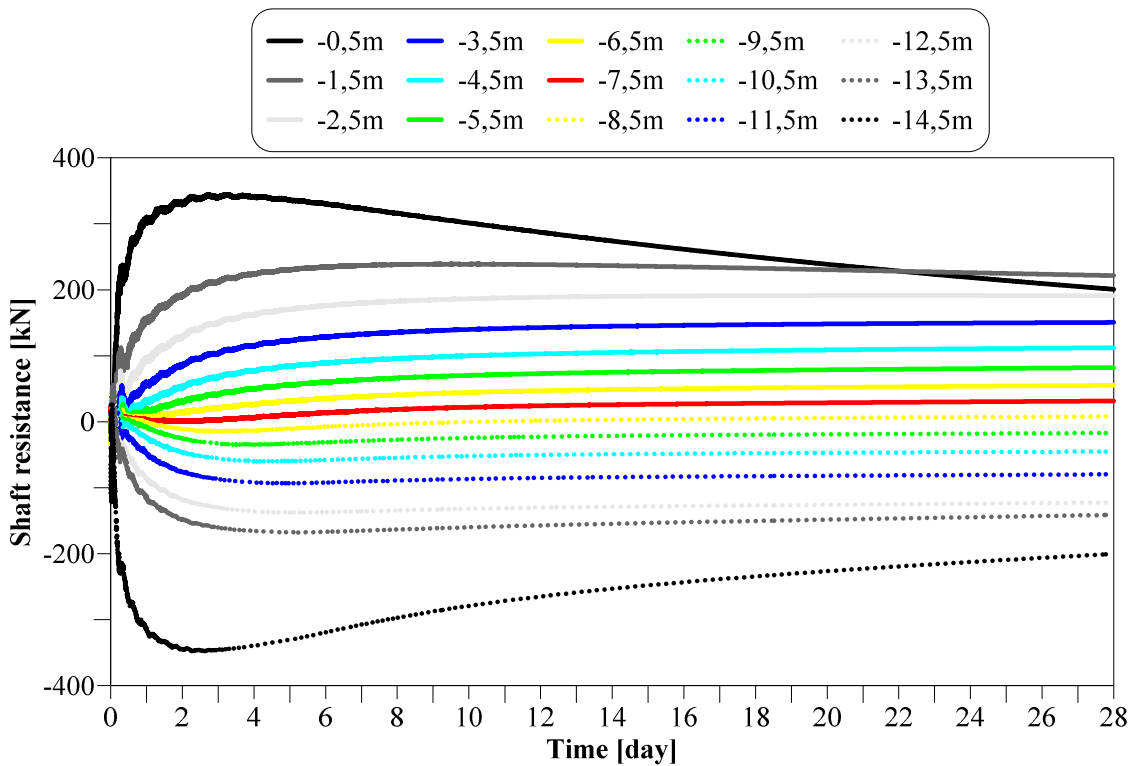


Figure 4-19 - Shear stress along the pile circumference



a)



b)

Figure 4-20 – Shaf resistance versus time for a couple of pile embedded in dense homogeneous soil with $s/d=2$ for different depths a) after 7 days; b) after 28 days

4.4 Conclusion

In this chapter, two types of numerical analysis are presented and discussed. In the first one the thermomechanical response of an isolated end-bearing pile subjected to thermal loads with different time resolutions and different thermal surface boundary condition is analysed. An axisymmetric model is used to model the pile by the finite element software Plaxis 2D. The model is contextualized in the Neapolitan area both for the geotechnical model and for thermal loads applied over the time. The effects on pile-soil interaction have been evaluated in terms of pile head displacements and axial forces along the pile shaft.

A first analysis regarded a comparison in terms of mechanical response between the application of the thermal loads considering a daily or an hourly variation. It was found that greater pile head displacements are induced by an hourly temperature variation than the daily variation while the axial forces distribution along the pile shaft is very similar in both cases. Anyway, comparing the high computational effort connected to the numerical simulation using an hourly temperature variation with the small difference on the induced effects by daily and hourly variation lead to conclude that a simulation with a daily temperature variation is the most convenient assumption in this case.

Moreover, in the second part of the analysis, the effects of different thermal surface boundary were investigated considering or the outdoor or the building indoor temperature. The latter assumption provides a simplified method to indirectly involve the superstructure heat flows in the problem. It is noted that the differences between the two assumptions are more evident in the modelled recovery phases observing the pile head displacements over the time. During the recovery phases the thermal surface boundary is the only thermal load indirectly acting on the pile while, during the heating and cooling phases, the differences between the two hypothesised boundary conditions are rather small. Anyway, seems that outdoor temperature leading to greater pile head displacements an axial force variation.

The second analysis described in this chapter, concerns the analysis of a group of energy piles and the interaction for applied thermal loads. A parametric study was carried out by the difference commercial software FLAC3D using a three-dimensional model.

The aim of the study is to investigate the behaviour of energy pile groups via the interaction factors method. For this reason, a couple of piles was modelled and elastic model both for pile and the surrounding soil was used. The analysis was carried out crossing different parameters regarding both the pile distance and the soil layering.

Previously, a mechanical analysis was carried out and interaction factors were determined and compared with results present in literature (Poulos abacus). A good agreement was found.

After, a thermomechanical analysis was carried out to obtain interaction factors for energy piles applying a thermal load on only a pile of the couple. It was found that soils with constant stiffness with the depth showed greater values of the interaction factor than the soils with stiffness variables with the depth. This phenomenon was also found for the mechanical case and documented by Poulos. Moreover, it was also observed that the interaction factor decreases with the pile distance increase. It is in accordance with the mechanical results. Anyway, it should be noticed that contrary to what happens in the mechanical case, in the thermal one the interaction factor decreases with the K coefficient increase.

However, comparing the mechanical and thermal cases, it should be noticed that for same group geometry and soil properties, mechanical interaction factors are always greater than the thermal one. Regarding the axial force it was observed that the distance of the pile and the type of soil could change the magnitude of the axial forces along the pile shaft.

4.5 References

- Bourne-Webb, P.J., Amatya, B., Soga, K., Amis, T., Davidson, C., Payne, P., 2009. Energy pile test at Lambeth College, London: Geotechnical and thermodynamic aspects of pile response to heat cycles. *Geotechnique* 59, 237–248. <https://doi.org/10.1680/geot.2009.59.3.237>
- Jeong, S., Lim, H., Lee, J.K., Kim, J., 2014. Thermally induced mechanical response of energy piles in axially loaded pile groups. *Appl. Therm. Eng.* 71, 608–615. <https://doi.org/10.1016/j.applthermaleng.2014.07.007>
- Marone, G., Di Girolamo, L., Pirone, M., Russo, G., 2020. Numerical modelling of heat exchanger pile in pyroclastic soil. *E3S Web Conf.* 205, 1–7. <https://doi.org/10.1051/e3sconf/202020505014>
- Poulos, H. G. 1968. Analysis of the settlement of pile groups. *Geotechnique*, 184, 449–471
- Poulos, H.G., Aust, M.I.E., Mattes, N.S., 1971. Settlement and load distribution analysis of pile groups. *Aust. Geomech. J.* 55, 18–35.
- Rotta Loria, A.F., Laloui, L., 2018. Group action effects caused by various operating energy piles. *Geotechnique* 68, 834–841. <https://doi.org/10.1680/jgeot.17.P.213>
- Rotta Loria, A.F., Laloui, L., 2017a. The equivalent pier method for energy pile groups. *Geotechnique* 67, 691–702. <https://doi.org/10.1680/jgeot.16.P.139>
- Rotta Loria, A.F., Laloui, L., 2017b. Thermally induced group effects among energy piles. *Geotechnique* 67, 374–393. <https://doi.org/10.1680/jgeot.16.P.039>
- Rotta Loria, A.F., Laloui, L., 2016. The interaction factor method for energy pile groups. *Comput. Geotech.* 80, 121–137. <https://doi.org/10.1016/j.compgeo.2016.07.002>
- Rotta Loria, A.F., Vadrot, A., Laloui, L., 2018. Analysis of the vertical displacement of energy pile

- groups. *Geomech. Energy Environ.* 16, 1–14. <https://doi.org/10.1016/j.gete.2018.04.001>
- Russo, G., 2013. Experimental investigations and analysis on different pile load testing procedures. *Acta Geotech.* 8, 17–31. <https://doi.org/10.1007/s11440-012-0177-4>
- Russo, G., 1998. Numerical analysis of piled rafts. *Int. J. Numer. Anal. Methods Geomech.* 22, 477–493. [https://doi.org/10.1002/\(SICI\)1096-9853\(199806\)22:6<477::AID-NAG931>3.0.CO;2-H](https://doi.org/10.1002/(SICI)1096-9853(199806)22:6<477::AID-NAG931>3.0.CO;2-H)
- Tsetoulidis, C., Naskos, A., Georgiadis, K., 2016. Numerical investigation of the mechanical behaviour of single energy piles and energy pile groups. *Energy Geotech. - Proc. 1st Int. Conf. Energy Geotech. ICEGT 2016* 569–576. <https://doi.org/10.1201/b21938-90>
- Russo G., Marone G., 2018. Experimental comparison on different pile load testing methods. *Experimental comparison on different pile load testing methods. DFI-EFFC Int. Conf. on Deep Found. and Ground Improvement: Urbanization and Infrastructure Development-Future Challenges*, Rome, 11
- Schmertmann J.H. 1975. Measurement of in situ shear strength. State of the art report. ASCE speciality conference on in situ measurements of soil properties, vol 2, pp 57–138
- Kulhawy F.H., and Mayne P.W. 1990. Manual on estimating soil properties for foundation design. Research Project 1493-6, Electric Power Research Institute, Palo Alto, California

Chapter 5

5 Tests on small-scale model of energy pile embedded in pyroclastic soil

5.1 Introduction

Thermomechanical tests on a 1 g small-scale energy pile model were carried out at the Geotechnical Laboratory of the University of Naples Federico II.

The aim was to simulate the behaviour of an energy pile with an aspect ratio (AR) of about 13, installed in the Neapolitan area.

Small-scale tests have some advantages over field tests such as greater cost-effectiveness and more control over the boundary conditions during testing. The main purpose is to carry out the test applying to the pile real boundary conditions to which a full-scale energy pile can be subjected in the Neapolitan area both in terms of type of soil and in terms of thermal loads.

The soil used for the test was *Pozzolana*, a pyroclastic sand typical of the Neapolitan area produced over the centuries by the volcanic activity.

On the other hand, thermal loads assigned during the small-scale tests to the pile were extrapolated from numerical simulations carried out by the building thermal simulation software Design Builder as shown in previous chapters.

The small-scale pile was reproduced by an aluminium tube installed inside a square-plan Plexiglas box filled with pozzolana using the rain technique. The soil was rained at a density of $9,30 \text{ kN/m}^3$ to obtain a loose state ($e = 1,65$).

Sensors have been installed both on the pile and in the surrounding soil to measure and record the deformations and displacements of the pile, as well as changes in temperature and water content within the soil.

A series of different thermomechanical tests were carried out on the model to investigate the stress and strain distributions in the pile, the displacements of the pile head and the temperature distribution in the surrounding soil under different levels of mechanical loads and type of thermal loads.

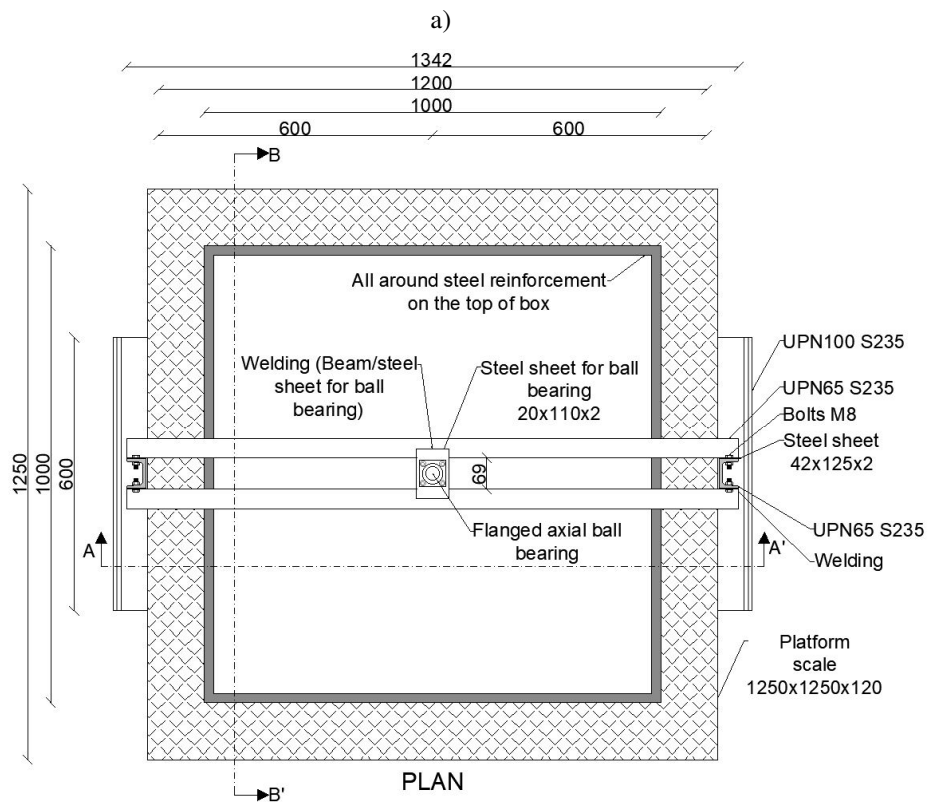
5.2 Laboratory scale test layout

This section describes the stages involved in the design and construction of the laboratory prototype for small-scale pile experiments. After a brief overview of the pile installation phases, each individual component of the prototype and the sensors used are described in detail.

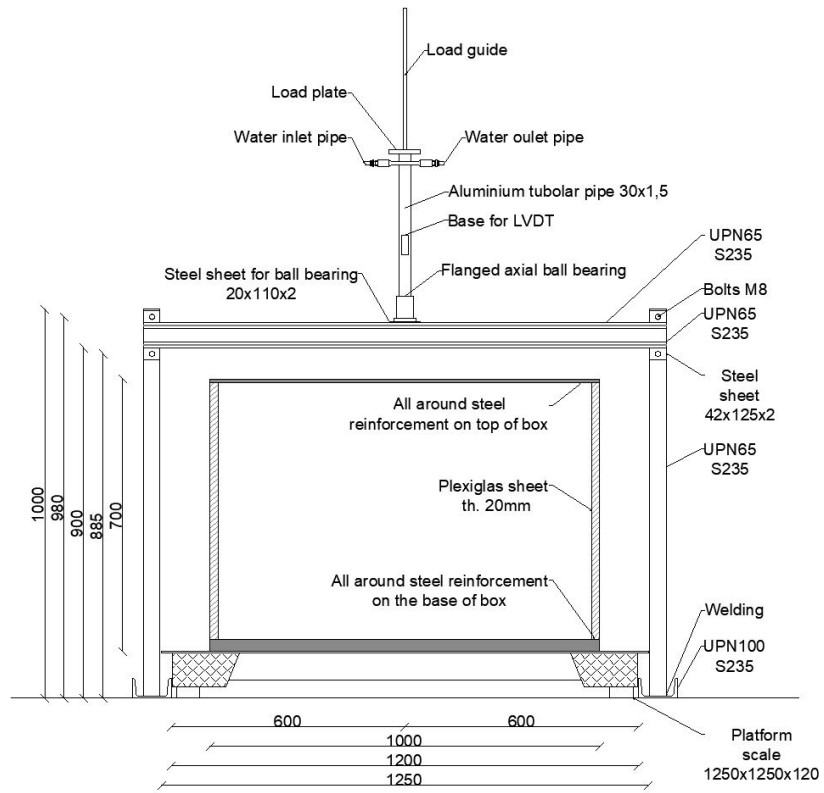
5.2.1 Test setup stages

Figure 5-1 shows the layout of the test carried out in the Federico II geotechnical laboratory in Naples and the individual components of the test.

The test setup followed several stages of both design and installation. First, the dimensions of the pile and the material used to make it were chosen. Subsequently, based on the dimensions of the pile, a box was designed and built to contain the soil inside which the pile was installed. Finally, the way the pile was installed, the application of thermo-mechanical loads and the way the soil was put inside the box were considered. In the following paragraphs the components of the tests and their set up are detailed explained.

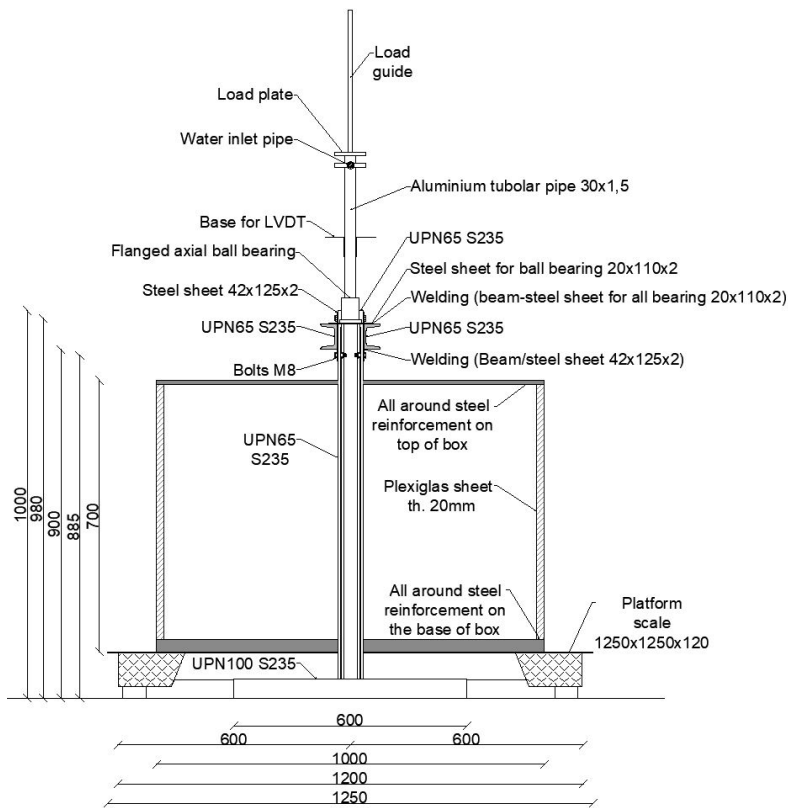


b)



SECTION A-A'

c)



SECTION B-B'

d)

Figure 5-1 – Realisation and design of the small-scale test apparatus. a) realisation of the box (in the picture the pile was suspended from the frame beam while the box was filled with soil). Design: b) plant; c) section AA'; d) section BB'

5.2.2 The pile

The small-scale pile was obtained by using an EN AW-6060 extruded aluminium alloy tube with an external diameter of 30 mm and a thickness of 1,5 mm characterized by Young's modulus of 69000 MPa, a medium tensile strength of 120 MPa, a linear expansion coefficient of $23 \cdot 10^{-6} \mu\epsilon^{\circ}\text{C}^{-1}$ and a thermal conductivity of 200 W/m°C. The ratio between the diameter of the pile and the D_{50} of the sand particles should be greater than 50 to avoid the effects of the grain size scale (Fioravante 2002). Since the soil had a D_{50} equal to 0,2 mm, it was largely exceeded because the ratio resulted 3 times higher than that recommended by the literature. The total length of the aluminium tubular was 950 mm. The part of the tubular embedded in the sand and equipped with strain gauge sensors corresponded to the last 400 mm of the tubular. The remaining part was necessary for the loading and guiding system of the pile during the test. At the tip of the tubular, a cap was inserted. The main function of the tip was to provide a sealing system for the water circulating inside the aluminium tubular. For this reason, the tip was fitted with a rubber O-ring which guarantees perfect water tightness (Figure 5-2).

To simulate the behaviour of a concrete pile, it was necessary to increase the roughness of the lateral shaft of the aluminium pile. Therefore, the external area of the pile and pile's tip were covered with gypsum and sand mortar (Figure 5-3).



Figure 5-2 – Cap for the pile tip with O-ring for the water tightness



Figure 5-3 – Gypsum and sand mortar on pile shaft

The mobilisation and the ultimate value of the shaft friction depend on the interface zone between pile and soil (Fioravante 2002). The thickness of interface depends on the pile roughness and varies between $(2 \text{ to } 5) \times D_{50}$ for smooth pile up to $(10 \text{ to } 15) \times D_{50}$ for rough pile. To define the difference between a smooth and a rough pile, a normalized roughness is defined as:

$$R_n = \frac{R_{max}}{D_{50}}$$

Equation 5-1

The normalized roughness is defined as the ratio between the Maximum surface roughness (measured as the height between two sequent peaks over a skin length from 0,8 mm to 2,5 mm) and the mean particle size of the sand D_{50} . For $R_n < 0,02$ the interface is considered as smooth while for $R_n > 0,1$ the interface is considered as totally rough (Fioravante 2002). Because the soil used for the tests had a D_{50} of 0,2 mm and the same soil was used to cover the pile in the gypsum and sand mortar, assuming an average roughness of the pile corresponds to D_{50} , R_{max} could be equal or greater of D_{50} and so R_n would be at least 1. So, the pile interface in the tests could be considered totally rough.

5.2.3 The thermal and mechanical loading system

The thermo-mechanical loading system was installed with a sealing mechanism into the upper part of the aluminium tube. With this system it was possible to provide the pile with both a mechanical load, using cast iron disks, and thermal loads, through the circulation of temperature-controlled water. The load system consisted of a part outside the pile and a part inside the pile. The external part was made by a plate 80 mm in diameter called *load plate* on which iron disks for the mechanical load were placed. A cylindrical bar called *load guide* was welded to the centre of this plate to make it easier and safer for the weights to remain on the pile head. About 19 mm below the load plate, welded to another plate, the inlet and outlet of the heat carried fluid were placed. The part of the loading system that fitted inside the pile was the water circulation part. It was a circulation system consisting of two concentric cylinders. The outermost cylinder had a diameter of 27 mm, a thickness of 2,5 mm and a height of 50 mm. On the other hand, the inner cylinder had an external diameter of 16 mm and a height of 300 mm.

A rubber O-ring was located inside a groove in the centre of the outer cylinder, mainly to prevent water leaking from the pile top, but also to ensure perfect adherence between the aluminium tube (the pile) and the loading system. The inner cylinder, instead, collected the water from the bottom of the pile via a pipe about 540 mm long, to bring it back to the head and allow it to exit via the return pipe to the circulating bath (Figure 5-4, Figure 5-5).

Watertightness tests of both the head and tip loading systems were carried out on the pile prior to installation in the box.

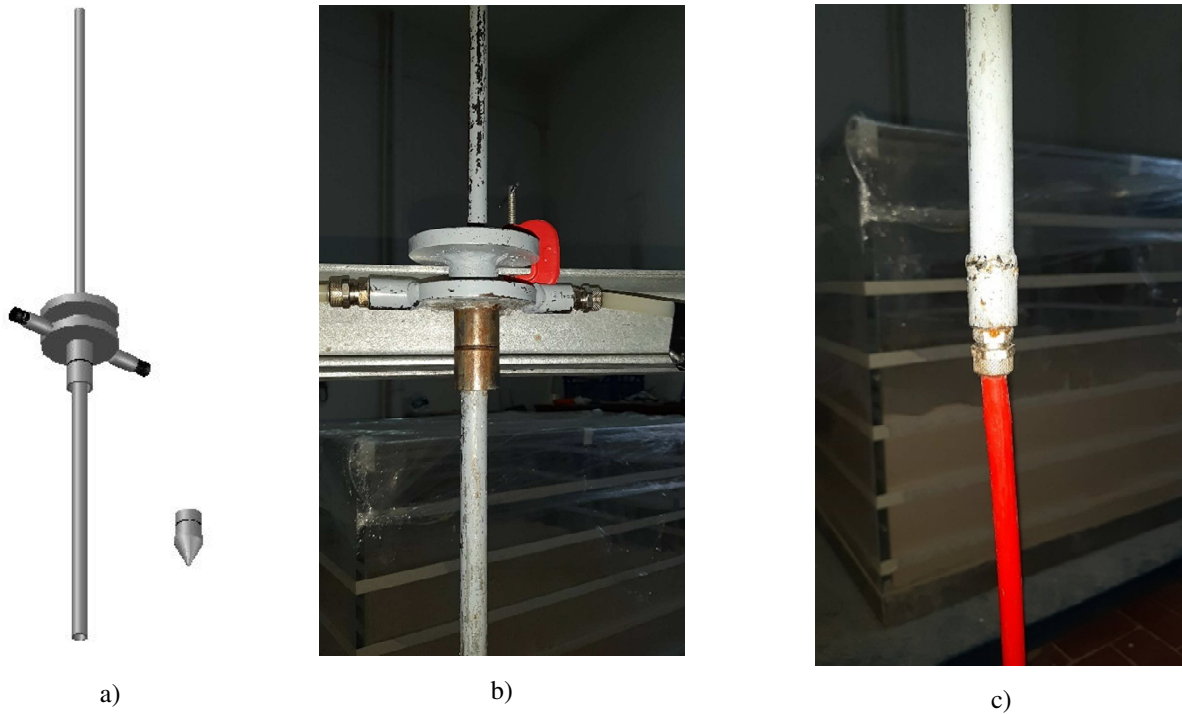


Figure 5-4 – a) 3D view of the load system design with the cap for the pile tip b) upper part of the loading system where it is possible to see the plate for mechanical loading, the second plate where the in and out of the water circulation system is connected, the cylinder from which the water goes down into the pile and the stem for returning the water from the bottom of the pile; c) the lower part of the loading system where there is the pipe that draws water from the bottom of the pile)

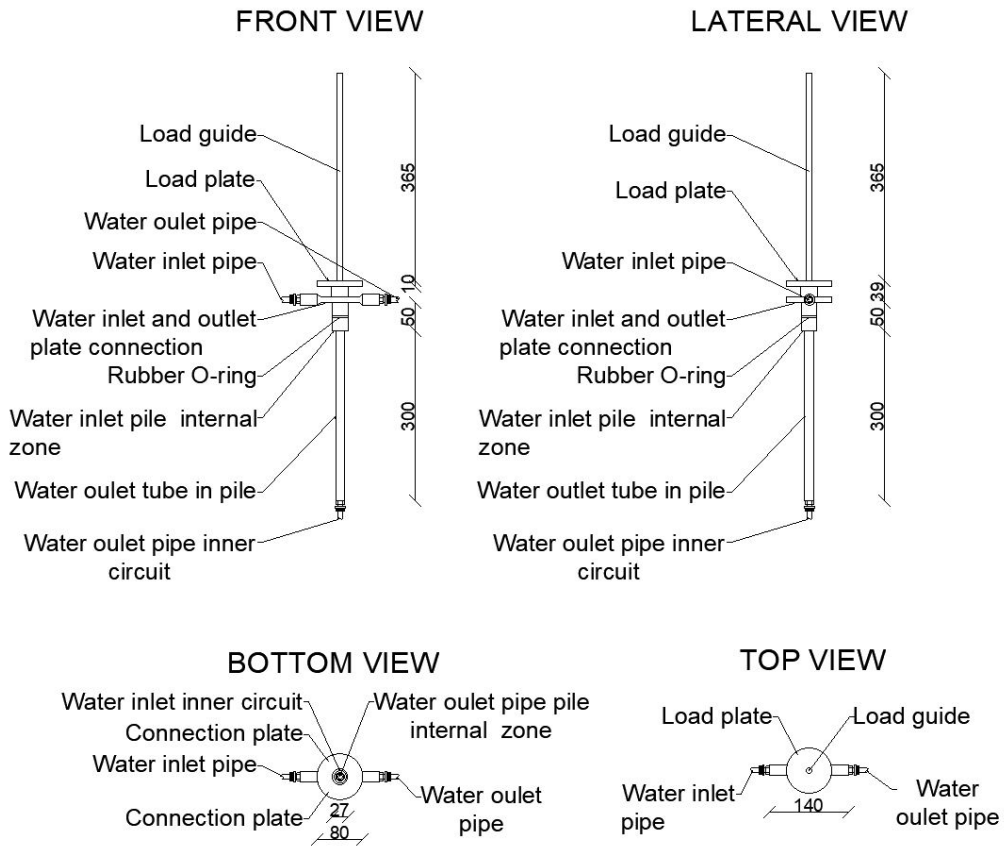


Figure 5-5 – Design and description of the thermal and mechanical load system

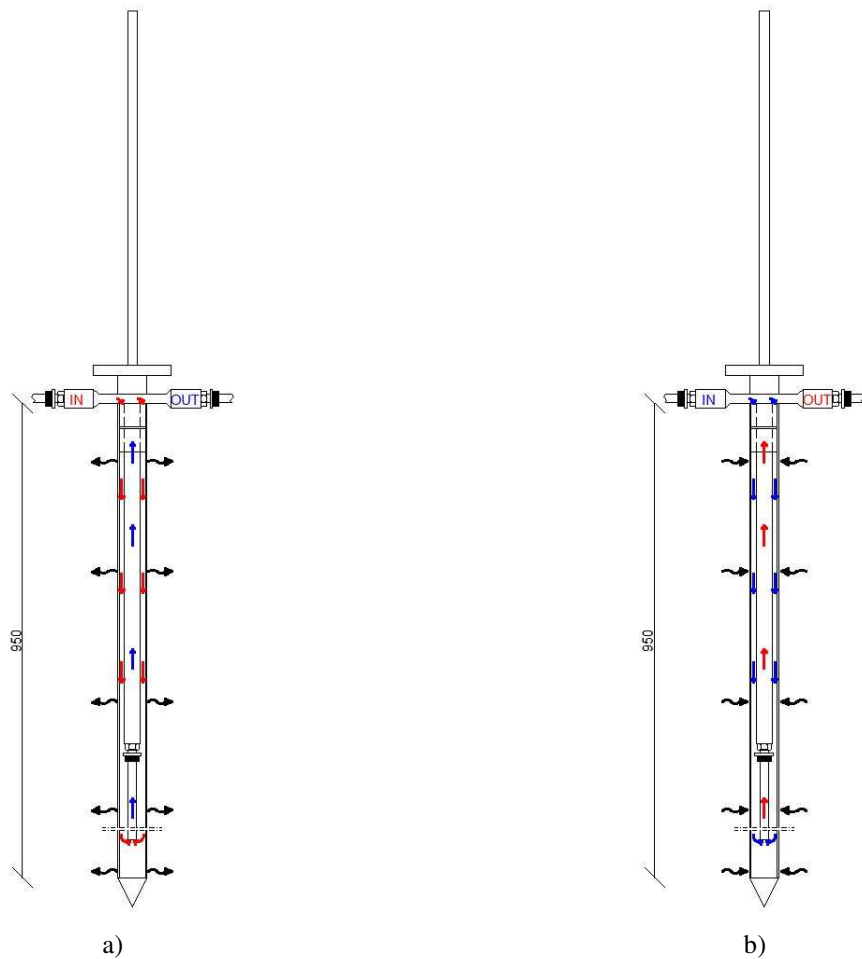


Figure 5-6 – Heat transfer mechanism between pile and soil a) during the pile heating phase (heat injection in soil); b) during the pile cooling phase (heat extraction from soil)

5.2.4 The water temperature and circulation control system

To assign thermal loads to the pile, it was necessary to control both the temperatures of the heat carrier fluid and its circulating times into the pile. To achieve these objectives, the circulating bath by Lab Companion was used. The output and input of the circulating bath, in fact, were connected by two thermally insulated semi-rigid plastic pipes, with the input and output of the thermo-mechanical loading system. In this way, it was possible to create a closed loop for the circulating heat carrier fluid. By the circulating bath it was also possible to set the flow rate of water entering the pile. In Figure 5-7 is shown the heating and cooling capacities that can be reached by the device and the volumetric flow rates that can be provided by the circulating bath.

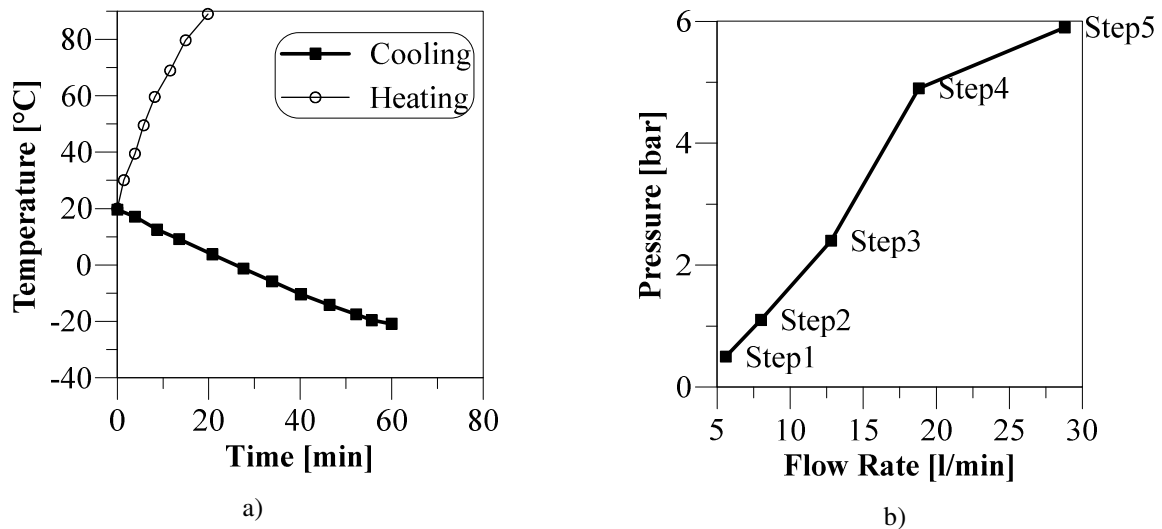


Figure 5-7 – Performances of the circulating bath a) thermal variation against time in both heating and cooling phase b) flow rate and pressure for the different steps

5.2.5 The soil – Pozzolana sand

Pozzolana was the soil used for the tests. The main characteristics of this pyroclastic soil have already been described in chapter 3. It came from a site located north of the city of Naples in the Pascarola ASI industrial zone in the town of Caivano (Na). The characterisation of the subsoil in this area was carried out both indirectly, through bibliographic studies, and directly, by means of in situ surveys. According to the Geological Map of Italy in sheet 183-184 (Island of Ischia-Naples) at a scale of 1:25000, the stratigraphy of the sampling area is characterised by a succession of mainly finely stratified cineritic deposits with interspersed levels of pumiceous lapilli resting on a thick ochre paleosol.

An initial characterisation of the subsurface of the site was provided by CTPs and core tests carried out by Raucci (2017) as shown in Figure 5-8.

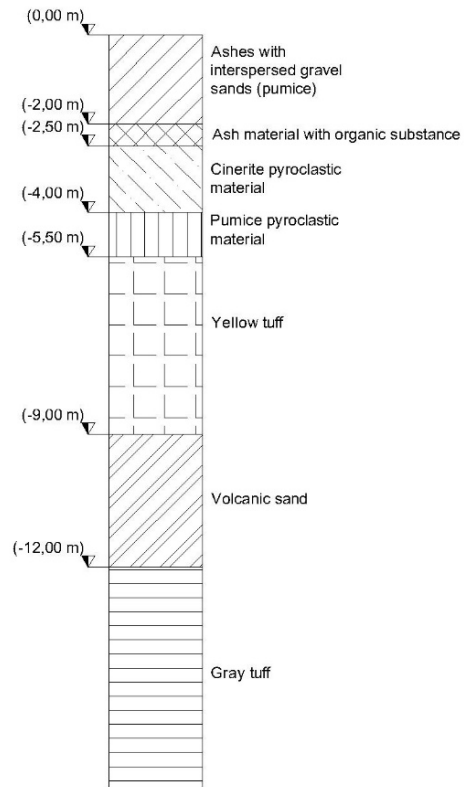
Further investigations were carried out directly on site to investigate in detail the stratigraphic succession of the chosen soil sampling site. A core drill was carried out to a maximum depth of approximately 6,00 m. The investigation confirmed the literature data. An alternation of silty sands and volcanic ashes (*Pozzolana*) was found between approximately 1,00 m and 4,20 m, while at a depth between 5,00 m to 5,60 m, a tuffaceous formation alternating with fractured Neapolitan Yellow Tuff was detected. The water table was intercepted at a depth of approximately 3,80-3,90 m from the ground surface in the layer characterised by the presence of Pozzolana (Figure 5-9). After a granulometric study of some samples of the stratigraphy taken at different depths, it was decided to use pozzolanic sand lying at a depth between 2,00 m and 2,50 m from ground level for the laboratory tests.



a)



b)

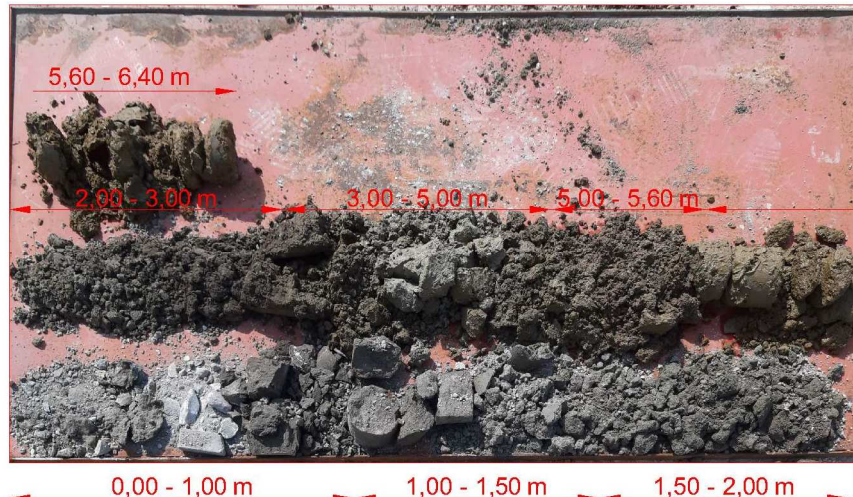


c)

Figure 5-8 - a) Geographical overview of the extraction area; b) extraction area according to the Geological Map of Italy; c) stratigraphy (after Raucci 2017)



a)



b)

Figure 5-9 – a) Core drilling machine used during the soil investigation phase; b) visual analysis of the stratigraphic succession immediately after coring

5.2.5.1 Mechanical properties

A first characterisation about the mechanical properties of the soil was already carried out by Raucci (2017) by two core drillings (S1 and S2) and four CPTs (Figure 5-10). Moreover, also CID (drained

triaxial consolidated tests) and oedometric tests on undisturbed samples were carried out in laboratory.

From in situ tests it was obtained a friction angle of 35° using the methods of Durgunoglu and Mitchell (1975) and Robertson and Campanella (1983). On the other hand, by CPTs it was obtained a relative density of 44% using the method of Lancellotta (1983) and Baldi et al (1986). Furthermore, a Young's modulus of 3.1 MPa and an oedometric modulus of 3,7 MPa were estimated using De Beer's method (1965).

The laboratory tests were carried out on samples of borehole S2. Two samples were taken from this borehole at different depths: sample S2-1 (between 2,00 m and 2,50 m), and sample S2-2 (between 4,00 m and 4,50 m).

Three CID tests were performed at three different cell pressures: 50 kPa, 100 kPa and 200 kPa. Figure 5-11 shows the results of the tests. The critical and peak state angles were determined to be $29,4^\circ$ and $33,3^\circ$ respectively.

The investigations directly carried out during this research on the soil taken from the site concern the stratigraphy between 2,00 m and 2,50 m. Firstly, the granulometric curve was determined (Figure 5-12).

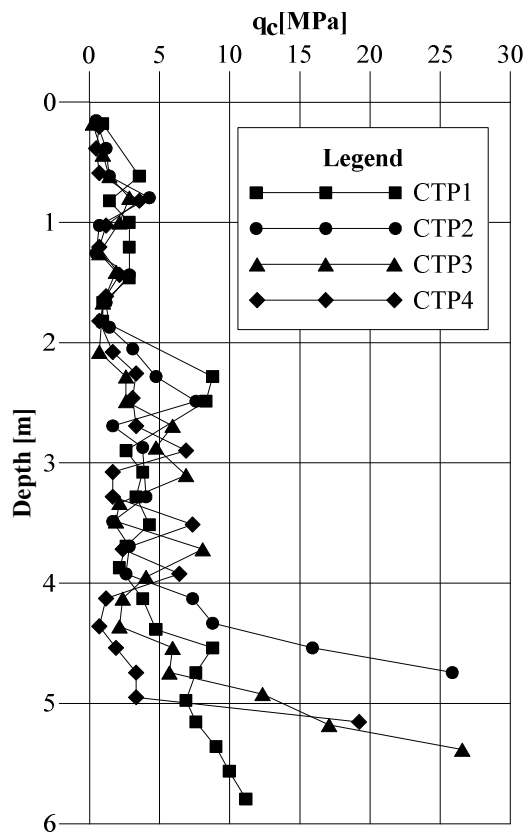


Figure 5-10 - Pascarola CPTs test (after Raucci 2017)

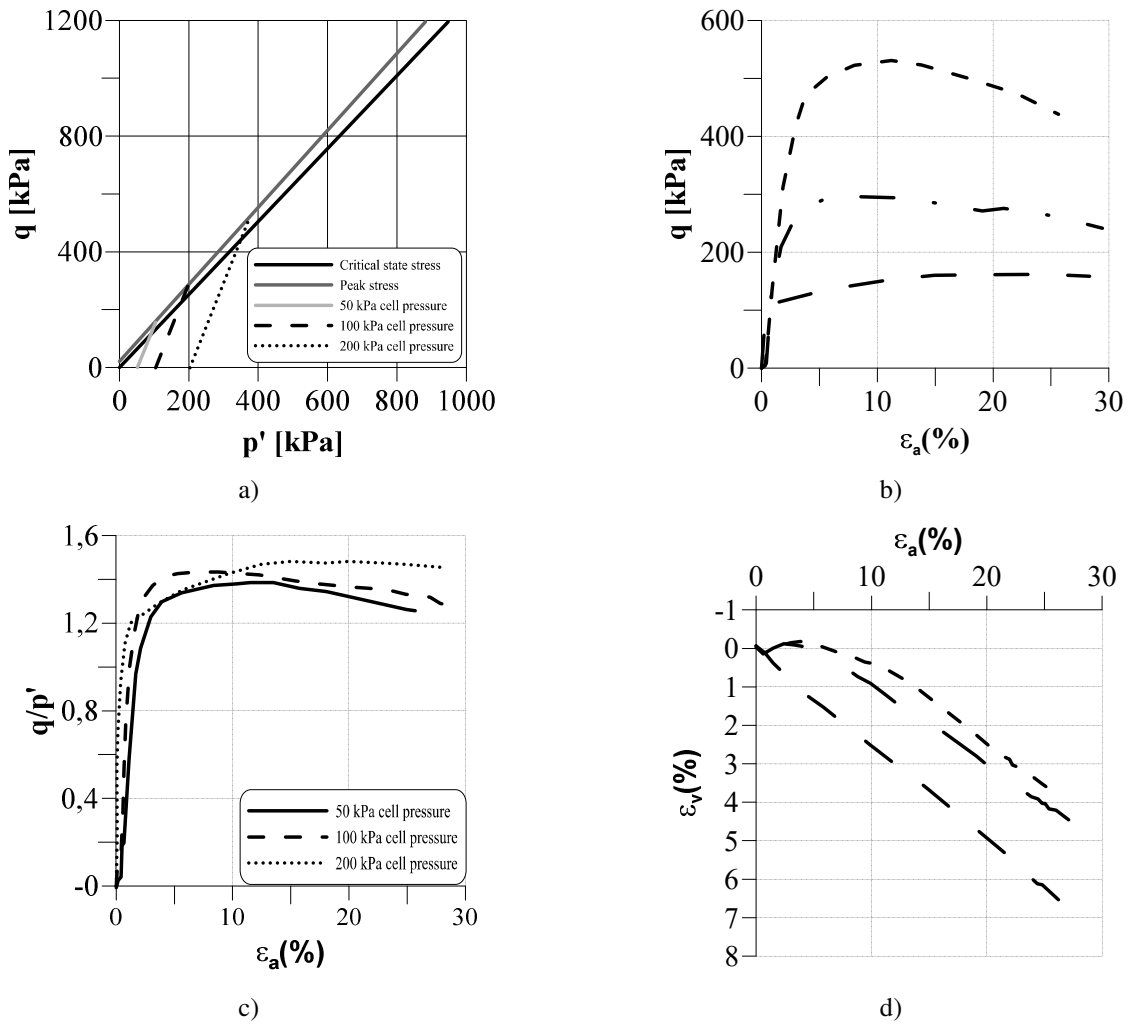


Figure 5-11- a) stress path; b) deviatoric stress versus axial strain; c) deviatoric stress - mean effective stress ratio versus axial strain; d) volumetric strain versus axial strain (after Raucci 2017)

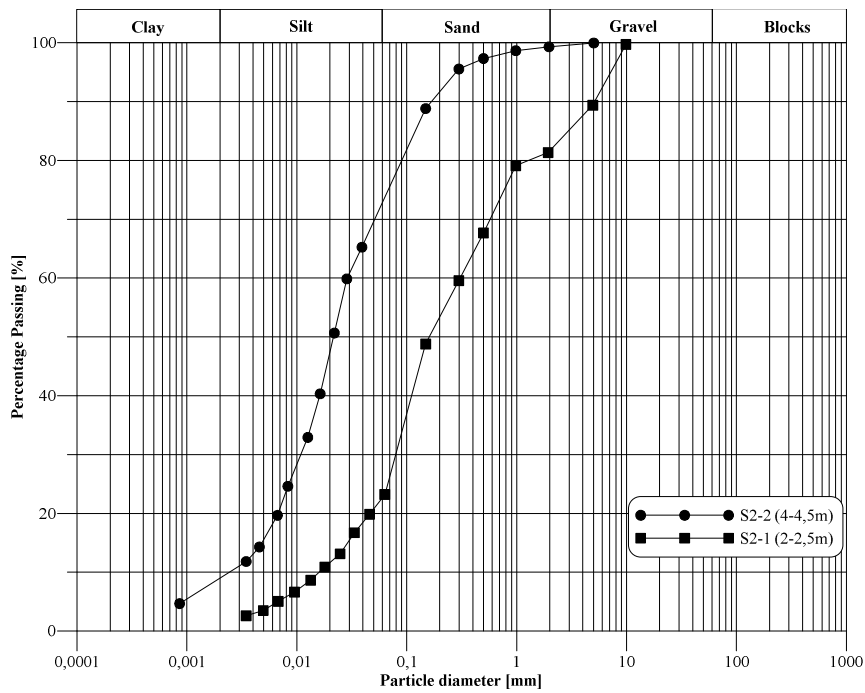


Figure 5-12 - Grain size distribution for different sampling depths

Subsequently, a particle density $G_s=2,54 \text{ g/cm}^3$, a maximum void index $e_{\max}=1,70$ and a minimum void index $e_{\min}= 1,08$ were determined. The maximum void index was determined by following one of the four standard specifications of ASTM 4253-00. It was chosen the method in which the oven-dried soil is placed on a vibrating table because it is applicable when the soil can contain up to 15%, in dry mass, of soil passing through $75 \mu\text{m}$. On the other hand, the minimum void index, was obtained dropping the soil from above through a funnel into the die. This method is the most recommended by the above-mentioned regulation.

The results obtained were compared with the literature. Nicotera (2002) reports a series of data obtained from the study of soil from more than 44 sites in the Neapolitan area. The data collected was divided into 3 classes (Table 5-1):

- CLASS A: data from samples less than 15 m in depth;
- CLASS B: data from samples between 15 m and 25 m in depth;
- CLASS C: data from samples deeper than 25 m;

Table 5-1 - Maximum and minimum particle density (G_s), initial void index (e_0), dry weight (γ_d), total weight for unit of volume (γ), water content (w_0) for CLASS A, CLASS B and CLASS C samples divided by the water content

		<i>A Natural water content</i>	<i>B Natural water content</i>	<i>C Natural water content</i>	<i>A Saturated in lab</i>	<i>B Saturated in lab</i>
G_s [g/cm ³]	min	2,25	2,23	2,23	2,45	2,43
	max	2,66	2,6	2,54	2,52	2,5
e_0	min	0,573	0,739	0,653	0,998	1,095
	max	2,344	2,412	2,251	1,603	1,765
γ_d [kN/m ³]	min	7,59	7,44	7,814	9,27	8,79
	max	15,64	14,26	15,36	12,22	11,71
γ [kN/m ³]	min	9,24	9,02	10,38	12,15	10,61
	max	18,44	17,27	18,41	17,19	14,29
w_0	min	0,101	0,051	0,131	0,183	0,191
	max	0,618	0,515	0,615	0,301	0,478
Sr_0	min	0,211	0,147	0,334	0,332	0,285
	max	0,888	0,878	0,90	1,00	0,766

The values of particle density, natural water content and void indices obtained on the sample taken on site are comparable with those grouped by Nicotera (2002) in class A.

The particle size analysis of the soil sampled on site provided a D_{50} in agreement with the prescriptions given by Weinstein (2008) on the ratio of pile size to soil grain size. However, to facilitate the installation of the soil, it was decided to cut the grain size curve to a maximum of 5 mm. The soil with the new grain size curve was subjected to further tests to determine the new G_s , e_{max} and e_{min} . By the tests, carried out with the same criteria as before, were obtained G_s values of 2,52 gr/cm^3 , e_{max} of 1,7 and e_{min} of 0,9. These values indicate the soil is still comparable with class A natural water content soils provided by Nicotera (2002).

The voids index is fundamental for the reproduction in the laboratory test on a smaller scale of denser or looser soils. As can be seen from Table 5-1, the maximum void indices that can be reproduced in the laboratory are smaller and far from those that can be obtained from a natural sample, since the naturally occurring laying and stratification process for this type of pyroclastic soil is difficult to reproduce artificially. Therefore, to reproduce a loose state, $e = 1,65$ was assumed as void index for the soil pluviated in the box.

To simulate the behaviour of an energy pile in loose soil during the test, a void index of 1,55 was used. The mechanical properties of the material used in the test box were also evaluated by means of direct shear tests using the AUTOSHEAR 27-WF2160 device. These tests were carried out on both loose and dense material samples.

A reconstituted sample of dry sand was prepared inside a 60 mm x 60 mm box by the air pluviation method to obtain a final dry specific gravity of 9,8 kN/m^3 . The sample was prepared by pluviating it in two 11 mm layers by gently tamping it through a pad (Figure 5-13)



a)



b)

Figure 5-13 – Shear test box a) arrangement of sand inside the shear box; b) tamping of soil in the box shear

According to ASTM D3080/D3080M (Standard Test Method for Direct Shear Test of Soils Under Consolidated Drained Conditions) the shear rate must be sufficiently slow to ensure drained conditions so that insignificant excess interstitial pressure exists at failure. In the present case the tests were carried out at a speed of 0,133 mm/min considering that it was carried out on dry samples, thus reaching, after one hour, a final relative displacement between the two parts of the shear box of about 8 mm.

The tests were carried out on reconstituted specimens with the same void index subjected to different normal stresses. In particular, the normal stresses applied were 8,17 kPa, 17,03 kPa, 32,02 kPa and 63,34 kPa and three tests were carried out for each stress state.

The results obtained in terms of tangential stresses/displacement/specimen height variation are shown in Figure 5-14.

As can be seen from the diagram, as the normal tension increases, the shear stresses and the initial stiffness increase and there are no peak phenomena. In fact, for all the stress states, once τ_{\max} has been reached, it remains about constant throughout the test. The same behaviour can be observed for the trend of the height of the test piece (and therefore of the volumetric variation) in which an almost contracting behaviour of the test piece can be noted, due, above all, to the very loose state of thickening with which it was placed.

From the data obtained, it was possible to derive an angle of friction for these dry pozzolana samples of 41°. This value is slightly higher than the range indicated by Nicotera (2002) of 32°- 40° for saturated or unsaturated pozzolana. Anyway, the explanation for this can be found in the substantial difference in terms of mechanical properties that can exist between a dry soil sample such as that of the experiment carried out, and saturated soil samples. This statement is supported by the experiments by Wils et al. (2015) and Miura and Yamanouchi (1975) by comparing the mechanical properties of saturated and dry samples. Wils et al. (2015) stated that specimens containing water showed lower peak deviatoric stress and peak shear angle than dry specimens while Miura and Yamanouchi (1975) stated that water in saturated specimens increased compressibility and decreased shear strength.

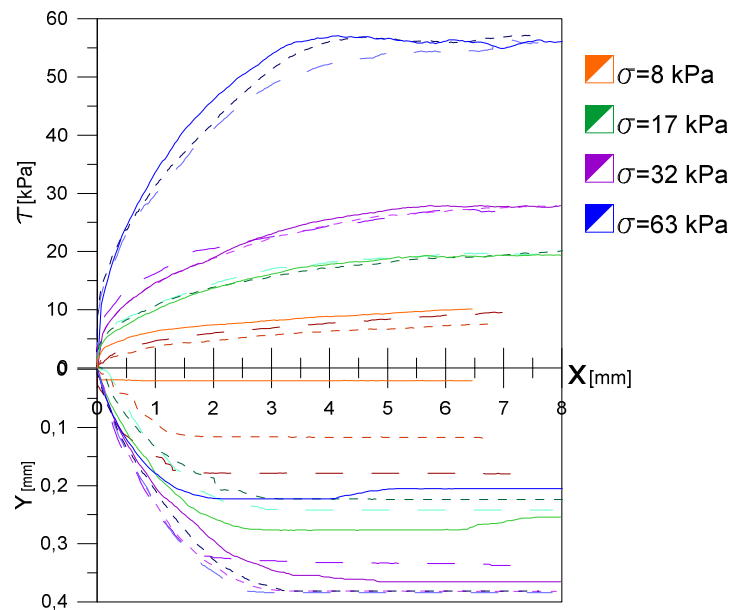


Figure 5-14 - shear stress and vertical displacement plotted against the shear displacement at different level of nominal normal stresses.

5.2.5.2 Thermal aspects

The soil used in the small-scale test was characterised from a thermal point of view by measuring its thermal resistivity (and thus indirectly its thermal conductivity). The measurement was carried out at the GEOFISICA s.r.l. laboratories (CS, Italy) using as acquisition instrument a MAE A5000T control unit. The measurement method complies with ASTM D 5334 and IEEE 442-1981 and is based on the so-called transient line heat source or transient heated needle method. In the test a probe, also called a thermal needle, with a length much greater than the diameter was used to simulate the hypothesis of an infinite linear source. This probe incorporated both a heating wire and a temperature sensor and was inserted into the soil. From its response to a heating cycle for a few minutes, thermal resistivity (or vice versa, conductivity) could be calculated. In practice, a current and a known voltage were circulated through the probe and the temperature increase over a given period was recorded. According to the theory of the infinite line source model (ILSM) if a constant amount of heat is applied to a heater of zero mass over a period, the temperature response is:

$$\Delta T = \frac{q}{4 \cdot \pi \cdot \lambda} \cdot Ei \left(\frac{r^2}{4 \cdot a_s \cdot t} \right)$$

Equation 5-2

Where:

t is the time elapsed since the start of heating [s];

ΔT is the temperature increase since time zero [°C];

q is the input power per unit length of the heater [W/m];

r is the distance to the heated needle [m];

α_s is the soil thermal diffusivity [m²/s];

λ is the thermal conductivity [W/m°C].

Ei is the exponential integral.

From the previous equation α_s and λ cannot be determined explicitly. However, assuming that the exponential integral can be approximated by the natural logarithm, that the probe was infinitely long with respect to the infinitely small diameter, and that the ambient temperature was constant during the measurement, the exponential integral can be neglected for long periods and therefore:

$$\Delta T \cong \frac{q}{4 \cdot \pi \cdot \lambda} \cdot \ln(t)$$

Equation 5-3

Considering two instants of time, the conductivity can be calculated as:

$$\lambda = \frac{q(\ln t_2 - \ln t_1)}{4\pi(T_2 - T_1)}$$

Equation 5-4

For the soil used in the small-scale test, two dry pozzolan specimens with two different states of thickening (loose and dense) were prepared to evaluate the possible difference in thermal conductivity. Indeed, the state of thickening of the soil and so different void ratios, can result in different thermal conductivity values. The void ratios used for the two samples were, respectively, 1,27 for the loose sample and 1,05 for the dense sample.

The specimens were prepared in accordance with the provisions of ASTM D53334 which suggests compacting the material to the desired dry density and gravimetric water content within a thin-walled metal or plastic tube with a minimum diameter of 50 mm, length of 200 ± 30 mm and using a suitable compaction technique.

For this purpose, plastic tubes with a height of 700 mm and a diameter of 200 mm were used. Both the loose and the dense sample were prepared by air pluviation. In the case of the preparation of the loose sample ($e=1,27$), there was a slight mechanical thickening after pluviation from a very small height. On the other hand, in the case of the dense sample, the drop height of the sand by precipitation occurred from a height of about 700 mm followed by a strong mechanical compaction. Both samples,

however, were prepared in seven layers, i.e., every 100 mm mechanical compaction was carried out to achieve a constant relative density over the whole height of the sample.

The thermal tests were carried out by means of a 300-second test from which 248 temperature measurements were taken. The thermal conductivity obtained for the loose samples is 0,222 W/m°C and for the dense samples is 0,226 W/m°C.

5.2.6 The box

The box in which the soil was pluviated consisted of 20 mm thick Plexiglas sheets, 700 mm high and 1000 mm wide glued together to form a box 1000 mm wide, 1000 mm long and 700 mm high. The bottom of the box was made of 2 mm thick steel sheet which folds up 20 mm to accommodate the plexiglass side walls.

The design of the dimensions of the box, the material used, and the thickness of the Plexiglas sheets was based on the need to reduce both mechanical and thermal boundary effects during the tests. The first step was based on the literature prescriptions for a general design of the system and then on numerical simulations to verify the design.

As far as the literature is concerned, Parkin and Lunne (1982) prescribe minimum dimensions for the ratio between the diameter of the pile and the diameter of the box (in the case of the square box, the measurement of the side of the square was chosen) to allow the behaviour of the confined soil inside the box to be equal to that of an unbounded soil. For loose sands the authors prescribed the ratio must be 20.

Le Kouby et al. (2013) on the other hand, makes suggestions regarding the distance between the tip of the pile and the bottom of the box. According to the author, this distance should be ten times the pile diameter. In this case, the dimensions of the box (1000 mm x 1000 mm x 700 mm) make it possible to eliminate edge effects, considering that the pile had a diameter of 30 mm and the tip is 300 mm from the bottom of the box.

From a thermal boundary conditions point of view, the dimensions of the box provided a ratio of pile diameter to box width of approximately 1:30. This ratio was almost double the ratio of 1:18 used in the test by Kramer et al. (2015).

In addition to the indications provided in the literature, numerical simulations with finite-difference software were carried out to understand the distribution of temperatures (and so the heat flow) inside the box. Numerical simulations with FEM software were carried out to design the thickness of the PMMA walls according to the maximum permissible deformations.

The results obtained from the numerical thermal analysis show that, by simulating a 24-hour test with continuous operation mode of the pile and a ΔT of 20 °C between the temperature of the ground and the pile, the dimensions of the box are such that they reproduce the behaviour of a real-sized pile in

a soil with undefined dimensions. However, it had to be considered that the thermal boundary conditions of the part of the soil in contact with the outside air could not to be designed in advance. As suggested by Wang et al. (2011), the effects of the air temperature in the laboratory room were considered by monitoring it and comparing it with the ground temperatures, both during the tests and several hours before the test started.

From a mechanical point of view, on the other hand, it was found that 20 mm thick plexiglass walls were sufficient to contain the thrust of the soil (even at densities of the soil higher than those used in the laboratory tests) and that the maximum deformations are equal to 0,64 mm (Figure 5-15).

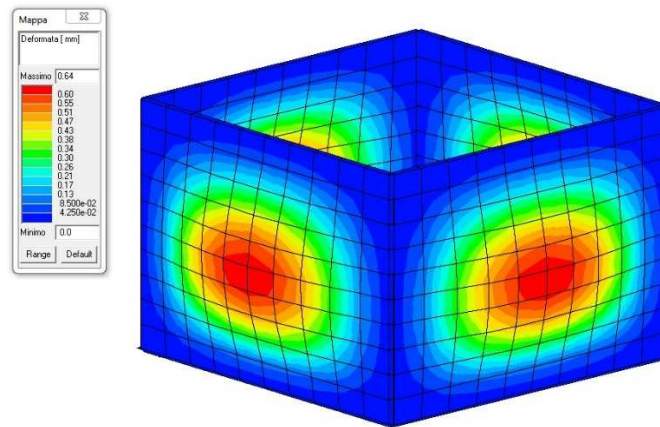


Figure 5-15 - Maximum deformations of the plexiglass walls of the box calculated with FE software

Table 5-2 - Mechanical and thermal properties of PMMA

Density [g/cm ³]	E [MPa]	Ten. strength [MPa]	Comp. strength [MPa]	α [°C ⁻¹]	λ [W/m°C]	Specific heat [kJ/kg°C]
1,2	3200	75	125	8x10 ⁶	0,19	148

A steel frame consisting of two columns and two coupled beams, both UPN 65 S235, was built around the box. The purpose of the frame was to create a support that was independent of both the box and the pile and that supported the sliding of the pile inside a double cylinder with rectangular flanged linear bushing bolted between the two beams of the frame.

The plexiglass box was placed on a platform scale with a maximum capacity of 1500 kg. The function of the scale was to control the weight of the soil during the soil pluviation phases inside the box until a dry density of 9,30 kN/m³ was reached. Since the volume of the box was known, the density of the soil was indirectly controlled. The soil was not pluviated in a single step but in seven steps of 100 mm each to ensure a homogeneous density over the entire height of the box. To facilitate the operations, the height intervals of 100 mm were marked on the plexiglass walls of the box with adhesive tape. These intervals were also useful for determining the heights at which the various sensors were to be located.

After filling the box to a height of 300 mm, the pile was introduced into the centre of the square plan of the box. The tubular was kept on axis and in position, preventing it from sliding inside the rectangular flanged linear bushing bolted to the metal frame outside the box. The remaining 400 mm of the box was then backfilled. This method of installing the pile in the ground was carried out to simulate the installation of a non-displacement pile and therefore not generate horizontal surges within the ground.

5.2.7 Sensors

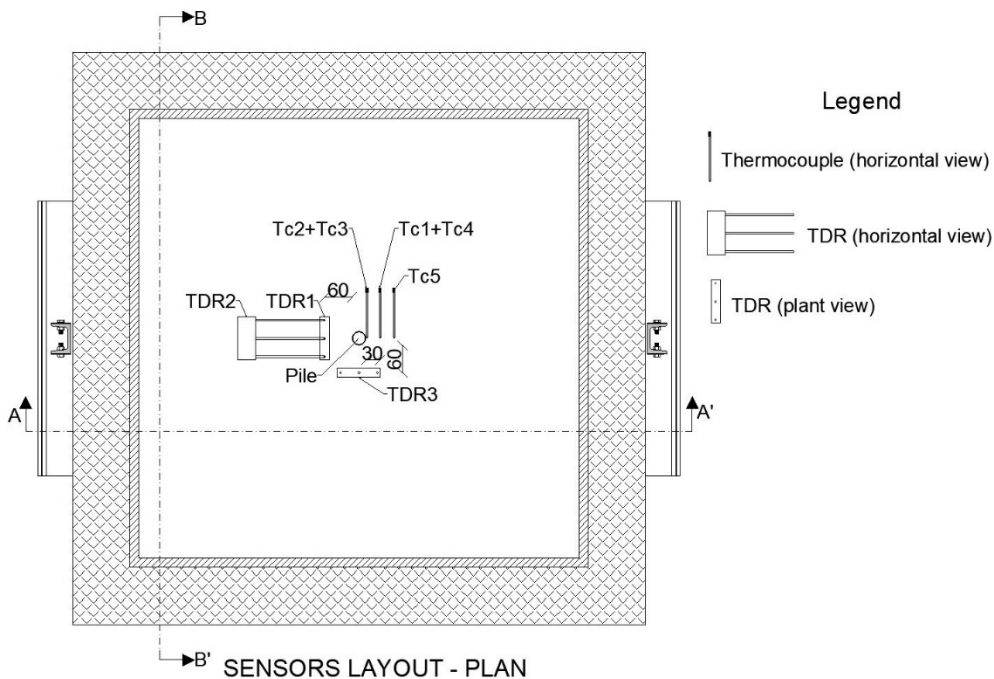
To measure the pile and surrounding soil thermal and mechanical behaviour, different sensors were placed both on pile shaft surface, on pile head and in the soil.

To measure strains induced by thermal and thermo-mechanical loads, a total of 9 strain gauges were glued to the outer lateral surface of the pile, 7 were arranged for measuring longitudinal strains and the other 2 were arranged for measuring transverse strains.

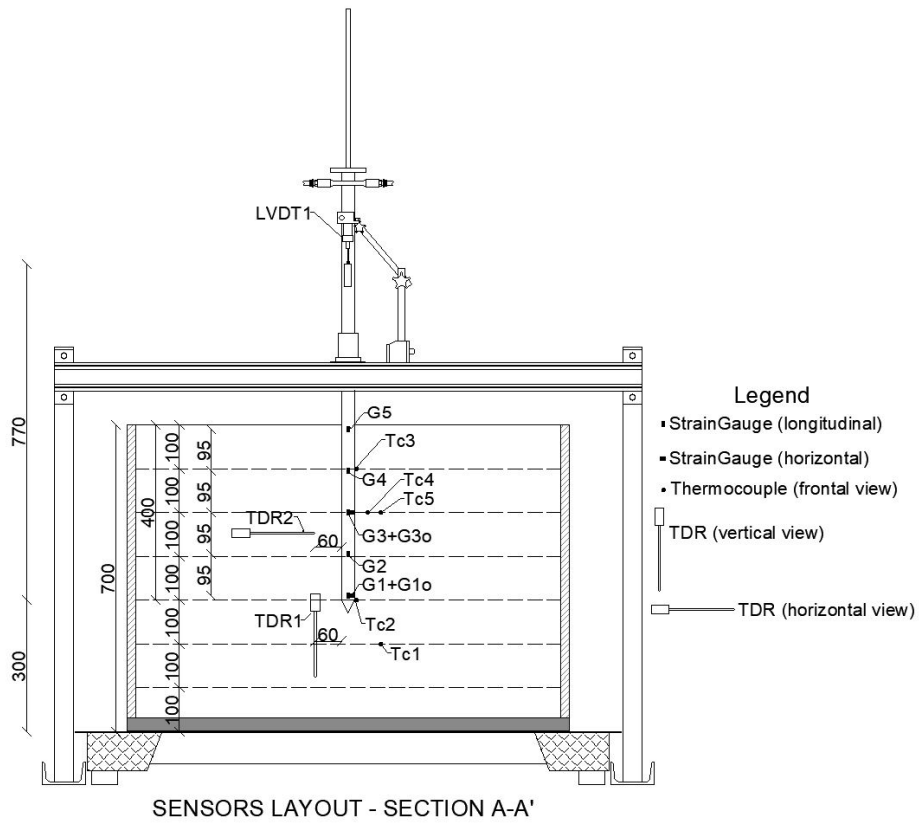
The pile head displacements were measured by a couple of LVDT (Linear Variable Differential Transducer) placed on the steel frame beam around the Plexiglas box. The LVDT were supported by telescopic magnet arms.

Soil temperatures during the tests and in the recovery time after the active phase of the tests, were monitored by a set of thermocouples placed in different zones of the box. Figure 5-16 shows the complete sensor configuration of the model.

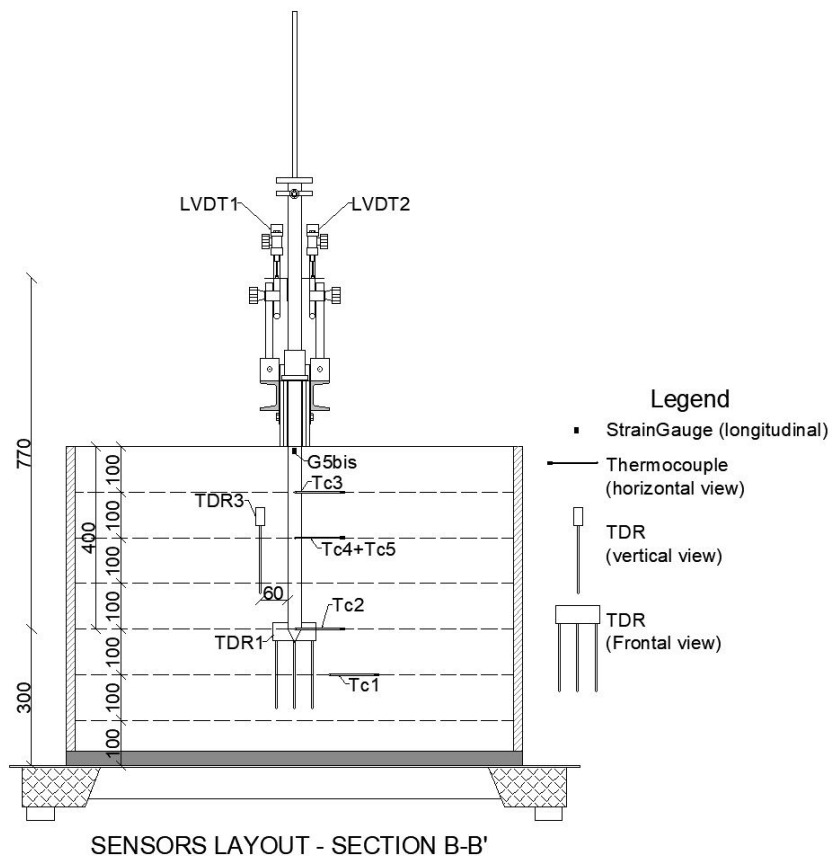
However, each sensor listed has been described in detail in the following paragraphs.



a)



b)



c)

Figure 5-16 – Sensor positioning a) plant; b) section AA'; c) section BB'

5.2.7.1 Strain gauges

On the lateral surface of the pile, a total of 9 electric quarter bridge three-wire strain gauges were applied to measure both longitudinal and radial deformations of the pile during the tests. The 7 longitudinal sensors were named SG1, SG2, SG3, SG4, SG5, SG5bis and SG5tris and were applied to the pile tip at distances of 10 mm, 105 mm, 200 mm, 295 mm and 390 mm respectively. The 2 horizontal sensors, named SG1O and SG3O, were applied at a distance from the tip of 10 mm and 200 mm respectively. Because of the nature of the material used to simulate the pile (aluminium), the strain range to be measured during the test was considered homogeneous. For these reasons it was decided to use strain gauges from the Tokyo Measuring Instrument Lab type FLAB-6-23-3LJCT-F with a gauge length of 6 mm with a coefficient of thermal expansion of $23 \cdot 10^{-6} \text{ } ^\circ\text{C}^{-1}$ (the same of the aluminium) and a gauge resistance of $120 \text{ } \Omega$. The strain gauges were subsequently coated with a silicon rubber-based protective coating specific for this type of instrumentation to prevent accidental damage during the preparation of the test or during the test itself. Finally, prior to the installation of the pile in the ground, to provide a roughness to the side surface of the aluminium tubular, the part of the aluminium tubular embedded into soil was covered with plaster and sand mortar.

A strain gauge is a resistance whose ohmic value varies with strain. Bonded to the surface of any structure, it can measure the strain when the structure is stressed. The main elements of a strain gauge are the matrix and the grid (Figure 5-17).

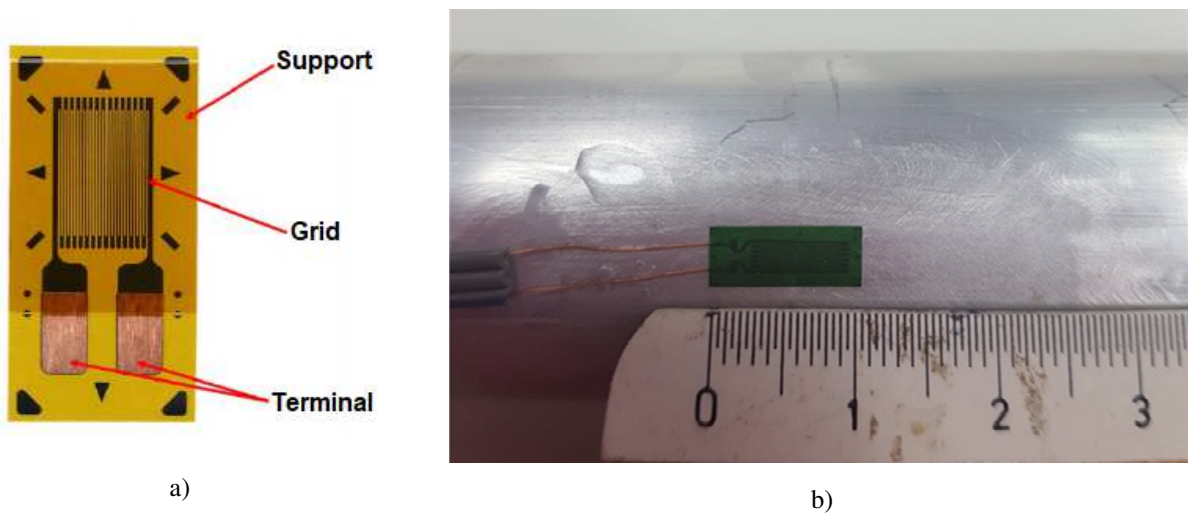


Figure 5-17 - a) strain gauge structure b) dimension of strain gauge used during the tests

The strain produced on the surface of an object at the point of application of the strain gauge are transmitted to the grid, which changes its electrical resistance as it deforms. This change in electrical resistance, which is proportional to the strain, can be measured with great accuracy by special instruments. When a filiform conductor is subjected to traction, it is observed experimentally that its electrical resistance increases in proportion to the force exerted.

$$R = \frac{\rho l}{A}$$

Equation 5-5

Where R is the resistance for a filiform conductor, A is the cross section of the conductor, l is the total length of the conductor and ρ is its resistivity. Differentiating and dividing the by R gives:

$$\frac{\Delta R}{R} = \frac{\Delta \rho}{\rho} + \frac{\Delta l}{l} - \frac{\Delta A}{A}$$

Equation 5-6

$\Delta\rho/\rho$ is the variation in relative resistivity, $\Delta l/l$ is the strain of the conductor in the longitudinal direction and $\Delta A/A$ is the relative change in cross section of the conductor.

Considering the conductor attached to the surface on which the strain is to be measured, it is possible to relate the change in resistance to the longitudinal strain of the strain gauge using the following relationship:

$$\frac{\Delta R}{R} = \frac{\Delta \rho}{\rho} + (1 + 2\nu) \cdot \varepsilon_l$$

Equation 5-7

With ν Poisson's modulus and ε_l longitudinal strain of the strain gauge.

The relationship between strain and relative change in strength is expressed as follows:

$$\varepsilon_l = \frac{1}{k} \frac{\Delta R}{R_g}$$

Equation 5-8

where k is the gauge factor, a dimensionless quantity that is obtained experimentally, $\Delta R[\Omega] = R_f - R_g$ is the change in resistance of the strain gauge (R_f is the final resistance of the strain gauge $[\Omega]$ and R_g is the initial resistance of the strain gauge $[\Omega]$) and ε the strain measured by the strain gauge $[\mu\varepsilon]$.

With electrical strain gauges, strains measured with a resolution of the order of one micrometer/meter, i.e., one part in a million. Therefore, changes in resistance can be very small. To be able to measure the value with good accuracy, a connection circuit is used which can provide an amplified signal such as that of the Wheatstone bridge. It is the most common and simplest bridge network to find the resistance. This bridge is used where small changes in resistance are to be measured like in sensor applications. This is used to convert a resistance change to a voltage change of a transducer.

Wheatstone bridge consists of four legs, each containing one resistance (Figure 5-18). Generally powered by a constant voltage generator V_{IN} , it is used to determine the unknown value of one of the

four resistances by reading the difference in potential U_e , known as the unbalance voltage, which is generated at the unpowered ends of the bridge.

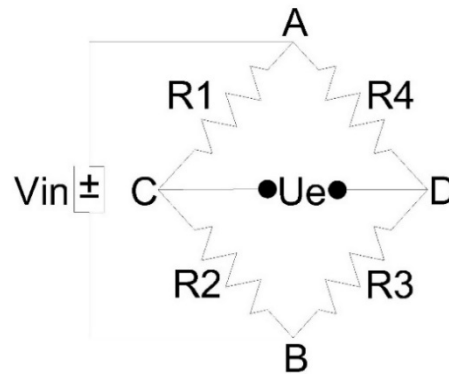


Figure 5-18 - Wheatstone bridge scheme

The AB diagonal is referred to as the power diagonal and the CD diagonal as the signal diagonal. The bridge is formed with strain gauges and complementary resistances depending on the measurement to be made. By replacing one or more resistances with as many strain gauges we obtain the following measuring circuits:

- Quarter Wheatstone bridge configuration when a single resistor is replaced with a strain gauge.
- Half Wheatstone bridge configuration when two resistors are replaced by two strain gauges.
- Full Wheatstone bridge configuration when all four resistors in the circuit are replaced by four strain gauges.

The choice of the type of bridge to be used depends on the purpose of the measurement. In the case of the test carried out in which it was necessary to calculate deformations induced by thermo-mechanical loads, it was decided to use the quarter bridge (Figure 5-19).

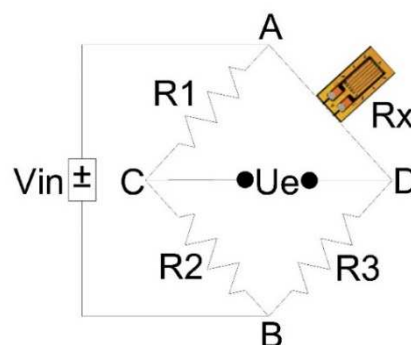


Figure 5-19 - Quarter bridge configuration

To measure and record the induced strain, two Vishay model D4 Data Acquisition Conditioners with four input channels were used for the tests. From an analytical point of view, to measure the induced

strain inside the strain gauge, it is therefore necessary to be able to evaluate the unbalance generated in the diagonal output (signal) CD of the Wheatstone bridge. To assess this, it is assumed that C and D are voltage dividers and so:

$$V_C = \frac{R_2}{R_2 + R_1} \cdot V_{in}$$

Equation 5-9

$$V_D = \frac{R_3}{R_x + R_3} \cdot V_{in}$$

Equation 5-10

When the Wheatstone bridge is in equilibrium

$$V_{DC} = 0$$

Equation 5-11

And because,

$$V_{DC} = V_C - V_D$$

Equation 5-12

For the equilibrium:

$$\frac{R_2}{R_2 + R_1} \cdot V_{in} = \frac{R_3}{R_x + R_3} \cdot V_{in}$$

Equation 5-13

After some mathematical passages it results that the Wheatstone bridge is in equilibrium when:

$$R_2 \cdot R_x = R_3 \cdot R_1$$

Equation 5-14

And so:

$$R_x = \frac{R_1 \cdot R_3}{R_2}$$

Equation 5-15

By imposing a known value on the two resistors R_2 and R_1 and assuming that their ratio is constant, in the case of an unbalanced Wheatstone bridge, it will be sufficient to vary only the resistance R_3 until V_{CD} returns a zero value and consequently to obtain the value of the unknown resistance (strain gauge).

$$\frac{R_2}{R_1} = c$$

Equation 5-16

$$R_x = c \cdot R_3$$

Equation 5-17

Another property that characterises strain gauges is the error due to cable resistance. The cables used to connect the strain gauges to the control unit can cause changes in resistance or induce additional resistance as they are subjected to changes in temperature, leading to so-called "apparent deformations". By using appropriate connection diagrams, however, such errors can be eliminated. Considering the quarter-bridge connection, this can be made via a two-wire (Figure 5-20) or three-wire connection (Figure 5-21).

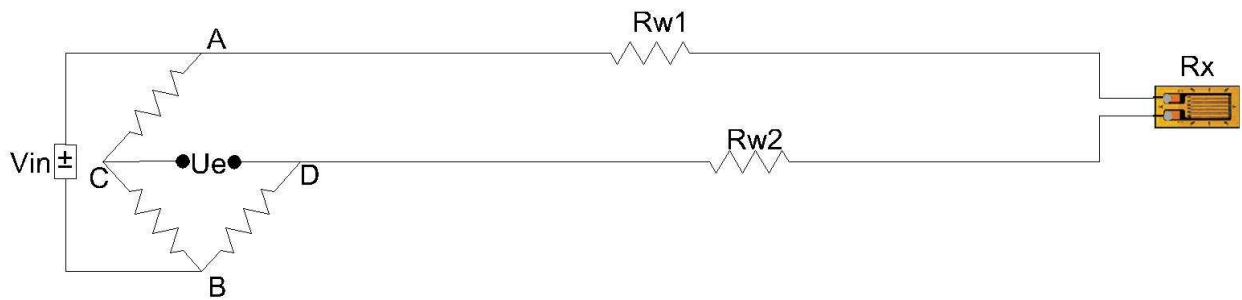


Figure 5-20 - Quarter bridge connection via two-wire

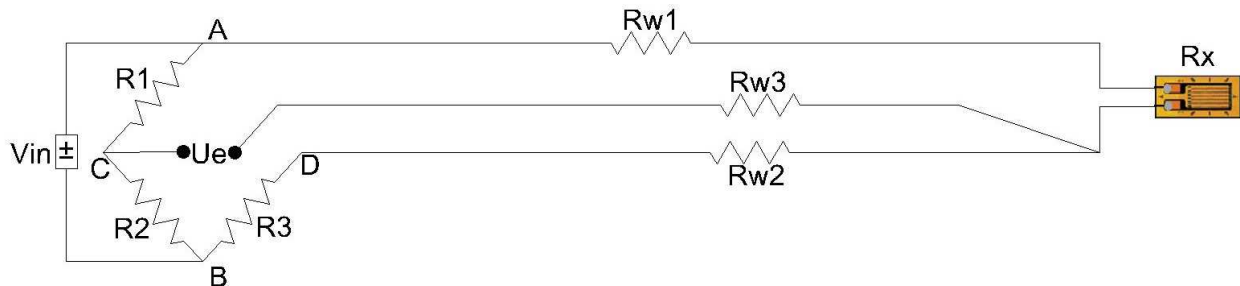


Figure 5-21 - Quarter bridge connection via three-wire

The two-wire connection produces an incorrect strain measurement because it introduces apparent strains all on the same side and therefore not compensated. Equation 5-14 shows that the bridge is balanced when:

$$\frac{R_x}{R_1} = \frac{R_3}{R_2}$$

Equation 5-18

for the case of the two-wire connection:

$$\frac{R_x + R_{w1} + R_{w2}}{R_1} \neq \frac{R_3}{R_2}$$

Equation 5-19

The three-wire connection, on the other hand, eliminates the apparent deformations because both cable w₂ and w₁ are connected in series on one of the two adjacent branches of the bridge, while cable w₃, which is used to read the unbalance of the bridge, does not introduce any errors because since no current is circulating in it the voltage drop at its ends is negligible. So, from an analytical point of view, as far as the three-wire connection is concerned:

$$\frac{R_x + R_{w1}}{R_1 + R_{w2}} = \frac{R_3}{R_2}$$

Equation 5-20

5.2.7.2 Strain gauge calibration: shunt calibration

The strain gauges used for the test have their own gauge factor. However, to be able to connect the strain gauges to the control units responsible for reading the measurements, it was necessary to adapt the connections between the original connection wire welded onto the strain gauge directly by the parent company and the control unit. It was necessary to adapt the terminals of the strain gauge cable with RJ45 plugs supported by the control units. This procedure entailed a change in terms of resistance reading by the strain gauge and therefore a recalibration of the gauge factor was carried out.

A method used to determine the correct k value was to apply shunt calibration, a function already implemented in the control units used. Shunt calibration is a method by which it is possible to parallel the strain gauge with a resistor (or rather with the branch of the bridge adjacent to the strain gauge) with a known ohmic value and to simulate a precise strain value. If the strain read by the bridge is different from that applied to the shunt resistor, then it will be necessary to vary the gauge for the correction to take place. The shunt resistance for a given simulated strain value is a function of the strain gauge resistance.

$$R_{sh} = \frac{R_x + 10^6}{k \cdot \varepsilon_s} \cdot R_x$$

Equation 5-21

R_{sh} is the shunt resistance, R_x is the resistance of the bridge branch to be shunted, k is the gauge factor and ε_s is the simulated strain measured in µε. In Figure 5-22 is shown the scheme of the shunt calibration.

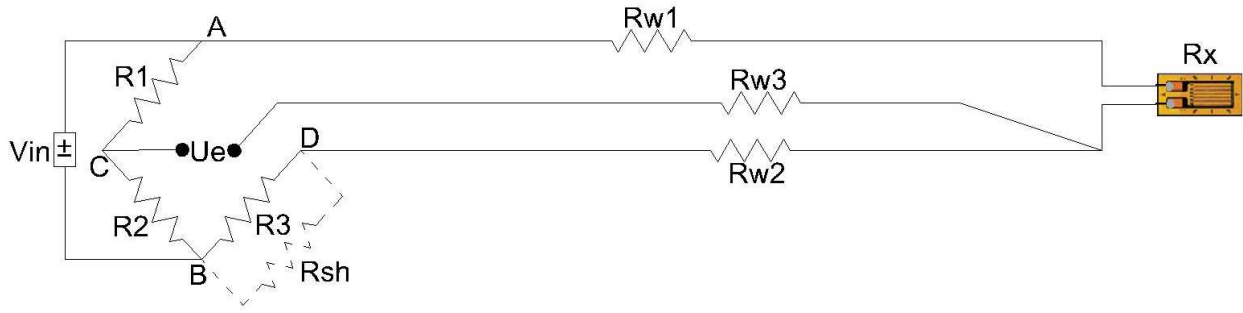


Figure 5-22 -Shunt calibration configuration

5.2.7.3 Strain gauge thermal calibration

In order to consider the effects of the temperature on the strain gauges measurements, a preliminary test before inserting the pile into the box was carried out. The grid conductor electrical resistivity and the thermal expansion between the grid conductor and the object surface at the which the strain gauges are glued, are certainly the main algebraic effects the affect the thermal output.

$$\frac{\Delta R}{R_0} = \beta_G \Delta T + \left[K_G \left(\frac{1 + K_t}{1 - \nu_0 K_t} \right) (\alpha_M - \alpha_G) \right] \Delta T$$

Equation 5-22

Where:

- $\beta_G \Delta T$: gauge resistance with temperature
- $\left[K_G \left(\frac{1 + K_t}{1 - \nu_0 K_t} \right) (\alpha_M - \alpha_G) \right] \Delta T$: Resistance change proportional to the differential expansion
- $\frac{\Delta R}{R_0}$ Unit change in resistance from the initial reference resistance, R_0 , caused by change in temperature resulting in thermal output.
- β_G Temperature coefficient of resistance of the grid conductor
- K_G Gauge factor of the strain gauge
- K_t Transverse sensitivity of the strain gauge for its gage factor
- ν_0 Poisson's Ratio of the standard test material used in calibrating the gauge
- α_M Thermal expansion coefficient of the test material
- α_G Thermal expansion coefficient of the grid
- ΔT Temperature change from an arbitrary initial reference temperature
- $\left(\frac{1 + K_t}{1 - \nu_0 K_t} \right)$ is the correction factor for transverse sensitivity to account that the strain in the gage grid due to differential thermal expansion is biaxial.

In Equation 5-22 the first term represents the grid conductor electrical resistivity while the second term takes into account the thermal expansion coefficients of gauge and measured material.

$$\varepsilon_T = \frac{\frac{\Delta R}{R_0}}{K} = \frac{\left[\beta_G + K_G \left(\frac{1 + K_t}{1 - \nu_0 K_t} \right) (\alpha_M - \alpha_G) \right] \Delta T}{K}$$

Equation 5-23

By Equation 5-23 it is possible to obtain the thermal output in strains units for a strain gauge under thermal variations (ΔT) in free thermal condition of contraction or expansion for the investigated specimen substrate (pile surface). Because the coefficients are temperature-dependent the temperature output should not be linear with the temperature change. The thermal output results only function of the gage resistance variation with temperature in the case of self-temperature compensated gauges. In fact, because the thermal expansion coefficients of the gauge and the measured object material are the same, by the Equation 5-22 it is clear that the thermal output depends on only by the temperature coefficient of resistance of the grid conductor.

To take into account of the possible thermal corrections to make for every strain gauge applied on the pile shaft, a series of heating and cooling thermal tests were carried out with the pile in nearly free expansion condition (i.e. putting the pile vertically on a rigid base). During the tests the strain gauges thermal outputs were recorded for different heat carrier fluid inlet temperature.

5.2.7.4 Thermocouples

To measure and control temperature in soil, a set of MgO-insulated stainless steel thermocouple K stems 100 m long and 3 mm in diameter were used. One of these thermocouples was used to measure the outlet water temperature from pile during the tests. This info was very important to calculate the effective heat power exchanged between pile and soil.

Thermocouples were placed in soil to obtain a measure about temperature distribution near the pile and other adjacent zones. The first thermocouple called Tc1, were placed 100 mm under the pile toe and 500 mm from the ground surface at two diameters (60 mm) from the pile surface. Other two thermocouples, called Tc2 and Tc3, were placed in contact with the pile surface. While Tc2 measured pile toe temperatures, Tc3 was placed 100 mm from the ground surface and measured the temperature near pile head. To control what happened far from pile surface, other two thermocouples, Tc4 and Tc5, were placed respectively one diameter (30 mm) and two diameters (60 mm) from pile surface. These sensors were 200 mm from ground surface i.e., at the same height as the centre of gravity of the pile.

Before the sensor was installed in the ground, to obtain a precise measurement, only the tip of the thermocouples was uncovered by a layer of insulating material, which was placed on the remaining part of the stem (Figure 5-23).

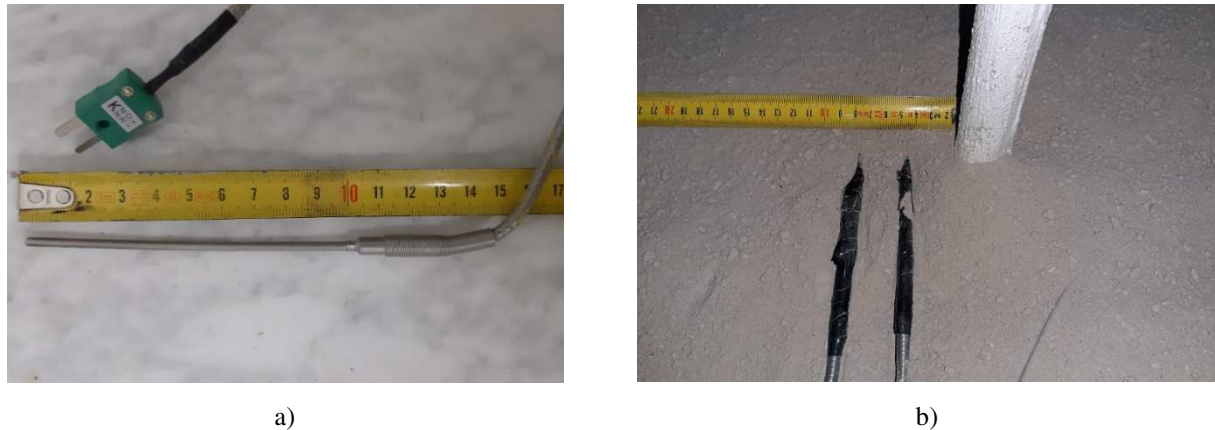


Figure 5-23 – a) thermocouple dimensions; b) location of Tc4 and Tc5 near the pile and stem thermal insulation system

5.3 Small-scale test program

To analyse the thermomechanical behaviour of the small-scale energy pile and the surrounding soil, a series of mechanical, thermal, and thermomechanical loads were applied to the model. The thermal and mechanical loads were chosen with different criteria. Regarding the thermal load, it was chosen between the inlet temperatures simulated by Design Builder software for a building placed in the city of Naples as already explained in detail in previous chapter 3. The inlet temperature trend, already showed in previous chapter, is reproduced in Figure 5-24.

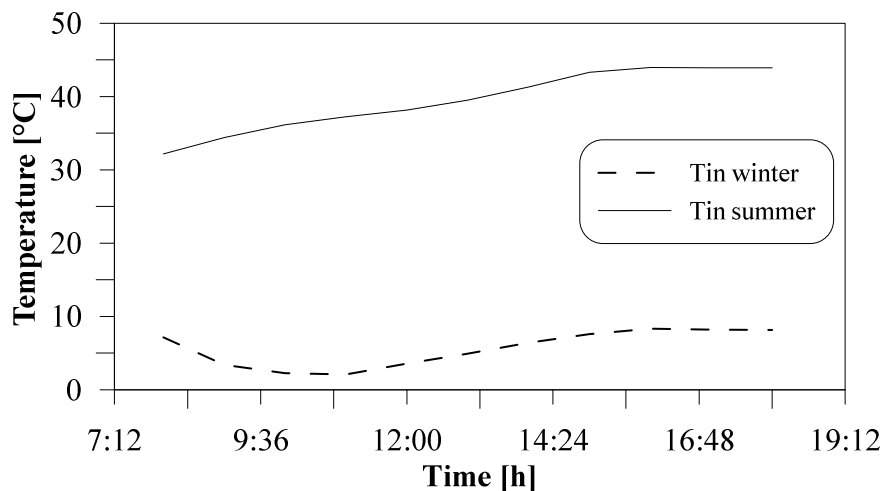


Figure 5-24 - Inlet temperature used during the tests for heating and cooling thermal loads

Regarding the mechanical load, on the other hand, the pile ultimate bearing capacity was estimated by a load test better explained in next sections. The ultimate capacity of the pile was assumed as the mechanical load that provided a pile head settlement equal to the 10% of the pile diameter (i.e. 3 mm). For the tests carried out during the experimentation, generally the mechanical load applied on pile head corresponded to a service load equal to approximately the 30% of the ultimate load bearing capacity.

On the ground level three circular loads were applied. The aim was to reproduce in small-scale not only the geometric sizes of the model respect to a field test but also to try to make more compatible

the soil stresses in the laboratory box with the soil stresses that can be found in full scale piles installations.

A test program was established to investigate the pile/soil behaviour. The program provided for three different test modes depending on the way of the thermal load application.

In the first one a purely mechanical load was applied on the pile head to establish the bearing capacity. After, a series of cyclic thermomechanical tests were carried out with a thermal load extrapolated from the energy simulation both for the heating and cooling case. In the heating case, also the effects of a time recovery between two consecutive cycle was investigated.

Finally, a series of tests in which the heating thermal load was provided continuously and with a regular law were carried out. The minimum and the maximum temperatures of the thermal loads corresponded to the maximum and minimum temperatures recorded for the monotonic heating histories used in the previous tests. The aim was to analyse the effects on the pile head displacements of the same continuous cyclic regular thermal loads under different mechanical loads applied on the pile head. Below a scheme with the test program is reported in Table 5-3.

In any thermal and thermomechanical test, the behaviour of the small-scale model was monitored both during the active phase (i.e. when the circulating bath worked) and for some hours after the circulating bath stoppage (monitoring phase).

Moreover, during the active phase, the thermal power injected/extracted into/from the ground was also evaluated both for heating and cooling thermal loads. The evaluation of the thermal power was carried out using the Equation 5-24:

$$Q = \rho C_p \Delta T \nu$$

Equation 5-24

Where:

Q is the heat output exchanged between the pile and the ground [W];

ρ is the density of the heat transfer fluid (water 997 kg/m³);

C_p is the specific heat (water 4186 J/kg °C);

ν is the fluid flow rate (for the tests performed 9,33x10⁻⁵ m³/s)

ΔT is the temperature difference expressed in °C between the inlet and outlet temperatures.

A thermocouple was inserted at the output side of the circulating bath circuit to evaluate and record the output temperature. The inlet temperature, instead, was directly provided by the thermal sensor inside the circulating bath. Using these data, it was possible to establish the inlet and outlet temperature difference during the tests.

In next sections, the tests carried out with the thermal history designed on the basis of the energy analysis simulation are called “long-term”. On the other hand, the tests carried out with regular thermal histories are called “S” followed by a letter indicating the level of mechanical load applied during the test.

It should be noticed that during the pile installation in the box, the strain gauge 1 was damaged. Consequently, it was not possible to obtain strain data about the pile toe.

Table 5-3 – Test program scheme

Test modes	Type of test	Mechanical load	Thermal load	Duration
Mechanical	Mechanical load test (Q_{im})	$Q_{max} = 283$ N	no	1,98 h
Cycle with designed thermal history	Long-term Thermomechanical heating (9 cycles with recovery)	97 N	$T_{max} = 44,0$ °C $T_{min} = 32,2$ °C	Active phase: 106 h Monitoring phase: 95 h
	Long-term Thermomechanical cooling (10 cycles)	97 N	$T_{max} = 2,1$ °C $T_{min} = 8,3$ °C	Active phase: 80 h Monitoring phase: 60 h
Regular and continuous cycle	SA: Heating 0% of the Q_e (11 cycles)	no	$T_{max} = 44,0$ °C $T_{min} = 32,2$ °C	Active phase: 66 h Monitoring phase: 81 h
	SB: Thermomechanical heating 50% of the Q_e (11 cycles)	49 N	$T_{max} = 44,0$ °C $T_{min} = 32,2$ °C	Active phase: 66 h Monitoring phase: 106 h
	SC: Thermomechanical heating 100% of the Q_e (11 cycles)	97 N	$T_{max} = 44,0$ °C $T_{min} = 32,2$ °C	Active phase: 66 h Monitoring phase: 38 h
	SD: Thermomechanical heating 150% of the Q_e (11 cycles)	146 N	$T_{max} = 44,0$ °C $T_{min} = 32,2$ °C	Active phase: 66 h Monitoring phase: 101 h

5.3.1 Stresses in soil

To increment the stresses level in the soil for a more realistic comparison with a field case three circular loading batteries were arranged around the pile at ground level. Each load battery had three cast iron discs. The circular load area had a radius of 350 mm and resulted in a load of 6,63 kPa.

In Figure 5-25 the stress trend with the depth is reported according the results obtained by the Defrel software. It can be noticed that the major stress increment is obtained for the first 100 mm of the box. However, the loads placement at the ground surface have effects until the box bottom where a vertical stress of about 1,5 kPa was calculated.

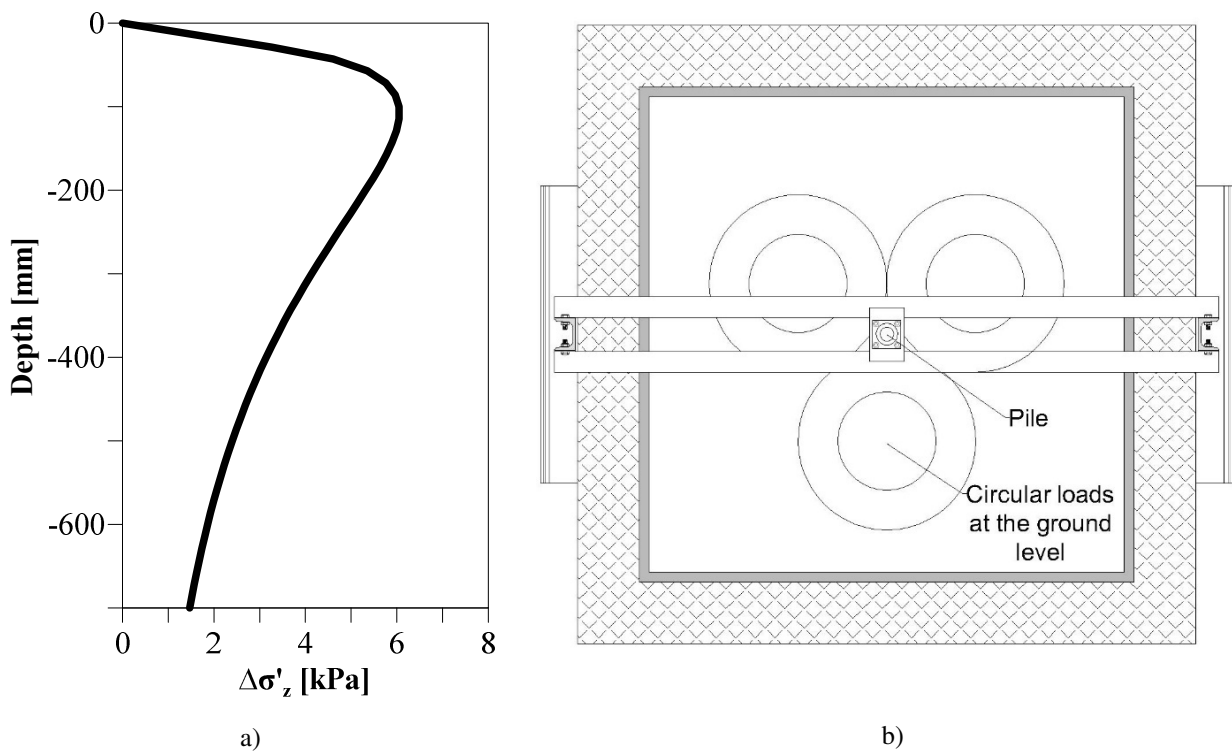


Figure 5-25 – a) increase in vertical stresses after application of the load at ground level; b) scheme of the weight placement at the ground level in the box

5.3.2 Mechanical test. Determination of the ultimate capacity of the pile

A mechanical test was carried out to establish the ultimate load capacity of the pile. The test was performed in 11 load and 11 unload steps in which circular cast iron weights were applied to the pile head. Weights of about 3,1 kg were applied for the first 3 load steps. For the following steps every load had a weight of approximately 2,4 kg. Each step had an application time of approximately 5 minutes (Figure 5-26).

The ultimate capacity load of the pile is established as the load corresponding to a final pile displacement equal to 10% of the diameter. Because the pile had a diameter of 30 mm, the ultimate capacity load is evaluated for a final settlement of 3 mm.

The Figure 5-27 shows that the ultimate load capacity of the pile was approximately 28,8 kg (about 282 N). Moreover, from the Figure 5-27, it is also possible to notice that for the first two load steps, the settlements had a different trend compared to the rest of the test. It was due to a preload of approximately 6,0 kg applied on the pile head before that the was carried out.

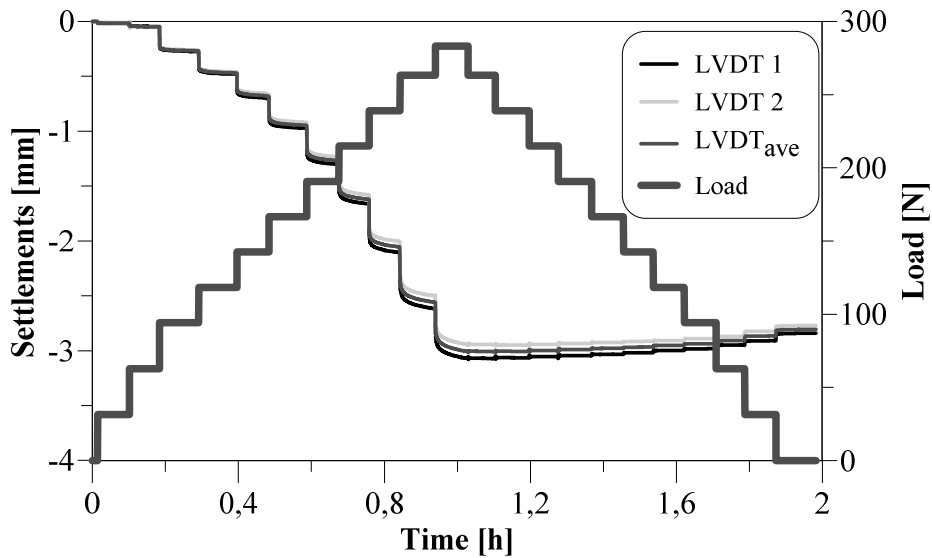


Figure 5-26 - Pile settlements and load steps versus the time during the mechanical load test

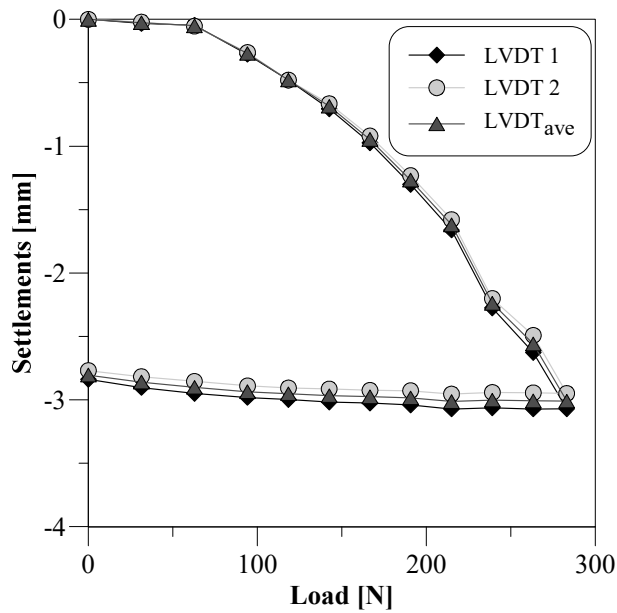


Figure 5-27 - Load-settlements curve during the mechanical test

The mobilized shear stresses were evaluated starting from the axial loads. The pile was subdivided in 4 segments 95 mm in length since it was the distance between two consecutive strain gauges. Because the gauge G1 was damaged, only 3 zone could be considered. The pile head displacements versus the mobilised friction are shown in Figure 5-29.

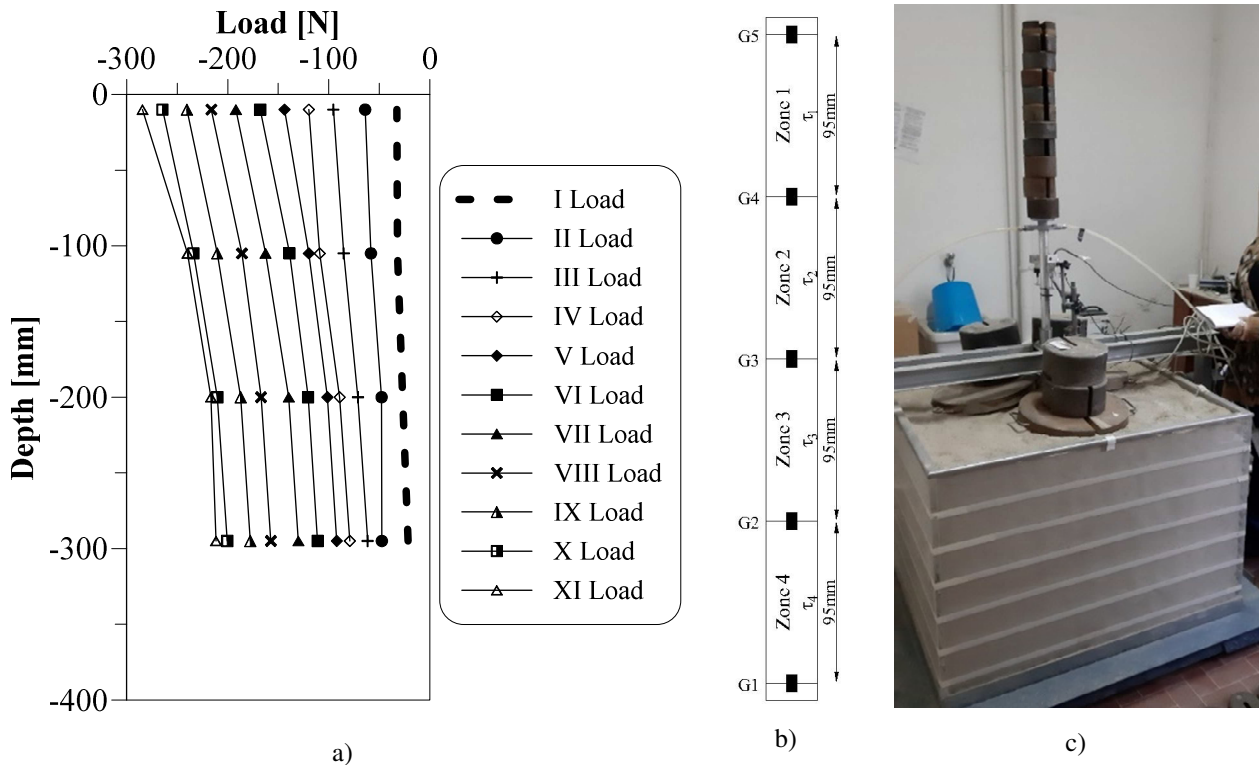


Figure 5-28 - a) axial force distribution along the pile depth for the different load steps; b) scheme of the zones of the pile with the depth; c) the final load step during the mechanical load test

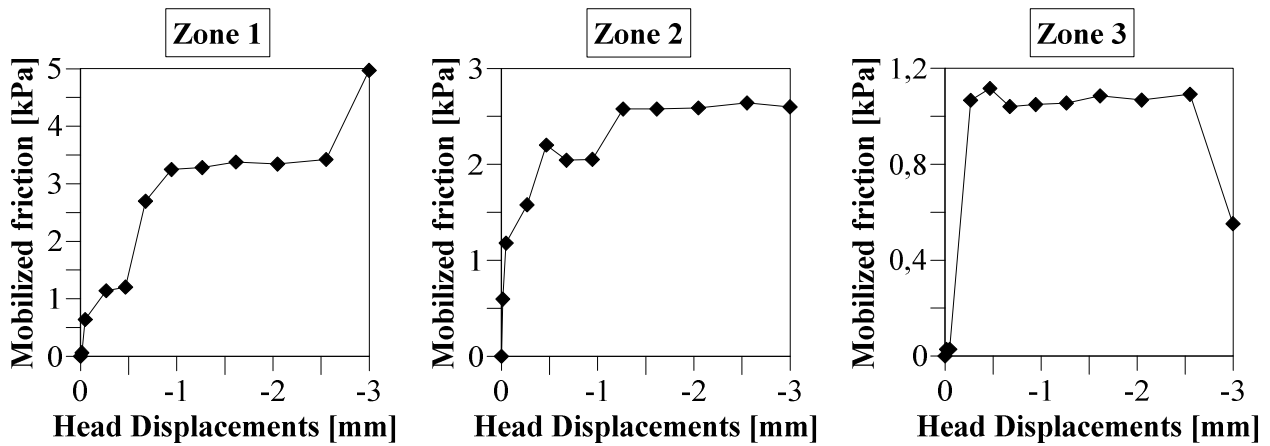


Figure 5-29 - a) Mobilized friction versus the pile head displacements during the mechanical load test

5.3.3 Long-term thermomechanical heating test

The long-term thermomechanical heating test was carried out in two different steps. In the first one only the mechanical load of 96,7 N (approximately the 30% of the ultimate capacity bearing) was applied on the pile head. After some minutes the thermal loads were applied to pile via circulating bath. The thermomechanical loads were applied for approximately 5 day (106 hours). As shown in Figure 5-30 the same thermal history is replayed for 9 times. Between two cycles repeated consecutively a time of recovery of about 2 hours occurred.

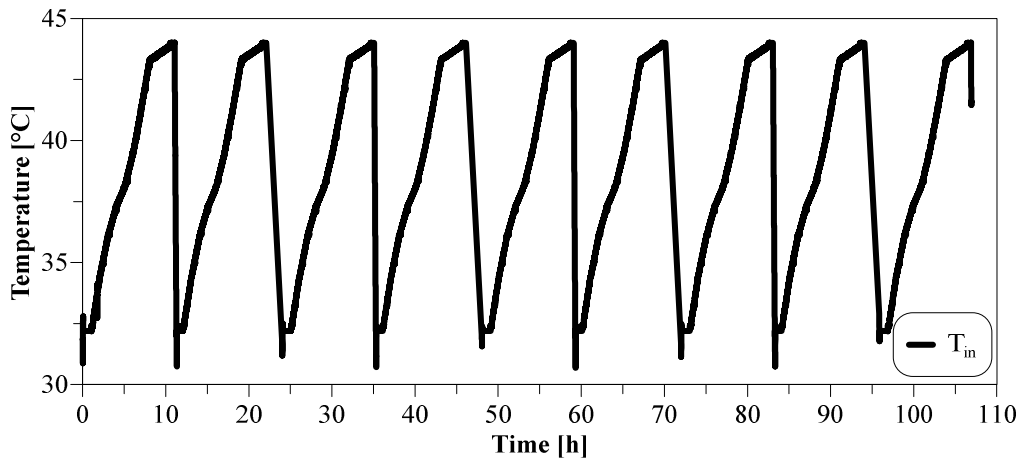


Figure 5-30 - Thermal loads for the thermomechanical heating long term test

The active phase of the test, i.e. when the circulating bath worked and provided thermal loads to pile, carried out for about 106 h. After this phase a monitoring phase both for head displacements and for the soil temperatures occurred for a total time of the measures of about 201 hours.

5.3.3.1 Soil temperature distribution for Long-term thermomechanical heating test

In Figure 5-31 the trends of the soil temperature and the inlet and outlet temperatures of the circulating baths are reported. Despite the recovery time each two cycles, it is possible to notice an increase in soil temperature over the time. This trend is observed both for the thermocouples closest to the pile (Tc2 and Tc3) but also for Tc4 placed 1-diameter from pile.

Seems that the ambient temperature is affected by the operation of the circulating bath. In fact, it is evident a change in trend of the air temperature in correspondence of the end of the double cycles before the recovery time.

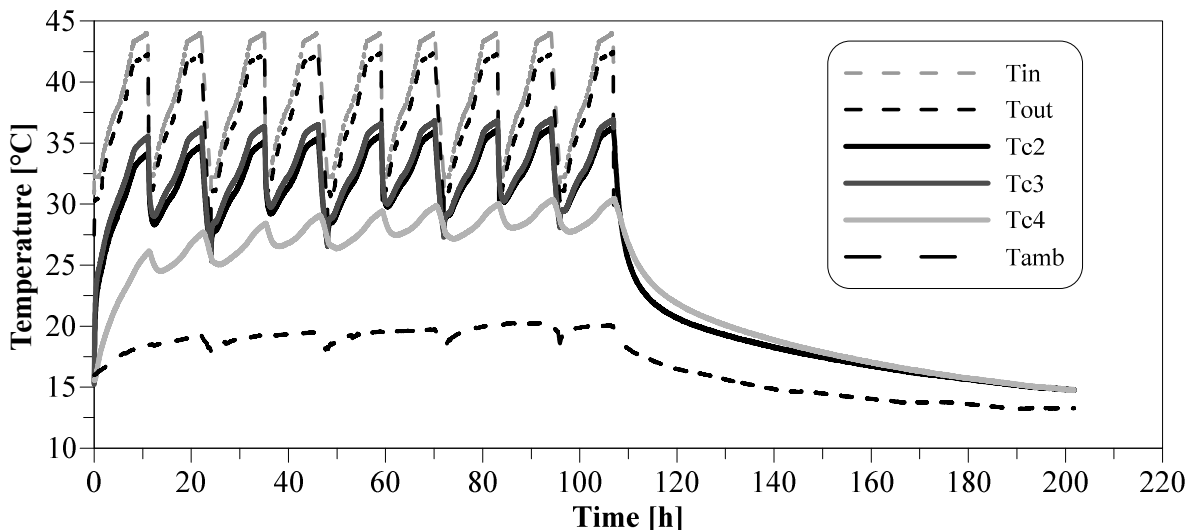


Figure 5-31 - Soil, ambient and heat carrier fluid temperature versus the time for the thermomechanical heating long term test

Other ways to analyse the soil temperature trend are Figure 5-32. Bar diagrams with the temperature of each thermocouple at the end of every cycle for the active mode and approximately every 24 h for 4 days at the end of the active mode are reported.

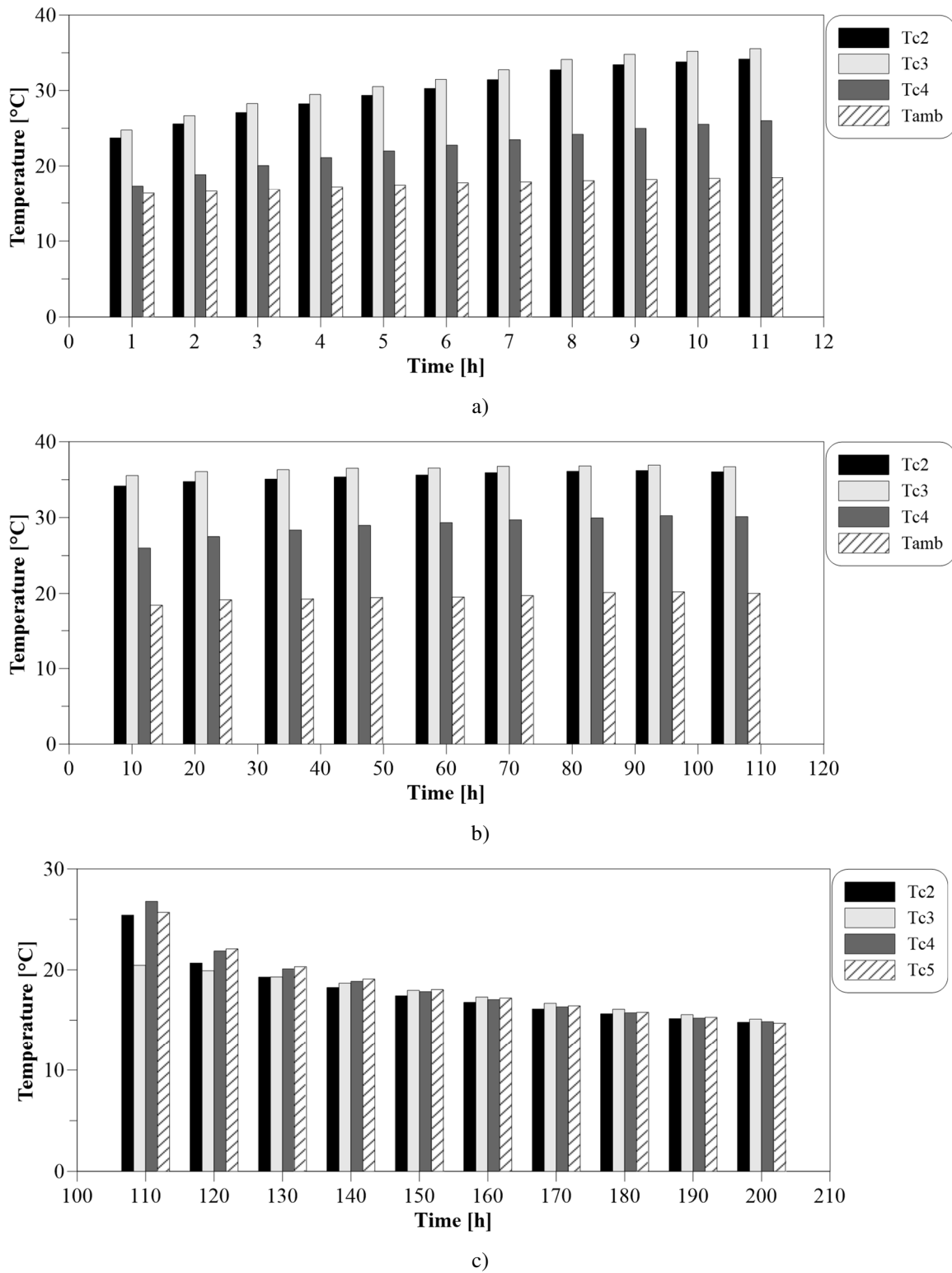


Figure 5-32 - Soil temperature a) during the first cycle of the test; b) at the end of every cycle; c) from the end of the active phase of the test until the end

The temperature difference between the thermocouple placed in the highest and lowest position of the pile surface, Tc3 and Tc2 respectively, is maximum at the end of the first cycle with a value of about 1,37 °C. Anyway, the initial gap tends to decrease as the number of cycles increase, with a temperature difference recorded between the two thermocouples of about 0,66 °C at the end of the

ninth cycle. The temperature variation between the upper part of the pile and the lower part is an indication of a non-uniform distribution of the temperature along the pile shaft and it is a clear sign of the thermal exchange between the pile and the surrounding soil along the pile depth. This phenomenon was also confirmed by the inlet and outlet temperatures of the water from the pile which oscillated between 1,76 °C of the first cycle to 1,52 °C of the last one.

On the other hand, the soil temperature recorded 1-diameter from the pile (Tc4) at the end of the first cycle is about 8,8 °C lower than the temperature measured at the pile surface in the same instant of time. Anyway, at the end of the first cycle, Tc4 measures a temperature increase of approximately 10,4 °C respect the initial undisturbed soil temperature while, at the end of the last thermal cycle Tc4 measures a temperature increase of about 4,1 °C compared to the end of first cycle. At the end of the last cycle the temperature difference between the pile surface and 1-diameter from the pile decrease to 7,88 °C. Anyway, 24 hours after the end of the test, the soil temperature at 1-diameter from the pile was higher than the pile surface. This phenomenon demonstrates that the conduction of thermal energy is still occurring also after the circulating bath stoppage, and the thermal inertia of the soil is playing a role. After 3 days from the end of the test the temperatures of the soil in measured at the pile surface and 1-diameter from the pile were approximately equal. It is the signal of a condition of equilibrium achievement and the beginning of the process of restoration to undisturbed temperature conditions in the soil. After 4 days from the application of the last thermal load, in fact, the soil temperature reaches 14,8 °C, lower than the initial average temperature measured before the beginning of the test (15,4 °C).

5.3.3.2 Heat thermal power for Long-term thermomechanical heating test

It is observed that after every recovery time when the system restarted to work there is a peak in heat power exchanged. It depended on the higher inlet and outlet temperature difference due to pile cooling. On the other hand, a slightly decreasing trend of the heat exchanged is noted with time. With the passing of the cycles, in fact, despite the recovery time, the initial temperature of the pile is always higher due to a thermal accumulation (Figure 5-33).

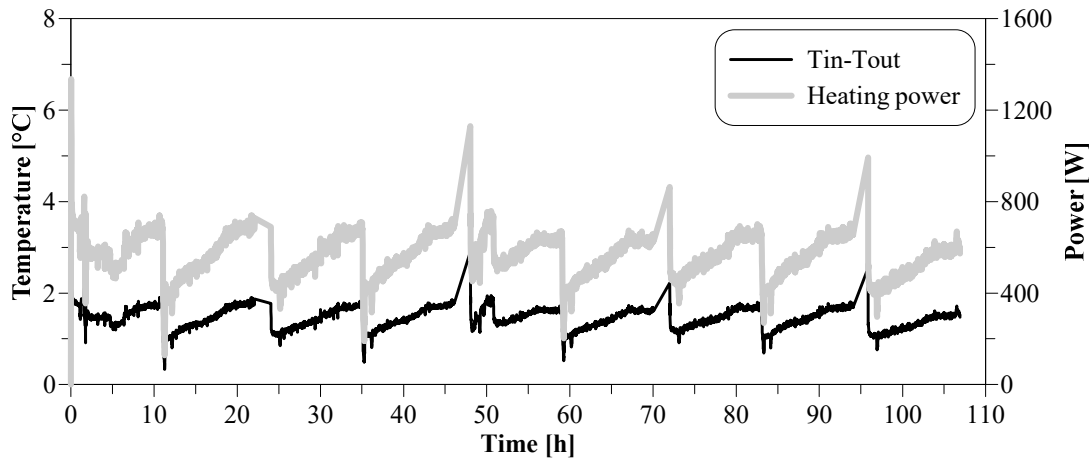


Figure 5-33 - Heat power exchanged between pile and surrounding soil and the difference of inlet and outlet temperature versus the time

5.3.3.3 Pile head displacements for Long-term thermomechanical heating test

The effects of thermomechanical loading on the pile in terms of head displacements are recorded by a LVDT couple. The final value of the displacement trend over time is derived from the arithmetic mean of the values of each individual LVDT for each time instant. Using the principle of superposition of effects, it is possible to separate the thermal displacement from the thermo-mechanical one by subtracting from the latter the value of the mechanical settlement before the application of the thermal load. In Figure 5-34 both the trend of the thermomechanical displacements (LVDT ave) and the derived thermal displacements from them are reported.

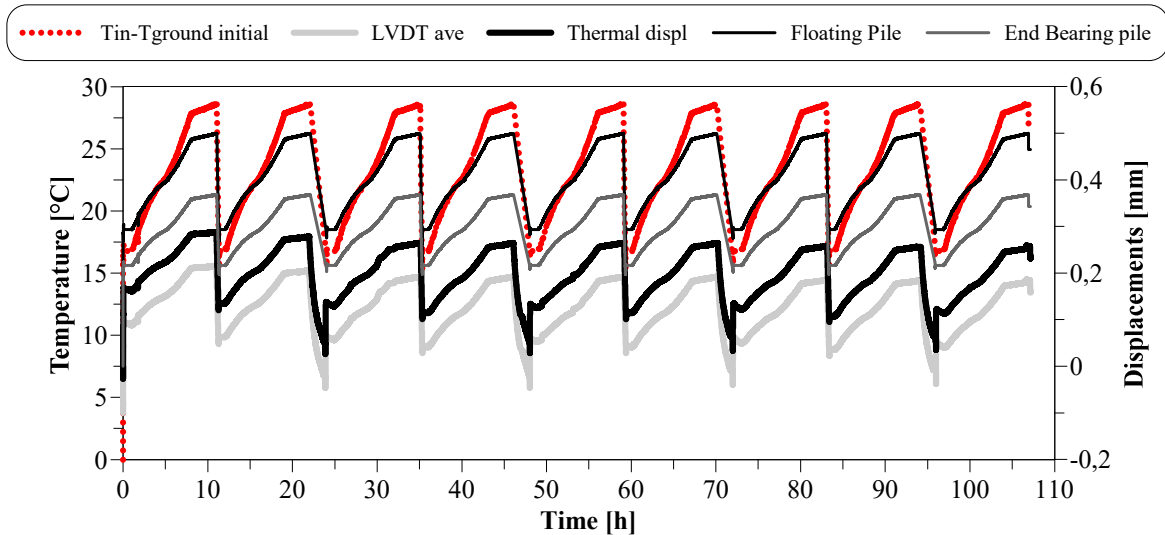


Figure 5-34 - Pile head displacements and inlet temperature trend versus the time for the long-term thermomechanical heating test

At the start of the test, in time zero, the application of the mechanical load (96,7 N) on the pile head cause an instantaneous settlement of -0,11 mm. At the same instant of time, since no thermal load had yet been applied to the pile, the purely thermal contribution is zero. However, as soon as the thermal load was applied to the pile it is possible to notice both an upward displacement of the pile head of about 0,2 mm. Moreover, the trend of both thermal and thermo-mechanical displacements

followed the trend of the thermal loads with maximum displacement values obtained at the end of each cycle. For the first cycle, the maximum thermal and thermomechanical lifts were 0,31 mm and 0,22 mm, respectively.

As described previously, at the end of two cycles there is a recovery phase of about 2 hours in which no thermal load is applied to the pile. In these phases, it is possible to notice a tendency for the pile to cool down with consequent settlements of the head in terms of displacements. However, it is noted that the assigned recovery time is not sufficient for the complete restoration of the initial conditions. In addition, the value of the pile head settlement is not constant with the succession of thermal cycles. In the recovery time at the end of the application of the first couple of cycles, in fact, the maximum settlement recorded is -0,04 mm while at the end of the eighth cycle (fourth couple of cycles) the settlement increase to 0,06 mm.

The maximum thermal displacement is observed at the end of the first thermal cycle with a value of 0,22 mm. Increasing the number of the thermal cycles the thermal displacement has a decreasing trend. At the end of the ninth heating cycle, in fact, with a recorded value of 0,18 mm, the thermal displacement has a decrease of 17 % compared to the beginning of the test.

The thermal displacement corrected from mechanical settlement is then compared with the trend of thermal displacements that the pile would have, subjected to the same temperature differences between heat carrier fluid and the initial conditions, in the case of different restrain configurations. In particular, the two extreme cases of floating pile, in which the null point is placed in the pile middle, and the case of end bearing pile in which the null point is placed in the pile toe, are considered. The temperature difference applied during the test is denoted as $T_{in}-T_{out}$ and it is obtained as the difference between the inlet fluid temperature and the initial soil temperature of 15,14 °C.

It is possible to notice that from the pile head displacements trend recorded during the test, the behaviour of the pile is very close to that of a floating pile.

However, the location of the null point could also be derived from the trend of the pile axial forces with depth.

5.3.3.4 Axial forces for Long-term thermomechanical heating test

In Figure 5-35 the axial forces considering both the thermomechanical effects and the only thermal one is showed. It should remember that with the negative sign the compression forces were assumed. By the graphs it is possible to notice the great compressive axial force increment in the case of the thermomechanical test respect the only mechanical test. Moreover, it should be observed that the maximum compressive values were measured in the pile middle. In fact, considering the only thermal effects the compressive axial force values were between -279 N and -216 N for the upper and lower

bound, respectively. On the other hand, in the same point, considering the thermomechanical effects, values between -326 N and -264 N for the upper and lower bound, respectively are reached.

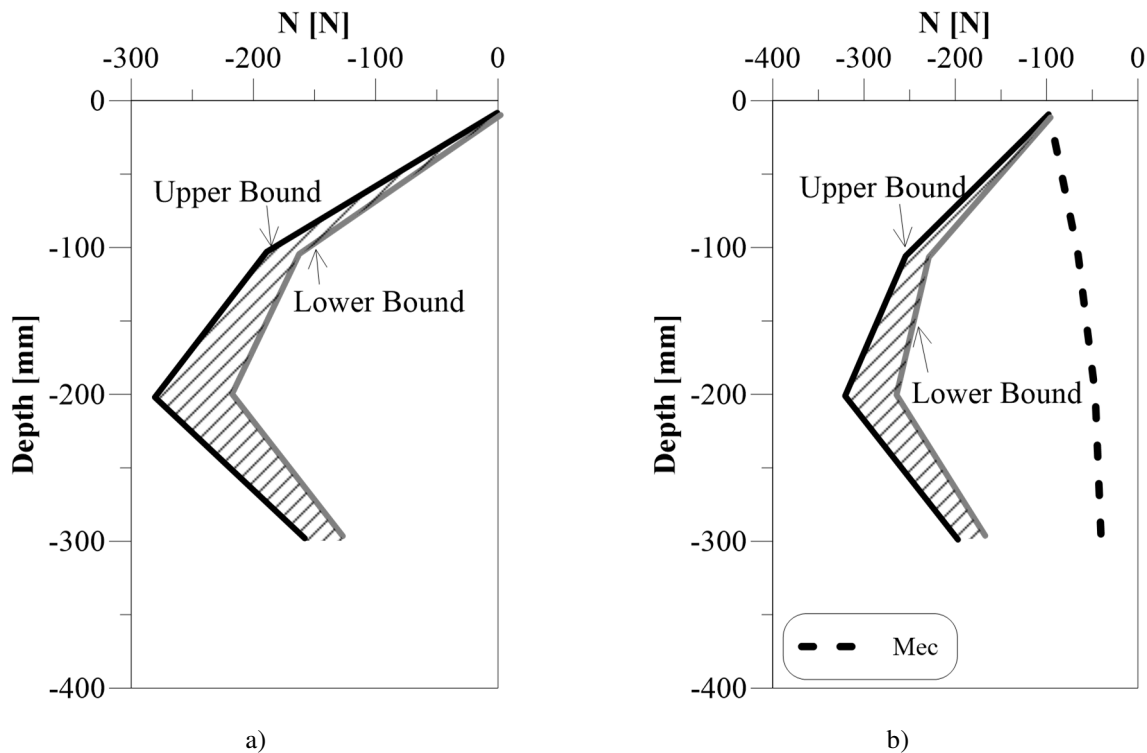


Figure 5-35 - Axial forces along the pile length for long-term hating test a) Thermal values; b) Thermomechanical values

5.3.4 Long-term thermomechanical cooling test

Just as performed for the long-term thermomechanical heating test, long-term thermomechanical cooling test was performed in two steps. The first involved the application of mechanical load only (96,7 N). The second, on the other hand, involved the addition of the thermal loads to the mechanical load by running the circulating bath.

Compared to the heating test, in the cooling test, it is intended to investigate the behaviour of the pile without any recovery period between cycles. Therefore, the applied thermal load consists of the successive application of 10 cooling cycles of 8 hours duration each. The total duration of the test in which thermal loads are applied is about 80 hours with minimum and maximum temperatures ranging between 2,10 °C and 8,3 °C. The initial temperatures of the soil inside the box and air inside the test room is 15,85 °C and 18,82 °C respectively. The imposed thermal load is shown in Figure 5-36.

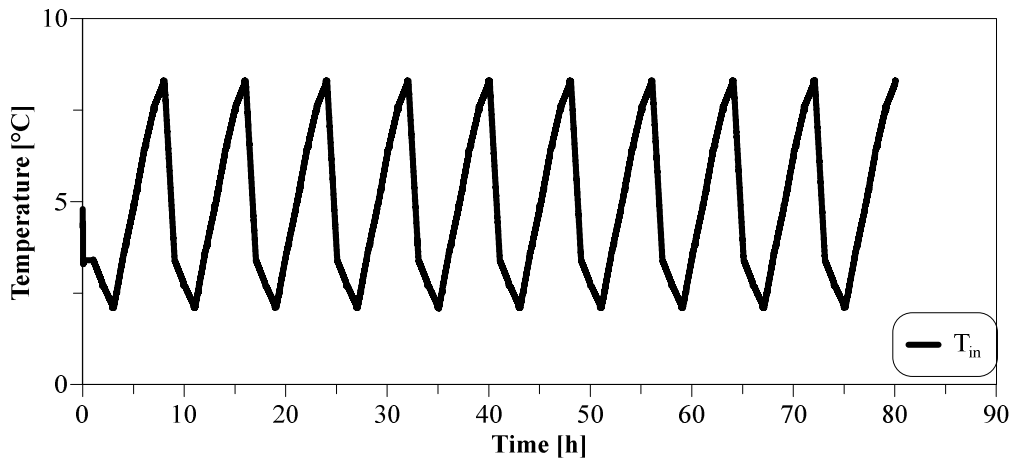


Figure 5-36 - Thermal loads for the thermomechanical cooling long term test

5.3.4.1 Soil temperature distribution for Long-term thermomechanical cooling test

Once the active part of the test finished (i.e. when the thermal loads were applied to the pile) the pile and the surrounding soil were monitored for another 63 hours in order to evaluate the evolution of the heat transfer process inside the soil, taking into account the thermal boundary conditions. Figure 5-37 shows the trends of the inlet and outlet temperatures of the water circulating inside the pile, the temperatures of the soil at the pile and at a distance of one diameter from it, and the ambient temperature of the test room.

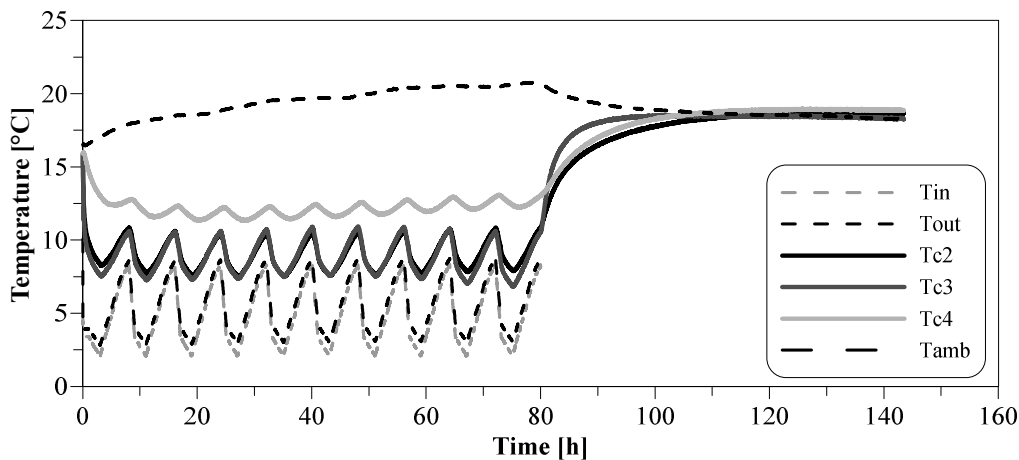
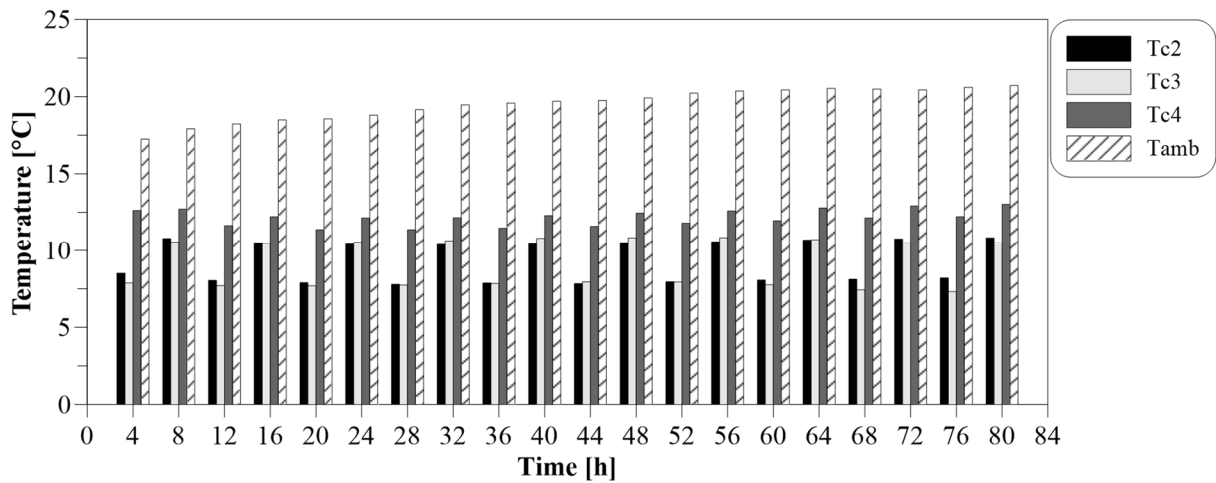


Figure 5-37 - Soil, ambient and heat carrier fluid temperature versus the time for the thermomechanical cooling long term test

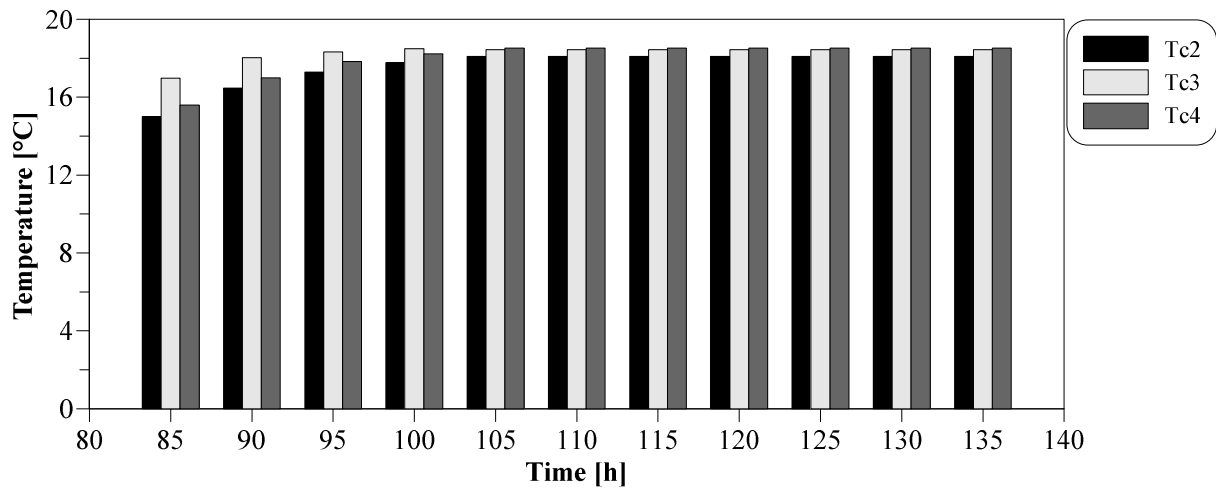
As for the long-term thermomechanical heating test, also in this case the distribution of the temperatures for the length of the pile is not uniform. Obviously, for the cooling test the Tc2 thermocouple located near the pile and at the height of the tip recorded a higher temperature than the Tc3 located near the pile head. This temperature difference is 0,64 °C at the beginning of the test while at the end of the test it decreases to 0,33 °C. This result confirms what has already been discussed in the previous paragraph for the heating test. The difference is the result of the heat exchange between the pile and the ground and the decrease in time denote the tendency of the system to reach thermal equilibrium.

The temperature at 1-diameter from the pile and at a height corresponding to the middle of the pile is measured by Tc4. After the first 4 hours, the temperature recorded by Tc4 was 2,73 °C higher than that calculated at the pile surface considering the same height from the ground surface (arithmetic mean between Tc2 and Tc3). At the end of the 10th cycle, the same temperature difference is 1,34 °C. This result denotes the cooling of the surrounding soil.

In Figure 5-38 are shown the temperatures of thermocouples Tc2, Tc3 and Tc4 at the middle and at the end of every cycle of the active phase of the test (i.e. when the thermal loads are applied in pile). Moreover, the temperature trend of the same sensors from the end of the active phase to the end of the test are also shown by the bar graph.



a)



b)

Figure 5-38 - Soil temperature distribution a) during the active phase of the test; b) from the end of the active phase to the end of the test

After 63 hours from the end of the application of the thermal cooling loads, the average soil temperature is 18,42 °C. It means that the cooling effects are practically completely dissipated. Furthermore, the ambient temperature at the end of the test is 18,55 °C. This data confirms the thesis

that the soil temperature is exclusively influenced by the environmental conditions and that the effects induced by the pile are completely absent after about 2,6 days.

5.3.4.2 Heat thermal power for Long-term thermomechanical cooling test

As shown in Figure 5-39, also for the cooling mode, as already viewed in the heating case, the trend of the heat power exchanged between the pile and the surrounding soil tends to decrease due to thermal accumulation by the pile over time. It provides a consequent decreasing of temperature difference between the inlet and outlet heat carrier fluid. Furthermore, comparing the cooling test with the heating test in which a recovery period was provided every two cycles, it is possible to note that the thermal accumulation in the pile occurs in a more linear way and that the thermal power trend does not undergo any peak during the test.

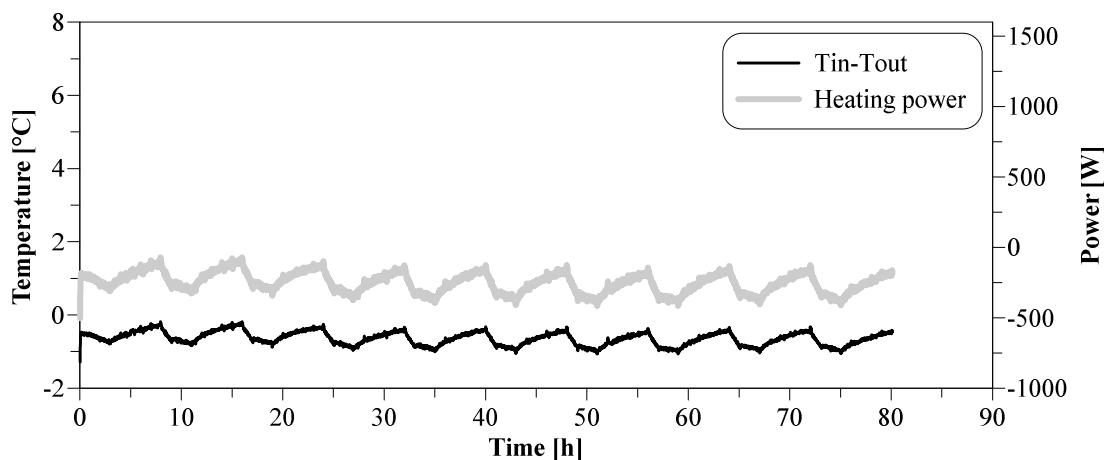


Figure 5-39 - Heat power exchanged between pile and surrounding soil and the difference of inlet and outlet temperature versus the time

5.3.4.3 Pile head displacements for Long-term thermomechanical cooling test

Regarding the displacements measured at the pile head, in Figure 5-40 both the thermomechanical and thermal displacements are represented. As for the heating case, also in this case, at the initial instant of the test, only the effects induced by the mechanical load are detected since the thermal load had not yet been applied to the pile. The value of the settlement for the application of the only mechanical load is 0,08 mm.

The trend of the thermal displacement measured during the test, the thermal displacement calculated in the hypothesis of floating pile and end bearing pile and the difference between the inlet temperature and the average initial temperature of the soil versus the time are reported in Figure 5-40.

The maximum settlement induced by the application of thermal loads, however, tends to increase with the number of thermal cycles with a progressive accumulation of settlements cycle by cycle. At the end of the first cooling cycle, the recorded thermal settlement is 0,1145 mm. At the end of the tenth thermal cycle, instead, the measured settlement is 0,133 mm.

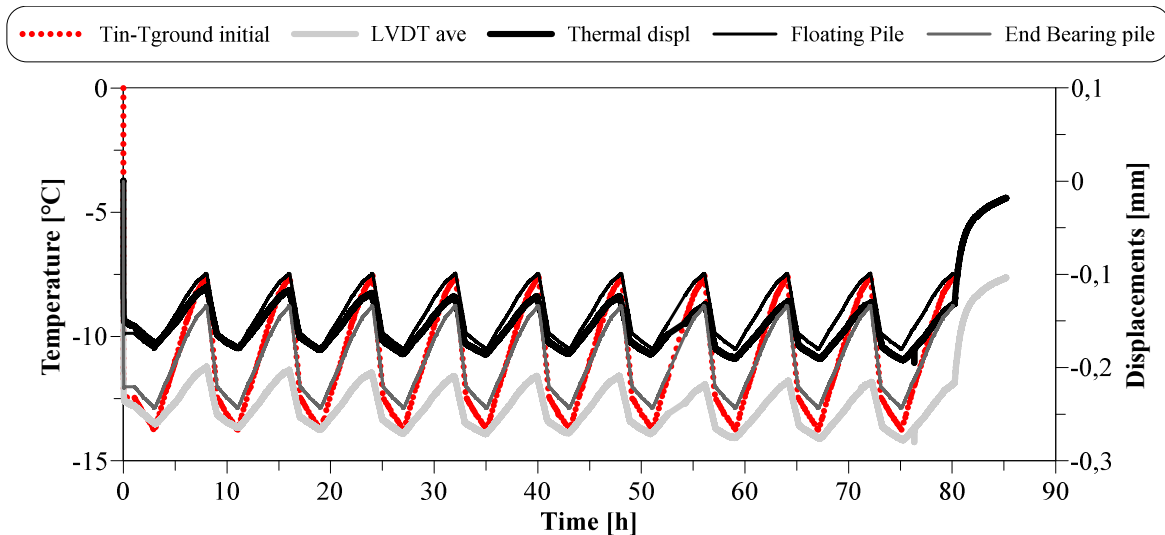


Figure 5-40 - Pile head displacements and inlet temperature trend versus the time for the long-term thermomechanical cooling test

It is noticed that the measured thermal displacement denotes a very similar behaviour of floating pile. It means that the null point is very close to the middle of the pile. This observation is also confirmed by the trend of the axial forces.

In Figure 5-41 the difference of displacements respects the first cycle are plotted both for the cooling and the heating phase of the test. It can be observed a trend that seemed to not stabilize during the first 10 cycles.

Anyway, mathematical functions were extrapolated both for the cooling (Equation 5-25) and the relative heating phase (Equation 5-26).

$$\delta_{(n)} = \left(\frac{0,5}{n}\right)^{\alpha} - 1 [mm]$$

Equation 5-25

$$\delta_{(n)} = \left(\frac{1}{n}\right)^{\alpha} - 1 [mm]$$

Equation 5-26

Where n represents the number of the cycle at which investigate the displacement increment and α is a coefficient that change according to the cooling ($\alpha = 0,008$) or relative heating ($\alpha = 0,006$) phase. The terms “relative” is used because the maximum temperature reached by the pile at the end of the relative heating phase are lower than the initial undisturbed soil temperatures and so are relative only to a phase of the thermal cycle.

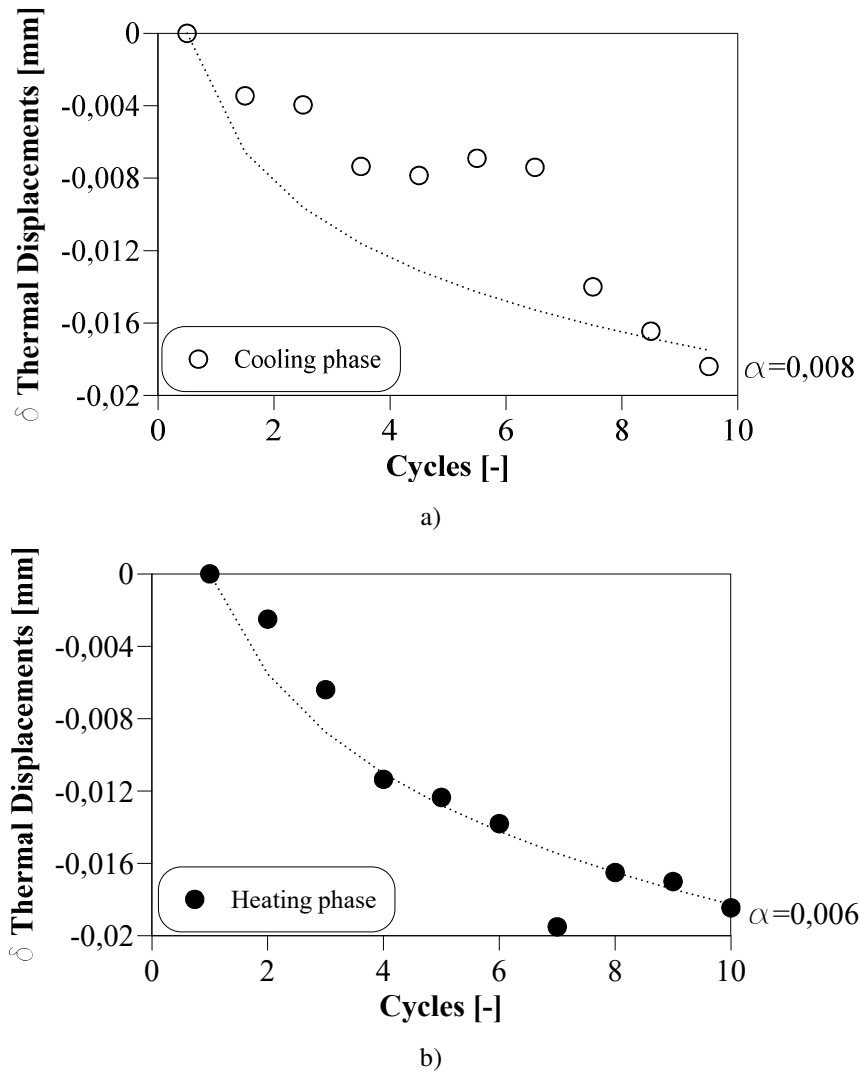


Figure 5-41 - Pile head displacement trend for the long-term cooling test considering a) the cooling phase; b) the heating phase of the test of each cycle

5.3.4.4 Axial forces for Long-term thermomechanical cooling test

In Figure 5-42 the axial forces measured at the end of each cooling cycle are reported. Contrary to what observed for the thermomechanical heating test, the graphs in Figure 5-42 shows a reduction in compressive axial force between the application of mechanical load only and the application of the cooling loads. Moreover, it is observed that in the middle of the pile the greater values of axial forces are reached and have always positive sign (tensile axial forces).

In the pile middle, in fact, the thermomechanical axial force values are between 130 N and 99 N. Without the influence of the mechanical load these values would reach 188 N for the upper bound and 157 N for the lower bound.

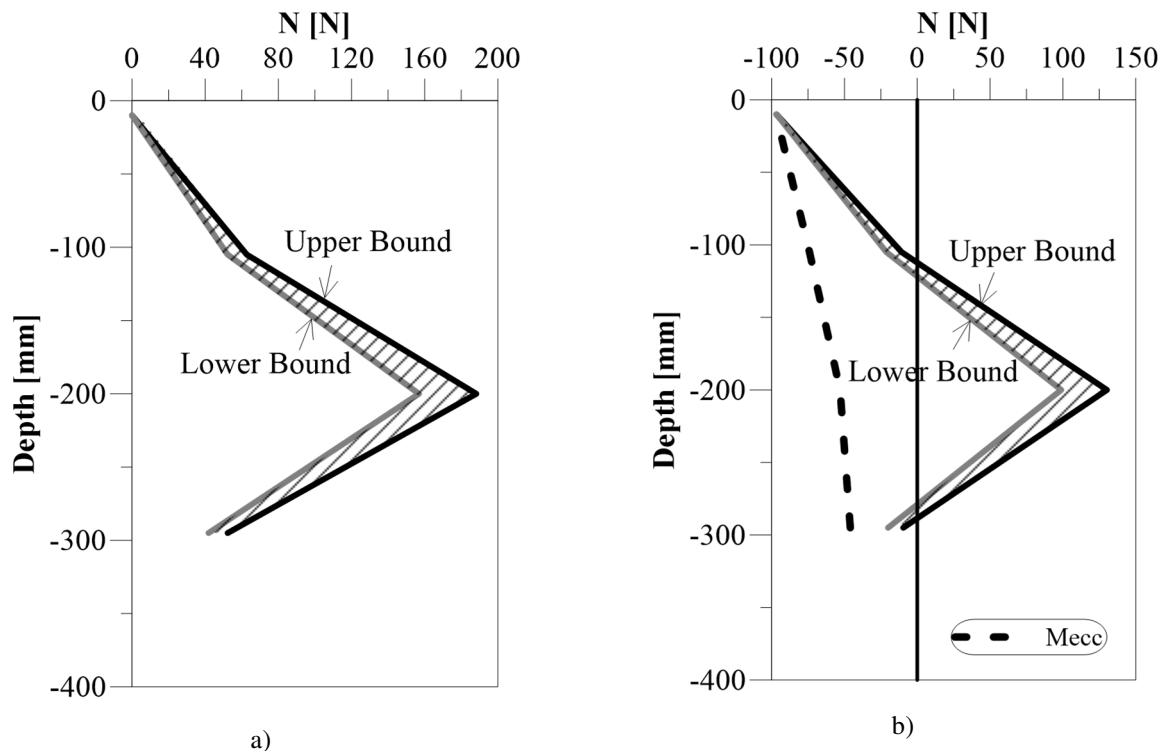


Figure 5-42 - Axial forces along the pile depth for the long-term cooling test a) Thermal values; b) Thermomechanical values

5.3.5 Regular cyclic tests

A series of thermal and thermo-mechanical tests using a regular and continuous thermal heating function over the time were carried out to analyse the behaviour of the pile. The aim was to evaluate the stress-strain and displacement response of the pile subjected to the same thermal load but with different values of mechanical load applied at the pile head. A total of four tests were carried out. One test involved the application of the thermal load only, while in the other three tests the pile was also subjected to mechanical and thermal loads. The value of the mechanical load chosen was 50% of the service load (approx. 48,4 N), 100% of the working load (approx. 96,7 N) and 150% of the working load (approx. 145 N). To simplify the discussion, tests will be referred to as SA, SB, SC, and SD for tests performed at 0%, 50%, 100% and 150% of the service load respectively.

For all four tests, the thermal load applied to the pile during the experiment was always the same. It was a continuous regular thermal history repeated 11 times with a trend that varied from a minimum of 32,2 °C to a maximum of 44 °C in 3 hours and from maximum to minimum in another 3 hours. The maximum and minimum temperature values considered were extrapolated from the thermal history of inlet temperatures to the heat exchangers evaluated through the dynamic thermal simulation carried out with Design Builder. The total duration of the thermal load application was 66 hours. In Figure 5-43 the trend of the inlet temperature during the tests was shown.

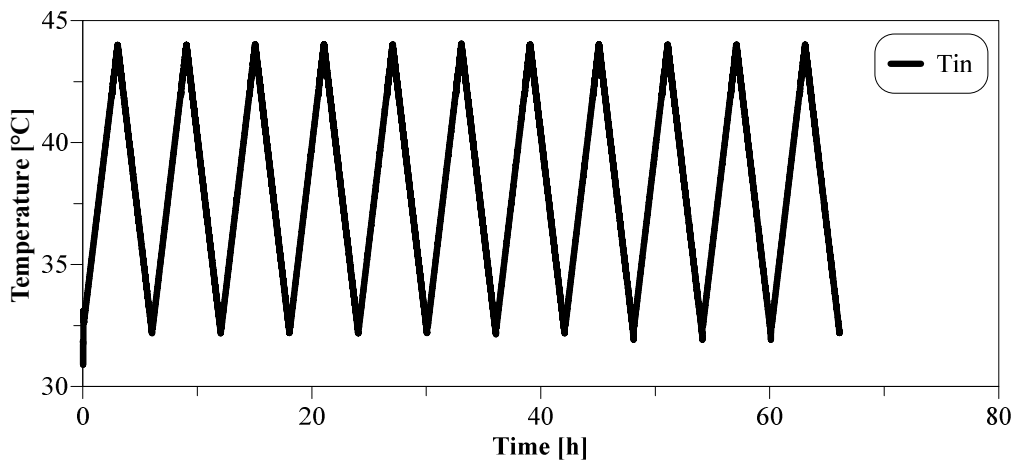


Figure 5-43 - Heat carrier fluid inlet temperature for the regular tests

The test was monitored both during and after the application of the thermal loads. In particular, the inlet and outlet temperatures of the heat carrier fluid, the soil temperatures, the displacements of the pile head and the axial loads on the pile were monitored.

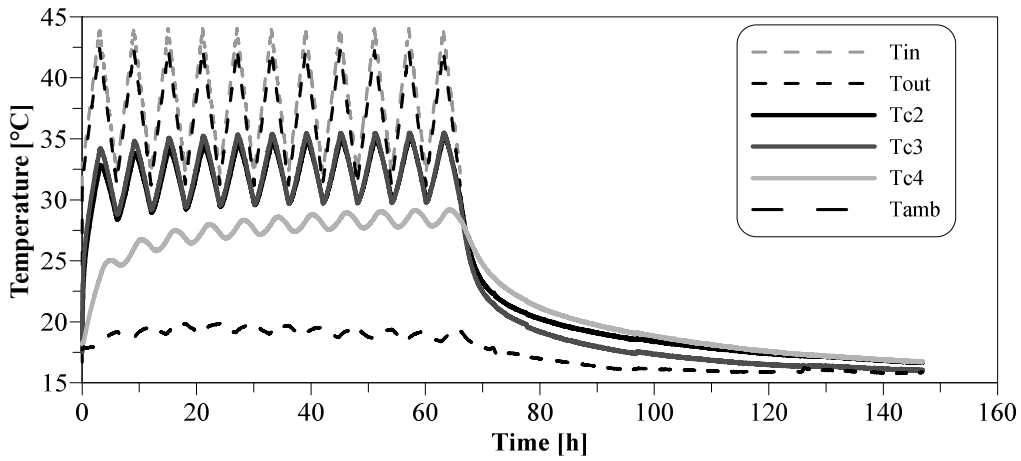
5.3.5.1 Soil temperature distribution for regular tests

From Figure 5-44 to Figure 5-48 the soil temperature distribution for the regular tests are shown. Generally, it can be observed that the trend is the same for all tests because of the same thermal load histories for all the tests. Both from the curves and the histograms graphs it is observed that during the active phase of the heating tests, the tendency of temperature at the pile surface and at one diameter from pile gain over the time. Moreover, always for all the tests, there is a certain temperature gap between the head and the toe of the pile surface with a greater temperature measured at the pile top. It is attributed to the heat exchange between the pile and the soil. This hypothesis is also confirmed by the decrease of the temperature gap between the top and the toe of the pile over the time because of the tendency of the system to the thermal equilibrium. It is also observed that the initial slope of the temperature gain in the active phases of the tests is very different between the pile surface and the soil at 1-diameter from the pile.

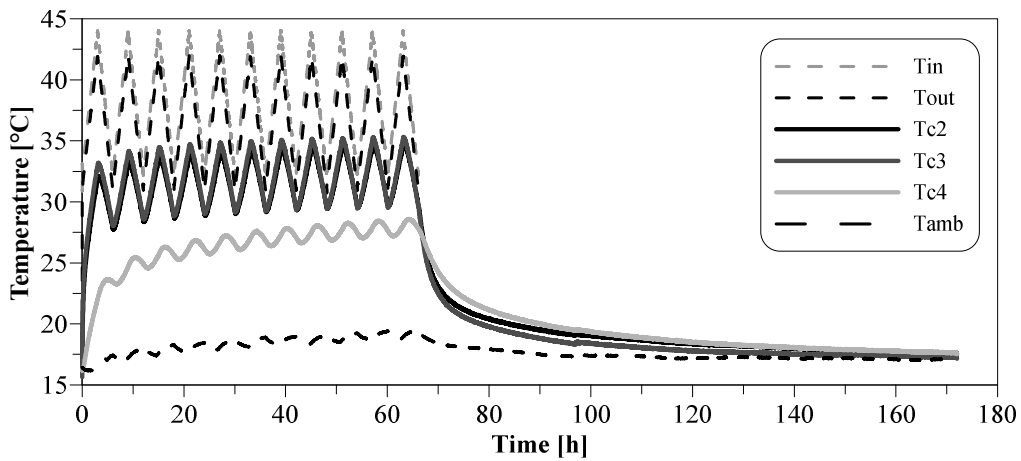
When the active phase of the tests ends and the heating is stopped, it is noticed in all tests that the temperature at one diameter from the pile is always higher than the pile surface. It is also observed a very heavy slope of the thermocouples Tc2 and Tc3 as soon as the heating stopped while, in the case of the thermocouple Tc4 the slope is gentler. Moreover, in cooling phase, after some hours from the heating stop, it is also observed a lower temperature near the pile surface for the pile top respect the pile toe zone.

These phenomena are linked to soil thermal inertia and to the thermal boundary condition. In the first hours of the cooling phase, the higher temperatures measured by Tc4 is due to the delay of the heat transfer from the heat source to the thermocouple. These differences between Tc2 and Tc4 tend to

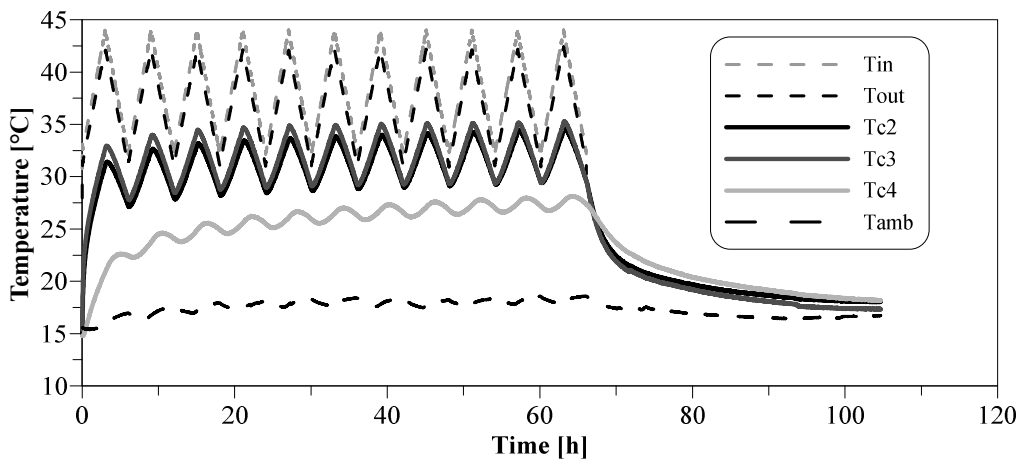
zero out over time. In any case Tc3 measured always lower temperatures also at the end of the measurements. It depends on the position of the thermocouple. In fact, Tc3 is placed very close to ground level and therefore much more influenced by the outside air temperature trend. This was demonstrated by the fact that at the end of the measurements, the temperature of the outside air and Tc3 were very close to each other while on the other hand, Tc2 and Tc4 placed in deeper position in the soil, maintained slightly higher temperatures maintained slightly higher temperatures.



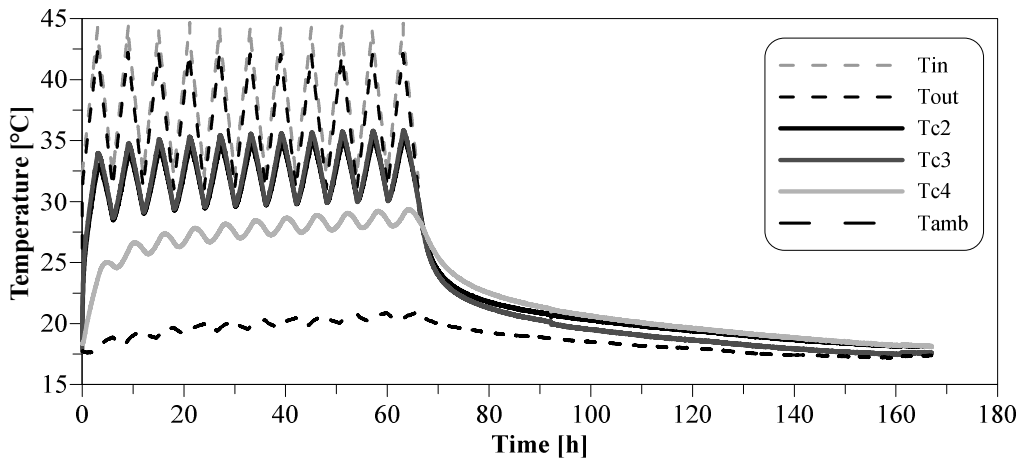
a)



b)

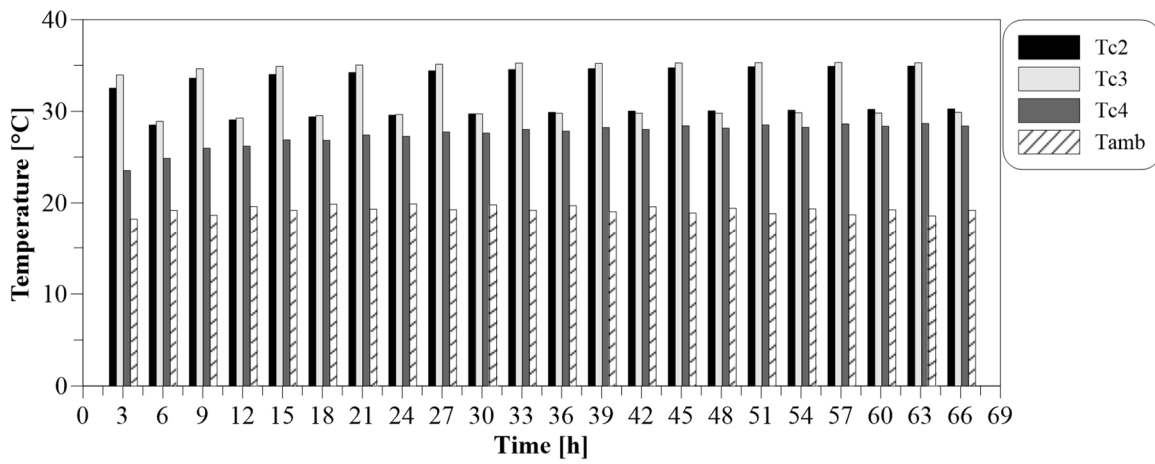


c)

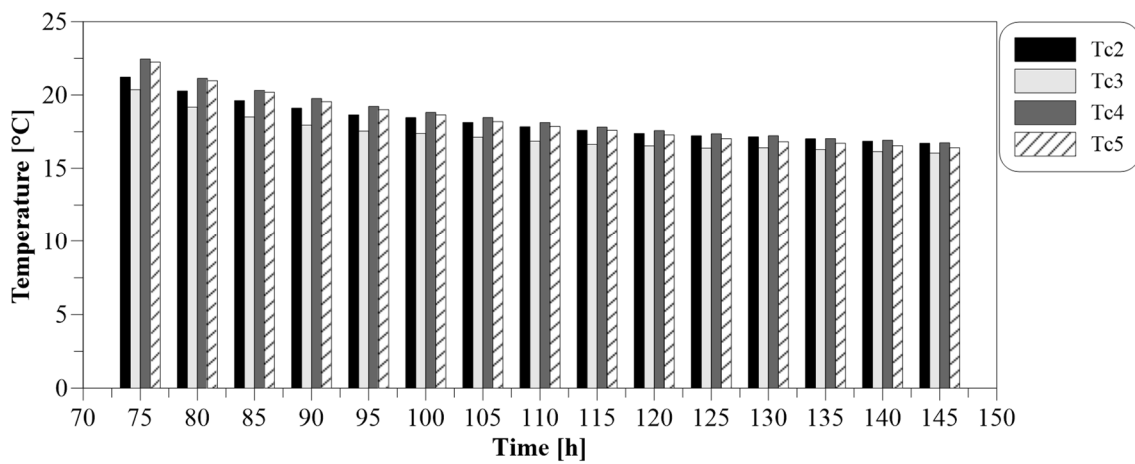


d)

Figure 5-44 – Soil and heat carrier fluid temperature trends versus the time for the small-scale pile subjected to a regular cyclic thermal load. Mechanical load on pile head (percentage respect the service load) a) SA b) SB) c) SC d) SD

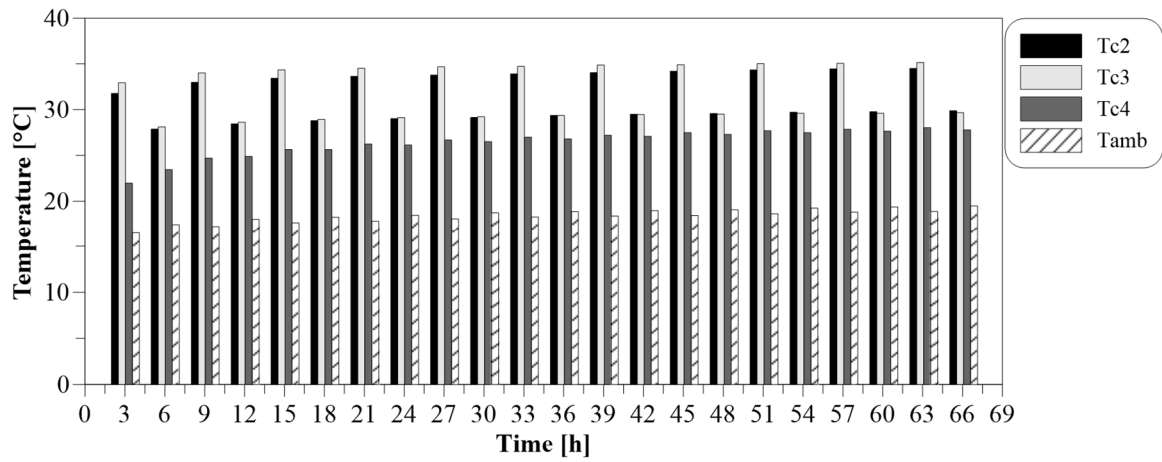


a)

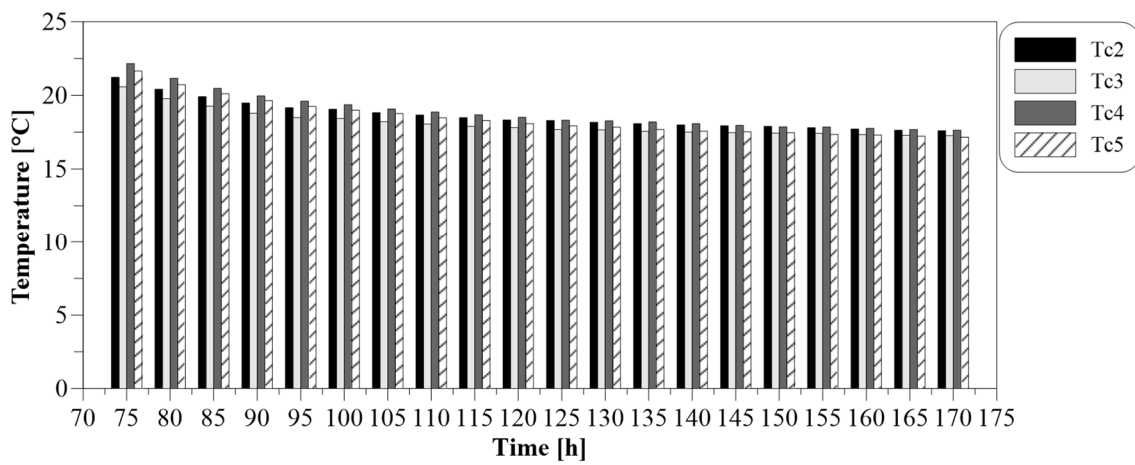


b)

Figure 5-45 - Soil temperature at different distance from the pile for the test SA. a) During the application of thermal loads b) After the application of thermal loads

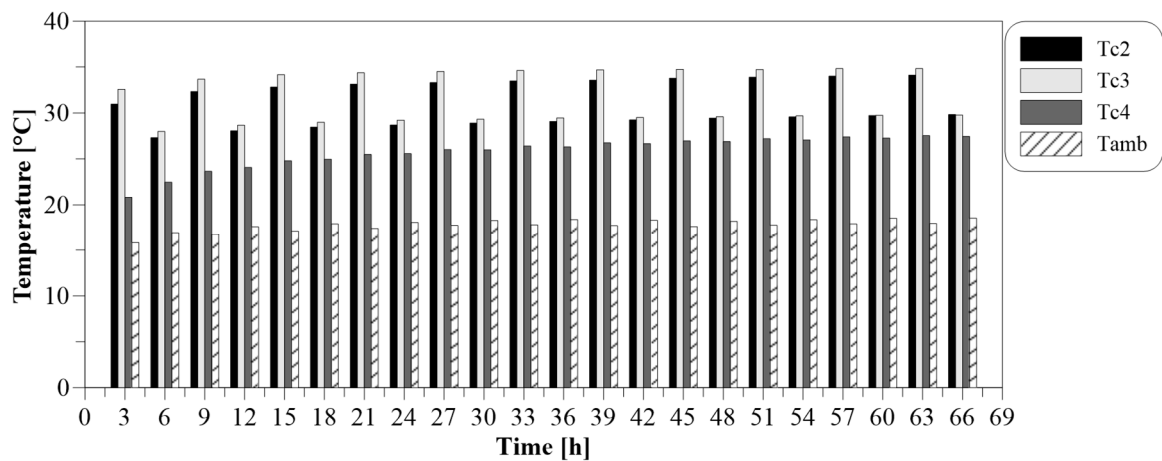


a)

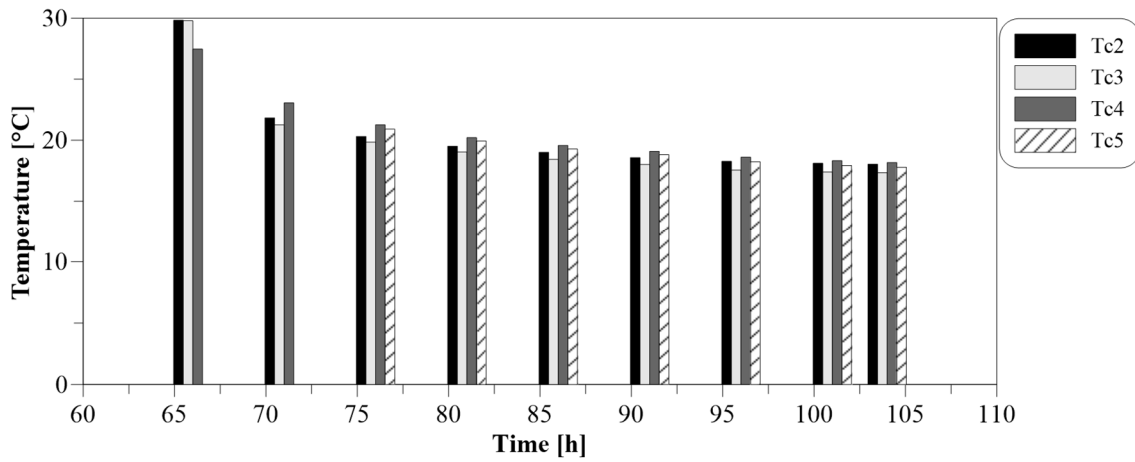


b)

Figure 5-46 - Soil temperature at different distance from the pile for the test SB. a) During the application of thermal loads b) After the application of thermal loads

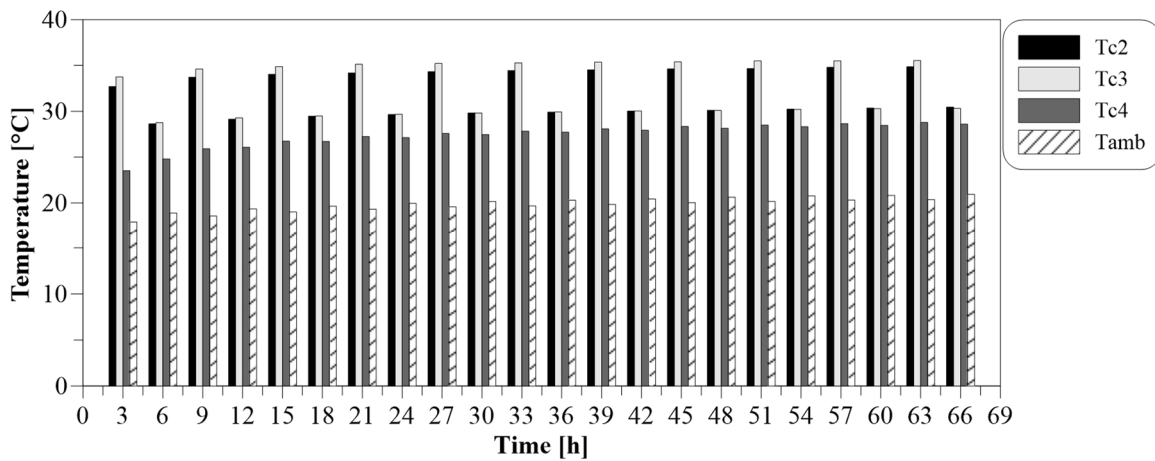


a)

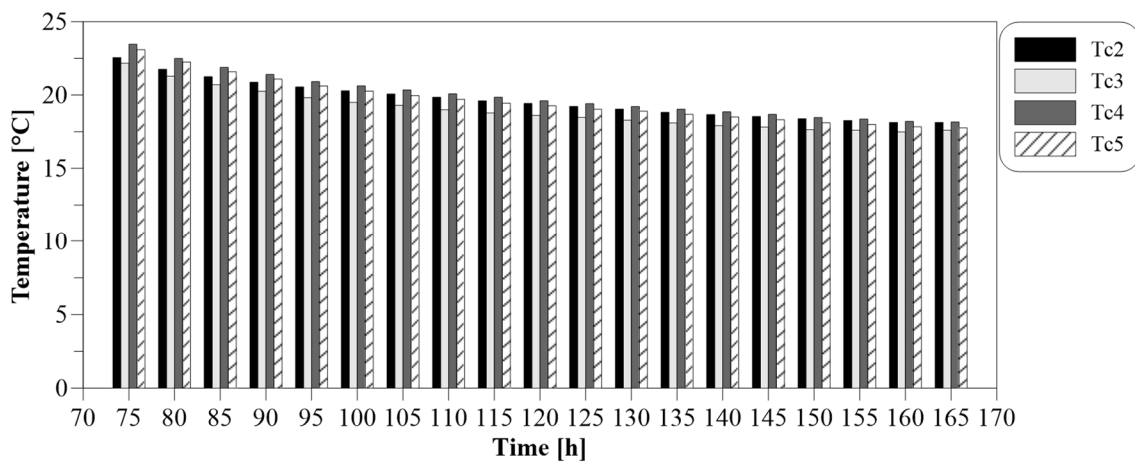


b)

Figure 5-47 - Soil temperature at different distance from the pile for the test SC. a) During the application of thermal loads b) After the application of thermal loads



a)



b)

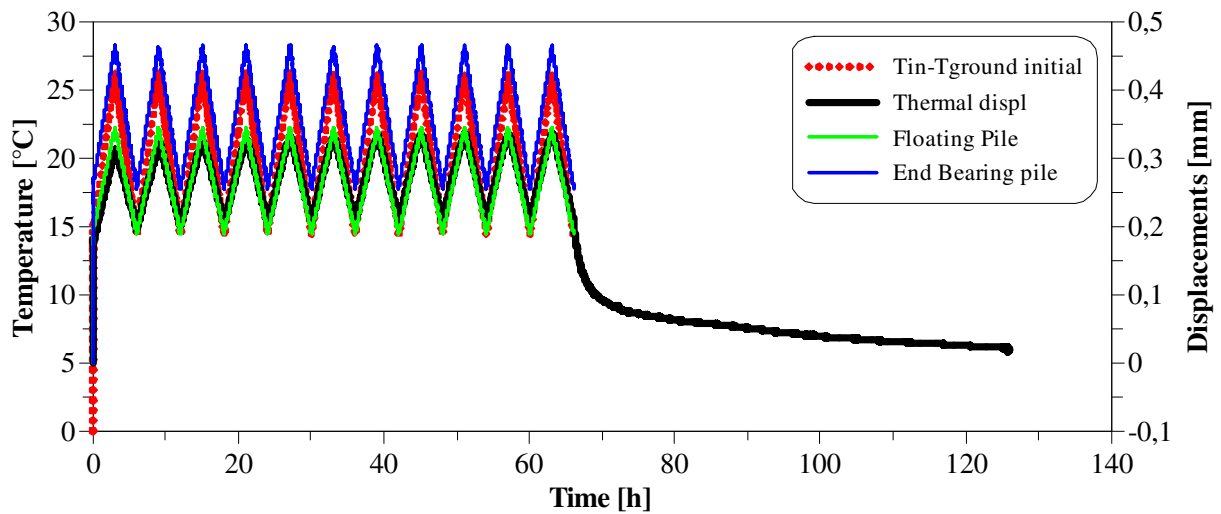
Figure 5-48 - Soil temperature at different distance from the pile for the test SD a) During the application of thermal loads b) After the application of thermal loads

5.3.5.2 Pile head displacements for regular tests

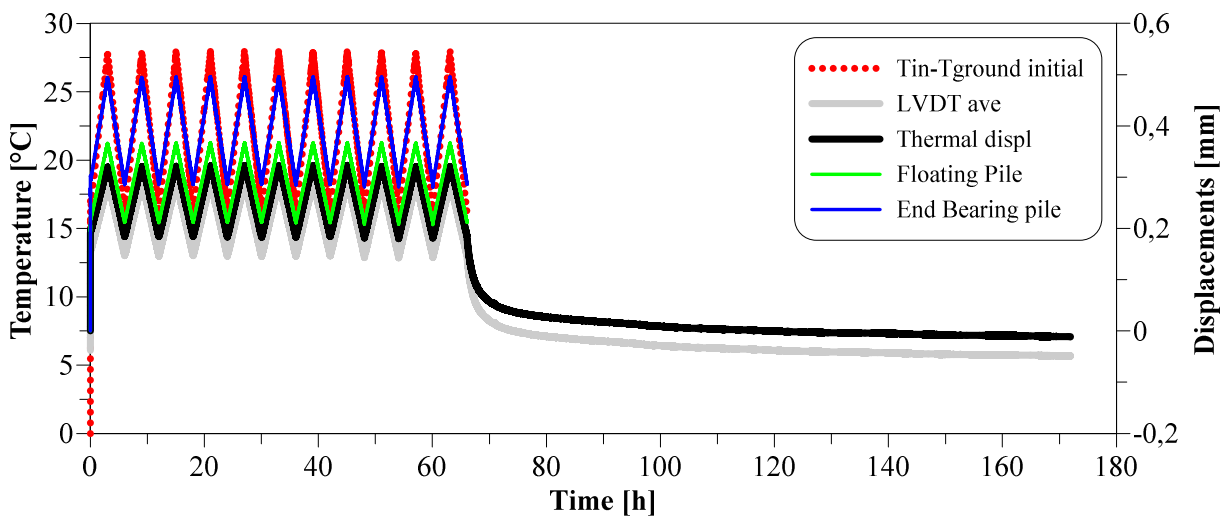
From the Figure 5-49 it is possible to notice that the magnitude of the mechanical load applied on the pile head changes the behaviour of the model. In fact, as shown, for no mechanical load applied the

pile head a behaviour very close to a theoretical floating pile is observed. On the other hand, as the mechanical loads increase, the thermal settlements of the pile, i.e. the measured displacements by LVDT reduced by the initial settlements due to the application of the mechanical load, move away from the theoretical behaviour of floating pile cycle after cycle.

It is possible to observe also a non-constant value of the pile head displacements. In fact, while for the test where the pile is subjected to a thermal load only the displacements trend seemed to have an increasing trend with the passing of cycles, on the other hand, the application of a mechanical load seemed to produce irreversible settlements cycle by cycle.



a)



b)

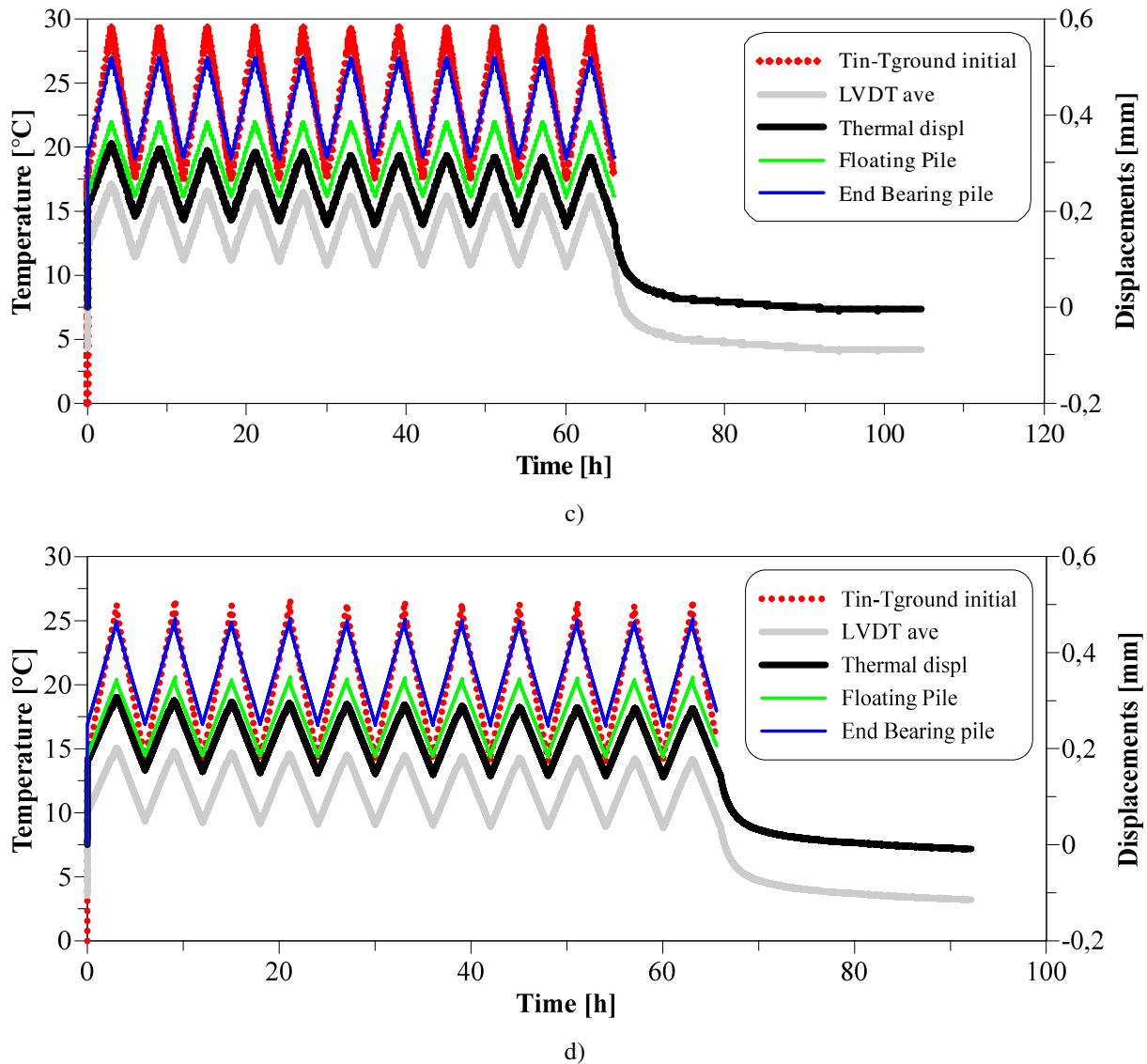


Figure 5-49 -Displacements and temperature trends versus the time for the small-scale pile subjected to a regular cyclic thermal load. Mechanical load on pile head (percentage respect the service load) a) SA b) SB c) SC d) SD

In Figure 5-50 the pile head displacement versus the temperature for the regular thermomechanical tests are reported to better investigate this phenomenon. It is possible to observe that as the mechanical load increases, the behaviour of the pile tends to deviate from the floating pile trend. For the SA test can be observe a coincidence with the straight line representing the floating pile also in terms of slope. As the number of cycles increase the displacements of the head continue to increase. On the other hand, when a mechanical load is applied, the pile behaviour changed in function of mechanical load magnitude. For SB test, in fact, the pile is always under the floating pile theoretical behaviour and the 50% of service load seemed to create a sort of equilibrium between pile head heaves and settlements cycle by cycle. It is showed in Figure 5-50 b where this behaviour lead to a series of cycles that almost coincide with each other as the temperature varies.

When the mechanical load increase to 100% and 150% of the service load, i.e. considering SC and SD tests, a very different pile behaviour is observed. In contrast to the two previous cases, an increase

in pile settlements is noted as the number of cycles increased. Anyway, it can be also observed that for SC test, in the last cycles the displacements seem to have stabilised at a very similar value between cycles. On the other hand, for the SD test, it is noticed that the value of the eleventh cycle displacements are quite far from those of the tenth cycle. Probably much more cycles needed for this mechanical load level to stabilize the displacements.

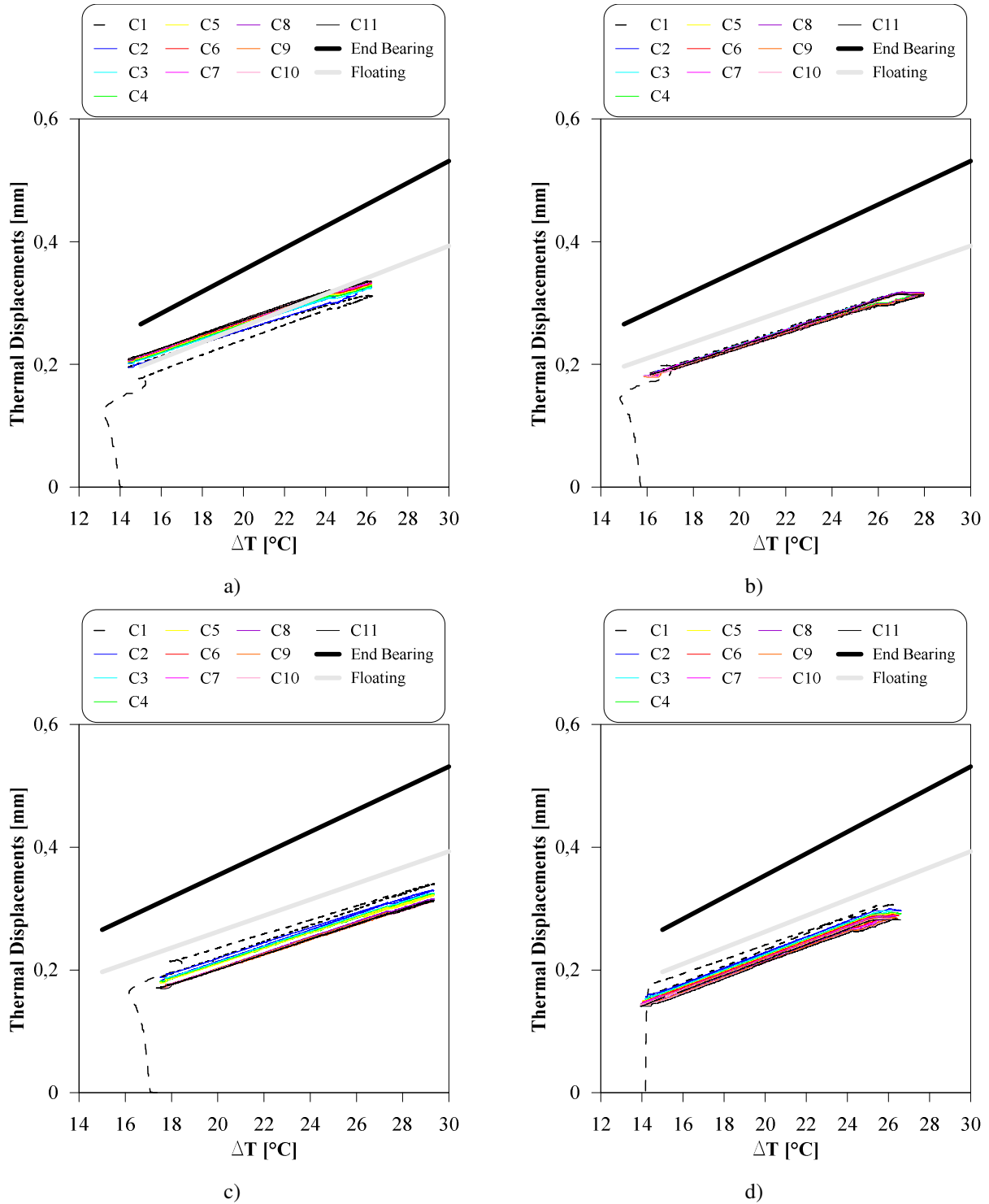


Figure 5-50 – Pile head displacements versus the difference of temperature for the 11 cycles of the regular test. Mechanical load on pile head (percentage respect to service load) a) no mechanical load (0%) b) 48,4 N (50%) c) 96,7 N (100%Qs) d) 145 N (150%Qs)

The thermal displacement evolution of the pile head with the number of the cycles considering the different mechanical load level of each test is investigated.

In Figure 5-51 the displacements increment trend respect the first cycle for all the test is reported.

It is observed that the presence of a mechanical load produces different effects on the displacement's increments.

In Figure 5-49 and Figure 5-50 the downward pile head trend coupled with a mechanical load has been already showed.

Anyway, by Figure 5-51 it is possible to mathematically investigate the phenomenon. In fact, for every mechanical load stage it is possible to describe the displacement increments as a mathematical law function of the mechanical level applied on the pile head.

It is observed that at the end of the heating phase the trend could be described as:

$$\delta_{(n)} = \left(\frac{0,5}{n}\right)^\alpha - 1 [mm]$$

Equation 5-27

On the other hand, at the end of the relative cooling phase the trend can be described as:

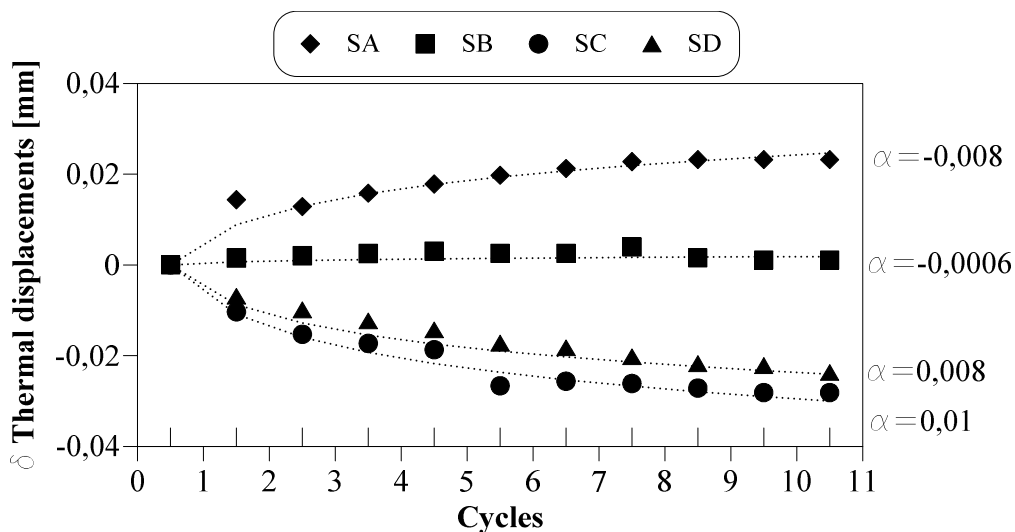
$$\delta_{(n)} = \left(\frac{1}{n}\right)^\alpha - 1 [mm]$$

Equation 5-28

the meaning of relative was already explain in previous sections.

Where n represents the number of the cycle at which investigate the displacement increment and α is a coefficient that change for the mechanical load level and in function of the heating or cooling phase of the pile.

The α coefficients are summarized in Table 5-4



a)

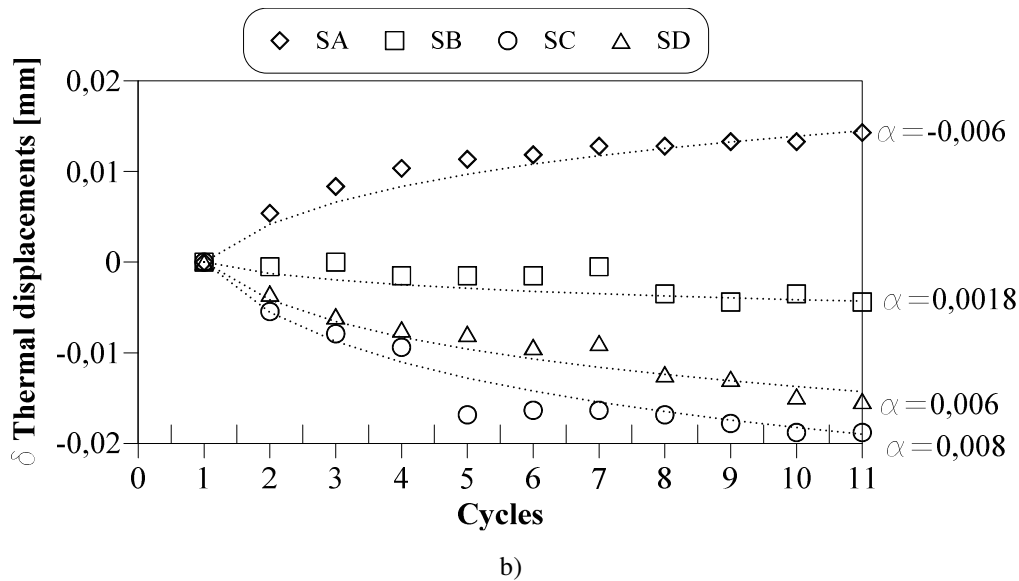


Figure 5-51 – Head pile displacements trend after the first cycle a) at the end of the heating phase; b) at the end of the cooling phase

Table 5-4 – α coefficient values. Q_s is the service load applied on the pile head

Mechanical stage	Heating phase	Cooling phase
0% of Q_s	-0,008	-0,006
50% of Q_s	-0,0006	0,0018
100% of Q_s	0,01	0,008
150% of Q_s	0,008	0,006

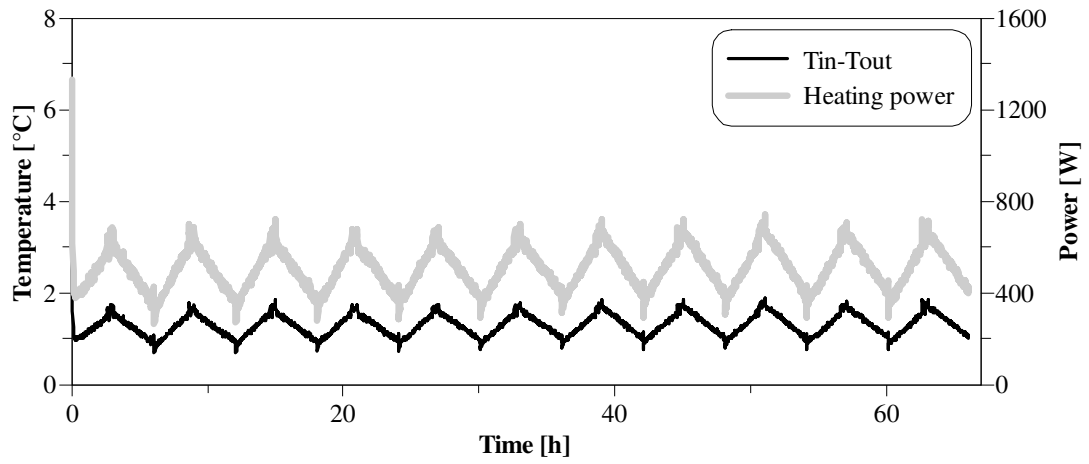
5.3.5.3 Heat power exchanged for regular tests

In Figure 5-52 the trend of the heating power exchanged between the pile and the soil and the difference in temperature between the inlet and outlet fluid are plotted.

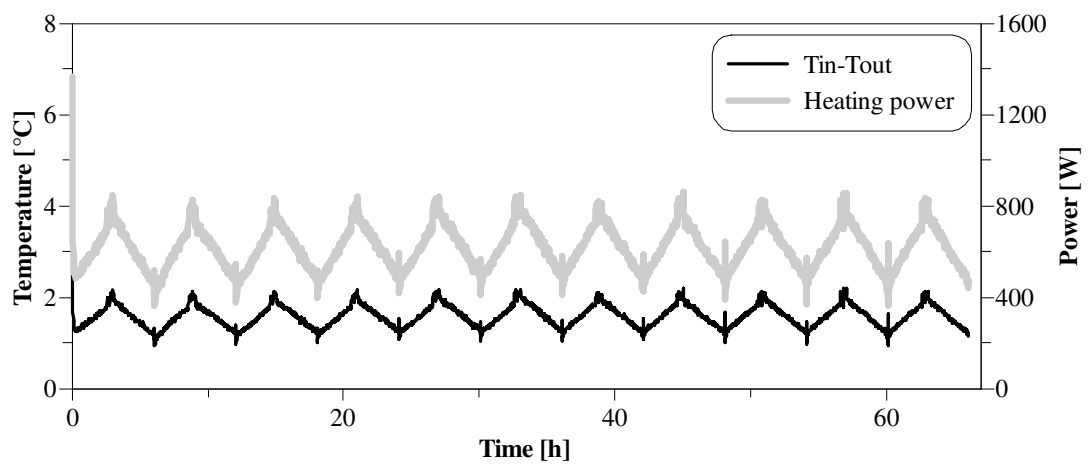
Because the applied thermal loads were the same for all the regular tests, the behaviour is approximately the same for all the considered tests. The only differences that occurred depend on the environmental condition of the room in which the tests were carried out.

Heat power trend is linked to the inlet-outlet temperature difference. It is observed an approximately regular trend due to the thermal load application mode. In fact, a regular and “symmetrical” division between the maximum and minimum supplied temperature over the time, seems to not produce strong thermal imbalances in the surrounding soil. In this way, the difference of temperature between the inlet and the outlet fluid seems to not decrease over the time cycle by cycle.

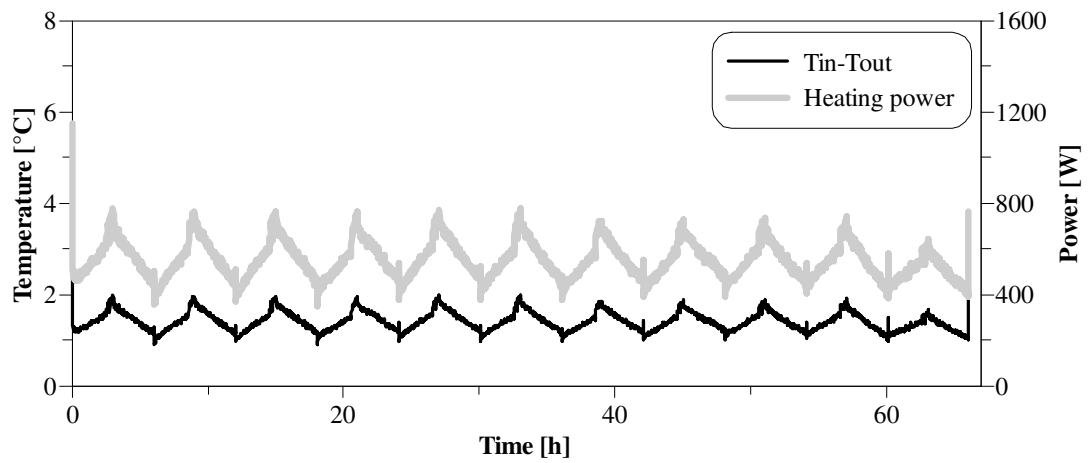
Anyway, for all the tests, the heat power followed the applied thermal loads. The initial value of heat power depended on the initial difference of temperature between soil and inlet fluid and it is noticed also that the ambient temperature could affected the measures.



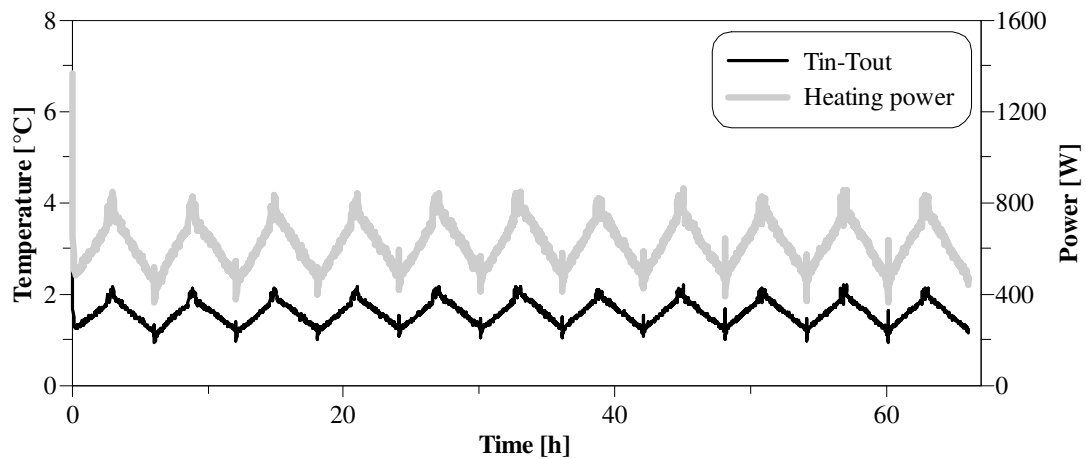
a)



b)



c)



d)

Figure 5-52 – Inlet and outlet heat carried fluid temperature difference and heat power exchanged between pile and soil trends versus the time for the small-scale pile subjected to a regular cyclic thermal load. Mechanical load on pile head (percentage respect the service load) a) SA b) SB c) SC d) SD

5.3.5.4 Axial forces for regular tests

In Figure 5-53 and Figure 5-54 the thermal and thermomechanical axial forces trend are reported for all the test.

The convention used for the axial force is negative sign for compression.

During the tests, the axial forces values tend to change. For this reason, in the graphs an upper and a lower bound and the relative area of axial force reached during the test are indicated.

The position of the maximum axial force was associate with the position of the null point.

By the comparison of the axial force thermal effects trend of all the tests, it can be noted that the maximum axial force values are measured generally at a depth from the ground level of -105 mm. During the cycles it tends to change in value than the others depth level, but generally it remained the higher value along the pile.

In some cases, in fact, the axial force value at -105 mm is very similar to the value record at -200 mm such as the SD case where, it seems that a change of the null point is occurring.

At the end of every cycle, the trend of the axial forces produced by the only thermal effects was very different between the considered tests.

Comparing the axial forces of the tests also considering the presence of mechanical load, it is observed a shift from purely mechanical axial forces with a significant increase in compressive stresses. This phenomenon is observed especially when the inlet temperature of the heat carrier fluid is the higher. It should be noted that the trend of mechanical axial force is not constant with the depth. In fact, it tends to decrease with the depth. It brought in thermomechanical trend to final values of axial forces in the upper part of the pile larger than the only thermal trend.

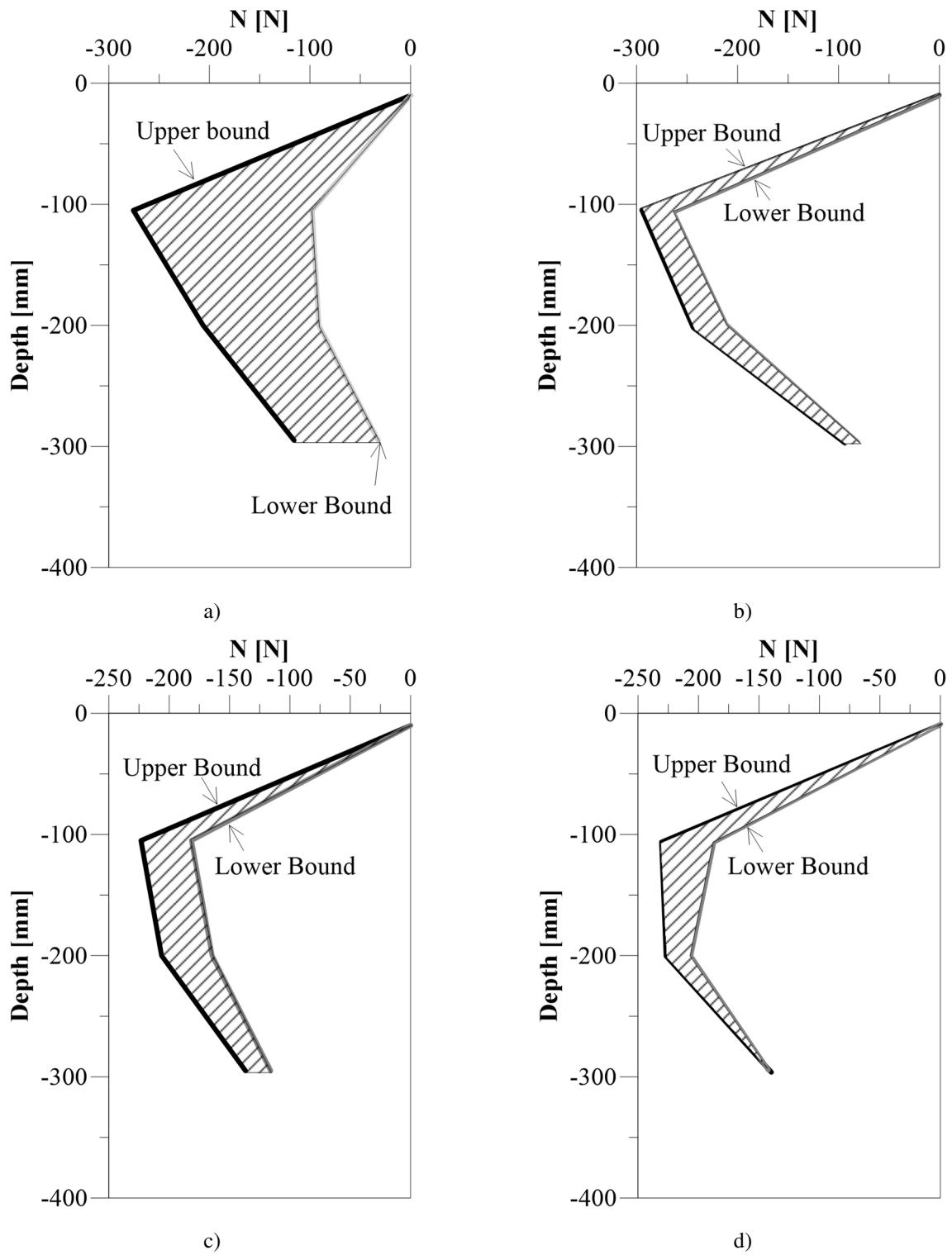


Figure 5-53 – Thermal axial forces for the test a) SA; b) SB; c) SC; d) SD

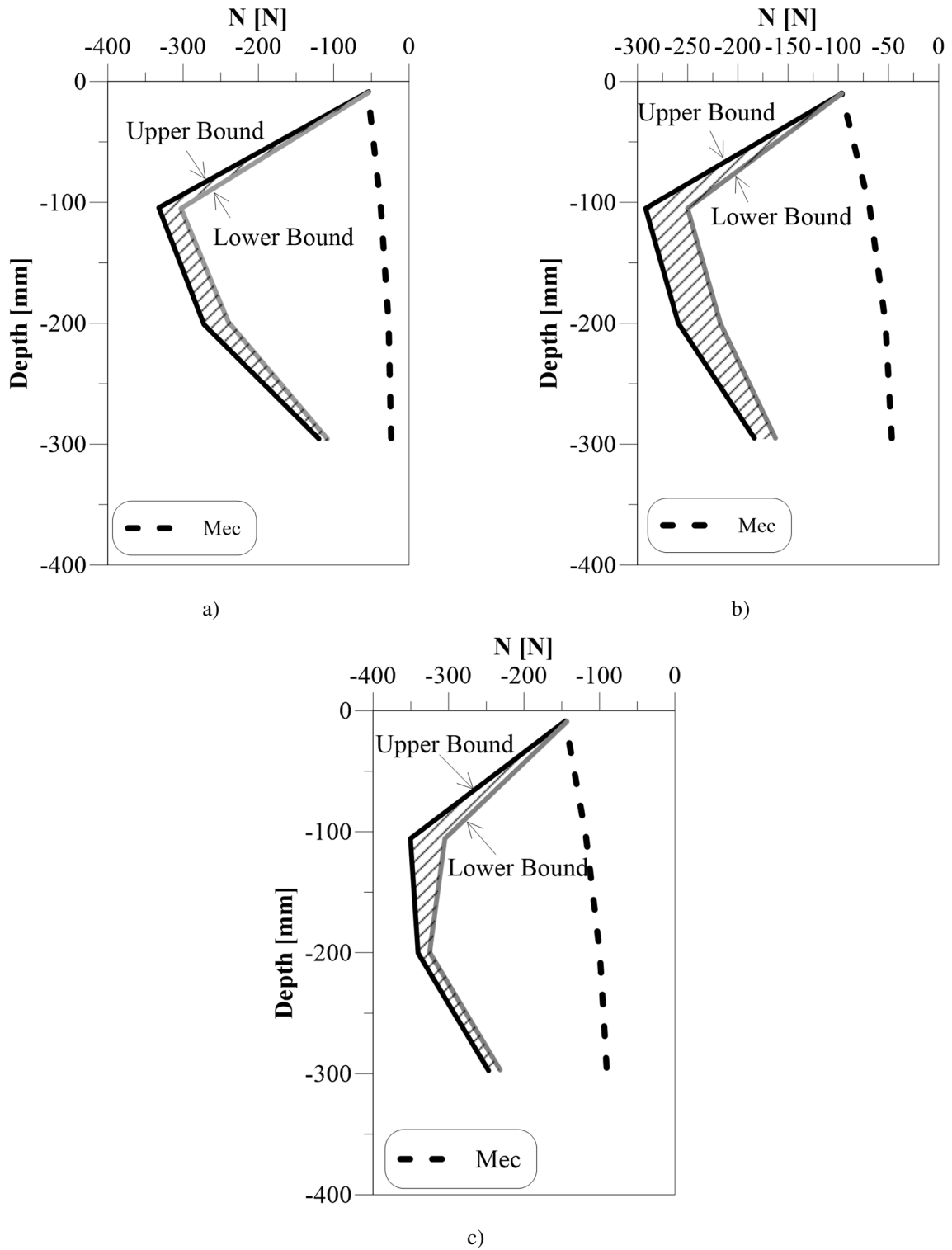


Figure 5-54 - Thermomechanical axial forces for the test a) SB; b) SC; c) SD

5.4 General discussion

Different aspects are analysed for the thermal and thermomechanical small-scale tests described in this chapter such as the temperature distribution along the pile and the soil, the stress distribution along the pile, the exchanged heat power between pile and soil and the pile displacements with the number of the cycle.

As regarding the first aspect, from the tests it is noted that both in heating and cooling mode, the temperature distribution along the pile is not uniform. In fact, the upper part tends to have a temperature closer to the inlet temperature that change with the pile depth. In the heating mode, the temperature tends to decrease with depth. Vice versa, the opposite happened in cooling mode. It is due to the heat exchange that takes place between pile and surrounding soil.

Moreover, when the thermal loads are applied to the pile, the surface temperature of the pile rises over the time (decrease in the case of cooling thermal loads) with a very high gradient. Maybe it is also due to the material of the small-scale pile and to its thermal conductivity. On the other hand, the temperature measured one diameter from the pile surface have a gentler gradient of temperature when the thermal loads are applied and a time delay in temperature change can be noticed. These are all aspects linked with the soil thermal inertia. This phenomenon, indeed, can be observed also at the end of the tests. In fact, at the end of the application of the thermal loads, it can be noted an inverse trend. The pile surface temperatures tend to decrease quickly (increase in the cooling mode) and, on the other hand, at one diameter from the pile the temperature change starts later and with a gentler gradient. The time needed to return to initial temperature condition depend on the magnitude and time application of the thermal loads.

As regard the heat power exchanged between the pile and surrounding soil, them are not comparable with similar piles in literature. Anyway, the heat power values are strongly affected by the inlet carrier fluid flow rate, the circulation system of the heat carried fluid, the distance between circulating system and the pile surface and the thickness of the pile surface. As said in chapter 2, these are all factor that could affect the energy pile thermal performances. For this small-scale model an aluminium tube 1,5 mm in thickness with a direct system of water circulation with a flow rate of 5,6 l/min was used. Some values of exchanged heat power for small-scale tests could be found. Yang et al. (2016) coiled a spiral shaped pipe around a PVC cement filled tube with a heat carrier fluid flow rate of 0,67 l/min. Kramer et al. (2015) equipped a concrete pile with an U-tube shaped pipe in which heat carrier fluid circulated with a flow rate that ranged between 0,8 l/min and 4,78 l/min or Elzeiny et al. (2020) equipped a concrete pile with an double U-tube shaped pipe in which heat carrier fluid circulated with a flow rate of 0,8 l/min. Anyway, these tests can be compared with the small-scale model used in this research.

As regarding the stress distribution along the pile, the trend of the axial forces is reported for all the carried-out tests. It is possible to notice that the axial forces provided by thermal loads are larger than the axial forces provided by the mechanical loads. It is evident especially in the thermomechanical cases in which it is possible to observe the difference of magnitude between the two kind of load. In any case, in heating mode a gain of the compressive axial forces is obtained, while in cooling mode

the opposite happened. The cooling thermal loads used during the long-term provided not only a decrease of the compressive axial forces of the mechanical load but provided a tensile state along the pile. The maximum axial forces have been found -105 mm from the ground surface or in the pile middle (-200 mm) depending on the type and magnitude of the thermal and mechanical loads.

Finally, the pile head displacements for cyclic application of thermal loads has been analysed both in the long-term cooling test and in the regular tests.

The pile head displacements for aluminium pile embedded in dry sand was also investigated by other authors in literature (Kalantidou et al. 2012; Yavari et al. 2014; Nguyen, Tang, and Pereira 2017). The small-scale model used in this research seems to follow the literature results. In fact, cyclical thermal loads provide irreversible pile displacements cycle by cycle for the aluminium pile embedded in pyroclastic soil. However, the magnitude and the verse of the displacements depends on the magnitude of the mechanical load applied on the pile head. It was noted that when no mechanical loads are applied on the pile head, an increase of pile heave displacements are measured. On the other hand, when the magnitude of the mechanical load is not greater than the 50% of the service loads, a not definite trend was observed for the pile head displacements. It seems to be in a sort of equilibrium between the pile head heave for some cycles and the pile head settlements in other one. When the mechanical load exceeds that values, irreversible settlements are observed for the pile with the increase of the number of the cycles.

In this chapter also a relation was provided to try to predict the relative displacements that occurs after n cycles for piles with different mechanical loads.

5.5 Conclusion

In this chapter a series of small-scale test carried out on an aluminium pile embedded in dry Neapolitan pyroclastic soils and subjected to thermal loads typical of the Neapolitan area are described.

After a detailed description of the materials and methods used for the test, the test program and relative results are presented.

Two type of thermal cyclic loads were applied to the pile. In the first one, a thermal history obtained by an energy dynamic simulation by the software Design Builder was repeated for 9 times both for the heating and for the cooling mode. Heating test was characterized by a recovery time between two consecutive cycles. These kinds of tests were called “long term” test.

In the second type of thermal cycles, instead, the behaviour of the small-scale energy pile was investigated under a continues and regular heating thermal law.

Different energy pile design aspects are discussed in the chapter.

A first analysis regards the temperature distribution in soil and along the pile over the time for the different tests. Some aspects, such as the soil recovery time to return to initial temperature conditions or the difference of temperatures in different point of soil during the tests are discussed. Moreover, one of the most important aspects treated in the chapter regards the pile head displacements. Irreversible pile settlements are noted to increase cycle by cycle and trend of the settlements depends on the mechanical load magnitude. A mathematical relation is found to predict the settlement magnitude after n number of cycles and for different mechanical load magnitudes. This relation is found both for the cooling and heating thermal loads both for the heating and the cooling phase of a thermal cycle.

Finally, the stress distribution in terms of axial forces are discussed for all the test. The results are analysed both the thermal and the thermomechanical effects and lower and upper bound of the axial forces variations are reported.

5.6 References

- Durgunoglu H.T. and Mitchell J.K. (1975). Static penetration resistance of soils, evaluation of theory and implication for practice. In: Proceedings of the in-situ measurement of soil properties, Raleigh, NC, ASCE, New York, NY.
- Elzeiny, Rehab, Muhannad T. Suleiman, Suguang Xiao, Mu’Ath Abu Qamar, and Mohammed Al-Khawaja. 2020. “Laboratory-Scale Pull-out Tests on a Geothermal Energy Pile in Dry Sand Subjected to Heating Cycles.” *Canadian Geotechnical Journal* 57 (11): 1754–66. <https://doi.org/10.1139/cgj-2019-0143>.
- Fioravante, V. 2002. “On the Shaft Friction Modelling of Non-Displacement Piles in Sand.” *Soils and Foundations* 42 (2): 23–33. https://doi.org/10.3208/sandf.42.2_23.
- Kalantidou, A., A. M. Tang, J. M. Pereira, and G. Hassen. 2012. “Preliminary Study on the Mechanical Behaviour of Heat Exchanger Pile in Physical Model.” *Geotechnique* 62 (11): 1047–51. <https://doi.org/10.1680/geot.11.T.013>.
- Kouby, Alain Le, Jean Claude Dupla, Jean Canou, and Roméo Francis. 2013. “Pile Response in Sand: Experimental Development and Study.” *International Journal of Physical Modelling in Geotechnics* 13 (4): 122–37. <https://doi.org/10.1680/ijpmsg.13.00005>.
- Kramer, Cory A., Omid Ghasemi-Fare, and Prasenjit Basu. 2015. “Laboratory Thermal Performance Tests on a Model Heat Exchanger Pile in Sand.” *Geotechnical and Geological Engineering* 33 (2): 253–71. <https://doi.org/10.1007/s10706-014-9786-z>.
- Nguyen, Van Tri, Anh Minh Tang, and Jean Michel Pereira. 2017. “Long-Term Thermo-Mechanical Behavior of Energy Pile in Dry Sand.” *Acta Geotechnica* 12 (4): 729–37. <https://doi.org/10.1007/s11440-017-0539-z>.
- Nicotera, M.V. 2002. Resistenza a taglio delle pozzolane del napoletano: analisi statistica di dati sperimentali. Università degli Studi di Napoli Federico II, febbraio 2002.
- Miura N., and Yamanouchi T. 1975. Effect of water on the behavior of quartz-rich sand under high stresses. *Soils and Foundations, JSSMFE*, 15 (4) (1975), pp. 23-34

- Raucci, M. 2017. “Comportamento Di Platee Su Pali in Terreni Sabbiosi.”
- Robertson P.K. and Campanella R.G.,(1983). SPT-CPT Correlations. *Journal of Geotechnical Engineering* Volume 109 Issue 11.
- Weinstein, G.M. 2008. Long-term behaviour of micropiles subject to cyclic axial loading.Ph.D. thesis, Polytechnic University, Brooklyn, Newyork. 373 pages.
- Yang, Weibo, Pengfei Lu, and Yongping Chen. 2016. “Laboratory Investigations of the Thermal Performance of an Energy Pile with Spiral Coil Ground Heat Exchanger.” *Energy and Buildings* 128: 491–502. <https://doi.org/10.1016/j.enbuild.2016.07.012>.
- Yavari, Neda, Anh Minh Tang, Jean Michel Pereira, and Ghazi Hassen. 2014. “Experimental Study on the Mechanical Behaviour of a Heat Exchanger Pile Using Physical Modelling.” *Acta Geotechnica* 9 (3): 385–98. <https://doi.org/10.1007/s11440-014-0310-7>.

Chapter 6

6 Field tests: effects of thermal loads on a concrete energy pile

6.1 Introduction

In this chapter the results obtained from field tests carried out on a full-scale concrete energy pile embedded in pyroclastic soils are discussed.

The site where the tests were carried out is in an under-construction area in the municipality of Crispano, in the province of Naples, where an industrial shed was to be built.

Three thermal tests were carried out on an energy pile 0,60 m in diameter and 12 m in length equipped with a spiral shaped thermal pipe. The aim was to analyse the behaviour of the pile foundation subjected to different thermal and thermomechanical loads in terms of strains, displacements, and stresses. For a number of reasons partially connected to the restrictions of the Covid period only thermal tests were carried out.

In the first part of the chapter, the site stratigraphy, the energy pile and its construction phases, the sensors used for the monitoring during the tests are described.

In a second part, a detailed description of the three test and the data results are analysed.

In the third and last part of the chapter the continuous monitoring of pile and surrounding soil temperature over the time is discussed. Indeed, for about seven months, the data logger recorded the hourly temperatures of the pile and the soil sensors. These temperatures were also compared with the air temperature recorded nearby. The aim was to analyse the trend and evolution of the temperatures both over the time and with the depth, inside a pyroclastic soil deposit, one of the most widespread soil types in the Neapolitan area.

Such data are important for fixing boundary conditions for the design of energy piles in our climatic zone. Efficiency of the GSHP system and soil-pile mechanical interaction are influenced by such temperature initial profile.

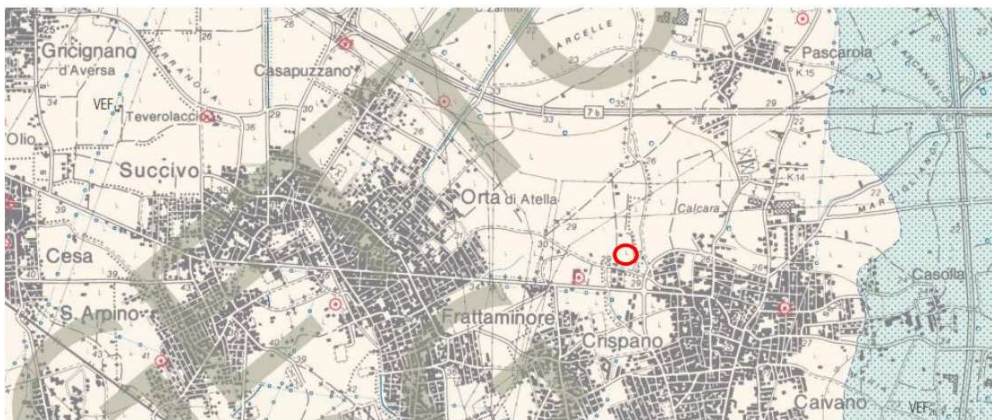
6.2 The area of the field test

The field tests on the energy pile were carried out in the municipality of Crispano in the province of Naples.

The geographical location of the area is shown below along with the information from the geological map of Italy on sheets 446-447 (Figure 6-1).



a)



Pyroclastic deposits
 svi_p pyroclastic stratified with millimetric to centimetric pumiceous and stony elements, more abundant at the base, varying in colour from light grey to light yellow, locally with a compact basal level of the volcanic breccia type, with ages ranging from 39 to 15 ky

b)

Figure 6-1 – a) geographical overview of the extraction area b) geological map

To establish the stratigraphy of the site, core drilling was carried out with soil retrieval (Figure 6-2). In Figure 6-3, grain size distribution for different depths as obtained by laboratory tests are reported. The borehole investigated down to a depth of about 15 m (approximately 3 m below the tip of the pile). The water table was not detected.

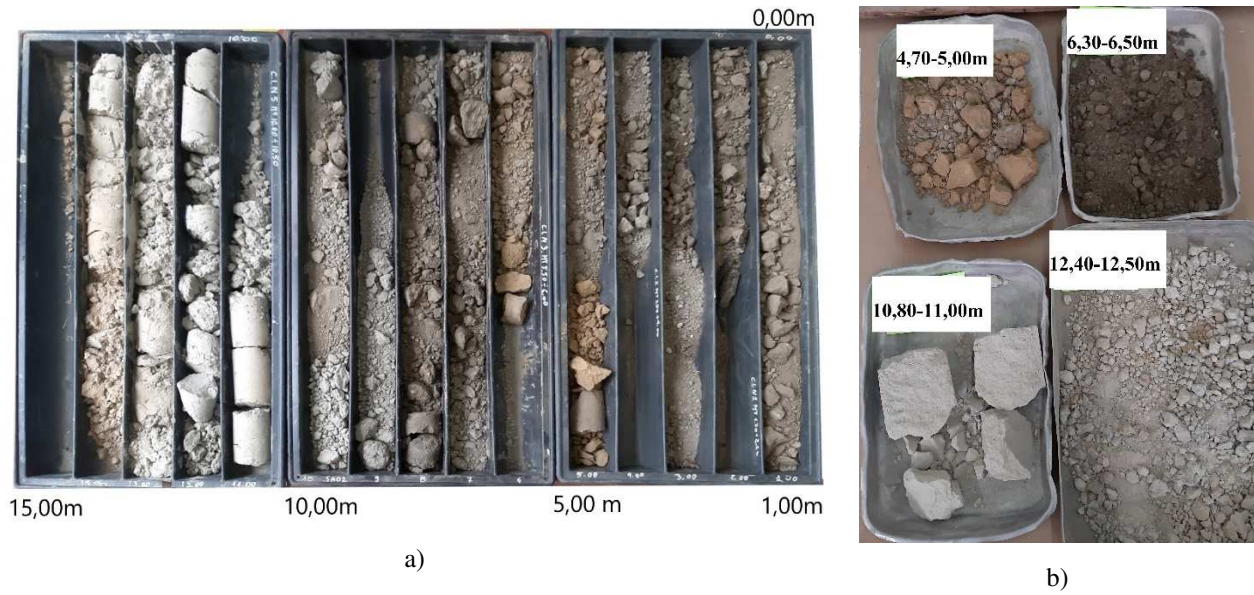


Figure 6-2 – a) material from on-site coring; b) sampling of material at different depths for particle size analysis

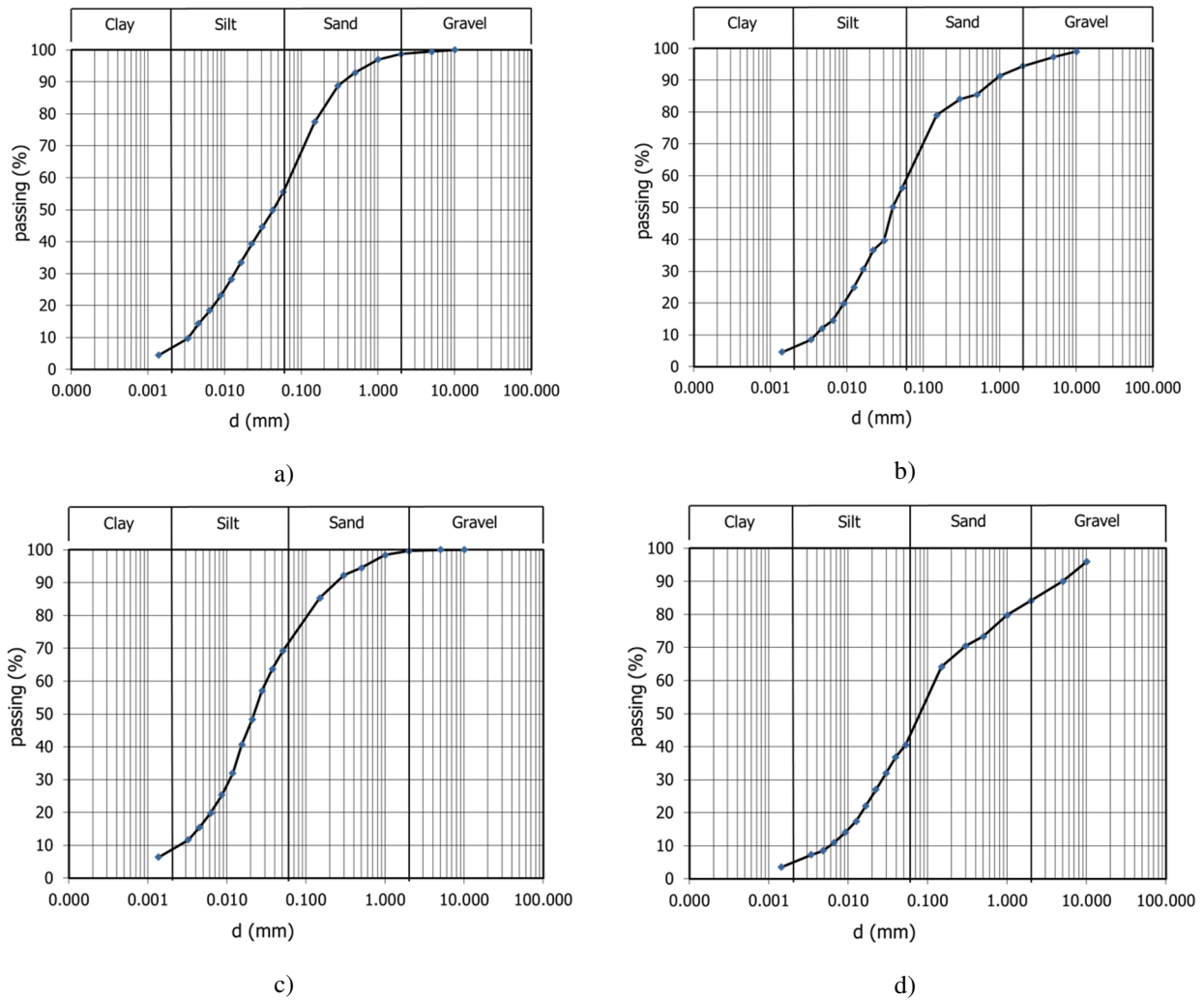


Figure 6-3 - Grain size distribution for different depths: a) 4,70-5,00 m; b) 6,30-6,50 m c)10,80-11,00 m d) 12,40-12,50 m

On the basis of the visual inspection of the samples the following layers were detected:

- From 0 m to 1,60 m: Top soil;

- From 1,6 m to 5,80 m: very loose yellow-ochre ashes. By the grain size distribution, it could be identified as a silt with sand slightly clayey.
- From 5,80 m to 10,80 m: weakly cemented grey pyroclastic ashes. By the grain size distribution, it could be identified as a silt with slightly gravelly sand.
- From 10,80 m to 12,20 m: pumices in a white to yellow ochre sandy-loam matrix interbedded by homogeneous ashes. By the grain size distribution, it could be identified as a silt with slightly clayey sand.
- From 12,20 m to 14,40 m: very fine yellowish silt. By the grain size distribution, it could be identified as a slightly gravelly sand with silt.

To establish the soil mechanical properties, a Cone Penetration Test (CPT) was carried out. The results of the CPT, i.e. the tip resistance, the soil strata subdivision and the mechanical properties for every stratum were reported in Figure 6-4.

The soil specific weights of strata were determined by laboratory measurements on undisturbed samples taken during the site coring. On the other hand, the elastic modulus and the friction angle were determined by widely used relationships.

Regarding the Young modulus it was determined by the Equation 6-1:

$$E = kq_c$$

Equation 6-1

Where q_c is the CPT tip resistance and k is a parameter function of the soil type. Meyerof and Fellenius (1985) suggest the values reported in Table 6-1.

Table 6-1 – k values

Soil	silty sand	medium-dense sand	dense sand	sand and gravel
k	1,5	2	3	5

On the other hand, the friction angle was determined according to the Durgunouglu-Mitchell equation (Equation 6-2):

$$\varphi = 14,4 + 4,8 \ln q_c - 4,5 \ln \sigma$$

Equation 6-2

Where q_c is the CPT tip resistance and σ is the effective lithostatic stress.

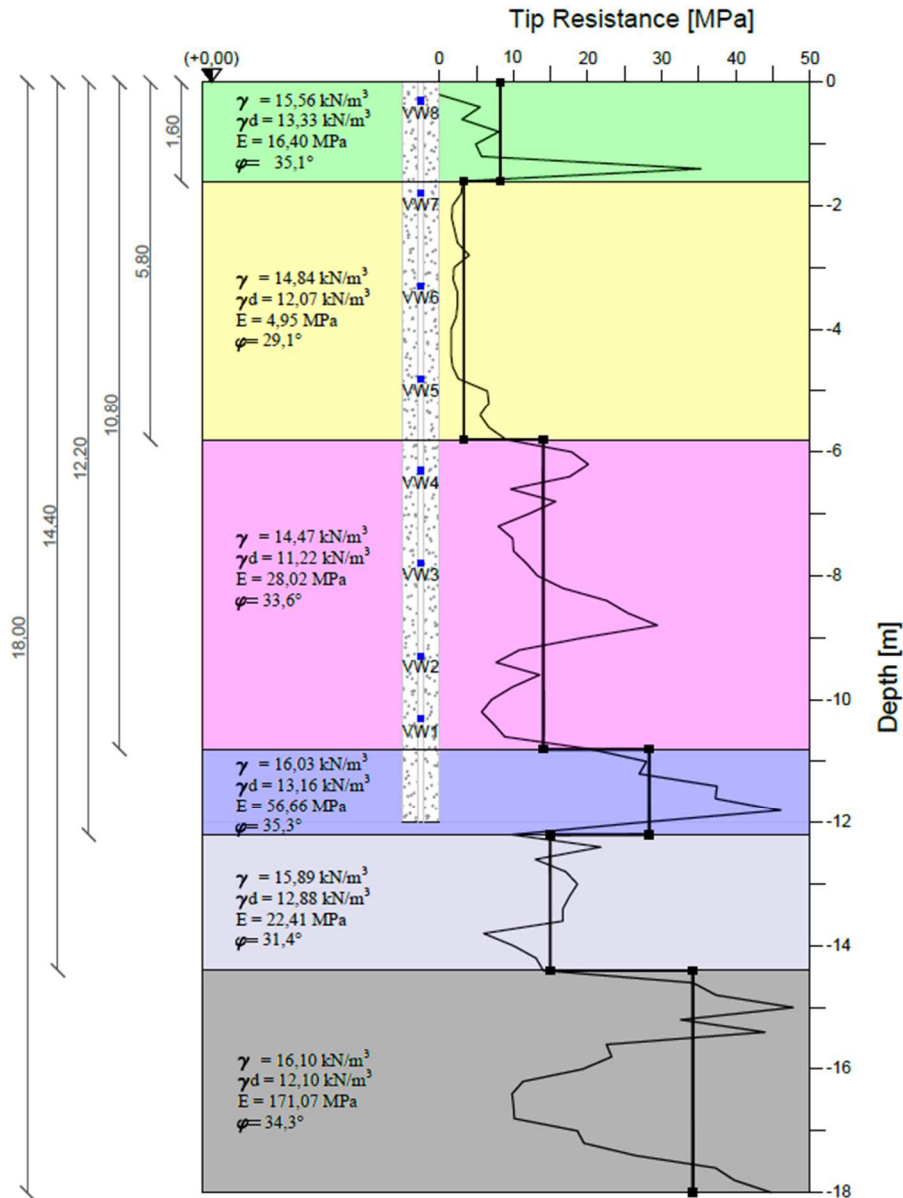


Figure 6-4 – Soil layering and average mechanical properties along the pile shaft (with the location of the vib. wires)

6.2.1 Test Pile

The field tests were carried out on an in-situ reinforced concrete pile with a diameter of 0,60 m and a length of 12,0 m. The pile was reinforced with a steel cage consisting of 8 longitudinal bars Φ 14 and spiral ties Φ 8 with a pitch of 0,20 m. The water circulation system was fixed to the reinforcement, consisting of a single HDPE pipe with a diameter of 0,02 m and a total length of about 85 m. The pipe was inserted into the steel cage in a spiral configuration with a pitch of approximately 0,20 m between the turns. Once got to the pile tip the pipe was brought upwards with a linear stretch. The water circulation system was designed to let the water enter inside the spiral part of the pipe at controlled temperature (T_{in}) and to let the water rise through the linear pipe stretch (Figure 6-5). With this layout a total pipe length 6,5 times the effective total length (12 m) of the pile was installed. This solution increased the area of the heat exchangers inside the pile which is a factor to play with in

order to maximise heat exchange between the pile and the ground. Moreover, following the indications provided by the literature and discussed in the Chapter 2, the pitch of the spiral was selected to get as low as possible the thermal interference between the pipes.

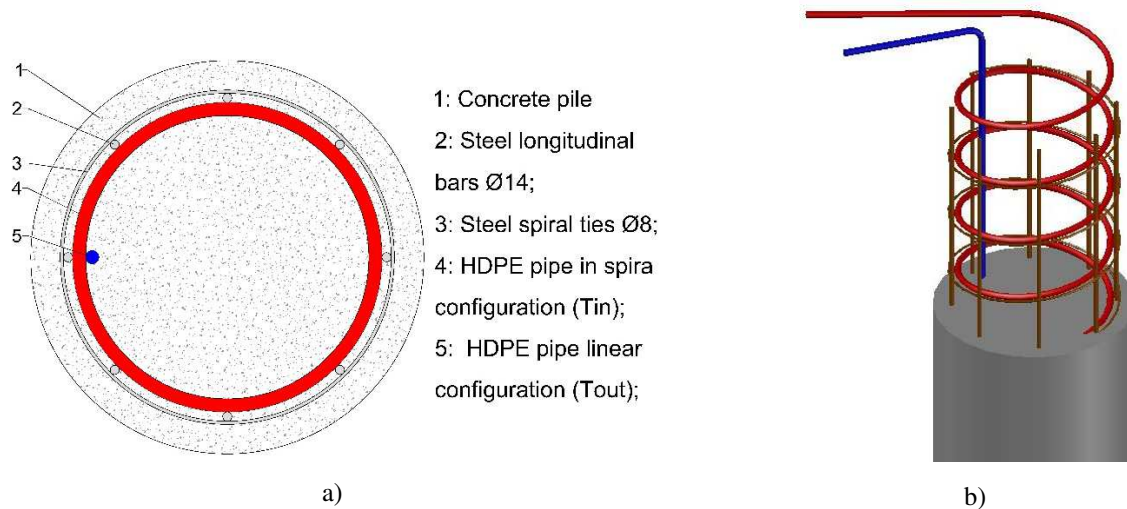


Figure 6-5 – Design of concrete energy pile: a) scheme of the components; b) 3D design

The pile was installed in two distinct phases. In the first one, which took place in the workshop, the reinforcement cage was assembled and then the HDPE pipes were inserted. These were carefully shaped to obtain the spiral form, taking great care to avoid any bottlenecks in the pipe during installation that might have formed in the pipe due to excessively tight bending radii. Once the pipe was prepared, it was fixed to the reinforcement cage by plastic cable ties. In addition, a 0,08 m diameter PVC pipe was inserted into the centre of the reinforcement cage to accommodate the vibrating wire gages during the post-casting phase (Figure 6-6). Anyway, the instrumentation and sensors with which the pile was equipped will be discussed in more detail in the following paragraphs.



Figure 6-6 – PVC pipe inserted inside the reinforcement cage for positioning the vibrating wires

On the reinforcement cage also the thermometric strings consisting of 4 NTC thermocouples were fixed.

The second phase involved the construction of the pile in situ. It was a bored pile with the removal of a cylindrical volume of soil from the ground by a bucket. Because the bored pile was installed in

dry silty sand soil (over the ground water table) there was no need of excavation supports as the bore walls were self-standing. Once the excavation was carried out, the reinforcement cage, equipped with pipes, was lowered into the hole and then the concrete was poured from above (Figure 6-7). Before and after the pile construction operations, the correct functioning of the pipes was always verified by means of water circulation tests.



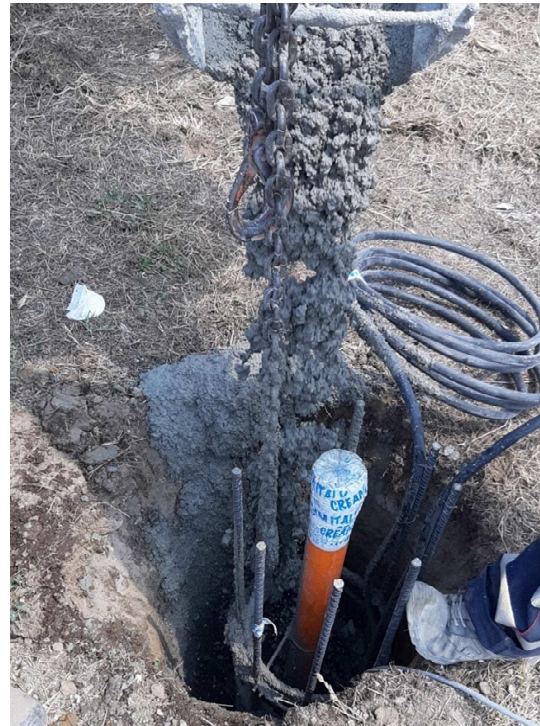
a)



b)



c)



d)

Figure 6-7 - Machines used and construction phases of the energy pile: a) bucket; b) excavation of the hole with soil removal; c) lowering of the reinforcement cage previously prepared in the workshop; d) concrete casting

6.2.2 The mechanical resistance of the pile

To determine the stresses induced by the thermal loads inside the pile, in addition to the geometric characteristics of the pile, already discussed in the previous paragraph, it was essential to know the mechanical properties of the materials constituting the pile. Since the vibrating wires provide frequency change which are related to strains in the material where they are embedded in, to know the stress acting in the pile, it was essential to know its elastic modulus E_p .

The elastic modulus of a structural element in reinforced concrete, and therefore of the pile, was obtained by means of the following standard equation:

$$E_p = \frac{A_c E_c + A_s E_s}{A}$$

Equation 6-3

Where:

- E_p is the elastic modulus of the pile;
- E_c is the elastic modulus of the concrete;
- A is the cross-sectional area of the pile;
- A_s is the area of the reinforcement of the pile;
- A_c is the concrete area of the pile section equal to difference between A and A_s ;

In this case, the elastic modulus of the steel was certified and equal to 210000 MPa. The strength and the elastic modulus of the concrete were determined by means of uniaxial compression tests on three cubes taken during the casting of the pile and cured for 28 days (Figure 6-8).



a)



b)



Figure 6-8 – a) sampling of concrete during casting; b) collection of three specimens to be matured for 28 days; c) crushing test; d) specimen after crushing test

From the compression tests, the cubic strength of each specimen was determined. The average of the strength measured on three specimens was 35,10 MPa.

The average elastic modulus of the material could be determined using the following formula in accordance with the Italian technical standards for construction (Ministerial Decree 17/01/2018 Chapters 4 and 11):

$$E_{cm} = 22000 \cdot [f_{cm}/10]^{0,3}$$

Equation 6-4

where:

$$f_{cm} = 0,83 \cdot R_{cm}$$

Equation 6-5

Calculations show an average concrete elastic Young's modulus of **30319 MPa**.

Using equation (3) the elastic equivalent Young's modulus of the piles was estimated as **31100 MPa**.

6.2.3 Sensors and measuring instruments used for test

To determine the stresses induced by the thermal loads during the tests and the temperature variations inside the pile and in the soil, deformation and temperature sensors were set up. Two thermometric strings consisting of 4 NTC (negative temperature coefficient) thermistors spaced 3 m apart were used, one located close to the reinforcement cage of the pile and another located in a specially created borehole at one 0,90 m from pile to monitor the temperatures in the soil. In addition, 8 vibrating wires positioned in the centre of the pile, placed in a phase following the casting of the pile inside the PVC pipe specifically positioned and left closed during the casting phase (Figure 6-9). The sensors and the

relative dimensions have been differentiated with different acronyms and colours for a clearer reading of the diagram:

- the vibrating wires inserted in the centre of the pile were named **VW** and indicated in blue;
- the NTC thermistors inside the pile were named **TP** and indicated in red;
- the NTC thermistors inside the soil and were named **TS** and indicated in green;
- the geometric dimensions of the pile and distances were indicated in black.

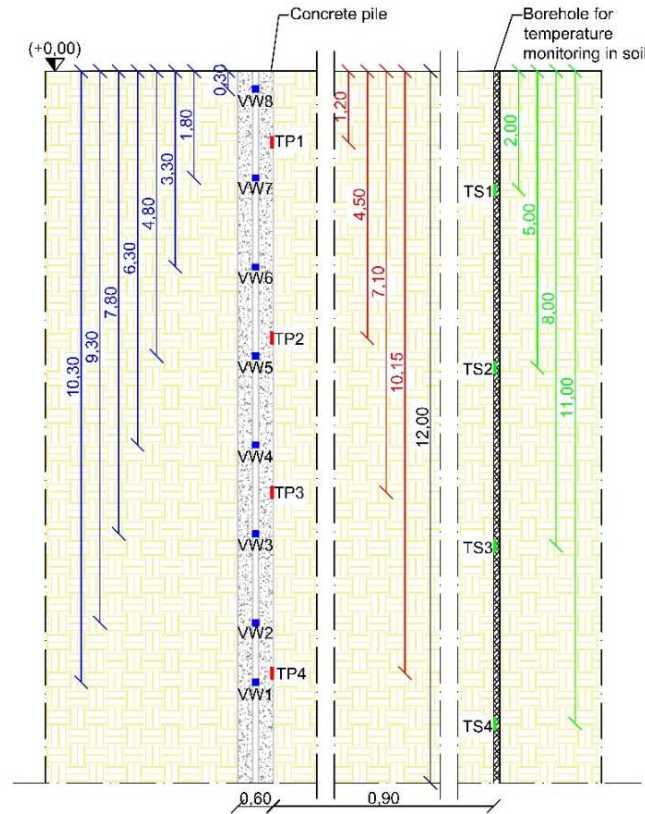


Figure 6-9 - Sensor location

The vertical displacements at the pile head were measured using an optical tacheometer. The measurements were carried out by comparing the displacements of a benchmark located on the pile head with a with another benchmark sufficiently far away from the test pile.

Figure 6-10 shows the orthophoto of the site with the location of the equipment used for the test.

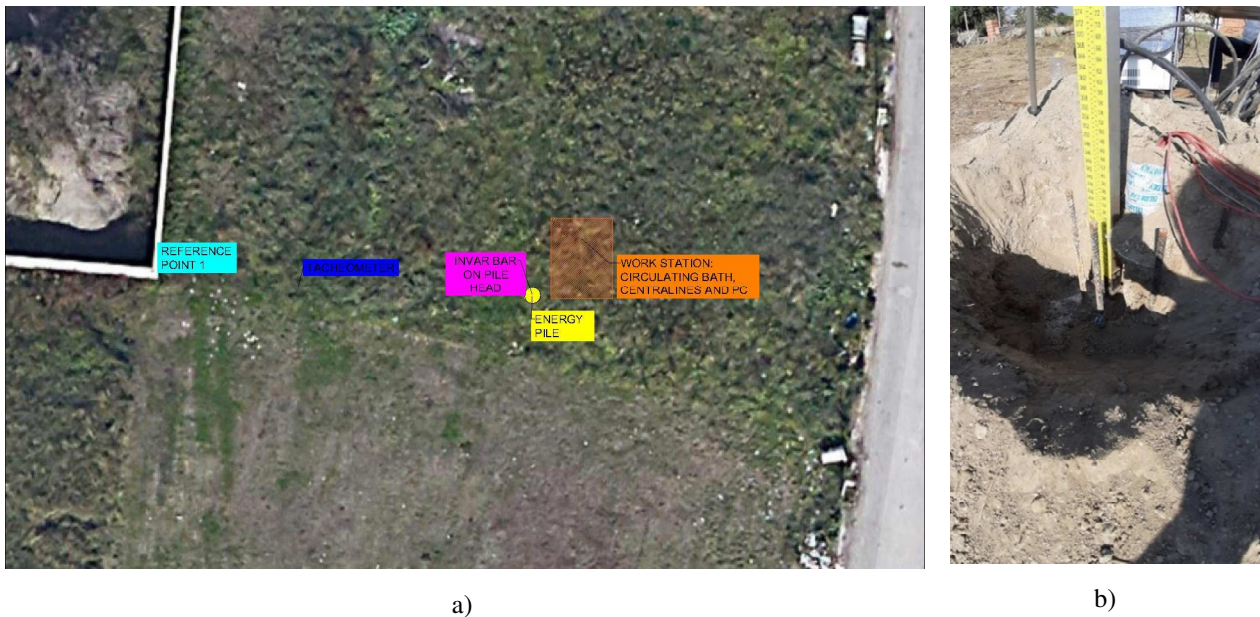


Figure 6-10 – a) overview and location of instrumentation used during testing; b) level staff located on the pile head

6.2.3.1 The vibrating wires

To measure the deformations induced during the test, 8 SISGEO model 0VK4200VC00 vibrating wires, specific for installation inside concrete structures, were used. These sensors are equipped with an internal thermocouple. For these reasons they have four wires: two are used for the vibrating wire sensor and the other two are for the NTC thermocouple. As mentioned in the previous paragraphs, these sensors were in the central part after the construction of the concrete pile inside a borehole with a diameter of 0,08 m. The vibrating wires were prepared in advance to form a strain gauge string with well-defined distances between the sensors (Figure 6-11). Once the wiring of the sensors was completed, they were immersed in the borehole in the centre of the pile and simultaneously poured with cement mortar. Once the mortar has got sufficient strength (i.e. 7/14 days) it is possible to measure pile's shaft strains which are assumed to be equal to the strains measured at the central vib. wire locations.

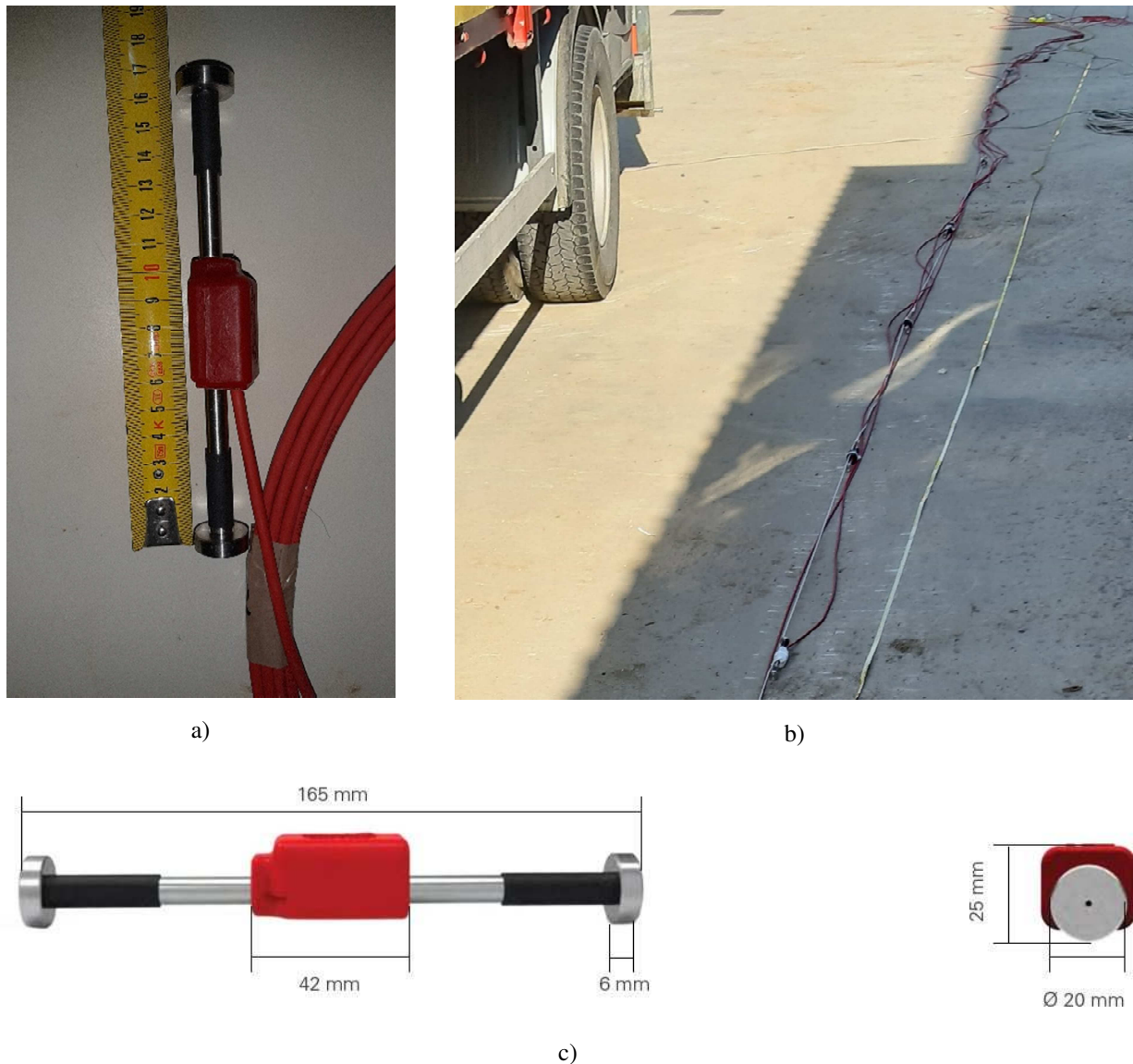


Figure 6-11 – a) vibratig wire used in test; b) construction of the strain gauge chain to be inserted inside the pile; c) geometric dimensions of the vibrating wire

It is widely known that these gauges are made by a steel wire tensioned between two blocks anchored to the structural element to be monitored (embedded in concrete in this case). A relative movement between the two blocks cause a change in the wire tensioning, resulting in a change in the resonance frequency of the wire. In proximity to the centre of the wire, a pair of coils electrically stimulated induce the vibration of the wire. The reading of the relative resonance frequency by dedicated readouts determines the tensional state and therefore the deformation of the gauge (and therefore of the structural element to which it is attached).

This argument could also be examined from an analytical point of view. In fact, the operating principle of these sensors is based on the theory of the vibrating string whereby the fundamental frequency f [Hz] of an ideal string fixed at the ends is:

$$f_w = \frac{1}{2L_w} \sqrt{\frac{T_w}{\mu_w}}$$

Equation 6-6

Where:

- L_w is the wire length [m];
- T_w in the wire tension [N];
- μ_w is the wire linear density [kg/m].

the wire tension is directly proportional to its deformation because:

$$T_w = A_w E_w \varepsilon$$

Equation 6-7

- Where:
- A_w wire section [mm²];
- E_w wire elastic modulus [MPa];
- ε is the strain [$\mu\varepsilon$].

So, after deducting the characteristics of the wire from the above equation:

$$\mu \varepsilon = G f_w^2 10^{-3}$$

Equation 6-8

G is the gauge factor of the sensor and very often, ($f^2 \times 10^{-3}$) is also referred to as "Digit".

The adopted vib. wires had a gage factor of 3,814.

The sensors have a zero reading corresponding to the frequency at the moment of the installation.

The change in the tension of the wire (i.e. the strains from the zero reading) may be calculated with the following formula and is obviously directly proportional to the difference of the square of the frequency:

$$\Delta\mu\varepsilon = (f^2 - f_0^2) \cdot G \cdot 10^{-3}$$

Equation 6-9

where:

- f is the wire vibration frequency [Hz]
- f_0 is the reference wire vibration frequency [Hz]
- G is the sensor gauge factor.

Depending on the convention adopted generally positive values of strains indicated sensor extension.

Anyway, the frequency recorded at the beginning of each test was chosen as the reference vibration frequency f_0 . At the same instant of time, the reference temperature T_0 , introduced later, was also chosen.

Since thermal loads were applied in the tests, the effects of temperature on the measurements of the vibrating string are to be considered as influencing the final measurements.

A change in temperature affects the tensional state of the vibrating wire. For example, an increase in temperature with both ends locked corresponds to a reduction in the tension of the wire. There are also transient phenomena which occur while the heat moves through the structural body and get around the vib. wire and finally get into the body of the sensor where the TC is located. These phenomena can be very complex to be analysed.

To consider, the decrease in frequency due to the thermal elongation of the wire (in case of heating), it is possible to introduce the deformations named by Marshall and Hunter (Marshall and Hunter 1980) as "real" or "true" and expressed as:

$$\varepsilon_{Real} = (f^2 - f_0^2) \cdot G \cdot 10^{-3} + \alpha_s(T_1 - T_0)$$

Equation 6-10

and:

$$\varepsilon_{real} = \varepsilon_{read} + \Delta T \alpha_s$$

Equation 6-11

where:

- α_s is the linear coefficient thermal expansion of the steel vibrating wire [$\mu\varepsilon/^\circ\text{C}$];
- T_0 is the reference temperature [$^\circ\text{C}$];
- T_1 is the temperature at the instant of measurement [$^\circ\text{C}$].

With this report it was possible to determine the actual deformations undergone by the pile during thermal loading.

However, even if during the tests carried out the pile was not mechanically loaded at the top, it was not a structural element free to deform in space, since it was restrained by the soil both laterally and at the toe. This restrain gives rise to stresses inside the pile that were evaluated as the difference between the deformations that the pile could have had if it had been in free conditions and the actual deformations read.

In free conditions pile would have strains calculated as:

$$\varepsilon_{Pfree} = \Delta T \alpha_c$$

Equation 6-12

where:

- α_c is the linear coefficient thermal expansion of the concrete [$\mu\epsilon/^\circ\text{C}$];
- ΔT is the difference in temperature [$^\circ\text{C}$].

And so:

$$\epsilon_{rest} = \epsilon_{real} - \Delta T \alpha_c$$

Equation 6-13

And considering previous equations:

$$\epsilon_{rest} = \epsilon_{read} + \Delta T (\alpha_s - \alpha_c)$$

Equation 6-14

From ϵ_{rest} it was possible to determine the normal stresses within the pile using the following equation:

$$N = E_p \cdot A \cdot \epsilon_{rest}$$

Equation 6-15

6.2.3.2 Thermistors strings

The pile edge and soil temperatures were measured using a thermometric string consisting of 4 NTC (negative temperature coefficient) thermistors, i.e. resistors that change their electrical resistance as a function of temperature, spaced 3 m apart (Figure 6-12). A thermometric string was placed on the pile reinforced gage, while another thermometric string was placed in a borehole purposely drilled at one diameter far from the pile.



Figure 6-12- NTC thermistor used during the test

6.3 Parameters and interpretation of the thermal field test results

In the following sections some parameters are introduced, and their calculation procedure is outlined. These parameters will be used for the interpretation and the analysis of the thermal field test results reported in the section 1.4.

6.3.1 The concrete thermal expansion coefficient determination

The thermal load applied on pile induced thermal strains. Because the effects of the soil at toe and surrounding the pile, a part of the strain were restrained and contributed to providing stress to the pile.

For the shallower vibrating wire VW8, placed only 0,30 m from the ground surface, the effects of the surrounding soil could be considered negligible. Moreover, because there was no restraint at the pile head, the gauge was considered free to expand under heating thermal loads. Plotting the read strain measurements versus the difference of temperature read by the vibrating wire thermistor in the same instant of time, it was possible to determinate a slope (Figure 6-13). The mobilized coefficient of thermal expansion is defined as the slopes of the thermal axial strain versus temperature.

$$\alpha_{mob} = \frac{\epsilon_{real}}{\Delta T}$$

Equation 6-16

In other words from Equation 6-14, considering that ϵ_{rest} was null, the ratio between true strain (i.e. ϵ_{real}) and the difference of temperature read in the same instant of time (i.e. the slope of the plot) is the difference between the two thermal expansion coefficient.

The conventional sign used was negative for contractive strain/compressive stress.

Considering the results obtained from the T2 and T3 tests and assumed the coefficient of thermal expansion of the steel of the vibrating wire as $12,2 \mu\epsilon/^\circ\text{C}$, it resulted an average concrete mobilized coefficient of thermal expansion of $9,5 \mu\epsilon/^\circ\text{C}$. This was in the range of values reported in literature between $9 \mu\epsilon/^\circ\text{C}$ and $15 \mu\epsilon/^\circ\text{C}$ (Laloui, Nuth, and Vulliet 2006; Stewart and McCartney 2014).

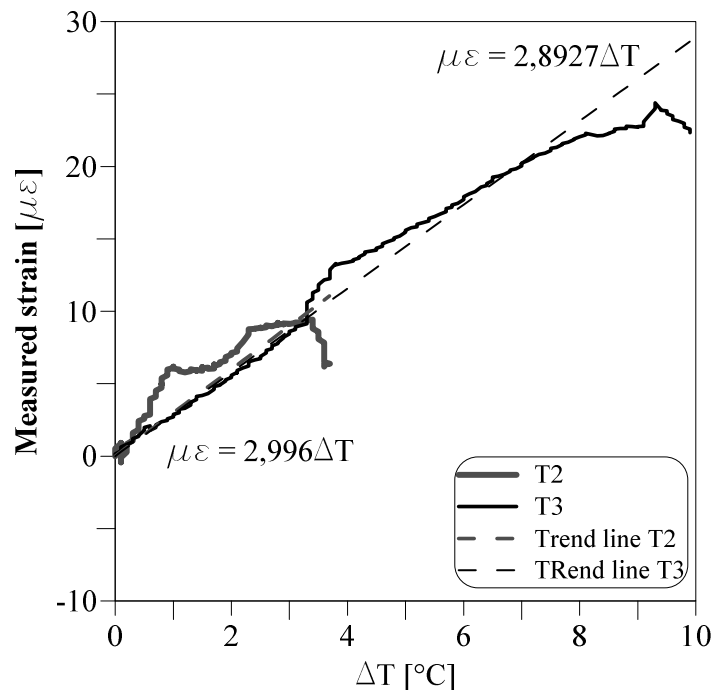


Figure 6-13 - Determination of the concrete thermal expansion coefficient through the strain analysis of VW8

6.3.2 The exchanged heat power between pile and soil

An important aspect of any experiment with piles used as heat exchangers is the evaluation of the energy exchange between pile and soil. Typically, as already clarified in previous chapters the

exchange starts between the pipe where the carrier fluid is pumped to flow and the concrete section of the pile and after from the pile towards the surrounding soil. For a number of practical reasons only short-term field tests were arranged and the discussion in the following paragraphs is oriented towards such cases.

In order to fix a procedure to evaluate such an exchange the following equation was adopted:

$$Q = \rho C_p \Delta T v$$

Equation 6-17

where:

Q is the heat power exchanged between the pile and the surrounding soil [W];

ρ is the density of the heat carrier fluid (water 997 kg/m³);

C_p is the carrier fluid specific heat (water 4186 J/kg °C);

v is the carrier fluid flow rate defined in each test;

ΔT is the temperature difference in °C between the inlet and outlet temperatures.

Because for all the tests water was used as carrier fluid, the exchanged heat power differences between could be affected only by the flow rate and the difference of temperature over the time during the test.

6.3.3 Axial forces and mobilized side shear stress

As said in previous sections, the pile surrounding soil restrained the thermal pile strain. Starting from the restrained strain (Equation 6-13) it was possible to determine the induced axial force in the pile by Equation 6-18:

$$N_i = \mu \varepsilon_{rest,i} E A$$

Equation 6-18

Where:

N_i is the axial force for a depth i [10⁻³ kN];

$\mu \varepsilon_{rest,i}$ is the restrained strain at the depth i [10⁻⁶];

E is the concrete Young modulus [MPa]

A is the pile section [mm²].

For the following tests the adopted convention was negative sign for compressive and positive for tensile forces.

From the axial force values, it was possible to calculate for different pile depth the mobilized side shear stress. The pile was divided into six segments defined by two subsequent VWGs. In each segment the mobilized side shear stress is computed with the Equation 6-19:

$$\tau_{si} = \frac{(N_i - N_{i+1})}{(\pi D L_s)}$$

Equation 6-19

Where:

τ_{si} is the mobilized side shear stress in the i-th segment [kPa]

N_i and N_{i+1} are the axial forces evaluated into the upper part and lower part of every segment [kN];

L_s is the segment length [m];

D is the pile diameter [m].

During the tests looking at the pile side downward shear stress were considered as positive and obviously upwards directed were considered as negative.

6.3.4 The degree of freedom

The degree of freedom was already introduced in the chapter one. It is defined as the ratio between the real and free axial strains, $\varepsilon_{T,real}$ and $\varepsilon_{T,free}$ and is denoted with “n”. The degree of freedom value range between 0 and 1. For a null n the pile results completely blocked while for a unitary value of n the pile is completely free to move. By the way, in real cases, n is always an intermediate value between the two limits, and it depends on the restraint at the two extremities of the pile and mobilized shaft friction (Knellwolf, Peron, and Laloui 2011)

$$n = \frac{\varepsilon_{real}}{\varepsilon_{T,free}}$$

Equation 6-20

6.4 The test program

Three tests were carried out on the pile applying only heating thermal loads. Thermo-mechanical load tests could not be organized for problems related to the Covid emergency. The aim of the tests was to analyse the pile and surrounding soil response in terms of temperature changes, strains and stresses. For each test, a constant heating temperature was provided to pile by the circulating bath with a magnitude typical for the operation of the GSPH in Neapolitan area.

For a number of reasons, the tests could not last the same amount of time. Where opportune the results were reported against a normalised time expressed as a percentage of the total duration of the test. The results at 35%, 50%, 80%, 95% and 100% of the total time test duration were considered as the most representative. These instants were labelled A, B, C, D and E, respectively.

Tests T1 and T3 were performed for longer time than T2. In fact, in the T2 case a system power lacks stopped the inlet flow of the heat carrier fluid. When possible, the test monitoring continued for some hours after the stop. The aim was to investigate on the transient phenomena that occurred after the heat supply ended.

During the installation procedure two sensors were damaged. In fact, no measurements were recorded by the vibrating wire 4 located at 6,30 m from the ground level and by the NTCG3 thermistor located in the ground at a depth of 11,0 m from the ground level.

6.4.1 Test T1

The duration of the test was approximately 5,13 hours and it was carried out using a maximum inlet temperature of 35 °C with a heat carrier fluid flow rate of 12,8 l/min. The outlet temperature was measured by two thermocouples inserted in the output heat carrier fluid circuit.

The temperature trend versus the time measured in the pile axis and in the surrounding soil at one diameter from pile is reported in Figure 6-14. In Figure 6-15 the temperature profiles with the depth at the pre-labelled instants of time are plotted.

During the test the inlet temperature varied from 26,5 °C to 35,1 °C with an increasing trend throughout the duration of the test. A constant temperature of 35 °C was reached from the instant C to the instant E of the test.

Before the test start, the pile and surrounding soil temperatures were measured (Table 6-2). For comparable depth of sensors, it was observed that the pile temperature was slightly higher than the soil one, likely because of the different thermal properties of the concrete and the soil. On the other hand, comparing the temperature measurement at the edge and in the central zone of the pile section, a substantial uniformity is found. The upper sensors showed higher temperatures at the beginning of the test with the maximum difference of about 9 °C between the upper vibrating wire and the deepest one. This difference is of course related to the seasonal cycles of the undisturbed ground temperatures. At the end of the test (instant E) it was observed that the vibrating wire VW8 placed 0,3 m from the ground surface and the thermistor NTC1 placed 1,20 m from the ground surfaced measured the same temperature of 31,10 °C. On the other hand, considering the VW7, placed 1,8 m from the ground surface a temperature of 28,8 °C was measured.

In following sections is demonstrated that the temperature read by the VW8 was strongly affected by the external environmental temperature. Vice versa, the higher temperatures measured by the NTCPs were certainly depending on the proximity of the sensors to the spiral pipe with the fluid carrier.

When the test started the temperature distribution in the pile changed over the time. Figure 6-15 allow to highlight two main aspects regarding the temperature distribution in the pile in the radial and in the longitudinal direction. NTCP1, NTCP2, NTCP3 and NTCP4, can be assumed approximately at the same depth of VW7, VW5, VW3 and VW1. Considering these sensors, it can be observed that at any time during the test an expected temperature gradient was indeed recorded between the edge and the axial zone of the pile. Table 6-3 reported the measured temperatures by the pile sensors in the instant E. Moreover, comparing Figure 6-15 a) and Figure 6-15 b) it is evident the response over the

time of the edge zone and the axial zone of the pile. At the test start the thermistors placed near the pipes suddenly registered an increase in temperature. The temperature sensors on board of the vibrating wires in the pile centre took several tens of minutes to move upwards.

The delay of temperature is noticed also after the test stoppage. While NTCPs measured a nearly instantaneous temperature decrease, on the other hand, the VWs kept showing an increasing trend. This is of course associated to the concrete thermal inertia that affected the heat transfer from the pipes to the pile centre. Moreover, the temperature was not uniform also with the pile depth. In fact, the upper parts of the pile resulted warmer at the end of the test and the temperature gap between the sensors decreased with the depth. It could be the effect of the proximity of higher pile zone to the inlet temperature. As matter of fact, it should be noted that the temperature recorded by NTCP1 at the end of the test was only 0,7 °C lower than the inlet temperature measured in the same instant time. Anyway, it is also observed that near the pile toe, the VW1 measured the larger temperature differences from the start of the test already at time instant A. At the end of the test the ΔT difference between VW1 and VW2 was relevant.

Finally, at the distance of the thermistors chain in the ground, surrounding soil was not affected by the imposed temperature in the pile during the test. As shown in Figure 6-15 b) no temperature changes occurred in the soil with the depth.

Table 6-2 - Temperature values in pile and surrounding soil before the start of the test T1

z [m]	Sensor	T [°C]	z [m]	Sensor	T [°C]	z [m]	Sensor	T [°C]
-0,3	VW8	27,5	-1,2	NTCP1	25,5	-2	NTCG1	23,3
-1,8	VW7	24,5	-4,5	NTCP2	20,4	-5	NTCG2	18,7
-3,3	VW6	21,2	-7,1	NTCP3	19,8	-11	NTCG4	17,6
-4,8	VW5	19,9	-10	NTCP4	18,8			
-7,8	VW3	19,5						
-9,3	VW2	19,2						
-10	VW1	18,4						

Table 6-3 - Temperature values in similar depth for VWs and NTCPs at the end of the test T1

z[m]	VW	T[°C]	z[m]	NTCP	T[°C]
-0,3	VW8	31,1			
-1,8	VW 7	28,8	-1,2	NTCP1	31,1
-4,8	VW 5	25,2	-4,5	NTCP 2	28,3
-7,8	VW 3	24,5	-7,1	NTCP 3	26,5
-10,3	VW 1	24	-10,15	NTCP 4	25,3

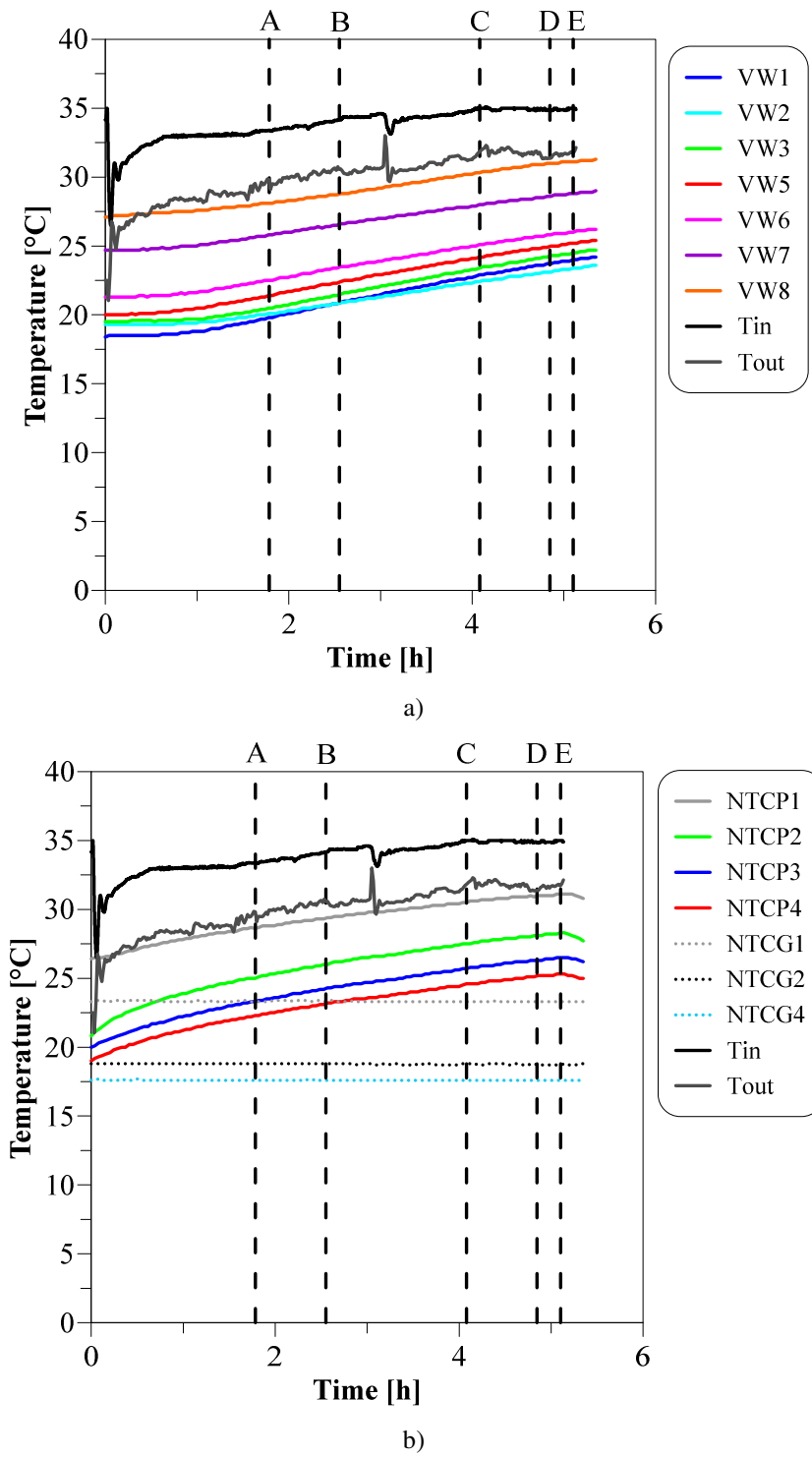


Figure 6-14 - T1 temperature trend versus the time measured a) in the pile centre by vibrating wire; b) in the pile edge by the NTCP and in the soil one diameter from pile by the NTCG

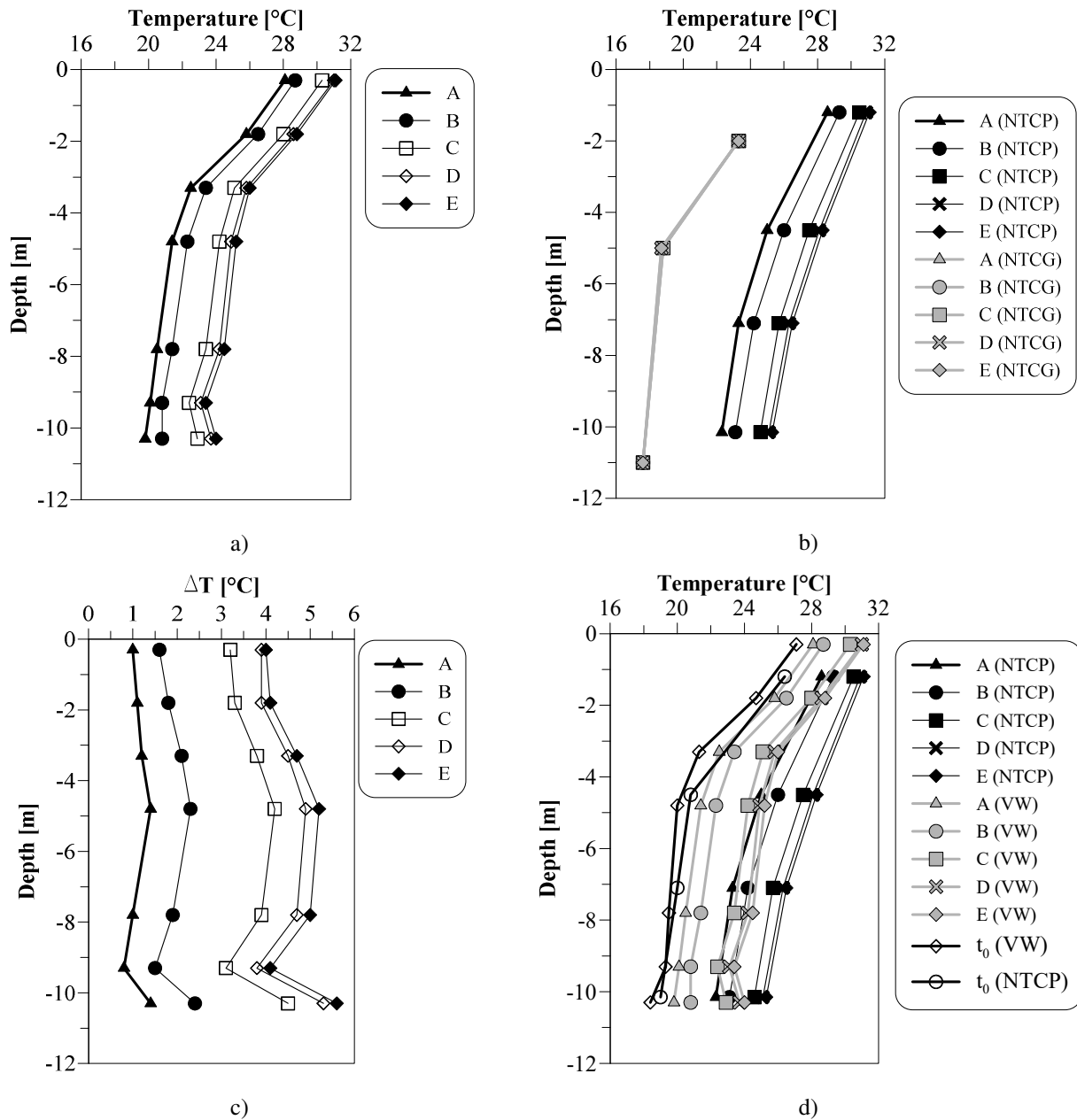


Figure 6-15 - Measured temperature in 5 instants of time during T1 for different depths a) measured by vibrating wire along the pile axis; b) along the pile edge and in surrounding soil one diameter from the pile by the NTC; c) difference of temperature along the pile axis; d) comparison of the different temperatures profile in the pile and in surrounding soil

By the temperature difference between inlet and outlet heat carrier fluid, it is possible to calculate the heat power exchanged between the carrier fluid in the pipe and the pile with the surrounding soil.

The maximum difference of temperature between inlet and outlet temperature is measured at the start of the test when for the first 3 minutes a mean difference of 11,2 °C is reached. After the system had reached its full operating capacity, as can be seen by the Figure 6-16 the mean difference of temperature over the time was approximately 3,8 °C. The trend of the difference decreased with the time and so, the power trend also tends to decrease (Equation 6-17). Anyway, at the end of the test the trend seems to stabilize, but longer time would occur to confirm the trend. The mean heat power normalized respect the pile length was 287 W/m.

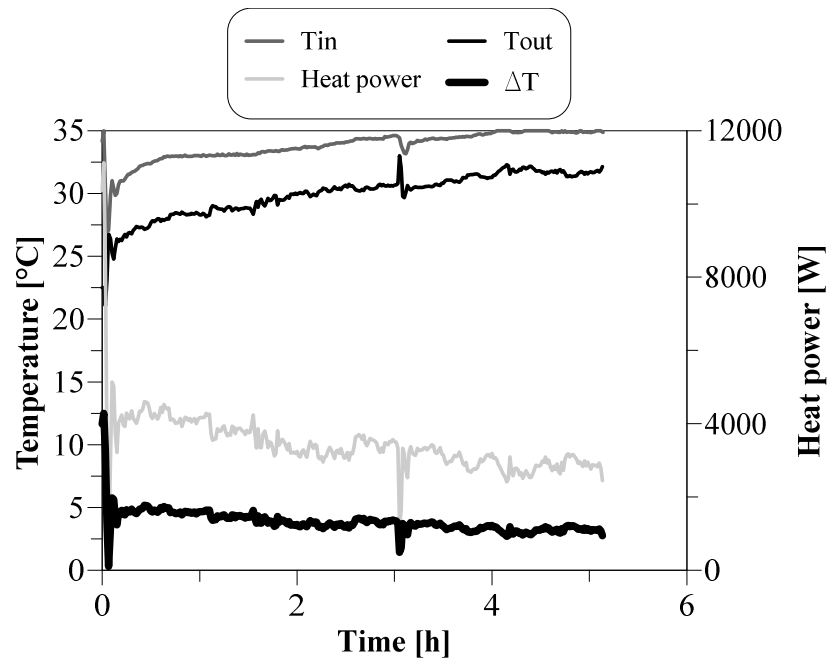


Figure 6-16 - Inlet and outlet temperature difference and heating power trend for T1

In Figure 6-17 the axial force and the mobilized side shear stress trend are showed for different depth and different instant of time. Because it was a thermal test and no restraint were applied on the pile head, the axial force results null in the upper part of the pile for all the considered time instant. It was noted that the pile was all subjected to compressive axial forces only after the 50% of the test duration. On this aspect it should be kept in mind the transient nature of the experiment and the fact that when heated the vibrating wire would show initially false tensile strain due to the fact that the body of the sensor follow the strains of the heated concrete but the wire is not yet at the same temperature.

In Figure 6-17 b) only the instant of time in which on the average compressive strains are developed along the pile shaft are plotted. Nevertheless, there are along the shaft portion of the piles that show inverted sign of the mobilised shaft friction.

In Figure 6-18 the real strain and degree of freedom trend along the pile depth are reported. The instants of time A and B is not considered in the n plot.

Regarding the degree of freedom of the pile it is observed that the stronger restrains offered by the soil occurred at 1,8 m and 7,8 m. In effect, the depth of these points had a correspondence with the depth in whit the CPT offered the stronger cone tip resistance as described in previous paragraphs and as shown in Figure 6-4.

In Figure 6-19 the pile head displacements trend compared with the heat carrier fluid inlet temperature versus the time is reported and can be observed that the pile head displacements followed the inlet temperature trend over the time and a final displacement of 0,26 mm is measured.

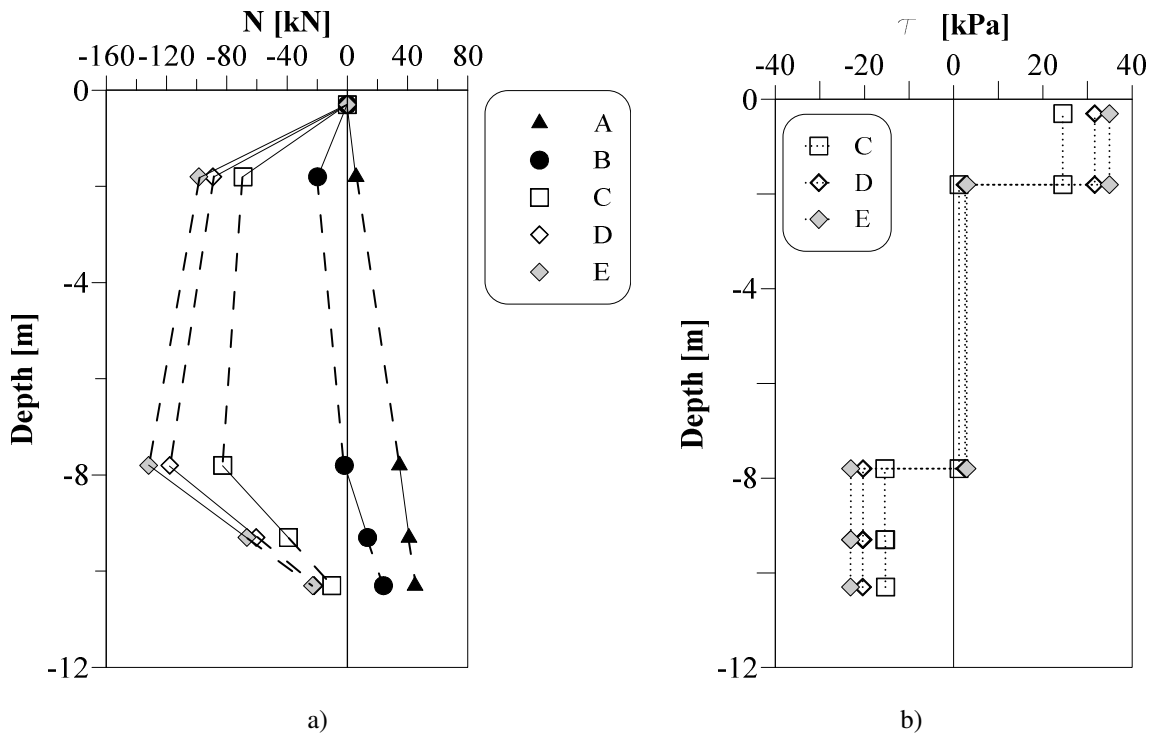


Figure 6-17 - a) Pile axial forces with the depth; b) mobilized side shear stress for T1

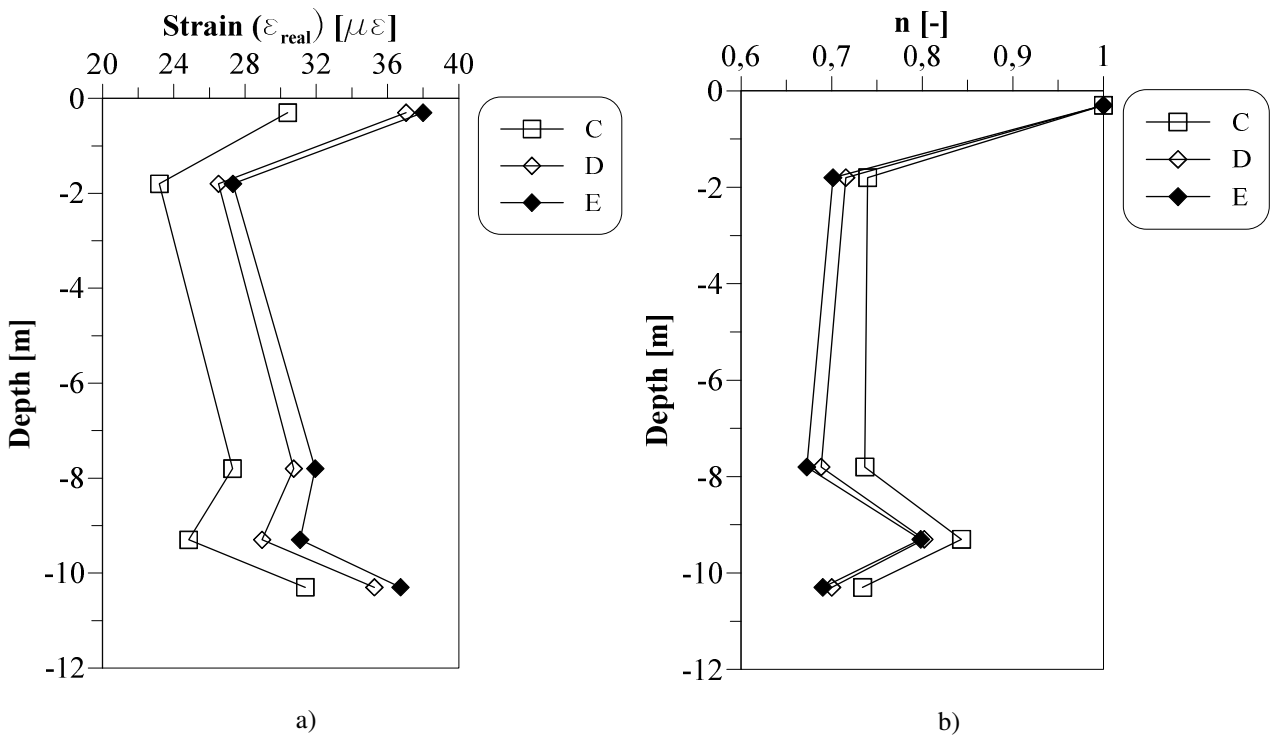


Figure 6-18 - Test T1 a) Real strain versus the depth for different instants of time; b) Degree of freedom trend versus the depth

The Figure 6-17 shows that when the circulating bath turned off the maximum axial force values is measured at 7,80 m from the ground surface and at the pile toe. To investigate on the displacement's magnitude measured during the test, it is chosen to express them as a percentage of the maximum theoretical pile displacements for the same time instant of the measured displacements. It is chosen

to refer the percentage for the time instant E. The ΔT is considered as the average value measured along the pile in the considered time instant. For time instant considered E a $\Delta T = 4,67\text{ }^{\circ}\text{C}$ occurs. Considering a null point located 7,8 m from the ground surface the measured displacement results 75% of the maximum theoretical.

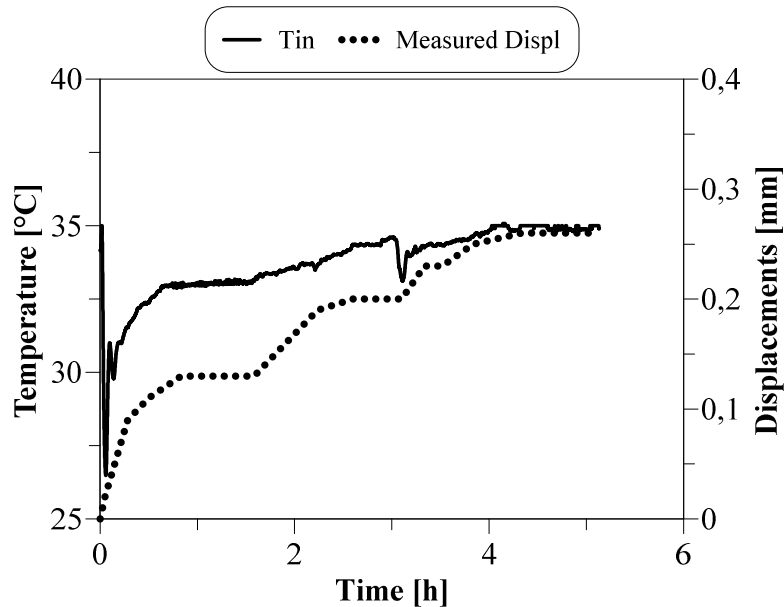


Figure 6-19 – Measured thermal displacements and inlet temperature values versus the time for test T1

6.4.2 Test T2

The duration of the test was approximately 4,80 hours but only for 1,63 hours the heat carrier fluid was provided to pile because of an unexpected technical problem with the circulating bath due to a lack of electrical power.

Anyway, for about 3,25 hours after the system stoppage, temperatures both in the pile and in the surrounding soil were measured. Compared to the T1, this test made it possible to appreciate the behaviour of the pile in the phase after the circulating bath stopped working.

During the test the heat carried fluid flow rate was 12,8 l/min and respect the T1, in this test in addition to the two thermocouples inserted in the output heat carrier fluid circuit, other two thermocouples were used to measure the air temperature during the test.

As the T1, also in this case the pile and surrounding soil initial temperature were measured before the test started. In Table 6-4 the measured temperatures 2,85 hours before the test start are reported.

As already observed in T1, a certain temperature uniformity between the edge and the axial zones of the pile in the radial direction is detected. On the other hand, a temperature decreases with the depth increase is noticed. Moreover, for the same depth, the surrounding soil temperatures have lower values than the temperature measured into the pile.

In Figure 6-20 and in Figure 6-21 the temperature trend versus the time measured in the pile axis and in surrounding soil at one diameter from pile and the temperature for different instant of time versus the depth are reported, respectively.

During the test the inlet temperature varies from 25,1 °C to 33,5 °C with an increasing trend throughout the duration of the test. An increasing trend in inlet temperature is observed at the time A when the circulating bath turned off.

In Table 6-5 it possible to compare the temperature values of the axial and edge zone sensors placed in comparable depth at the time instant A.

Like in the test T1, also in this case a certain temperature difference occurs in radial and longitudinal directions of the pile during the test. Anyway, the longer monitoring carried out in T2 after the system stoppage hallow to observe the evolution of the temperatures into the different pile zones.

Comparing Table 6-5 and Table 6-6 it is possible to observe that at the end of the pile heating phase (instant A) the same higher temperature is measured both in VW8 and NTCP1. Anyway, in both cases the values are very far from the inlet carrier fluid temperature measured in the same instant of time (33,5 °C). Moreover, by Figure 6-20 is evident the effects of the external climatic conditions on VW8 than the other sensor and partially also on NTCP1 the shallower sensors of the pile. As shown, after the time instant A, all vibrating wire increased their temperature approximately until the time instant B. On the other hand, as soon as the circulating bath turned off (instant A), all the NTCPs have a temperature decrease. The only exception is VW8 that after the instant B continued rising the temperature and the NTCP1 where a constant value trend is measured.

As happened in T1, also in this case the VW1 placed near the pile toe measures the larger temperature differences from the start of the test already after the time instant A. At the end of the test the ΔT difference between VW1 and VW2 is relevant.

As expected, the temperature inlet time was too short to impact on the surrounding soil as shown in Figure 6-21 b).

Table 6-4 - Temperature values in pile and surrounding soil before the test T2 start

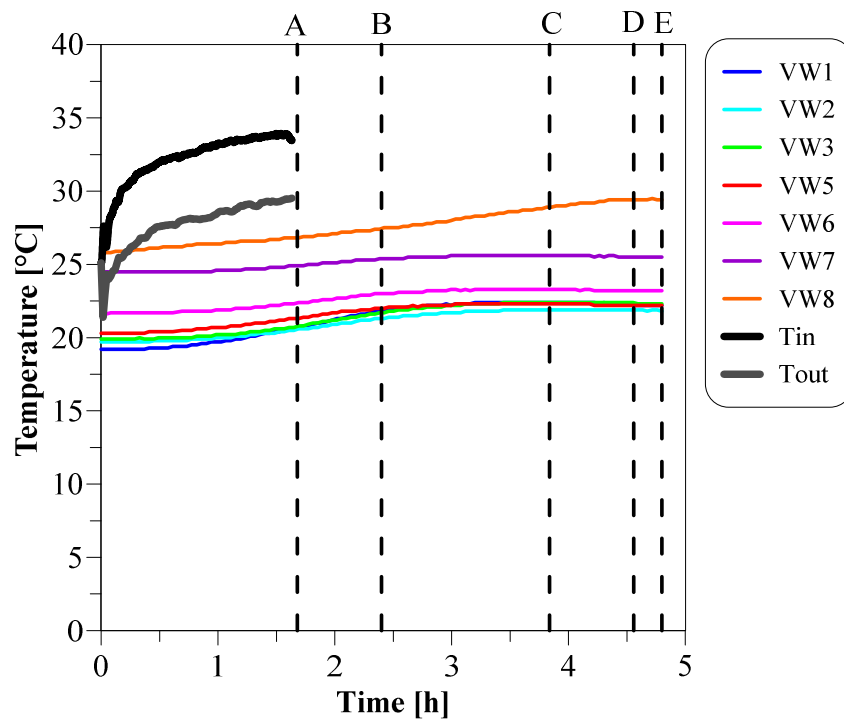
z [m]	Sensor	T [°C]	z [m]	Sensor	T [°C]	z [m]	Sensor	T [°C]
-0,3	VW8	25,6	-1,2	NTCP1	25,6	-2	NTCG1	23,1
-1,8	VW7	24,7	-4,5	NTCP2	20,8	-5	NTCG2	18,5
-3,3	VW6	21,6	-7,1	NTCP3	20	-11	NTCG4	17,4
-4,8	VW5	20,1	-10	NTCP4	19,1			
-7,8	VW3	19,7						
-9,3	VW2	19,4						
-10	VW1	18,5						

Table 6-5 - Temperature values in similar depth for VWs and NTCPs at the end of the test T2 (time instant A)

z [m]	Sensor	T [°C]	z [m]	Sensor	T [°C]
-0,3	8	26,8			
-1,8	7	24,9	-1,2	1	26,6
-4,8	5	21,3	-4,5	2	24,2
-7,8	3	20,7	-7,1	3	23,3
-10,3	1	20,6	-10,15	4	23,1

Table 6-6 - Temperature values in similar depth for VWs and NTCPs at the end of the test T2 (time instant E)

z [m]	Sensor	T [°C]	z [m]	Sensor	T [°C]
-0,3	VW8	29,4			
-1,8	VW7	25,5	-1,2	NTCP1	26,2
-4,8	VW5	22,2	-4,5	NTCP2	22,8
-7,8	VW3	22,3	-7,1	NTCP3	22,2
-10,3	VW1	22,2	-10,15	NTCP4	21,6



a)

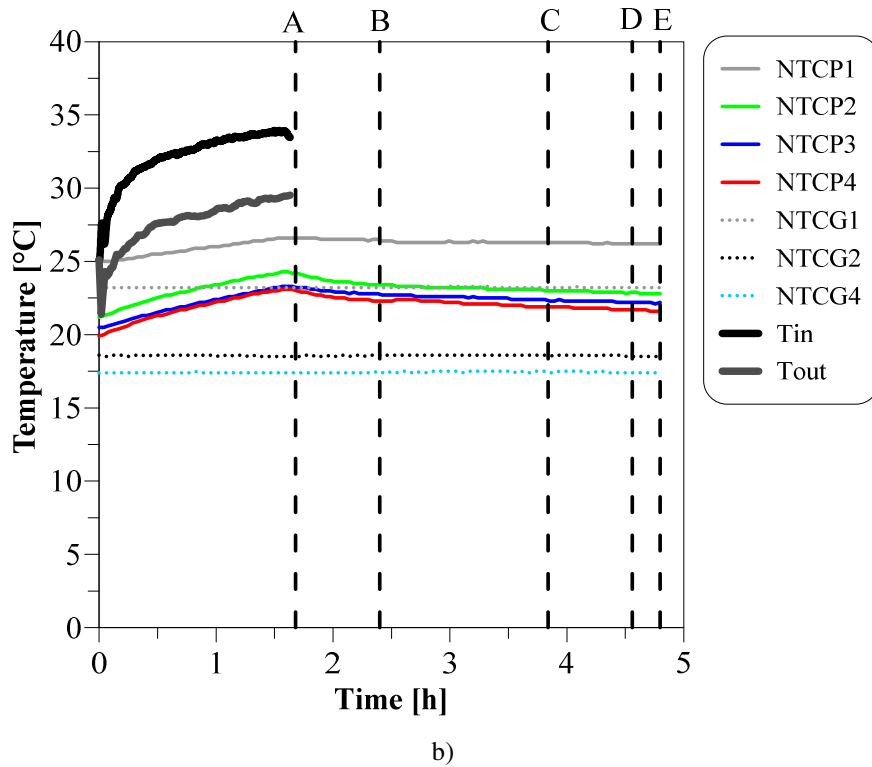


Figure 6-20 – T2 temperature trend versus the time measured a) in the pile centre by vibrating wire; b) in the pile edge by the NTCP and in the soil one diameter from pile by the NTCG

It is noticed that the temperature in the pile axis started to rise approximately after one hour from the test start. As said before, the pile temperature does not result constant with the depth and the VWs started from different temperature levels. Anyway, it is possible to notice that the deeper VW1 shows a slope trend greater than the other VWs also after the temperature supply into the pile. In fact, just after the time instant A, the temperature in VW1 is comparable or higher than the upper VW2 and VW3 and at the instant of time B it reaches the temperature level of the VW5. As also observed in Figure 6-21 c) the VW1 ΔT from the start of the test is the greater (without considering that of the VW8 which, as mentioned, was affected by external climatic factors).

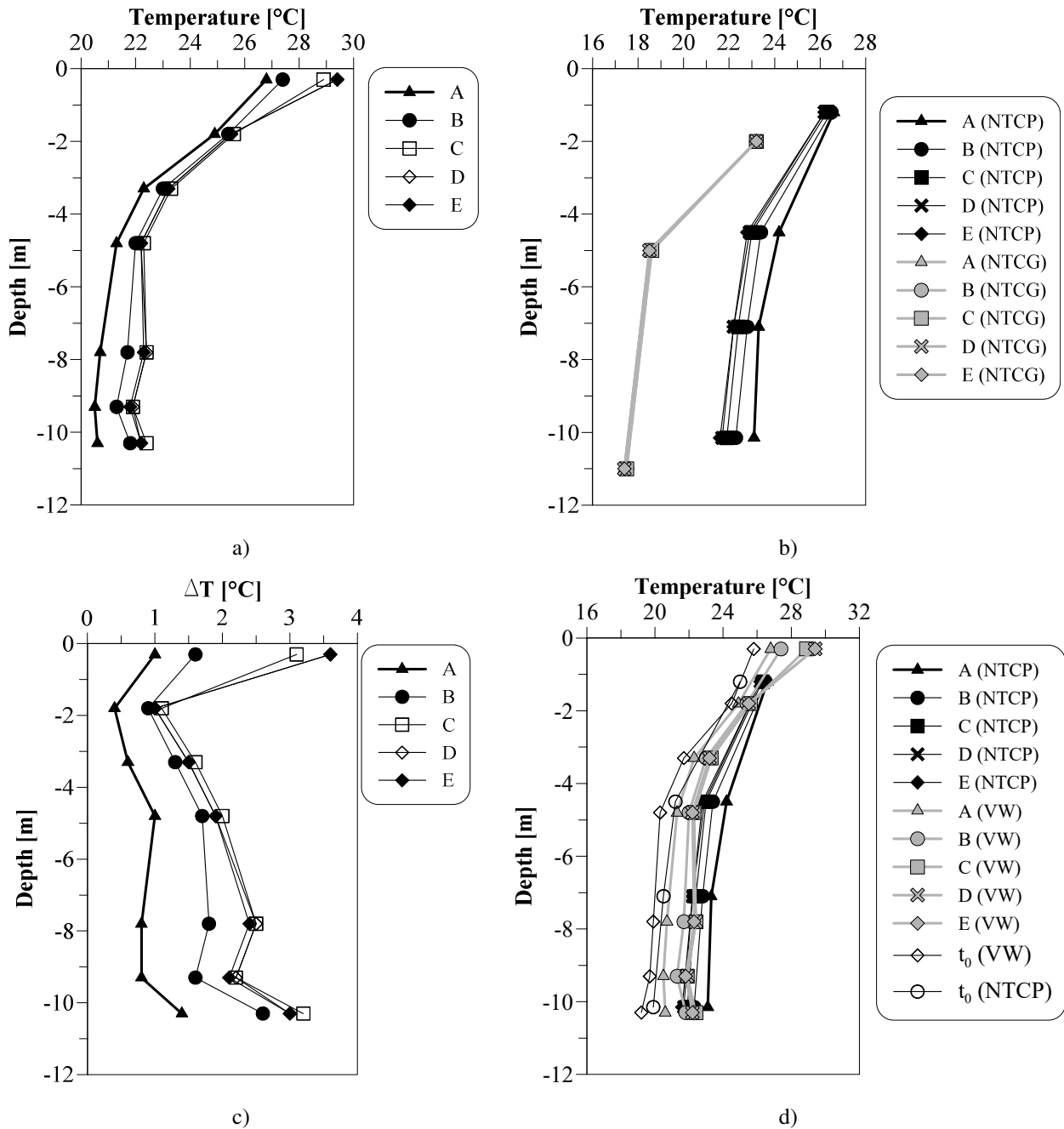


Figure 6-21 - Measured temperature in 5 instant of time during T2 for different depths a) measured by vibrating wire along the pile axis; b) along the pile edge and in surrounding soil one diameter from the pile by the NTC; c) difference of temperature along the pile axis; d) comparison of the different temperature in the pile and in surrounding soil

Figure 6-22 shows the inlet, outlet, external ambient temperatures, and heat power trend versus the time. This test demonstrates the greater energy performances of short time operation mode in energy pile. In fact, comparing the T1 and T2 results it can be observed that over the time the T2 test has a mean difference between inlet and outlet temperature of 4,5 °C and a mean heat power exchanged normalized respect the pile length of approximately 330 W/m. On the other hand, in T1 a mean temperatures difference over the time was approximately 3,8 °C and the mean heat power normalized respect the pile length was 287 W/m. Moreover, it should be observed that in T2 the heating power

trend is still in the increasing phase. It means the test was interrupted when the pile was in the initial transient phase.

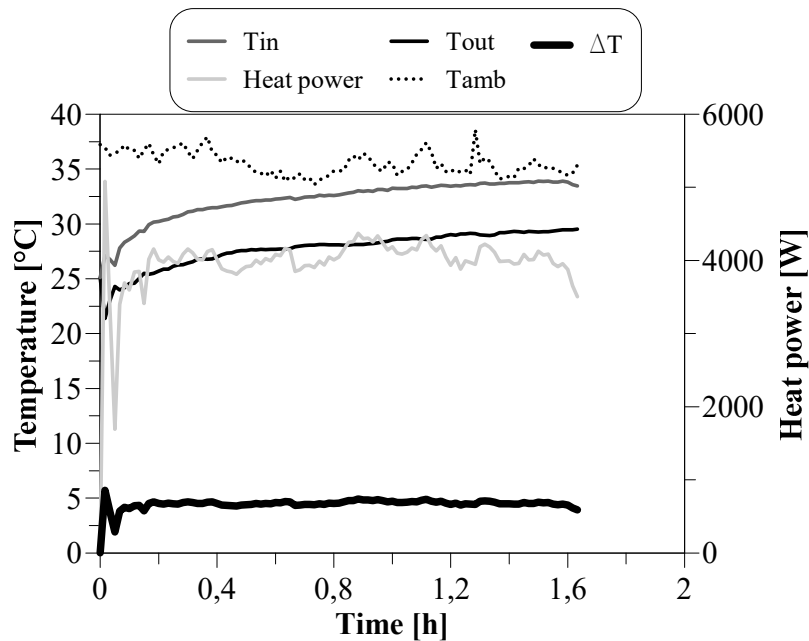


Figure 6-22 – Inlet, outlet and external ambient temperature difference and heating power trend for T2

In Figure 6-23 the axial force and the mobilized side shear stress trend were showed for different depth and different instant of time. Because it was a thermal test and no restraint were applied on the pile head, the axial force is null in the upper part of the pile for all the considered time instant. Considering the magnitude and the time application of thermal loads, the axial forces shows a different trend than the T1. It should be noted the stop occurred in instant A and from the axial forces graph could be appreciate the thermal delay between the application of loads in edge zones and the axial response. In fact, still tensile axial forces there are in the time instant A. Only for consequent time instants the heat reached the vibrating ware and induced effects. So, the compressive axial forces reached during a no active thermal load supply. Moreover, it was also observed that the axial force maximum value is reached for the time instant E at a depth 7,8 m from the ground surface.

In Figure 6-23 b) only the instant of time in which on the average compressive strains are developed along the pile shaft are plotted . Nevertheless, there are along the shaft portion of the piles that show inverted sign of the mobilised shaft friction. It is also observed that respect the T1 tests, in T2 likely because of the shorter time in which the thermal loads were applied, the mobilized side shear stress had lower values.

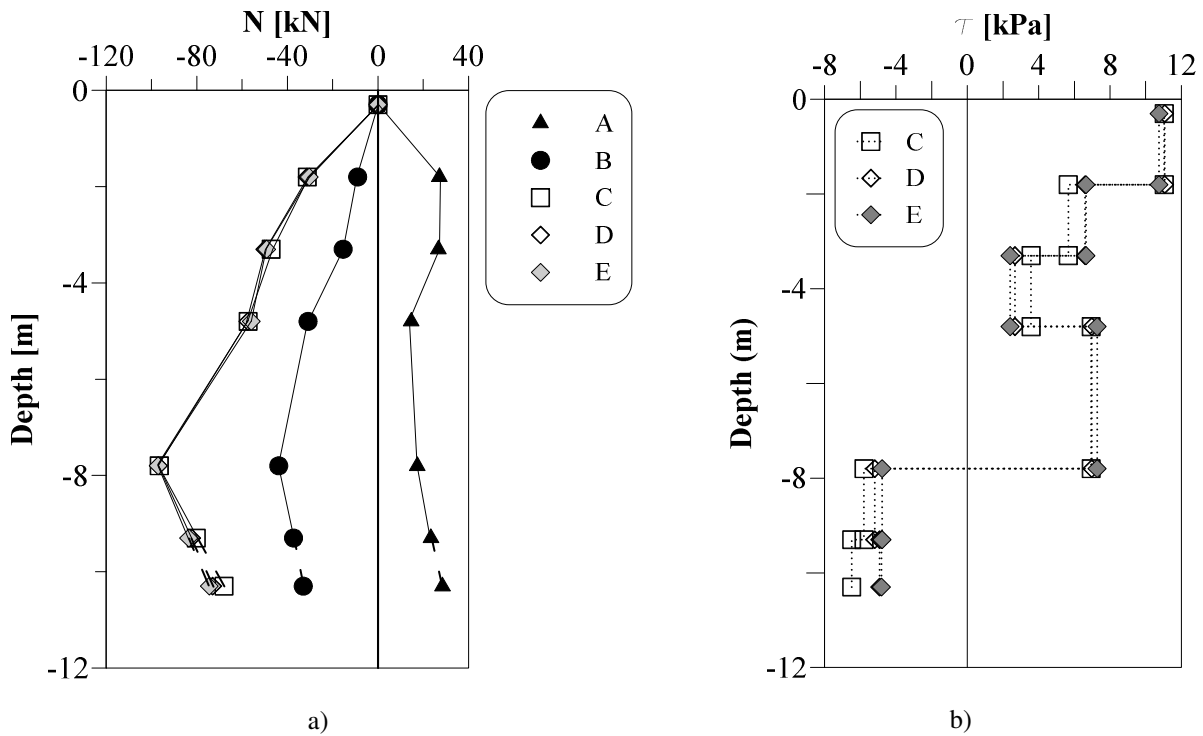


Figure 6-23 - a) Pile axial forces with the depth; b) mobilized side shear stress for T2

In Figure 6-24 the real strain and degree of freedom trend along the pile depth were reported. The instants of time A and B was not considered in n plot because of the previous considerations.

Regarding the degree of freedom of the pile it is observed that the values ranged between approximately 0,6 for the upper part of the pile and approximately 0,5 for the deeper part.

Respect the T1 test, maybe due to the applied thermal loads magnitude and duration the trend of real strain and n did not present any evident trend change.

In Figure 6-25 the pile head displacements trend compared with the heat carrier fluid inlet temperature versus the time is reported. The measured displacements in the instant of time A, when the circulating bath turned off is 0,09 mm.

As said, in this time instant the null point is placed at 7,8 m from ground surface.

The same procedure carried out for the test T1 was adopted in this case and the maximum measured displacement is expressed as percentage of the maximum theoretical displacement that could have the pile respect the maximum theoretical displacement. In this case a length of 7,8 m and an average ΔT value of 1,6 °C is considered. The measured displacement was the 76% of the theoretical thermal expansion.

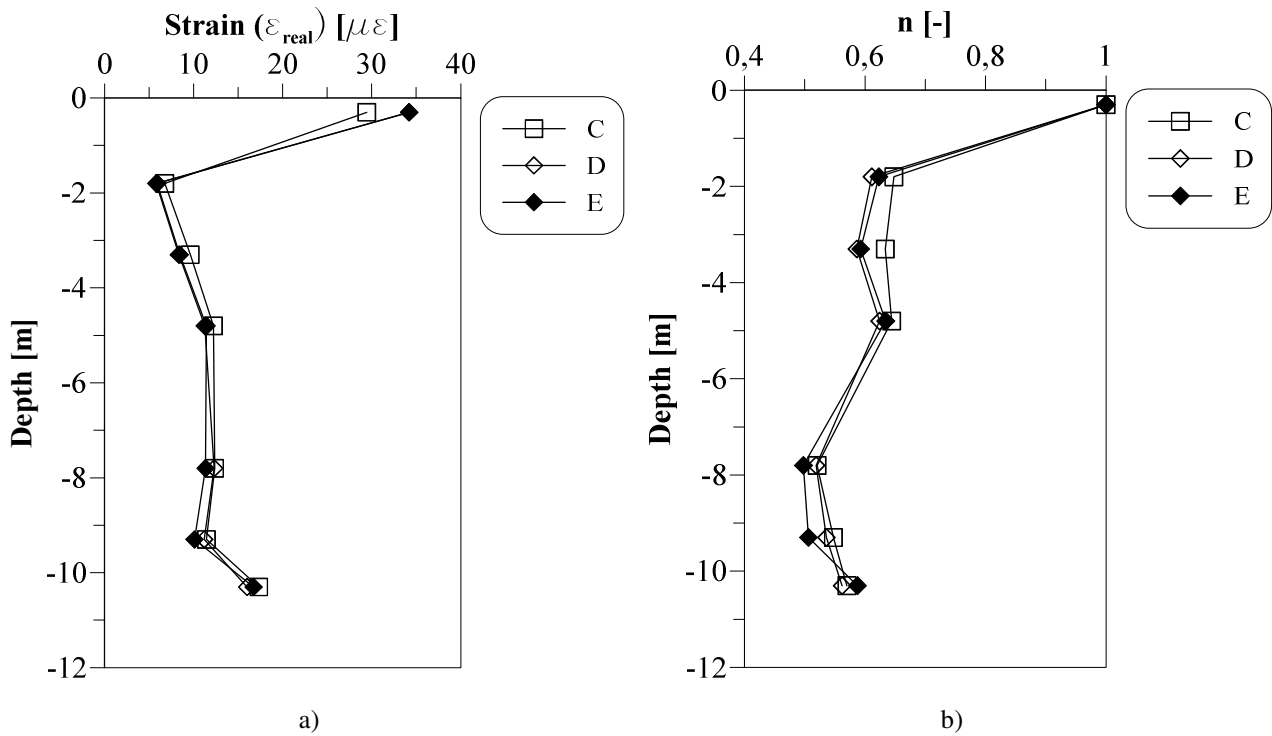


Figure 6-24 – Test T2 a) Real strain versus the depth for different instants of time; b) Degree of freedom trend versus the depth

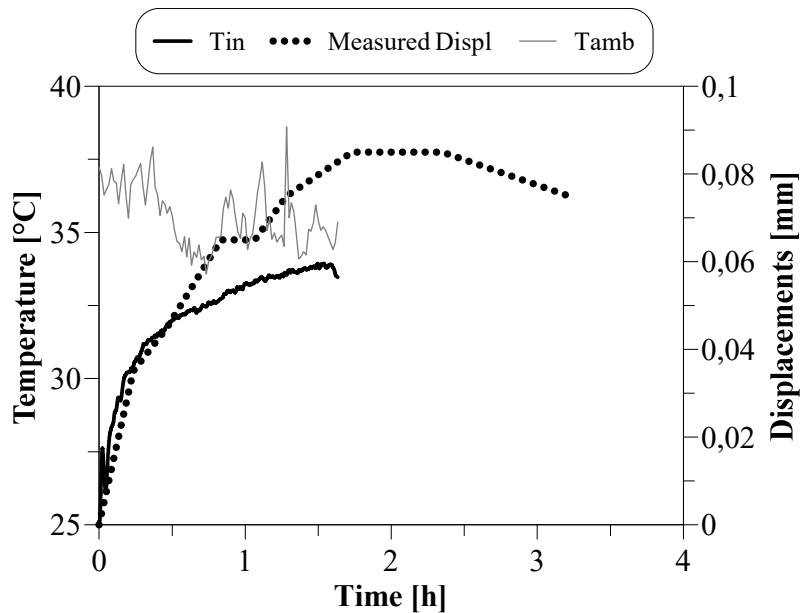


Figure 6-25 - Measured thermal displacements and inlet temperature values versus the time for test T2

6.4.3 Test T3

T3 was the last of the three field tests carried out. The duration of the test was approximately 7,1 hours in which thermal loads were applied for 6,1 h. The last hour was used to monitor the effects after the circulating bath turned off. As for T2, in this test both the outlet carrier fluid and the external ambient temperature were measured.

Test T3 were carried out the day after the T2 test. The aim of the test was to investigate the effects of daily applied thermal loads on pile.

The inlet heat carrier fluid temperature increased until the value of approximately 30 °C

As for the other tests, before the start the initial temperatures of pile and surrounding soil were measured.

In Table 6-7 and

Table 6-8 the pile and surrounding soil temperatures before the test start and the pile temperature for similar depth in the edge and the axis are reported, respectively.

Comparing the results showed in Table 6-7 with the result obtained in the other tests, it is observed that the effects of the T2 on pile were still evident the day after. While in T1 and T2 a generally uniform radial temperature and a temperature decrease with the depth was observed, in T3, on the other hand, the results are different. In fact, while a sort of radial temperature uniformity is preserved, along the pile the temperature trend resulted very variable. In the upper part of the pile, VW8 is strongly affected by the morning air temperatures and measured values 4,7 °C lower than temperature measured 1,5 m deeper. Moreover, seemed that the transient phenomena of the heat transfer and the capacity of heat storage is evident above all in the deeper part of the pile. While the initial temperature measured in the depth range between -1,8 m and 4,8 m are similar to tests T1 and T2, from 7,8 m and 10,3 m higher initial temperatures are measured. These values are few Celsius degree lower than the temperature measured in the same points at the end of the T2.

When the test started the temperature measured by sensors were monitored over the time (Figure 6-26). As already observed in the previous tests, also in T3 a different response is observed between the edge of the pile and the axial zone. As soon as the test started, the thermistors placed on the reinforced cage near the pipes measured a temperature increase. The vibrating wire, as for the other tests, started to measure a temperature increment only approximately 1 hour after the test start and the behaviour was different for each sensor. It is observed the VW8 placed in the upper part of the pile was strongly affected by the external air temperature. It has the most sloping trend of all the vibrating wire and reached the maximum pile temperature of 29,3 °C at the circulating bath stoppage and 30,7 °C at the end of the test. The other vibrating wire were characterised by a somewhat similar trend except for VW1 located at the pile toe. This sensor, indeed, was characterized by a greater slope of the trend over the time than the upper sensors. Even if VW1 at the beginning of test started from a lower temperature, both at the instant of time in which circulating bath was stopped and end of the test reached higher temperatures than other vibrating wire (except for the upper sensors VW7 and VW8). This trend was also confirmed by the ΔT measurements reported in Figure 6-27 c).

From Figure 6-27 d) and

Table 6-8 is observed the difference of temperatures between the different pile zones. As observed in previous tests, the edge had higher temperatures than the axial zones and a difference of temperatures occurred with the pile depth between the upper and lower part of the pile. Anyway, respect the T1

and T2 tests, in T3 the differences of temperatures in radial direction are lower and above all the deeper part of the pile reached the higher value at the end of the test. In addition, a temperature difference of only 0,6 °C occurred in the pile axis from the pile toe to a depth of 4,8 m from the ground surface.

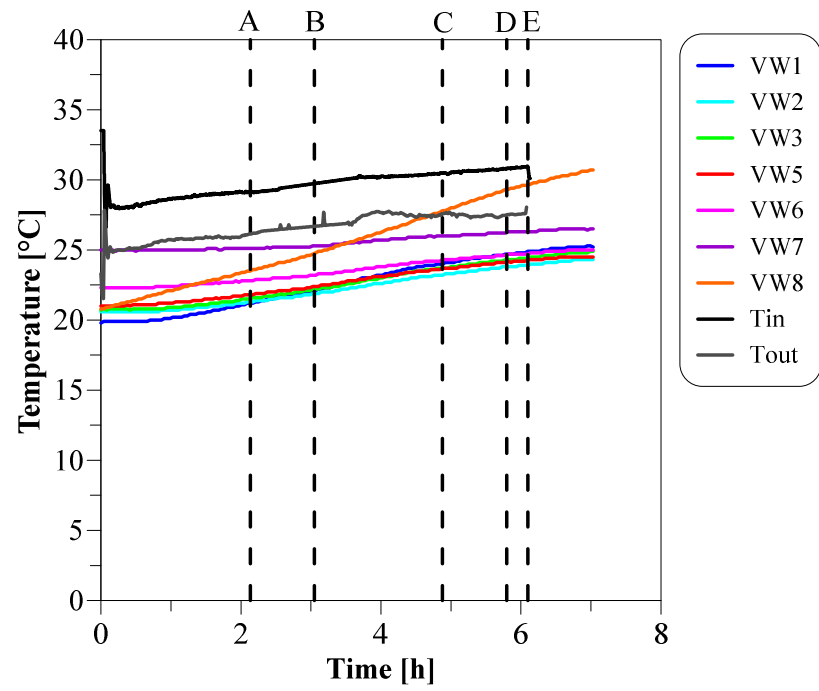
These differences depended on the initial condition of the test that were affected by the test T2 carried out about 24 hours before.

Table 6-7 - Temperature values in pile and surrounding soil before the test T3 start

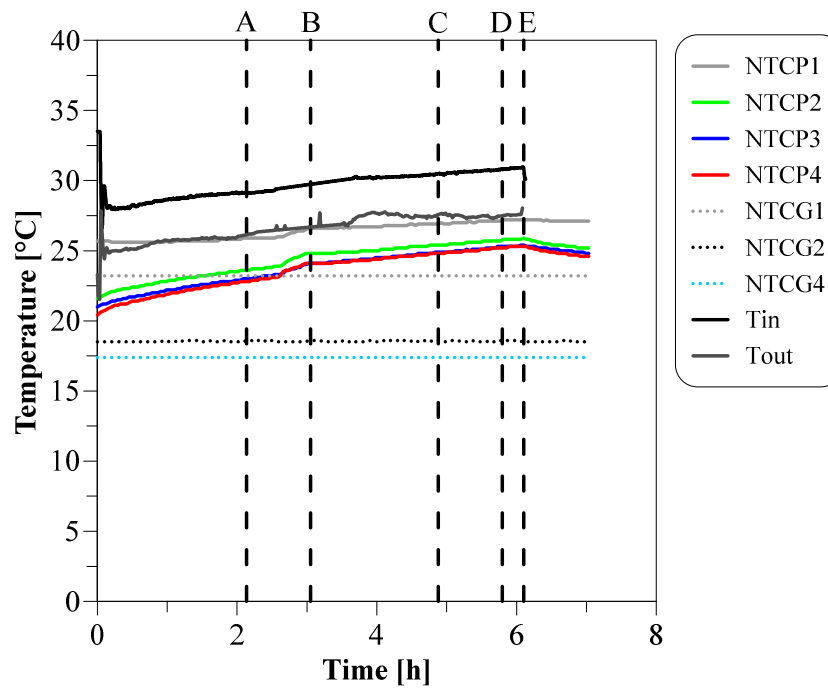
z [m]	Sensor	T [°C]	z [m]	Sensor	T [°C]	z [m]	Sensor	T [°C]
-0,3	VW8	20,2	-1,2	NTCP1	25,7	-2	NTCG1	23,2
-1,8	VW7	24,9	-4,5	NTCP2	21,6	-5	NTCG2	18,5
-3,3	VW6	22,3	-7,1	NTCP3	21	-11	NTCG4	17,4
-4,8	VW5	21	-10	NTCP4	20,3			
-7,8	VW3	20,7						
-9,3	VW2	20,5						
-10	VW1	19,8						

Table 6-8 - Temperature values in similar depth for VWs and NTCPs at the end of the test T3 (time instant E)

z [m]	Sensor	T [°C]	z [m]	Sensor	T [°C]
-0,3	VW8	29,6			
-1,8	VW7	26,3	-1,2	NTCP1	27,2
-4,8	VW5	24,3	-4,5	NTCP2	25,9
-7,8	VW3	24,4	-7,1	NTCP3	25,4
-10,3	VW1	24,9	-10,15	NTCP4	25,3



a)



b)

Figure 6-26 – T3 temperature trend versus the time measured a) in the pile centre by vibrating wire; b) in the pile edge by the NTCP and in the soil one diameter from pile by the NTCG

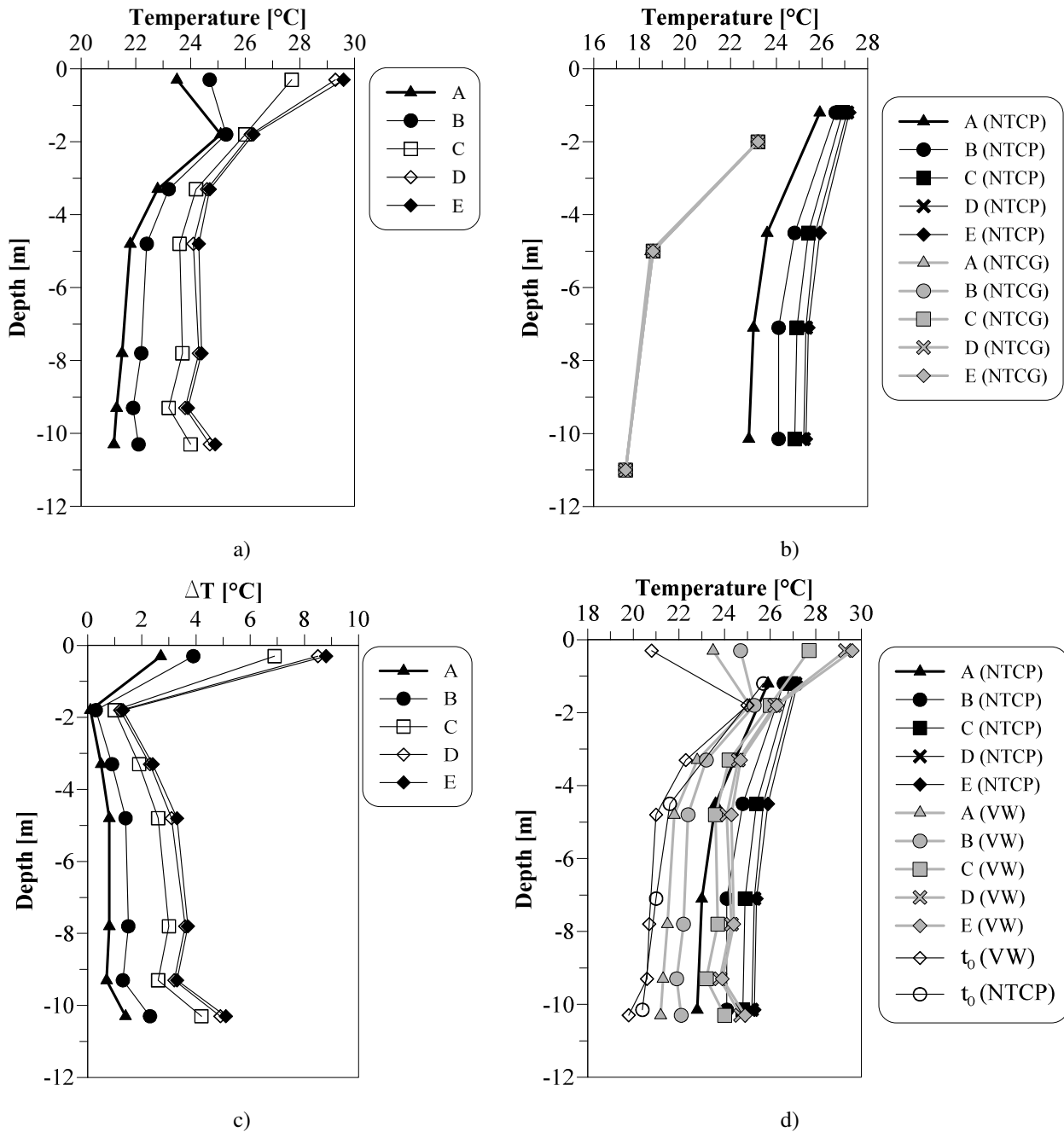


Figure 6-27 - Measured temperature in 5 instant of time during T3 for different depths a) measured by vibrating wire along the pile axis; b) along the pile edge and in surrounding soil one diameter from the pile by the NTC; c) difference of temperature along the pile axis; d) comparison of the different temperature in the pile and in surrounding soil

The Figure 6-28 shows the development of the thermal powers and the inlet, outlet and ambient temperatures over time. It is possible to note that after an initial peak due to the great difference in temperature between the circulating bath and the temperature in the pile, the power trend alternates between small increasing and decreasing phases, resulting in a final average value of heat exchanged normalized respect the pile length of approximately 228 W/m.

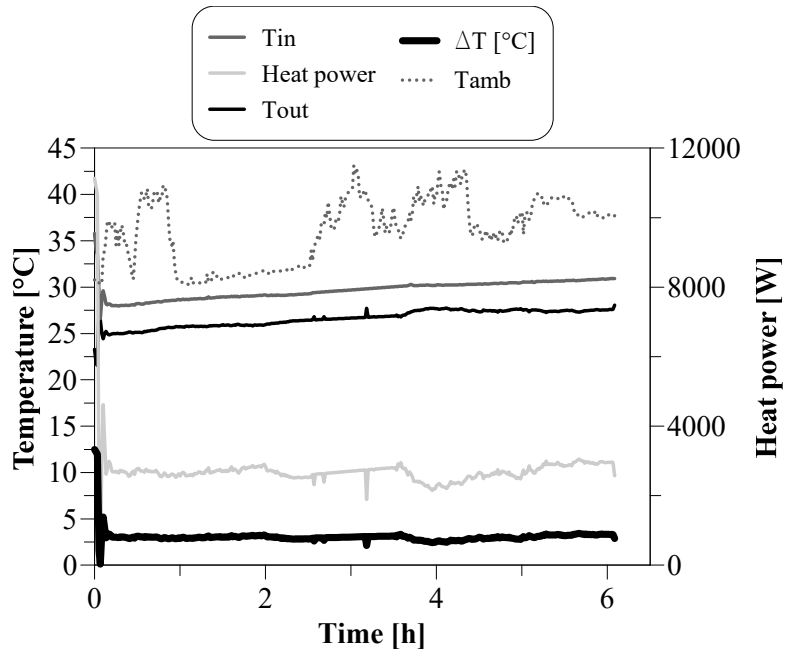


Figure 6-28 - Inlet, outlet and external ambient temperature difference and heating power trend for T3

In Figure 6-29 the pile axial forces trend with the depth and the mobilized side shear stress are reported. It is observed that an effective compressive state of the pile occurs only in the final parts of the test. It could be the combined effects of the previously carried-out test T2 and the inlet temperature values reached during the test. However, in T3 for the final phases of the test, compressive axial forces increased with the depth increase until 7,9 m. From this point a trend inversion was observed as shown also in Figure 6-29 b) where only the most representative instants of time are reported.

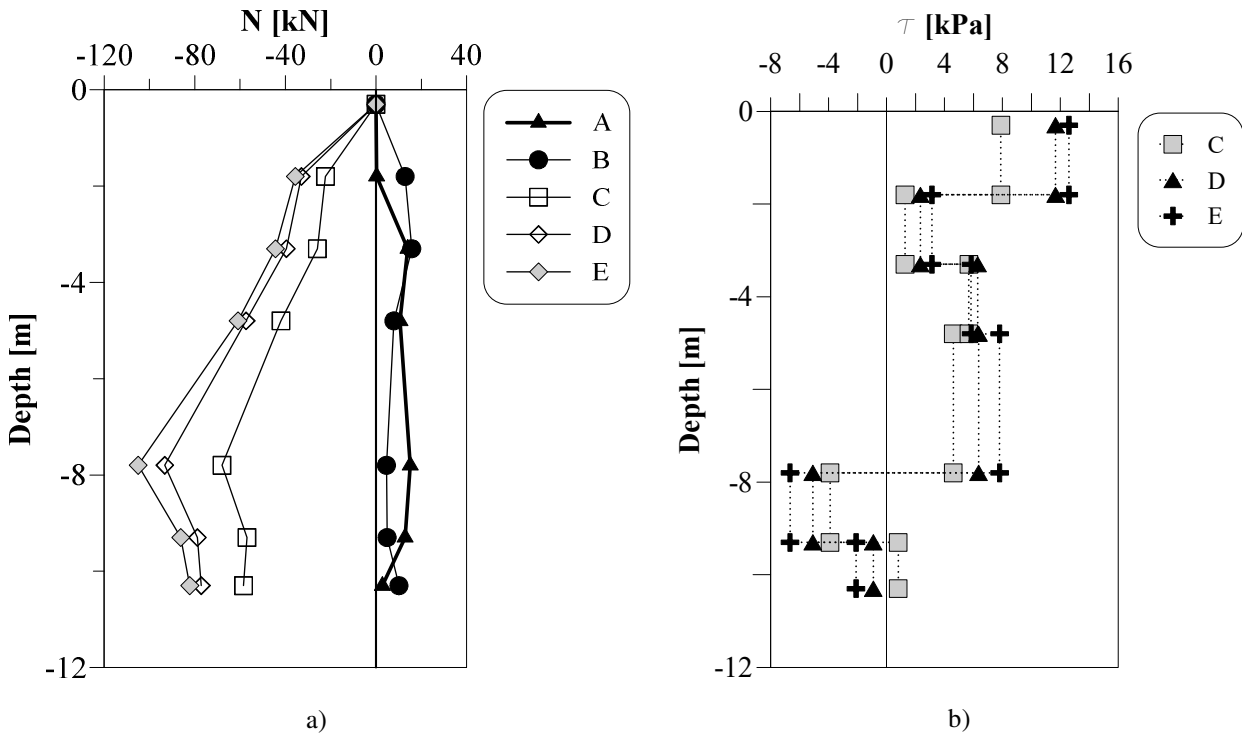


Figure 6-29 - a) Pile axial forces with the depth; b) mobilized side shear stress for T3

In Figure 6-30 the real strain and the degree of freedom n versus the depth are reported. It is observed that apart from the pile head which had no restraints, the highest degree of freedom is observed in the central part of the pile. Anyway, no great n variation was observed along the pile depth. The maximum measured pile head displacements are observed at the end of the test. When the circulating bath stopped to work a pile head displacement of 0,23 mm was measured (time instant E). From the axial force diagram, it could be concluded that the null point was at 7,8 m from the ground surface. Considering an average ΔT value of = 4,0 °C the measured displacement was 78% of the free column theoretical expansion with an equivalent length of the pile from the head to the null point.

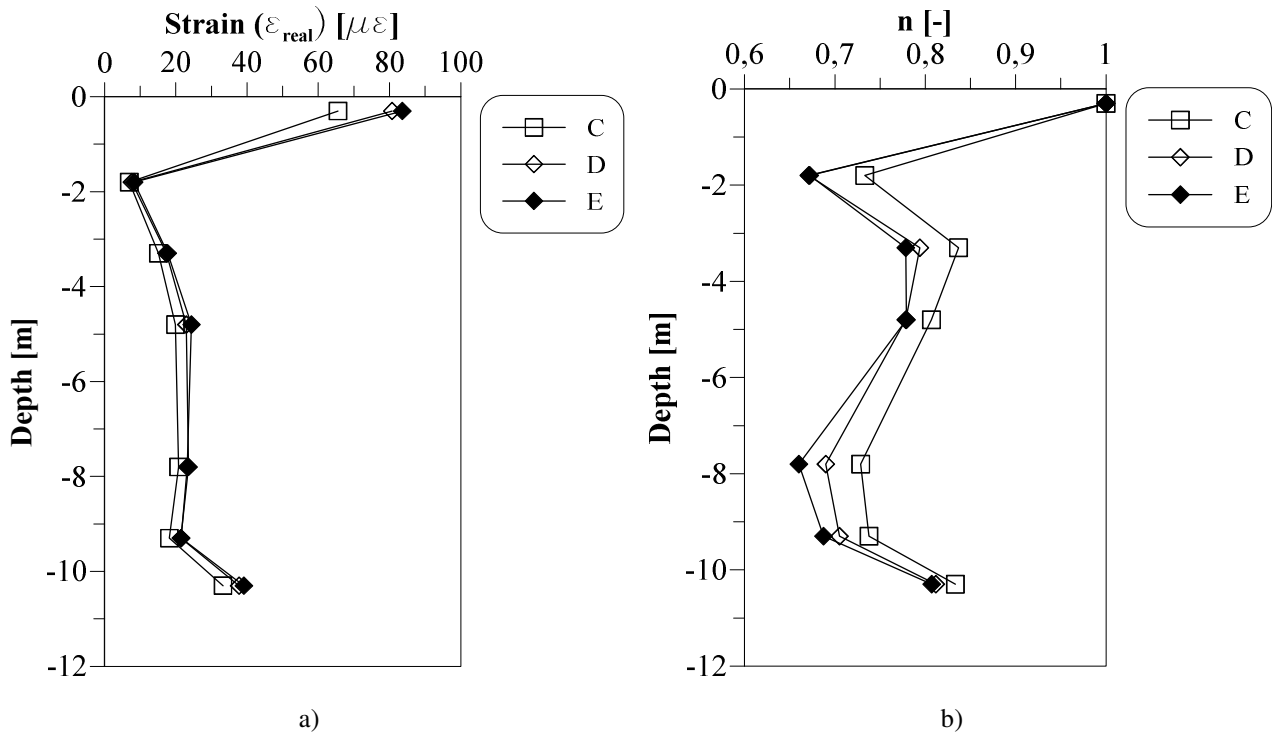


Figure 6-30 - Test T3 a) Real strain versus the depth for different instants of time; b) Degree of freedom trend versus the depth

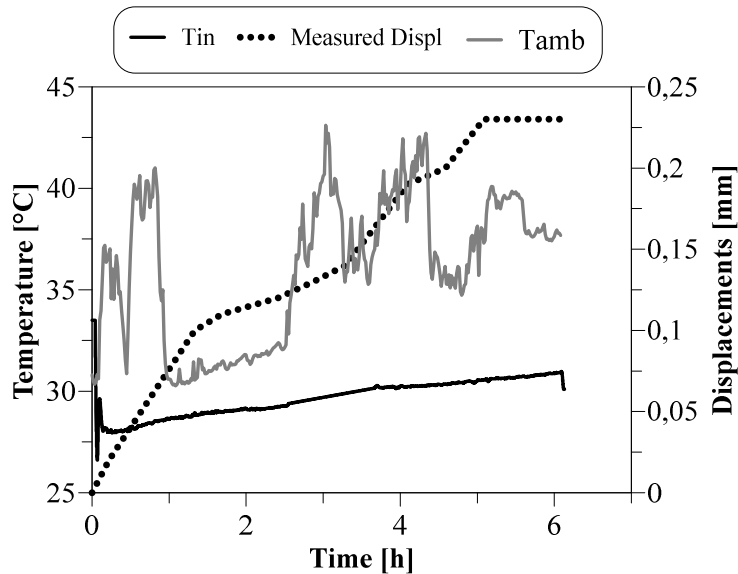


Figure 6-31 - Measured thermal displacements and inlet temperature values versus the time for test T3

6.5 Long term temperatures monitoring

As observed from the carried-out field test, for daily thermal loads under 35 °C no effects occurred in surrounding soil. Anyway, with a long-term temperature monitoring of the pile and soil it is observed that, as expected, for the shallower soil zone, during the months sensible temperatures changes occur because of the environmental climatic conditions.

The collected data are showed with a monthly basis to be clearer. Both temperature variation with the depth and temperature variation over the time for every sensor are presented both for pile and surrounding soil (Figure 6-32).

The depth diagrams show that for all the zones considered, as expected from theory, the sensors closest to the surface are significantly affected by the variation of the external air temperature. VW8, located only 0,30 m from ground level (the most exposed to external thermal fluctuations, as also highlighted by Figure 6-33), has thermal excursions that vary between 6,2 °C in January to 15,7 °C in April.

The NTC1 located in the pile edge shows the same trend. Anyway, because of their greater depth of installation than VW8 (1,2 m from ground level) it managed to maintain a greater thermal inertia. Consequently, the temperature range values over the time of NTC1 is reduced compared to VW8. It is interesting to note that even the first thermocouple installed in the ground at about 2 m above ground level, despite its greater depth compared with the other sensors and the different material in which it is immersed, nevertheless suffers from significant seasonal fluctuations, going from 22,6 °C measured in October to 12,6 °C measured in March.

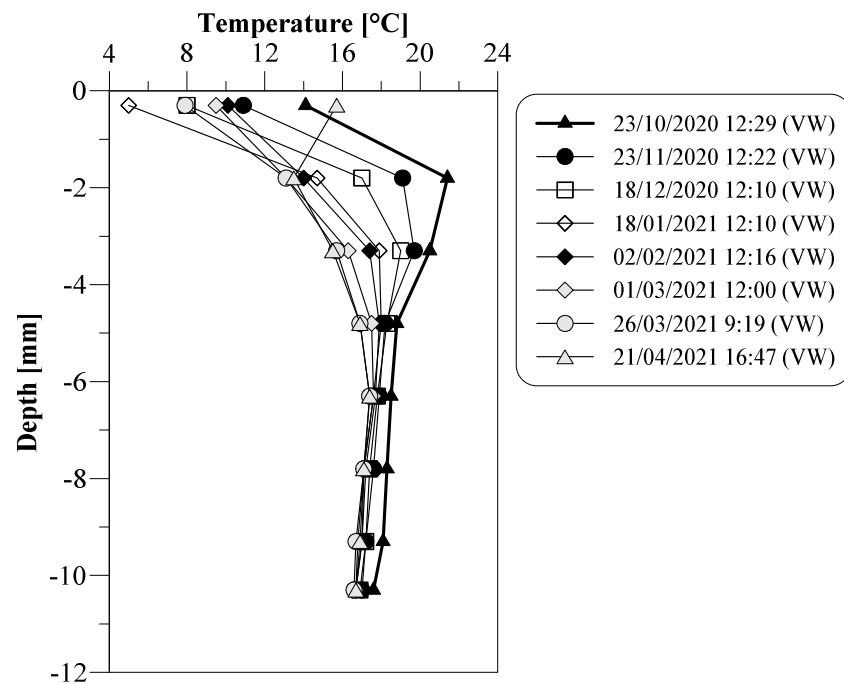
As regards the temperature trends with depth, it is noticed that up to a depth of 4 metres there are different temperature slopes in the pile, depending on the considered month. After this depth, it was possible to notice an almost similar trend for all months, which moves towards progressively colder temperatures. At the pile toe, the temperature rose from the approximately 17,6 °C measured in October to the 16,7 °C recorded in January.

As regard the thermistors installed in soil, it is observed a great behaviour difference between the NTCG1 placed 2 meters from the ground surface and NTCG2 placed 4 m from the ground surface. In fact, the former shows more variable temperatures values over the time then the latter that, on the other hand, has an almost constant value ranged between 18 °C and 17 °C. Furthermore, it is interesting to notice that the values recorded at greater depths (approximately 11 m from ground level) are subject to variations in temperature, varying between 17 °C and 16,6 °C.

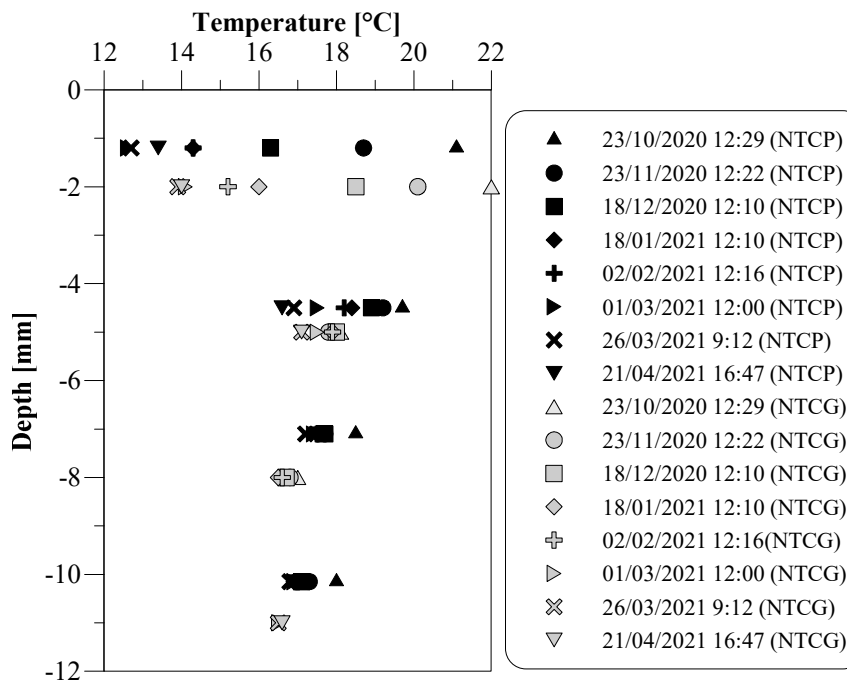
In Figure 6-33 the variability of the shallower sensors whit the external condition is more evident. In fact, it should be noted how the vibrating ware 8 and partially the NTCP1 tended to follow the external

air temperature. It is a further demonstration of how for the first sensors the measurements made during testing were strongly influenced by uncontrollable boundary conditions.

Finally, it is interesting to notice also that the slope of the curves is function of the ground surface proximity and that the trend change depended on the same factor. Excluding VW8, the shallower sensors started to change the trend between February and March while, the deeper sensors still followed the same trend.



a)



b)

Figure 6-32 - Temperature versus the depth on monthly basis a) in pile axis; b) in pile edge and surrounding soil

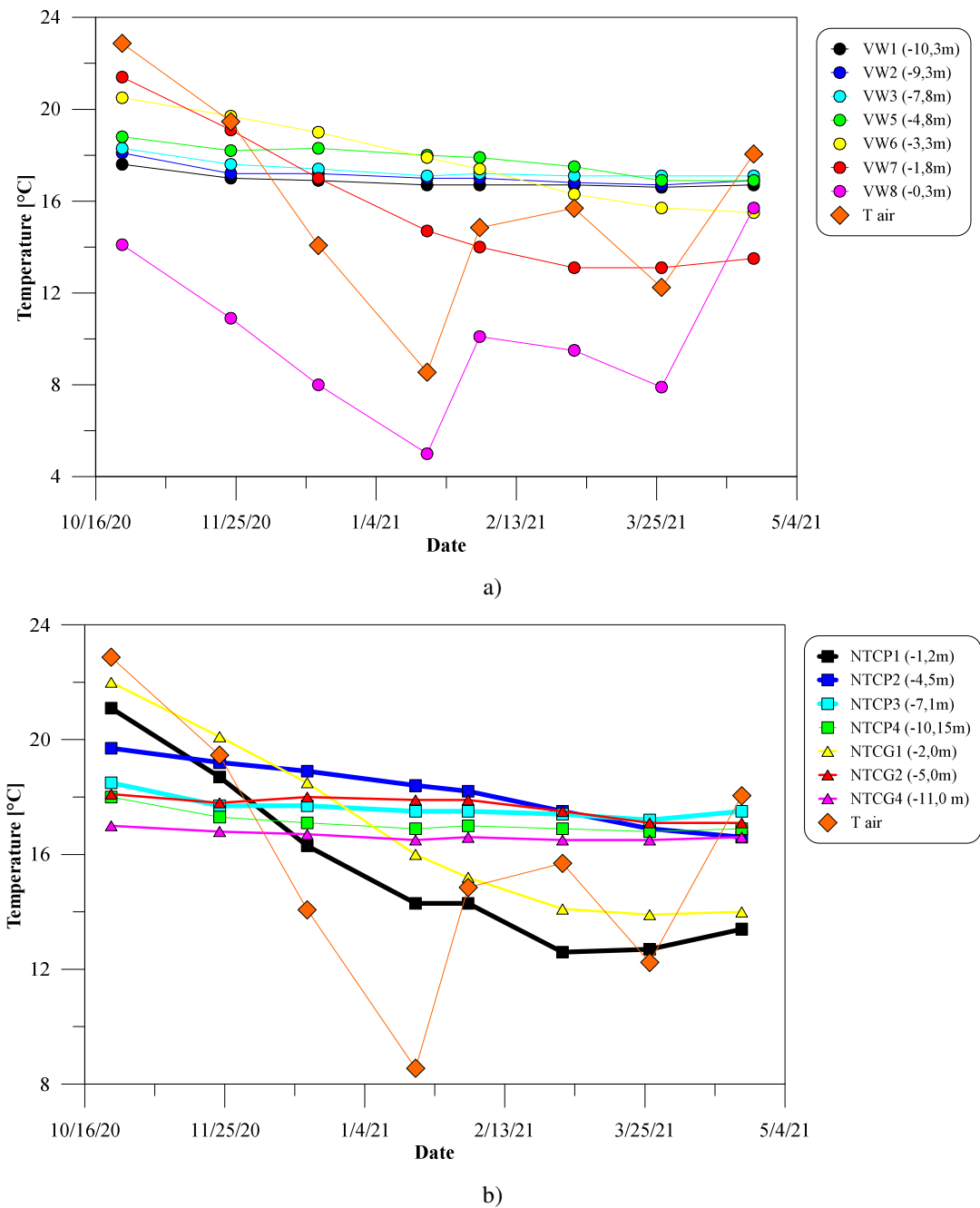


Figure 6-33 - Temperature trend versus the time a) vibrating wire in the pile axis; b) thermistors in the pile edge and surrounding soil

According to the theory reported in chapter 1, it is possible to determinate the trend of the soil temperature for different time and different depth using the mathematical relation proposed by Hillel. In this case, the relation has been used in two ways. Frist, starting from the measured values reported above, it is calculated the soil average thermal diffusivity along the soil depth. After, considering the calculated data, a yearly temperature trend for the site subsoil is predicted.

As previously detailed reported in chapter 1, according to (Hillel 1982), the soil temperature in function of time and depth. Considering an arbitrary zero point (t_0):

$$T(z, t) = T_m + A_0 e^{-z/d} \left[\sin\left(\omega(t - t_0) - \frac{z}{d} - \frac{\pi}{2}\right) \right]$$

Equation 6-21

Where:

$T(z, t)$ is the temperature of soil at time t and depth z ;

T_m is the average temperature of the soil;

z is the considered soil depth;

t is the considered time;

A_0 is the amplitude at the soil surface;

$\varphi(z)$ is the phase angle at depth z .

ω is the radial frequency defined as $2\pi/P$;

P is the period;

d is called damping depth and it is defined as the depth at which the temperature amplitude decreases to the fraction $1/e$ (37%) of the A_0 . Damping depth is linked to thermal diffusivity and radial frequency ω :

$$d = \sqrt{\frac{2\alpha_s}{\omega}}$$

Equation 6-22

Where α_s is the soil thermal diffusivity [m^2/s].

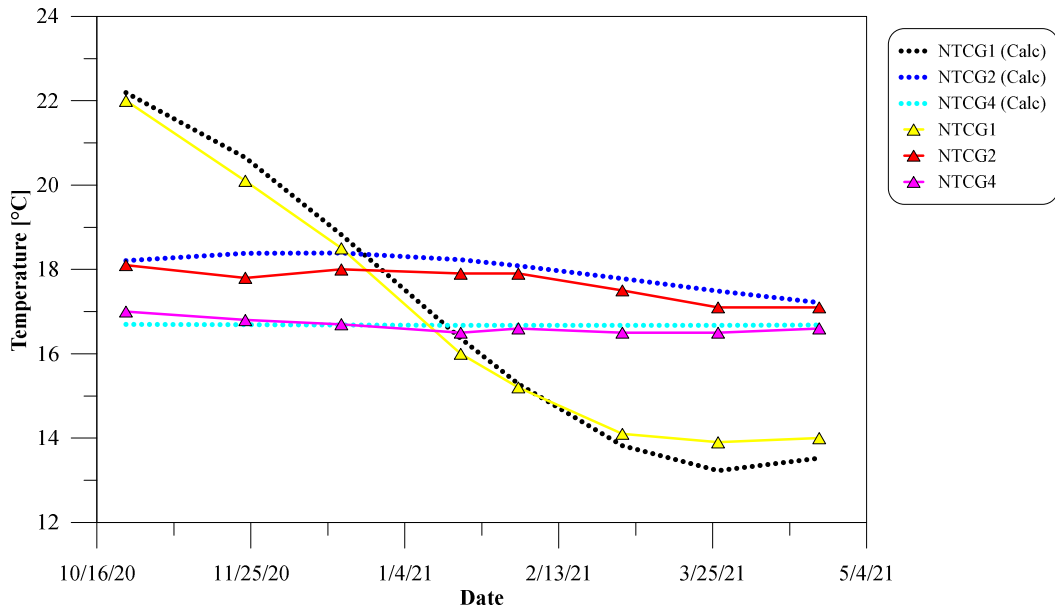
The average temperature of soil is provided by the field measures over the time while the air temperature is used to calculate the amplitude at the soil surface.

The best fitting from the measured and calculated values have been obtain for a soil thermal diffusivity of $0,0216 m^2/day$. This is comparable with the values of thermal diffusivity derived from the VDI 4640, 2001 for dry sand (chapter 1). The values derived from VDI 4640, indeed, ranged between $0,020$ and $0,049 m^2/day$. The fitting results are showed in **Errore. L'origine riferimento non è stata trovata.** considering the temperature trend for each depth with the time and in Figure 6-34 comparing the calculated and the measured values for each depth in some instant of time.

Obtained the soil thermal properties it possible to use the mathematical approach to predict the temperature trend for different time instants and different depths.

In this case, the soil average temperature has been measured from the data while the amplitude at the soil surface has been obtained considering the daily air temperatures of the Neapolitan area in the last 4 years. For each year has been calculated the amplitude. The mean of the four amplitude values has

been considered in the calculation. The aim is to obtain a result free from possible yearly thermal anomalies of the environmental conditions.



Errore. L'origine riferimento non è stata trovata.

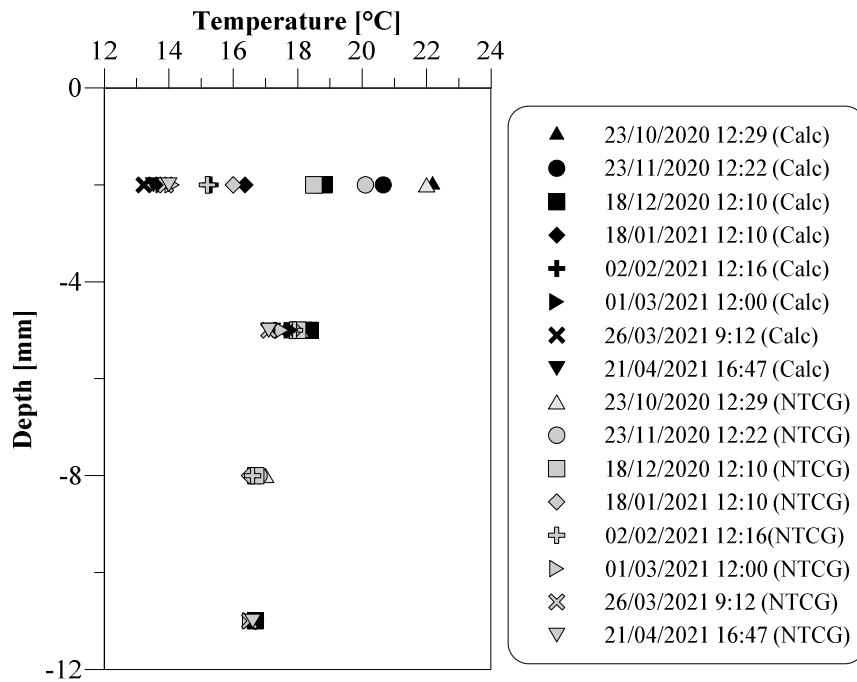


Figure 6-34 - Comparison between the measured temperatures in soil and the trend obtained with the Hillel's formula for different depths

In Figure 6-35 and Figure 6-36 the predicted temperature versus the time for different depths and the predicted average monthly temperatures for different time are reported, respectively.

As expected, and as noticed for the measured values, it is possible to notice that with the depth there is a decrease of the maximum and minimum soil temperature values. Moreover, also a shift in time is observed of the maximum and/or minimum values. Anyway, as also measured approximately

around 7 m from the ground surface, the variations are so small that the temperature can be considered constant with an average value of approximately 17 °C.

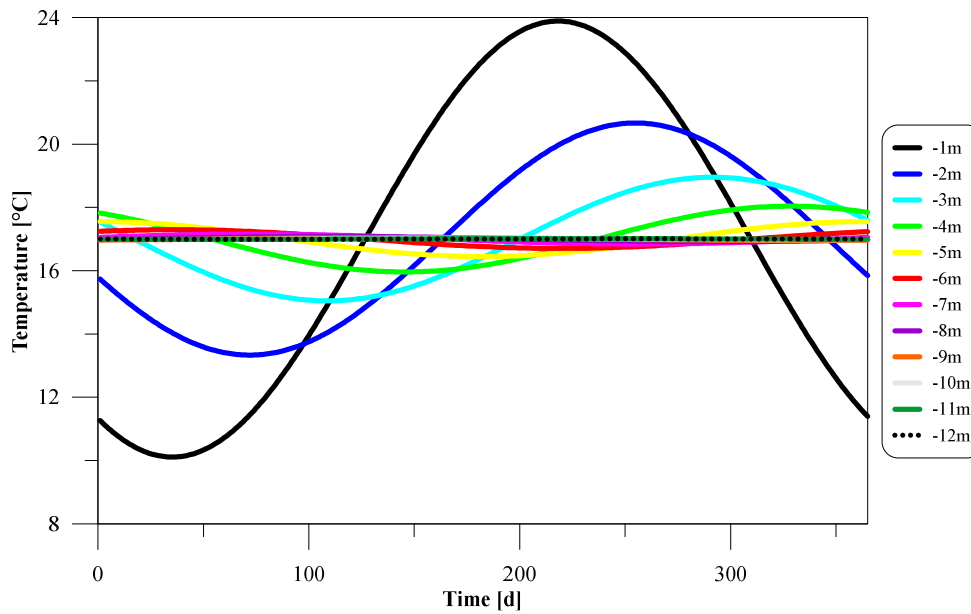


Figure 6-35 - Predicted average temperature versus the time for different depths

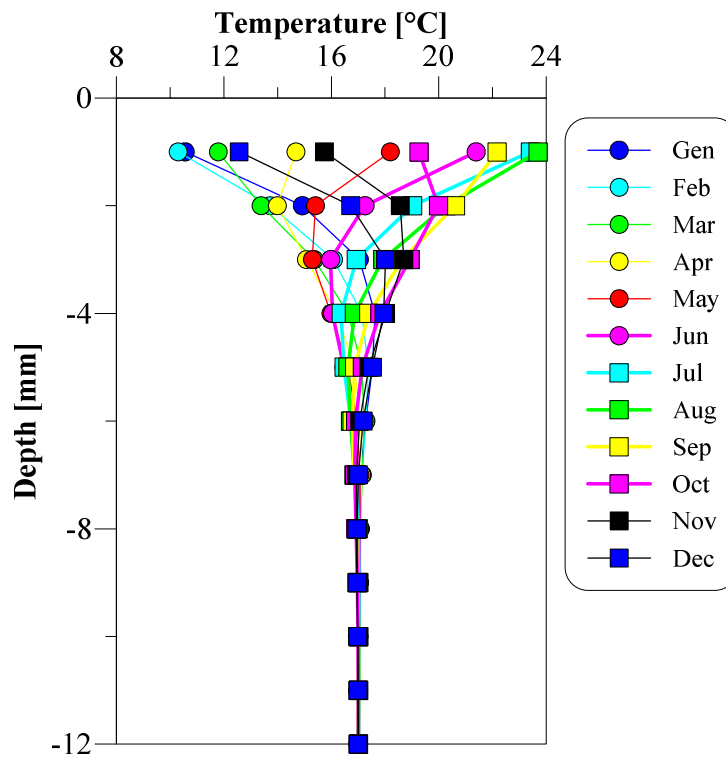


Figure 6-36 - Predicted monthly average temperature with depths

6.6 Results discussion

The three field tests reported in the chapter are carry out simulating an “on/off” operation mode for a GSHP, (i.e. thermal loads for short time). The pile was not loaded mechanically and no restrains occurred at the pile head so, it is interesting to observe the pile response in terms of stress/strains, displacements, and temperature distribution.

Operation time shorter than 6 hours, in fact, seems to not influence the surrounding soil temperatures. It means that the thermal soil reservoir is still fully usable. This phenomenon results in a higher energy efficiency of the system, which is also demonstrated by the results of the heat exchanged between the pile and the ground during the tests. In fact, normalized values of the mean heat power respect the pile length for T1, T2 and T3 are 287 W/m, 330 W/m and 228 W/m, respectively. These values are comparable with literature results obtained by (Park et al. 2015) that ranged between 285 W/m and 252 W/m for concrete energy piles equipped with spiral pipes.

The time duration of the test T2 affects the heat power value. In fact, the maximum heat transfer between pile and surrounding soil is obtained in the first hours the operation. Because T2 lasted only 1,63 hours the average value result very high.

Anyway, these results confirms the high thermal performances of concrete pile equipped with spiral pipes (Zarrella, De Carli, and Galgaro 2013).

The thermal performances of the pile are also in accordance with the literature consideration about the differences in heat exchange rate between the “on-off” and “continuous” operation mode (Park et al. 2015; 2016; 2017), (Faizal, Bouazza, and Singh 2016), (Batini et al. 2015) where is demonstrate that the “on-off” operation mode have higher thermal performances than the “continuous” one.

However, it seems that the transient phenomena do not influence only the thermal performances.

Test T2 was the shorter test. The pile was subjected to the heating phase for only 1,63 hours but the pile monitoring continued until 4,80 hours. Form the it is observed that after that the heat source is turned off, the heat continues to propagate in the in the pile section. Consequently, an increase of the stress in the pile is observed.

The concrete heat storage is also another an interesting phenomena thar could be observed during the tests. T3 and T2, in fact, were performed within a few hours of each other. At the T3 start, a different initial pile temperature is observed than the other tests. In radial direction, in fact, especially in the deeper parts of the pile the temperature differences result more uniform and higher than the other tests. It was due to the heat storage effects from the previous thermal test T2.

The mechanical behaviour of the pile is similar for all the test both for stress and for displacements. In all cases, heating thermal load provides compressive axial forces along the pile shaft. The difference of the axial force magnitude depends on the magnitude and on the duration of the

application of the thermal loads. In fact, it should be noticed that in test T1, where higher inlet temperature was used for longer time than the other tests, the maximum values of axial forces are measured (-132 kN). In test T2, inlet temperature was comparable with T1 but the time of application was approximately a quarter than T1. On the other hand, in test T3 the inlet temperatures were lower than T1 during the test approximately 4 °C, but the time of application was comparable with T1. The maximum axial forces measured in T2 and T3 were -97 kN and -105 kN, respectively. These values are not too far apart but, however, are smaller than the maximum value obtained in T1.

In all tests the maximum values of axial forces are measured 7,8 m from the ground surface. It corresponds with the null point of the pile when subjected to thermal load. From the null point it is possible to calculate the theoretical thermal strain that the pile could have if no restraints are offered. For each test, the maximum measured displacement during the test were compared with the theoretical thermal strain and was reported as a percentage. For all the tests the percentage of measured displacements respect the theoretical free range between 75% and 78%.

Even if the tests did not affect the soil temperature, by a long monitoring it was possible to appreciate how the environmental phenomena could influence the soil temperature.

The reported results are very interesting because provide a view of the temperature distribution over the time. Moreover, also provide a result about the separation between the ground surface zone and the swallow zone (as defined in chapter 1). Results show the for the investigated site, the environmental effects influence the temperature variation until 7 m from the ground surface. After this depth a constant temperature of 17 °C seems occur.

6.7 Conclusion

Field tests carried out in the province of Naples on a full-scale concrete energy pile embedded in pyroclastic soils have been discussed in this chapter.

Three thermal tests were carried out on an energy pile 0,60 m in diameter and 12 m in length equipped with a spiral shaped thermal pipe.

After a brief site description, the results of the field tests and the results of a long-term site measurements were reported and discussed in the chapter.

All the field thermal tests had different durations but, however, them was characterized by a short-time operation mode.

This kind of test have allowed to study the effects of the heat transfer transient phase on the thermal and mechanical energy pile performances when subjected to thermal loads for only some hors. This kind of thermal loads, anyway, are very common in the practice especially when the GSHP plant is used with an “on-off” operation mode.

The results highlighted the great thermal performances that reached the pile in the first hours of its work. On the other hand, it was also observed a gain of the concrete stress also some hours after the heat source turned off.

Moreover, it was found that the pile had a null point between the middle point and the toe and that measured displacement ranged between 75% and 78% of the free thermal displacements.

Finally, the subsoil thermal profile was analysed, and the thermal diffusivity was detraind analytically from the measured values.

With the obtained results a prediction of the subsoil temperature distribution over the time and for different depth in the investigated site was carried out. It was observed that after 7 m from the ground surface the soil temperature could be considered undisturbed from the environmental climatic conditions.

6.8 References

- Batini, Nicolò, Alessandro F. Rotta Loria, Paolo Conti, Daniele Testi, Walter Grassi, and Lyesse Laloui. 2015. "Energy and Geotechnical Behaviour of Energy Piles for Different Design Solutions." *Applied Thermal Engineering* 86: 199–213. <https://doi.org/10.1016/j.applthermaleng.2015.04.050>.
- Faizal, Mohammed, Abdelmalek Bouazza, and Rao M. Singh. 2016. "An Experimental Investigation of the Influence of Intermittent and Continuous Operating Modes on the Thermal Behaviour of a Full Scale Geothermal Energy Pile." *Geomechanics for Energy and the Environment* 8: 8–29. <https://doi.org/10.1016/j.gete.2016.08.001>.
- Hillel, Daniel. 1982. "Soil Temperature and Heat Flow." *Introduction to Soil Physics*. <https://doi.org/10.1016/b978-0-08-091869-3.50013-5>.
- Knellwolf, Christoph, Hervé Peron, and Lyesse Laloui. 2011. "Geotechnical Analysis of Heat Exchanger Piles." *Journal of Geotechnical and Geoenvironmental Engineering* 137 (10): 890–902. [https://doi.org/10.1061/\(asce\)gt.1943-5606.0000513](https://doi.org/10.1061/(asce)gt.1943-5606.0000513).
- Laloui, Lyesse, Mathieu Nuth, and Laurent Vulliet. 2006. "Experimental and Numerical Investigations of the Behaviour of a Heat Exchanger Pile." *International Journal for Numerical and Analytical Methods in Geomechanics* 30 (8): 763–81. <https://doi.org/10.1002/nag.499>.
- MARSHALL, J. K., and P. HUNTER. 1980. "Effect of Temperature on Vibrating Wire Strain Gauges." *Strain* 16 (1): 37–44. <https://doi.org/10.1111/j.1475-1305.1980.tb00313.x>.
- Park, Sangwoo, Dongseop Lee, Hyun Jun Choi, Kyoungsik Jung, and Hangseok Choi. 2015. "Relative Constructability and Thermal Performance of Cast-in-Place Concrete Energy Pile: Coil-Type GHEX (Ground Heat Exchanger)." *Energy* 81: 56–66. <https://doi.org/10.1016/j.energy.2014.08.012>.
- Park, Sangwoo, Dongseop Lee, Seokjae Lee, Alexis Chauchois, and Hangseok Choi. 2017. "Experimental and Numerical Analysis on Thermal Performance of Large-Diameter Cast-in-Place Energy Pile Constructed in Soft Ground." *Energy* 118: 297–311. <https://doi.org/10.1016/j.energy.2016.12.045>.
- Park, Sangwoo, Seokjae Lee, Dongseop Lee, Sean S. Lee, and Hangseok Choi. 2016. "Influence of

Coil Pitch on Thermal Performance of Coil-Type Cast-in-Place Energy Piles.” *Energy and Buildings* 129: 344–56. <https://doi.org/10.1016/j.enbuild.2016.08.005>.

Stewart, Melissa A., and John S. McCartney. 2014. “Centrifuge Modeling of Soil-Structure Interaction in Energy Foundations.” *Journal of Geotechnical and Geoenvironmental Engineering* 140 (4): 04013044. [https://doi.org/10.1061/\(asce\)gt.1943-5606.0001061](https://doi.org/10.1061/(asce)gt.1943-5606.0001061).

Yoon, Seok, Seung Rae Lee, Jianfeng Xue, Kai Zosseder, Gyu Hyun Go, and Hyunku Park. 2015. “Evaluation of the Thermal Efficiency and a Cost Analysis of Different Types of Ground Heat Exchangers in Energy Piles.” *Energy Conversion and Management* 105: 393–402. <https://doi.org/10.1016/j.enconman.2015.08.002>.

Zarella, Angelo, Michele De Carli, and Antonio Galgaro. 2013. “Thermal Performance of Two Types of Energy Foundation Pile: Helical Pipe and Triple U-Tube.” *Applied Thermal Engineering* 61 (2): 301–10. <https://doi.org/10.1016/j.applthermaleng.2013.08.011>.

General conclusion

In the last years the European union policies are increasingly focused on limiting energy consumption and climate-changing gas emissions. In this context, energy piles represent a rather innovative technology that couples the role of the structural foundation with the role of the heat exchangers for Geotherm Source Heat Pump (GSHP) plants to satisfy the building heating and cooling needs by the use of the of the Shallow Geothermal Energy (SGE).

This PhD thesis has dealt with physical and numerical investigation on the thermomechanical behaviour of energy piles operating in the Neapolitan context. Experimental investigations were carried out at field scale and at small scale in a laboratory box. The Neapolitan context was considered both for the soil in which the energy pile was embedded and for the qualitative and quantitative definition of the thermal loads applied to energy piles. The annual thermal loads were obtained from a dynamic energy simulation of an office building contextualized in the Neapolitan geographic area, carried out by the software Design Builder.

In the first chapter of the thesis the energy pile technology was described and contextualized in the European socio-political context. First of all, a brief overview about the principal energy European Directive regulating limits for the energy design of buildings and the use of renewable energy sources was carried out. In addition, an analysis of the main energy consumption sources in the world was carried out. Subsequently, the SGE and the GSHP were described in detail. After, an overview about the energy pile technology, the theoretical principles of pile/soil interaction under thermomechanical loads were described. Finally, the soil thermal properties, the heat transfer mechanism and the soil temperatures distribution with the depth were detailed described and analysed for the energy piles design.

The second chapter of the thesis concerned the energy pile literature review. The chapter can be split ideally in two main parts. In the first one the review was focused about the structural/geotechnical results obtained from filed tests and small-scale tests. In the second part of the chapter an energy/technological review was done comparing the main results of field tests, small-scale tests and numerical analysis. In the first part of the chapter, a lot of field test were compared considering the differences in terms of the pile degree of restrain. Both the trend of the pile axial stress against the temperature variation and the pile head settlements against the temperature variation for the different authors were analysed. From the results it was observed that, depending on the degree of restrain of the pile, the axial stress increment was included, in heating phase, between 106 kPa/°C and 333 kPa/°C while the pile head settlements were included between 0,07 mm/°C and 0,18 mm/°C. Regarding the small-scale tests, the literature results were compared in terms of pile head settlements against the temperature variation. In this case, the effects of cyclical thermal loads were analysed

distinguishing tests in which the piles were embedded in sand and test in which the piles were embedded in clay. It was observed an increase of irreversible pile settlements with increasing number of cycles for the tests in sand depending on the mechanical load magnitude applied on the pile head. On the other hand, by the tests in clay it was observed that, considering the same mechanical load, the state of the soil (small or high overconsolidation ratio) and the pile type of restrains (i.e. floating or end bearing pile) could vary significantly the final settlement value after a number of thermomechanical cycles.

In the second part of the chapter, the energy performances of the energy pile, considered in terms of power exchange per unit length (W/m), was related to technological aspects such as the heat exchangers pipe configuration, the pile aspect ratio, the inlet thermal carrier fluid flow rate and the inlet thermal carrier temperature. The first factor was observed as a very influent one the spiral shape heat exchanger showing the best thermal performances. It was also observed that high inlet carrier fluid flow rate and high temperature differences between the inlet carrier fluid and the surrounding soil improved the energy piles thermal performances. Finally, high thermal conductivity of the pile materials and a not continuous operation mode during the day increased the energy pile thermal performances.

The Neapolitan context both from a geological, geotechnical, and climatic point of view was addressed in the third chapter. In the first part of the chapter, the typical geological and geotechnical features of the Neapolitan subsoil were described and analysed. It is characterized by two main volcanic formations. The first one has lithified facies and it is called *Neapolitan Yellow Tuff* while the other one is a silty sand by a granulometric point of view, is generally not cemented and it is called *Pozzolana*. The main mechanical and thermal parameters of these formations were described. In the second part of the chapter, the climatic zone of the Neapolitan area was analysed. In this part, moreover, it was carried out an energy simulation by the software Design Builder. It was modelled a multi-storey office building in the Neapolitan climatic context equipped with a geothermal plant. By the energy simulation it was possible to obtain the annual geothermal heat exchangers thermal loads for the Neapolitan climatic zone. The obtained results were used as thermal loads for the numerical analysis and physic experiment carried out during the PhD research.

The results of numerical analyses carried out both for the study of a single pile and for a couple of piles were discussed in the chapter four. In the first case a finite element model was carried out by the software Plaxis 2D. An axisymmetric 2D model was used to investigate the effects of different assumptions on the boundary conditions at ground surface on the thermomechanical behaviour of a single energy pile embedded in Neapolitan pyroclastic soils. The subsoil and pile mechanical properties were obtained by a trial and error procedure based on experimental data of a site

investigation and conventional design pile load test carried out in a site in the East of Naples. The effects of different thermal surface boundary were investigated considering or the outdoor or the building indoor temperature. The latter assumption provided a simplified method to indirectly involve the superstructure heat flows in the problem. The effects on pile-soil interaction have were evaluated in terms of pile head displacements and axial forces along the pile shaft. From the analysis it was observed that:

- Hourly temperature variation caused greater pile head displacements than the daily variation (approximately 10%). In any case, compared with the mechanical case, the hourly temperature variation and the daily temperature variation led to increase the final displacement of 51% and 37% respectively. On the other hand, considering the axial forces distribution along the pile shaft the results between the two cases were not so far. In the point of maximum stress, in fact, it was observed that during the heating phase the hourly temperature variation caused an increase in axial force of approximately 14% than the mechanical case. At the same depth, the daily variation increased the axial force values approximately of 6%. In any case the differences between the daily and hourly variation resulted approximately of 8%. The difference in results was however rather small and it was concluded that as first approximation also a simple daily variation for long term analyses (i.e. one year or more) could be enough accurate thus requiring much smaller computational efforts.
- Outdoor temperature surface boundary condition led to greater pile head displacements and greater axial force variation especially during the recovery phases of the analysis. Anyway, the maximum pile head displacement considering indoor temperature variations at the soil surface was 4,31 mm, not so far from the value obtained when the outdoor temperature variations at the soil surface was considered. As regarding the differences in axial forces, it was of about 10% to 15% on the average between the two cases. Finally, it was observed that the recovery phases had a more pronounced effects on the axial loading distribution.

The other numerical simulation involved studying the behaviour of a couple of energy piles by the analysis of the interaction factor. A multiparametric analysis was carried out using the commercial finite-difference code FLAC3D. Some variable parameters were considered such as the different distances between the piles, the different soil state (loose and dense) and considering soil properties homogeneous or not homogeneous with the depth. An elastic model both for the pile and the surrounding soil was used. The interaction factor was determined both for the mechanical and for the thermal case. In any case, the procedure was to load (mechanically or thermally) a pile of the couple and analyse the behaviour of the unloaded pile in terms of displacements. The mechanical interaction

factors values were compared to the thermal interaction factors. It was observed that also in the case of thermal loads, the effects in pile groups were amplified than a single pile. In fact, it was found that the trend with the spacing was similar both for the mechanical and thermal cases with larger interaction factors occurring at smaller spacing. Furthermore, the interaction factors due to thermal loadings were slightly lower but similar to the interaction factors used for ordinary pile groups under vertical mechanical loads.

In chapter 5 the small laboratory box designed and instrumented to carry out small scale tests is first presented. A prototype of small-scale energy pile model was equipped with sensors and a rather huge testing program was carried out. This experimental part of the thesis was carried out in order to study the energy pile behaviour under cyclic thermomechanical loads. An aluminium tube was embedded in *Pozzolana* sand and was subjected to thermal loads from carried out by the energy analysis. Both cooling and heating thermal loads and different mechanical loads were used. By the small-scale it was possible to better investigate about the temperature distribution in soil and pile. It was observed that the temperature along the pile was not uniform during the test, with temperatures closer to inlet temperature on the pile head. Moreover, it was also possible to investigate the effects of the soil thermal inertia both during the active phase of the test and monitoring the temperatures when no thermal loads were applied on pile. In addition, it was observed that the shallower part of the soil was affected by the outside environmental conditions. Generally, it was observed that cyclical thermomechanical loads led to irreversible pile head displacements cycle by cycle. The magnitude and the trend of the displacements depended on the magnitude of the mechanical load applied on the pile head. A regression analysis provided in chapter 5 an analytical formula to predict the relative displacement after some number of cycles. In short, the results obtained by the tests showed that:

- In cooling phase, with the applied thermal loads, pile head settlements resulted 1,92 greater than the purely mechanical case under service load ($SF = 3$). Moreover, in cooling phase the compressive axial forces of the mechanical case decreased and changed in tensile axial forces i.e. the axial force decreased from a minimum of 1,9 times to a maximum of 2,5 times compared to the purely mechanical case.
- In heating phase, with the applied thermal loads, the axial force increased from a minimum of 3 times to a maximum of 9 times compared to the purely mechanical case under service load, depending on the mechanical load applied to the head. From the cyclical tests carried out in laboratory it was observed that the residual value of the settlements (pile downward) depend on the magnitude of the mechanical load applied in the preliminary stage. The ratio between the pile head thermal displacements during the thermal loads peak and the initial pile head

settlements due to mechanical loads, varied from 8,45 and 2,88. Higher values are reached under service load with higher SF.

In chapter 6 the results of three field tests carried out on a prototype bored pile in a typical site north of Naples are presented. The pile is 12 m in length and 0,6 m in diameter and embedded in pyroclastic soil. Moreover, the pile was equipped with a heat exchanger spiral shaped fixed to the reinforcing cage. The strain and the temperature in the pile and in the surrounding soil were measured by vibrating wire strain gauges and thermistors strings. The subsoil was investigated by a CPT and by a continuous coring.

During the test the pile was not mechanically loaded and was subjected only to thermal loads for short time in order to simulate a daily “on/off” operation mode of the GSHP. The three tests were called T1, T2 and T3 and they had not the same duration. In addition, for a period of about seven months the temperatures of the pile and the surrounding soil were monitored and measured. From the collected data it was possible to analyse the temperature soil profile with the time and the depth for the first seven month of monitoring, to deduce the thermal diffusivity of the soil and finally to predict the annual soil temperature with the depth and the time using analytic mathematical relations provided by the literature. It was possible to observe that:

- The mechanical behaviour of the pile was similar for all three tests. During the heating tests, in fact, compressive stress was measured along the pile shaft. For all three tests the null point was located at a depth of 0,65 L (where L is the pile length). The maximum values of axial forces, -132 kN, were measured during the test T1 while the maximum axial forces measured in T2 and T3 were -97 kN and -105 kN, respectively. Because T1 was the test with a slightly higher inlet temperature, it was evident the effect of the inlet heat carrier fluid temperature.
- During the test the temperature of the soil surrounding the soil did not change. Maybe it was due to duration of the tests (less than 6 hours) and to the inlet temperature (approximately 35 °C for all tests). On the other hand, the average heat power rates exchanged between pile and surrounding for the tests T1, T2 and T3 are 287 W/m, 330 W/m and 228 W/m. Moreover, it was also observed that the temperature distribution along the pile is not uniform with the depth.
- The concrete pile exhibited displacements ranging in between 75% and 78% of the theoretical “free displacement” during the tests.
- From the long-term monitoring of the pile and surrounding soil temperature variation over the time it was found that the environmental effects influence the temperature variation until 7 m from the ground surface. From this zone an average temperature of approximately 17 °C was measured. The soil thermal diffusivity obtained from site measurements was approximately

of 0,0216 m²/day. It could be considered as a reference value for designs in areas adjacent to the field tests carried out during the research

In conclusion, from the study carried out in this PhD thesis it can be observed that from an energy point of view energy pile for the Neapolitan context can represent a great opportunity to add sustainability in the field of building climatization. This could occur both for heating and for cooling purposes. These last could be also more important taking into account the specific context of the geographical area. Energy pile can be realized every time that a superstructure needed of pile foundation for the structural safety without overcharging for additional excavation and drilling compared to the structural design. The results obtained about the thermomechanical behaviour of energy piles by physical tests and the numerical analysis carried out in this research are a useful support to design decision to be taken when a pile foundation is used also for heating and cooling purposes where single piles are just individuated to act also as heat exchangers.

Anyway, some studies and analysis can be carried out in future in order to broaden knowledge of the behaviour of energy piles in Neapolitan area. First of all, application of the interaction factors calculated via FLAC in a classical computer programs for the analysis of pile groups under thermal loadings is possible. Further numerical analysis could better investigate about the interaction factor in energy pile groups by adding in multiparametric analysis some variables such as different magnitude and time duration of the thermal loads. It could be interesting to analyses the interaction factor simulating different operation mode of the GSHP plant.

Regarding the small-scale test, the designed prototype could be used to continue the investigation about cyclical loads considering a number of cycles much larger than the 10 considered in this research. Different magnitude of mechanical loads, also, could be applied on the pile head to investigate the pile-soil system behaviour for longer time application of thermal loads analysing the pile head displacements trend. Also, the test bored pile could be further used to carry out other and more complete tests that were partially stopped due to the difficulties connected to the Covid events.